Transactions of the ASME®

Transactions of the ASME, Journal of Engineering for Gas Turbines and Power (ISSN 0742-4795) is published quarterly (Jan., Apr., July, Oct.) for $130.00 per year by The American Society of Mechanical Engineers, 345 East 47th Street, New York, NY 10017. Second class postage paid at New York, NY and additional mailing offices. POSTMASTER: Send address changes to Transactions of the ASME, Journal of Engineering for Gas Turbines and Power, c/o THE AMERICAN SOCIETY OF MECHANICAL ENGINEERS, 22 Law Drive, Box 2300, Fairfield, NJ 07007-2300.
CHANGES OF ADDRESS must be received at Society headquarters seven weeks before they are to be effective. Please send old label and new address.
PRICES: To members, $40.00, annually: to nonmembers, $136.00.
Add $15.00 for postage to countries outside the United States and Canada.

INDEXED by Applied Mechanics Reviews and Engineering Information, Inc.
Canadian Goods & Services Tax Registration #126148048

Journal of Engineering for Gas Turbines and Power

Published Quarterly by The American Society of Mechanical Engineers

VOLUME 114 • NUMBER 3 • JULY 1992

TECHNICAL PAPERS

ANNOUNCEMENTS

1991 Soichiro Honda Lecture

Energy, Efficiency, and the Environment: Three Big Es of Transportation

K. J. Springer
Southwest Research Institute,
San Antonio, TX 78228

The three big Es of transportation are Energy, Efficiency, and the Environment. As the clouds of global climate change and the desire to rely less on Mid-East crude builds, how do manufacturers and refiners reconcile the needs of consumer acceptance and governmental regulation? How can policies and practices be united so that everyone involved works to the common goal of personal mobility? This lecture traces recent events that have resulted in paradox on top of paradox. As industry continues to react to the latest round of air pollution regulations, where are we headed as far as new CAFE limits and the potential for additional longer term controls related to the greenhouse effect? These are issues that will affect those in the equipment and oil industry, as well as the consumer, in the days ahead.

Introduction

This is a comment on current and future road transportation, as influenced by sometimes contradictory and paradoxical policies of government and responses by industry. In no other major segment of our society have government regulations roamed so at will than in on-highway transportation, regulating everything from the fuels to the tailpipe emissions with safety and fuel economy thrown in for good measure. For the past 20 years,the thrust of these regulations has been principally at the car makers. Because car making and fuel refining are very competitive businesses, the industry had to have common targets to justify the enormous redirection of effort and additional expenditures to reduce energy consumption and emissions. The threat of "you cannot sell cars in the U.S. after a given date unless they met certain emission, safety, or economy requirements" got the attention of upper management. Perhaps this approach was necessary to get action on items generally considered as additional costs to make and sell a product, but were not perceived as a reason for a customer to decide to buy that make of car. Therein was the great argument that deeply divided the industry from the government. The car and equipment making and fuel refining industries resented the government and its regulators intruding into their business. They resented the agency employees telling them how to make cars, trucks, and buses, and how to refine crude oil. It made little difference that the Environmental Protection Agency (EPA) or Department of Transportation (DOT) were, in fact, carrying out the wishes of Congress. In many cases, the Federal law was re-interpreted through Federal court decisions as a result of lawsuits by one or more environmental or consumer groups.

In retrospect, the industry has been able to comply with these numerous regulations, albeit at enormous cost in resources of people, equipment, and facility, a cost eventually passed to the consumer. Only in a few instances were time delays necessary. Thus, the lawmakers and regulators can take some measure of satisfaction in saying, "See, I told you you could do it" and "my technology-forcing regulations were achievable after all." There is little doubt that we now have more environmentally friendly, safe, and efficient cars at an earlier date than we would have had if the industry had been left to its own timetable. Perhaps this is the one saving feature, the one redeeming value in the system of confrontation, regulatory requirements, and reactive response that characterized each of the areas of environment, fuel, and safety improvements. It would be sufficient to end this lecture at this point if the saga of regulation of the automotive industry was at a standstill, as it was during the eighties. Everyone could take credit for winning, in their own way, since everyone won: manufacturer, refiner, and consumer. The products are definitely better, and the consumer did not have to pay as much as some forecast he would, even though he is paying more.

There are new U. S. and state laws, however, that portend enormous changes to transportation that affect makers, refiners, and consumers in the future. It is these new requirements and the changes, conflicts, contradictions, and paradoxes that need debate and discussion. Fresh from that extra good feeling of accomplishment by the Clean Air Act Amendments of 1970 and 1977 and the Energy Policy and Conservation Act of 1975 establishing Corporate Average Fuel Economy (CAFE), the lawmakers have tasked the industry with even more technology-forcing requirements for the decade of the nineties and beyond. It is these forces, clearly the drivers of technology improvement for the foreseeable future, that will shape the types of products to be used by consumers in the U.S. and to some extent in other parts of the world. So far, safety regulations for the future have concentrated on extending the passenger car rules to other classes of motor vehicles. Safety remains important, however, as the car is made even smaller and lighter, or must use a new fuel or an existing fuel under

Contributed by the Internal Combustion Engine Division and presented at the 13th Annual Fall Technical Conference, Muskegon, Michigan, September 30–October 2, 1991. Manuscript received by the Internal Combustion Engine Division September 15, 1991. Associate Technical Editor: J. A. Caton.

different circumstances. The remainder of this lecture will focus on energy, efficiency, and environmental issues, the three big "Es" or "biggies," as they are expected to affect on-highway cars, trucks, and buses.

Energy

The automotive car, truck, and bus engine has been married to crude oil derived gasoline and diesel fuel almost since inception. Development and use of the internal combustion engine powered vehicle has been linked directly with a relatively inexpensive, abundant, and available refined product. This marriage of fuel and engine has had its rocky times, as in 1967 when Exxon [1] showed the auto industry that activated carbon could serve to collect vapors from the tank and engine. This resulted in a Federal Regulation [2] to control evaporative emissions during diurnal heating as well as after engine shut-off. Another instance was when, at the request of the auto makers, the EPA required unleaded gasoline for catalyst-equipped cars beginning July 1974. Yet another instance was in 1985 when General Motors urged fuel refiners to make cleaner gasoline that would not make troublesome port fuel injector deposits [3]. Sometimes, the relationship seemed troubled, marked by lengthy silences, as if the partners had quit talking to each other. The marriage appeared headed for the divorce court when an interloper, alcohol fuel, entered the scene with strong Federal encouragement in June 1989. The car companies had developed flexible fuel vehicles (FFVs) able to run on any combination of methanol and gasoline, up to 85 percent by volume methanol, called M-85.

Auto-Oil Fuel Effects Project. In Oct. 1989, the 14 million dollar, Phase I Auto-Oil Program of 1990–1991 was announced [4]. Perhaps the turning point was the June 1989 Bush Administration proposal [5] to mandate millions of FFVs in nine nonattainment areas on a time-phased schedule. Maybe the turning point was the Sept. 1989 introduction of a reformulated fuel by ARCO called EC-1 to replace leaded gasoline in Southern California [6]. Perhaps there was the growing realization of a need to see what might be possible with gasoline composition in conjunction with the modern computer-controlled passenger car [7]. In Nov. 1990, Phase II of the Auto-Oil Program was authorized. It is a 25 million dollar project expected to be completed in mid-1994.

There was little doubt on anyone's part that the automobile had made truly remarkable, revolutionary gains in all the regulated areas of emissions, economy, and safety, while still burning the same basic unleaded gasoline for the past 15 years. Was it time for the possibilities of improved gasoline to be revisited? It had been over 20 years since the last in-depth research on fuel effects on emissions and air quality had been performed. The 1970 Clean Air Act Amendments directed major reductions in tailpipe emissions with goals of 90 percent HC and CO and 70 percent NO_x. The oil industry was left out of such technology-forcing limits for good reason. Changes in fuels, while producing some reductions in some pollutants by perhaps 10–15 percent, were trivial compared to the 70 and 90 percent requirements placed on the manufacturer. As a consequence, little was asked from the refiner other than to take out the lead (starting in July 1974) and add deposit control additives (1985) and control vapor pressure (1989) [8].

Energy Consumption. What does all this have to do with energy other than that gasoline and diesel fuel are made from crude oil? As shown in Fig. 1 [9], approximately 11 million barrels of crude oil are consumed by transportation in the U.S. each day. About 45 percent is imported, affecting more or less the U.S. balance of trade. These statistics do not mean much until one realizes that it was transportation, principally the popularity of the automobile, that increased our need for crude oil. The U.S., it seems, will do almost anything to get oil. How different the U.S. and the world might be had the personal freedom of mobility provided by the privately owned car been restricted by a lower availability of crude oil. The availability of crude oil to the U.S. market was somewhat dependent on the advent of cheap transport in huge supertankers, the technical innovation that permitted oil from relatively inaccessible sources to reach the U.S. market. Post-World War II government policies that supported urban sprawl, endless highway construction, the suburbs, and low-density housing away from the city [10] also take much credit for the car becoming a necessity to life, society, and civilization as we know it today.

The major driving force for the mixed fuel-energy strategy of today is concern over environmental effects, termed micro and macro. It happens that nearly every city of over 1 million people has some type of air pollution problem dependent more or less on transportation along with the other activities of the city. This is termed the micro effect. Relative to the seven mile thickness of the troposphere, the layer of atmosphere that surrounds the planet Earth, the city-related pollution is regarded by some as isolated. Depending on the gas or vapor, however, all have some life in the atmosphere regardless of whether generated in the city or in the country. This is the macro effect.

Carbon-Based Fuels—Global Warming. Consumption of energy, principally from fossil fuel, means a carbon-based economy, one in which the standard of living is proportional to the amount of carbon consumed, whether from wood, charcoal, coal, oil, or natural gas. The increasing population of the Earth, the desire for a better lifestyle, including all the material goods and services, plus the freedom of personal mobility afforded by the car, mean more carbon consumption, at an ever-increasing rate. Figure 2 [11] shows that more and more CO_2 is released as the carbon in the fuel is burned, whether in a boiler or in an internal combustion engine.

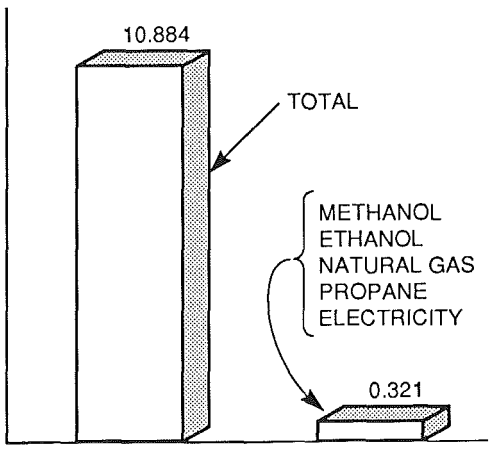

Fig. 1 Transportation energy, estimated 1989 U.S. daily average (millions of barrels per day oil equivalent [9])

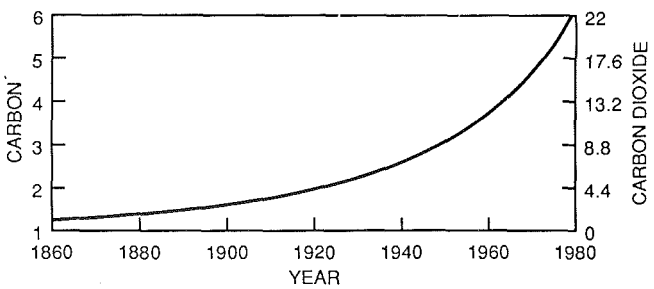

Fig. 2 Worldwide carbon and carbon dioxide production from fossil fuel combustion (billions of tons per year [11])

An ever-increasing CO_2 concentration gives rise to concern over global warming and the potential for global climate catastrophe. Carbon dioxide, along with methane, chlorofluorocarbons (CFCs), nitrous oxide, tropospheric ozone, and water vapor, absorbs the reflected infrared energy from sunlight that strikes the Earth. Like panes of glass in a greenhouse, the absorption of this energy is responsible for a livable earth environment of about 15°C (59°F). Too much greenhouse gas emission portends disaster according to a growing number of scientists. Since CO_2 is believed to contribute to half of the greenhouse gas effect, the ever-increasing consumption of carbon-containing fuels is suspect and is being scrutinized by world opinion. In the U.S., transportation accounts for 4.2 percent, of which cars are responsible for 2.8 percent of the CO_2 emissions.

More than 130 nations took part in the Feb. 4–14, 1991, Chantilly, Virginia International Negotiating Committee on a Framework Convention on Climate Change [12]. It is expected that in 1992, the U.S. may enter into some type of international agreement on limiting CO_2 emissions. When this happens, it will likely include transportation and especially the passenger car, a favorite target for CO_2 reduction. There are many strategies under consideration that involve, in the ultimate, a move away from carbon-containing gasoline, diesel, or alcohol fuels to electricity and hydrogen made from non-CO_2 producing sources of energy such as the sun, nuclear, or wind. The staggering amount of energy used each day in the U.S. for transportation makes any alternative look like the proverbial "drop in the bucket." Thus, such transportation strategies will likely include major efforts to conserve, in terms of improved efficiency, reduction in vehicle miles traveled as in a change in lifestyle and perhaps limitations in auto registrations or fuel rationing. Much has been published on this subject, and [13–16] are helpful for further study.

Efficiency

There are some common misconceptions about fuels and what influence environmental rules have had and continue to have over engine efficiency as well as the ubiquitous corporate average fuel consumption (CAFE) regulations.

Spark-Ignited Engines. The spark-ignited (Otto cycle) engine thermal efficiency is dependent on compression ratio among other factors. Figure 3, from [17], shows the historical trend of compression ratio in the U.S. Spark ignition engine compression ratio is determined by the mechanical octane number of the combustion chamber design such as high swirl, fast-burn systems and is limited by the fuel quality or chemical octane number. In the design of engines that have greater efficiency, gasoline with higher octane is essential. An engine's tendency to knock audibly under low-speed, relatively mild conditions is measured by ASTM D 2699 for research octane number (RON) and under high-speed, high-severity conditions by ASTM D 2700 for motor octane number (MON).

Sometimes cars will have low-speed knock during light acceleration or knock audibly during hard acceleration as in entering a freeway or during hill climb. Usually one cylinder is responsible because of excessive combustion chamber deposits, overadvancement of the spark timing, or some change in EGR or air–fuel mixture. Such knock is of limited duration and is rarely harmful to the engine. The use of higher octane, premium grade gasoline usually eliminates the annoying knocking sound, but does little to improve the engine thermal efficiency or vehicle fuel economy, contrary to popular belief. EPA has determined that only 5 percent of the cars actually need premium or midgrade unleaded, although those grades are as much as one-third of the gasoline sold.

In 1921, tetraethyl lead (TEL) was shown to decompose during the combustion cycle to form a cloud of catalytically

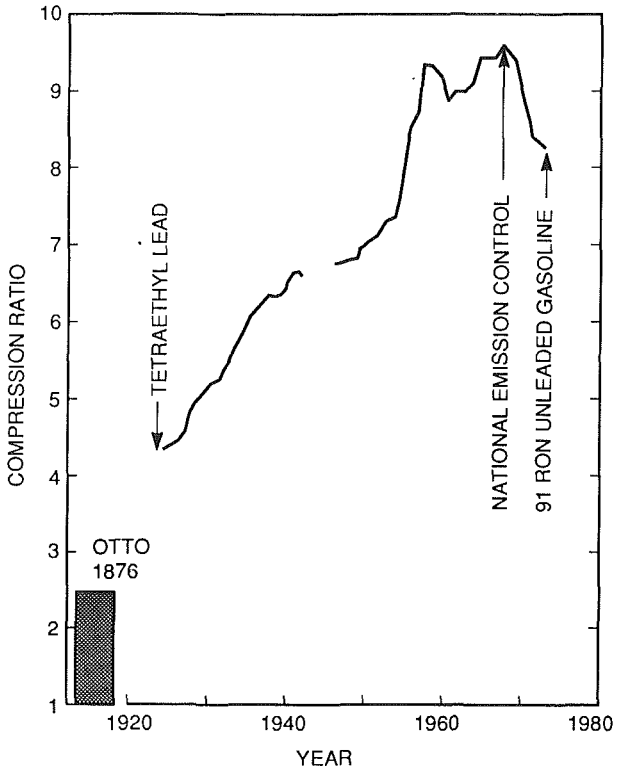

Fig. 3 Average U.S. compression ratio, historical trend [17]

active lead oxide particles. These particles interrupt the chain-branching reactions that lead to too-rapid combustion known as knock. The maximum lead content of gasoline was initially established by the U.S. Surgeon General at 4.0 ml of lead compound per gallon (4.23 g of lead per gallon) based on health considerations in handling the fuel. The economical use of lead resulted in a practical maximum of about 3 g per gallon. The effectiveness of TEL and TML lead compounds is dependent on fuel composition. TEL, and more recently TML (tetramethyl lead), with appropriate bromine and chlorine-based scavengers, have been widely used in gasoline in the U.S. Considerable advances were also made in refining processes such as thermal cracking, catalytic cracking, and reforming, so that by about 1955, 95 RON gasoline was available.

Compression Ignited Engines. This type of engine, which normally operates on diesel fuel, is the most efficient of any heat engine yet devised. Diesel fuel has an ignition quality, called cetane number, which is a measure of the readiness of the fuel to ignite spontaneously. It is opposite in effect to that of the octane quality of gasoline. The higher the cetane number, the shorter the delay between injection and ignition of the fuel under the pressure and temperature in the combustion chamber of the engine. Fuel cetane number for type 2-D fuel, popularly used in on-road trucks and buses, is specified by ASTM D 975-81 to be 40 minimum, as measured by ASTM D 613. Sometimes low cetane levels results in increased combustion noise, emissions, and poor starting. The effect of cetane on efficiency is more dependent on the fuel composition and heating value with an average U.S. cetane of 45, common for on-highway type 2-D fuel. Merely increasing cetane number does not necessarily allow a higher compression ratio or result in lower fuel consumption. Diesel engines use a compression ratio high enough for starting, yet optimum for best engine efficiency and durability. One compression ignition engine that runs on methanol features a compression ratio as high as 23:1, plus ignition aids such as glow plugs because of the much higher auto-ignition temperature of methanol relative to diesel fuel [18].

Air Pollution and Unleaded Gasoline. During the fifties and sixties, air pollution over some cities in the U.S., notably Los Angeles, got progressively worse as photochemically reactive hydrocarbons and oxides of nitrogen combined in sunlight to yield ozone and cause eye irritation. The best strategy for meeting the stringent requirements of the 1970 Clean Air Act Amendments was to reduce engine-out emissions as much as possible and then add an oxidation catalyst to further reduce CO and HC. Retarded ignition timing and exhaust gas recirculation were popularly used ways to reduce NO_x.

In order to use the oxidation catalyst, the car makers needed a lead-free fuel. It was known that lead combustion products glaze the porous surface of the exhaust catalyst, a poisoning effect that rendered the device less efficient. The U.S. car makers, led by GM President Edward Cole, redesigned engines for 1975 with lower compression ratio. In this way, the engines could operate on regular grade gasoline without lead. On Jan. 10, 1973, the EPA issued regulations requiring unleaded gasoline be sold starting July 1, 1974 for catalyst equipped cars. The unleaded gasoline was to have 91 RON, later defined as octane index $(R+M)/2$ of 87.

The car makers did not ask the oil refiners to change composition or reformulate, merely take out lead. This was not easily accomplished, however, since lead was a blending agent that was not used to the same amount in all gasolines; nor was the phase-in of unleaded cars all that the refiner had to deal with. The EPA soon issued rules to phase out lead content in the remaining gasoline beginning Jan. 1, 1975, which did result in changes in refinery processing and fuel composition, now known as reformulation. Many times, these changes adversely affected refinery yield, requiring more energy consumption to produce more and more unleaded or lower lead gasoline; another loss in the overall energy efficiency. Some of the engine efficiency loss was regained through continued combustion research, improved mixing, and combustion process control, an improvement in mechanical octane number. In some cases refinery yields likewise were improved. However, the advent of lower compression engines and the refining of unleaded gasoline are still considered to have increased overall energy consumption, a paradox of some significance.

OPEC, the Energy Crisis and CAFE. In 1973, OPEC limited production to increase the price of crude oil. OPEC said it was trying to do us a favor with higher prices to reduce consumption and become more self-reliant. In the energy crisis that resulted, the CAFE regulations required makers of cars and light trucks to produce more fuel-efficient vehicles, ultimately reaching 27.5 miles per gallon (MPG) average in 1985. Figure 4 [19] tracks the sales-weighted CAFE, in miles per gallon, since 1974 for both domestic and imported cars. Interestingly, the engine design improvements played a minor role, although engine power to vehicle weight were of major importance. The tried-and-true methods to achieve better economy through lower vehicle weight, smaller displacement engines, i.e., 4 cylinder in place of 6 and a 6 in place of a V8, lower engine speeds, by use of overdrive transmissions, and lower wind and rolling resistance, all helped. At no time did the fuel itself become a subject of reformulation or change. Compression ratios remained at a level compatible with $(R+M)/2$ of 87 (91 RON). There was little thought given to raising fuel octane and compression ratio. With the crisis conditions of shortages, gas lines, and higher prices, people were glad there was fuel enough to burn. Alternatives such as diesel fuel made a brief appearance in U.S.-made passenger cars as a means to preserve the large car in some vehicle line-ups. Diesel cars have superior fuel economy; however, few diesel-powered cars are still sold in the U.S. because of the stringent exhaust particulate standards.

At the same time as the safety standards and CAFE standards were taxing the car makers, another, more significant reduction

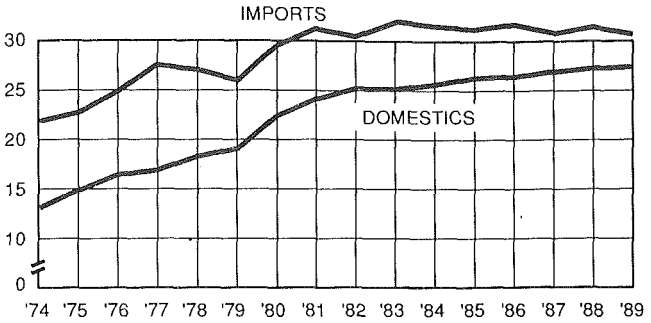

IMPORTS
22.2 23.2 25.4 27.7 27.3 26.1 29.6 31.5 31.1 32.2 31.8 31.5 31.7 31.1 31.2 30.6

DOMESTIC
13.2 14.8 16.6 17.2 18.7 19.3 22.6 24.2 25.0 24.6 25.6 26.3 26.6 27.0 27.3 27.1

Source: U.S. Department of Transportation

Fig. 4 CAFE since 1974 [19]

in emissions was promulgated. As a result of the Clean Air Act Amendments of 1977, the car maker needed to roll back HC, CO, and NO_x emissions even more. Effective with model year 1981, HC/CO/NO_x limits were 0.41/3.4/1.0 g per mile. To do so required a major technical breakthrough, the oxygen sensor. This sensor permitted use of a three-way catalyst, one that simultaneously could promote oxidation of HC and CO to CO_2 and water vapor and reduction of NO to N_2, water vapor, and CO_2. To make this happen, the oxygen sensor acted as a fast-acting switch at the stoichiometric air:fuel ratio, about 14.7:1 for gasoline, to provide feedback to the engine. It happens that the use of platinum (for oxidation) and rhodium (for reduction) in the same catalyst system would reduce all three regulated emissions if the air:fuel ratio was controlled to 14.7: $\pm$0.1. Unleaded gasoline remained a requirement for long life of both the porous zirconium dioxide oxygen sensor and the catalytic device. A variety of system controls for fuel and air resulted. With individual port fuel injectors directing a fuel spray on the underside of the intake valve and utilizing the error signal from the oxygen sensor for feedback, the possibilities of computer control of the engine continue to be explored to achieve long-term drivability and customer acceptance. Such systems, considered revolutionary just a few years ago, are considered commonplace and even taken for granted today.

Now possible are sensors that detect knock before it can be heard and automatically determine which cylinder is knocking. Using a smart ignition system, the timing of just the knocking cylinder is retarded for the usually brief knocking duration and then readjusted back to standard programmed timing. This engine of today has the ability to be octane insensitive, i.e., run on a fairly wide range of fuels. Of course, the lower the octane, the later the ignition in more and more cylinders and although the engine will still run, the performance and efficiency will be poor. Too bad these same smart engines cannot advance the timing to take advantage of the higher octane in some fuels. Rarely is this permitted because the increase in engine-out NO could overload the three-way catalyst. The engine featuring manifold fuel injection, oxygen sensor, and three-way catalyst with adaptive feedback computer control and knock sensor has a trivial effect on engine efficiency, even though there are momentary retarded timings where the occasional cylinder knock occurs.

To some engineers, the three-way catalyst represents a major obstacle to improved efficiency, an improvement of as much as 10 percent promised from very lean-burning engines. Engines that operate with air:fuel ratios of greater than 22:1

qualify as lean burn and are possible with today's technology. The fact that three-way stoichiometric burn engines are already available and in common use for many years in the U.S. has been reason enough for the European community to adopt the same stringent standards for its member countries. These standards are sufficiently difficult to rule out, at least for the time being, serious consideration of the lean burn engine. So far, lean burn engines cannot achieve the NO_x standard and being lean, cannot make use of three-way catalytic aftertreatment because of the excess oxygen in the exhaust. Such regulations are seen by the European and Japanese to deter and perhaps block further development of lean burn engines, another obvious efficiency-environmental paradox.

Optimum Octane—Efficiency and Energy Use. It requires more energy to raise gasoline to the same octane number without benefit of TEL or TML. The current unleaded 91 RON level is not necessarily optimum for overall best energy use in the refinery and in the engine. For example, a 95 RON fuel is sufficient to allow the compression ratio to be increased a full number from, say, 8.5 to 9.5:1. However, it is pointless to make higher compression engines achieve better combustion efficiency if the gains are more than offset by efficiency losses in the refinery. A 1983 study on the rational utilization of fuels in private transport [20] indicated 94.5 RON is optimum. Similar studies in the U.S. need to take advantage of the latest technical improvements in refinery processes and engine possibilities. The optimum fuel octane value could help the auto-oil program to define a recipe for future gasoline and, of course, be central to any energy plan or policy. A "rule of thumb" is that an increase in one octane number will permit a one percent fuel economy improvement.

Future Efficiency Improvements. The major improvements in engine efficiency, expected in the future, will lie with reduced friction losses, reduced pumping losses, preservation of heat through insulating films, and coatings coupled with improved expansion processes [21]. Heat conservation within the engine does little good if it is not converted to useful work in the expansion process or collected in some type of regenerative turbo-compound expander, where exhaust heat is converted into torque. Of all these potential areas, the remaining major improvements in engine efficiency are thought to be related to engine friction. Significant efforts are in progress and more, much more, is expected in terms of design, materials, and lubricants. Even so, all these changes will be minor and almost trivial when compared to further improvements in engine and vehicle weight, vehicle power to weight, size, and shape, as the car maker struggles to keep gasoline cars in the mix of vehicles of the expected future stringent CAFE regulations.

Safety concerns already are voiced as vehicle size is further reduced. The small car injury statistics and the concern over vehicle size and head-on collisions may place some lower limit on vehicle size and weight for safety reasons. If all cars were underpowered and the same weight, then the problem would not be as severe. This is obviously not going to be the case in the near future any more than in the past. The car designer will be forced to the limit of technology in the use of materials and structures for occupant protection as vehicles are further reduced in weight [22].

Another major area for continued improvement is in drive train torque management. There is a limit to how slowly the engine can run with acceptable torque. However, the more speeds in the automatic transmission, the greater the ability of the computer to match the transmission to the engine for the drive torque required. Computer management of engine and transmission will lead to further improvements in the quality of drive, the ultimate test of customer satisfaction, and this is affected by the fluid as well as the friction materials. It is believed that the computer controlled automatic transmission passenger car can achieve superior fuel economy to the manual transmission except when driven by an expert test driver. The computer control will consistently decide on the best drive gear for fuel economy and drivability and thus be important in achieving future CAFE limits.

Regardless of all these expected improvements in efficiency, the gasoline-powered car will find itself in a mix of vehicles powered by other types of fuels and engines. The mix could include FFVs or vehicles with engines designed to burn methanol only or natural gas. Depending on future CAFE regulations and provisions to give credits to alternative fuels, electric, gasoline-electric hybrids, and even hydrogen-fueled vehicles could appear. One suggestion that encourages alternatives is to compute fuel economy on the basis of the amount of crude oil derived gasoline consumed. For a FFV operating on M-85, 15 percent gasoline, 85 percent methanol, getting 20 mpg (gasoline energy equivalent), its fuel economy could be 133 mpg if based only on the gasoline fraction [23]. Such calculations presume that the FFV will always operate on M-85, an uncertain possibility.

Future of CAFE. Major increases in CAFE are expected to make major changes in vehicles. This is thought to be the single most important issue facing the auto makers. As mentioned earlier, there are still some technical improvements possible. However, these will not be, in themselves, sufficient to meet improvements proposed by Senator Bryan of 20 percent (to 34 mpg) and 40 percent (to 40 mpg) in 1996 and 2001 [24], or Senate Bill 279, a bipartisan bill to increase CAFE to 40 mpg by 2001. CAFE should be considered as one of several aspects of conservation. To some, it is the only "safe" or convenient policy to follow regarding reduced reliance on foreign crude oil, global warming, trade imbalance, and air pollution. To others, it is a way to encourage alternatives through creative fuel economy incentives.

Those against CAFE regulation argue that the best policy would be to increase the price of gasoline sharply through taxation, as do many European countries. Others believe a reduction in vehicle miles traveled by increasing the number of passengers per car from the current average of about 1.5 is the answer. This strikes at a lifestyle based on freedom of mobility and the cost and convenience of personal vehicle operation. Since no one wishes to interfere in these, the major burden of fuel economy improvements continue to be the responsibility of the car maker.

Heavy Duty Engine and Vehicle Efficiency. EPA classifies as heavy duty those engines used in trucks and buses having a gross vehicle weight (GVW) of over 8500 lb or a frontal area larger than 45 ft^2. Such engines and vehicles have no fuel economy or CAFE standards. The value of HD engines is in their ability to produce flywheel power and torque, and not carry on the average of 1.5 persons, as with cars and many pickup trucks. Engines usually are specified on the basis of specific fuel consumption (lb of fuel per bhp hour) at rated speed and load, useful in comparing engines such as gasoline and diesel. The energy crisis of the midseventies brought out many new engine and vehicle features such as engine speed derating, greater use of turbochargers, wind deflectors for less wind resistance, and lower rolling resistance tires. To what extent future regulations will impact on truck and bus fuel economy over typical driving cycles, that are somewhat analogous to the passenger car city and highway cycles, is unknown. The EPA transient engine certification cycle results in fuel consumption at the same time the emissions of HC, CO, NO_x, and particulate (diesel only) are obtained. However, the analogy with the CAFE procedure ends there since engine fuel consumption is only one part of HD vehicle fuel consumption, a value not readily obtained as is the case for light duty vehicles where the entire vehicle is tested on a chassis dynamometer.

On-road fuel economy can be measured; however, the wide variety of HD vehicles means lots of testing.

The Unleaded Fuel Paradox

Taking lead out of gasoline had some good effects as in lower lead levels in the atmosphere and along roadways, and facilitating exhaust emission control by catalytic devices. However, taking lead out resulted not only in higher energy consumption in the refinery (lower yield), but a reformulation of gasoline toward use of more volatile and aromatic components. These were consequences that neither the government nor the car makers appeared to take into consideration in 1973, and resulted in what may be termed the unleaded fuel paradox. Cars are certified by EPA for sale in the U.S. based on unleaded reference fuels for emissions and durability testing [26]. These fuels, originally selected in the late sixties, were intended to typify fuels then sold commercially.

Volatility, Vapor Pressure and Volatile Organics. Volatile organic compounds (VOCs) are the major drawback to the future use of gasoline in the U.S. One reason gasoline is a good fuel is that its volatility makes it relatively easy to vaporize and mix with air and ignite, especially when cold. Thus, the volatility is adjusted regionally and seasonally following ASTM D 4814. The emissions certification gasoline is 9 psi vapor pressure and this was not atypical of the late sixties summer grade of gasolines. Except for California, which always enforced 9 psi summer vapor pressure, gasolines sold in the U.S. gradually increased in vapor pressure during the 1975–85 period to about 11.5 psi (summer grade). Although most cars ran satisfactorily, some of the vapor from the fuel tank and engine during diurnal heating and after engine shutdown was not collected by the activated carbon canisters. The increased vapor pressure was usually a result of blending butane [27] and more volatile aromatics into the fuel to achieve the octane specification. Butane has low primary atmospheric activity and is of little consequence in the photochemical reactions to form ozone. However, some of the evaporative emissions not collected include other VOCs, thought to be more photochemically reactive.

Thus, the fuel reformulation that occurred to produce increasingly larger quantities of unleaded fuel each year generally brought about more and different VOCs than those in the certification fuel. Their escape routes into the atmosphere became better understood as in refueling losses, the release of gasoline vapors equal in volume to the amount of fuel pumped into the tank. Running losses, vapors emitted from the vehicle while in operation other than tailpipe HC, were defined. Work on behalf of EPA [28] and unpublished results indicate that some of the best octane improving ingredients of gasoline do not oxidize easily by the exhaust catalyst. This had led to further speculation that perhaps some gasoline compositions resulted in tailpipe emissions with higher overall photochemical reactivity than was anticipated. Perhaps the way the unleaded gasoline was made could have had an unexpected impact on resulting air quality in terms of ozone.

In the mideighties, various alcohols were used to supplement and extend gasoline, sometimes to the point motorists began complaining of impaired drivability in terms of surge and stretch-lean operation and lack of power from their cars during warm summer months. These symptoms of vapor lock resulted when blend vapor pressure of some summer gasoline grades reached as high as 13.5 psi. However, when the cars were fueled with a 9 psi gasoline, the cars ran fine.

The initial response to these complaints came from the government. More states began regulating vapor pressure and alcohol content while the EPA published rules [8] to limit summer vapor pressure to 10.5, 9.5, or 9 psi starting on May 16, 1989 (Stage I) and to 9, 7.8, or 7 psi on May 16, 1992 (Stage II) following regions as defined in ASTM D 4814. The California Air Resources Board (CARB) Stage I reformulated fuel requirements beginning Jan. 1, 1992 is 7.8 instead of 9 psi. These changes will further impair refinery operation since a change in 1 psi has been estimated to lower the industry's gasoline capacity by about 2 percent [29].

Another response to the VOCs was to require additional Stage II refueling loss recovery as well as vehicle on-board recovery. The on-board recovery system would likely involve a much larger activated carbon canister than is currently used and could also collect vapors emitted by the fuel system and vehicle during operation (running loss). The on-board system is under review by the U.S. Department of Transportation (DOT) for possible vehicle fire safety implications.

A third response was the introduction by ARCO in Sept. 1989 of EC-1, a reformulated fuel to replace leaded fuel in Southern California [6]. This fuel contains fewer of the lightest compounds such as butane, and only about one-third of the heavier forms of two classes of hydrocarbons,the aromatics and olefins. Compared with leaded regular, EC-1 has about one-third of the aromatics (including 50 percent of the benzene). It has reduced vapor pressure to 8 psi, 1 psi below the then existing California standard. As a result, tests show EC-1 to emit fewer reactive hydrocarbon VOCs [29]. Perhaps more than any other fuel's development in recent years, ARCO EC-1 reawakened the industry to the potential of further environmental improvements possible by reformulating gasoline. With the exception of MTBE, all these changes had been investigated in the sixties.

A fourth response to the VOCs has been to investigate ways to improve gasoline through reformulation and use of additives. Phase I of the Auto-Oil Program, started in 1989, makes use of an extensive matrix of fuel formulas, cars, and measurements of regulated and unregulated emissions, including comprehensive HC speciation. Air quality modeling studies assess the anticipated improvement in air quality in terms of HC, ozone, CO, and NO_x. It is thought that one or more reformulated fuels will be identified for use in existing as well as new cars.

A fifth response to the VOCs concern was the CARB regulations of Sept. 1990 establishing standards based on nonmethane organic gases (NMOG) adjusted for individual component reactivity as the method of expression for tailpipe and evaporative hydrocarbons. Using detailed HC speciation, and the relative reactivities on Table 1 [30], the ozone making potential of gasoline HC can be computed. NMOG, adjusted for photochemical reactivity, is then a common basis for comparison and provides a "level playing field" for various reformulated gasolines, alcohols, and natural gas.

A sixth response to the VOCs was the continued pressure to use more and more alternative fuels instead of gasoline. The encouragement given FFVS and alcohol fuel, primarily M-85, by the Bush Administration in 1989 [5] illustrates the extent of the concern. Other alternatives such as natural gas (compressed or liquid) and liquid petroleum gas gain credibility by replacing the volatiles that characterize today's gasoline and its atmospheric reactivity. Another response, but weakly voiced, is to use diesel fuel, which, because of its higher boiling range and general lack of volatile components that vaporize easily, would obviate the need for diurnal, hot engine soak, refueling, or vehicle running losses. However simple such a solution to the reactive VOCs from gasoline, the diesel has its own set of problems, which will be discussed in more detail later.

After review of this litany of responses to gasoline VOCs, is there any doubt that this is the major problem faced by refiners? The paradox is that VOC emissions from gasoline-powered vehicles were partially affected in quantity and type by an earlier reformulation, brought on when lead was removed.

Importance of Octane Improving Additives. Refinery yield,

Table 1 Maximum incremental reactivities of selected VOCs [30]

Compound (VOC)	Mol. Wt.	Kinetic Reactivity	Mechanistic Reactivity	Overall Reactivity
		fraction VOC reacted	gm.O_3/gm VOC reacted	gm.O_3/gm VOC emitted
Carbon Monoxide	28	0.051	1.9	0.097
Methane	16	0.002	18.6	0.036
Ethane	30	0.24	8.3	0.49
Propane	44	0.43	4.3	1.00
N-Butane	58	0.58	2.8	1.85
N-Pentane	72	0.58	2.8	1.64
N-Hexane	86	0.69	2.2	1.50
N-Octane	114	0.83	1.2	0.98
N-Decane	147	0.91	0.8	0.77
Branched C-6 Alkanes	86	0.70	3.3	2.32
Branched C-8 Alkanes	114	0.85	2.0	1.71
Branched C-9 Alkanes	128	0.90	1.7	1.52
Ethene	28	0.93	16.4	15.25
Propene	42	1.00	12.7	12.66
1-Butene	56	1.00	12.0	11.98
Trans-2-Butene	56	1.00	13.4	13.35
C-8 Alkenes	112	1.00	6.2	6.16
Benzene	78	0.25	4.0	1.00
Toluene	92	0.73	7.3	5.31
P-Xylene	106	0.96	11.2	10.73
Tnalkyl Benzene	120	1.00	11.5	11.50
Acetylene	26	0.16	6.6	1.05
Methanol	32	0.19	7.4	1.40
Ethanol	46	0.51	4.4	2.25
t-Butanol	74	0.22	4.1	0.91
Formaldehyde	30	1.00	16.5	16.46
Acetaldehyde	44	1.00	11.6	11.55

energy consumption, and operational flexibility are enhanced to the extent the octane requirements can be met through additives. The search for substitutes for TEL and TML goes on. But the continued reluctance of CARB and EPA to consider metal-containing additives such as methylcyclopentadienyl manganese tricarbonyl (MMT) has curtailed such research. The current concerns relate to increased engine-out particulates and health effects of MMT combustion products in the atmosphere. The uphill battle to obtain approval and acceptance of potent octane improvers such as MMT [31] has forced refiners to search for different and improved processing methods that achieve required octane at reduced vapor pressure. These interrelationships are very complex and are different for different refineries, crudes, and product mixes. Complicating the issue further is the mandated addition of oxygen to the fuel by use of alcohols or ethers. For example, the increase in vapor pressure when using an alcohol to achieve the required oxygen content is only partially offset by the octane blending value of the alcohol. Table 2 lists the vapor pressure and octane blending values for several alcohols and ethers, classed oxygenates.

Environmental Laws

Since the first Federal tailpipe regulations for model year 1970 cars, the government has had its way with the car, truck, and bus industry through progressively more stringent, technology-forcing standards. Except for the lead phase-out and requirements to control gasoline vapor pressure, the government has not attempted to regulate the refiners in the same way as the manufacturers; that is, until the Clean Air Act Amendments of 1990 (CAA'90) [32].

Federal Standards. Table 3 is a brief listing of standards for passenger car (LDV), defined as 6000 lb GVW or less, and light truck (LDT), vehicles with more than 6000 lb up to 8500 lb GVW. The CAA'90 requires further reductions for LDV by 1994 in NO_x of 0.4 g/mile (same as CARB 1989). The existing standards for LDTs are essentially halved and begin in 1995. Tier II of the CAA'90 provides for 50 percent reductions in CO, NMHC, and NO_x in 2004, unless EPA finds the new standard is not (1) necessary, (2) technologically feasible, or (3) cost effective.

Table 2 Some characteristics of oxygenates

Characteristic	Alcohols		Ethers		
	Methyl[1]	Ethyl	MTBE	ETBE	TAME
Oxygen Content, Weight %	50	35	18.2	15.7	15.7
Blending Vapor Pressure, psi	4.6	2.3	9	4	4.4
Octane Blending Value[2]					
Research, R	131.5	117.5	118	119	113.5
Motor, M	101.5	103	102	103	101.5
(R+M)/2	116.5	110.3	110	111	107.5
Volume % Required to Reach:					
2% O_2 by Weight	4	5.4	11	12.7	12.7
2.7% O_2 by Weight	5.4	7.3	15	17.1	17.2

[1] Must be blended with a cosolvent to be used as a gasoline additive
[2] Midrange octane blending values are approximate and vary with gasoline blendstock[20]

Table 3 U.S. vehicle pollution limits

	Grams/Mile		
	CO	HC	NO_x
	Existing Limits		
LDV 1989	3.4	0.41	1.0
LDT 1989	10.0	0.8	2.3
Evaporative	2.0 g/test		
Diesel LDV P.M.	0.2 g/mile		
	Clean Air Act Amendments of 1990		
		NMHC	
Tier I			
LDV 1994	3.4	0.25	0.4
LDT 1995	5.0	0.39	1.1
Tier II			
LDV 2004	1.7	0.125	0.2

Doubled Durability. The major problem expected with the Tier I regulations is the 100,000 mile durability demonstration, instead of the current 50,000 mile test. The manufacturer sees perhaps triple the recall liability, an ever-present threat. In reality, cars usually are not recalled for repair beyond about 25,000 miles because by the time the "fix" is determined, and the owners notified, the remaining life of the vehicle may not be worth the trouble, or at least this is one argument. If cars are not recalled for emissions repair after, say, 75,000 miles, the recall life is about threefold over current practice. This forces manufacturers not only to perform much longer durability testing, but to take all steps possible to guard against deterioration or failure on a vehicle that gets progressively less attention, less miles per year, and will be in service much longer with sometimes two or more owners.

Evaporative and Other LDV/LDT Needs. With regard to evaporative losses, the new Federal limits remain unchanged at 2 g HC per test. This limit will be joined in 1996 by standards for vehicle running and refueling HC losses. Diesel cars currently must meet 0.2 g particulates per mile. Tier I diesel particulates for 1994 LDV will be 0.08 g/mile and 1995 LDT will be 0.12 g/mile.

Other on-highway LDV/T provisions in the CAA'90 relate to the allowance of other states to imitate the same CARB stringent car emissions standards. Also required will be expansion of inspection and and maintenance requirements from 70 to 110 of the most affected areas, with improvements required in on-board diagnostics for emissions problems. LDV coldstart (20°F) CO standards begin in 1994 (Tier I) and become more stringent in 2001. In 1998, fleets of 10 or more centrally fueled vehicles in ozone nonattainment areas of over 250,000 population are encouraged to use alternative fuels such as methanol or natural gas in order to meet California low emission vehicle (LEV) standards.

Table 4 U.S. EPA heavy-duty diesel emission regulations [1] (g/hp-h)

	NO_X		PM
1988 (all)	10.7		0.6
1990 (all)	6.0		0.6
1991 (all)	5.0		0.25
1993 (urban buses)	5.0		0.10
1994 (trucks)	5.0		0.10
1994 (urban buses)	2.5	or	0.05
1998 (trucks)	4.0		0.10

(1) HC of 1.3 and CO of 15.5 g/hp-hr unchanged since 1988

HD Truck and Bus. The Federal emission standards for HD diesel engines were changed by the CAA'90. Listed in Table 4 are the current and future limits. The CAA'90 revised the urban bus limits, allowing the 0.1 g/hp-h particulate limit to be delayed until 1993 with the change in 1994 to 0.05 g/hp-h particulates or 2.5 g/hp-h NO_x. Halving the already stringent 0.1/5 g/hp-h particulates/NO_x limits requires buses to use fuels such as methanol or natural gas. A possible alternative, although one that may not be competitive, will be a low-emission diesel fitted with a flow-through catalyst plus a highly efficient particulate trap. Another "surprise" was the further lowering of the HD NO_x standard to 4.0 g/hp-h in 1998. By way of comment, some believe this to be the limit for in-cylinder NO_x reduction without increasing engine-out particulates.

Heavy-Duty Clean Fuel Vehicles. Section 245 of the CAA'90 requires vehicles above 8500 and up to 26,000 lb gross vehicle weight (GVW) to have, starting model year 1998, combined NO_x + NMHC of 3.15 g/hp-h. This is equivalent to 50 percent of the 1994 HD diesel limits. This weight category includes two-axle trucks and small buses. This, plus the city bus limits of 2.5 NO_x or 0.05 particulates, portends perhaps even more stringent regulations for trucks and buses used in and around cities. The advent of a nonmethane standard for HD engine HC encourages natural gas since the HC part of the regulation will not be as technology forcing. It is speculated that once the 1994 limit of 0.05 g particulate or 2.5 g NO_x is demonstrated for urban buses, other diesel-powered vehicles used in sensitive areas that continue to have pollution problems, will have such regulations. Perhaps there will be a 0.05 g/hp-h organic particulate standard for all HD by 2000. This will remain to be seen and may depend on if and when efficient and durable aftertreatment systems are developed.

Potential Methane Standard. The adoption of a methane HC standard is of interest if:

1 International agreement on reduction of greenhouse gases is reached that would require control of methane emissions,
2 Natural gas HD vehicles become popular, and
3 Many cars and light trucks are converted to natural gas fuel.

The likelihood of the above is not completely clear, yet they are distinct possibilities, making NMHC standards that intentionally delete methane as another potential paradox. Some currently evaluated trucks converted to natural gas have very high hydrocarbons. Assuming 90 percent of the exhaust HC is methane, the NMHC standard will allow the engine to emit up to 13 g HC per bhp-h. Discounting unburned lubricant, 11.7 g would be methane and the NMHC would be 1.3 g, the diesel standard. In the event a methane standard is promulgated, there is some possibility of catalysts being developed for oxidation of methane. However, applications to vehicles and durability remain to be demonstrated. Thus, a NMHC standard encourages waste of fuel as well as permitting greater emission of a greenhouse gas that has one-tenth the life of CO_2 and is 30 times more effective than CO_2 [13].

Table 5 CARB car standards, gasoline fueled, g/mile (50,000 mile)

	NMHC	CO	NO_X	PM(2)	
1989	0.39	3.4	0.4	0.08	
	NMOG(1)				HCHO(3)
1993	0.25	3.4	0.4	0.08	0.015
TLEV	0.125	3.4	0.4	0.08	0.015
LEV	0.075	3.4	0.2	0.08	0.015
ULEV	0.040	1.7	0.2	0.04	0.008
ZEV	0	0	0	0	0

(1) Non-methane organic gases (NMOG) includes HC, oxygenated HC such as alcohols, aldehydes, ketones, and ethers and would be adjusted for clean fuels reactivity
(2) PM: diesel vehicles only
(3) HCHO: methanol (M-85) vehicles only

Off-Road and Locomotives. The CAA'90 also calls for regulation of nonroad engines and vehicles greater than 175 hp starting in 3 years. Locomotives are to be regulated in 5 years. Regulations for off-road and locomotives are to be based on the greatest degree of emissions reduction achievable.

CARB Standards. Continuing their self-appointed role as leader in vehicle air pollution regulations, the CARB adopted standards in 1990 for model years out to 2003 [33]. Table 5 lists four new standards for transitional low-emission vehicle (TLEV), low-emission vehicle (LEV), ultra-low-emission vehicle (ULEV), and zero emission vehicle (ZEV) beginning with the 1993 model year.

Hydrocarbons Redefined as NMOG Adjusted for Reactivity. Future hydrocarbon limits subtract the methane content, a negligible emission from the micro-environmental viewpoint for gasoline-powered cars. CARB redefines hydrocarbons for post-1993 low-emission vehicles as nonmethane organic gases (NMOG). NMOG includes the usual HC plus the oxygenated HC such as alcohols, aldehydes, ketones, and ethers. The important twist in the use of NMOG is the requirement to analyze the HC for its constituents and then to apply their relative reactivities, to determine ozone-forming potential. California has based its standards on currently specified certification gasoline, described in Table 6 [26]. Through the adjustment of the various HC components for their relative reactivity, a basis for comparison with other fuels such as M-85 or natural gas or with various reformulated gasolines is provided.

For example, using certification gasoline, on which the 0.075 g/mile LEV NMOG is based, FFV burning M-85 could be allowed to meet a higher standard, perhaps 0.1 to 0.15 g NMOG/mile, depending on the specific FFV emissions. Instead of M-85, maybe a modified car operating on a reformulated gasoline could achieve reduced reactivity adjusted NMOG. This is one important outcome expected to be identified in the Auto-Oil Program.

ULEV-NMOG Limit Achieved. Alternative fuels, such as M-85 or natural gas, may not be necessary for manufacturers to meet the ULEV limits of 0.04 g NMOG/mile. It has been shown, at least to the CARB satisfaction, that cars have the potential for achieving 0.04 g NMOG/mile operating on certification gasoline. This feat was accomplished by Southwest Research Institute's Emissions Research Department in 1990 [34]. By injecting air into an electrically heated catalyst during the first 60–80 seconds of cold-start, HC were effectively controlled until the main exhaust catalyst reached operating temperature.

Table 6 Specification of unleaded gasoline used in U.S. emissions certification [26]

Item	ASTM	Unleaded
Octane, research, minimum	D2699	93
Sensitivity, minimum		7.5
Lead (organic), grams/U.S. gallon		0.00-0.05
Distillation Range:		
IBP[1], °F	D86	75-95
10 percent point, °F	D86	120-135
50 percent point, °F,	D86	200-230
90 percent point, °F	D86	300-325
EP, °F (maximum)	D86	415
Sulfur, weight percent, maximum	D1266	0.10
Phosphorous, grams/U.S. gallon, max		0.005
RVP[2,3] pounds per square inch	D323	8.7-9.2
Hydrocarbon Composition:		
Olefins, percent, maximum	D1319	10
Aromatics, percent, maximum	D1319	35
Saturates	D1319	([4])

[1]For testing at altitudes above 1,219 m (4,000 ft) the specified range is 75-105.
[2]For testing which is unrelated to evaporative emission control, the specified range is 8.0-9.2.
[3]For testing at altitudes above 1,219 m (4,000 ft) the specified range is 7.9-9.2.
[4]Remainder.

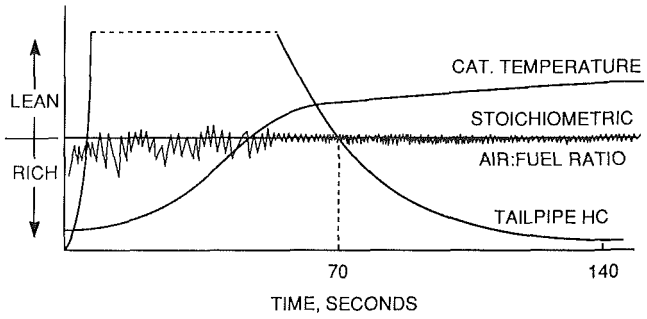

Fig. 5 Typical 1990 model FTP cold-start catalyst and hydrocarbon behavior

For many years, it has been known that the cold start emissions during the first few minutes of the Federal Transient Procedure (FTP) after cold start, remained uncontrolled and could contribute more HC than the remainder of the test. To get the engine to start, most fuel control systems go "open-loop" during which time a richer than stoichiometric mixture is provided in order for the engine to start and run. As better catalysts and controls were developed, the open loop time has been steadily reduced to about 1 min. Figure 5 illustrates the cold start control of HC from a 1990 catalyst-equipped car.

In the SwRI studies, it was found that by preheating a small metallic oxidation catalyst located in front of the main catalyst, and controlling the injection rate of supplemental air for combustion, the excess hydrocarbons can be catalytically burned. In Sept. 1990, two cars achieved 0.03 g NMOG/mile in laboratory tests at SwRI and at CARB [35].

Although there are many questions remaining on practicality, durability, and customer acceptance of the preheat delay time plus battery requirements, a method has been shown to achieve the ULEV NMOG using certification gasoline and without necessarily resorting to an alternative fuel. This development also re-identifies the one remaining tailpipe emissions problem for gasoline cars, the cold-start, an old problem that has progressively been reduced by the manufacturer. There are many alternative ways to reduce the cold-start HC, such as better precylinder air–fuel mixture preparation through improved injectors and location, mechanical and thermal vaporizers, and relocated oxidation catalysts with even lower light-off temperatures.

Table 7 CARB fleet average NMOG car schedule (percent sales in California)

Model Year	NMHC 0.39	NMOG 0.25	TLEV 0.125	LEV 0.075	ULEV 0.040	ZEV 0	Fleet Avg
1994	10	80	10				0.250
5		85	15				0.231
6		80	20				0.225
7		73		25	2		0.202
8		48		48	2	2	0.157
9		23		73	2	2	0.113
2000				96	2	2	0.073
1				90	5	5	0.070
2				85	10	5	0.068
3				75	15	10	0.062

CARB Fleet Average NMOG Schedule. Table 7 shows percent sales of cars in California by model year to achieve the fleet average NMOG. This is an example since the manufacturer can use other introduction dates and even skip TLEV cars, as long as the fleet average is attained. LEVs are expected to be the dominant car in the product mix between 1988 to 2003. Some hybrid engine-electric and pure electric cars such as the GM Impact [36] could start selling before the year 2000 as a part of the strategy to meet the fleet average NMOG.

Fuels. Why are so many of the major air pollution areas of the U.S. still "out of attainment" for ozone and CO? This recurring question is central to the CAA'90 and will be for the decade of the nineties and perhaps beyond. "Out of attainment" means the locale still has atmospheric levels that exceed the National Ambient Air Quality Standards (NAAQS) for one or more primary pollutants. Local, regional, and state implementation plans were intended to achieve such limits under deadlines imposed by the EPA by a mix of controls on stationary and mobile sources. Why did such plans, models, and controls fall short in so many cities on ozone and CO? The NAAQS for ozone is 235 mg/m^3 (0.12 ppm) on an annual basis while CO is 10 mg/m^3 (9 ppm) on an 8-h basis [37].

Federal Regulations, Gasoline. The CAA'90 has two major fuel requirements: a reformulated gasoline for ozone control and a gasoline with increased oxygen for CO control. A reformulated gasoline is to be sold starting in 1995 in the nine worst ozone nonattainment cities in the U.S. These cities are Baltimore, Chicago, Hartford, Houston, Los Angeles, Milwaukee, New York, Philadelphia, and San Diego. They represent about 30 percent of the U.S. population and account for about 25 percent of gasoline sales. The reformulated fuel must contain 2 percent by weight oxygen, limit aromatics to 25 percent by volume, and limit benzene to 1 percent by volume. The fuel, as well as all gasoline sold in the U.S., must contain an additive to prevent injector and intake system deposits. In addition to these "recipe" specifications, the fuel must be qualified as to its effect on emissions of VOCs and toxics. A 15 percent reduction in VOCs and a 15 percent reduction in toxics is required by the reformulated fuel in 1995 with a target of 25 percent in each category in 2000. The EPA is expected to issue procedures by which these reductions are to be demonstrated and the reformulated fuels are qualified for sale. The basis for reduction will be a 1990 baseline fuel in a 1990 model car.

To reduce CO during winter months in 41 cities with CO problems, i.e., greater than 9.5 ppm CO ambient levels, the oxygen content in gasoline is to be increased to 2.7 percent by weight. This fuel is to be available in 1992, but may be delayed for up to 2 years by EPA if a shortage of oxygenates exists in a given area. This regulation makes use of the favorable Denver Front Range (Ft. Collins to Colorado Springs) experience of Jan. 1 to Feb. 28, 1988. During this time, gasoline containing 1.5 percent oxygen reduced ambient CO by 9 percent, the

intended result [38]. Since then, the requirement has been to add 2 percent oxygen by weight during Nov. 1 to Feb. 28 each winter. During the first year, MTBE, rather than methanol, was used in 94 percent of the gasoline because of its superior blending characteristics, vapor pressure, and cost.

One way to achieve 2.7 percent O_2 by weight, required by the CAA'90, is to blend in 15 percent by volume of MTBE. Other oxygen containing chemicals, such as ETBE, TAME, ethanol, or methanol may also be used to increase fuel oxygen content. The use of oxygenates can result in increased octane of the blend depending on the oxygenate and blendstock (Table 2). Perhaps this will allow components to be used in such formulas that result in fewer reactive NMOGs in the exhaust and from evaporation. Alcohols tend to increase blend vapor pressure through formation of azeotropes. This is expected to compensate for changes in the volatile components, as in fewer volatile aromatics.

Reformulated Gasoline Observations. Technical Bulletin No. 1 of the Auto/Oil Air Quality Improvement Program [39] provided the initial results and effects of fuels on emissions in two fleets of vehicles: current (1989) and older (1983–85) models. This report was widely quoted as to the varying effect fuel composition changes had on regulated emissions of HC, CO, and NO_x. Emissions from some cars would increase and some would decrease and the effect was termed a "mixed bag." The only consistent effect was that of fuel oxygen content on CO production.

The real significance in reformulation lies with the newly regulated species, the reactive HC, the VOCs, and the toxics. It would be nice if a fuel change resulted in less NO_x. Just as important, perhaps even more important, would be reduced reactive HC. The possibilities of this should be available soon from air quality modeling of the extensive tailpipe and evaporative HC speciation. For reformulated fuel to compete with alternatives, the potential to form ozone is crucial. In the meantime, General Motors recommended, effective Mar. 18, 1991, the use of reformulated gasoline in all its existing and future model cars and trucks. Preferring not to wait until 1995 for the CAA'90 requirements, the 1992 GM Owners Manuals will contain the reformulated fuels recommendation [40].

The Auto-Oil results to date confirm that learned at SwRI in independent studies. Observations from many fuel-vehicle matrix projects may in general be summarized as follows:

Fuel modification	Emission effect
Decrease volatility	Decrease exhaust and evaporative HC emissions
Decrease aromatic content	Decrease exhaust and evaporative aromatic emissions
Add oxygenates	Decrease CO Increase iso-butylene (MTBE, ETBE) Increase formaldehyde (MTBE) Increase acetaldehyde (ETBE, ethanol) Reduce fuel economy
Decrease olefins	Decrease unburned fuel olefins

Except for the effect of oxygenates, there are exceptions to all of the above in that HC, CO, and NO_x can vary up to threefold with fuel modification. Another observation was that high octane components in the fuel, such as iso-octane, toluene, xylenes, ethylbenzene, and benzene, are the most difficult to remove with catalytic aftertreatment while 1,3-butadiene in the exhaust is easy to remove during the cold-start with an air-injected, electrically heated catalyst [34, 35].

Federal Regulations, Diesel Fuel. The importance of diesel fuel sulfur content on sulfuric acid particulate emissions of the diesel engine has been well established [41]. Figure 6 illustrates the importance of reducing fuel sulfur content on achieving the 0.1 g/hp-h standard, as well as allowing use of a flowthrough oxidation catalyst. This type of aftertreatment

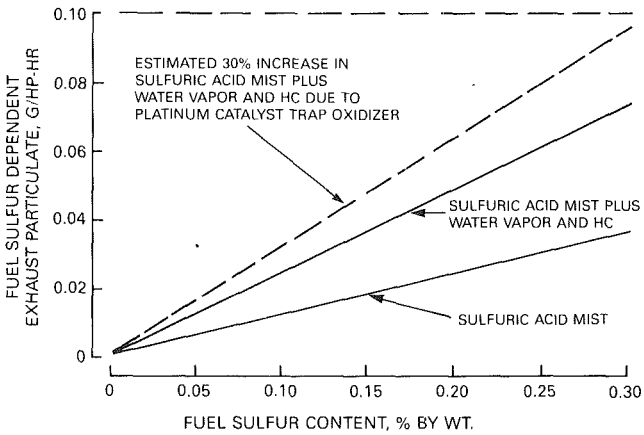

Fig. 6 Collectible fuel sulfur dependent particulate as a function of fuel sulfur content

is expected to be sufficient for most engines to meet the 1994 regulation. In an unprecedented action, the Engine Manufacturers Association (EMA) and American Petroleum Institute (API), plus two other industry groups, held a series of meetings on the need to reduce sulfur and aromatics in diesel fuel. A joint report [43] issued in July 1988 recommended that EPA require all on-highway type 2-D fuel be reduced in sulfur content to 0.05 percent by weight maximum effective Oct. 1, 1993. Furthermore, it was recommended that aromatics be controlled by requiring such fuels to have a minimum cetane index of 40, the current minimum cetane number according to ASTM D 975-81 for type 2-D fuel. The relationship between calculated cetane index and engine cetane number is very close, unless cetane improving additives are used.

On Aug. 21, 1990, EPA issued a rule [44], since confirmed by the CAA'90, that endorsed the industry recommendations and added an alternative 35 percent aromatics maximum [44]. This is expected to be about 2 to 3 cents per gallon more at the pump overall. The price increase will depend on the size and type of refinery, crude oil available, and product mix in the refinery.

CARB Gasoline Regulations. In Sept. 1990, the CARB issued their Phase I regulations for gasoline effective Jan. 1, 1992. The summer vapor pressure (Apr.–Oct. 13) is lowered from 9 to 7.8 psi, with limits of 0.05 g/gal lead and 0.005 g/gal phosphorus. The lead and phosphorus limits are to reduce deterioration of oxygen sensor and catalyst life. The gasoline must also control port fuel injector deposits to a maximum flow loss of 5 percent, using the Coordinating Research Council (CRC) 15 min run–45 min off (soak) cycle car test [45]. A Shell bench test for port fuel injector deposits holds promise for predicting stay-clean and clean-up performance of additive-treated gasolines. Its development at SwRI has been supported by CRC and industry. The method is very similar to that described in [46].

Intake valve deposits must also be controlled to a maximum of 100 mg/valve average using the 10,000 mile SwRI-BMW intake valve deposit (IVD) test [47]. In order to achieve vaporization of the injected fuel spray before ignition, the fuel is intentionally directed onto the hot underside of the intake valve. The valve surface temperature can approach 600°F. If the fuel decomposes and leaves a residue in the intake system, it can, over time, cause customer complaint during the crucial cold-start, drive-away type of vehicle operation. The fuel, during cold-start, tends to be adsorbed by the deposits during idle and initial acceleration. In this way, the engine can operate so lean that the engine stalls, stumbles on acceleration, lacks power, and has a rough idle. As soon as the engine reaches operating temperature, adsorption-desorption equilibrium is

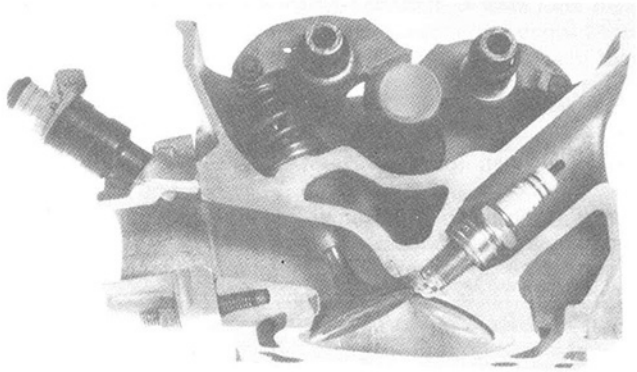

Fig. 7 Intake port of fuel-injected gasoline engine [48]

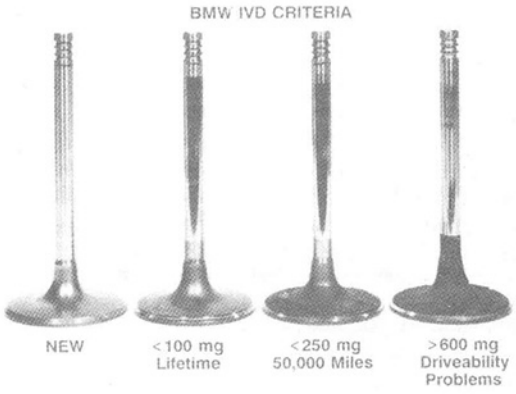

Fig. 8 Pass/fail criteria for gasoline qualification 10,000 mile BMW-SwRI Intake Valve deposits [48]

achieved. Figure 7 is a cutaway of an intake port showing the fuel injector and intake valve relative to the fuel injector [48].

There were sufficient complaints about Bavarian Motor Works (BMW) car drivability, due to IVD, that work to develop a *fuel qualification procedure* was begun in 1986. Like GM, BMW went public with their problem and convinced the refiners to qualify their gasolines using a 10,000-mile car test based primarily on intake valve deposits and secondarily on drivability and other car performance factors. Pass/fail limits for the gasoline of <100 mg average deposit acceptable for unlimited use and 250 mg for 50,000 miles use were established. Figure 8 shows the typical deposits for the pass/fail acceptance criteria.

At the Feb. 28, 1991 CRC Intake Valve Deposit Group meeting, Ford Motor Company reported that 97 percent of 1990 model year cars and 100 percent of 1990 model year light trucks were designed for regular grade unleaded gasoline, $(R+M)/2$ of 87. Ford further reported that the fuel quality statement in the Owners Guide will be revised to state:

- "All grades of unleaded gasoline should contain an effective intake system deposit control additive
- Do not use a higher octane grade unleaded gasoline than recommended in the Owners Guide"

By way of explanation, Ford said that premium grade unleaded fuels in vehicles designed for regular grade unleaded may aggravate drivability symptoms. They requested a gasoline deposit performance test procedure be included in SAE J312/ASTM D 4814 requirements [49]. Fuel additives, as described for example by [50], will play a major role in maintaining excellent drivability of cars through improved gasoline performance [51].

Gasoline will be further modified, perhaps reformulated,

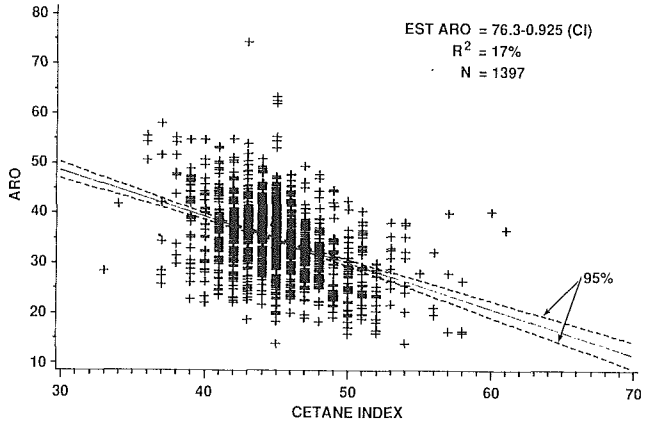

Fig. 9 Aromatics and calculated cetane index for 1397 samples summer 1983 to winter 1988 diesel fuel survey [48]

following CARB Phase II rule making expected in Sept. 1991. Under consideration will be new specifications on aromatic content, vapor pressure, olefins, distillation, benzene, oxygen content, and ozone-forming toxic potential. Some of the expected changes are in the same direction as the CAA'90 fuel for the nine worst O_3 nonattainment areas and would take effect perhaps in 1994, 1995 at the latest.

CARB Section 2345, Substitutes for Clean Fuels, specifies what a gasoline must achieve if it is to be a substitute for a "clean fuel." Primary "clean fuel" examples are methanol (M-85 or M-100), ethanol (E-85), compressed/liquid natural gas (C/LNG), or liquid petroleum gas (LPG). The rules are effective from 1994 to 1996 in the Los Angeles Basin for large refineries ($>50{,}000$ BPSD) and in 1997 statewide, all suppliers.

The substitute fuel, termed "deeply formulated" by the author, must demonstrate emissions equal to or less than a LEV operating on one of the primary "clean fuels." Reactivity adjusted tailpipe and evaporative NMOG, NO_x, CO, and the aggregate toxic-weighted benzene, 1,3-butadiene, formaldehyde, and acetaldehyde are the emissions on which the comparison will be made. Particulates will also be used for comparison if diesel fuel against a low-emission FFV burning M-85 is a major test for reformulated gasoline. The NMOG, adjusted for atmospheric reactivity, is intended to allow direct comparison.

CARB Diesel Fuel Requirements. On Nov. 22, 1988, CARB adopted regulations for on-highway type 2-D fuel sold beginning Oct. 1, 1993. The low sulfur limit of 0.05 percent by weight is the same as EPA [47]. However, CARB specifies that the fuel have less than 10 percent aromatic content for large refineries of greater than 50,000 barrels per stream day. Figure 9 illustrates the aromatic content of some 1393 samples collected over a 5-year period. As may be seen, few diesel fuels were sold below 20 percent aromatics, with the average of about 35 percent evident.

In the CRC VE-1 project, it was found that aromatic content had little effect on particulates, but an increased effect on NO_x for a 1991 prototype diesel engine (Detroit Diesel Corporation Series 60) [52]. Both particulates and NO_x from then current technology engines were sensitive to aromatics as shown in Fig. 10 [48, 53]. Apparently to achieve both low particulates and NO_x from future diesel engine fuels, a 10 percent aromatics content was specified; even though none are made at that level and the cost to do so in refinery energy and yield may prove very expensive, even prohibitive for some suppliers. One estimate indicated that making 10 percent aromatic fuel could increase the price by as much as 20 cents per gallon for those refiners that elect to do so.

CARB, however, leaves a way out for the refiner in that he

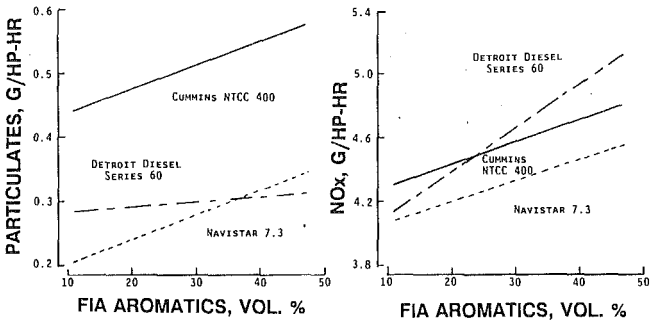

Fig. 10 Effect of aromatics on particulates and NO_x from three HD diesel engines by EPA transient test [48, 53]

can, if he wishes, offer a reformulated type 2-D diesel fuel if it gives emissions equal to or less than would be obtained from a 10 percent aromatics fuel [54]. The test procedure is basically the same as that used in the CRC VE-1 project, namely the Detroit Diesel Corporation direct injected Series 60, an 11.1 liter, four-stroke cycle turbocharged and aftercooled engine of 330 hp at 1800 rpm. The procedure involves replicate transient cycle tests using the EPA HD diesel engine certification procedure, in which the 10 percent aromatic reference fuel is run back-to-back with the candidate fuel. The CRC VE-1 work was continued by the Western States Petroleum Association to look at the effect of cetane level from natural and chemical additive with 10 percent aromatic content. Table 8, calculated the data of [55], indicates that the natural cetane could substitute for reduced aromatics more effectively than a cetane improver such as 2-ethylhexyl nitrate.

For example, to make a diesel fuel with 20 percent aromatics equivalent in particulate emissions to the 10 percent aromatics, 48 cetane CARB reference fuel requires a fuel with a natural 50 cetane or a cetane-improved fuel by chemical additive of 53. This is not so difficult to achieve, considering national average diesel fuel is 45 cetane number. However, in the case of NO_x, the 20 percent aromatics fuel will require either a 58 natural cetane or a cetane by chemical additive of 70. These calculations indicate natural cetane is a more effective substitute for aromatics on particulate and NO_x than 2-ethylhexyl nitrate. To produce equivalent NO_x to that from the 10 percent aromatic reference fuel will require substantial cetane improvement for the examples shown. It is believed that for most refineries, production of diesel fuel containing less than 20 percent aromatics will require major refinery change and be quite expensive.

The above, plus other possibilities of diesel fuel reformulation for California, are being investigated by several oil refiners to establish sensitivity of emissions to various reformulated, low sulfur, diesel fuels. So far, the possibilities of reformulation and its impact on price and availability of diesel fuel in California are largely unknown. Reference [54] provides details on the CARB procedure used for a reformulated type 2-D fuel qualification as alternative to the 10 percent aromatics, 0.05 percent sulfur by weight fuel.

Alternative Fuels. The major force driving regulations that encourage alternative fuels is environmental improvement. Other reasons such as less reliance on foreign crude oil or global warming have been used, but the concern over VOCs from gasoline and organic particulates from diesel and their toxicity appear to be the root causes. The subject is of immense importance and has far reaching implications beyond the scope of this lecture. A few points need to be made in summary, however.

Table 8 Substitution of cetane for aromatics[1]

	Natural Cetane	Improved Cetane[2]	Aromatics %FIA
Particulates:	52	55	25
	50	53	20
	49	51	15
NO_x:	65	88	25
	58	70	20
	52	57	15

[1] Examples calculated to achieve emissions equivalent to 48 CN, 10% aromatic reference fuel

[2] Improved with 2-ethylhexyl nitrate. 45 CN national average used as baseline fuel

Methanol. Methanol promises to be a convenient way to get remotely produced natural gas to the U.S. market. From an energy-efficiency standpoint, it becomes attractive when the engine is designed to run with the fuel undiluted, as M-100, where compression ratio is increased and optimized. Mixtures of methanol and gasoline, intended to bridge the transition from gasoline to methanol, are not more fuel efficient and are questionable so long as gasoline is available and inexpensive. Environmental improvements seem a paradox. Everyone is aware of the claims for lower NO_x, volatiles, and reactivity adjusted NMOG. The major reactive component in M-85 fueled FFV exhaust is formaldehyde. According to Table 1, formaldehyde is 457 times more reactive in forming ozone than methane. Although some current technology catalysts are capable of efficient conversion of formaldehyde when new [56], such efficiencies have yet to be demonstrated with extended mileage. As shown in Table 5, the 50,000 mile CARB formaldehyde standard is 0.015 g/mile (TLEV and LEV) and 0.008 g/mile (ULEV).

Natural Gas. If methanol is a liquid form of natural gas, perhaps it would be more energy efficient to just liquify the gas and ship it to market in LNG tankers rather than make it into methanol. Then, it could be used in liquid or compressed state in vehicles. Aside from storage density and other concerns, natural gas makes sense if gasoline and diesel fuel are to be replaced. Again, to achieve the efficiency of this high-octane fuel, the engine needs to take full advantage of the special features of natural gas while designing for low NO_x, the major problem expected. Depending on global warming requirements, a methane standard may be the only way to reduce methane emitted into the atmosphere from the engine or leaks. Regardless of the price and abundance of natural gas, its adverse potential as a greenhouse gas means that care must be taken in converting car and heavy duty engines.

Ethanol. Its major use remains as a 10 percent mix in gasoline as Gasohol. Ethanol and other alcohols such as tertyl butyl alcohol remain as gasoline fuel supplements and are used more or less depending on availability and price. It remains to be seen the extent to which ethanol will be used to achieve the 2 or 2.7 percent by weight oxygen requirements of future gasolines.

Ethers. Considered by some refiners as the most effective and easily blended oxygenates, methyl tertiary butyl ether (MTBE), ethyl tertiary butyl ether (ETBE), and tertiary amy methyl ether (TAME) are popularly used to add oxygen to gasoline. Beyond use in winter months in Colorado to reduce CO, these oxygenates will find increasing use in CAA'90 requirements for gasoline in the 9 worst ozone cities and in the 41 highest CO cities. Other uses for oxygenates are known. For example, two-stroke cycle gasoline powered motorcycles in Taiwan operate on fuel containing 2 percent oxygen by weight for more complete combustion and less CO. Additive treatment through oxygenates has great possibilities for improved, more complete combustion, and fewer emissions. Sim-

ilar additives may likewise help to reduced emissions from diesel engines. The regulations seem to encourage deposit control and combustion improving type chemicals as long as they are not metal based.

Action Items

More than a wish list, the following action items will serve as discussion and summary:

1 Gasoline Octane—The importance of this single fuel property on refinery and vehicle efficiency and energy consumption cannot be minimized. For example. the use of metal-containing octane booster additives such as MMT needs to be resolved as to their acceptance by EPA and CARB.

2 Optimum Octane and Energy—The optimum octane number of gasoline for overall energy efficiency is a delicate balance between protroleum processing, environmental requirements, and engine thermal efficiency. A continuing study and optimization of the overall best octane quality for energy and efficiency is needed. It should make use of recent findings by the Auto-Oil Program, new refinery technology, and fuel additives development. The results of this study would be important in the national energy strategy.

3 Global Catastrophe—In any response to future agreements to reduce greenhouse gases because of global warming fears, standards for methane and CO_2 emissions are options as well as encouragement to conserve and reduce energy consumption.

4 CAFE—Energy conservation in transportation means CAFE to many, while it is efficiency that is important. There is a need to consider innovative means of expressing and achieving economy beyond simply percentage roll-back or arbitrary miles per gallon levels. What, if anything, can be done to increase truck and bus fuel efficiency and economy? How to prepare CAFE rules that are appropriate for alternative fuels for FFVs, natural gas powered vehicles and electric or hybrid-electric cars? CAFE, to be meaningful, must reflect safety, customer, and society needs, as well as conservation of energy.

5 HD Particulates—The flow-through oxidation catalyst appears the technology of choice for HD diesel truck engines to meet stringent 1994 particulate standards. Long life of the catalyst, up to 290,000 miles for the largest trucks, will require identification of lubricants that are compatible with the catalyst operation, as well as work well in low oil consumption engines of the future.

6 Alternative Fuels—Lower particulate emissions, such as the 0.05 g/hp-h required of city buses in 1994, will require alternative fuels such as methanol and natural gas or extensive exhaust aftertreatment. It is speculated that a flow-through catalyst plus a system of dual wall flow type ceramic filters, located as far from the engine as possible, to promote condensation of organics and aerosols on the collected carbon, might make the advanced technology diesel engine burning diesel fuel acceptable in environmentally sensitive applications [57].

7 Particulate Control—The flow-through catalyst plus cool exhaust wall filter is expected to remove nearly all particulates and organics. To what extent this technology can be applied to the diesel-powered car is uncertain, since NO_x is an emission that must also be controlled. However, if the exhaust of the direct-injected diesel car engine was benign, then its greatly reduced exhaust and evaporative VOCs, relative to gasoline, could be taken advantage of. Other well-understood improvements in fuel economy and lower CO_2 emissions (global warming) could be realized.

8 Reformulated Fuels—Reformulated gasoline and diesel fuel cry out for definition beyond that afforded by the CAA'90 or CARB regulations. There is much confusion over just what a reformulated fuel is, much less how to demonstrate effectiveness of injector and intake system deposit control as well as the required 15 percent reductions in VOCs and toxics. Much more appears needed to define NMOG reactivity as required by the CARB for broad acceptance by industry.

The fundamental question of why so many cities failed to attain ozone and CO NAAQSs remains unanswered. All that is certain is the industry has another round of vehicle standards and recipes for reformulated fuels. Ten years from now, will these areas still be "out-of-attainment" and continue to elude our best efforts at control? It would be instructive to the future to understand the effect various factors had in the past such as deficiencies in modeling, emission factors, vehicle usage, vehicle miles traveled, maintenance, tampering, fuel quality, atmospheric interactions, hydrocarbon reactivity, evaporative losses, and other variables such as unregulated sources and pollutants in the mobile source pollution estimates. Perhaps such a look back will be valuable in the design of control programs and assessing progress toward environmentally acceptable and efficient transportation of the future.

References

1 Clarke, P. J., Gerrard, J. E., Skarstrom, C. W., Vardi, J., and Wade, D. T., "An Adsorption-Regeneration Approach to the Problem of Evaporative Control," SAE Paper No. 670127, 1967.

2 40 CFR, Part 86, Subpart A, para. 86.130-78, p. 503, Protection of the Environment, July 1, 1985.

3 Kehrl, H. H., General Motors Vice Chairman, letter to Chief Officers of twenty-two petroleum companies, Nov. 18, 1985.

4 *Chicago Tribune*, "Oil, Auto Industries to Test Reformulated Gasoline," Oct. 18, 1989.

5 *Automotive News*, "Industry Awaits Details of Air Plan," p. 49, June 19, 1989.

6 *New York Times*, "ARCO Offers New Gasoline to Cut up to 15% of Old Cars Pollution," Aug. 15, 1989.

7 Colluci, J. M., "Automotive Fuels for the 1990's Challenges and Opportunities," General Motors Research Laboratory Report GMR-6589, F&L-882, Mar. 9, 1989.

8 40 CFR, Part 80, EPA Volatility Regulations for Gasoline and Alcohol Blends Sold in Calendar Years 1989 and Beyond; Final Rule, Mar. 22, 1989.

9 "Alternative Transportation Fuels: No Simple Solutions Available," *Energy Focus*, Society of Petroleum Engineers, Apr. 1990.

10 *Bus Ride*, "A Farewell to Responsibility," May 1990.

11 *National Wildlife Federations Conservation 90*, Vol. 8, No. 6, Aug. 17, 1990.

12 *The Oil Daily*, "Negotiations, Estimations and Rhetoric Leave Greenhouse Gas Issue Clouded," Feb. 12, 1991, p. 5.

13 Springer, K. G., "Global What? Control Possibilities of CO_2 and and Other Greenhouse Gases," ASME JOURNAL OF ENGINEERING FOR GAS TURBINES AND POWER, Vol. 113, 1991, pp. 440-447.

14 Hammerle, R. H., Shiller, J. W., and Schwarz, M. J., "Global Climate Change," ASME JOURNAL OF ENGINEERING FOR GAS TURBINES AND POWER, Vol. 113, 1991, pp. 448-455.

15 Amann, C. A., "The Greenhouse Effect," SAE Paper No. 902099, 1990.

16 NRC, "1990 Fuels to Drive Our Future," National Research Council Report, National Academy Press, Washington, DC.

17 Amann, C. A., "The Automotive Spark-Ingition Engine—An Historical Perspective," *History of the Internal Combustion Engine*, ASME ICE-Vol. 8, 1989, pp. 33-45.

18 Carroll, J. N., Ullman, T. L., and Winsor, R. E., "Emission Comparison of DDC 6V-92TA on Alcohol Fuels," SAE Paper No. 902234, 1990.

19 *Automotive News*, "Environmental Groups to Seek Boost in CAFE," Dec. 24, 1990, p. 9.

20 CONCAWE, Ad Hoc Group Automotive Emissions Fuel Characteristics," Assessment of the Energy Balances and Economic Consequences of the Reduction and Elimination of Lead in Gasoline," R. Kahsnitz et al., Report 11/83, Den Haag, Concawe, 1983.

21 Heywood, J. B., "Future Engine Technology: Lessons From the 80's for the 1990's," ASME 1990 Soichiro Honda Lecture, ASME JOURNAL OF ENGINEERING FOR GAS TURBINES AND POWER, Vol. 113, 1991, pp. 319-330.

22 *Automotive News*, "Mitsubishi: Weight, Not Size, is MPG Ticket," Apr. 1, 1991, p. 1.

23 *Automotive News*, "Bush's Dual-Fuel Plan Spells CAFE Relief," Feb. 18, 1991, p. 2.

24 *Automotive News*, "With War as Ammunition, Bryan Shoots for a CAFE Win," Feb. 4, 1991, p. 3.

25 *USA Today*, "Use Law to Demand More Efficient Cars," Apr. 4, 1991.

26 40 CFR, Part 86, Subpart A, para. 86.113-82, p. 482, *Protection of the Environment*, July 1, 1985.

27 Frank, M. E., "Gasoline Volatility Regulations: the Impact on the US Refining Industry," *Hydrocarbon Technology International*, 1990.

28 Warner-Selph, M. A., and Smith, L. R., "Assessment of Unregulated Emissions From Gasoline Oxygenated Blends," EPA Report No. 460/3-91-002, Mar. 1991.

29 *Oil & Gas Journal*, "New Transportation Fuels: The Challenges Ahead," OGJ Special, Nov. 13, 1989.

30 Lowi, A., Jr., and Carter, W. P. L., "A Method for Evaluating the Atmospheric Ozone Impact of Actual Vehicle Emissions," SAE Paper No. 900710, 1990.

31 Lenane, D. L., "Effect of a Fuel Additive on Emission Control Systems," SAE Paper No. 902097, 1990.

32 Clean Air Act Amendments of 1990 Senate Bill 1630 as passed by the U.S. House of Representatives and Joint House-Senate Conference Agreement, Oct. 10, 1990, Title II, signed by President George Bush, Nov. 5, 1990, pp. 77-145.

33 Resolution 90-58 State of California Air Resources Board Agenda Item 90-14-1 Low Emission Vehicles/Clean Fuels Amending Title 13 California Code of Regulations, Sept. 28, 1990.

34 Heimrich, M. J., "Air Injection to an Electrically-Heated Catalyst For Reducing Cold-Start Benzene Emissions From Gasoline Vehicles," SAE Paper No. 902115, 1991.

35 Heimrich, M. J., Albu, S., and Osborn, J., "Electrically-Heated Catalyst System Conversions on Two Current-Technology Vehicles," SAE Paper No. 910612, 1991.

36 *Automotive News*, "GM Develops Group to Build and Market Electric Car Line," Mar. 11, 1991, p. 1.

37 40 CFR, Part 50, Ch. 1, 7-1-87 Edition, p. 538-541.

38 Colorado Air Quality Control Commission Regulation No. 13 Implemented Jan. 1, 1988.

39 *Auto/Oil Air Quality Improvement Research Program*, Technical Bulletin 1, Initial Mass Exhaust Emission Results From Reformulated Gasolines, Dec. 1990.

40 Reuss, L. E., General Motors Corporation News Release Regarding Use of Reformulated Gasoline, Mar. 18, 1991.

41 Springer, K. J., "Diesel Lube Oils—Fourth Dimension of Diesel Particulate Control," ASME JOURNAL OF ENGINEERING FOR GAS TURBINES AND POWER, Vol. 111, No. 3, 1989, pp. 355-360.

42 Springer, K. J., "Low Emission Diesel Fuel for 1991-1994," ASME JOURNAL OF ENGINEERING FOR GAS TURBINES AND POWER, Vol. 111, No. 3, 1989, pp. 361-368.

43 Recommended Federal On-Highway Diesel Fuel Specifications to Assist Engine Manufacturers in Meeting the 1991 and 1994 Particulate Standards, submitted by American Petroleum Institute, National Petroleum Refiners Association, Engine Manufacturers Association, and National Council of Farmer Cooperatives, July 19, 1988.

44 40 CFR, Parts 80 and 86, Regulation of Fuels and Fuel Additives: Fuel Quality Regulations for Highway Diesel Fuel Sold in 1993 and Later Calendar Years: Final Rule, Aug. 21, 1990.

45 CRC Report No. 565, "A Program to Evaluate a Vehicle Test Method for Port Fuel Injector Deposit-Forming Tendencies of Unleaded Base Gasolines," Feb. 1989.

46 Richardson, C. B., Gyorog, D. A., and Beard, L. K., "A Laboratory Test for Fuel Injector Deposit Studies," SAE Paper No. 892116, 1989.

47 Bitting, B., Gschwendtner, F., Kohlhepp, W., Kothe, M., Testroet, C. J., and Ziwica, K. H., "Intake Valve Deposits—Fuels Detergency Requirements Revisited, SAE Paper No. 872117, 1987.

48 Springer, K. J., "Gasoline and Diesel Fuel Qualification—A National Need," ASME JOURNAL OF ENGINEERING FOR GAS TURBINES AND POWER, Vol. 112, 1990, pp. 398-407.

49 "Intake Valve Deposit/Driveability Investigations CRC IVD Group," Ford Engine, Fuels and Lubricants CAC; Feb. 28, 1991.

50 *Oil & Gas Journal*, "Additives to Have Key Role in New Gasoline Era," Feb. 11, 1991.

51 *Consumers Report*, "Which Gasoline for Your Car?" Jan. 1990.

52 Ullman, T., "Investigation of the Effects of Fuel Composition on Heavy-Duty Diesel Engine Emissions," SAE Paper No. 892072, 1989.

53 Springer, K. J., "Diesel Fuels and the Future of Diesels in the U.S.," presented at the Xth AGELFI European Automotive Symposium, Ostend, Belgium, Oct. 11-12, 1990.

54 Title 13, California Code of Regulations Section 2256, Aromatic Content of Diesel Fuel Subsection(g) Certified Diesel Fuel Formulations Resulting in Equivalent Emission Reductions, Apr. 17, 1989, amended Dec. 13, 1990, Feb. 8 and Apr. 15, 1991.

55 Ullman, T. L., Mason, R. L., and Montalvo, D. A., "Effects of Fuel Aromatics, Cetane Number, and Cetane Improver on Emissions From a 1991 Prototype Heavy-Duty Diesel Engine," SAE Paper No. 902171, 1991.

56 Newkirk, M. S., Smith, L. R., and Ahuja, M., "Formaldehyde Emission Control Technology for Methanol-Fueled Vehicles," SAE Paper No. 902118,

57 Springer, K. J., "Particulate Trap for Two-Stroke Cycle Detroit Diesel Powered City Bus," *Engine Design, Operation and Control Using Computer Systems*, ASME ICE-Vol. 9, 1989.

G. E. Doughty

S. R. Bell

K. C. Midkiff

Department of Mechanical Engineering,
University of Alabama,
Tuscaloosa, AL 35487

Natural Gas Fueling of a Caterpillar 3406 Diesel Engine

A Caterpillar 3406 turbocharged diesel engine was converted to operate in a natural gas with diesel pilot ignition mode and was evaluated for performance and emission characteristics for both diesel and natural gas operation. Full-load power was achieved with natural gas fueling without knock. Similar fuel efficiencies were obtained with natural gas fueling at high loads, but efficiencies were lower for low loads. Bosch smoke numbers were reduced by over 50 percent with natural gas fueling for all cases investigated. NO_x emissions were found to be lower at low loads and at high speeds under high load. CO emissions were significantly increased for natural gas fueling while CO_2 concentrations in the exhaust were reduced for natural gas fueling.

Introduction

Petroleum, since the turn of the century, has been an inexpensive and readily available energy source. Experts for some years now have predicted the end of this era. There may not be agreement as to exactly when the petroleum supply will be depleted, but the concern is great enough to warrant research in alternative fuels. A successful alternate fuel should be inexpensive, abundant, and the products of combustion of the fuel must be environmentally acceptable or be such that they can be cleansed to acceptable levels.

Concern with exhaust emissions pollution from internal combustion engines has become a major driving force in new engine designs and new fuel development for engines. Environmental problems have been particularly severe in urban areas where high concentrations of vehicles and people result in the exposure of a large population to high levels of pollutant emissions. Current enacted and proposed legislation by several governmental bodies across the United States is aimed at addressing this environmental concern. For pre-1990 diesel engines, the EPA allowed 10.7 g/bhp-hr of NO_x emissions. This limit was reduced to 6.0 g/bhp-hr in 1990 and to 5.0 g/bhp-hr in 1991. In January of 1988 and for the first time, the EPA began regulating particulate emissions from diesel engines. The initial standard for particulates is 0.6 g/bhp-hr with a final proposed standard of 0.1 g/bhp-hr beginning in 1994 [1, 2]. These emission standards are extremely demanding and potentially extend beyond the current marketplace technology for diesel engines. New and innovative concepts with relatively short developmental times must, therefore, be sought if their impact is to be realized in the market in a timely manner.

The use of alternative fuels and in particular natural gas has been identified as a potential design choice for engines [1, 2]. The performance of natural gas engines has been investigated with promising results at The University of Alabama and by others [3–8]. The emissions aspects are less well investigated, but preliminary results from testing are encouraging for the particulate and NO_x emission levels.

An advanced and promising concept of natural gas fueled engines is the lean burn engine. The lean burn engine, as the name implies, operates with a significant fraction of excess air. The primary potential advantages offered by the concept are lower local temperatures in the cylinder, which yield lower NO_x emissions, less potential for knock, and the potential for improved thermal efficiencies. Conventional spark-ignited gas engines operate close to the stoichiometric fuel/air ratio, which results in higher peak local temperatures, which increases the chances of dissociation reactions for forming NO_x and often results in incomplete combustion. While conventional fueled diesel engines operate at an overall lean condition, the in-cylinder fuel injection results in actual burning occurring at conditions ranging from rich to lean, thereby producing products characteristic of rich burning (particulates) and of stoichiometric burning (NO_x). The application of natural gas fueling to a diesel-type engine is a lean burn concept if the fuel is either aspirated or injected prior to entering the cylinder so that there is a near-premixed mixture at ignition. Ignition of lean methane mixtures is difficult to achieve and can result in incomplete combustion or total misfire [9]. For ignition to be successful, the energy release rate in the early stages of ignition must be greater than losses from the ignition flame kernel. If not, the flame extinguishes prematurely. For lean mixtures, the energy release per unit volume is less because the fuel charge is diluted with excess air. This is a major concern for lean burn engines and is a concern that warrants careful study. Concepts suggested for achieving stable ignition include using a pilot diesel charge, high energy spark, plasma jets and stratified charge/spark designs [9–11]. The objective of this work was to investigate the emissions and performance characteristics of a commercial diesel engine being operated on natural gas with pilot diesel for ignition. For the results reported, the engine design and operating conditions were not specifically modified to minimize emissions for operations on natural gas. However, the engine did exhibit strong emissions dependency on those operational parameters varied. The following sections of this report include a discussion of the testing facilities and discussion of results and conclusions.

Contributed by the Internal Combustion Engine Division and presented at the 13th Annual Fall Technical Conference, Muskegon, Michigan, September 30–October 2, 1991. Manuscript received by the Internal Combustion Engine Division September 1, 1991. Associate Technical Editor: J. A. Caton.

Facility Description

The engine used in this study was a Caterpillar 3406 diesel. The engine was factory equipped with a turbocharger and retrofitted with an intercooler to allow operation using natural gas without encountering knock. The basic engine characteristics of the test engine are summarized in Table 1 [6].

A drawing of the engine test facility is shown in Fig. 1 and includes the major equipment and support systems for the facility. A coolant tank was constructed of stainless steel to hold coolant water for the test engine. The tank was equipped with a water inlet and an overflow drain such that the tank temperature could be controlled by the flowrate of the water. The tank was also equipped with a thermocouple and digital readout so that coolant temperature could be monitored. All engine tests were conducted with the coolant water at approximately 180°F. The intercooler used city water to cool the intake air-fuel mixture so that natural gas might be used as a fuel without knock. Inlet water temperatures at the intercooler and the coolant tank were approximately 67°F.

The natural gas used was pipeline natural gas from the local gas utility and was introduced into the intake air stream just prior to the turbocharger. Natural gas flow rates were controlled using a manual, variable area, fine control needle valve. A gas analysis was preformed to determine the gas composition and theoretical heating value of the natural gas; see Table 2. The higher heating value of the natural gas was taken to be the sum of the weighted averages of the higher heating values of each constituent. To determine the lower heating value of the natural gas the heat of vaporization of the water contained in the products was subtracted from the theoretical higher heating value. This gave a lower heating value for the gas of 20,600 Btu/lbm.

Engine intake air was filtered and passed through a laminar flow element and surge drum before entering the engine; see Fig. 1. For tests where the air-to-fuel ratio was varied, the air flow rate was controlled using a butterfly valve upstream of the natural gas inlet and the turbocharger. Diesel fuel was stored in a 55 gallon drum that was higher in elevation than the fuel pump on the engine. The diesel fuel was supplied by the university and had a cetane number of approximately 49. The lower heating value of the fuel was estimated to be 18,280 Btu/lbm [12]. The diesel fuel flow rate for pilot ignition was measured using a positive displacement flow meter, which provided an analog output for the data acquisition system. Several temperatures were monitored in the engine including each exhaust port, pre- and post-turbo, inlet air, coolant in, and coolant out. Pressure measurements included laminar flow element differential, pre- and post-turbo and exhaust manifold.

The test dynamometer was a directly coupled, water cooled, traction brake. It was equipped with a digital readout of engine speed, torque, and power, A strain gage amplifier was placed in parallel with the dynamometer strain gage and a frequency-to-voltage circuit was placed in series with the magnetic pick-off on the dynamometer. These modifications allowed engine speed and torque to appear on the dynamometer digital readout and to be recorded by the computer data acquisition system simultaneously.

Continuous sampling exhaust gas analyzers were used to measure the levels of NO_x, CO, CO_2, and SO_2 in the exhaust. Sample lines were connected to the exhaust manifold directly behind the turbocharger and the gas was conditioned used a Thermo Electron Corporation model 600 sample gas conditioner. The conditioner passes exhaust gas through a filter and a 37°F bath to cleanse and dehumidify the gas. Each instrument is equipped with a 0–100 mV output. The voltage output from each instrument is proportional to the concentration of pollutant in the exhaust. Particulate concentration in the exhaust was monitored using the Bosch smoke number method. Samples were taken in the exhaust pipe approximately 4 ft from the exhaust manifold. A Bosch sample pump was used to pass a fixed amount of exhaust gas over a filter to trap the particulates. A Bosch smoke meter was then used to assign a smoke number for each filter paper.

The data acquisition system used was a Swan XT10 computer equipped with a Metra Byte Corporation Das-16 high-speed analog-to-digital interface board. The operating parameters including temperatures, pressures, flow rates, engine speed,

Table 1 Engine specifications

Cylinders	6, inline
Bore	5.4 in.
Stroke	6.5 in.
Displacement	893 in.^{3}
Compression ratio	14.5
Combustion system	Direct injection
Maximum engine speed at full load	2100 rpm
Rated brake power	280 hp
Fuel injection	Variable time

Table 2 Chemical composition and analysis of natural gas

Component	Formula	Volumetric analysis, percent
Hexanes +	C_6 +	0.13
Propane	C_3H_8	0.57
Iso-butane	i-C_4H_{10}	0.11
Normal butane	n-C_4H_{10}	0.15
Iso-pentane	i-C_5H_{12}	0.05
Normal pentane	n-C_5H_{12}	0.06
Carbon dioxide	CO_2	0.28
Ethane	C_2H_6	3.29
Oxygen	O_2	<0.01
Nitrogen	N_2	0.96
Methane	CH_4	94.39
Carbon Monoxide	CO	<0.01

Compressibility factor $Z = 0.99785$
Specific gravity (air = 1.0) ideal = 0.5910
HHV @ 60°F and 14.73 psia dry gross ideal = 1047.0 Btu/ft^3

Specific gravity (air = 1.0) saturated = 0.5921
HHV saturated = 1031.0 Btu/ft^3

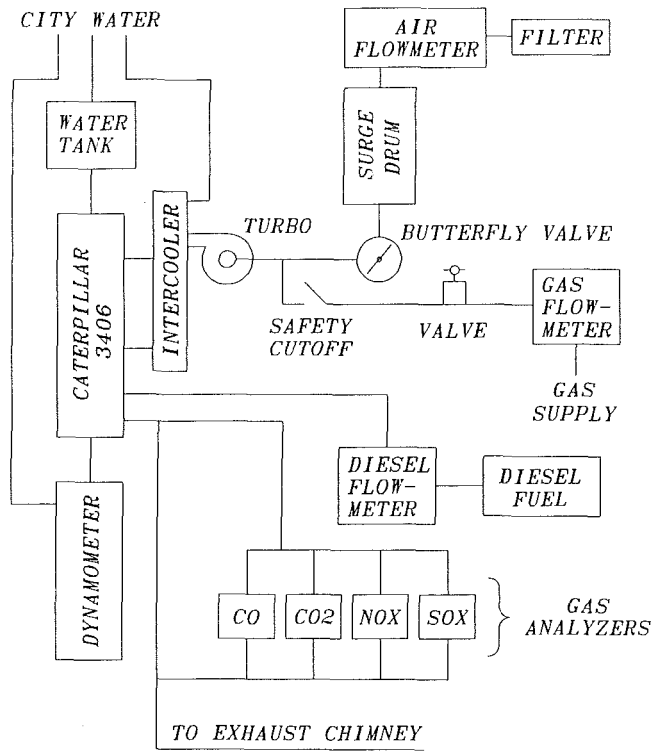

Fig. 1 Schematic of experimental setup

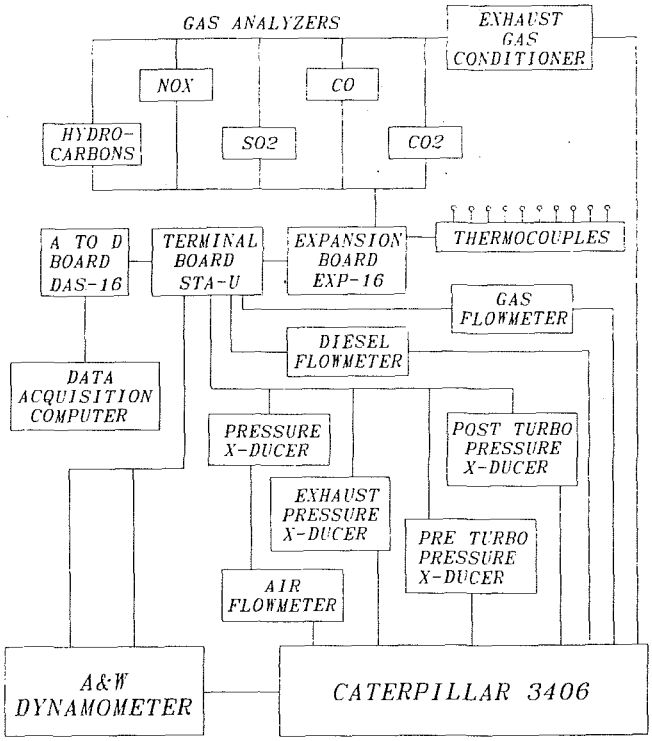

Fig. 2 Schematic of data acquisition system

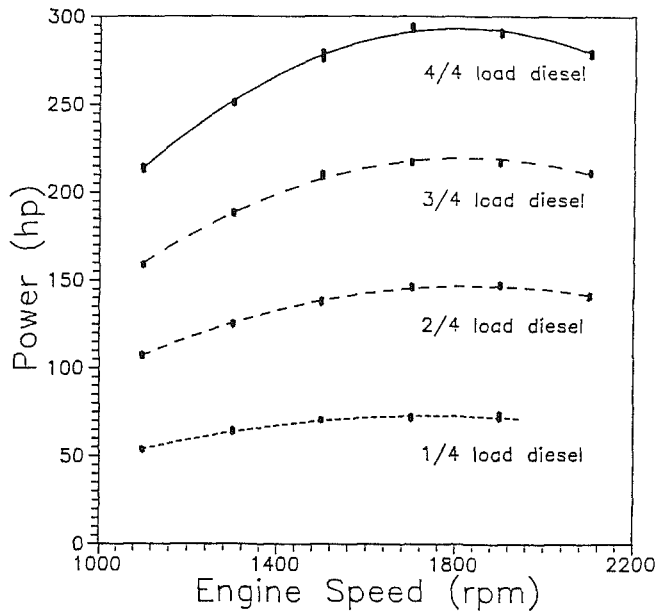

Fig. 3 Power as a function of engine speed for full, three-quarters, one-half, and one-quarter loads

torque, and pollution content (NO_x, CO, CO_2, SO_2) of the exhaust gas are monitored and recorded in data files using this system. The software program converts bit values returned by the DAS-16 to data readings such as torque and fuel flow rate and calculates from these power, fuel efficiency, and emissions. A schematic of the instrumentation and data acquisition is shown in Fig. 2.

Results and Discussion

Two separate groups of tests were conducted in this study. In the first group of tests, the effects of varying the speed and load of the engine on the emissions and performance were investigated. The engine load was varied in percentages of full load in 25 percent increments as engine speed was varied in

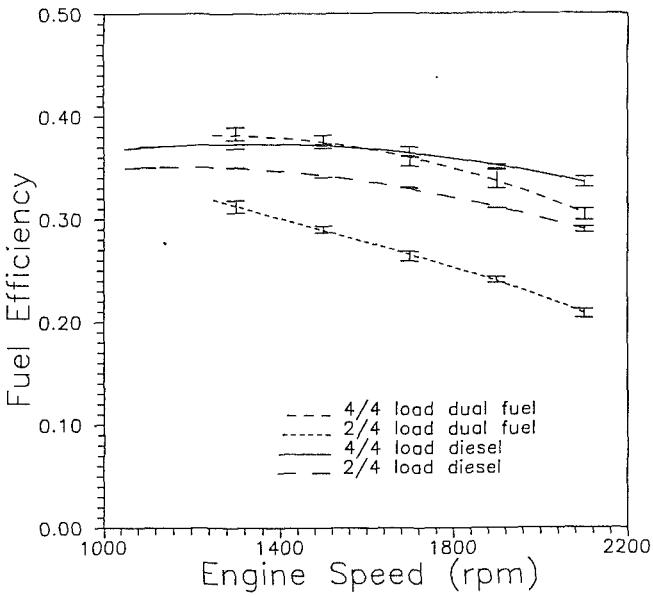

Fig. 4 Fuel efficiency as a function of engine speed for full and one-half loads

200 rpm increments. Figure 3 illustrates the power curves for each load. This graph represents actual data from a diesel baseline test and compared closely to manufacturer's data. The power results for natural gas and diesel runs were similar as the natural gas flow rate was adjusted to produce the diesel performance at each speed and load. In all cases, the diesel pilot flow rate was held near 15 percent of full load flow rate on a mass basis. For this paper, only the full and one-half load data are presented graphically. Trends exhibited for the other loads closely followed the full and one-half load cases.

In the second group of tests the intake air was restricted using the valve located upstream of the turbocharger. This allowed investigation of the effect of air-to-fuel ratio on engine performance and exhaust emissions. Engine speed was held constant for each test while loads and air-to-fuel ratios were adjusted. The tests were conducted at three engine speeds, 1300 rpm, 1700 rpm, and 2100 rpm, although only the 2100 rpm data is presented in figures.

Figures constructed with all recorded data were difficult to read due to overlapping. Therefore, graphic representation of test data presented in this paper is given in the form of best-fit curves. Error bars representing the standard deviation are included in graphs where feasible in order to give an indication of the data deviation. For all cases, approximately 12 data points at each operating condition were used to determine the curves and the standard deviation.

Diesel curves represent the combination of two sets of data taken on separate days after recalibration of the equipment. Dual-fuel curves that give data as a function of load and rpm represent the combination of three sets of data taken on separate days after recalibration of the equipment. Dual-fuel curves that give data as a function of fuel/air equivalence ratio and load represent the combination of two sets of data taken on different days after recalibration of the equipment.

Performance Results

The performance results presented include the brake fuel efficiency and fuel-air equivalence ratio. Other parameters measured include brake torque, brake power, and volumetric efficiency. Fuel conversion efficiency was taken to be equal to the brake power divided by the total injected energy rate (pilot diesel + natural gas). Because fuel heating values are different for diesel and natural gas, brake specific fuel consumption comparisons were not made. However, these can be calculated from the material presented.

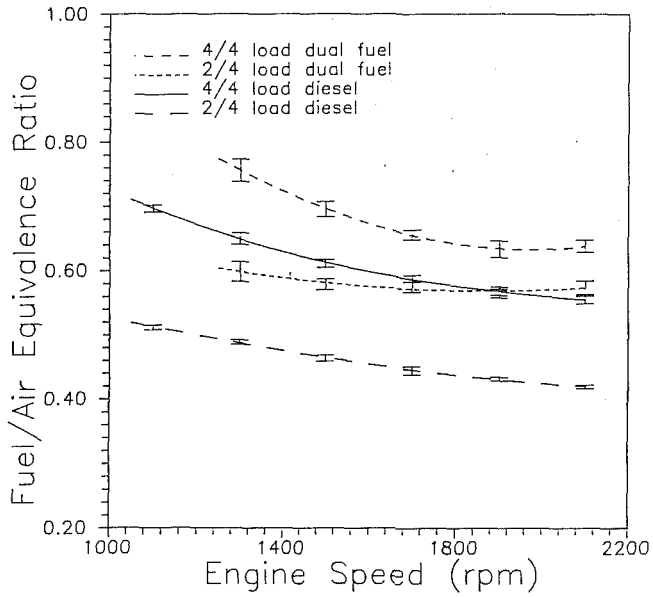

Fig. 5 Fuel-air equivalence ratio as a function of engine speed for full and one-half loads

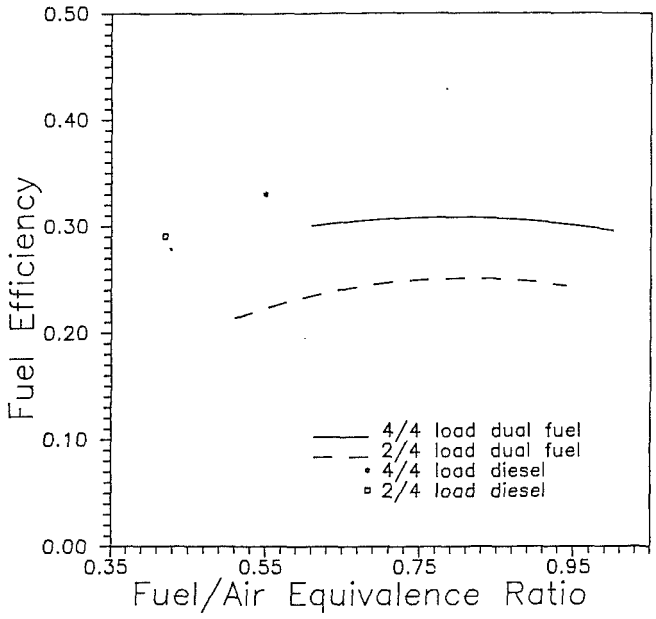

Fig. 6 Fuel efficiency as a function of fuel/air equivalence ratio for full and one-half loads and 2100 rpm

Figure 4 shows the brake fuel conversion efficiency as a function of engine speed for full and one-half load for both diesel and natural gas fueling. The full-load fuel efficiency closely matches the diesel full load, being slightly higher at speeds below 1500 rpm and lower at speeds above 1500 rpm. As the speed of the engine is increased, the combustion event is prolonged (in terms of crank angle duration) and moves further into the expansion stroke. The pilot injection timing is analogous to spark timing in that it determines the start of the combustion event. For natural gas fueling, no modifications to the injection timing of the pilot diesel were made over standard diesel timings. It is expected that the performance as a function of engine speed results could be optimized using pilot timing for natural gas. This, however, was not done in this study. For one-half load, the natural gas fuel conversion efficiencies were lower than the corresponding diesel efficiencies by 8 to 30 percent over the operating speeds investigated. Again, this was partly attributed to the nonoptimized pilot timing. Cylinder pressure data taken previously for this engine for natural gas fueling showed the peak pressure occurring between 5 and 10 crank angles later (depending on load and speed) than the corresponding peak pressure for diesel fueling. In some cases a double hump on the pressure trace could be seen, which is explained as combustion of the pilot diesel charge followed by the methane combustion [6]. A Caterpillar 3208 engine was also previously tested using natural gas and similar dual peak pressure traces were found under some conditions. With a 7.5 crank angle advance in the 3208, a 10 percent increase in fuel conversion efficiency at higher speeds was seen for natural gas fueling. For diesel fueling, the same advance decreased the fuel efficiency by about 45 percent at higher speeds [6]. For the 3406 engine tested here, it is envisioned that advancing the timing for natural gas fueling would lead to performance improvement. As discussed later, emission optimization would likely require timings different to best performance timings.

As engine load is further reduced, the fuel efficiency continues to drop. The worst case recorded was one-quarter load at 1900 rpm with the fuel efficiency of diesel being approximately 24 percent and natural gas being approximately 17 percent. As the load is decreased, the fuel-air equivalence ratio in the engine is leaned. The strong dependence of flame speed for methane-air mixtures (as well as other combustion characteristics, such as required ignition energy) on equivalence ratio impacts the engine performance [13-15]. As a methane-air mixture is leaned from stoichiometric, the flame speed is decreased, and for a fixed ignition timing will lead to longer or delayed combustion. The delayed peak cylinder gas pressure relative to TDC and lean quenching of the methane-air mixtures in the periphery of the combustion chamber are probable explanations for the reduction of efficiencies. Although not included in this study, it would be expected that an increase in unburned methane would be found at the light loads.

An important parameter for consideration is, therefore, the fuel-air equivalence ratio, which is defined as the stoichiometric air-to-fuel mass ratio divided by the measured air-to-fuel mass ratio. Figure 5 shows the equivalence ratio as a function of engine speed for full and one-half load for both diesel and natural gas fueling. As shown, the natural gas fueling compared to diesel fueling leads to slightly higher (less lean) equivalence ratios for a given load and speed condition. This occurs for two reasons. First, the natural gas is aspirated into the engine where it mixes with air, thereby displacing some portion of air, which could have moved into the cylinder. As less air is inducted, the equivalence ratio increases. Secondly, as load is decreased, the engine is less efficient using natural gas (as discussed earlier) and more natural gas must be added to produce the fixed load-speed condition. The increased fueling then increases the equivalence ratio of the engine.

For natural gas fueling, increasing speeds and decreasing loads resulted in leaner mixtures. As shown in Fig. 4, this also led to lower fuel conversion efficiencies. Worth noting here is that for diesel fueling the fuel and air are not in a premixed form for combustion and the equivalence ratio is an overall ratio. Actual combustion occurs in fuel-rich to stoichiometric to fuel-lean regions. Therefore, direct comparisons between the diesel equivalence ratios and natural gas equivalence ratios can be misleading as one is natural gas-air and the other is diesel sprayed into air.

The fuel-air equivalence ratio impacts the combustion process, which in turn affects engine performance and emission characteristics of the engine. To investigate the effect of equivalence ratio on fuel efficiency, the inlet air to the engine was throttled, thereby allowing control of the equivalence ratio. Figure 6 shows the fuel conversion efficiency as a function of fuel-air equivalence ratio for natural gas fueling at full and one-half load at 2100 rpm. Also shown in the figure for comparison are the full and one-half load points for the base diesel

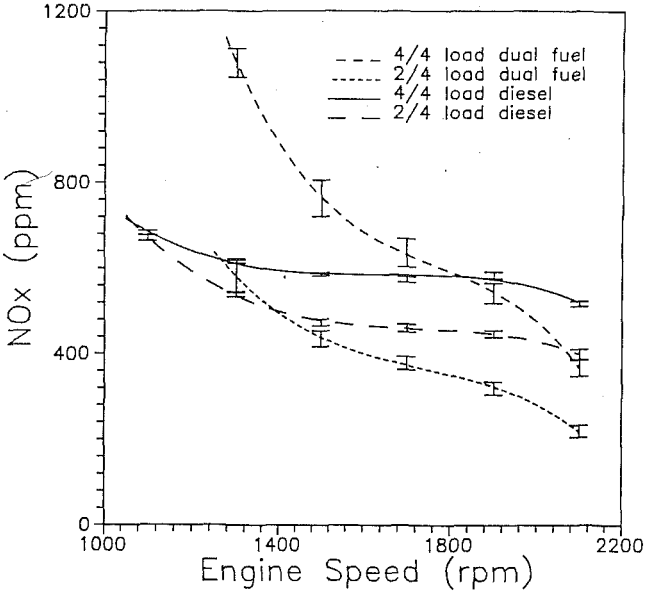

Fig. 7 NO_x emission as a function of engine speed for full and one-half loads

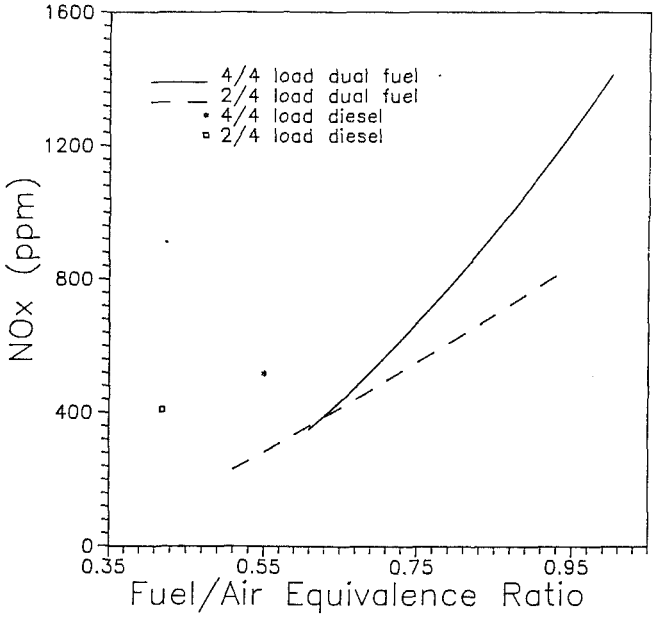

Fig. 8 NO_x emission as a function of fuel/air equivalence ratio for full and one-half loads and 2100 rpm

cases. For full-load natural gas fueling, only modest improvement of efficiency could be attained by increasing the equivalence ratio. For half-load, efficiency improvement was more pronounced, increasing from 21 percent at 0.51 equivalence ratio to 25 percent at about 0.80 equivalence ratio. The best fuel efficiencies appear to occur at equivalence ratios near 0.75 to 0.80 for these cases. For both loads, the natural gas fuel efficiencies are lower than the corresponding diesel case. Again, it is expected that optimizing the pilot charge timing for best fuel efficiency would lead to better natural gas fuel efficiencies. As the equivalence ratio is decreased, the flame speed of the leaned mixture decreases, which results in lowered engine performance. As the equivalence ratio is increased, a point would eventually be reached where further increase leads to lowered fuel efficiency. For both load cases in Fig. 6, a slight downturn in efficiencies was seen at equivalence ratios above about 0.9. Two possible explanations follow. First, it is expected that a best pilot injection timing for a given mixture equivalence ratio exists. In these results, the timing was not changed and therefore, the performance would decrease from a best value as the equivalence ratio is changed. Second, as the equivalence ratio is increased, to near or above 1, it is more difficult to achieve adequate air to all fuel locations in the cylinder leading to longer combustion times and possibly unburned fuel. This would also result in lowered efficiencies.

In summary, for performance, the engine was operated without knock with gas substitution percentages of about 85 percent on a mass basis. Full-load power was easily achieved at all operating speeds. At lower loads a decrease in fuel efficiency was found, although adjusting the fuel-air equivalence ratio can moderate this effect. It was determined the pilot timing should be further investigated and hydrocarbon emissions data would be useful in determining partial burn limitations.

Emission Results

NO_x emission concentrations measured in the exhaust gas as a function of engine speed for full and one-half load for diesel only and natural gas fueling are shown in Fig. 7. At full load and for speeds greater than about 1800 rpm, natural gas fueling reduced the NO_x emission concentrations from the engine compared to the full-load diesel fueling NO_x concentrations. Below 1800 rpm, NO_x concentrations are increased over diesel fueling levels for full-load natural gas fueling. For half-load conditions, the NO_x concentrations are lower for

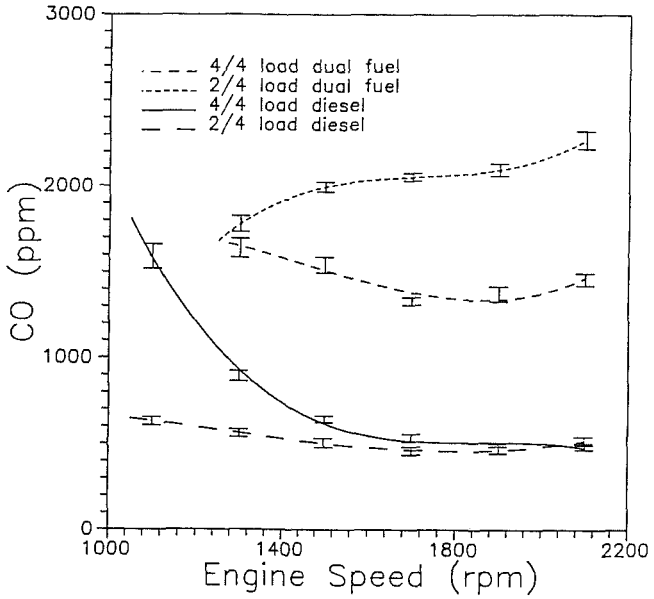

Fig. 9 Carbon monoxide emission as a function of engine speed for full and one-half loads

natural gas fueling for speeds above about 1400 rpm and slightly higher than the diesel levels for lower speeds. In both load cases, the general trend is decreasing NO_x concentrations with increasing speed. These results are consistent with the fuel–air equivalence ratio data presented earlier, which showed natural gas–air mixture leaning with increasing engine speed. Mixture leaning for the near-homogeneous natural gas cases would lead to lower in-cylinder temperature and thus, decreased NO_x formation. Also, the leaner mixtures would result in slower flame propagation, also resulting in lowered peak in-cylinder temperatures. The fuel efficiency data presented earlier are also consistent with this explanation with an overall decreasing trend with increasing speed. The nonoptimized pilot timing (with respect to fuel efficiency) leads to lowered performance. However, the NO_x engine characteristics were improved. This is interesting in that it points to the trade-off between emissions and performance.

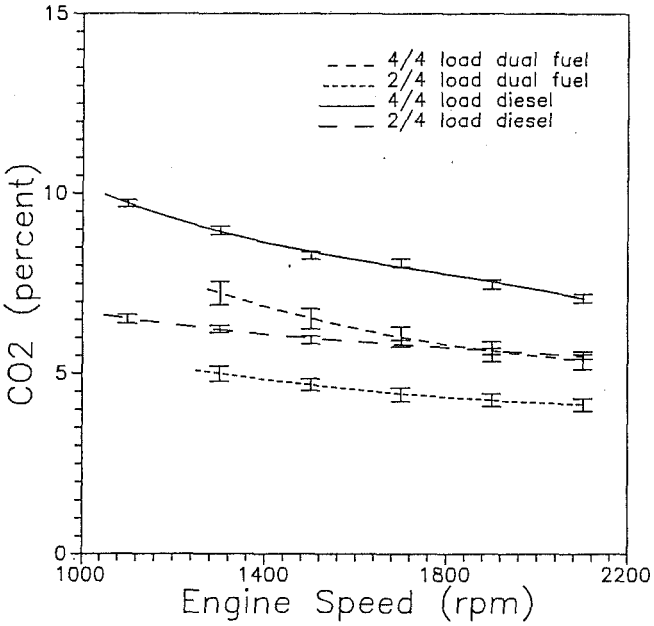

Fig. 10 Carbon dioxide emission as a function of engine speed for full and one-half loads

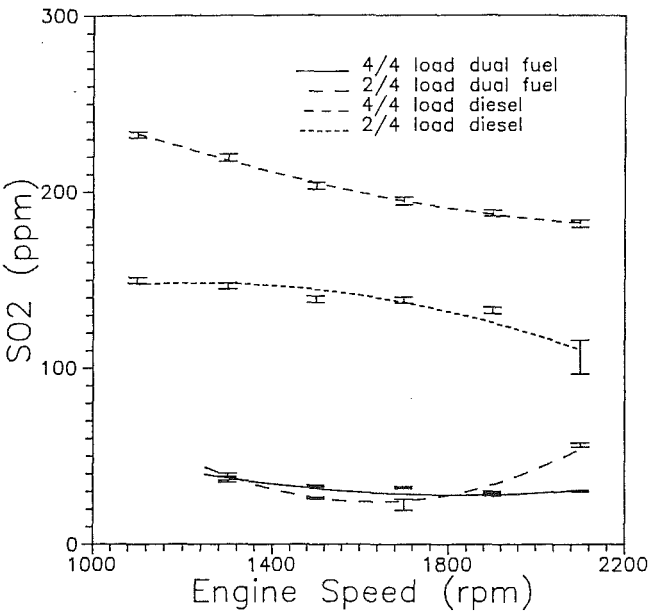

Fig. 11 Sulfur dioxide emission as a function of engine speed for full and one-half loads

Figure 8 shows the effect of varying the fuel–air equivalence ratio on NO_x concentrations for full and one-half load natural gas fueling at 2100 rpm. Again, the corresponding diesel-only points are noted on the figure for reference. The left limit for the full and one-half load data lines corresponds to no throttling of the intake air, which results in the leanest mixture conditions and lowest NO_x concentrations. As the air is throttled, less air is used to charge the cylinder and thus a more fuel-rich mixture occurs. As would be expected, higher equivalence ratios yield higher in-cylinder temperatures and thus, higher NO_x concentrations. The NO_x concentrations are also affected directly by the change in dilution air to the engine. That is, as excess air is decreased, less dilution occurs, thereby increasing the NO_x concentrations. For half-load, increasing the equivalence ratio from 0.5 to 1.0 would reduce the number of product moles by approximately half. For a given NO_x production, this would increase the concentration of NO_x by 2 or double the NO_x. The measured NO_x concentration changes

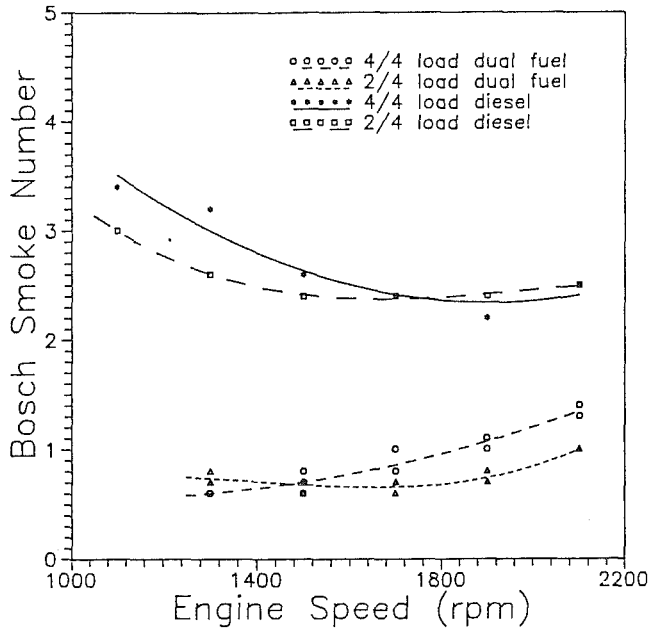

Fig. 12 Bosch smoke number as a function of engine speed for full and one-half loads

by a factor of about 4 for this equivalence ratio range and thus, about one-half of the NO_x change can be attributed to dilution changes. For full-load conditions, dilution appears to play a less significant role in the NO_x concentration levels.

Figure 9 shows the concentrations of CO in the exhaust as a function of engine speed for full and one-half load conditions for both diesel and natural gas fueling. For all speeds, natural gas fueling resulted in higher CO emissions. This is consistent with the fuel efficiency results and explanations for nonoptimized pilot timing and flame quenching or partial burning. It is expected that the elevated CO concentrations would be accompanied by higher unburned hydrocarbons. Although not presented graphically, varying the fuel–air equivalence ratio allowed CO emissions to be lowered; however, the best CO emission levels for full and one-half loads (occurring at an equivalence ratio of 0.75 to 0.80) were still higher than the corresponding diesel-only levels. It is expected that pilot charge timing could also be used to control CO concentration levels.

The CO_2 concentration in the exhaust gas was lowered for natural gas fueling. These results are shown for full and one-half loads in Fig. 10. The decrease in CO_2 concentrations results from the higher H to C ratio of natural gas, which directly impacts the number of moles of each product constituent. As the H to C ratio is decreased, more carbon product, CO_2, is formed compared to hydrogen product, H_2O, thereby increasing CO_2 concentrations for diesel over natural gas fueling. The natural gas used in the study was low in sulfur and thus, its use also significantly reduced SO_2 concentrations as shown in Fig. 11. For the cases investigated, the SO_2 emissions were reduced almost linearly with diesel fuel reduction. For full-load natural gas, about 15 percent diesel pilot was used and the SO_2 concentration for full-load natural gas fueling is about 15 percent of the diesel concentration. Because the diesel pilot flow rate per engine stroke was not varied, the SO_2 concentrations for natural gas fueling were near constant.

Particulate emissions from the engine were monitored using a Bosch smoke number method whereby a sample of exhaust was pulled through a filter paper and particulate concentration was indicated using light reflectivity from the sample filter paper. The smoke number plotted as a function of engine speed for full and one-half load conditions for diesel and natural gas fueling is shown in Fig. 12. For natural gas fueling, the Bosch smoke numbers are reduced to 1/2 to 1/3 of the corresponding

diesel only cases. These results indicate a significant reduction in particulate emissions. The reduction of particulate formation is expected since the homogeneity of the air–fuel mixture improves for the natural gas fueling cases. This minimizes the occurrence of locally rich zones, which can produce particulates. A dilution tunnel has been developed to monitor particulate emission levels more accurately for future reporting.

Conclusions

The Caterpillar 3406 engine was operated with natural gas as the primary fuel and diesel as the pilot or ignition fuel. The engine was operated at one-quarter, one-half, three-quarters, and full-load conditions without encountering knock. The following observations were made for comparing engine operation using natural gas versus diesel:

- For full-load operation, the fuel efficiency for natural gas operation was similar to diesel operation.
- For lower loads the fuel efficiency was decreased for natural gas fueling for fixed pilot injection timing.
- NO_x concentrations in the exhaust were reduced at low loads and at high speeds for high loads for natural gas fueling.
- CO emissions were increased for natural gas fueling.
- CO_2 emissions were decreased for natural gas fueling.
- SO_2 concentrations were decreased for natural gas fueling.
- Particulate emissions were decreased for natural gas fueling.

Other observations that suggest future research include: The pilot injection quantity and timing is an important parameter for performance and emissions optimization, and additional analysis of emissions would be useful including unburned hydrocarbon measurement and use of a dilution tunnel for particulate measurements.

References

1 Gill, A. P., "Design Choices for 1990's Low Emission Diesel Engines," SAE Paper No. 880350.

2 Richards, R. R., and Sibley, J. E., "Diesel Engine Emissions Control for the 1990's," SAE Paper No. 880346.

3 Acker, G., Brett, C. E., Schaetzle, W. J., and Song, Y. K., "LNG (Liquid Natural Gas) as a Fuel and Refrigerant for Diesel Powered Shrimp Boats," ASME Paper No. 88-ICE-21.

4 Xianhua Ding and Hill, P., "Emissions and Fuel Economy of a Prechamber Diesel Engine With Natural Gas Dual-Fueling," SAE Paper No. 860069.

5 Barbour, T. R., Crouse, M. E., and Lestz, S. S., "Gaseous Fuel Utilization in a Light-Duty Diesel Engine," SAE Paper No. 860070.

6 Acker, G., "A Study of the Combustion Characteristics of the Dual-Fuel Diesel Engine," Ph.D. Dissertation, The University of Alabama, 1986.

7 Tesareck, H., "Investigation Concerning the Employment Possibilities of the Diesel-Gas Process for Reducing Exhaust Emission Especially Soot (Particulate Matters)," SAE Paper No. 750158.

8 Boisvert, J., Gettel, L. E., and Perry, G. C., "Particulate Emissions of a Dual-Fuel Caterpillar 3208 Engine," ASME Paper No. 88-ICE-18.

9 Pitt, P. L., "An Ignition System for Ultra Lean Mixtures," *Combustion Science and Technology*, Vol. 35, 1984, pp. 277–285.

10 Quader, A. A., "Lean Combustion and the Misfire Limit in Spark Ignition Engines," SAE Paper No. 741055, 1974.

11 Anderson, R. W., and Lim, M. T., "Investigation of Misfire in a Fast Burn Spark Ignition Engine," *Combustion Science and Technology*, Vol. 43, 1985, pp. 183–196.

12 Heywood, J. B., *Internal Combustion Engines*, McGraw-Hill, New York, 1988, p. 915.

13 Heywood, J. B., *Internal Combustion Engines*, McGraw-Hill, New York, 1988, p. 302.

14 Obert, E. F., *Internal Combustion Engines and Air Pollution*, Harper and Row Publishers, New York, 1973, pp. 234–235.

15 Heywood, J. B., *Internal Combustion Engines*, McGraw-Hill, New York, 1988, pp. 372–375, 400–478.

Emission Reductions Through Precombustion Chamber Design in a Natural Gas, Lean Burn Engine

M. E. Crane

S. R. King

Southwest Research Institute,
San Antonio, TX 78228

A study was conducted to evaluate the effects of various precombustion chamber design, operating, and control parameters on the exhaust emissions of a natural gas engine. Analysis of the results showed that engine-out total hydrocarbons and oxides of nitrogen (NO_x) can be reduced, relative to conventional methods, through prechamber design. More specifically, a novel staged prechamber yielded significant reductions in NO_x and total hydrocarbon emissions by promoting stable prechamber and main chamber ignition under fuel-lean conditions. Precise fuel control was also critical when balancing low emissions and engine efficiency (i.e., fuel economy). The purpose of this paper is to identify and explain positive and deleterious effects of natural gas prechamber design on exhaust emissions.

Introduction

As natural gas becomes an increasingly attractive alternative to conventional energy sources such as gasoline, diesel fuel, and even electricity, combustion systems designed to exploit the advantages associated with natural gas have risen to the forefront of engine research. One advantage of natural gas is its wide flammability limits, especially to the fuel-lean side where ignition of natural gas can occur in the presence of more than 200 percent theoretical air [1]. Operating in this regime translates into improved fuel economy and lower NO_x emissions; however, these improvements are usually at the expense of exhaust HC. The objective of this research was to develop and experimentally verify ways to reducing total HC emissions from prechamber, stratified charge engines operating on natural gas. The effects of these combustion strategies on NO_x were also measured.

A conventional natural gas prechamber is shown in Fig. 1. The prechamber usually replaces the diesel fuel injector and seats flush with the firedeck. Communication with the main combustion chamber occurs through a small orifice or throat near the base of the prechamber. A spark plug is located in this area for ignition of the prechamber mixture. During the intake stroke, a very fuel-lean, gaseous mixture is introduced into the main chamber. The subsequent compression stroke forces a fraction of the lean main chamber mixture into the smaller volume prechamber, where it is supplemented with raw natural gas supplied through the gas inlet valve. The mixture in the prechamber, often near chemically correct, is then ignited via a conventional spark plug and ignition system.

The mixture in the prechamber burns rapidly with a corresponding sharp rise in prechamber pressure. A high-energy, burning mixture exits the prechamber through the orifice and initiates combustion of the very lean mixture in the main combustion chamber. This process has the ability to operate under overall leaner conditions than open chamber configurations due to the higher ignition energy of the prechamber jet when compared to conventional spark ignition. Ultimately, lower NO_x and CO emissions, less cyclic variability, and reduced combustion duration are realized.

Research was directed at the development and understanding of novel prechamber designs, with the goal of reducing light load/fuel lean HC emissions. This was achieved by understanding what had been investigated in the past, considering those findings in this study's designs, and incorporating novel ideas to address problem areas. As a result, several unique

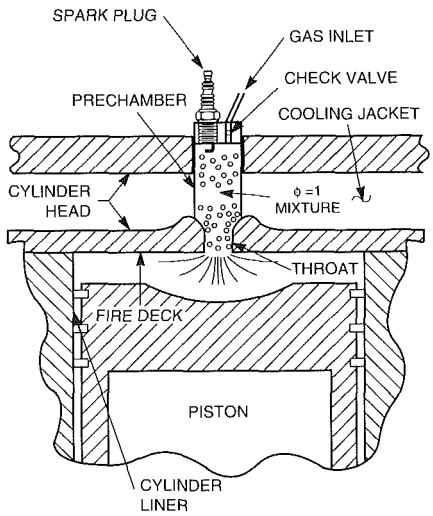

Fig. 1 Typical natural gas prechamber installed in a diesel engine cylinder head

Contributed by the Internal Combustion Engine Division and presented at the 13th Annual Fall Technical Conference, Muskegon, Michigan, September 30–October 2, 1991. Manuscript received by the Internal Combustion Engine Division September 20, 1991. Associate Technical Editor: J. A. Caton.

Table 1 Engine features and dimensions

Bore, mm	137.2
Stroke, mm	165.1
Stock Displacement, L	2.4
Induction	Naturally Aspirated
No. of Cylinders	1
Valve Train	4 vlvs actuated w/pushrods
Compression Ratio	14.5:1 (stock)
Piston Type	Re-entry w/ 3 rings

prechambers were designed, fabricated, and characterized on a single-cylinder research engine. This report explains the underlying combustion mechanisms resulting in designs that simultaneously reduced HC and NO_x.

Experimental Apparatus and Procedures

Experimental Engine Setup. A Caterpillar 1Y540 (CAT 1Y540), single-cylinder engine was chosen for this investigation. This engine configuration is typically used for oil characterization testing and was well suited to prechamber evaluation due to its inherent size and flexibility. Specific engine features and dimensions are presented in Table 1.

The induction system used the CAT 1Y38 surge tank with a heater mechanism to control inlet air temperature. An exhaust system using piping and an exhaust barrel as specified by the Caterpillar 1Y540 Engine 1-J Test Procedure [2] was also installed. Exhaust back pressure was minimal for all test conditions.

Several modifications were made to the engine prior to testing. A new cylinder head was modified to accept the experimental precombustion chambers in what was formerly the unit injector hole. Modification involved removing the injector and machining a small spot-face on the backside of the firedeck to allow the prechamber base gasket to seat. Furthermore, the injector hole was threaded to provide clamping force on the prechambers.

Additional modifications were required to accept a specially fabricated spark plug near the prechamber throat. A hole was bored that permitted a 195-mm-long spark plug to be inserted through the side of the cylinder head and into the prechamber base for throat ignition or flame ionization detection. Water intrusion was sealed out with a high-temperature silicone sealer around the outside of the plug's sealing surfaces. Firing pressures were contained with a standard, 14 mm spark plug gasket. This approach worked quite well; there was no evidence of water leakage during any inspections or testing. Final cylinder head modification involved a change to the firedeck to accept a flush-mounted, cylinder pressure transducer.

Instrumentation and Cell Setup. A summary of the engine test setup and associated instrumentation is shown schematically in Fig. 2. The CAT 1Y540 research engine is shown in the center of the figure. Engine temperature was maintained to within 2°C by a shell and tube heat exchanger and was critical since the prechamber was surrounded by coolant.

Natural gas was metered into the engine through regulators providing independent control of flow into the main and precombustion chambers. Main chamber gas was introduced to the intake air supply downstream of the surge tank, approximately 750 mm away from the intake port. Control of gas flow into the prechamber was accomplished by regulating the gas pressure upstream of the prechamber. Gaseous flow rates were adequately measured with positive displacement, Roots-type meters.

Ignition of the inducted fuel and air mixture occurred in the precombustion chamber through either a conventional, 10 mm spark plug gapped to 0.38 mm or the extended length plug gapped to about 0.51 mm (manufacturer's specifications). An

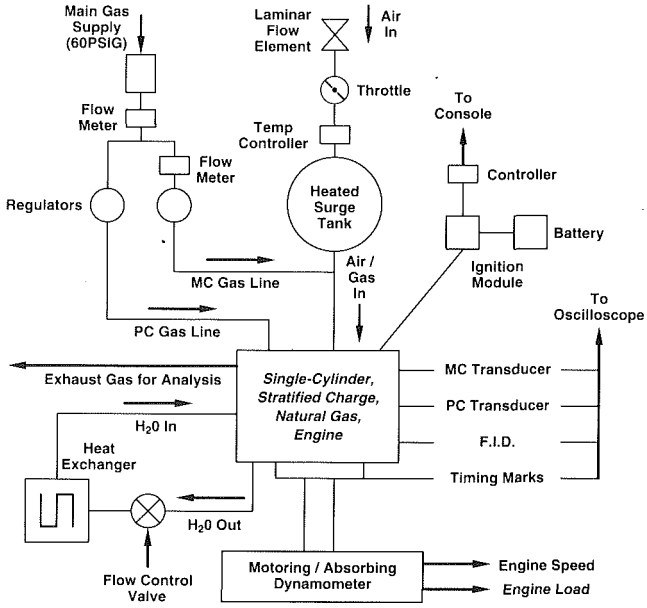

Fig. 2 Schematic of engine instrumentation and associated hardware used for evaluation of natural gas prechamber designs

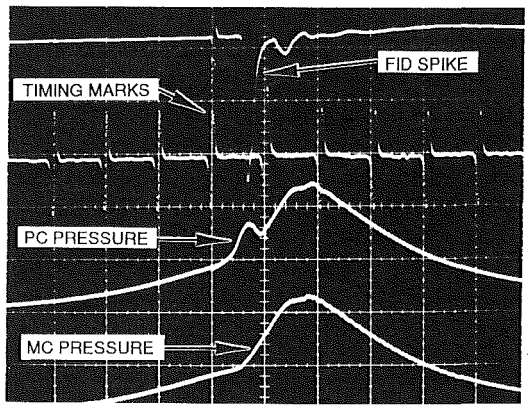

Fig. 3 Sample oscilloscope trace showing (from top to bottom): FID pulse, 10 deg increment timing marks (center line is TDC), prechamber pressure trace, and main chamber pressure trace

Electromotive HPV1 high energy ignition system provided necessary voltage in both cases. A 60-tooth pick-up wheel mounted onto the crankshaft nose served as a shaft encoder for accurate spark timing changes.

Gaseous exhaust emissions including CO, CO_2, total HC, NO_x, and O_2 were measured by a Beckman emissions cart through a heated sample line. Hydrocarbon emissions were measured on a carbon basis (ppm C) and are three times those reported on a straight propane basis.

High-speed data encompassed cylinder pressure traces from the precombustion chamber, the main combustion chamber, and a Flame Ionization Detector (FID) signal. Flush-mounted and cooled, Kistler 6121A cylinder pressure transducers were used to measure cylinder pressures. Resulting signals were conditioned through Kistler 5004 charge amplifiers and observed through a four-channel oscilloscope. Storage of these traces for posttest analysis was accomplished with a Norland "Prowler" A-D converter/storage scope.

The final piece of high-speed data acquired during this study made use of the aforementioned FID. Supplying a voltage potential across the spark plug not being used for prechamber ignition allowed characterization of the time necessary for the flame to travel a certain distance within the prechamber. This was accomplished by monitoring the time between the ignition event and flame arrival at the FID. The latter event was evident

on the oscilloscope as a distinct voltage drop as shown in the upper portion of Fig. 3.

Experimental Test Procedure. It was difficult to test all prechambers under identical conditions. Their unique designs expectedly changed their behavior in terms of emissions, lean limit, and combustion stability. However, items that were consistent from test to test are presented in Table 2.

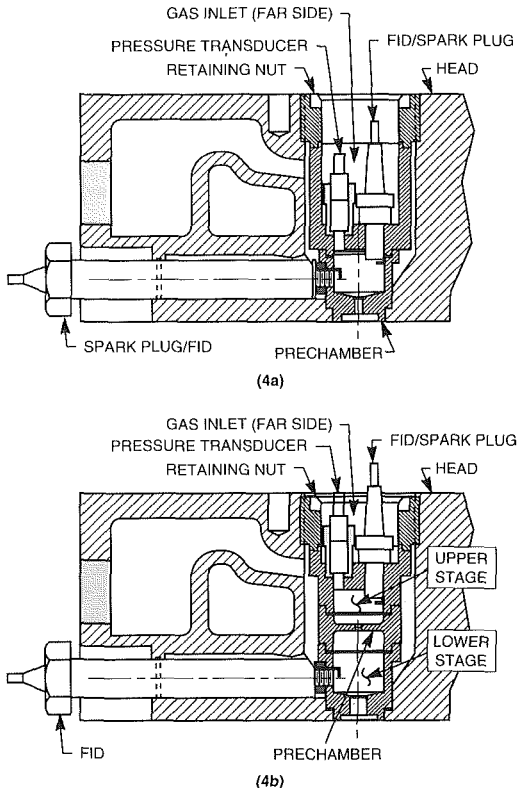

Fig. 4 Basic prechambers designs tested for hydrocarbon reductions: (*a*) conventional design, and (*b*) staged prechamber assembly

Table 2 Standard test condition

Oil Sump Temperature, C	72
Coolant Out Temperature, C	85
Engine Speed, rpm	1000
Inlet Air Temperature, C	35
Exhaust Backpressure	Minimal
Inlet Air Humidity, grains	50 - 90
Throttle Position	Wide Open Throttle
PC Fueling Rate	Min, Mid, Max
MC Fueling Rate	That necessary to achieve desired load
Ignition Timing	Sweep
A/F Ratio	~ 30:1
Load	50 psi BMEP

The CAT 1Y540 was broken in on natural gas with the baseline prechamber configuration. This allowed power and friction to stabilize.

Prechamber Design and Strategy

Design objectives focused on physically incorporating the most successful and state-of-the-art strategies from past investigations into these low emission prechambers. This was accomplished by adopting a modular design that allowed different configurations to be evaluated in a time-effective manner without fabricating each prechamber individually.

The first step in the prechamber design process was to determine what aspects of prechamber design would be addressed. It was decided to concentrate on specific design parameters that the literature identified as critical. Parameters that were deemed critical and were accommodated during the design phase included ignition site [3, 4], prechamber stoichiometry [5], main chamber stoichiometry [6, 7], prechamber volume [3, 8, 9], orifice size [8, 10, 11], orifice design [3, 4], and fuel mixing [9, 12]. Each prechamber design had a role in determining the relative effect of these parameters.

Conceptual approaches were designed to conform to the CAT 1Y540 cylinder head. The cylinder head was sectioned and reproduced on a CAD system to allow for specific prechamber designs. Using the modular approach mentioned earlier, four basic designs were developed to fit the CAT 1Y540 cylinder head and accommodate the necessary instrumentation.

Basic Modular Prechamber. This basic prechamber scheme is shown schematically in Fig. 4(*a*) and was used in various forms for Tests 1-4. The spark plug, fuel inlet valve, and pressure transducer are located in the top part of the prechamber assembly. This interchangeable component is labeled the prechamber cap. The prechamber orifice was fixed in the prechamber base, which was seated on a modified portion of the cylinder head. The assembly was held together by a prechamber retainer that compressed the cap and base. Threads in the cylinder head secured the retainer and allowed sufficient clamp load.

Each component of the modular design had a specific function. The prechamber base seated securely in the cylinder head and accommodated various orifice sizes and configurations. In addition, it was designed to allow use of a throat-mounted spark plug or an FID. Ignition of the bulk gas or the gases near the throat wall (i.e., Tests 2, 3, and 4) could be achieved with this system. When the top-mounted spark plug was used for prechamber ignition, the throat plug was used as the FID. The prechamber cap stacked neatly on the base through an annular groove and no threads. Threadless contacts were desired to prevent seizure and difficult disassembly.

The CAT 1Y540 cylinder head conveniently provided for a wet prechamber since the injector hole communicated with the cylinder head coolant jacket. A wet prechamber helped to

Table 3 Prechamber design summary

	Prechamber Configuration (by Test Number)							
	1	2	3	4	6	8	9	10
Vol, total pc (ml)	13.27	13.27	13.27	13.27	17.86	17.86	17.86	n/a
Vol, lower pc (ml)	n/a	n/a	n/a	n/a	15.26	15.26	15.26	n/a
Vol, upper pc (ml)	n/a	n/a	n/a	n/a	2.60	2.60	2.60	n/a
% of TCV	6.8	6.8	6.8	6.8	9.0	9.0	9.0	n/a
Dia, prim orifice (mm)	4.75	4.75	9.53	9.53	4.75	9.53	4.75	n/a
Dia, sec orifice (mm)	n/a	n/a	n/a	n/a	9.40	3.18	3.18	n/a
Compression Ratio	13.5	13.5	13.5	13.5	13.1	13.1	13.1	14.4
Ignition Site	TOP	THROAT	THROAT	BULK GAS	TOP	TOP	TOP	CENTRAL MC

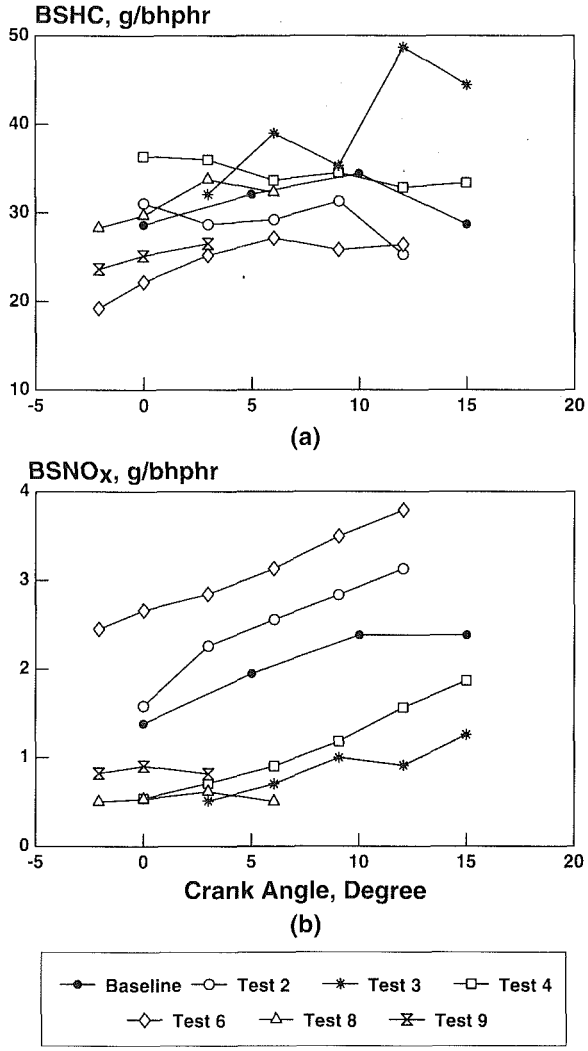

Fig. 5 Prechamber design effects on (*a*) total exhaust HC and (*b*) oxides of nitrogen (1000 rpm, WOT, "maximum" prechamber fuel flow rate at 50 psi bmep)

Table 4 Individual test *A/F* ratios

	Test							
	1	2	3	4	6	8	9	10
Avg. Equiv. Ratio	0.56	0.55	0.52	0.55	0.57	0.55	0.59	N/A
Range	±.015	±.015	±.025	±.005	±.005	±.015	±.005	N/A

Table 5 Light load emissions summary (results relative to baseline test)

Test Number	HC	NO_X	Efficiency
Baseline	–	–	–
Test 2	-16%	+25%	+7%
Test 3	+26%	–72%	-2%
Test 4	+13%	–56%	+4%
Test 6	–30%	+50%	–2%
Test 8	+3%	–69%	–4%
Test 9	–14%	–47%	–14%
Open Chamber	n/a	n/a	n/a

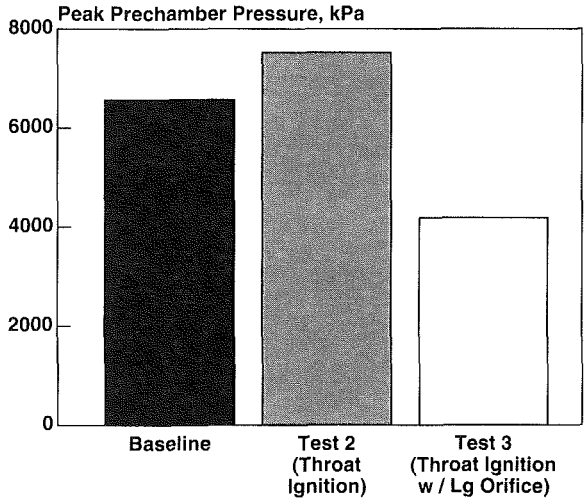

Fig. 6 Designs effects on peak pressure within the prechamber (5 deg BTDC, 1000 rpm, WOT, equivalence ratio = 0.54)

prevent detonation, but required that sealing surfaces resulting from the modular design seal against prechamber firing pressures and coolant leaks. The former was accomplished with annealed copper gaskets at every juncture. Each gasket was designed to be approximately 0.08 mm oversized so that the prescribed clamp load would provide adequate crush of each gasket. In this manner, prechamber combustion pressures were sealed from escaping into the cylinder head coolant jacket.

Preventing coolant leaks into the prechamber was crucial since it would have significantly modified characteristic prechamber combustion. These leaks were avoided by simply applying a thin bead of silicon sealer to the circumference of individual mating surfaces. This approach proved to work well.

Combinations of these modular pieces allowed straightforward changes in prechamber volume, orifice diameter, plug location, and prechamber geometry. Design characteristics and test combinations presented in this report are given in Table 3. All prechambers were fabricated from 421 stainless steel.

Staged Prechamber. One of the novel prechambers designed and fabricated for testing was labeled "Staged Prechamber" (Fig. 4*b*). This design features two auxiliary chambers communicating with one another through a secondary orifice. Similar to the previous designs, a premixed fuel and air charge is inducted into the main chamber and subsequently compressed into the Staged Prechamber assembly. Supplemental gas is added to the upper stage of the Staged Prechamber where ignition first occurs through a conventional spark plug.

It was hypothesized that the developed flame kernel in the upper chamber would release a high-energy, preliminary torch to ignite the lower stage fuel and air charge. An FID was located near the throat of the lower stage to indicate when the flame front had arrived. Torch ignition in the main combustion chamber was achieved through a primary orifice connecting the main chamber and prechamber assembly.

Two upper stages were designed and fabricated so that the effects of secondary orifice size could be evaluated. Table 3 details the design of the staged prechambers (ref. Tests 6, 8, and 9).

Experimental Results

Nine natural gas combustion systems were evaluated as part of this effort:

- Baseline configuration (Test 1)
- Prechamber with throat-mounted spark plug (Test 2)
- Prechamber with throat-mounted spark plug and large orifice (Test 3)
- Prechamber featuring ignition of the bulk gas (Test 4)
- Staged prechamber with large secondary orifice and small primary orifice (Test 6)
- Staged prechamber with small secondary orifice and large primary orifice (Test 8)

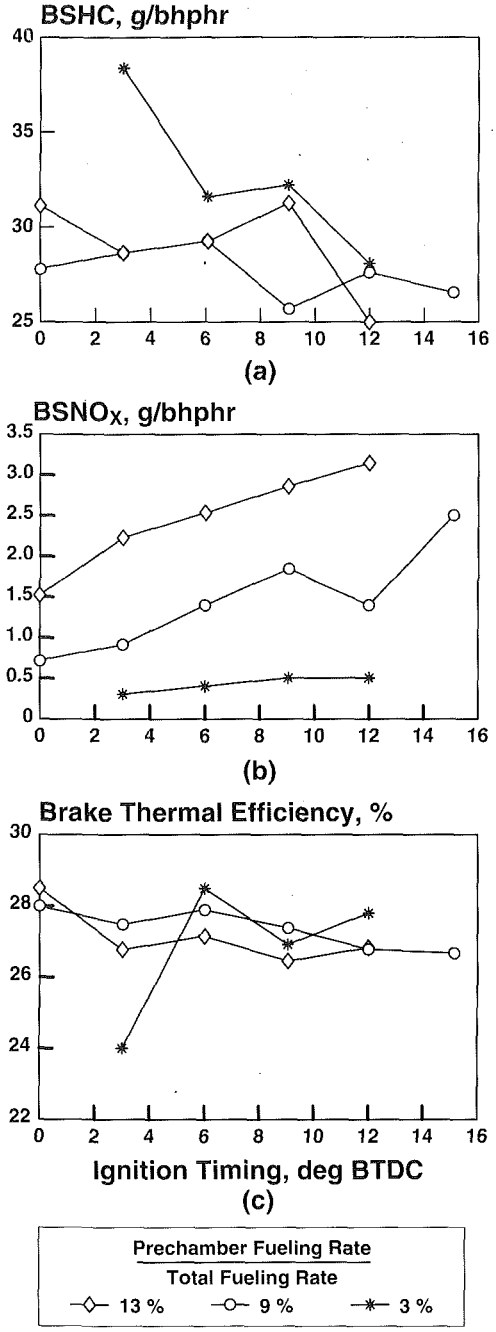

Fig. 7 Prechamber fueling rate effects on (*a*) total exhaust HC, (*b*) NO_x, and (*c*) brake thermal efficiency (Test #2, 1000 rpm, WOT, 50 psi bmep)

- Staged prechamber with small primary and secondary orifices (Test 9)
- Open chamber combustion system (Test 10)

Characteristic HC and NO_x result are briefly summarized for the first seven tests in Fig. 5. These curves were generated under the relatively light load of 50 psi BMEP and a minimum HC prechamber fueling rate. Prechamber and total engine air/fuel ratios were held nearly constant during testing; however, as spark timing was increased or prechamber fueling rates were changed, main chamber fueling rate was adjusted accordingly to maintain a constant load. Overall equivalence ratios[1] for each test configuration are given in Table 4. Equivalence ratio

[1]Equivalence ratio = $(A/F)_{stoich}/(A/F)_{actual}$.

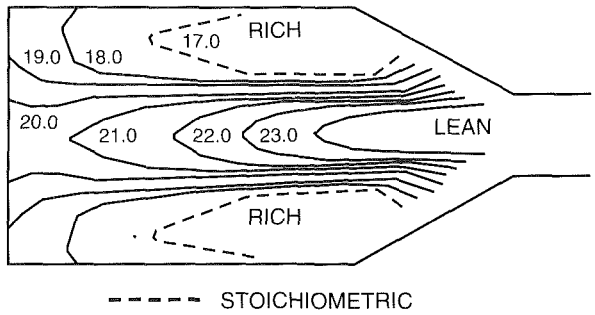

Fig. 8 Typical spatial variation of air-fuel ratio in the prechamber of a natural gas engine as predicted by computational fluid dynamics code (12 deg BTDC) [9]

was set to maintain 50 psi bmep and did not vary more than ±0.025 during any given test.

Results in Table 5 represent a summary of the average emission trends shown in Fig. 5. Prechamber designs used in Tests 2, 6, 8, and 9 lowered or maintained total HC emissions relative to the baseline curve. Test 6 demonstrated the greatest improvement by reducing exhaust HC by almost 30 percent. Oxides of nitrogen were reduced relative to the baseline prechamber in Tests 3, 4, 8, and 9. The typical HC-NO_x tradeoff is apparent in the first four tests. The latter staged prechambers simultaneously lowered exhaust NO_x and HC and appear very promising. The only change in fuel consumption was improved fuel economy in Test 2 and significantly worse efficiency in Test 9. Test 9 efficiency decreased due to increased pumping losses across the small diameter orifices in the staged prechamber.

Open chamber results are not shown because this configuration would not operate under such lean conditions (average of 0.55 equivalence ratio). Emissions and combustion stability degraded with the open chamber configuration and required that it be run at richer air/fuel ratios and heavier loads at wide open throttle. However, open chamber tests were conducted in an "unoptimized manner." Compression ratio was approximately 10 percent higher than that used in prechamber testing due to reduced clearance volume. Also, the open chamber test was run unthrottled and there was no effort to ensure adequate mixture preparation for the incoming charge. The spark plug was centrally located between the four valves where the prechamber orifice usually resided.

Analysis of Experimental Results

Analytical and experimental data are presented to explain mechanisms underlying observed HC, NO_x, and general prechamber performance behavior. Several theories are presented to explain observations related to different prechamber designs.

Hydrocarbon Emissions. Copious amounts of emissions and performance data were taken under various operating conditions during testing. However, HC emissions have been documented to be worst under light-load conditions where frequent misfire, poor volumetric efficiency, and/or poor combustion stability prevail. Consequently, the following analyses focus on the relatively light-load operation of 50 psi BMEP at 1000 rpm.

Baseline Prechamber. The advantage of operating with a prechamber is evident by realizing that open chamber emissions data are absent from the light load results in Fig. 5. Load was controlled solely by main chamber and prechamber fuel metering and it was found that the open chamber configuration was not able to operate under the required, fuel-lean, light load conditions. Attempts to do so resulted in excessive amounts

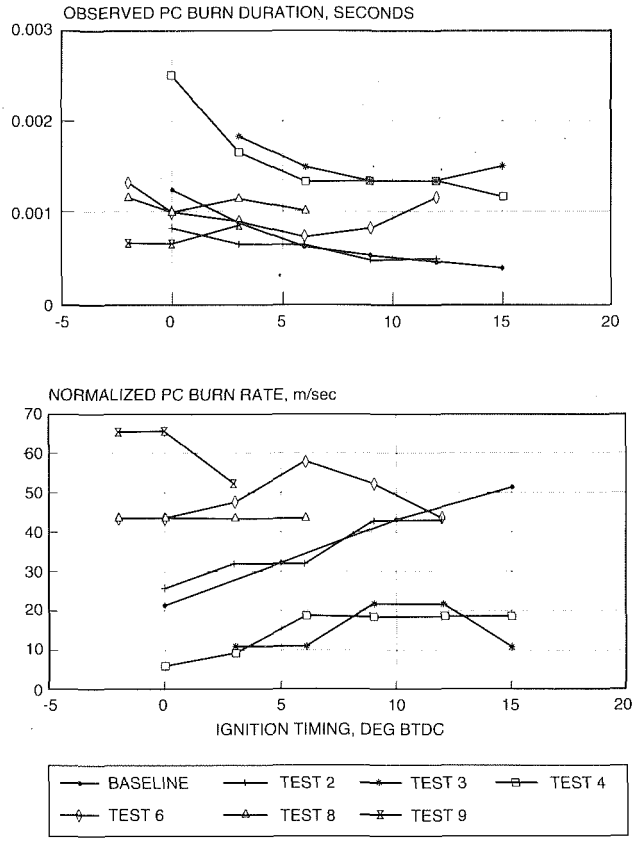

Fig. 9 The effect of prechamber design and operating conditions on (*a*) prechamber burn time, and (*b*) normalized burn rate

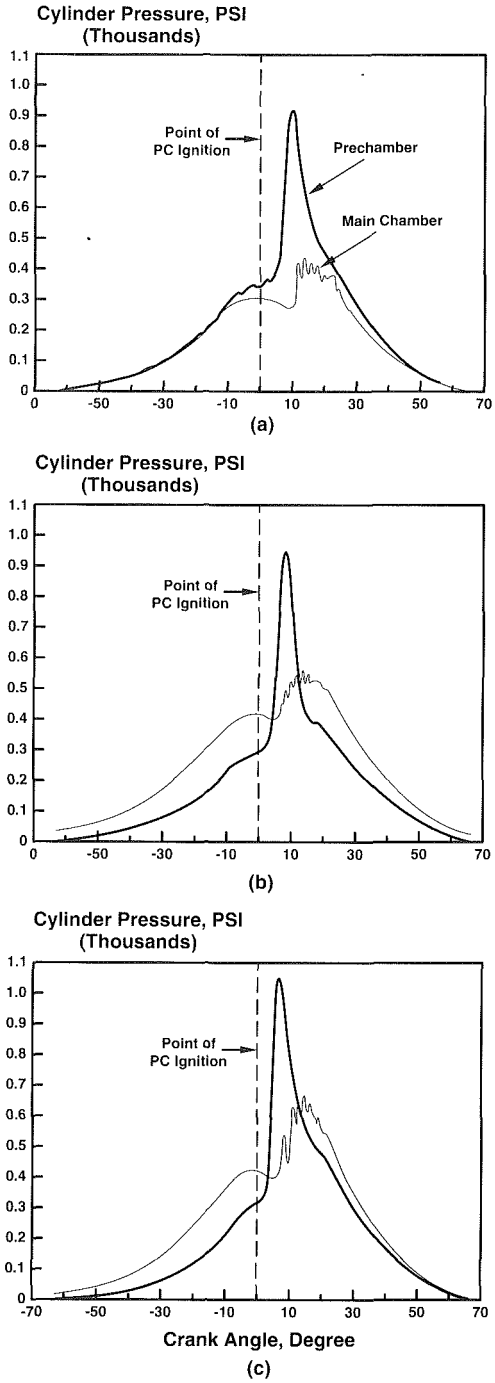

Fig. 10 Representative prechamber and main chamber pressure traces for configurations tested in (*a*) Test 6, (*b*) Test 8, and (*c*) Test 9 (0 deg BTDC, 1000 rpm, WOT, "maximum" prechamber fueling rate at 50 psi bmep)

of unburned fuel due to frequent misfires. The conventional prechamber served its intended purpose of extending the lean operating limit and thereby reducing NO_x. Unfortunately, these reductions in NO_x are accompanied by unacceptably high HC emissions.

Test 2 Prechamber. It has been proposed that a strong factor contributing to excessive HC is the location of the spark plug in the prechamber design [3, 4, 9]. Conventional natural gas prechambers place the spark plug at the top of the prechamber as was the case in the baseline testing. This allows for stable ignition but happens to be the farthest point from the prechamber throat. The result is that unburned prechamber fuel can be forced into the main combustion chamber before it is oxidized.

The prechamber design of Test 2 was identical to the baseline prechamber except that the spark plug was relocated near the prechamber throat. This strategy was successful at reducing HC under light loads by up to 16 percent. Relocating the spark plug near the prechamber throat reduced HC through two controlling mechanisms: reduction of unburned fuel and improved scavenging near the spark plug.

Conventional prechambers force significant fractions of raw prechamber gas into the main combustion chamber as a result of increased pressure ahead of the advancing flame front [4, 14]. The result is less fuel energy in the prechamber to generate the desired high-energy ignition source for the main chamber. Initiating combustion near the prechamber orifice results in a flame front that travels back into the prechamber—exactly the opposite direction that the baseline prechamber promoted. Unburned fuel is trapped in the high-temperature and high-pressure, prechamber end gas where it is more completely burned. This is indicated by increased prechamber cylinder pressures (Fig. 6). Ultimately, this increase in peak prechamber pressure and rate of pressure rise helps light-load operation where HC are worst [4].

The second factor contributing to the observed results in Test 2 is improved, preferential scavenging [3, 14]. Locating the spark plug at the top of the prechamber makes it vulnerable to stagnant, burned gases that are difficult to purge during the exhaust event. Lean limit extensions have been reported with throat-mounted plugs that benefit from improved scavenging in the vicinity of the spark plug. This reduces cycle-to-cycle combustion variability by promoting ignition of a fresh air/fuel mixture.

Although prechamber fueling strategy is an operating variable rather than a design variable, its effect was so pronounced

that it warrants mention. Test 2 prechamber fueling effects on HC, NO_x, and thermal efficiency are shown in Fig. 7. These results are typical for light-load operation and demonstrate how prechamber fueling rate must be optimized and tightly controlled. Part (*a*) shows that approximately 9 to 13 percent of the total fuel charge, by mass, should be admitted to the prechamber for optimal control of exhaust HC. Significantly reduced prechamber fueling rates, such as the 3 percent curve, resulted in too little prechamber energy and erratic engine operation even at advanced ignition timings; hence, the erratic HC and thermal efficiency curves in Fig. 7.

Test 3 Prechamber. Brake specific HC and cyclic variability increased with the prechamber design of Test 3. Doubling the prechamber orifice diameter (with respect to Test 2) reduced the prechamber peak pressure by an average 50 percent (Fig. 6) and the main chamber peak pressure by 30 percent under light-load conditions. The effect was most pronounced by the lack of a characteristic prechamber pressure spike. This is the same result found by previous investigators [8, 10]. Increased HC production is the result of reduced in-cylinder turbulence and correspondingly slower burn rates.

These results strongly suggest that turbulence intensity in the main chamber, generated by the kinetic energy of the prechamber jet, can be adjusted by the orifice diameter. A small orifice such as used in Test 2 produces higher in-flow velocities to the main chamber due to the greater pressure differential between prechamber and main chamber. Higher in-flow velocities lead to faster burns caused by greater in-cylinder turbulence. Previous testing with different throat diameters has shown that smaller diameter orifices also provide greater main chamber torch penetration [8, 11].

Results also support earlier suggestions that raw prechamber fuel may be forced into the main chamber ahead of the advancing flame front. Recognizing that the prechamber in Test 3 was fueled almost identically to the prechamber in Test 2, the lower cylinder pressure in Test 3 must be the direct result of liberating less fuel energy. This was probably due to raw fuel escaping into the main chamber and out the exhaust before it could be more fully oxidized. This scenario effectively lowers the prechamber's energy-producing ability.

If smaller diameter orifices provide greater torch penetration and higher main chamber turbulence, which result in reduced HC, then how small is too small for a prechamber orifice? The factor limiting reductions in prechamber orifice diameter is quenching distance of the exiting jet. A flame propagating between two walls (i.e., an orifice) can be extinguished due to high heat transfer if the walls are too close; therefore, it is necessary to identify and relate the effects of pressure, stoichiometry, temperature, and other variables in prechamber design. An excellent, quantitative measure of quenching distance was devised by Adams and used in this study to ensure that orifice diameters were not less than calculated quenching distances [11]. In practice, orifice erosion may also present a practical limit.

Test 4 Prechamber. Prechamber design effects in Test 4 produced higher HC emissions than the baseline prechamber at light load. An extended tip spark plug was installed to initiate combustion in the bulk of the prechamber gas, similar to a centrally located spark plug, which reduces combustion duration by allowing the flame kernel to develop radially in all directions rather than unidirectionally within the prechamber.

Cylinder pressure traces showing frequent misfires and high cyclic variability indicated that flame initiation was not readily achieved with this configuration causing excessive HC emissions, possibly due to inhomogeneities within the prechamber. It has been shown [9] that significantly fuel-deficient regions exist along the centerline of the prechamber in a natural gas engine. An example of this is shown in Fig. 8 where air–fuel ratios as lean as 23:1 are observed along the centerline of the prechamber. This problem is further aggravated by high prechamber flow velocities induced through high engine speeds and/or small orifice diameters.

Staged Prechamber Analysis. Unique staged prechambers were evaluated in Tests 6, 8, and 9 and showed promise in their ability to reduce HC emissions. Test 6 and Test 9 prechambers reduced HC by approximately 30 percent and 14 percent, respectively, when compared to the baseline configuration. Test 8 maintained the same HC output as the baseline chamber. Differences in NO_x emissions are discussed in the next section.

Although staged prechambers differed in secondary and primary orifice diameters, they shared an important characteristic—very fast prechamber burn rates. This is most evident by noticing that the staged prechambers are the only chambers run at spark timings *retarded* of TDC (Fig. 5). Furthermore, the staged prechambers of Tests 6, 8, and 9 reached MBT 3, 4, and 7 deg sooner than the baseline configuration, respectively.

FID traces (Fig. 9*a*) support the fast prechamber burn hypothesis. Physically, these traces represent the time between prechamber ignition and arrival of the flame front at the prechamber throat. During this time, flame initiation and propagation occur; therefore, these curves provide a time measure of the sum of these two mechanisms.

However, there is another variable that must be accounted for when analyzing these curves. Relative locations of ignition site and FID were not necessarily the same. For instance, the baseline chamber used a top-mounted spark plug for ignition and the throat-mounted plug as the FID. The inverse was true in Test 2, although the distance between the two was equivalent. The staged prechambers always used the upper stage's spark plug for ignition and the throat plug in the lower stage as the FID. The distance separating these instruments was approximately twice the distance within the conventional type prechambers. To normalize these curves, the distance between the ignition source and FID was divided by the observed prechamber burn duration in Fig. 9(*a*). Results (Fig. 9*b*) represent psuedo-averaged flame speeds for each of the prechambers. The fastest burning prechambers are represented by curves from Tests 9, 6, and 8, respectively.

The staged prechamber's ability to burn faster and reduce HC, relative to conventional designs, is further supported by comparing prechamber and main chamber pressure traces. Peak pressure in the upper prechamber stage of Test 6 was almost 950 psi while the peak pressure of the prechamber in Test 2 was only 780 psi under similar conditions. This represented an increase of 22 percent. This extra "potential energy" translates into a more energetic ignition system for the lower stage and, ultimately, the main chamber.

Staged prechamber pressure traces in Fig. 10 reveal that secondary and primary orifice diameters significantly affect prechamber and main chamber combustion. Test 8 featured a small-diameter (3.2 mm) secondary orifice and large-diameter (9.4 mm) primary orifice. The large-diameter primary allowed some combustion of the main chamber mixture before peak pressure was reached in the prechamber. Results are similar for Test 6 except that main chamber combustion occurred more abruptly. This is evident from the higher rate of pressure rise. In both cases, ignition of the main chamber charge is due to large diameter secondary or primary orifices allowing the upper stage jet to penetrate prematurely into the main chamber. Two small-diameter orifices, such as in Test 9, inhibit early penetration of the jet into the main chamber, allowing the burning prechamber mixture to liberate the fuel's chemical energy more completely and supply a stronger ignition source to the main chamber. High-energy ignition of the main chamber mixture is evident from the abrupt and highly agitated main chamber

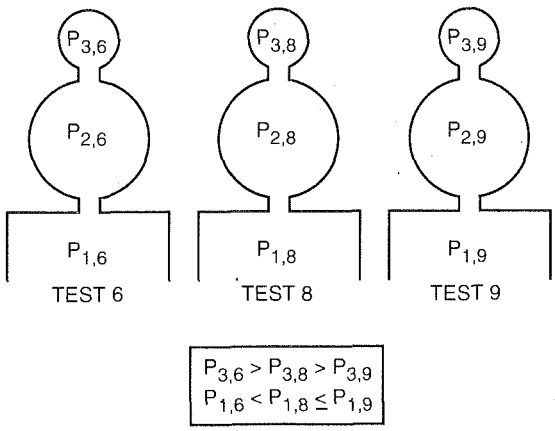

Fig. 11 Staged prechamber and main chamber pressure (and temperature) behavior during prechamber and main chamber ignition, respectively

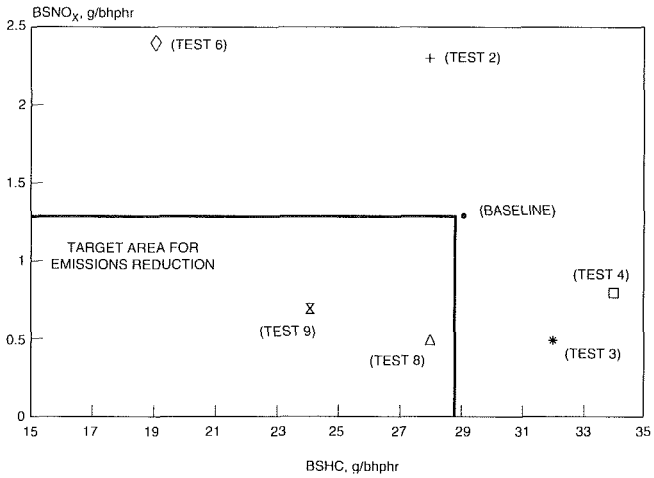

Fig. 12 Average NO_x-HC trade-offs for "minimum" HC fueling rate in prechamber (1000 rpm, WOT, 50 psi bmep)

pressure trace in Fig. 10(*c*). These main chamber pressure fluctuations represent flow reversals between the lower stage and main chamber. Flow reversals were evident in all prechamber tests, but to lesser extents.

Conditions for stable ignition are different between staged prechambers as well. Labels in Fig. 10 show typical staged prechamber "motoring" pressures (pressure prior to ignition). Prechamber and main chamber pressures in Test 6 were almost identical at the time of prechamber ignition. Conversely, main chamber pressures in Tests 8 and 9 were much higher than their respective upper stage pressures. Results show that prechamber pressures and temperatures at the time of prechamber ignition are highest for Test 6, Test 8, and Test 9, respectively. High prechamber pressures (and temperatures) increase flammability limits and make spark ignition easier in the upper stage. The schematic in Fig. 11 demonstrates that main chamber pressures are highest for Tests 8 and 9 (they are nearly equal) and lowest for Test 6 at the time of main chamber ignition. Again, flammability limits have been widened by these high-pressure conditions which require lower ignition energies (i.e., temperatures) in the main chamber. The advantage in this scenario lies with prechambers from Tests 8 and 9. The air/fuel mixture in the upper prechamber stage is easily ignited without the air of increased pressure. However, the main chamber mixture is relatively fuel lean and therefore, benefits greatly from the increased pressures that require lower ignition temperatures for flame initiation. Pressure differentials with the small secondary orifices are even greater at more advanced spark timings. Higher main chamber pressures at the time of main chamber ignition could have reduced ignition delay and may explain the higher main chamber pressures in Test 8 (relative to Test 6) for almost equivalent prechamber jet strength (as judged by peak prechamber pressures).

Oxides of Nitrogen Emissions. The previous discussion on HC would not be complete without an explanation of the effects on NO_x emissions. NO_x emissions at the light-load test condition were shown earlier in Fig. 5. An obvious trend is the dependence of NO_x on ignition timing. Retarded ignition timings drastically cut NO_x emissions in almost every case through the reduction of combustion pressures and temperatures.

Typical NO_x-HC trade-offs are apparent for prechambers tested in Tests 2, 3, 4, and 6: NO_x were reduced at the expense of HC for equivalent ignition timings. An example of the NO_x-HC trade-off under light-load operation is shown in Fig. 12, where NO_x emissions are plotted against minimum observed HC emissions for a given configuration. Although Test 6 produced the minimum HC, Tests 8 and 9 did the best job of minimizing both NO_x and HC.

The promise of the staged prechamber approach surfaces when reviewing these HC-NO_x points. Test 8 and 9 prechambers not only reduced or maintained HC emissions relative to the baseline prechamber, but also reduced NO_x by approximately 70 percent and 50 percent, respectively, relative to the baseline prechamber. This may be due to several mechanisms.

Previous research has proposed that the bulk of NO_x emissions are generated primarily in the prechamber and not in the main chamber. Earlier discussion showed that the prechambers generated high pressures and rates of pressure rise, especially when compared to the main chamber. This subjected the relatively small volume of prechamber gases to high temperatures. NO_x generation is governed by the Zeldovich mechanism [15] and is primarily a function of temperature. Thus, the relatively rich prechamber is capable of producing very high pressures and temperatures resulting in the significant production of NO_x emissions. This supports the conclusion that a small prechamber volume is better than a large prechamber volume. Smaller prechambers lower prechamber-derived NO_x and also minimize thermal losses (by reducing surface-to-volume ratio).

Prechamber fueling rates were just as effective in controlling NO_x production as they were in controlling exhaust HC. Low prechamber fueling rates approaching 3 percent of the total gaseous charge in Test 2 (ref. Fig. 7) minimized NO_x emissions due to partial burns that ultimately lowered prechamber and in-cylinder temperatures.

These curves support the theory that NO_x are prechamber-derived. Reduced prechamber fueling meant enriched main chamber mixtures to maintain the same load. Therefore, the overall air/fuel ratio was held relatively constant (approximately 29:1) while NO_x were observed to drop. Prechamber-derived NO_x drop with fuel-lean prechamber mixtures and dominate overall engine-out NO_x production. Similar tendencies were found for the staged prechamber in Test 6. Test 8 and 9 results, which featured small-diameter (3.2 mm) secondary orifices, contradicted these results. In fact, progressively lower levels of prechamber fueling coupled with higher main chamber fueling rates resulted in progressively higher NO_x under all load conditions.

These latter results suggest that NO_x are not solely prechamber-derived when the secondary orifice is of very small diameter. The small mass of upper stage charge simply is not capable of producing significant amounts of NO_x despite producing very high pressures and temperatures. Rather, it appears that a significant fraction of the engine-out NO_x are created in the lower stage or the main chamber. Analysis of cylinder pressure data suggests that the main combustion chamber is

capable of producing significant NO_x when operating with these staged prechambers. The peak prechamber pressure for Test 2 (0 deg BTDC) is only 100 psi higher than the main chamber pressure (0 deg BTDC) for Test 9. If prechamber-derived NO_x are significant for the Test 2 prechamber due to high operating pressure/temperature, then it can be inferred that the main combustion chamber in Tests 8 and 9 is capable of producing similarly significant NO_x results. Furthermore, prechamber fueling rate comparisons found that the small secondary orifice chamber tolerated less upper stage fuel than the large secondary orifice of Test 6. To maintain stoichiometry, main chamber fuel was added, which further aggravated main chamber-derived NO_x. The role of the lower stage in these processes remains largely undefined.

Conclusions

1 Prechamber combustion systems can extend the lean operating limit in natural gas engines. This was shown by operating several natural gas prechambers at an average equivalence ratio of 0.55 where a comparable, open chamber design exhibited frequency misfires and unstable torque.

2 Relocating the spark plug to the throat of a conventional prechamber reduced light-load HC emissions by 16 percent but increased NO_x emissions by 25 percent.

3 Staged prechambers, incorporating upper and lower stages separated by an orifice, where shown simultaneously to reduce engine-out HC and NO_x emissions up to 14 percent and 47 percent, respectively.

4 Prechamber fueling strategies in conventional or staged prechambers must be optimized and tightly controlled to attain desired emissions and efficiencies under varying speeds and loads.

5 Prechamber orifice diameter should be sized to optimize torch penetration, jet strength, main chamber turbulence, and durability.

6 Stage prechamber designs require more development to confirm the results presented here and to exploit their proposed advantages.

Acknowledgments

The author would like to thank W. Liss and A. Wells of the Gas Research Institute for their support of this work and their technical direction; R. Netting (SwRI) whose meticulous technical work made possible the quality results presented in this report; and, A. Brenholtz of Stitt Spark Plugs for supplying the specially designed spark plugs used for throat ignition.

References

1 Kanury, A. M., *Introduction to Combustion Phenomena*, Combustion Science and Technology—Vol. 2, Gordon and Breach, Science Publishers, Inc., 1975.

2 "Caterpillar 1Y540 Engine 1-J Test Procedure," Apr. 1985.

3 Noguchi, M., Sanda, S., and Nakamura, N., "Development of Toyota Lean Burn Engine," SAE Paper No. 760757.

4 Varde, K. S., and Lubin, M. J., "Combustion of a Stratified Charge in a Chamber," *The Journal of Automotive Engineering*, IMechE, 1974, pp. 7–10.

5 Beaty, K. D., "Natural Gas Low Emission Engines for Buses; A Scandinavian Project," 2nd International IANGV Conference—Vol. II, Buenos Aires, Argentina, Oct. 1990, Paper No. 27.

6 Storrar, A. M., "A Combustion Chamber to Combine High Efficiency, Low Emissions and Wide Fuel Tolerance," *Automotive Engineer*, June/July 1983, pp. 13–15.

7 Wood, C. D., Personal Communications, 12/10/90.

8 Snyder, W. E., Wright, M. R., and Dexter, S. G., "A Natural Gas Engine Combustion Rig With High-Speed Photography," ASME JOURNAL OF ENGINEERING FOR GAS TURBINES AND POWER, Vol. 110, pp. 334–342.

9 Charlton, S. J., Jager, D. J., Wilson, M., and Shooshtarian, A., "Computer Modelling and Experimental Investigation of a Lean Burn Natural Gas Engine," SAE Paper No. 900228.

10 GRI Final Report, "Development of Advanced Combustion Technology for Medium and High Speed Natural Gas Engines," Section I, Copy No. 3 of 10, Feb. 1989.

11 Adams, T. G., "Theory and Evaluation of Auxiliary Combustion (Torch) Chambers," SAE Paper No. 780631.

12 Adams, T. G., "Torch Ignition for Combustion Control of Lean Mixtures," SAE Paper No. 790440.

13 Melton, R. B., Jr., "Minefield Clearance Using Focused Repetitive Shock Waves (U)," SwRI Final Report No. AR-958, Sept. 1974.

14 Shahed, S. M., Personal Communication, 1/19/91.

15 Glassman, I., *Combustion*, Academic Press, Inc., New York, 1977.

R. C. Meyer

D. P. Meyers

S. R. King

Engine, Fuel, and Vehicle Research Division,
Southwest Research Institute,
San Antonio, TX 78228

W. E. Liss

Gas Research Institute,
Chicago, IL 60631

Effects of Spark Plug Number and Location in Natural Gas Engines

Combustion experiments were conducted on a spark-ignited single-cylinder engine operating on natural gas. A special open chamber cylinder head was designed to accept as many as four spark plugs. Data were obtained to investigate the effects of spark plug quantity and location on NO_x, HC, CO emissions, brake and indicated thermal efficiency, MBT timing, combustion duration, ignition delay, peak cylinder pressure, peak cylinder temperature, and heat release over a wide range of equivalence ratios.

Introduction

Natural gas-fueled engines are widely employed in stationary applications and are gaining acceptance in mobile applications because of emissions reduction potential and alternative energy source concerns. A variety of combustion techniques for achieving low emissions and acceptable performance characteristics can be applied to natural gas engines. Some of the techniques include: stoichiometric burn with three-way catalyst exhaust aftertreatment; lean-burn prechamber; and lean-burn open-chamber with and without oxidation catalyst. This paper seeks to investigate combustion characteristics suitable for a variety of combustion technologies associated with natural gas.

It has long been understood that NO_x production is a function of time, temperature, as well as oxygen and nitrogen concentration [1]. Also well documented are the effects of combustion characteristics [2]. However, although demonstrated on gasoline-fueled engines [3–5], it has not been shown how natural gas combustion, emissions, and performance are interrelated by these parameters in terms of ignition source location.

The work conducted in this program looks at the effects of varying spark plug quantity and location on the aforementioned parameters in a natural gas-fueled engine. This program was sponsored by Gas Research Institute (GRI) and conducted at Southwest Research Institute (SwRI).

Technical Approach

In order to achieve the desired objective of the project, a single-cylinder engine was chosen as the test engine. A single-cylinder engine was desired in order to alleviate cylinder-to-cylinder combustion variations and coincident data anomalies.

The engine used in these tests had a bore of 3.8125 in. and a stroke of 3.750 in. Other pertinent engine specifications are shown in Table 1 [6].

The primary objective of this project was to determine the effects of the number of spark plugs and their location on emissions and performance of a natural gas engine. A cylinder head was designed with multiple spark plug locations (see Fig. 1). The head has a flat fire deck, which was used with a flat-top piston, giving a disk-shaped combustion chamber.

Table 1 Engine specifications

Engine	LABECCO
No. Cylinders	1
Bore	3.8125 in.
Stroke	3.750 in.
Compression Ratio	10.5:1
Engine Speed	1800 RPM

A single centrally located plug (configuration A) is typical of many diesel engine conversions where the fuel injector is directly replaced with a spark plug. Multiple ignition sources and faster burn rates were anticipated by using all four plugs (configuration B) while slowest burn rates were expected by using a single plug located as far from the center as possible (configuration C). A legend as to plug location in reference to the cylinder head is shown in Fig. 2.

Equivalence ratio sweeps from 1.00 to 0.65 were performed for each of the three plug configurations at 1800 rpm. For each point in the equivalence ratio sweep, MBT (minimum best torque) spark timing was determined and data were taken.

The reader should bear in mind that brake-specific emissions and efficiency data contained in this report at lean equivalence ratios are not representative of values obtainable with optimized, turbocharged lean-burn natural gas engines due to low brake power.

Experimental Setup

Monitored variables included fuel, coolant, and lubricant temperatures, pressures at several points, intake air temper-

Contributed by the Internal Combustion Engine Division and presented at the 13th Annual Fall Technical Conference, Muskegon, Michigan, September 30–October 2, 1991. Manuscript received by the Internal Combustion Engine Division September 25, 1991. Associate Technical Editor: J. A. Caton.

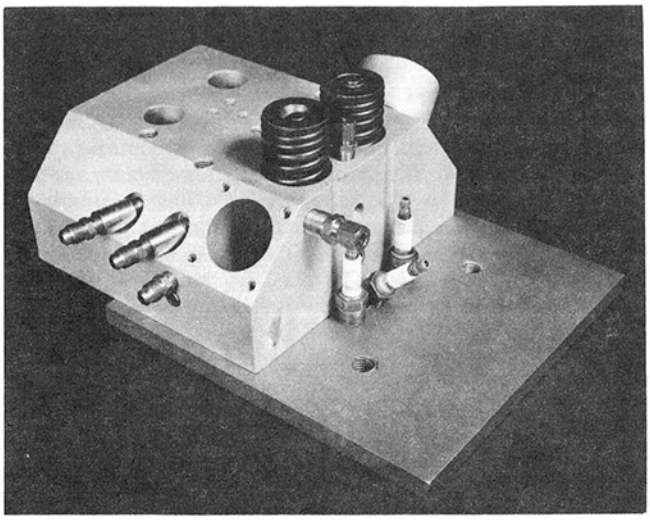

Fig. 1 Cylinder head

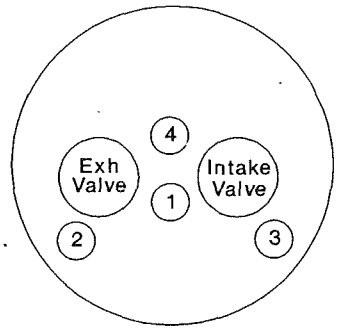

CONFIGURATION	PLUG QTY	PLUG LOCATION
'A'	1	1
'B'	4	1, 2, 3, 4
'C'	1	2

Fig. 2 Spark plug location legend

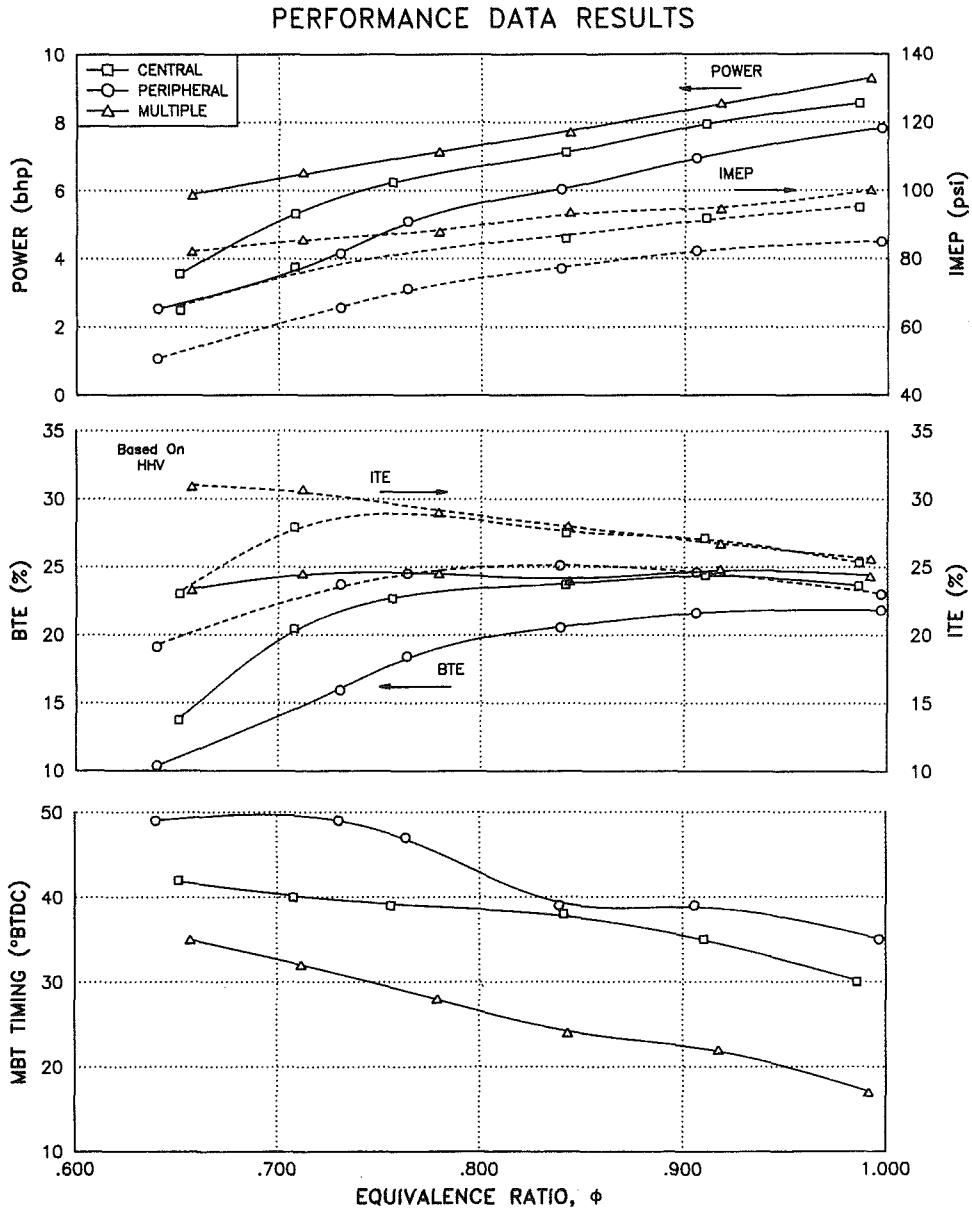

Fig. 3 Performance results

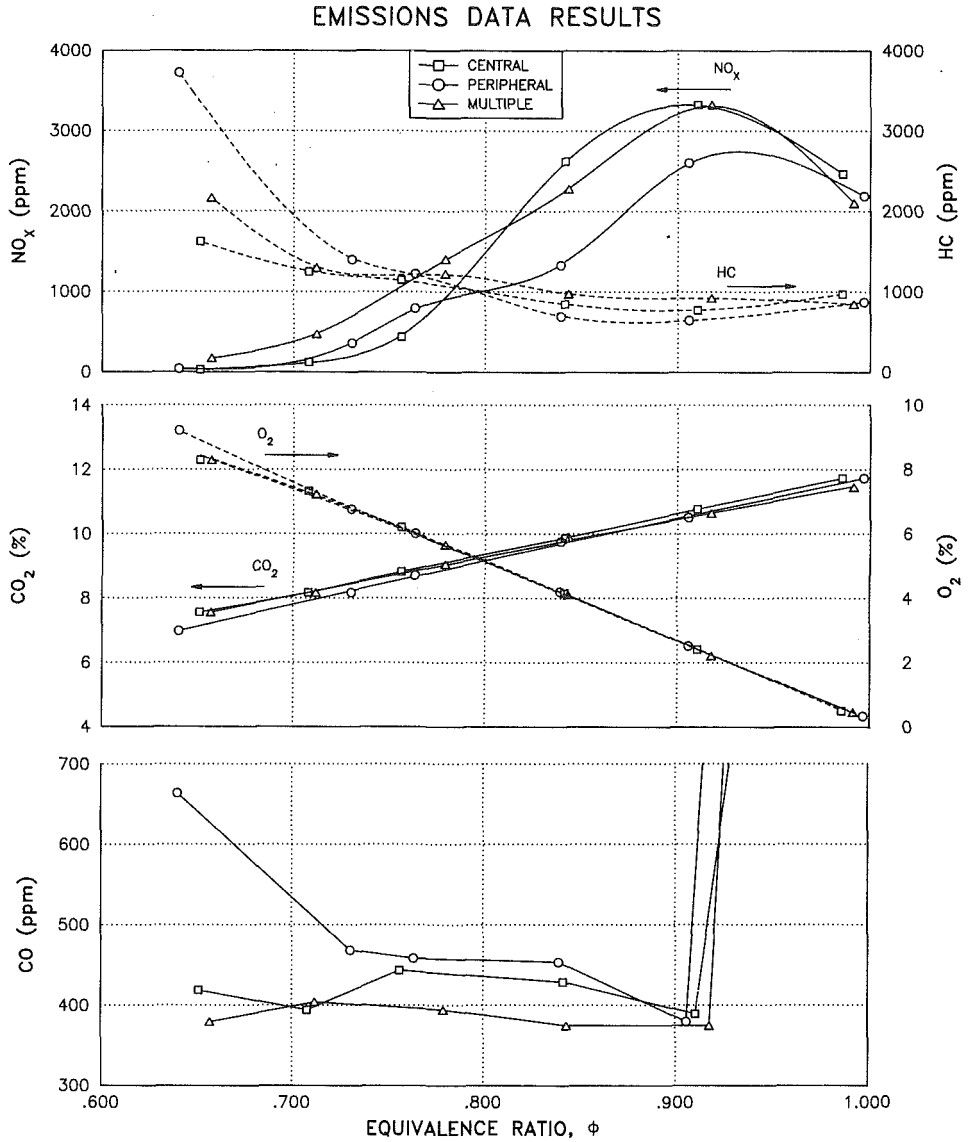

Fig. 4 Emissions results

ature, and exhaust temperature at the exhaust port. The computer data collection and analysis system was programmed to calculate brake horsepower (BHP), brake and indicated thermal efficiency, IMEP, in-cylinder gas temperature, ignition delay, combustion duration, heat release, and standard deviation of peak cylinder pressure.

The fuel mass flow rate, engine rpm, fluid and component temperatures and pressures were recorded by a Hewlett-Packard 3497 low-speed data acquisition system, which is tied to an HP 1000 Series E minicomputer. Each of the engine parameters was recorded by the HP 3497 once every 15 seconds. Ten of these samples were averaged for each of the test runs.

High-speed data were obtained for each test point using a cylinder pressure transducer (Kistler model 6121) and a shaft encoder. These data were based on a hundred cycle average for each half degree of crank angle. All indicated data were obtained by use of this high-speed data acquisition system. IMEP, heat release, gas temperature, and combustion duration were determined using Heywood's "Fully Mixed Model" [7].

The natural gas fuel combustion changed with time in SwRI's laboratory to the extent that corrections to equivalence ratio, Btu content, and fuel flow rate were made on all data using gas composition measured by an on-line gas chromatograph. It was observed that the methane concentration varied from 92 percent to 96 percent (mole fraction).

Results

Performance Results. Figure 3 shows the performance results of the three different spark plug configurations tested. It can be seen that for maximum brake horsepower and IMEP, the multiple B plug configuration is better than the centrally located A configuration, which in turn is better than the peripheral C configuration.

Analysis of the ITE and BTE shows that while the centrally located A plug configuration and the multiple B plug configuration are considerably better that the peripheral C configuration, the multiple B configuration is actually no better than the centrally located A plug configuration rich of 0.75 equivalence ratio. Below 0.75 equivalence ratio the multiple plug configuration B is able to extend the lean misfire limit, presumably due to the multiple ignition sources, which yield a higher probability of initiating combustion.

It should be noted that all thermal efficiencies depicted in Fig. 3 are based on the higher heating value of the fuel. This was done in accordance with the natural gas utility industry standard of basing everything on higher heating value.

Emission Results. Figure 4 shows the emissions results taken for the three configurations tested. Examination of Fig. 4 reveals that NO_x production for the centrally located A and

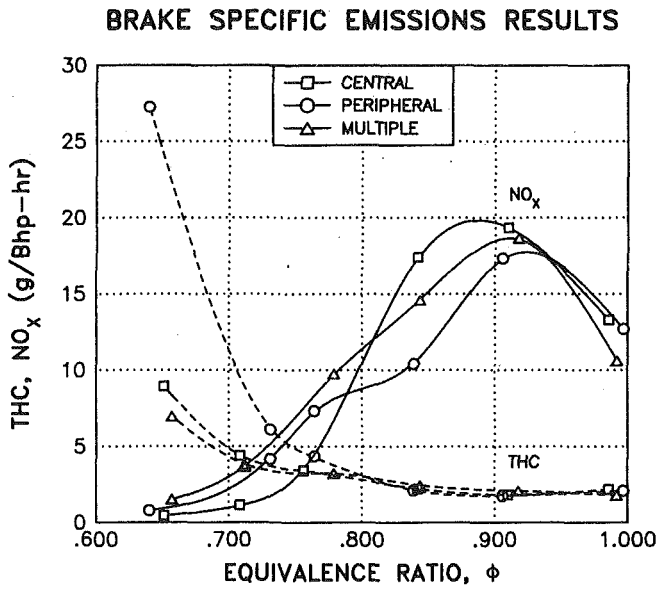

Fig. 5 Brake specific emissions results

multiple B configurations is very similar. The combustion duration and peak cylinder temperatures discussed in the next figure are also very similar for the centrally located A and multiple B configurations. NO_x production for the peripheral C configuration is significantly lower and can be attributed to the fact that, while the combustion duration is longer, the peak cylinder temperature is not as high. This lower NO_x result illustrates the pronounced sensitivity of NO_x production to temperature rather than time since this "slow-burn" peripheral C configuration exhibits much longer burning duration.

Examination of hydrocarbon emissions reveals an interesting condition. The different plug configurations yield almost inverse results whether rich or lean of approximately 0.80 equivalence ratio. Above 0.80 equivalence ratio, the peripheral C configuration produces the least hydrocarbons, while below 0.80 equivalence ratio this configuration produces the most hydrocarbon emissions. The cause of this phenomenon is again associated with the combustion duration. This may be thought of in the following way: There is a certain quantity of fuel-air mixture trapped in the crevice volume above the top ring land but below the piston crown surface. The quicker burn times associated with the multiple plugs result in the main chamber combustion being completed early while there is still

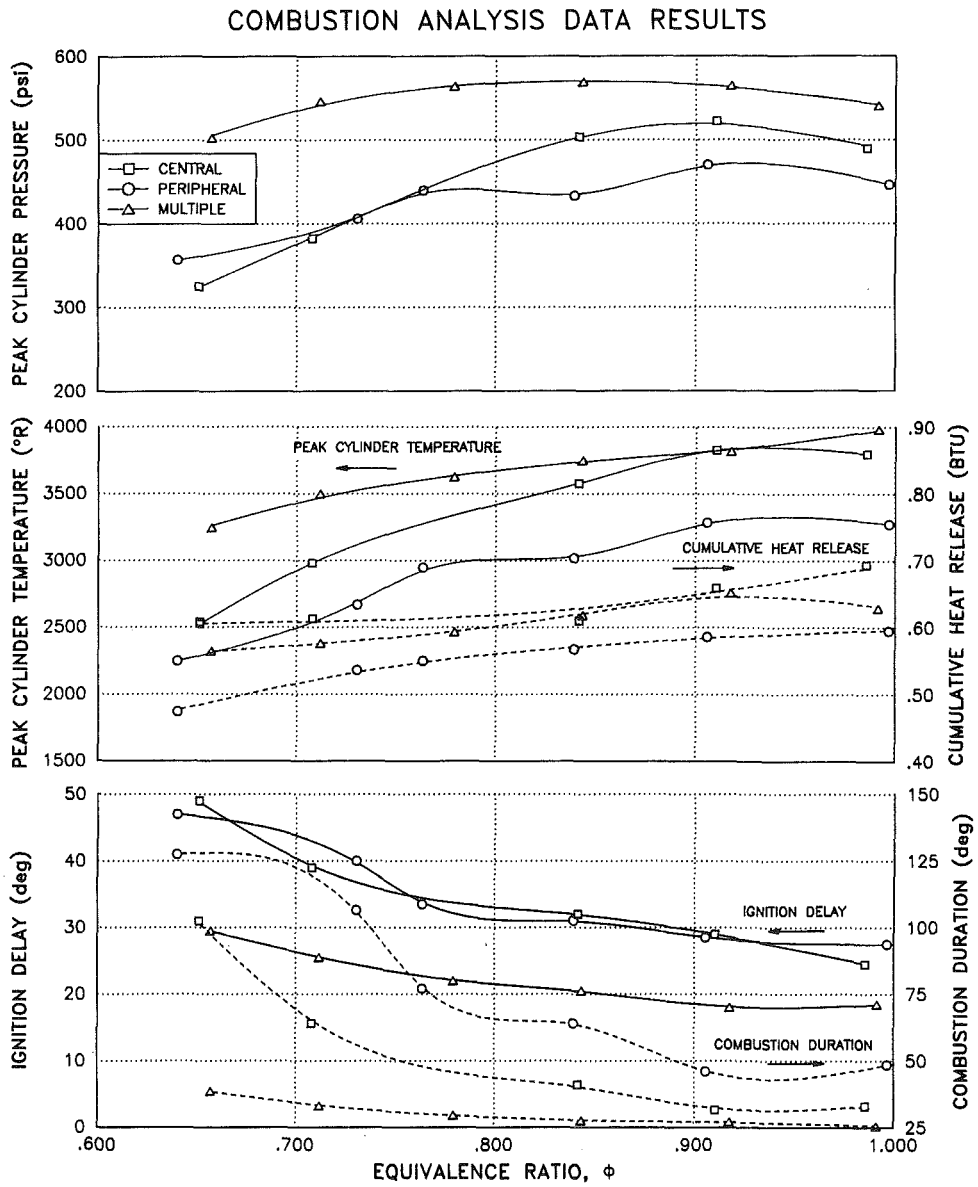

Fig. 6 Combustion analysis results

a considerable mass of fuel-air mixture caught in the crevice volume. Conversely, the peripheral C configuration with its longer burn time allows more time for the crevice mixture to escape, thus enabling it to be burned with the main charge. Below 0.80 equivalence ratio this slow-burning mechanism detrimentally effects hydrocarbon emissions. For this case the duration of burn at the peripheral C plug configuration is sufficiently long that the end of combustion is not complete prior to the exhaust valve opening and flame quenching. However, the centrally located A and multiple B plug configurations with their relatively fast burn rates are able to complete combustion before the exhaust valve is opened.

The CO_2 and O_2 trends verify the accuracy of the equivalence ratio determination. The fact that the data points fall consistently on top of one another and in a straight line indicates that the changes in fuel composition have been dealt with accurately.

As for CO emissions, we wee that the peripheral C plug configuration exhibits the highest CO. This is a result of the relatively poor combustion characteristics of this configuration. Again we see that the centrally located A configuration exhibits characteristics very similar to that of the multiple B plug configuration.

All emissions data shown in Fig. 4 are shown on a volume fraction basis. On a brake specific basis (Fig. 5), the centrally located A plug configuration shows the most benefits in the extremely lean region for NO_x production. The multiple plug configuration shows the highest specific NO_x production and can be attributed to peak cylinder temperature as is explained in the next section. As expected, the multiple plug configuration has the lowest specific HC production, which is, as stated earlier, due to its lower incidence of misfire.

Combustion Analysis Results. Figure 6 is a summary of the results of the combustion analysis. The peak cylinder pressures for the multiple B plug configuration are consistently higher than either the centrally located A or peripheral C configurations. This is due to the faster burn rate associated with the multiple plug configuration, which has the peak pressure occurring closer to top-dead-center and therefore high peak cylinder temperatures. Since at the leaner equivalence ratios the multiple plug configuration is still firing more consistently and closer to TDC, the average peak cylinder pressure is higher.

Analysis of peak mass-averaged cylinder temperatures shows that the multiple plug configuration produces higher temperatures than the other configurations. This was caused by the relatively short combustion durations near TDC. Conversely, the centrally located A and peripheral C configurations have considerably lower temperatures due to longer combustion durations occurring well after TDC.

Analysis of the cumulative heat release results reveals that the multiple B plug configuration actually released slightly less heat than the centrally located A configuration. This is believed to be due to the fact that, although almost identical amounts of total heat were released, the higher peak in-cylinder gas temperatures and the earlier occurrence of combustion for the multiple plug configuration allowed more heat to be transferred through the combustion surfaces; therefore, the apparent heat release was lower. The relatively low heat release associated with the peripheral C plug location is due to the relatively slow combustion and lower gas temperatures of that configuration.

The remaining graphs of Fig. 6 depict ignition delay (0–10 percent cumulative heat release) and combustion duration (10–90 percent cumulative heat release) for the three configurations. Interestingly, at equivalence ratios greater than 0.75 the centrally located A plug configuration burns as fast as the multiple B plug configuration. Yet, in terms of ignition delay, the centrally located A configuration is comparable to the peripheral C configuration. The peripheral C configuration produces significantly longer combustion durations when compared to the other two configurations. This is believed to be the main cause of the performance and emissions effects presented above.

Conclusion

In conclusion we see that the multiple plug configuration B has the largest advantage in performance, in that it produces greater horsepower and higher thermal efficiencies for all equivalence ratios. It also has lower HC production at the leaner equivalence ratios due to its reduced misfire rate. However, its "ultrafast" burn rates result in higher NO_x production than the other configurations at equally lean equivalence ratios. The peripheral C plug location exhibited both poor performance and high emissions production over most of the range except between 0.80 and 1.0 equivalence ratio where it actually produced slightly lower NO_x and hydrocarbon emissions. The centrally located A plug configuration offers the best compromise in that it has adequate performance and low emissions production when compared to the other configurations.

Finally, if the different plug configurations are associated with different combustion rates it is evident that there is an optimal burn rate for each equivalence ratio. This optimal burn rate must be slow enough to minimize NO_x production and yet fast enough to produce adequate performance characteristics. It appears fortunate for those converting existing diesel engines to natural gas that the single centrally located spark plug produces burn rates near this optimum.

Acknowledgments

The authors of this paper would like to thank the following people whose efforts have made this paper possible: Allen Wells (GRI); Chip Wood (SwRI); Shannon Vinyard (SwRI); Steven King (SwRI); John Hedrick (SwRI); Elvan Sekula (SwRI); Dennis Kneifel (SwRI); David Dowell (SwRI); and Janie Gonzalez (SwRI).

References

1 Lavoie, G., and Heywood, J., "Experimental and Theoretical Study of Nitric Oxide Formation in Internal Combustion Engines," *Combustion Science and Technology*, Vol. 1, 1970, pp. 313–326.

2 Fleming, R., and O'Neal, G., "Potential for Improving the Efficiency of a Spark Ignition Engine for Natural Gas Fuel," SAE Paper No. 852073, 1985.

3 Thring, R., "The Effects of Varying Combustion Rate in Spark-Ignited Engines," SAE Paper No. 790387, 1979.

4 Johnson, J. H., "Effect of Swirl on Flame Propagation in a Spark-Ignition Engine," SAE Paper No. 565C, 1962.

5 Sakai, Y., and Miyazaki, H., "Effect of Combustion Chamber Shape of Nitrogen Oxides," JSAE Paper No. 6 1974, 1973.

6 Ainsley, W., and Cleveland, A., "CLR Oil Test Engine," presented at SAE Fuels and Lubricants Meeting, Paper No. 641, 1955.

7 Heywood, J., *Internal Combustion Engine Fundamentals*, McGraw-Hill, New York, 1988.

Development of the Cooper-Bessemer CleanBurn™ Gas-Diesel (Dual-Fuel) Engine

D. T. Blizzard
Cooper-Bessemer Reciprocating Products Division,
Cooper Industries,
Grove City, PA 16127

F. S. Schaub

J. G. Smith

Cooper-Bessemer Reciprocating Products Division,
Cooper Industries,
Mount Vernon, OH 43050

NO_x emission legislation requirements for large-bore internal combustion engines have required engine manufacturers to continue to develop and improve techniques for exhaust emission reduction. This paper describes the development of the Cooper-Bessemer Clean Burn ™ gas-diesel (dual-fuel) engine that results in NO_x reductions of up to 92 percent as compared with an uncontrolled gas-diesel engine. Historically, the gas-diesel and diesel engine combustion systems have not responded to similar techniques of NO_x reduction that have been successful on straight spark-ignited natural gas burning engines. NO_x levels of a nominal 1.0 g/BHP-h, equal to the spark-ignited natural gas fueled engine, have been achieved for the gas-diesel and are described. In addition, the higher opacity exhaust plume characteristic of gas-diesel combustion is significantly reduced or eliminated. This achievement is considered to be a major breakthrough, and the concept can be applied to both new and retrofit applications.

Background

The following is a brief background regarding Cooper-Bessemer's history of exhaust emission control programs. The CleanBurn™ low-NO_x level natural gas burning engine was introduced in 1977 for integral engine compressor units serving the gas industry. This low-NO_x integral two-stroke gas engine uses a jet cell chamber operating on the fuel-rich side of stoichiometric. The main chamber operates with very fuel-lean combustion by virtue of high scavenging air supercharging level. The net result of the diverse combustion is to reduce the NO_x from a range of 15–20 g/BHP-h to 1–3 g/BHP-h. Over 165 integral gas engine compressors have been sold by Cooper-Bessemer since 1977. Because of this technology, virtually every engine of this type sold today is of the CleanBurn™ configuration.

The four-cycle gas–diesel (dual-fuel) engine is a popular driver for generators in municipal, sewage treatment, and base-load cogeneration power plants because of its durability and because of its ability to burn 94 percent natural gas as the most economical fuel, yet change over to full diesel should the gaseous fuel supply be interrupted for any reason. Operating in the dual-fuel mode, approximately 6 percent fuel oil is injected and compression ignited, which in turn ignites the remaining 94 percent gaseous mixture. By contrast to the straight gas engine, equivalent low-emissions technology for large slow-speed four-cycle dual-fuel engines had never been developed. Best Available Control Technology (BACT) levels were achieved by certain parametric adjustments including retarding injection timing of the approximately 6 percent pilot fuel oil. BACT NO_x levels were typically 5 g/BHP-h and gas–diesel opacity levels were within the mandated limit of 20 percent.

However, even though opacity levels met all requirements, the inherent yellowish colored exhaust plume exhibited during dual-fuel operation presented a psychological problem with customers and the general public feeling that anything visible is bad and not acceptable. Complaints received regarding these legal but visible emissions became one of the major driving forces behind our R&D Program.

This paper contains relevant detail regarding the type engine being marketed with the new combustion system, the development engine and facility, the extensive effort set forth to the gas–diesel engine in prior years using more conventional reduction techniques, and the significance to the dual-fuel CleanBurn™ program of having earlier applied to two-cycle spark-fired integral engine reduction system to the four-cycle power engine.

The LSB-6 Laboratory Engine

The operating data that follows, unless noted, was generated using a six-cylinder in-line 15-1/2 in. bore 22 in. stroke engine. The model series is LSB-6 and it is fitted with top end parts identical to the LSVB series. The LSVB series has enjoyed a comparatively high new engine production in the past several years, particularly in the cogeneration market; see Fig. 1.

The LSB-6 was installed in the Mount Vernon, OH, Research and Development Laboratory in mid-1988 and has been fitted for quick conversion to spark-gas, diesel, or gas–diesel modes. The laboratory setup provides precise recording of data by one-quarter crank degree encoding and series 900 Hewlett-Packard computer equipment provides display and hard copy

Contributed by the Internal Combustion Engine Division and presented at the 13th Annual Fall Technical Conference, Muskegon, Michigan, September 30–October 2, 1991. Manuscript received by the Internal Combustion Engine Division September 16, 1991. Associate Technical Editor: J. A. Caton.

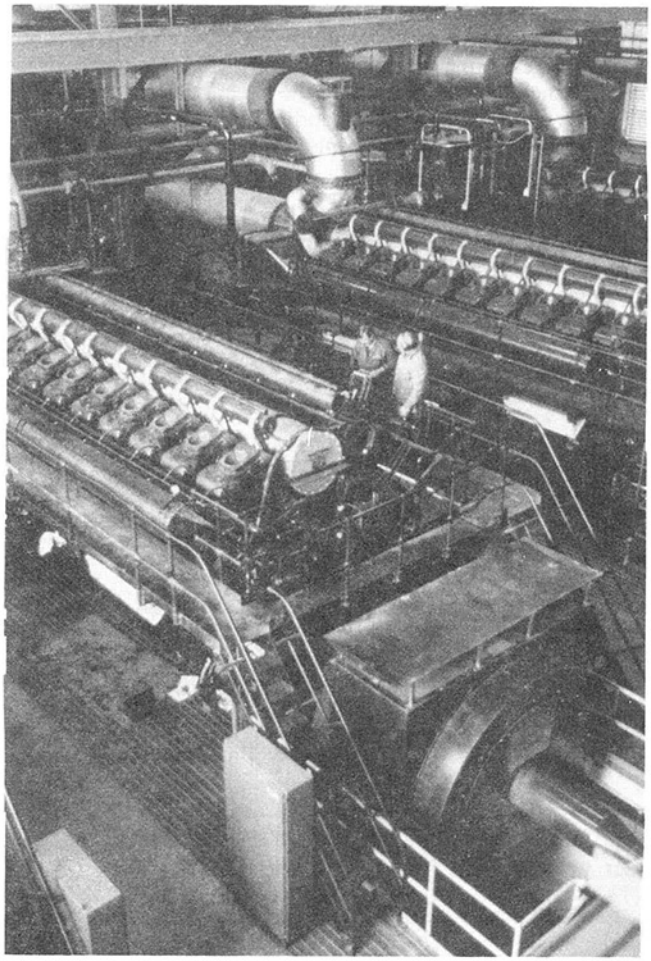

Fig. 1 Cogeneration installation of Cooper-Bessemer LSVB dual-fuel engines delivering 8386 BHP per engine

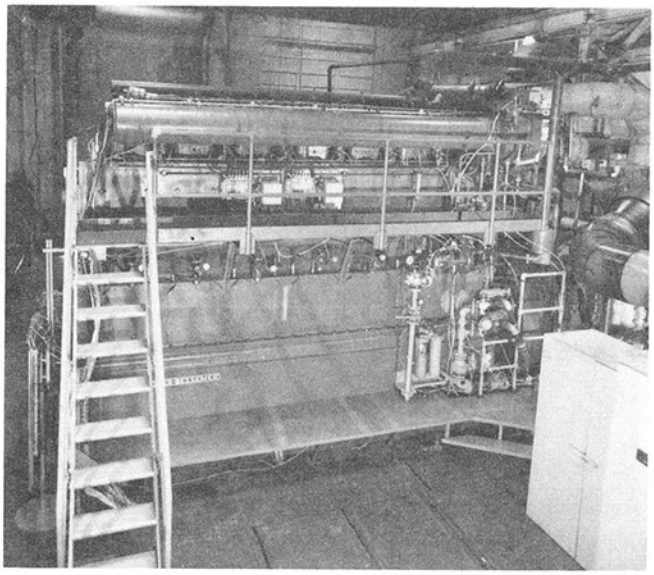

Fig. 2 Laboratory installation of LSB-6 power engine

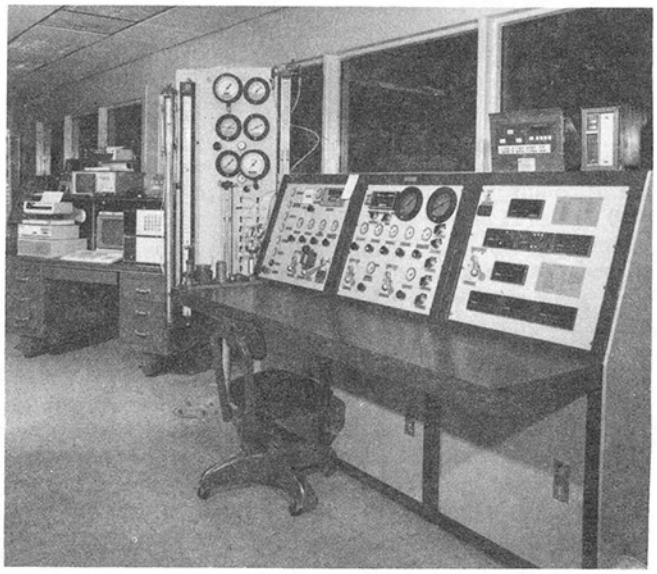

Fig. 3 Data acquisition and control room for laboratory LSB-6 power engine

pressure-time and rate-of-heat-release data for each test condition. Fuel selection is pipeline quality natural gas, propane, and methanol. Blending equipment is on-site for normal butane to study sensitivity [1], as well as a twenty-ton source of CO_2 to simulate digester gas. Figures 2 and 3 illustrate the laboratory installation of the LSB-6 and identify supporting systems. Figures 4 and 5 are sectional drawings showing general engine design of the LSVB and LSB.

The six vertical cylinders of the laboratory LSB-6 engine allow quick, cost-controlled changes to combustion components, and hydraulic shrink cams permit a timing change for one group of cams that can be accomplished in two hours.

Correlation of data between the Mount Vernon Laboratory six-cylinder unit and the production sixteen- and twenty-cylinder units has been excellent regarding turbocharger matching pressure and air mass flows, emission levels, and general performance. The slightly higher friction of the proportionally larger bottom end of the LSB-6 (LSVB-12 crankshaft) requires a 1.5 percent downward fuel correction to project the V angle production units. This correlation not only provides credible projection of new technology to production units, but also allows accurate and inexpensive handling of marketing quotes to address nonstandard ratings, fuels, and emission requirements.

Nomenclature

AMB = ambient temperature, °F
AMP = air manifold pressure, in. Hg absolute
BMEP = brake mean effective pressure, psi
BSFC = brake specific fuel consumption, Btu/BHP-h
BTC = before top center
CO = carbon monoxide, g/BHP-h
DEV = deviation, firing pressure, psi
FP = firing pressure, psig
HCt = total hydrocarbons, g/BHP-h
IGN = ignition timing, crank degrees before top center
kW = kilowatt
NO_x = oxides of nitrogen, g/BHP-h
NBN = normal butane number, a measure of fuel sensitivity
NOP = nozzle opening pressure
PC = port closure, fuel pump, in crank degrees before top center
PO = pilot oil
psig = pounds per square inch gage
PTT = preturbine temperature, °F
rpm = revolutions per minute
Y = yellow

Gas-Diesel Open Chamber Activity

Preliminary Work. Extensive effort was pursued with gas-diesel open chamber emission control techniques, which have been of interest in prior years since the birth of the Clean Air Act. Reference [2] includes data recorded twenty years ago using readily available NO_x reduction methods including ignition timing retard, reduced air manifold temperature, increased air rate, and torque reduction. More recent work has included tests using a four-valve 13-in. bore, 16-in. stroke single cylinder laboratory engine with a combustion chamber geometry and fuel admission system, similar to that of the LSVB. Tests were completed exploring reduced pilot oil, various nozzle configurations, very high pilot oil injection rate, high injection pressure, and cylinder swirl. High injection rate was provided by utilizing a nonstandard injection pump with a 50 percent increase in plunger area. High injection pressure was accomplished by back pressuring the injection nozzle and raising the pressure from a conventional 7000 psig to double that level. Swirl was provided by inlet valve shrouding, which is described later in this paper.

Work Using the Laboratory LSB-6. The most promising of these tests were repeated using the LSB-6 Laboratory engine. Figure 6, lines 1–5, illustrates for the standard gas-diesel engine the single effect of controlling air manifold pressure through a range limited by detonation on the low-pressure end and by high fuel consumption or combustion roughness on the high

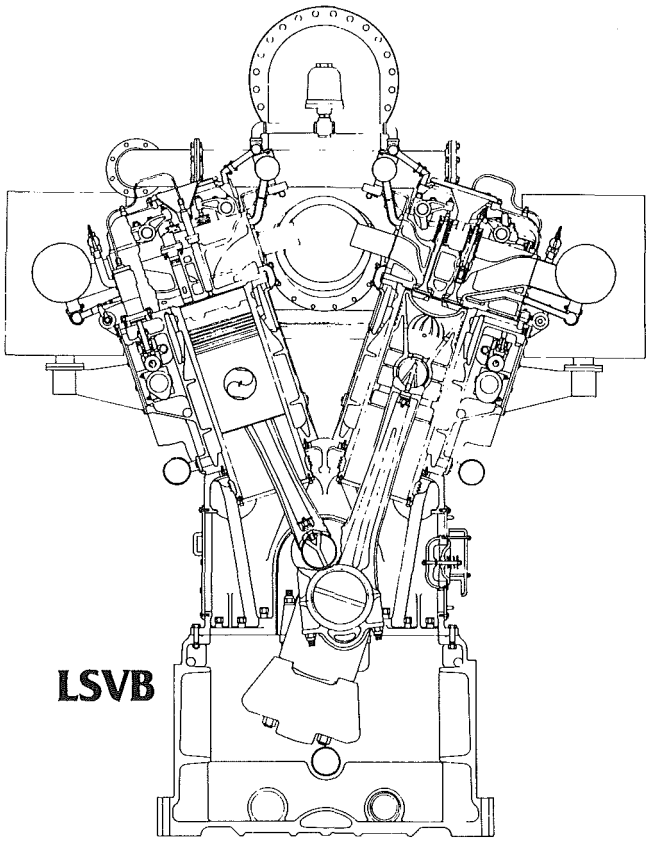

Fig. 4 Sectional drawing of the LSVB engine

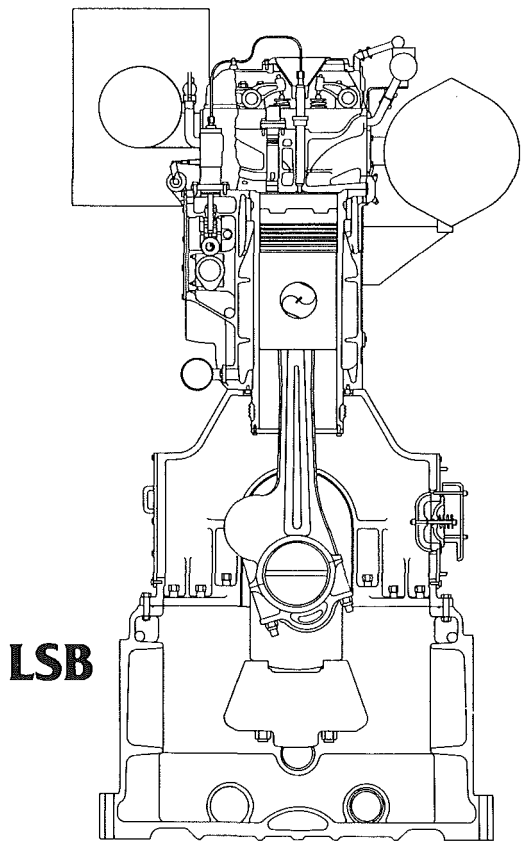

Fig. 5 Sectional drawing of the LSB engine

LSB-6 80°F AMBIENT
Gas-Diesel Mode - 200 BMEP

Line	Detail	% PO	AMP	NOx	HCt	BSFC	FP	DEV	Smoke % Opacity	PTT
1	Std Noz 18° PC	5.7%	55	11.5	1.0	6231	1301	49	20Y	1207
2	Std Noz 18° PC	5.6%	59	8.2	1.8	6254	1249	52	20Y	1158
3	Std Noz 18° PC	5.7%	63	5.2	3.3	6352	1207	49	15Y	1095
4	Std Noz 18° PC	6.8%	67	4.4	4.9	6528	1196	48	15Y	1054
5	Std Noz 18° PC	5.5%	72	4.1	7.3	6592	1203	40	10Y	1014
6	Reduced PO	3.8%	67	3.2	4.6	6530	1165	71	15Y	1072
7	4 Hole .018, 18° PC	6.0%	67	3.2	6.1	6396	1168	55	15Y	1049
8	4 Hole .018, 18° PC	2.8%	67	2.2	4.3	6510	1110	78	15Y	1088
9	4 Hole .021, 18° PC	5.6%	67	3.9	4.8	6526	1180	51	10Y	1066
10	4 Hole .021, 18° PC	4.3%	67	3.2	4.7	6519	1141	53	10Y	1077
11	4 Hole .018, 15° PC	5.9%	67	3.2	4.6	6530	1126	69	10Y	1082
12	4 Hole .018, 15° PC	4.2%	67	2.8	4.6	6576	1090	69	10Y	1103
13	Raise NOP 5500 PSIG	5.5%	67	3.6	4.0	6618	1129	63	10Y	1103

Fig. 6 Summary of most promising open chamber data

LSVB-6-80 AMB
Gas-Diesel Mode - 200 BMEP
Shrouded Inlet Valves

Configuration "A"
Fuel Nozzle 9° PC

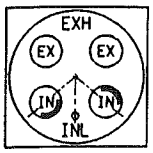

%PO	AMP	NOx	HCt	BSFC	FP
6.3	65	5.5	1.7	6455	1196

DEV	SMOKE % OPACITY	PTT
58	10Y	1130

Configuration "B"
Fuel Nozzle 9° PC

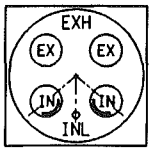

%PO	AMP	NOx	HCt	BSFC	FP
6.6	65	7.5	1.8	6382	1216

DEV	SMOKE % OPACITY	PTT
71	10Y	1141

Configuration "C"
Fuel Nozzle 9° PC

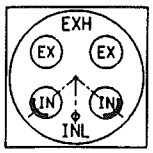

%PO	AMP	NOx	HCt	BSFC	FP
6.1	65	5.4	1.6	6530	1088

DEV	SMOKE % OPACITY	PTT
52	15Y	1186

Configuration "D"
Fuel Nozzle 9° PC

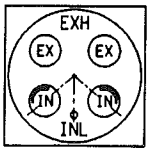

%PO	AMP	NOx	HCt	BSFC	FP
6.7	65	5.4	1.6	6443	1106

DEV	SMOKE % OPACITY	PTT
58	10Y	1179

Fig. 7 Summary of work investigating in-cylinder swirl

end. Note that NO_x can be reduced by increasing the air manifold pressure from 55 to 72 in. mercury absolute pressure; however, NO_x levels below 4 g/BHP-h could not be achieved, and a fuel consumption penalty of 5 percent accompanies the reduced NO_x. Also accompanying the reduced NO_x, at higher air manifold pressure, is a rise in unburned hydrocarbons and a rise in carbon monoxide (not shown). An incremental improvement in exhaust opacity is noted with increased air manifold pressure.

Line 6 of Fig. 6 shows the effect of reducing the pilot oil quantity to the standard gas-diesel nozzle while using line 4 air manifold pressure. NO_x is reduced an additional 20 percent compared to line 4; however, engine combustion regularity becomes limiting as the peak pressure standard deviation exceeds seventy.

Lines 7–12 were run with four-hole nozzles and illustrate the benefit of fuel nozzles available to those installations not requiring instant changeover to full diesel mode. The four-hole nozzle does not allow adequate fuel flow to operate 100

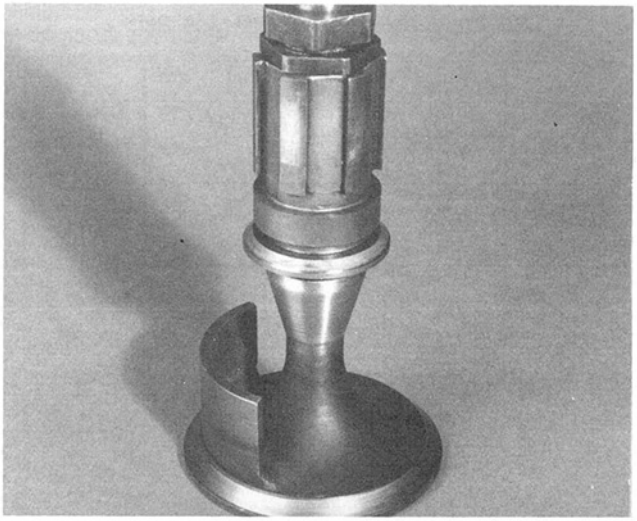

Fig. 8 Inlet valve with 115 deg shroud

percent diesel. All data were recorded with "line 4" air manifold pressure. Line 7 compared to line 4 shows a drop in NO_x for like quantities of pilot oil and a slight improvement in fuel consumption. The line 8 reduction in pilot oil to 2.8 percent drops the NO_x to 2.2 g/BHP-h, but engine combustion regularity is unacceptable at a standard firing pressure deviation of 78 psi.

Lines 9 and 10 using larger 0.021-in. diameter four-hole fuel nozzles show negligible change in numbers attributed to the nozzle configuration change, while lines 11 and 12 using 0.018-in. diameter four-hole fuel nozzles and 18 deg injection timing, compared to lines 7 and 8 show a negative fuel and NO_x benefit associated with further injection retard to 15 deg BTC.

Line 13 shows the negligible effect of increasing the nozzle opening pressure from 3500 psi to 5500 psi in the interest of improving penetration. The data show little change from lines 11 and 12.

Other test work performed using the standard open chamber gas-diesel configuration included variations of main valve timing to effect an improvement in either fuel mixing and/or fuel sweep (waste) during the valve overlap period. No reduction in fuel consumption, opacity, or NO_x was found as compared to the standard timing. (See discussion section of this paper for additional detail regarding role of unburned hydrocarbons.)

Figure 7 provides a summary of activity directed to the study of in-cylinder swirl. Figure 8 is a photograph of a standard inlet valve with a 115 deg shroud welded to the valve head. Configuration A of Fig. 7 illustrates the shroud position used to generate a clockwise in-cylinder mixture motion as viewing downward in the cylinder. Rate of combustion was increased significantly, requiring resetting of the pilot oil pump port closure from 18 deg BTC to 9 deg BTC to limit peak pressures at a 1200 psig level.

Comparison of Fig. 7 configuration A data to Fig. 6 line 4 data shows that high swirl improved BSFC level slightly but actually increased NO_x. Note that for the same approximate air manifold pressure, preturbine temperature has been increased, indicating the degree of flow restriction imposed by the shroud to the normal free flow, four valve configuration. Engine air flow data substantiates this observation. Unburned hydrocarbon levels are lower for Fig. 7 configuration A; however, we attribute this to exhaust oxidation at the higher preturbine temperature rather than to improved fuel air mixing or other factors accountable to the shrouds.

Configurations B, C, and D are included to show results of some of the other shroud positions evaluated. Configuration B, compared to Configuration A, produced slightly higher

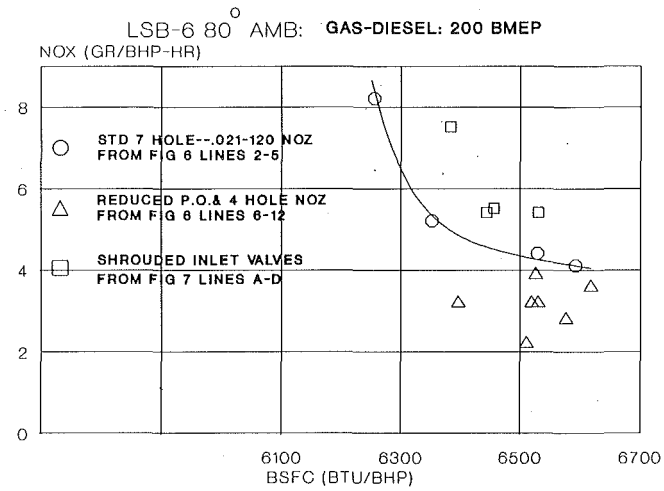

Fig. 9 NO_x/BSFC plot for gas-diesel mode

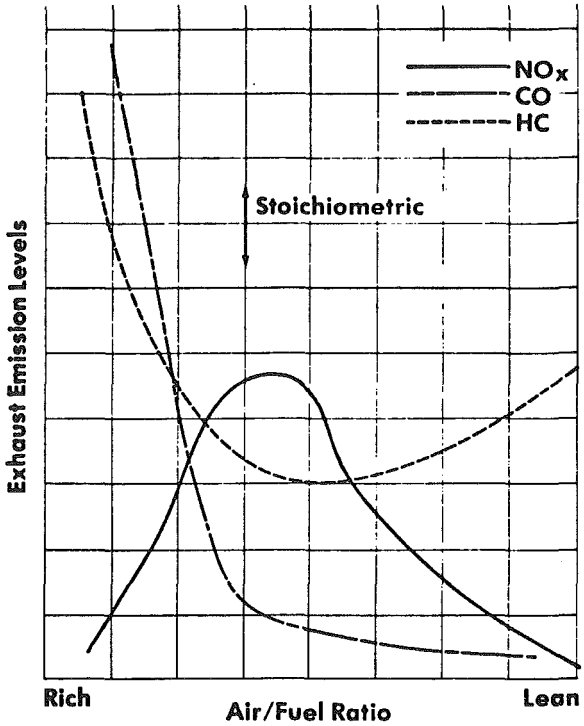

Fig. 10 Effect of air/fuel ratio on exhaust emissions internal combustion engines

peak pressures, lower BSFC, and higher NO_x, with increased combustion roughness. Configurations C and D show reduced peak pressures compared to Configurations A or B, and show comparable NO_x and total unburned hydrocarbon levels to Configuration A.

Figure 9 shows a plot of NO_x versus BSFC for the open chamber gas-diesel data lines of Figs. 6 and 7. The general trend is a sweep to the lower right-hand corner of the grid showing a conventional tradeoff of increased fuel consumption for beneficial reductions in NO_x. The target region for combined NO_x and BSFC improvement is of course the lower *left*-hand corner of the grid. Lines 6–12, working with reduced pilot, tend to move in the desired direction but meet the barrier of marginal combustion as indicated by peak pressure standard deviation numbers greater than 50. Lines A through D of Fig. 7 are clearly on the undesirable side of the standard engine variable air rate response curve shown by lines 2–5 of Fig. 6.

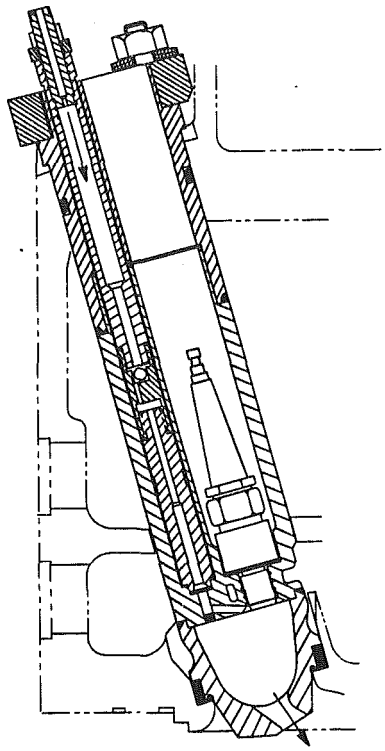

Fig. 11 Torch cell for spark-gas power engine

Application of the Spark-Fired Torch Cell to the Four-Cycle Engine

Commercial application of the two-cycle integral compressor engine torch cell concept to the LSV four-cycle power engine line was introduced in 1985 to Southern Energy Company at Elba Island, GA, in the interest of achieving acceptable power quality for a spark-ignited gas engine serving very tight frequency requirements. A later phase of this program included turbocharger modifications, resulting in a full CleanBurn™ package achieving not only precise power but also control of oxides of nitrogen to levels in the 2.0 g/BHP-h range. More recent development has extended this NO_x level to the 1 g/BHP-h level and has resulted in sale to date of fourteen units with ratings up to 180 BMEP and for fuels ranging from LNG to digester gas.

Fuel–Air Ratio and NO_x Formation. Figure 10 has appeared in many technical presentations [3] on the subject for NO_x control for combustion processes and shows NO_x formation as a function of fuel–air ratio. It provides the basic arguments for understanding the CleanBurn™ NO_x control mechanism. Essentially the cylinder main chamber is controlled to be very fuel lean and combustion temperatures are thereby controlled to levels sufficient to limit NO_x formation. The pilot or torch chamber is fuel rich and NO_x is thereby limited by the available oxygen. The main chamber is represented by the right side of Fig. 10, and the torch chamber is represented by the left.

Design and Performance Details of the Spark-Fired CleanBurn™ LSVB Engine. Figure 11 illustrates the spark-fired torch cell installation to the LSVB engine line. Cell geometry and volume are basically unchanged from that of the two-cycle integral engine line but nozzle direction is tailored to accommodate the more vertical access available for the LSVB engine line. As with the larger bore two-cycle engines, two cells per cylinder are used, which net combustion smoothness and BSFC/NO_x gains compared to one cell per cylinder.

LSB-6 80°F AMBIENT
Spark-Gas CleanBurn™ Mode 180 & 200 BMEP

Line	Detail	AMP	NOx	HCt	BSFC	FP	DEV	Smoke % Opacity	PTT
14	5° Ign 180 BMEP	60	1.5	4.2	6319	1040	41	< 5%	1077
15	5° Ign 180 BMEP	62	1.0	4.7	6400	1045	42	< 5%	1049
16	8° Ign 180 BMEP	64	1.0	6.3	6326	1177	29	< 5%	991
17	4° Ign 200 BMEP	75	1.0	5.4	6240	1206	51	< 5%	1020
18	4° Ign 200 BMEP	75	1.2	5.0	6250	1200	50	< 5%	1040

Fig. 12 Summary of spark gas CleanBurn™ data

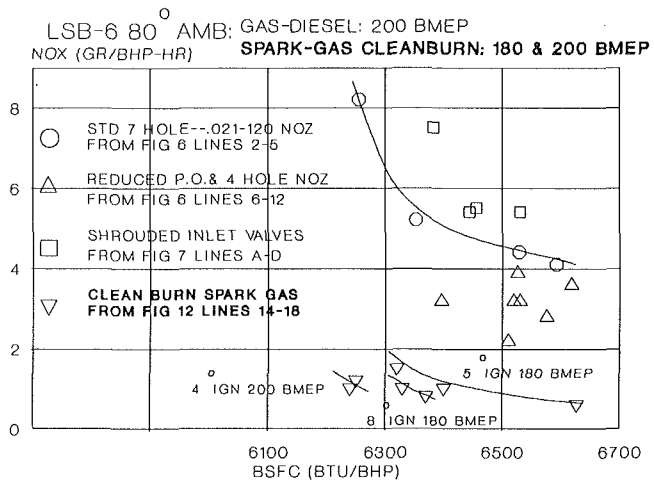

Fig. 13 NO_x/BSFC plot for gas-diesel and spark-gas CleanBurn™ modes

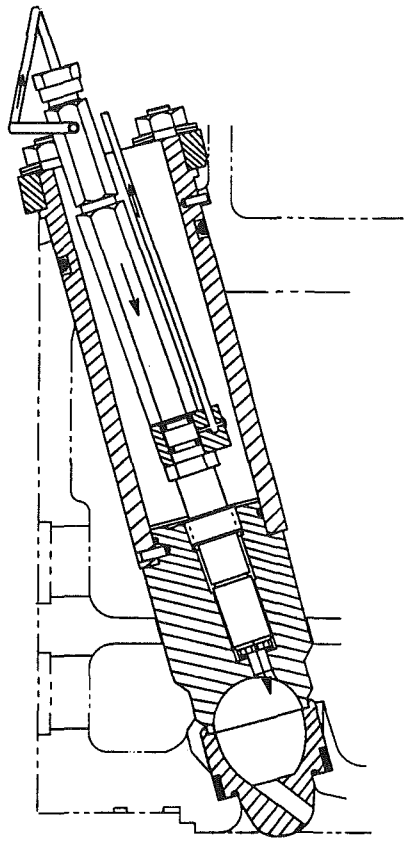

Fig. 14 Torch cell for gas-diesel engine

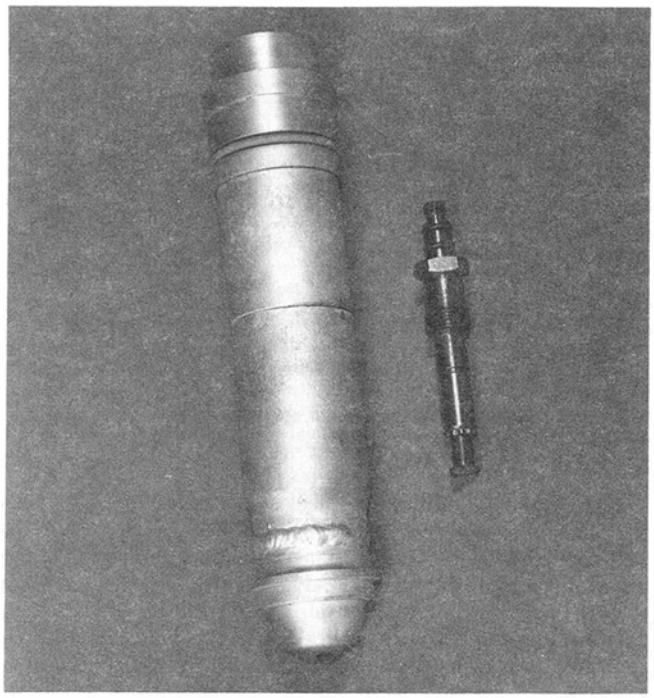

Fig. 15 Pilot oil torch cell and injector

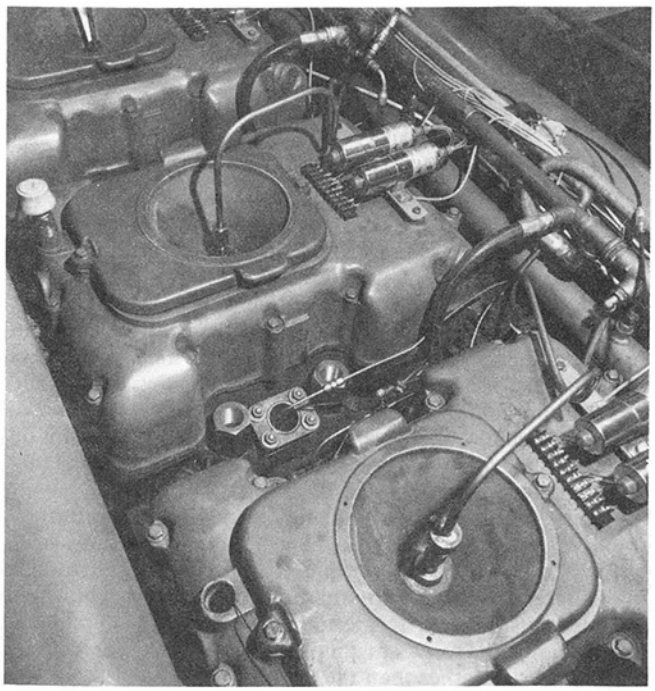

Fig. 16 Installation of pilot oil torch cells in LSB-6 cylinder heads

LSB-6 80°F AMBIENT
Gas-Diesel CleanBurn™ Mode 200 BMEP

Line	Detail	% PO	AMP	NOx	HCt	BSFC	FP	DEV	Smoke % Opacity	PTT
19	20° PC 200 BMEP	0.9%	67	1.36	3.9	6250	1266	48	< 5%	1021
20	20° PC 200 BMEP	0.9%	70	0.90	4.9	6330	1277	44	< 5%	991
21	23° PC 200 BMEP	0.9%	68	1.50	3.4	6210	1366	37	< 5%	942

Fig. 17 Summary of gas-diesel CleanBurn™ data

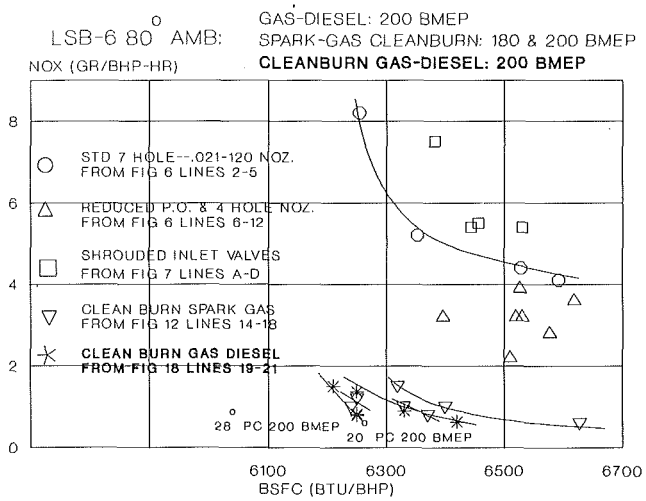

Fig. 18 NO_x/BSFC plot for gas-diesel, spark-gas CleanBurn™, and gas-diesel CleanBurn™ modes

The spark-plug and pilot gas check valve system are identical to that of the two-cycle.

Figure 12 tabulates performance numbers for variable air manifold pressure at two spark advances and Fig. 13 highlights the NO_x versus BSFC relationships against those of the open chamber gas-diesel shown earlier as Fig. 9. There is a marked reduction in NO_x levels and opacity levels for the spark-fired CleanBurn™ system. These data were generated on the same engine, using the same fuel gas admission system and the same combustion chamber. Only the method of ignition is different. The obvious dilemma was to account for the higher NO_x level that occurs, when only 3-6 percent of the total fuel used is number 2 fuel oil and the remainder is natural gas as compared with 100 percent natural gas.

The Pilot Oil Torch Cell

The Development Program. After exploring every practical avenue of open-chamber pilot oil injection options for the gas-diesel engine, it became apparent that diffusion burning of the pilot oil charge could not be tolerated. Pilot oil penetration and pattern variations did little to control NO_x. Cylinder swirl dramatically affected burning rate but not NO_x formation. Reduced pilot oil quantities either with the standard full diesel capability nozzles or with reduced area "gas-diesel only" nozzles produced unacceptable combustion quality and fuel consumption. It appeared that no matter how we handled the pilot injection, there was a significant quantity of pilot oil and associated main chamber fuel gas being burned in a manner contributing substantially to NO_x formation.

Experience and success with the spark-fired CleanBurn™ torch cell system, directed gas-diesel program effort away from open chamber diffusion burning. The desired benefit of the pilot oil torch cell was to not only control NO_x by rich burning, but also, it is hoped, to minimize the quantity of pilot oil involved, since its role as an ignition energy source would apply only to the cell rather than the main chamber.

Initial pilot oil torch cell work was assigned to the 13-in. bore, 16-in. stroke single-cylinder laboratory engine. In the interest of rugged design and low maintenance, a pintle type nozzle was suggested and a matrix of tests completed exploring cell size and geometry, cell nozzle diameter and length/diameter ratio, cell direction, and main chamber geometry. It was gratifying to find that, although these tests netted some gain in performance, the basic system displayed wide margin for operation and did not require precise control of operating parameters.

The program transition from the single-cylinder engine to the laboratory LSB-6 was easily accomplished. A series of tests were performed to establish final cell volume turbocharger matching pilot fuel quantity and timing, load acceptance, and fuel gas sensitivity (NBN) limits for an array of test parameters. Flame-out conditions were defined as a function of load and minimum air manifold temperatures.

System Description. Figure 14 illustrates the pilot oil fired torch cell installation in the LSVB cylinder head. The pilot oil injector is a modified commercial truck pintle nozzle. Typical pintle performance includes some blossom and ignition of the initial injection followed by the main penetrating injection, which intentionally strikes the uncooled nozzle portion of the torch cell. Cell charge motion as viewed in Fig. 14 is clockwise on the engine compression stroke as fuel lean main chamber mixture enters the cell, and counterclockwise during torch cell combustion. Figure 15 illustrates the cell and injector, and Fig. 16 shows the actual installation in the cylinder head. Pilot oil injection pumps are modified units chain driven from the engine camshaft.

Performance Results. Figure 17 tabulates performance data as a function of air manifold pressure for 20 deg BTC and for 23 deg pilot oil pump port closure. Comparison to Fig. 12 for the spark-gas CleanBurn™ mode shows excellent correlation. Figure 18 highlights the gas-diesel CleanBurn™ mode NO_x versus BSFC relationships against those of the open chamber gas-diesel and spark-fired CleanBurn™ engine.

Figure 19 makes a comparison between the present day uncontrolled gas-diesel engine and the CleanBurn™ gas-diesel engine. NO_x has been reduced 92 percent, opacity reduced from an objectionable yellow level to virtually a clear stack, and preturbine temperatures reduced over 200 deg. The jet cell allows a reduction of pilot oil from a nominal 6 percent to near 1 percent, yet retains an excellent ignition source for the fuel gas. The dual-fuel capability of this engine is still retained by this concept with full diesel rating being achieved by changeover to the conventional fuel system. During the gas-diesel mode the main fuel racks are set to zero delivery.

Load acceptance for the gas-diesel CleanBurn™ system is excellent and equals that of the conventional 6 percent pilot oil system. Variable ignition timing for the gas-diesel CleanBurn™ system is offered for non-base-loaded installations to provide peak efficiency throughout the load range.

Field Conversion

To achieve "proof of concept" of the gas-diesel CleanBurn™ engine on a large field operating cogeneration unit, two existing LSVB-20GDT engines rated 6000 kW, 200 BMEP were selected for the initial field conversions. Heads were re-

LSB-6 80°F AMBIENT
Gas-Diesel Mode - 200 BMEP

Line	Detail	% PO	AMP	NOx	HCt	BSFC	FP	DEV	Smoke % Opacity	PTT
1	Std. Gas-Diesel	5.7%	55	11.5	1.0	6231	1301	49	20	1207
21	CleanBurn™ Gas-Diesel	0.9%	70	0.90	4.9	6330	1277	44	< 5%	991

Fig. 19 Comparison of standard gas-diesel to CleanBurn™ gas-diesel

moved, reconditioned, and remachined for the torch cells; fuel and control system modifications assembled and installed; turbocharger upgraded and reinstalled; and the engine restarted within a three-week time frame. A formal field test using a third party emissions measurement firm was performed the week after initial start-up of the first unit. Test results are gratifying, with NO_x levels reduced to levels seen in the R&D engine, some reduction in CO levels and slight offset of hydrocarbons. The exhaust stacks are nearly totally clean with opacity improved from the 10–20 percent range of the non-CleanBurn™ gas-diesel engine, to 0 and 5 percent readings taken by a trained third party observer. Long-term reliability for the hardware appears to be excellent, with over 10,000 total hours logged.

Conclusion

The development of the gas-diesel CleanBurn™ engine is considered to be a major step forward in the advancement of emissions technology. It is expected that this is the new BACT level of emissions performance for dual-fueled engines.

Acknowledgments

The authors would like to thank the management of Cooper-Bessemer Reciprocating Products Division, Cooper Industries, for permission and support to publish this paper. Recognition for contribution should go to the Research and Development Laboratory staff, Engineering Design personnel, and Jack Kimberley, fuel system consultant.

Metric Equivalents

Readers more familiar with metric units are asked to use the following information to convert the nonmetric units used in this paper:

Nonmetric	Multiplied by	Yields metric
Btu	1055.06	J
hp	745.70	W
in.	0.0254	m
psi	6.894.76	Pa or N/m^2
sq. in.	0.006452	m^2
(°F − 32)	0.5556	°C
lb	0.4536	kg

References

1 Schaub, F. S., and Hubbard, R. L., "A Procedure for Calculating Fuel Gas Blend Knock Rating Large-Bore Gas Engines and Predicting Engine Operation," ASME Paper No. 85-DGP-5, 1985.

2 Schaub, F. S., and Beightol, K. V., "NO_x Reduction Methods for Large Bore Diesel and Natural Gas Engines," ASME Paper No. 71-WA/DGP-2, 1971.

3 Danyluk, P. R., and Schaub, F. S., "Emission Reduction by Combustion Modification in Two Stroke Spark-Ignited Gas Engines and by Catalytic Conversion," ASME Paper No. 81-DGP-7, 1981.

4 Kaiser, R., "NO_x Reduction Experience, Past and Planned, in Transamerica Delaval-Enterprise Engines," presented at the American Gas Association Transmission Conference, Seattle, WA, May 2, 1983.

5 Wilson, R. P. Jr., Mendillo, J. V., Gott, P. G., Danyluk, P. R., Schaub, F. S., and Wasser, J. H., "Single-Cylinder Tests of NO_x Control Methods for Spark-Gas Engines," ASME Paper No. 82-DGP-27, 1982.

6 Wilson, R. P., Jr., Mendillo, J. V., Genot, A., Bachelder, D. L., and Wasser, J. H., "Single-Cylinder Tests of Emission Control Methods for Medium-Speed Diesel Engines," ASME Paper No. 82-DGP-28, 1982.

The Effect of Injection Timing, Enhanced Aftercooling, and Low-Sulfur, Low-Aromatic Diesel Fuel on Locomotive Exhaust Emissions

V. O. Markworth
Department of Engine Research.

S. G. Fritz
Department of Emissions Research.

Southwest Research Institute,
San Antonio, TX 78228

G. R. Cataldi
Research and Test Department,
Association of American Railroads,
Washington, DC 20001

An experimental study was performed to demonstrate the fuel economy and exhaust emissions implications of retarding fuel injection timing, enhancing charge air aftercooling, and using low-sulfur, low-aromatic diesel fuel for locomotive engines. Steady-state gaseous and particulate emissions data are presented from two 12-cylinder diesel locomotive engines. The two laboratory engines, an EMD 645E3B and a GE 7FDL, are each rated at 1860 kW (2500 hp) and represent the majority of the locomotive fleet in North America. Each engine was tested for total hydrocarbons (HC), carbon monoxide (CO), oxides of nitrogen (NO_x), and particulate. Emissions were measured at three steady-state operating conditions: rated speed and load, idle, and an intermediate speed and load. Test results on the EMD engine indicate that a 4 deg injection timing retard, along with a low-sulfur, low-aromatic fuel and enhanced aftercooling, was effective in reducing NO_x from 10.5 g/hp-h to 7.2 g/hp-h; however, particulates increased from 0.15 g/hp-h to 0.19 g/hp-h, and fuel efficiency was 4.3 percent worse. Similar observations were made with the GE engine. This paper gives details on the test engines, the measurement procedures, and the emissions results.

Introduction

The program on which this paper is based is part of a multiyear locomotive engine research project funded by the Association of American Railroads (AAR) to characterize emissions from locomotive engines and to determine the effect of various control technologies on unburned hydrocarbons (HC), carbon monoxide (CO), oxides of nitrogen (NO_x), and particulates (PM). A previous study by Fritz and Cataldi [1] presented results of baseline locomotive engine emissions along with test results from a low-sulfur fuel currently used in southern California.

The current regulatory climate regarding engine emissions suggests that locomotive engine emissions (both gaseous and particulate) will soon be regulated beyond existing visible smoke standards. Regulation will likely begin in California where continuing nonattainment of National Ambient Air Quality Standards in many areas has resulted in consideration of extending mobile source emission regulations to off-highway sources (including locomotives). Assembly Bill AB234 was enacted in 1987 by the California Legislature and required the California Air Resources Board (CARB) to perform a study of locomotive emissions in the six nonattainment basins within California before any regulatory action could be taken. A contractor was selected to perform this study, and the final report [2] has recently been submitted to the CARB for final approval. This will clear the way for the rulemaking process for regulating locomotive emissions. The California Clean Air Act of 1988 called for a CARB staff report to develop recommendations for regulating off-highway emissions by the end of 1991. These regulatory recommendations are to include locomotives.

One recommendation to reduce locomotive exhaust emissions was presented in the CARB Locomotive Emissions Study [2]. It combined implementation of a 4 deg injection timing retard with the use of a low-sulfur, high-cetane diesel fuel for yard and switcher locomotives. The experimental efforts described herein were performed in an attempt to quantify the emissions and fuel economy implications associated with these recommended modifications.

The Federal Clean Air Act Amendments of 1990 required that the Environmental Protection Agency (EPA) study the air quality impact of locomotive emissions in nonattainment areas. It did not, however, set specific engine emission levels. It did include federal pre-emption for new locomotives and locomotive engines that excluded California or any other state from regulating new locomotives. This left the door open for CARB to pursue regulations on existing locomotives. As part of EPA's efforts, an initial survey of the contribution of locomotive emissions to air pollution in nonattainment areas is to be performed within one year. If the study concludes that

Contributed by the Internal Combustion Engine Division and presented at the 13th Annual Fall Technical Conference, Muskegon, Michigan, September 30-October 2, 1991. Manuscript received by the Internal Combustion Engine Division September 22, 1991. Associate Technical Editor: J. A. Caton.

locomotive emissions are significant, regulation must be in place within five years. Initial efforts in this area have focused on the EPA revising their methodology in state implementation plan guidelines for quantifying locomotive engine emissions.

In Canada, the Canadian Council of Ministers of the Environment, in their Phase I Management Plan for Nitrogen Oxides and Volatile Organic Compounds [3], will require railroads to reduce their total NO_x by 14 percent on a nationwide basis from the base year of 1985 by the year 2005. Current (1985) NO_x emissions from all rail transport were estimated at 7 percent of the national total. The NO_x/VOC Management Plan—Phase I represents the first phase of a three-phase NO_x and VOC control program aimed at fully resolving ground-level ozone problems in Canada by the year 2005. The Phase I plan is not expected to be sufficient to meet Canada's air quality goals, so the railroad industry's emission targets for 2005 could be lowered in a future phase. Because of the relatively small Canadian locomotive market, the government recognizes that they cannot exceed the stringency of U.S. regulations. After EPA and CARB act on new and existing locomotive engine regulations, the Canadian railroads could face more stringent regulations.

Background

There are effectively only two basic engines represented in the U.S. locomotive population. One of these is the two-stroke cycle engine manufactured by Electro-Motive Division (EMD) of General Motors Corporation. The majority of Class I U.S. locomotives (approximately 70 percent) are powered by a variant of this engine. Nearly all of the remaining U.S. locomotives use the four-stroke cycle engine manufactured by the Transportation Systems Division of the General Electric Company (GE). Two engine designs manufactured by Caterpillar Inc. are being field tested in a limited number of locomotives. A variety of other engine designs can be found on older switcher locomotives owned by short-line railroads and private industrial railroads.

A very limited amount of locomotive emissions information exists in the public domain. The Southern Pacific Transportation Company (SP) performed a study to develop certification procedures for visible smoke from locomotives in 1973 [4]. A field study was performed on GE locomotives by SwRI in conjunction with GE and the SP in 1975 [5]. Several studies of locomotive engine emissions were performed by SwRI for the U.S. Department of Transportation, the Federal Railroad Administration, and the EPA in the mid-1970s [6–10]. These studies focused on gaseous emissions and visible smoke (or percent opacity using light extinction smoke meters) and were performed on engines that are now two generations old. Most of these locomotives have been retired, upgraded, placed in switcher service, or sold to short line railroads where they are infrequently used.

A field study of in-service locomotive exhaust emissions was performed by the AAR in 1981 through 1983 [11]. Other studies

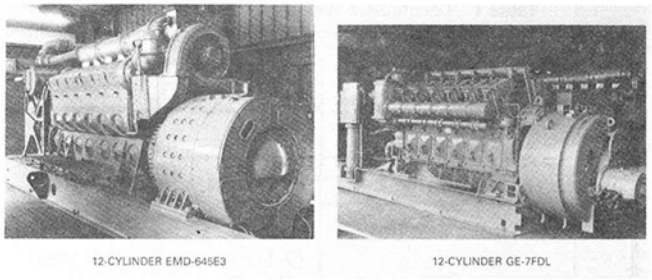

Fig. 1 Locomotive test engines at SwRI

by the AAR in the early and mid-1980s were performed primarily to determine engine performance while operating on alternative fuels, emulsions, or broadened specification diesel fuels. During some of these tests, gaseous emissions were recorded [12–16]. Since that time, however, significant engine upgrades in both the EMD and GE engine families have occurred, and a corresponding update of emission data is needed.

Experimental Test Plan

Description of Test Engines and Facilities. The EMD 12-645E3B engine shown in Fig. 1 is a two-stroke cycle engine, while the GE 12-7FDL operates on the four-stroke cycle. In the SwRI locomotive engine test facility, the EMD is loaded by a d-c generator and the GE by a d-c rectified alternator. The d-c power is absorbed by two sets of locomotive load grids equipped with cooling fans for heat dissipation. Both engines have their own cooling systems which are modified versions of the standard locomotive system. Pertinent specifications for each of the test engines are shown in Table 1.

Both engines are operated at conditions that simulate the notch operation of their respective line-haul locomotives. Locomotive engines operate only at specified speed/power combinations defined by throttle positions or "notches." Since the power output and speed are constant at each notch position, the fuel consumption rate is also constant and can be defined for each position. EMD and GE engines in line-haul service operate at eight power-producing notches. There are also idle and, in some locomotives, low idle operating positions. In dynamic brake throttle notch position, traction motors are used to brake the train. The d-c power generated during the dynamic brake operation is dissipated through resistive load grids located on the roof of the locomotive.

To facilitate laboratory testing, the notch positions were redefined in terms of speed and fuel mass consumption rate combinations. Notch 8 of each schedule represents rated speed and load of the engine. All other positions represent part-load conditions. To simplify emissions test work, only three notches were used. These are given in Table 2.

Nomenclature

AAR = Association of American Railroads
ASTM = American Society for Testing and Materials
bhp = brake horsepower
°C = degrees Celsius
CARB = California Air Resources Board
CO = carbon monoxide
CO_2 = carbon dioxide
d-c = direct current
EMD = Electro-Motive Division of General Motors Corporation
EPA = United States Environmental Protection Agency
°F = degrees Fahrenheit
g = grams
GE = Transportation Systems Division of General Electric Company
HC = hydrocarbons (total)
h = hour
kW = kilowatt
NO_x = oxides of nitrogen
PM = particulate matter
SAE = Society of Automotive Engineers
SwRI = Southwest Research Institute

Table 1 Locomotive test engine specifications

	EMD 12-645E3B	GE 12-7FDL
Number of Cylinders	12	12
Displacement L (in^3) / cyl	10.6 (645)	10.9 (668)
Bore and Stroke mm (in)	230 x 254 (9-1/16 x 10)	229 x 267 (9 x 10½)
Rated Speed (rpm)	904	1,050
Rated Power @ flywheel kW (bhp)	1,860 (2,500)	1,860 (2,500)
Compression Ratio	14.5:1	12.7:1
Cycle	2	4
Injection System	Unit Injector	Jerk Pump/ Nozzle

Table 2 Throttle notch schedules

	EMD 12-645E3B		GE 12-7FDL	
Notch Position	Engine rpm	Fuel Rate (kg/hr)	Engine rpm	Fuel Rate (kg/hr)
Idle	300	**	450	**
5	650	183	879	206
8	904	396	1,050	391
** - Observed at idle speed				

Table 3 Diesel fuel properties

Determinations		Test Method	Baseline	Low Aromatic - Low Sulfur
API Gravity @ 60°F		D1298	32.0	41.9
Flash Point °C (°F)		D93	64 (148)	77 (170)
Cloud Point °C (°F)		D2500	-8 (18)	-16 (4)
Viscosity @ 40°C (cSt)		D445	3.33	2.74
Sulfur (Wt%)		D2622	0.290	0.043
Cetane Number		D613	44.2	54.5
Heat of Combustion		D240		
Gross	MJ/kg		44.0	46.3
	BTU/lb		19,400	19,900
	BTU/gal		139,600	135,300
Net	MJ/kg		42.3	43.3
	BTU/lb		18,200	18,600
	BTU/gal		131,200	126,600
Carbon-Hydrogen Ratio		D3178		
% Carbon			87.3	85.7
% Hydrogen			12.2	14.2
Hydrocarbon Type		D1319		
Aromatics (%)			30.8	15.6
Olefins (%)			5.1	4.0
Saturates (%)			64.1	80.4
Specific Gravity			0.865	0.816
Distillation		D86		
% Recovered			Temp. °C (°F)	Temp. °C (°F)
IBP			188 (370)	191 (376)
5			221 (430)	208 (406)
10			237 (458)	216 (420)
20			246 (474)	228 (443)
30			254 (490)	242 (467)
40			263 (506)	253 (488)
50			280 (536)	263 (506)
60			289 (552)	273 (524)
70			299 (570)	283 (541)
80			311 (592)	294 (562)
90			329 (624)	311 (592)
95			340 (644)	326 (619)
EP			353 (668)	342 (648)

Gaseous Emission Measurement. Gaseous emission measurements during each steady-state test condition were obtained by sampling raw exhaust. Exhaust gases were analyzed for unburned hydrocarbons (HC), carbon monoxide (CO), oxides of nitrogen (NO_x), carbon dioxide (CO_2), and oxygen (O_2). Hydrocarbons were measured by a heated flame ionization detector unit built to specification as per SAE Recommended Practice J215. Carbon monoxide and carbon dioxide were measured by nondispersive infrared analyzers in a system that conforms to SAE Recommended Practice J177a. Oxides of nitrogen were measured using a chemiluminscent analyzer. For HC, CO, CO_2, and NO_x, all measurement instrumentation conformed to configurations typically used for EPA regulatory purposes.

Particulate Emission Measurement. The generally accepted test procedure for measurement of diesel particulate is specified by EPA for on-highway diesel engines. This procedure requires dilution of the total exhaust flow. Because of the size of locomotive engines, this "full-flow" dilution approach is not practical. Consequently, particulate measurements were made with a "split-then-dilute" system. This system samples a portion of the total exhaust flow and mixes it with filtered ambient air. Mixing occurs in the dilution tunnel prior to sampling the mixture for particulate. The dilution tunnel used in this work was 20 cm (8 in.) in diameter and approximately 5 m (15 ft) long. Samples of particulate were collected on dual (series) 90 mm Pallflex T60A20 fluorocarbon-coated glass fiber filters. The temperature of the diluted exhaust stream at the entrance to the particulate sample probe was regulated to 49°C ± 3 by varying the amount of raw exhaust entering the tunnel. All particulate filters were conditioned and weighed in a temperature and humidity-controlled chamber both before and after use.

Test Fuels Description. Two test fuels were evaluated in each of the 12-cylinder engines. For baseline measurements, an ASTM 2D diesel fuel was used. To assess the impact of low-aromatic, low-sulfur fuel on locomotive engine emissions, a second fuel was also tested. Both fuels were analyzed and the properties are given in Table 3. The low-aromatic, low-sulfur fuel was notably less dense, and has a substantially higher cetane number than the baseline fuel.

Duty Cycles. The engine test procedure used for the emissions measurements was essentially the same as has been developed for performance measurements. The engines were stabilized at rated conditions (Notch 8) for 2 hours prior to testing. One hour was spent at each notch position, with the first half hour being stabilization time. The emissions measurements took up to a full half hour at each test point.

The engine test procedure used for the emission measurements originally used a full-mode cycle and calculated the composite emissions using weighting factors for a line haul cycle provided by GE [1]. The full-mode test included the eight discrete power producing throttle positions or "notches," idle, low idle, and two dynamic brake notch positions. This cycle resulted from many studies performed by GE and EMD to determine actual operating modes of road locomotives.

Table 4 Comparison of full-mode versus three-mode duty cycles

Notch Position	Full-Mode Weighting Factor	3-Mode Cycle Weighting Factor
8	14	25
7	3	---
6	3	---
5	4	25
4	4	---
3	3	---
2	5	---
1	5	---
Idle	27.5	50
Low Idle	27.5	---
Dynamic Brake #1	2	---
Dynamic Brake #2	2	---
Total	**100 %**	**100 %**

Table 5 Full-mode versus three-mode composite baseline emissions

	weighted kW	Part. g/hp-hr	HC g/hp-hr	CO g/hp-hr	NO_x g/hp-hr
EMD 12-645E3B					
Full-Mode	432	0.28	0.33	0.80	11.7
3-Mode	661	0.27	0.29	0.60	11.3
GE 12-7FDL					
Full-Mode	436	0.26	0.60	2.24	10.7
3-Mode	703	0.22	0.41	1.88	10.8

Each emission test using the "full-mode" cycle required 10 to 12 hours to complete, and since multiple runs were necessary, an abbreviated cycle was desirable. Current emission data on the two locomotive engines were analyzed and a "three-mode cycle" was found to be representative. A comparison of the two cycles is given in Table 4 and a comparison of typical results obtained with the two cycles on the EMD and GE engines is shown in Table 5. Reference [1] gives a detailed description of the procedure for calculating the weighted composite brake-specific emissions.

For the EMD engine data given in Table 5, the three-mode cycle gives reasonable results for PM and HC, but it tends to yield NO_x results that are about 3 percent lower than that calculated with the full-mode cycle. For the GE engine, the NO_x results correlate closely while the PM results are about 15 percent lower and the HC results are about 30 percent lower

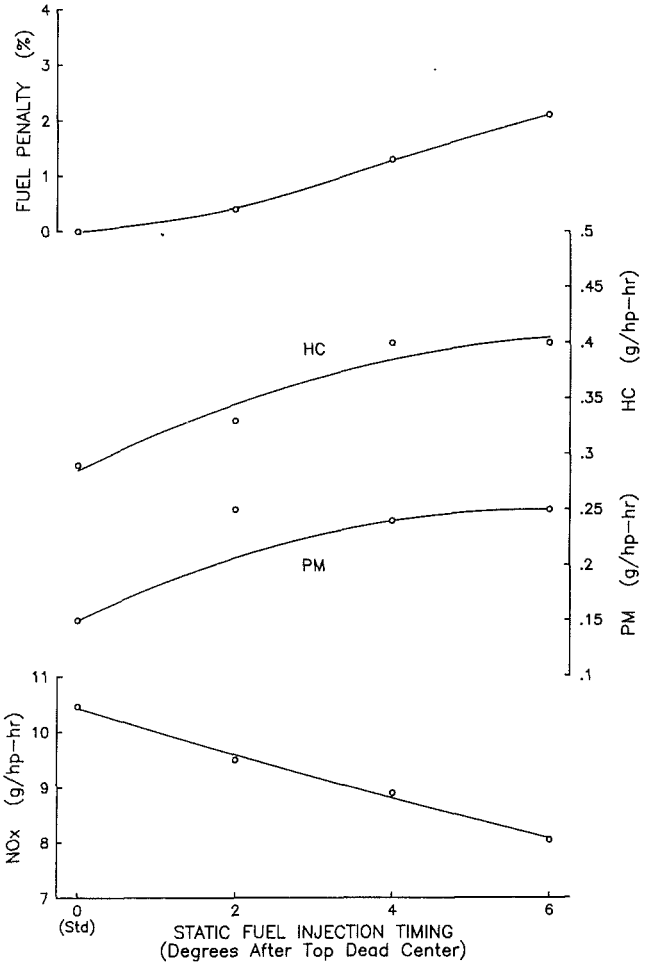

Fig. 2 The effect of fuel injection timing on emissions and fuel economy for a EMD 12-645 E3B locomotive engine

with the three-mode cycle. These differences in PM and HC are misleading, however, because these emissions are very low, whether calculated with the full-mode or three-mode method. Calculated CO emissions tend to be 13 to 25 percent lower on both engines using the three-mode duty cycle; however, this is considered acceptable since CO emissions are very low on these engines when compared to other mobile sources.

In the interest of maximizing the number of control techniques that could be evaluated, it was decided to use the three-mode cycle for all development testing. If a more accurate correlation with the full-mode cycle is desired, a detailed study of emission results may suggest a slight adjustment of the weighting factors.

Experimental Results

Presented below is a brief description of the engine and fuel modifications that were performed for this test program. A more detailed description of the hardware modifications is available [17, 18]. The highlights of the test results are summarized in the following sections, with comprehensive tabulated data given in the appendix for each test configuration. Emissions data for each individual test point are also available [18].

Injection Timing Effects. The effect of retarded timing was investigated by varying the static injection timing over the range of adjustment. In the case of the EMD engine, this was from standard (TDC) to 6 deg ATDC. For the GE engine, adjust-

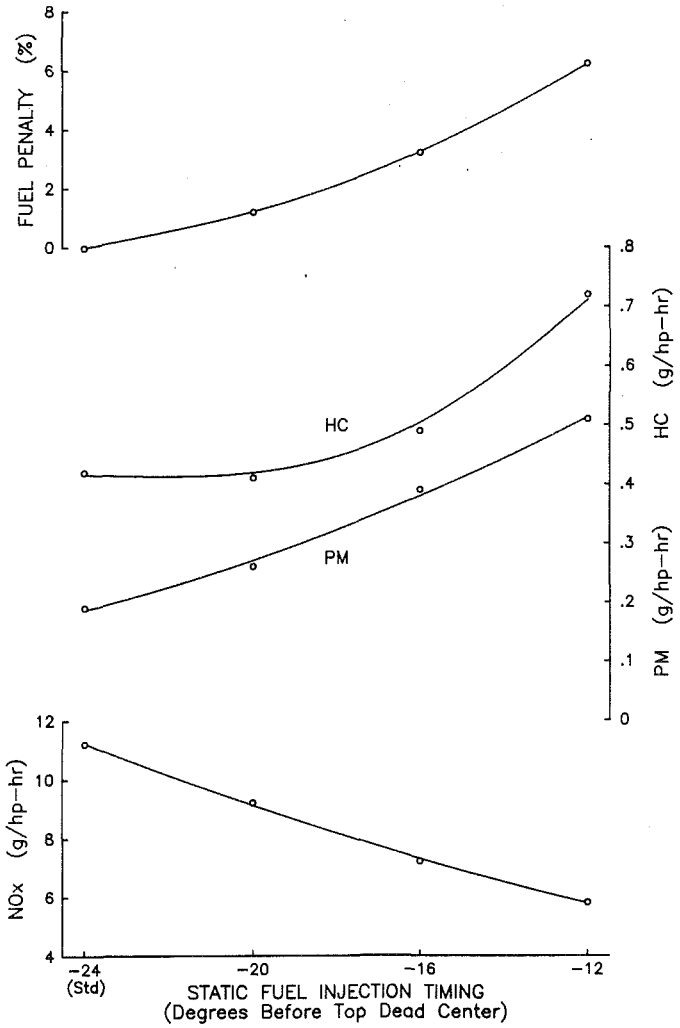

Fig. 3 The effect of fuel injection timing on emissions and fuel economy for a GE 12-7FDL locomotive engine

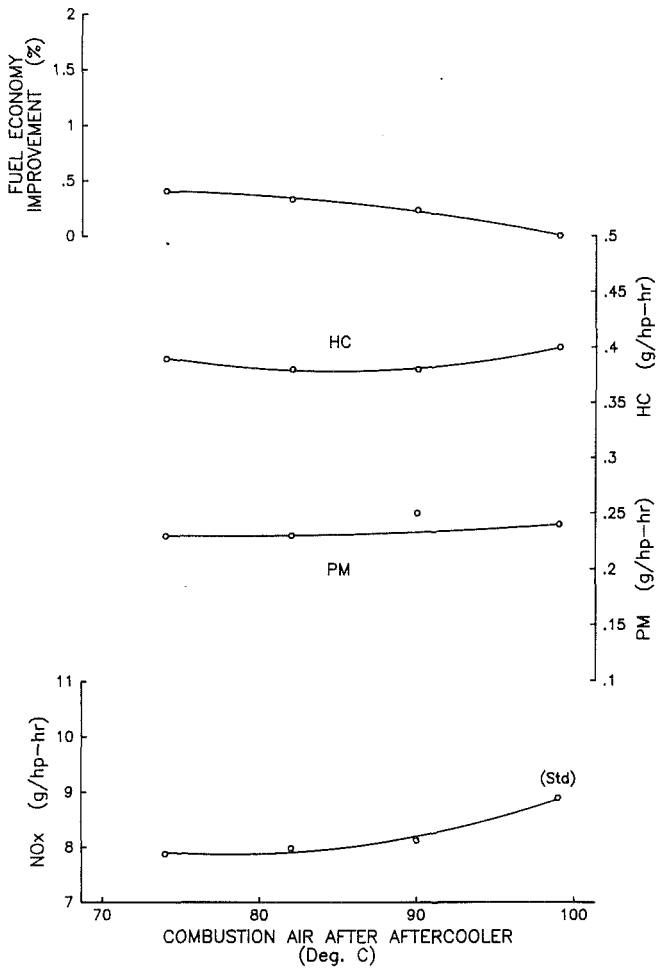

Fig. 4 The effect of aftercooler water temperature on emissions and fuel economy for a EMD 12-645 E3B locomotive engine with 4 deg retarded timing

ments were made from the standard injection timing of 24 deg BTDC to 12 deg BTDC.

The effects of fuel injection timing on NO_x and particulate for the EMD engine over the composite three-mode cycle results are shown in Fig. 2. Note that these test results were obtained with baseline diesel fuel and an unmodified aftercooler system. With a 4 deg retard, NO_x was reduced from a baseline level of 10.5 g/hp-h to 8.9 g/hp-h. Particulate, however, increased from 0.15 g/hp-h to 0.24 g/hp-h, and fuel consumption increased 1.3 percent for the EMD.

For the GE engine, fuel injection timing effects using baseline fuel are shown in Fig. 3. A 4 deg timing retard decreased NO_x from a baseline condition of 11.2 g/hp-h to 9.2 g/hp-h, while particulate increased from 0.19 g/hp-h to 0.26 g/hp-h, and fuel consumption increased 1.2 percent.

Enhanced Aftercooling Effects. For investigations on the effect of enhanced aftercooling, a separate aftercooler water system was fabricated. The existing engine-mounted aftercooler was utilized; however, engine cooling water no longer was used. Instead, utility water was the cooling medium, and the air temperature out of the aftercooler was varied by changing the water flow rate with a modulating valve. At Notch 8 and Notch 5, the reduced aftercooler temperatures were maintained, but at idle, the cooling water flow was shut off. Heating the intake air would have been required to maintain the target idle air temperature, and this would not have correctly simulated the field application. For all evaluations at Notch 8, Notch 5, and idle, three emission runs were made and the results averaged.

Enhanced intake air aftercooling experiments were performed on both the EMD and the GE engines with 4 deg timing retard. Results for the EMD engine are shown in Fig. 4. A slight reduction in NO_x emissions was demonstrated, with NO_x decreasing from 8.9 g/hp-h (with a typical boost air temperature after the aftercooler of 99°C) to 8.1 g/hp-h at 91°C (a 9 percent reduction). Further reductions in boost air temperature demonstrated only nominal reductions in NO_x emissions. Three-mode cycle particulates, CO, HC, and fuel efficiency were mostly unaffected by boost air temperature changes.

Results for the GE engine are shown in Fig. 5. The expected reduction in NO_x emissions was not as pronounced as observed for the EMD engine. NO_x decreased from 9.2 g/hp-h at a typical boost air temperature (after the aftercooler) of 85°C, to 8.7 g/hp-h at 77°C (a 5 percent reduction). Further reductions in boost air temperature also demonstrated slight reductions in NO_x emissions. Like the EMD engine, particulates, CO, HC, and fuel efficiency were mostly unaffected by boost air temperature changes, until boost air temperatures were forced below 68°C, where increases in CO and HC were observed.

Low-Sulfur, Low-Aromatic Fuel Effects. Low-sulfur, low-aromatic diesel fuel was tested at standard timing with unmodified aftercooling, and with 4 deg injection retard using enhanced boost air aftercooling for both engines. The results

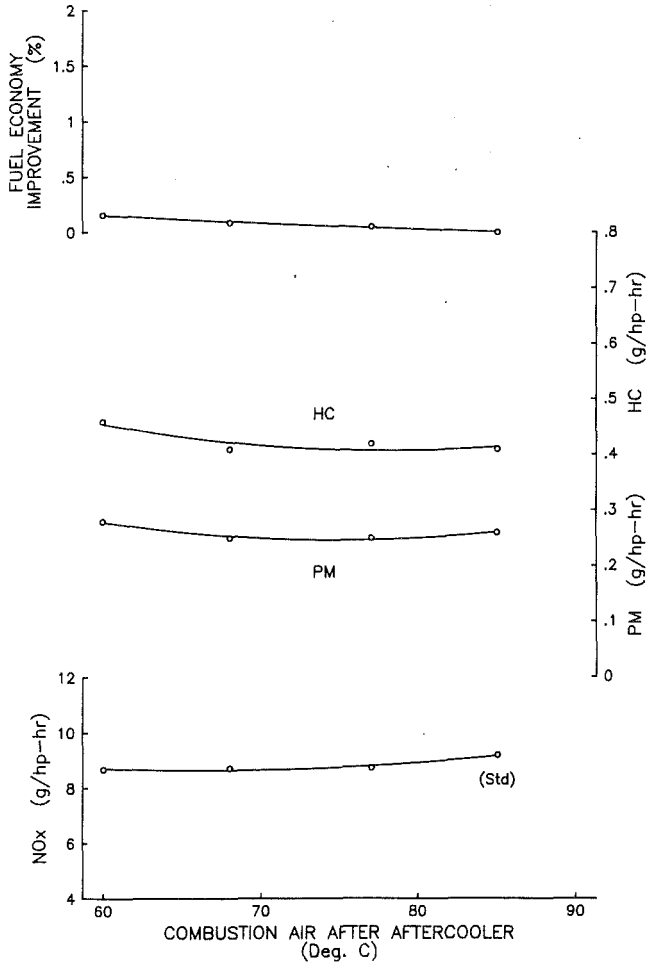

Fig. 5 The effect of aftercooler water temperature on emissions and fuel economy for a GE 12-7FDL locomotive engine with 4 deg retarded timing

of these tests are given in Table 6. The data indicate that at the standard injection timing, the low-sulfur, low-aromatic fuel did not significantly affect particulate emissions for either engine. This result is similar to results obtained in original baseline emission test work performed in 1989 using a very low sulfur fuel (0.01 wt. percent) [1]. However, when timing was retarded 4 deg, and enhanced aftercooling was in use, the low-sulfur, low-aromatic fuel was effective in reducing particulate emissions for both the EMD and GE engines.

The fuel penalty given in Table 6 represents any observed change in the engine brake specific fuel consumption, and the effect of the energy per unit volume difference of the low-sulfur, low-aromatic fuel compared to the baseline diesel fuel. Referring to Table 3, this difference is significant, with the low-sulfur, low-aromatic fuel having 3.5 percent less energy per gallon than the baseline fuel.

Discussion/Summary

One of the locomotive exhaust emissions reduction recommendations presented in the CARB Locomotive Emissions Study [2] was to use the combined implementation of a 4 deg injection timing retard and the use of a low-sulfur, high-cetane diesel fuel for yard and switcher locomotives. The experimental efforts described above were an attempt to quantify the emissions and fuel economy changes associated with performing these recommended modifications. Based on the laboratory

Table 6 The effect of low-sulfur, low-aromatic fuel on locomotive engine exhaust emissions

	PM (g/hp-hr)	HC (g/hp-hr)	CO (g/hp-hr)	NO_x (g/hp-hr)	Fuel Penalty (%)
EMD 12-645 E3B					
Baseline Fuel, Std. Timing	0.15	0.29	0.81	10.5	---
Low Aromatic Fuel, Std. Timing	0.17	0.33	0.83	10.4	3.5[a]
Baseline Fuel, 4° Retard, Enhanced Aftercooling	0.23	0.38	0.92	8.0	0.4[b]
Low Aromatic Fuel, 4° Retard, Enhanced Aftercooling	0.19	0.33	1.02	7.2	4.3[c]
GE 12-7FDL					
Baseline Fuel, Std. Timing	0.19	0.42	1.98	11.2	---
Low Aromatic Fuel, Std. Timing	0.18	0.36	1.87	9.9	3.5[a]
Baseline Fuel, 4° Retard, Enhanced Aftercooling	0.26	0.41	1.91	9.2	1.2[b]
Low Aromatic Fuel, 4° Retard, Enhanced Aftercooling	0.20	0.36	2.04	7.6	4.2[c]

Notes: All emissions are three-mode weighted composite.
a - Reflects btu/gallon difference only.
b - Reflects bsfc difference only.
c - Reflects bsfc and btu/gallon difference.

testing performed in this work, the following results can be expected by combining 4 deg injection timing retard; the use of a low-sulfur, low-aromatic (and high cetane); and enhanced aftercooling:

EMD 645 E3B:
- NO_x reduced 31 percent.
- Particulate increased 27 percent.
- CO increased 26 percent.
- HC increased 14 percent.
- Fuel consumption increased 4.3 percent.

GE 7FDL
- NO_x reduced 32 percent.
- Particulate increased 5 percent.
- CO increased 9 percent.
- HC decreased 12 percent.
- Fuel consumption increased 4.2 percent.

Inspection of these data shows that significant changes to emissions and fuel consumption can be expected by implementing the changes recommended in the CARB study. One important finding is that the two major locomotive engine types respond differently to the modifications. Although NO_x was reduced, other emissions increased. Therefore, emissions and fuel penalty trade-offs must be considered before proceeding with modifications for lower NO_x emissions alone.

Future Work

A standardized test procedure for measuring locomotive engine emissions does not exist. Recognizing that a formal duty-cycle based test procedure for measuring gaseous and particulate locomotive emissions *must* be established, the AAR has initiated an industry working group to establish these procedures. The working group is made up of representatives from EMD, GE, Caterpillar, AAR, and SwRI. It is anticipated that the standardized test procedure that evolves will be recognized by the locomotive engine manufacturers and will be adopted as an AAR Recommended Practice. This will ensure that future locomotive emissions are measured and reported in a consistent manner.

During the 1991 AAR research program, additional efforts will be made toward reducing exhaust emissions from locomotive engines. Studies will include determining the applica-

bility of existing NO_x correction factors for ambient air temperature and humidity; assessing the contribution of lubricating oil consumption to particulate emissions; further evaluating fuel effects on emissions; and evaluating various engine hardware configurations for emissions effects.

Acknowledgments

The AAR Phase XII Diesel Fuel Specification and Locomotive Improvement Program was performed at Southwest Research Institute for the Association of American Railroads. The AAR Project Technical Monitor was Mr. G. Richard Cataldi. Guidance for the Program was provided by the AAR Locomotive Efficiency Review Committee and the AAR Energy and Locomotive Program Steering Committee comprised of individuals from the member railroads of the AAR and locomotive manufacturers.

References

1 Fritz, S. G., and Cataldi, G. R., "Gaseous and Particulate Emissions From Diesel Locomotive Engines," *New Technology in Large Bore Engine*, ASME ICE-Vol. 13, B. Chrisman, ed., Oct. 1990, pp. 63-72.

2 "Locomotive Emissions Study," by Booz-Allen & Hamilton, Final Report for the California Air Resources Board, Jan. 1991.

3 "Management Plan for Nitrogen Oxides (NO_x) and Volatile Organic Compounds (VOCs)—Phase I," Canadian Council of Ministers of the Environment, CCME-EPC/TRE-31E, Nov. 1990.

4 "SP-AAR Program to Develop Certification Procedures With Respect to Visible Emissions From New and Out-Shopped Locomotives," SP Final Report, Aug. 1973.

5 Hoffman, J. G., Springer, K. J., and Tennyson, T. A., "Four Cycle Diesel Electric Locomotive Exhaust Emissions: A Field Study," ASME Paper No. 75-DGP-10, Apr. 1975.

6 Hare, C. T., and Springer, K. J., "Exhaust Emissions From Uncontrolled Vehicles and Related Equipment Using Internal Combustion Engines: Part 1—Locomotive Diesel Engines and Their Marine Counterparts," SwRI Report No. 11-2869-001, 1972.

7 Storment, J. O., and Springer, K. J., "Assessment of Control Techniques for Reducing Emissions From Locomotive Engines," SwRI Report No. AR-844, Apr. 1973.

8 Hare, C. T., Springer, K. J., and Huls, T. A., "Locomotive Exhaust Emissions and Their Impact," ASME Paper No. 74-DGP-3, May 1974.

9 Storment, J. O., Springer, K. J., and Hergenrother, K. M., "NO_x Studies With EMD 2-567 Diesel Engine," ASME Paper No. 74-DGP-14, May 1974.

10 Springer, K. J., and Davis, O. J., "Studies of NO_x Emissions From a Turbocharged Two-Stroke Cycle Diesel Engine," SwRI Report No. 11-2869-003, Oct. 1975.

11 Conlon, P. D., "Exhaust Emission Testing of In-Service Diesel-Electric Locomotives—1981 to 1983," AAR Report No. R-688, Mar. 1988.

12 Baker, Q. A., et al., "Alternative Fuels for Medium-Speed Diesel Engines Program, Fourth Research Phase Final Report," SwRI Report No. 03-7446-001, AAR Report No. R-569, Feb. 1984.

13 Wakenell, J. F., et al., "Alternative Fuels for Medium-Speed Diesel Engines Program, Fifth Research Phase Final Report," SwRI Report No. 03-7924, AAR Report No. R-602, Apr. 1985.

14 Wakenell, J. F., et al., "Alternative Fuels for Medium-Speed Diesel Engines Program, Sixth Research Phase Final Report," SwRI Report No. 03-8469, AAR Report No. R-615, Oct. 1986.

15 Wakenell, J. F., et al., "Diesel Fuel Specification and Locomotive Improvement Program, Eight Research Phase Final Report," SwRI Report No. 03-1542, AAR Report No. R-697, Dec. 1987.

16 Fritz, S. G., et al., "Diesel Fuel Specification and Locomotive Improvement Program, Ninth Research Phase Final Report," SwRI Report No. 03-2082, AAR Report No. R-731, Aug. 1989.

17 Fritz, S. G., et al., "Diesel Fuel Specification and Locomotive Improvement Program, Tenth Research Phase Final Report," SwRI Report No. 03-2695, AAR Report No. R-771, Dec. 1989.

18 Markworth, V. O., et al., "Diesel Fuel Specification and Locomotive Improvement Program, Eleventh Research Phase Final Report," SwRI Draft Final Report No. 03-3324, June 1991.

APPENDIX

Locomotive Engine Emissions Test Summary

GE 12-7FDL Emissions Data								
	Fuel Type	Timing Retard (Deg)	Boost Air Temp. (°C)	BSPM (g/hp-hr)	BSHC (g/hp-hr)	BSCO (g/hp-hr)	$BSNO_x$ (g/hp-hr)	Power/Fuel Loss (%)
Baseline	Baseline	0	85	0.19	0.42	2.0	11.2	0.0
4° Retard	Baseline	4	85	0.26	0.41	1.9	9.2	1.2[b]
8° Retard	Baseline	8	85	0.39	0.49	2.2	7.2	3.2[b]
12° Retard	Baseline	12	85	0.51	0.72	2.6	5.8	6.2[b]
Baseline - Low Aromatic Fuel	Low Aromatic	0	85	0.18	0.36	1.9	9.9	3.5[a]
Enhanced Aftercooling (4° Retard)								
85°C - Standard Condition	Baseline	4	85	0.26	0.41	1.9	9.2	0.0[b]
77°C	Baseline	4	77	0.25	0.42	1.9	8.7	0.1[b]
68°C	Baseline	4	68	0.25	0.41	2.0	8.7	0.2[b]
60°C	Baseline	4	60	0.28	0.46	2.0	8.7	0.3[b]
4° Retard, Low Aromatic, Enhanced Aftercooling	Low Aromatic	4	60	0.20	0.36	2.0	7.6	4.2[a]

Notes: a - Reflects bsfc changes and fuel btu/gallon differences.
b - Reflects only bsfc difference.

EMD 12-645E3B Emissions Data								
	Fuel Type	Timing Retard (Deg)	Boost Air Temp. (°C)	BSPM (g/hp-hr)	BSHC (g/hp-hr)	BSCO (g/hp-hr)	$BSNO_x$ (g/hp-hr)	Power/Fuel Loss (%)
Baseline	Baseline	0	99	0.15	0.29	0.81	10.5	0.0
2° Retard	Baseline	2	99	0.25	0.33	0.77	9.5	0.4[b]
4° Retard	Baseline	4	99	0.24	0.40	0.85	8.9	1.3[b]
6° Retard	Baseline	6	99	0.25	0.40	0.95	8.0	2.1[b]
Baseline - Low Aromatic Fuel	Low Aromatic	0	99	0.17	0.33	0.83	10.4	3.5[a]
Enhanced Aftercooling (4° Retard)								
99°C - Standard Condition	Baseline	4	99	0.24	0.40	0.85	8.9	0.0[b]
91°C	Baseline	4	91	0.25	0.38	0.95	8.1	0.2[b]
82°C	Baseline	4	82	0.23	0.38	0.92	8.0	0.3[b]
74°C	Baseline	4	74	0.23	0.39	0.93	7.9	0.4[b]
4° Retard, Low Aromatic, Enhanced Aftercooling	Low Aromatic	4	82	0.19	0.33	1.0	7.2	4.3[a]

Notes: a - Reflects bsfc changes and btu/gallon differences.
b - Reflects only bsfc difference.

Electrically Heated Catalysts for Cold-Start Emission Control on Gasoline- and Methanol-Fueled Vehicles

M. J. Heimrich
Department of Emissions Research,
Southwest Research Institute,
San Antonio, TX 78228

S. Albu
State of California
Air Resources Board,
El Monte, CA 91731

M. Ahuja
State of California
Air Resources Board,
Sacramento, CA 95814

Cold-start emissions from current technology vehicles equipped with catalytic converters can account for over 80 percent of the emissions produced during the Federal Test Procedure (FTP). Excessive pollutants can be emitted for a period of one to two minutes following cold engine starting, partially because the catalyst has not reached an efficient operating temperature. Electrically heated catalysts, which are heated prior to engine starting, have been identified as a potential strategy for controlling cold-start emissions. This paper summarizes the emission results of three gasoline-fueled and three methanol-fueled vehicles equipped with electrically heated catalyst systems. Results from these vehicles demonstrate that heated catalyst technology can provide FTP emission levels of nonmethane organic gases (NMOG), carbon monoxide (CO), and oxides of nitrogen (NO_x) that show promise of meeting the Ultra-Low Emission Vehicle (ULEV) standards established by the California Air Resources Board.

Introduction

Cold-start emissions are recognized as the greatest contributor to Federal Test Procedure (FTP) emissions for both gasoline- and methanol-fueled vehicles. Seventy to eighty percent of FTP exhaust emissions from current-technology vehicles are typically emitted during the first minute of cold operation. This is because the catalyst is too cold to be active during this period. One strategy to control cold-start emissions is to heat the catalyst electrically prior to cold starting the engine. Other strategies that have been researched include cold-start emission collection, close-coupled catalysts (close to the exhaust manifold), advanced catalyst formulations, and latent heat storage devices [1, 2]. This paper will review the electrically heated catalyst strategy for cold-start emission control and the California initiative to lower exhaust emission standards.

The State of California recently adopted new motor vehicle emission standards for 1994 and beyond [3]. These standards include limits for nonmethane organic gases (NMOG), carbon monoxide (CO), oxides of nitrogen (NO_x), and formaldehyde (HCHO). Nonmethane organic gases consist of all measurable reactive hydrocarbons (HC) and are defined as nonmethane hydrocarbons (NMHC), aldehydes and ketones, and alcohols containing 12 or fewer carbon atoms [4]. Table 1 provides certification emission standards for designated transitional low emission vehicles (TLEVs), low-emission vehicles (LEVs), and ultra-low-emission vehicles (ULEVs). Zero-emission vehicles (ZEVs) are a fourth category and produce no emissions of any pollutant. These standards were adopted in September of 1990.

Table 1 California exhaust emission standards for light-duty vehicles

Vehicle Category	Exhaust Emissions, g/ml			
	NMOG	CO	NO_x	HCHO
Adopted for 1993	0.250	3.4	0.40	--
TLEV	0.125	3.4	0.40	0.015
LEV	0.075	3.4	0.20	0.015
ULEV	0.040	1.7	0.20	0.008
TLEV, LEV, ULEV Standards Adopted September 1990				

The California Air Resources Board has sponsored research on several electrically heated catalyst applications at the Southwest Research Institute (SwRI). In two separate emission control studies, both gasoline- and methanol-fueled vehicles were modified by incorporating advanced catalyst technologies. One of the common objectives of these studies was to reduce the quantity of total organic gas emissions through the development of a total emission control system, without sacrificing control of other pollutants. The continued control of NO_x emissions was of special interest because of the NO_x contribution to smog formation.

A summary of the emission results from three gasoline-fueled vehicles and three methanol-fueled vehicles equipped with electrically heated catalysts systems is presented. The gas-

Contributed by the Internal Combustion Engine Division and presented at the 13th Annual Fall Technical Conference, Muskegon, Michigan, September 30–October 2, 1991. Manuscript received by the Internal Combustion Engine Division September 29, 1991. Associate Technical Editor: J. A. Caton.

oline-fueled vehicles were a 1986 Toyota Camry, a 1990 Buick LeSabre, and a 1990 Toyota Celica. The methanol-fueled vehicles selected for electrically heated catalyst application studies were a hybrid 1981 Ford Escort equipped with a 1983 methanol-fueled engine, a 1988 Chevrolet Corsica VFV, and a 1989 Ford Crown Victoria FFV. Emissions data generated by these vehicles have been used to demonstrate the feasibility of recent California low-emission vehicle standards.

Background

A cold start is defined in the Code of Federal Regulations (CFR) as an engine start following a 12- to 36- hour continuous vehicle soak in a constant temperature environment of 20°C to 30°C [5]. Electrically heated catalysts have been developed to assist conventional catalysts with cold-start emission control. An electrically heated catalyst is an automotive exhaust catalyst with an electrically conductive support. Electric current from the vehicle battery *directly* heats the catalyst support. Because the heated catalyst is hot prior to engine cranking, catalytic activity is possible and cold-start emissions can be controlled.

To initiate the catalyst heating sequence on today's demonstration vehicles, the ignition switch is placed in the "on" position. The driver then waits to start the engine while the catalyst is being heated. When the catalyst has reached a predetermined light-off temperature, the driver starts the engine. These heated catalyst systems modulate electrical power to the catalyst if the bed temperature drops below the light-off temperature. Additional electrical power is supplied to the catalyst for only a short time following the engine start. Typically, post-start heating continues for 10 to 50 seconds following a cold start and for less time following a hot start.

In a internal research study conducted by SwRI, a gasoline-fueled vehicle was equipped with an electrically heated catalyst. This study produced the initial finding that heating alone did not significantly improve emission control over an unheated catalyst test [1, 6]. With only electrical heating, cold-start catalyst activity was still impaired because of a lack of oxygen in the exhaust. In many vehicle fuel system calibrations, a cold engine is run fuel-rich to maintain drivability. Rich fuel-air ratios result in insufficient oxygen levels in the raw exhaust, limiting the oxidation of organic gases and CO.

To overcome this oxygen deficiency, secondary air was added for the conversion of organic gases and CO to carbon dioxide (CO_2) and water (H_2O). Pumps were used to inject air ahead of the heated catalyst following cold engine starting. On some vehicles, a short period of air injection following the hot start was beneficial. Emissions of NO_x cannot be controlled in the presence of excess oxygen. This lack of control occurs because oxygen-rich environments do not provide a suitable environment for the chemical reduction of NO_x. For this reason, short air injection periods are favored to maintain NO_x emission control. In the heated catalyst applications described in this paper, carefully defined air injection strategies were identified to minimize increases of NO_x emissions.

Gasoline-Fueled Vehicle Heated Catalyst Applications

Three gasoline-fueled vehicles were equipped with electrically heated catalyst systems at SwRI. These vehicles were a 1986 Toyota Camry, a 1990 Buick LeSabre, and a 1990 Toyota Celica. A summary of these heated catalyst installations and emission improvements is presented for each vehicle.

1986 Toyota Camry. A gasoline-fueled 1986 Toyota Camry was obtained for an electrically heated catalyst research study [1,6]. This vehicle was equipped with a 2.0 liter engine, electronic port fuel injection, and a three-way (only) catalytic converter. The original underbody stock catalyst was removed and replaced with an electrically heated catalyst, a three-way formulation designed as a total replacement for the stock catalyst. At the start of the heated catalyst research, this vehicle had almost 35,400 km (22,000 mi) on the odometer.

The electrically heated catalyst used on this vehicle was composed of two separate sections. The larger downstream section was a metal substrate catalyst without heating capability, while the smaller upstream section was a catalyzed metal substrate with the ability to be heated electrically. Figure 1 shows a schematic of this electrically heated catalyst. The electrically heated catalyst underwent 805 km (500 mi) of service accumulation on the Camry prior to experimentation. A photograph of the actual electrically heated catalyst unit is given in Fig. 2.

The Toyota Camry underwent several cold-start FTP experiments in order to determine the optimal air injection flow rate and duration. Air was injected ahead of the heated catalyst at a rate of 140 liters per minute (5.0 cubic feet per minute) for the first 140 seconds of the cold-start portion of the FTP. An off-vehicle electrically driven air pump was used for injecting air ahead of the heated catalyst. Standard catalyst heat-

Nomenclature

ARB = State of California Air Resources Board
CFM = cubic feet per minute
CFR = Code of Federal Regulations
CO = carbon monoxide
CO_2 = carbon dioxide
CRC = Coordinating Research Council
°C = degrees Celsius
EHC = electrically heated catalyst
EPA = United States Environmental Protection Agency
FFV = Flexible Fuel Vehicle produced by Ford Motor Company
FTP = EPA Federal Test Procedure
g/mi = grams per mile
HC = hydrocarbons
HCHO = formaldehyde
H_2O = water
km = kilometer
L = liters
LEV = low-emission vehicle
L/min = liters per minute
mi = mile
M85 = fuel consisting of 85 percent methanol and 15 percent gasoline
M90 = fuel consisting of 90 percent methanol and 10 percent gasoline
NMHC = nonmethane hydrocarbons
NMOG = nonmethane organic gases
NO_x = oxides of nitrogen
O_2 = oxygen
SAE = Society of Automotive Engineers
s = second
SwRI = Southwest Research Institute
TLEV = transitional low-emission vehicle
ULEV = ultra-low-emission vehicle
VFV = variable fuel vehicle produced by General Motors Company
V-6 = 6-cylinder engine with "V" configuration
V-8 = 8-cylinder engine with "V" configuration
w/ = with

ing times were established. Electrical heating was performed for 15 seconds before and for 30 seconds after the cold start. For hot starts, heating times were 5 seconds before and 10 seconds after hot cranking. Catalyst temperatures typically reached 500°C to 600°C prior to engine starting.

Federal Test Procedure emission tests were performed on the Camry with different combinations of catalyst heating and air injection. As described in [6], optimal heated catalyst performance occurred with both catalyst preheating *and* secondary air injection. These emissions results are compared to no-heat-no-air baseline emissions in Table 2. Significant reductions in NMHC and CO were obtained with the air-injected heated catalyst. Emissions of NO_x increased only slightly because of the secondary air.

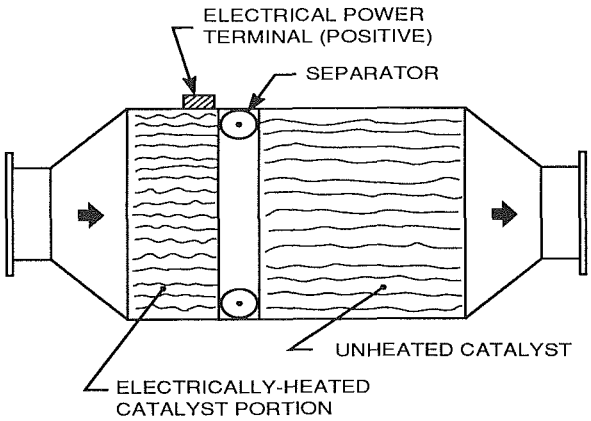

Fig. 1 Schematic of electrically heated catalyst used on Toyota Camry

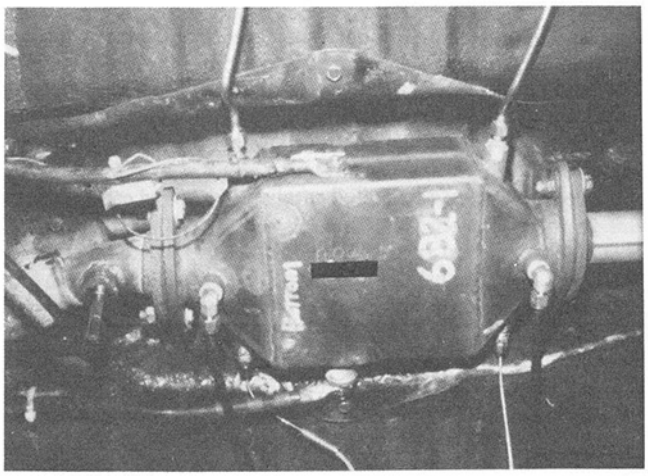

Fig. 2 Electrically heated catalyst on Toyota Camry

Table 2 Toyota Camry heated catalyst emissions compared to baseline

Catalyst Configuration	FTP Emissions, g/mi		
	NMHC	CO	NO_x
Baseline	0.12	1.13	0.22
EHC w/Air	0.03	0.38	0.25
Air Injection: 140 L/min, 140 sec. for cold-start. Baseline: Camet catalyst without heat nor air.			

1990 Buick LeSabre. A new 1990 Buick LeSabre equipped with a three-way underbody catalyst and a port fuel injected 3.8 liter engine was outfitted with a heated catalyst system for the California Air Resources Board [1, 7]. The electrically heated catalyst was mounted just ahead of the underbody production catalyst, as shown in Fig. 3. An electric air pump was mounted under the hood. An aftermarket battery with more energy capacity replaced the original battery. The heated catalyst power controller was mounted inside the vehicle.

A series of developmental air injection experiments was performed to determine the optimal air injection strategy. Cold-start and hot-start air injection strategies were investigated using the laboratory air injection pump. After several FTP emission tests, an air injection flow rate of 300 liters per minute (10.7 cubic feet per minute) was determined to be optimum. Cold-start air injection began as the engine cranked and continued for 75 seconds. Hot-start air injection began as the engine cranked and continued for 30 seconds.

Electrical heating of the catalyst on the Buick LeSabre was regulated by the on-vehicle power controller. This controller was programmed to maintain the catalyst bed above a temperature of 370°C. A thermocouple inside the heated catalyst provides a temperature feedback to the power controller. When the catalyst underwent prestart heating, the power controller heated the catalyst until the catalyst reached the programmed temperature. At this time this engine was started. After the engine started, the catalyst was electrically heated (as needed) to maintain the programmed temperature. The catalyst temperature was monitored by the controller for a period of up to three minutes following a hot or cold start, after which no additional electrical heating occurred.

Electrically heated catalyst emission test results are compared to the Buick stock catalyst emissions in Table 3. Emissions of NMHC and CO were reduced significantly while NO_x emissions were unchanged. Fuel economy decreased slightly due to additional (on-vehicle) battery recharging following the heating sequence.

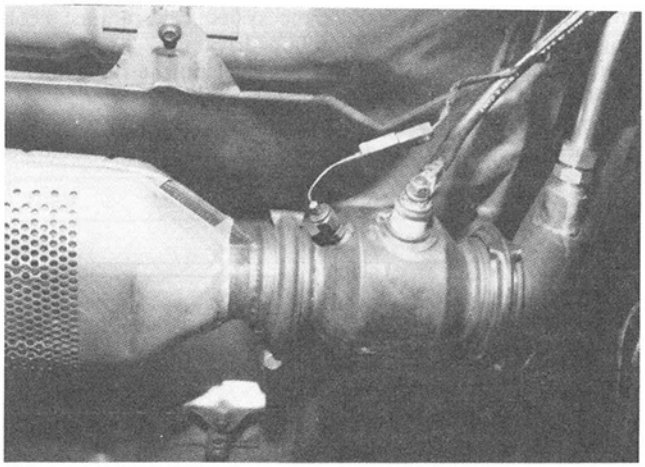

Fig. 3 Electrically heated catalyst mounted in front of production catalytic converter for Buick LaSabre

Table 3 Buick LeSabre heated catalyst emissions compared to stock

Catalyst Configuration	FTP Emissions, g/mi			Fuel Economy, mi/gal
	NMHC	CO	NO_x	
Stock (typical)	0.15	1.36	0.18	20.2
EHC w/air	0.02	0.25	0.18	19.7
Air Injection: 300 L/min; 75 sec. for cold-start, 30 sec. for hot-start.				

1990 Toyota Celica. An electrically heated catalyst system was also applied to a new 1990 Toyota Celica [1,7]. The Celica, shown in Fig. 4, was factory-equipped with a close-coupled catalytic converter plus a relatively small underbody catalyst. There was no air injection for the original catalyst configuration. This vehicle provided an opportunity to study the emission control potential of an electrically heated catalyst located downstream of a close-coupled catalyst. In this downstream location, the electrically heated catalyst would be expected to operate at lower overall temperatures than if located first in the exhaust stream. Long-term durability for the heated catalyst in this downstream location may be enhanced in this cooler location.

The close-coupled production catalyst was found to absorb engine exhaust heat, which caused the downstream electrically heated catalyst to warm up very slowly. Difficulties in maintaining the desired electrically heated catalyst temperature caused extended post-start heating times and contributed to increased engine emissions (because of the increased battery recharging load on the alternator).

The application of electrically heated catalyst technology to the Celica underwent several stages of optimization. Optimum air injection was determined to be 20 seconds following the cold-start and zero (no air injection) following the hot start. Post-start catalyst electrical heating was limited to 20 seconds in order to minimize battery discharge and subsequent recharging (energy replacement).

Toyota Celica emissions are given in Table 4 and show improved control of NMHC and CO, similar to other heated catalyst applications. For this application, the reduction in FTP NO_x emissions can be attributed to a relatively large heated catalyst volume [1,7]. The reduced post-start heating time contributed to a minimal fuel economy penalty, as compared to the extended heating times previously used. An in-depth analysis of this heated catalyst application is given in [7].

Fig. 4 1990 Toyota Celica

Table 4 Toyota Celica heated catalyst emissions compared to stock

Catalyst Configuration	FTP Emissions, g/mi			Fuel Economy, mi/gal
	NMHC	CO	NO_x	
Stock (typical)	0.09	0.68	0.08	25.6
EHC w/air	0.03	0.40	0.05	25.5

Air Injection: 300 L/min; 20 sec. for cold-start, no air for hot-start.
Post-start heating limited to 20 sec., no hot-start heating.

Methanol-Fueled Vehicle Heated Catalyst Applications

Three methanol-fueled vehicles were equipped with electrically heated catalyst systems. These vehicles were a 1981 Ford Escort (with a 1983 engine), a 1988 Chevrolet Corsica VFV, and a 1989 Ford Crown Victoria FFV. The Escort and Crown Victoria used air injection strategies that were incorporated in their original emission control system. The Corsica used the off-vehicle (laboratory) air injection pump for emissions testing. A summary of these heated catalyst applications is presented for each vehicle.

1981 Ford Escort. A 1981 Ford Escort was used to demonstrate electrically heated catalyst feasibility as part of an investigation into formaldehyde emission control for methanol-fueled vehicles [8]. The Escort had a 1.6 liter high-output methanol-fueled engine (1983 version). This engine was equipped with a carburetor and calibrated to run on M90 fuel (90 percent methanol, 10 percent gasoline).

Four manufacturer-supplied catalyst formulations were evaluated for formaldehyde emission control for the California Air Resources Board. Three of the four catalysts screened were conventional (nonelectrically heated) catalysts. The electrically heated catalyst was similar to the one used on the 1986 Toyota Camry. The catalyzed, heated metal substrate was located upstream of an unheated metal substrate catalyst within the same container. All four sample catalysts (each with different formulations) were designed and tested as a total underbody catalyst replacement. These catalysts represented current methanol catalyst technology.

For this discussion, two of the catalysts evaluated were selected for comparison. One was the electrically heated catalyst. The other was a conventional three-way plus oxidation catalyst with air injection between the pieces. This catalyst was selected because it demonstrated the best overall performance of the conventional catalysts.

Air injection and catalyst heating strategies were defined for the Escort. Cold-start secondary air was obtained using the air injection system from the preconversion (gasoline) 1981 Escort. Secondary air was delivered to the exhaust manifold (upstream of the electrically heated catalyst). The original on-vehicle air injection system was not optimized for this application. Fixed catalyst heating times were established for the Escort. For cold starts, the catalyst was heated for 15 seconds prior to engine starting. There was no hot-start catalyst preheating [8].

Emission tests were run on the Ford Escort with the methanol catalysts. Methanol and formaldehyde emissions were measured and used to calculate NMOG. A comparison between the electrically heated catalyst and the baseline FTP emission tests is given in Table 5. Formaldehyde, methanol, gasoline-derived hydrocarbons, and CO are primarily emitted during cold-start operation [8]. Generally, the electrically heated catalyst was

Table 5 Methanol Ford Escort heated catalyst emissions compared to baseline

Catalyst Configuration	Fuel	FTP Emissions, g/mi			
		NMOG	CO	NO_x	HCHO
Baseline	M90	0.44	2.12	0.38	0.0093
EHC w/Air	M90	0.10	1.85	0.46	0.0075

Air Injection: Escort production air injection strategy.
NMOG = Gasoline-derived hydrocarbons + methanol + formaldehyde - methane.
NMOG calculation uses stock catalyst FTP emissions of 0.04 g/mi methane.
Each value is the average of two emission measurements.

able to control formaldehyde, methanol, and CO emissions during the cold-start better than the other experimental catalysts used in this program, indicating that catalyst preheating and air injection made a significant improvement in cold-start emission control. This vehicle, however, still exhibited relatively high emissions of NMOG, probably because of its fuel system configuration and a limited heated catalyst optimization.

1988 Chevrolet Corsica VFV. A 1988 Chevrolet Corsica VFV was selected for study in a formaldehyde emission control program by the California Air Resources Board [8]. This variable fuel vehicle (VFV) could be run on any mixture of M85 fuel and gasoline. The Corsica was originally equipped with a 2.8 liter V-6 engine, port fuel injection, and an underbody three-way catalyst. The Corsica odometer displayed 3200 km (2,000 mi) at the time of the heated catalyst application.

The Corsica VFV was equipped with a laboratory electrically heated catalyst at SwRI. This catalyst system was similar to the one installed on the LeSabre and Celica, except that an off-vehicle battery and air pump were used. Corsica emissions with the production three-way catalyst are compared to electrically heated catalyst emissions in Table 6. Both emissions of NMOG and CO were reduced significantly. Even NO_x emissions were reduced moderately. Cold-start methanol and formaldehyde emission reductions contributed to lower FTP emissions with the heated catalyst and air injection [8]. Fuel economy figures were not compared on the Corsica because an off-vehicle battery (without recharging) was used to preheat the catalyst.

1989 Ford Crown Victoria FFV. A 1989 Ford Crown Victoria FFV was selected to study emissions from advanced technology methanol-fueled vehicles [8]. This flexible fuel vehicle (FFV) was capable of running on any mixture of gasoline and M85 fuel. The Crown Victoria was originally equipped with a close-coupled three-way catalyst and an underbody oxidation catalyst in each exhaust bank of a V-8 (5.0 liter) engine (for a total of four catalysts: two close-coupled and two underbody).

The Crown Victoria was modified by SwRI with an electrically heated catalyst system for laboratory emission demonstration tests. Electrically heated catalysts were placed in each exhaust bank upstream of the original underbody catalysts. Cold-start air injection was provided by the original-equipment secondary air pump (designed for the stock catalyst application). This air injection pump provided air ahead of the heated catalyst during cold-start operation and directly to the downstream oxidation catalyst afterward.

Emissions from both the heated and stock catalyst configurations, both running on M85 fuel, are given in Table 7. Significant improvements in NMOG and CO emissions were obtained with the heated catalyst system; however, NO_x emissions were similar to the baseline. Methanol emissions were reduced to undetectable levels with the heated catalyst configuration [8].

Table 6 Chevrolet Corsica VFV heated catalyst emissions compared to stock

Catalyst Configuration	Fuel	FTP Emissions, g/mi			
		NMOG	CO	NO_x	HCHO
Stock	M85	0.128	1.75	0.25	0.0213
EHC w/air	M85	0.03	0.40	0.17	0.0036

Air Injection: 100 sec for cold-start, 100 sec. for hot-start.
NMOG = gasoline-derived hydrocarbons + methanol + formaldehyde - methane.

Table 7 Ford Crown Victoria FFV heated catalyst emissions compared to stock

Catalyst Configuration	Fuel	FTP Emissions, g/mi			
		NMOG	CO	NO_x	HCHO
Stock	M85	0.13	0.72	0.53	0.0090
EHC w/air	M85	0.01	0.23	0.52	0.0012

Air Injection: Crown Victoria production air injection strategy.
EHC located in each exhaust bank of V-8.
NMOG = gasoline-derived hydrocarbons + methanol + formaldehyde - methane.

Summary

Electrically heated catalyst applications on three gasoline-fueled vehicles and three methanol-fueled vehicles have been reviewed. Based on the results of these experiments, the electrically heated catalyst with air injection has shown itself to be potentially capable of meeting future California emission standards. These heated catalyst systems, however, were unaged and were applied in a laboratory setting. Research into heated catalyst durability has begun [9]. In addition, four of the vehicles converted with heated catalyst emission control systems described in this paper will undergo on-road service accumulation by the State of California. Follow-up studies on these vehicles and data from other roadworthy fleets should provide insight into more durable and reliable heated catalyst systems.

Disclaimer

The statements and conclusions in this report are those of the authors and not necessarily those of the California Air Resources Board. The mention of commercial products, their sources, or their use in connection with material reported herein is not to be construed as either an actual or implied endorsement of such products.

Acknowledgments

This paper is based on work performed by the Department of Emissions Research at Southwest Research Institute under ARB Contract No. A6-204-32, "Control of Benzene Emissions From Light-Duty Motor Vehicles," and ARB Contract No. A732-148, "Formaldehyde Emission Control Technology for Methanol-Fueled Vehicles." Initial air injection research was performed in the SwRI Internal Research Study, "Experimentation to Determine the Feasibility of Air Injection on an Electrically Heated Catalyst for Reducing Cold-Start Benzene Emissions From Gasoline Vehicles," SwRI Project No. 08-9574. Use of the methanol-fueled Ford Escort was donated to SwRI and the ARB by the Coordinating Research Council (CRC). The electrically heated catalysts were provided by Camet Co. of Hiram, Ohio. The authors would like to recognize Juan Osborn and Sarah Santoro of the ARB and Lawrence Smith and Matthew Newkirk of SwRI for their contributions to the success of these programs.

References

1 Heimrich, M. J., "Control of Benzene Emissions From Light-Duty Motor Vehicles," Final Report for the State of California Air Resources Board, Contract No. A6-204-32, Release Date: June 1991.

2 Schatz, O., "Cold-Start Improvements With a Heat Store," SAE Paper No. 910305, 1991.

3 Staff Report, "Proposed Regulations for Low-Emission Vehicles and Clean Fuels," prepared by the State of California Air Resources Board, Mobile Source and Stationary Source Divisions, Release Date: Aug. 13, 1990.

4 Technical Support Document for "A Proposal to Amend Regulations Re-

garding Exhaust Emission Standards and Test Procedures for Passenger Cars, Light-Duty Trucks, and Medium-Duty Vehicles for the Control of Criteria Pollutant and Toxic Air Contaminant Emissions," by the State of California Air Resources Board, Mobile Source Division, Draft, Apr. 23, 1990.

5 Code of Federal Regulations, Title 40, Chap. 1, Part 86, Subpart B, Sections applicable to light-duty vehicles.

6 Heimrich, M. J., "Air Injection to an Electrically-Heated Catalyst for Reducing Cold-Start Benzene Emissions From Gasoline Vehicles," SAE Paper No. 902115, 1990.

7 Heimrich, M. J., Albu, S., and Osborn, J., "Electrically-Heated Catalyst System Conversions on Two Current-Technology Vehicles," SAE Paper No. 910612, 1991.

8 Current SwRI program, "Formaldehyde Emission Control Technology for Methanol-Fueled Vehicles," conducted by the Department of Emissions Research for the California Air Resources Board, Contract No. A732-148, SwRI Project 08-2346, 1991.

9 Whittenberger, W. A., and Kubsh, J. E., "Electrically Heated Metal Substrate Durability," SAE Paper No. 910613, 1991.

Coal-Fueled Diesel Engine Development Update at GE Transportation Systems

B. D. Hsu
General Electric Transportation Systems,
Erie, PA 16531

The U.S. Department of Energy is sponsoring a General Electric Company development program for using coal–water slurry (CWS) to power a diesel engine and to test it in a locomotive. The first locomotive system test was successfully completed in 1991 on GE/TS test track. The first-phase coal-fueled 12-cylinder diesel engine used in the locomotive test employed a modified positive displacement fuel injection system and developed 2500 hp in the engine laboratory. The final phase all electric controlled fuel injection equipment (FIE) diesel engine has completed individual component development phases. Combustion research evaluated a broad range of CWS fuels with different source coals, particle sizes, and ash contents. The electronic controlled FIE single cylinder test engine yielded 99.5 percent combustion efficiency. Envelop filters and copper oxide sorbent have been chosen to clean up the engine emissions after extensive evaluation of various hot gas cleaning methods. The projected removal rate of particulate is 99.5 percent and that of SO_2 is 90 percent. Over ten diamond insert injector nozzles performed well on the test engines. A bench test of one nozzle has been run for over 500 engine equivalent hours without significant wear. Tungsten carbide (WC) coated piston rings and cylinder liners were identified to be effective in overcoming power assembly wear. A matrix of WC spray parameters were investigated, and the best process was used to apply coatings onto full scale rings and liners. These and other test parts are currently running in two coal fuel operated cylinders on a converted eight-cylinder endurance test engine. All of these developed technologies will be applied onto the second phase engine and be used in the final phase locomotive test. An economic analysis was also completed on a concept locomotive design. Additional equipment cost and the level of diesel fuel price to repay the investment were analyzed. Thus the economic environment for the commercialization of the modern coal fueled locomotive is defined.

Introduction

Under the sponsorship of the U.S. Department of Energy (DOE), Morgantown Energy Technology Center (METC), the General Electric Company Transportation Systems is conducting a proof of concept program using coal–water slurry (CWS) fuel to power a locomotive. Some results of this study have already been reported in a previous paper (Flynn et al., 1990). In recent years, significant progresses were made in the completion of the first-phase multicylinder engine laboratory test and the first-stage coal-fueled diesel locomotive track test. CWS fuel, for the first time, was used successfully in powering a diesel engine at 1050 rpm and developed 2500 hp (16 MPa BMEP) in a GE-7FDL 12 cylinder engine (McDowell et al., 1991). This engine was transferred to a GE Dash 8 locomotive and completed preliminary system test on GE corporate test track.

A GE program is planned, in which four phases, "Technology R&D," "Engine Component Development," "Locomotive Integrated Systems Test," and "Conceptual Locomotive Design and Economic Analysis," are performed in parallel. At the core of the tasks, there are two phases of full-size 12-cylinder engine tests as well as two stages of locomotive systems tests. The highlights of the project are shown in Fig. 1. Briefly, the four phases are described as follows.

Technology R&D. The major technical areas, combustion, fuels, emissions, and durability, are to be investigated in bench-scale tests and on the single-cylinder research engine. The first task of the combustion R&D is to burn the coal–water slurry fuel with minimal modifications to the existing mechanical diesel fuel injection equipment (FIE) in order to gain the operating experience of a full-size multicylinder engine as quickly as possible. This experience is going to be used to guide the second task of developing an improved electronic controlled fuel injection system to be able to optimize the combustion of coal fuel in a diesel engine. The fuels R&D task is intended to identify some of the intrinsic CWS fuel parameters that influence engine combustion, as well as to broaden the engine ac-

Contributed by the Internal Combustion Engine Division and presented at the Energy-Sources Technology Conference and Exhibition, Houston, Texas, January 26–30, 1992. Manuscript received by the Internal Combustion Engine Division August 5, 1991. Associate Technical Editor: J. A. Caton.

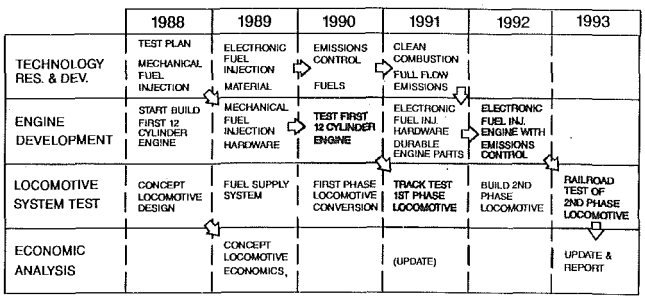

Fig. 1 Coal-fueled diesel locomotive project highlights

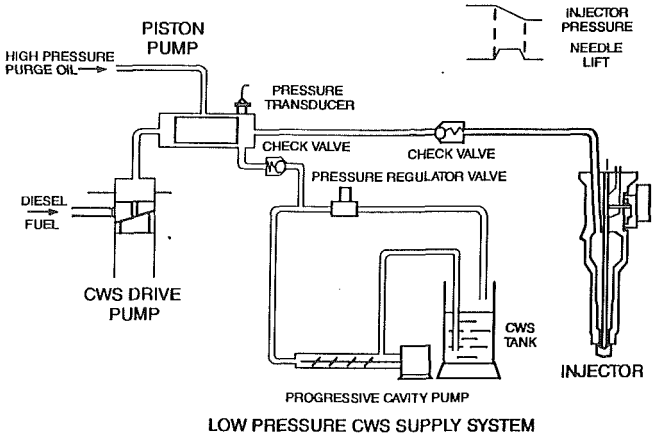

Fig. 2 Accumulator CWS injection system schematic

ceptance of the widest range of source fuel specifications. The emissions R&D objectives are first to characterize the coal-fired diesel engine emissions and then the develop the control system that will allow the engine to operate as clean as the original diesel fuel counter part. The durability objective is to develop the materials and processes that are needed to provide engine life comparable to today's oil-fueled diesel within reasonable cost.

Engine Component Development. The major technologies are to be scaled up to operate full-scale, multicylinder engines. Two consecutive phased 12-cylinder engines are to be built and tested on test stands. The first-phase engine uses mechanical FIE without any emission control equipment. As technology is developed, the second-phase engine will use the all electronic controlled FIE with fully developed emission controls system. Combustion, emissions, and operating data will be taken. In addition, two cylinders of another eight-cylinder engine are converted to CWS operation to provide a test bed for durability development. The engine for durability test will be operated for 1000 cylinder hours to collect long term component wear data.

Locomotive Integrated Systems Test. Two stages of locomotive development are to be conducted. The first-stage locomotive carries its CWS fuel on a tender. The first-phase engine was transplanted onto the first-stage locomotive and it has operated on GE Transportation Systems test track in 1991. The second-stage test locomotive will use the second-phase engine with all electronic control FIE, and will contain all the technologies developed during the project, included the emission control system. The track test will include operation in realistic railroad service.

Conceptual Locomotive Design and Economic Analysis. The coal-fueled locomotive that contains the technology to be developed in this program has been conceptually designed and its cost estimated. The investment in such a locomotive will be analyzed for different operating scenarios. This economic analysis will be updated at the end of the program.

This paper provides an update of the achievements obtained on the various aspects of the program.

Technology R&D

Combustion R&D. The combustion development for the mechanical CWS FIE and the mechanical pilot/starting diesel fuel system was completed in 1989. Its CWS fuel injection hardware was first developed under a previous DOE contract (DE-AC21-85MC22181) granted to GE and described in a paper by Hsu (1988). This system was not designed with durable parts and could only run for a short period of time. The combustion efficiency reached was only about 95 percent. The system and its main operation results on a single-cylinder engine were summarized in the earlier overview paper (Flynn et al., 1990). This system was subsequently built onto the first-phase 12-cylinder engine and completed full-scale engine test to be discussed later.

An electronically controlled accumulator CWS injection system, matched with an electronic start/pilot injector, has been developed on the GE single cylinder test engine. The basic CWS accumulator injection hardware was also developed under the previously mentioned earlier DOE contract and reported by Hsu et al. (1989). A schematic of the system is shown in Fig. 2. It can be briefly described as follows. A conventional jerk pump is used to pump diesel fuel oil onto the backside of a free floating piston in an CWS isolation pump. The CWS on the opposite side of the piston is thus pressurized and pushed into the accumulator injector. A check valve was included in the injector inlet to trap the high-pressure CWS in the injector on the refill cycle of the piston. A check valve is also included in the CWS fill line of the piston pump to keep it from reverse flowing during the pressurized cycle. The injector needle movement is controlled by servo oil pressurizing the appropriate side of a piston attached to the upper end of the injector needle. Thus, electronic signals feeding into a high-speed serve oil valve can provide the injection timing and duration in a prescribed manner.

An electronic start/pilot diesel fuel auxiliary injection system, developed by BKM, Inc., of San Diego, CA, is used together with the accumulator CWS hardware. The pilot diesel fuel system is of the common rail accumulator type. Therefore it does not require each cylinder to carry its own pump, thus simplifying the engine structural design. A general cross section layout of one cylinder with both the CWS and pilot fuel systems is shown in Fig. 3. This layout will be used on the second-phase 12-cylinder engine for each of the cylinders.

A computer model of CWS combustion in the engine has been completed by Ricardo, North America and described in detail in another published technical paper (Wahiduzzaman et al., 1990). It has contributed greatly in the understanding of the combustion performance of the engine. Further, it was also used to pursue the best ways to optimize the engine operation conditions (Wahiduzzaman et al., 1991). In-cylinder combustion photography and high-speed data systems were procured and the cylinder on the research engine was modified to accommodate the probes. This work will be completed later, and is expected to enhance significantly the knowledge of CWS in-cylinder combustion characteristics and further contribute to better combustion optimization.

Since Feb., 1990, the GE program has been expanded to include a study titled "Characterization of Coal-Water Slurry Fuel Sprays from Diesel Engine Injectors." It is performed by the Mechanical Engineering Department of the Texas A&M University. This work is closely coordinated with the development need at GE. Some results of the study have already

benefited the actual engine combustion design. Preliminary findings were published in a brief technical paper (Caton and Kihm, 1991). A thorough description of this work is also in press (Seshadri et al., 1992).

An extensive CWS combustion optimization study has been completed on the single-cylinder engine. The goal is to provide the highest combustion efficiency (burn-out rate) while not exceeding the firing pressure limit of engine components and having reasonable fuel consumption rates. It is also a goal to use the least practical amount of pilot diesel fuel. The parameters studied included CWS injection pressure, CWS and pilot injection timing, CWS injector hole size, number, shape and spray included angles, as well as engine inlet air conditions. Many interesting phenomena were noticed. For instance, for all practical purpose, CWS fuel ignites after its spray impinges on the combustion chamber walls. Impingement does not necessarily hamper combustion as long as it is not overly attached to the walls or hitting the cooler cylinder liner surface. Another interesting point that has been observed lies in the fact that, for optimum combustion, at the lower loads, the pilot diesel fuel is injected early in the cycle to serve as an igniter. However, at full load, pilot fuel should only be introduced late in the cycle to become a combustion enhancer after allowing a long delay time for the water in CWS fuel to evaporate before ignition ("Delayed Ignition"). Typical combustion heat release diagrams of low and high load operation are shown in Fig. 4. Achievements obtained so far include the following:

- The combustion efficiency at full engine load has reached 99.5 percent (as compared to 96 percent before), which greatly reduced the loading of the hot gas particulate removal system.
- The lowest load that can burn CWS fuel has been lowered from "Notch 5" load (960 rpm, 1.0 MPa MEP) to "Notch 2" load (620 rpm, 0.3 MPa MEP) and less pilot fuel under each load condition. As a result, the duty cycle CWS consumption increased from about 66 percent of the first-phase mechanical FIE engine to 80 percent, which exceeds the program goal of 75 percent (Flynn et al., 1990).
- The coal fuel diesel engine cycle efficiency is comparable to the oil fuel counterpart.

Details of findings are published in another paper (Hsu et al., 1992). All the above R&D results are presently being incorporated into a second-stage coal-fueled multicylinder engine.

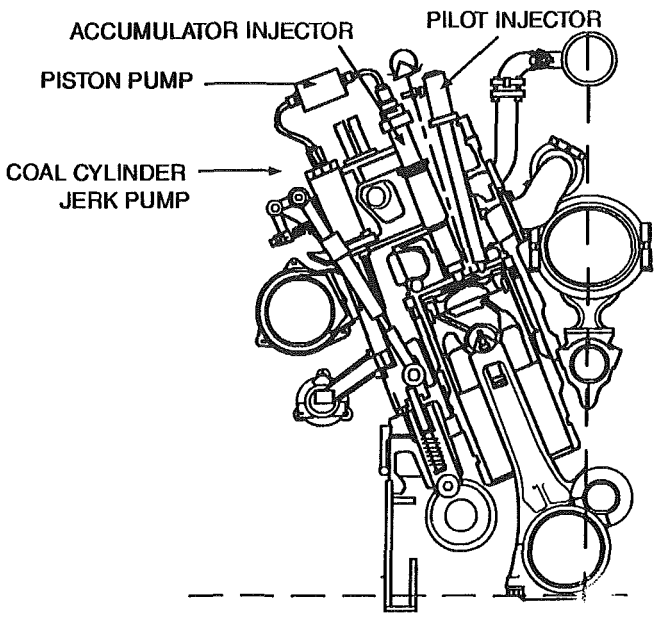

Fig. 3 Engine cross section layout of one cylinder

Fuels R&D. In the past, only one kind of domestic source bituminous coal (Kentucky Blue Gem) prepared by one fuel manufacturer into CWS (OTISCA Ind., of Syracuse, NY) was used on the GE engine. The fuel specifications are shown in Table 1.

One of the tasks of the project is to investigate the tolerance of injection hardware to CWS fuel variations. The CWS fuel comparison tests were completed during 1990. Fuels were procured from Otisca, AMAX of Golden, CO, and UNDERC of Grand Forks, ND. Source coals included bituminous coal from Kentucky and Pennsylvania and subbituminous coal from Wyoming. Cleaning methods ranged from heavy media cyclone to oil agglomeration, and chemical cleaning. Ash levels ranged from 0.7 to 2.8 percent. Mean particle sizes ranged from 3 to 15 μm. The GE diesel engine, using the accumulator fuel injection system, was able to burn all the CWS fuels at relatively high burnout levels (Table 2). However, the engine required different combustion parameters and some possible hardware modifications for optimum performance with each fuel (e.g., injector hole configurations, etc.). A more thorough description of the CWS fuel test results has been presented by Hsu and Confer in an ASME paper (1991).

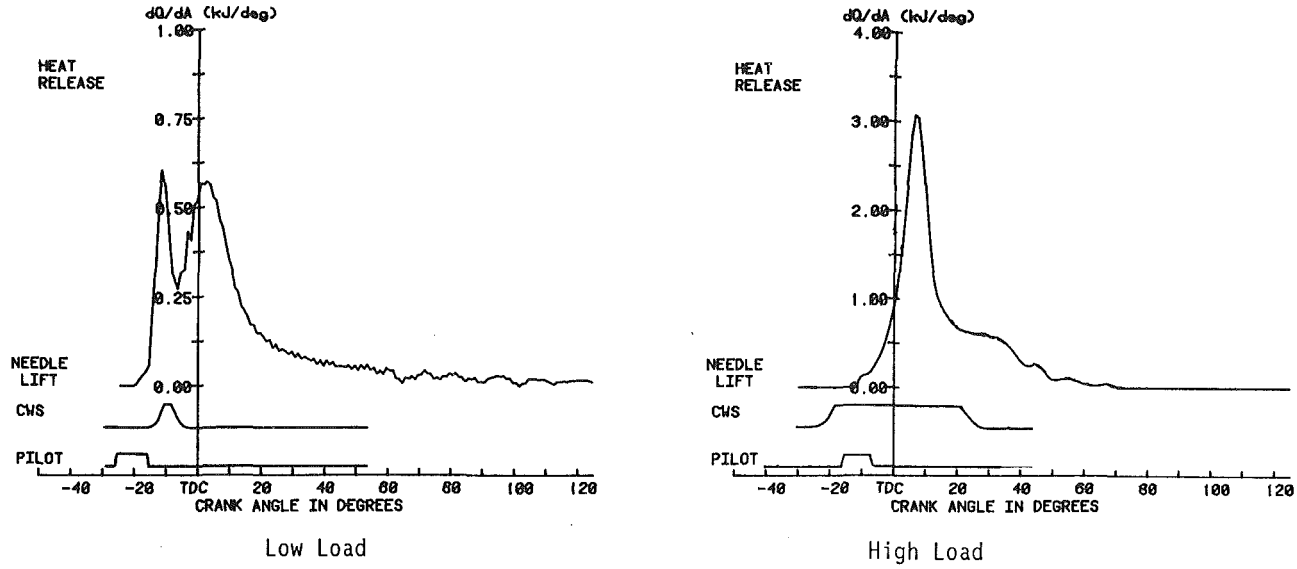

Fig. 4 Typical combustion heat release diagrams

Table 1 Kentucky Blue Gem coal nominal lot analysis

Proximate Analysis		Ultimate Analysis	
% Ash	0.80	% Carbon	82.59
% Volatile	39.40	% Hydrogen	5.34
% Fixed Carbon	59.80	% Nitrogen	2.08
		% Chlorine	0.18
Particle Size		% Sulfur	1.01
Mass Mean Diameter (microns)	5.47	% Oxygen (diff.)	7.58
Heating Value	High Heating Value (kJ/kg)		34630

Table 2 Test fuels and combustion results

Fuel No.	Fuel Vendor	Coal State Origin	Seam Name	Coal Type	Cleaning Process	Mean Micron Size	Ash %	Comb. Eff. %
1	OTISCA	Kentucky	Blue Gem	Bitum	Physical	4.6	0.7	99.2
2	OTISCA	Kentucky	Blue Gem	Bitum	Physical	4.8	0.8	98.8
3	OTISCA	Kentucky	Blue Gem	Bitum	Physical	3.1	0.7	98.7
4	OTISCA	Kentucky	Blue Gem	Bitum	Physical	3.2	0.7	99.2
5	OTISCA	Penn.	Pitt	Bitum	Physical	2.5	1.7	98.7
6	UNDERC	Wyoming	Kemmer	Subbit	Chemical	13.9	2.8	99.5
7	UNDERC	Wyoming	Sprg Crk	Subbit	Phys+Chem	14.7	2.1	99.0
8	UNDERC	Wyoming	Sprg Crk	Subbit	Chemical	14.9	2.8	99.2
9	AMAX	Kentucky	Splint	Bitum	Physical	8.2	2.5	97.7

Emissions R&D. Early in the program, an emissions sampling system was constructed to extract a small portion of the exhaust of the single cylinder engine. The system can test a subscale cyclone, fabric filter, or granular bed, singly or in combination. Calcium sorbents were also tested on engines to capture SO_2 from the exhaust. Lime was either mixed into the CWS fuel or injected into the exhaust manifold. Details of the findings have been reported by Slaughter et al. (1990).

At GE Corporate Research & Development, a small size Yanmar engine was set up with the exhaust gas passing through candle type stainless steel filters as shown in Fig. 5. The filters are equipped with reverse pulse air cleaning. The engine fuel was doped with carbon disulfide (CS_2) to increase the engine exhaust SO_2 concentration. Promising results were obtained using copper oxide (CuO) sorbent coupled with ammonia injection simultaneously to reduce SO_2 and NO_x emissions.

Based on findings of the above investigation, the cyclone was rejected for its inability to remove particulate with the required efficiency. Lime-based SO_2 sorbent was found to be insufficient. The granular bed option is potentially promising. However, in order to develop it into a locomotive engine system, the cost and time will be much more than the presently selected system. The final selected methods are:

- Regenerative CuO sorbent and ammonia injection downstream of turbocharger;
- High-temperature barrier filter downstream of sorbent injection;
- Off-line regeneration of sorbent.

The expected individual emission removal efficiencies of the system are:

- Particulate 99.5 percent
- SO_2 90 percent
- NO_x 90 percent

A cold flow facility of the envelope type barrier filter has been built and tested. It is now designed into a full-flow single-cylinder engine test system. Its fabrication is underway and will be later tested on actual engine. Details of this part of the program have been presented in another reference paper (Gal et al., 1991).

Durability R&D. The consistency of combustion and emissions testing has been greatly improved by the durability of the diamond compact nozzle, the development of which has been described in a previous paper (Flynn et al., 1990). Over ten diamond compact nozzles of different designs have since been tested on actual engines. Although the longest running time accumulated by one nozzle was no more than 100 hours, no sign of wear was detected and they all ran very reliably. Single diamond orifices have been tested for 500 hours on a research test stand with less than 0.5 percent increase in flow, as shown in Fig. 6. Previously, TiB_2 coating was also considered as a potential candidate for injector wear protection. TiB_2 coatings are very resistant to CWS erosion and two orifices have performed very well, but failure of the coating leads to catastrophic wear of the soft metal substrate. Work on developing alternate nozzle materials has thus been discontinued.

YANMAR CANDLE FILTER TEST

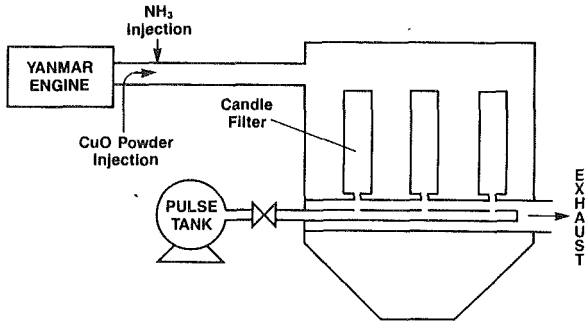

Fig. 5 Small-scale engine emission test configuration

After extensive bench scale test, it was identified that Tungsten Carbide (WC) coated piston rings and linear provide the best possibility to overcome the power assembly wear problem (Flynn et al., 1990). A development effort to define the relationships between plasma spray conditions and the properties of WC + Co and metal matrix composite coatings was completed. It was found that "Low-Pressure Plasma Deposition" (LPPD) processing can be used to produce piston rings with high quality WC + 12 percent Co coatings, particularly if the spray gun made by Electro-Plasma, Inc., was used. The findings can best be summarized as depicted in Fig. 7. A technical paper describing this effort has been presented to a DOE heat engines coating meeting (Rairden et al., 1990). A TiN coated piston ring was found to be very effective in preventing side wall wear. It was proven in a 165-hour run of the small Yanmar test engine using contaminated fuel.

Besides WC plasma coatings, piston crowns have been coated with nitride and boride coatings to reduce wear in the ring groove and monolithic exhaust valves and piston rings have been ordered. The R&D effort of durability is essentially complete. The technologies developed are presently being used to make full-size engine parts to be tested in the endurance engine.

Engine Development

Phase I 12-Cylinder Engine. This engine uses both mechanical pilot fuel injection and mechanical CWS injection hardware. Each cylinder has two injectors and two fuel injection pumps. The pilot pump is mounted on the side of the engine and the CWS jerk pump mounts on top of the engine. In each cylinder, a CWS injector is in the center and a pilot injector is on the side. These layouts are shown in Fig. 8.

The CWS injection system schematic is depicted in Fig. 9. Essentially, it is a conventional diesel jerk pump injection system with a pressure isolation pump between the pressurizing diesel fuel and the injected CWS fuel. The injector has backing fluid to keep the injector needle free from sticking.

For this mechanical FIE engine, both the pilot and CWS pumps are controlled by a single mechanical governor. A carefully conceived linkage system was designed to make the engine start on diesel fuel and switch to mostly CWS fuel through a secondary layshaft, which is manually operated at an appro-

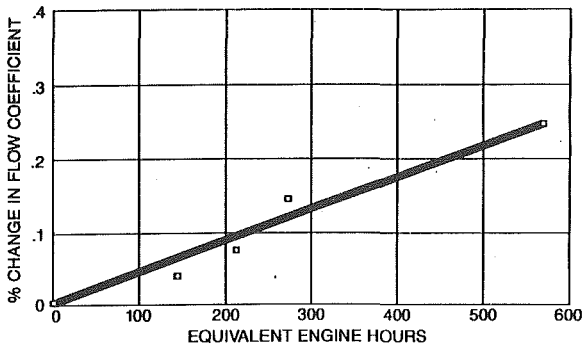

Fig. 6 Erosion rate of diamond compact orifice on test stand

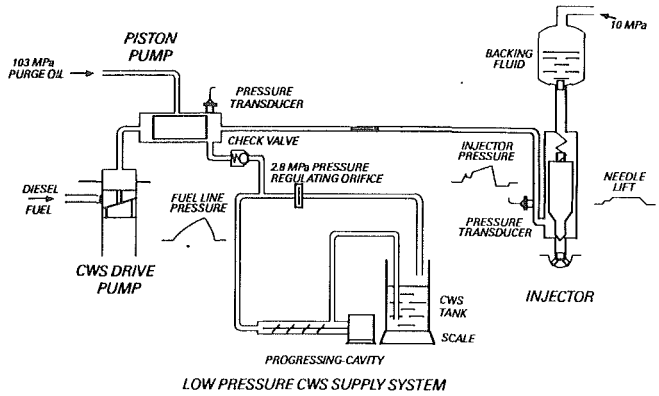

Fig. 9 Stage I coal-fueled engine CWS injection system schematic

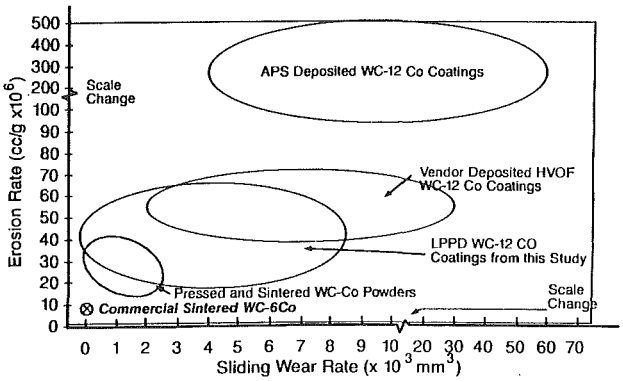

Fig. 7 Tungsten carbide plasma spray application

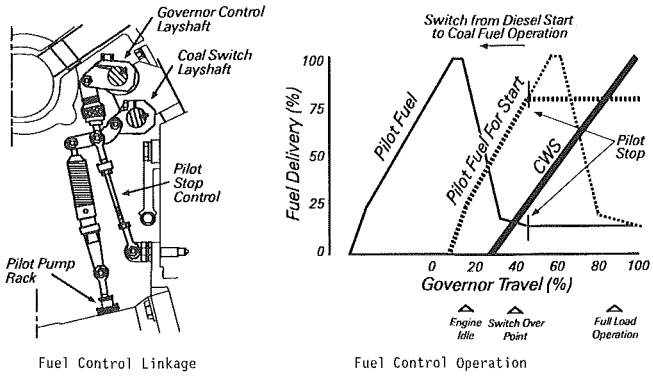

Fig. 10 Stage I coal engine fuel control schematic

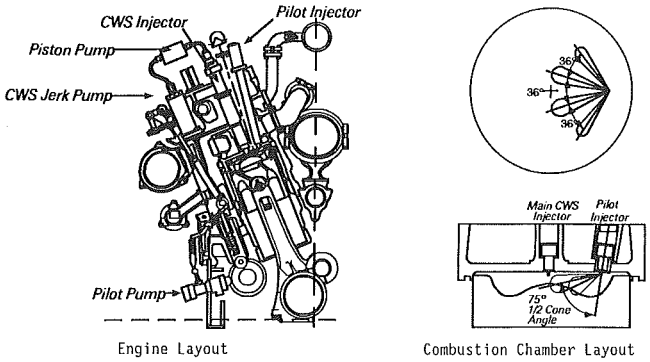

Fig. 8 Stage I coal-fueled diesel engine general layout

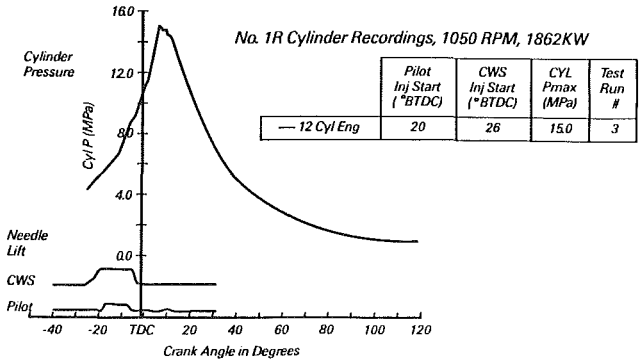

Fig. 11 Stage I coal engine full-load cylinder pressure

priate time. The linkage and fuel delivery schedule schematics are shown in Fig. 10.

After extended efforts were made, the switchover of the engine from diesel start to coal fuel operation was successful. The engine developed 2500 hp at 1050 rpm using mostly coal fuel. A typical cylinder firing pressure trace in one of the cylinders taken while the coal-fueled engine was running at 2500 hp is shown in Fig. 11. In the lower half of the figure of CWS fuel and pilot diesel fuel needle lifts are shown to indicate the fuel delivering timing schedule. It ran for approximately 10 hours in the engine laboratory and was moved onto the first-stage locomotive for a track test. Details of the testing of this engine were published in another technical paper (McDowell et al., 1991).

Phase II 12-Cylinder Engine. The second-phase 12-cylinder test engine will have all electronic controlled pilot and CWS FIE as described before. It will use all the durable engine parts developed in this program. The exhaust gas emissions cleanup system will also be built for this engine. At present, the building of the new engine is almost completed. It is scheduled to start testing in 1992.

Durability Engine Test. The endurance test engine has been operational since spring, 1991. Durable full-size engine parts built with the technologies developed in the R&D phase have been under test. They include WC coated liners, WC coated rings, and accumulator injectors with diamond compact inserted nozzles. The engine has accumulated over 100 hours of test time.

Recent full-size WC coated piston rings and liner run on the single cylinder combustion test engine for over 60 hours have shown very promising results. Figure 12 shows the top piston ring wear as expressed in ring gap comparison for a conventional production ring and a WC coated ring. Other coating process rings will continue to be evaluated.

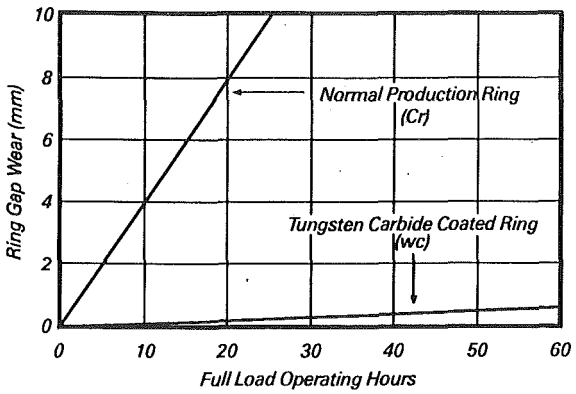

Fig. 12 Top piston ring wear comparison

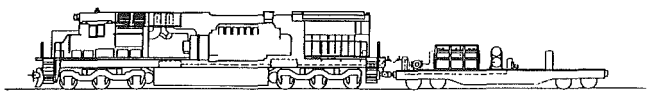

Fig. 13 Stage I test locomotive configuration

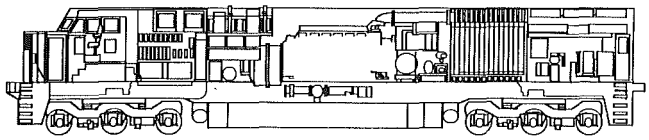

Fig. 14 Concept design of coal-fueled diesel locomotive

Locomotive Integrated Systems Test

First-Stage Locomotive Test. The first-phase locomotive system test is complete. For this stage locomotive test, the CWS fuel and its supply system are carried on a tender. Figure 13 is the test configuration schematic. The test was run for about 10 hours on the GE/TS test track. Since the first phase engine does not have durable engine parts or emission cleaning setup, it is mainly a design concept system checkout. The experience gained on the overall operation of a coal-fueled diesel engine, as well as its controls and supporting fuel supply system are being implemented onto the second-stage engine and locomotive design.

Second Stage Locomotive Test. The design of the second and final-phase locomotive is almost complete. After the first-phase locomotive test, the test locomotive will be modified. The overall length is to be extended to accommodate a larger CWS tank carried under the mainframe. Above the extended part of the main frame, the full-size emissions cleanup system will be installed. The second-phase all electronic controlled CWS fueled engine will be used. This engine also will have all the endurance parts developed under the program. The final locomotive test will include operation on commercial railroad tracks.

Conceptual Locomotive Design and Economic Analysis

Conceptual Locomotive Design. Earlier in the program a conceptual locomotive was designed (Flynn et al., 1990). It is shown in Fig. 14. The concept locomotive was based on a 4000 horse-power GE Dash 8 locomotive with additional systems necessary to support CWS operation. It was designed to complete a 50 hour mission without refueling or discharging its waste products. Its platform was lengthened by 10 feet to accommodate a larger fuel tank necessary to carry an adequate amount of the lower energy density fuel. This design carried all the CWS fuel on the locomotive. The extra length was also necessary to house the emission control system.

Table 3 Incremental cost increase of coal-fueled diesel locomotive

Engine Systems	$60,171
Emissions Control Systems	$160,446
Locomotive Structure	$58,195
Total	$278,812

Table 4 CWS fuel costs ($/MBtu)

	Eastern Bitum.	Western Subbit.
Otisca Physical Process		
Coal	$1.18	$ .57
Production	$ .79	$1.29
Transport	$ .95	$1.44
Total	$2.92	$3.30
Amax Physical Process		
Coal	$1.18	$ .57
Production	$ .92	$1.07
Transport	$ .95	$1.44
Total	$3.05	$3.08
Best Case:		
Coal		$ .35
Production		$1.29
Transport		$ .00
Total		$1.64

Economic Analysis. The concept locomotive was estimated to cost $280,000 more to the customer than the diesel oil fueled locomotive on which it was based. The majority of the cost increase was associated with emission control components. The second largest category was the engine components. The cost increases for the concept locomotive are itemized in Table 3.

Since the ability to burn coal increases the cost of the locomotive, the cost of the coal-based fuel must be lower than the oil-based fuel for the coal-fueled locomotive to be economically attractive. The CWS fuel cost was composed of raw coal cost, transportation cost, and processing cost. Three operating scenarios were evaluated in the economic analysis: Eastern, Western, and Best Case. The Eastern and Western cases served all the mainline track in their respective regions.

They required significant transportation costs to move the coal to the process plant and ship the processed slurry to the fueling depots. The best case scenario modeled a specific dedicated coal train serving the Powder River Basin. Since the coal was mined, processed, and used in the same location, no transportation costs were included. The CWS costs from the three regions are itemized in Table 4.

The return on an investment in coal-fueled locomotive was evaluated as a function of the cost of diesel fuel, as shown in Fig. 15. A diesel fuel price of $0.91, $0.81, and $0.59 per

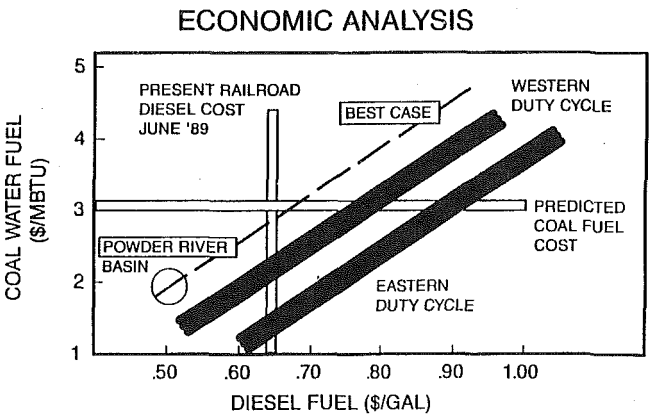

Fig. 15 Coal fueled diesel locomotive economic analysis

gallon would be necessary to repay the investment at a DCRR level of 15 percent, for the Eastern, Western, and best case duty cycles, respectively. The Eastern case requires the highest diesel price because of its lower average duty cycle. The Western case has a higher duty cycle, which causes more savings to be generated with the higher fuel use. The best case has the highest duty cycle due to its dedicated coal train operation. It also has the lowest CWS cost due to low western coal prices and the lack of transportation cost. For a more detailed description of the economic analysis, the reader is referred to the full report, which should be published by DOE in the near future.

Conclusions

Excellent progress has been made on all aspects of the coal-fired diesel locomotive program. The completion of the first-phase coal fuel locomotive track test marked a major milestone in the development of using coal fuel again since the disappearance of the steam locomotive. The R&D phase of the current program is essentially complete. Preliminary results of component development using the R&D technology findings are yielding promising returns. All signs indicate a successful second-stage locomotive test on commercial railroad to be highly possible. If the market environment predicted in the economic analysis of the program becomes a reality, the technologies will be there to support a modern coal-fueled diesel locomotive transition.

Acknowledgments

The support and permission to publish the results of this study from GE Transportation Systems and DOE Morgantown Energy Technology Center are gratefully acknowledged. The work on which this paper is based was conducted under DOE Contract No. DE-AC21-88MC23174. The support of the program from the other sponsors, Norfolk Southern Corporation, Pennsylvania State Energy Development Authority, and New York State Energy Research and Development Authority is also gratefully acknowledged. The author would like to thank his many colleagues at GE Transportation Systems, GE Corporate Research and Development, and GE Environmental Systems for their valuable contributions and hard work, without which there could not be any achievements. The author would also like to thank Mr. Leland Paulson, Contracting Officer Technical Representative DOE/METC for his comments and encouragements in the course of this study.

References

Caton, J. A., and Kihm, K. D., 1991, "Coal Water Slurry Atomization Characteristics," *presented at the DOE METC Heat Engines and Gas Steam* Cleanup Systems Contractors Review Meeting in Morgantown, WV, July.

Flynn, P. L., Hsu, B. D., and Leonard, G. L., 1990, "Coal Fueled Diesel Engine Progress at GE Transportation Systems," ASME JOURNAL OF ENGINEERING FOR GAS TURBINES AND POWER, Vol. 112, pp. 369-375.

Gal, E., Cohen, M., Van Kleunen, W., and Hamilton, R., 1991, "Coal Fueled Diesel Emissions Control Technology Development: A Status Report," presented at the DOE METC Heat Engines and Gas Stream Cleanup Systems Contractors Review Meeting in Morgantown, WV, July.

Hsu, B. D., 1988, "Progress on the Investigation of Coal-Water Slurry Fuel in a Medium Speed Diesel Engine: Part 2—Preliminary Full Load Test," ASME JOURNAL OF ENGINEERING FOR GAS TURBINES AND POWER, Vol. 110, pp. 423-430.

Hsu, B. D., Leonard, G. L., and Johnson, R. N., 1989, "Progress on the Investigation of Coal-Water Slurry Fuel in a Medium Speed Diesel Engine: Part 3—Accumulator Injector Performance," ASME JOURNAL OF ENGINEERING FOR GAS TURBINES AND POWER, Vol. 111, pp. 516-520.

Hsu, B. D., and Confer, G. L., 1991, "Progress on the Investigation of Coal-Water Slurry Fuel Combustion in a Medium Speed Diesel Engine: Part 4—Fuels Effect," *Coal Fueled Diesel Engines*, ASME ICE-Vol. 14.

Hsu, B. D., Confer, G. L., and Shen, Z. J., 1992, "Progress on the Investigation of Coal-Water Slurry Fuel Combustion in a Medium Speed Diesel Engine: Part 5—Combustion Studies," ASME JOURNAL OF ENGINEERING FOR GAS TURBINES AND POWER, Vol. 114, this issue, pp. 515-521.

McDowell, R. E., Basic, S. L., and Confer, G. L., 1991, "Design and Operation of a Coal Fueled 12 Cylinder Medium Speed Diesel Engine," presented at the DOE METC Heat Engines and Gas Stream Cleanup Systems Contractors Review Meeting in Morgantown, WV, July.

Rairden, J. R., Mehan, R. L., and Giammarise, A. W., 1990, "The Effects of Processing Conditions on the Wear Resistance of Plasma Sprayed WC-Co Coatings," *Proceedings of the DOE Conference on Coatings for Heat Engines*, meeting held in Castine, ME, Aug.

Seshadri, A. K., Caton, J. A., and Kihm, K. D., 1992, "Coal Water Slurry Atomization Characteristics of a Positive Displacement Fuel Injection System," ASME JOURNAL OF ENGINEERING FOR GAS TURBINES AND POWER, Vol. 114, this issue, pp. 528-533.

Slaughter, D., Cohen, M., Samuel, E., Mengel, M., and Gal, E., 1990, "Control of Emissions in the Coal Fueled Diesel Locomotive," *Coal Fueled Diesel Engines*, ASME ICE-Vol. 12, pp. 11-16.

Wahiduzzaman, S., Blumberg, P. N., Keribar, R., and Rackmil, C. I., 1990, "A Comprehensive Model for Pilot Ignited, Coal-Water Mixture Combustion in a Direct Injection Diesel Engine," ASME JOURNAL OF ENGINEERING FOR GAS TURBINES AND POWER, Vol. 112, pp. 384-390.

Wahiduzzaman, S., Blumberg, P. N., and Hsu, B. D., 1991, "Simulation of Significant Design and Operating Characteristics of a Coal Fueled Locomotive Diesel Engine," *Coal Fueled Diesel Engines*, ASME ICE-Vol. 14.

Features and Performance Data of Cooper-Bessemer Coal-Fueled Six-Cylinder LSB Engine

A. K. Rao
Cooper-Bessemer Reciprocating,
Grove City, PA 16127

E. N. Balles

R. P. Wilson, Jr.

Arthur D. Little, Inc.,
Cambridge, MA 02140

The six-cylinder Cooper-Bessemer LSB engine has been converted to operate with one cylinder on coal-water slurry (CWS) fuel and with five cylinders operating on diesel fuel. This development followed the successful operation of the single-cylinder JS engine on CWS for over 600 hours to date. The CWS injection system was scaled up about a factor of two in fuel volume from the JS system. A new cam box drive was fabricated for the LSB single-cylinder operation. The engine was operated and full power output was achieved from the CWS cylinder. Preliminary test results indicate good operate efficiency. An exhaust emission control system is in place for the proposed operation of all the six cylinders on CWS and major engine components are on hand. These results mark a significant milestone in the progress toward commercial readiness of the coal-fueled diesel engine system.

Introduction and Background

This research effort is being conducted as part of the Heat Engines Program of the Morgantown Energy Technology Center of the U.S. Department of Energy. The objective of this project is to demonstrate efficient and low-emission operation of the Cooper-Bessemer LSB-6 engine on CWS, as a proof-of-concept of the feasibility of using CWS as fuel for large stationary diesel engines. A 100-hour continuous proof-of-concept test is scheduled to be performed in 1993.

Over the past four years, the Cooper-Bessemer/Arthur D. Little team has gained experience in operating the single-cylinder laboratory JS-1 engine on CWS. The JS engine operation has helped to identify and resolve the problems in CWS handling, injection, and combustion as well as to develop highly durable combustion chamber components. Testing has also helped to identify the levels of pollutants in the untreated exhaust gas, thereby establishing realistic design targets for the emission control system.

Based on this experience, the six-cylinder LSB engine located at the Cooper-Bessemer R&D Laboratory in Mt. Vernon, OH, has been redesigned to operate on CWS and equipped with a full flow emission control system. The operation of the engine on CWS will be performed in two stages. First, the engine was operated with only the #1 cylinder fueled with CWS. The preliminary results of these tests are described in this paper. Once the various injection and combustion parameters are optimized, all six cylinders will be operated on CWS.

LSB Engine Parameters

The LSB engines come in 6- and 8-cylinder in-line configurations and are also available in the 12-, 16-, and 20-cylinder "vee" configuration (LSVB Model). The LSV series was first introduced in 1948 with a total installed capacity at the present time of over two million horsepower. This provides ample opportunity for retrofitting the engines already in the field, once the coal-fueled diesel technology becomes commercial.

The LSB engine, shown in Figs. 1 and 2, consists of a one-piece base, one-piece centerframe, and one-piece cylinder block. The engine has wet-type cylinder liners, which makes it convenient to coat the bore with hard materials for improved durability while operating on CWS. The cylinder head has two intake valves and two exhaust valves and a central diesel fuel injector. The camshaft is a single shaft that runs in a trough cast onto the side of the cylinder block. Cams are hydraulically mounted on the camshaft. The fuel is supplied by conventional jerk pumps driven by the camshaft. There is one fuel pump per cylinder. The pistons are two-piece pistons with forged steel crown and an aluminum skirt. A constant pressure turbocharger supplies the combustion air to the engine through an intercooler.

All the in-line and vee engines share a common bore and stroke of 15.5 in. × 22.0 in. The laboratory engine has six cylinders and the power generated is absorbed by a dynamometer. The operating speed range is 360–400 rpm. The rated maximum power output is 2605 bhp at a bmep of 208 psi.

LSB Design Modifications

Objective. An effort was made to keep the major components of the coal-fueled engine the same as those of the straight diesel engine. This would keep the cost of the components to be manufactured to a minimum, both for the prototype and production engines. Also, this would result in a high degree of reliability and predictable performance of the components. Design modifications to meet specific needs of the coal-fueled engine are described below.

Contributed by the Internal Combustion Engine Division and presented at the Energy-Sources Technology Conference and Exhibition, Houston, Texas, January 26-30, 1992. Manuscript received by the Internal Combustion Engine Division September 16, 1991. Associate Technical Editor: J. A. Caton.

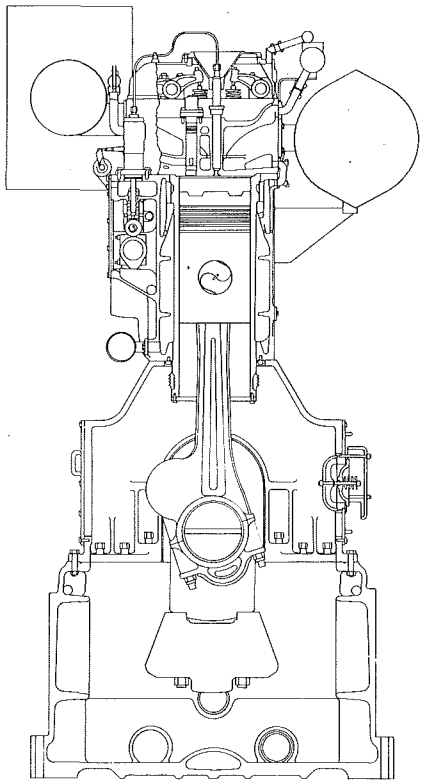

Fig. 1 Cooper-Bessemer LSB engine cross section

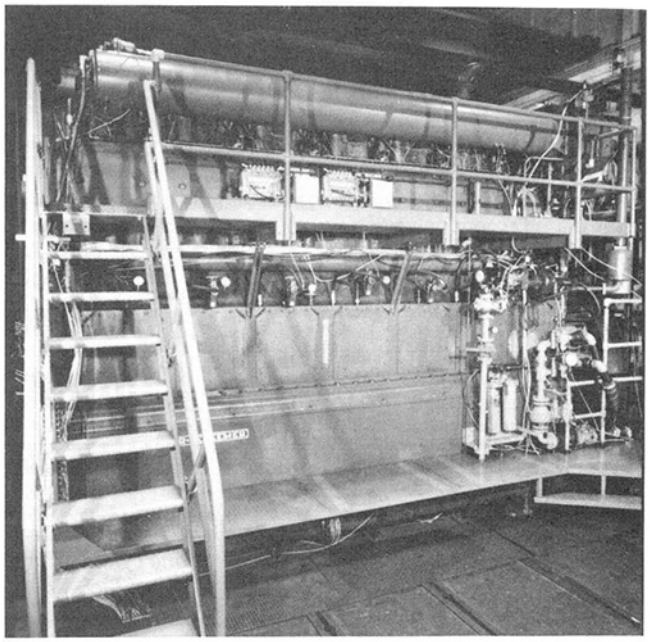

Fig. 2 Coal-fueled LSB-6 laboratory engine

Cylinder Block. The starting point for the design modifications was the coal slurry fuel itself. The baseline fuel has an average particle size of 12 microns, 1.5 percent ash on dry coal basis, and approximately 50 percent coal solids loading by volume. With its heating value of approximately half that of the diesel fuel, the fuel injection pump needed to deliver approximately twice the volume of CWS compared to the diesel fuel, in about the same duration, in order to develop the same horse-power output as a diesel engine. The fuel injection pump on the standard diesel engine has a 26 mm plunger and barrel. The fuel injection pump selected for coal fuel operation has a 36 mm plunger and barrel. The fuel injection system was designed for a peak injection pressure of up to 18,000 psi, although the normal operating value is about 10,000 psi in practice. This design value of peak injection pressure is substantially higher than that of the standard LSB diesel engine.

This combination of higher injection pressure acting on a larger plunger area has resulted in a substantially higher loading on the camshaft, which necessitated the increase of camshaft diameter from 4.125 in. to 6.5 in. Since the cylinder block houses the cylinder liners as well as the camshaft, the cylinder block was redesigned and substantially stiffened to accommodate the larger camshaft, larger cams, and higher loads from the fuel pumps.

The cylinder block was the only major casting to be redesigned. No changes were needed to the base, centerframe, crankshaft, main and connecting rod bearings, connecting rods, or air manifold.

Cylinder Head. The central hole in the cylinder head had to be slightly enlarged to accommodate the coal-fuel injector. The location or size of the air inlet and exhaust valves has not been changed. The jet cell openings in the cylinder head were used to accommodate the diesel pilot injector hardware. The result is that the cylinder head for the coal-fuelded engine can be machined from the same casting as the cylinder head for he diesel fuel engine. Because the two-cylinder heads are virtually identical, it is not anticipated that the CWS cylinder head would suffer any undue mechanical or thermal stresses if the peak firing pressures are kept within design limits.

Piston. The bowl-type combustion chamber used during JS engine tests gave remarkably good results. This is the standard combustion chamber shape for the dual-fuel LS engine (natural gas with diesel pilot) as opposed to the Mexican hat-shaped for DF2 engine. Therefore, a bowl-type combustion chamber in the piston will be used on the LSB engine as well. Currently, tests are being done on the JS engine to fine tune and optimize the combustion chamber shape, compression ratio and the CWS nozzle spray angle. Results from these tests will be used to revise the combustion chamber parameters on the LSB engine at a future date.

Nomenclature

ATC = After Top Center
BTC = Before Top Center
CWS = Coal–Water Slurry
DF2 = Number 2 Diesel Fuel
I.D. Fan = Induced Draft Fan
MAT = Manifold Air Temperature
NO_x = Oxides of Nitrogen
SCR = Selective Catalytic Reduction
bhp = brake horsepower
bmep = brake mean effective pressure
bsfc = brake specific fuel consumption
ihp = indicated horsepower
rpm = revolutions per minute

Conversion factors

1 Btu = 1.055 kJ
1 hp = 745.5 W
1 in. = 25.4 mm
1 psi = 6.895 kPa

Injection System

Main Injector. The concept for injecting CWS into the combustion chamber remains unchanged from that used on the JS engine, which was described by Rao et al. (1989). The JS system was scaled up to suit the LSB fuel requirements. The cam driven 36 mm jerk pump is used to time and meter diesel fuel, which supplies the pressure pulse to the top of the shuttle, which is a piston in the injector body that isolates diesel fuel and CWS. The shuttle in turn pressurizes and pumps the CWS trapped in the injector that was supplied at a low pressure through a nonreturn valve.

There are two successful nozzle designs that were used on the JS engine, with several different materials tested in each design. The first successful design had a "button" type nozzle tip. The most successful material used with this design to date is a tungsten carbide/cobalt cermet, which is an excellent working condition with over a hundred hours of operation on CWS. The other design had an "insert type" nozzle tip. In this design each of the injection holes is drilled into a very small and very hard cylindrical insert in a metal nut. Both sapphire and diamond inserts were tried. The sapphire insert tip had about 116 hours of CWS operation and is still in good working condition. The diamond insert tip was tested for its design integrity for over 20 hours on CWS with no apparent wear. The details of both these designs were described by Mayville et al. (1991).

Based on the above JS engine experience, the sapphire insert type nozzle was selected with 37 holes of 0.385 mm diameter for evaluation on the LSB engine. There are two rows of 18 holes each around the periphery and one hole pointing axially downward. The injector and nozzle were designed by AMBAC International. There are also plans to evaluate the single piece button type nozzle tip of tungsten carbide/cobalt cermet on the LSB engine.

Pilot Injector. Although auto ignition of CWS is possible and was demonstrated on the JS engine (Rao et al., 1988), a small quantity of diesel pilot (1 to 5 percent of total heat input) reduces the manifold air temperature required for timely ignition and combustion.

There are currently two choices available for the diesel pilot. First is a six-hole conventional pilot nozzle located in one of the jet cell holes in the cylinder head and injection the pilot fuel directly into the combustion chamber. The second choice is a diesel fuel fired jet cell shown in Fig. 3. A pintle nozzle is used to inject the diesel fuel onto the uncooled portion of the jet cell, igniting the fuel (Blizzard et al., 1991). The flame and hot gases emerge from the jet cell orifice into the main combustion chamber, igniting the CWS. The fuel to either of the pilot injectors is supplied by an auxiliary fuel pump, chain driven from the engine camshaft.

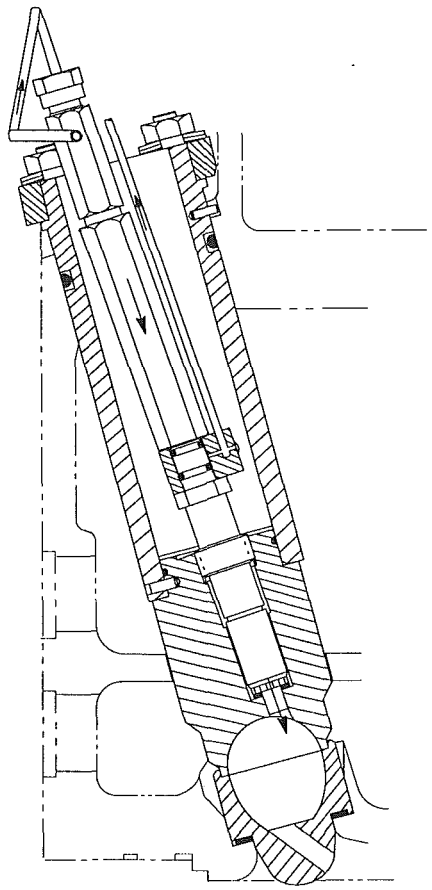

Fig. 3 DF2-fired jet cell

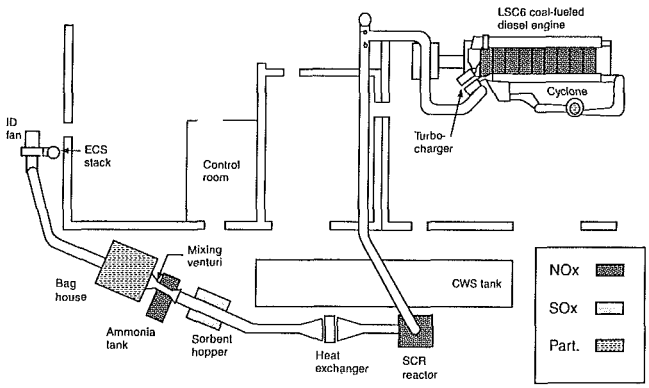

Fig. 4 Integrated emission control system for the LSC-6 coal-fueled diesel engine

Emissions Control System

The layout of the emissions control system is shown in Fig. 4. One of the main goals of the project is to reduce the emissions levels to be acceptable to cogeneration and electrical power production sites toward which this program is targeted.

Tests have been performed using the laboratory JS engine to optimize the CWS performance in terms of bsfc and NO_x levels by choosing the most favorable combination of combustion chamber shape, compression ratio, injection timing, pilot type, nozzle geometry, etc. Preliminary results indicate that some of these parameters have a significant impact on the NO_x levels, as well as bsfc. This information will be used to optimize the LSB engine combustion chamber parameters, making the in-cylinder combustion modification the first step in the NO_x reduction process. Based on the preliminary results, NO_x emission levels in the 0.8–1.2 lb/MMBtu range appear feasible before further reduction by exhaust gas treatment. With SCR, the coal diesel system is expected to achieve the design goal of 0.25 ± .05 lb/MMBtu.

The external exhaust gas treatment equipment consists of a cyclone, SCR reactor, heat exchanger, sorbent injection system, baghouse, and an I.D. fan. The cyclone is installed between the engine and the turbocharger, essentially to protect the turbocharger by removing relatively large particulate matter. The exhaust gases then pass through the turbocharger where heat is extracted from the gases to run the turbine. Then the gases pass through the SCR, where ammonia is injected, in the presence of a ceramic zeolite catalyst, resulting in 80–90 percent reduction of NO_x. Then the gases pass through a water-cooled heat exchanger simulating the heat recovery steam generator. After the heat exchanger, a sodium-based sorbent is injected into the exhaust gases, in a mixing venturi to capture

the sulfur. The mixture then enters the baghouse, where the remaining particulate along with the sorbent is filtered out. The next item in line, the I.D. fan, compensates for the additional pressure drop caused by the emissions control equipment, pushing the exhaust gases out the stack. Additional details have been reported by Staudt et al. (1991).

Provisions for LSB Engine Operation With One-Cylinder on CWS

Prior to the LSB engine conversion, considerable experience had been gained by operating the single-cylinder JS engine on CWS (Mayville et al., 1990; Benedek et al., 1989). To date, over 600 hours of JS engine operation on CWS have been accumulated. The JS-1 was a flexible and economic tool to evaluate various fuel injection systems, nozzle tip materials, different qualities of fuels and different coatings on the combustion chamber components subject to wear. However, with its bore and stroke of 13 in. × 16 in., it developed 215 bhp at 200 psi bmep and 400 rpm. The LSB engine, on the other hand, has a power output of 435 bhp per cylinder, requiring a 2:1 scale-up in injection hardware. It was decided first to operate the engine with one of the cylinders fueled by CWS while the other five would operate on DF2. This provided an opportunity to debug the scaled-up system and optimize the various injection and combustion parameters before going to six-cylinder operation.

In order to operate the engine on two different fuels, a separate cam box was fabricated and assembled, which was chain driven by the engine crankshaft. A 36 mm fuel injection pump was installed on the cam box. The diesel cylinder head was replaced by a CWS cylinder head fitted with a CWS injector and the diesel pilot jet cell described earlier.

On the JS engine, satisfactory combustion of CWS required a manifold air temperature (MAT) of about 270°F. This was achieved by heating the combustion air with an auxiliary electric heater. On the LSB it was believed that the MAT would have to be in the same range as for the JS. However, since the turbocharger compressor outlet temperature is in the 250–300°F range at full load, it was decided not to use an auxiliary heater, but instead disable the intercooler to maintain a high MAT. That meant the diesel cylinders would also run on high MAT. Therefore, the intercooler water was drained and the engine was run in full diesel mode. The engine carried satisfactory load without exceeding the peak cylinder pressures or preturbine limit.

A torsional vibration analysis was carried out to investigate the effect of no load on one cylinder. This condition could occur momentarily during fuel switching or if a CWS fuel line was plugged. The analysis showed the torsional stresses were well within design limits and there would be no catastrophic impact if the CWS cylinder stops firing for any reason.

The exhaust duct work was not altered in any way and therefore, the exhaust from all the six cylinders passed through the turbocharger.

Instrumentation

The instrumentation for recording and storing the data is similar to the instrumentation used on the JS engine (Rao et al., 1988). A high-speed data acquisition unit is used to scan and record all the pressures and temperatures, engine speed, load, etc., in digital form. Combustion and fuel injection pressures are measured and recorded every crankshaft degree. Cylinder pressure and heat release analysis is similar to that used for the JS engine (Balles et al., 1987). The CWS fuel was supplied to the engine from a 100 gallon day tank on a weight scale, which provided gravimetric fuel consumption data. CWS emissions data were not available during these tests because the exhaust from the CWS cylinder entered the same manifold as the exhaust from the five diesel cylinders.

Results and Discussion

The engine was first run with one cylinder on CWS and the other five cylinders on DF2 in July, 1991. However, CWS injection pressures were very high and full output from the CWS cylinder could not be achieved. Close examination of the CWS injection pressure traces and subsequent checking of the hardware revealed an error in the machining of the injector components. This was rectified and the tests with modified hardware are described below. In the run numbers that appear on the data, the first six digits refer to the date and the following four figures refer to the time of the day.

Excessive chain drive vibration limited the engine speed to approximately 380 rpm. Therefore, the data presented here pertains to an engine speed slightly lower than the design speed of 400 rpm. It should be noted that the six-cylinder operation on CWS will not require this chain drive.

Additional tests are planned to determine the relationship between the brake horsepower developed by the engine and the indicated horsepower calculated from the measured cylinder pressure data. Knowing the friction horsepower per cylinder as a function of speed and load will allow us to calculate the bhp of the CWS cylinder.

Repeatability. Figure 5 illustrates the repeatability of measured engine test data, and demonstrates consistent hardware performance while operating on CWS. The cylinder and injection pressure data shown in Fig. 5 are from nominally identical tests run three days apart. In both tests, the CWS cylinder used a 36 mm fuel injection pump timed for 27°BTC port closure, a 37-hole (0.457 mm hole diameter) main injector, and a six-hole (0.27 mm hole diameter) pilot injector. The measured slurry consumption rates for the two runs shown in Fig. 5 agreed within 2 percent (436 lb/hr versus 428 lb/hr), and the measured indicated specific fuel consumption agreed within 4 percent (6760 Btu/ihp•hr versus 6470 Btu/ihp•hr). This agreement is well within measurement accuracy bounds.

Effect of CWS Injection Timing. Figures 6 and 7 show the effect of CWS ignition timing on cylinder pressure, apparent heat release, and flame development. The start of main injection was varied from 14 deg. BTC to 22 deg. BTC, which had a dramatic impact on combustion. The 14 deg BTC timing proved to be so retarded that the peak cylinder pressure did not exceed the compression pressure (approximately 900 psia), the fuel did not burn fully, and heat release was late in the cycle, resulting in low efficiency. Advancing the start of CWS injection by 8 deg to 22 deg BTC substantially improved com-

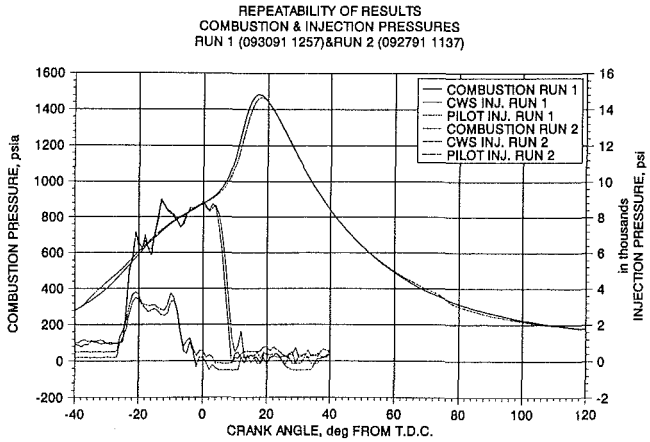

Fig. 5 CWS test repeatability: cylinder and injection pressure data from different runs under the same operating conditions

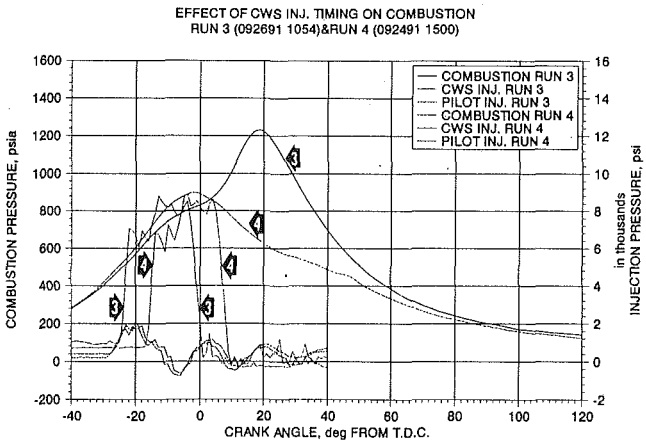

Fig. 6 Effect of CWS injection timing on cylinder pressure (run 3 start of injection at 22 deg BTC; run 4 start of injection at 14 deg BTC)

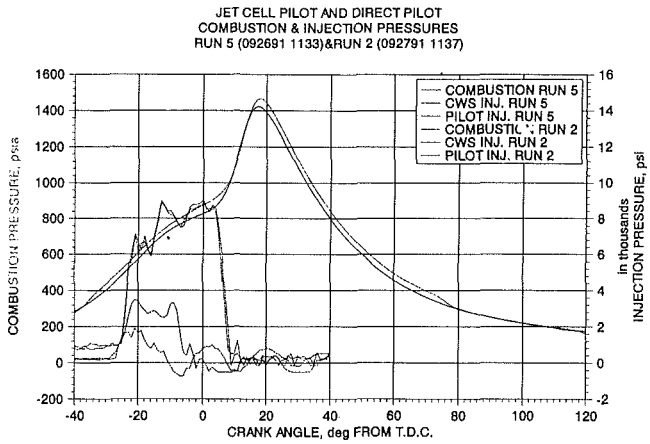

Fig. 8 Effect of pilot configuration on cylinder pressure: diesel fuel jet cell versus direct diesel pilot

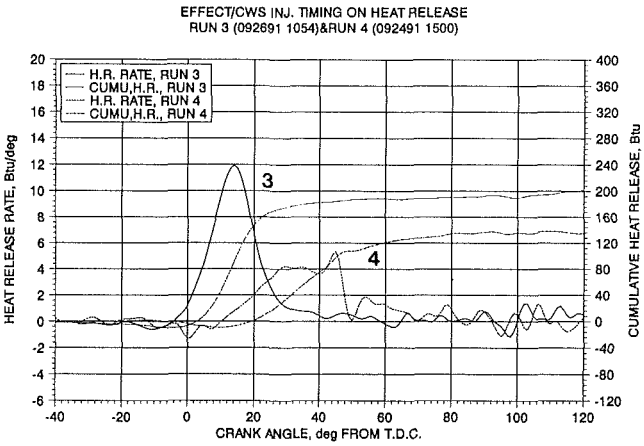

Fig. 7 Effect of CWS injection timing on heat release

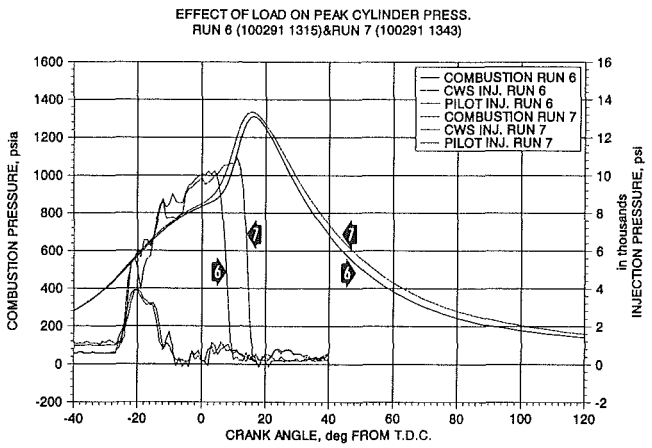

Fig. 9 Effect of engine load on cylinder pressure and injection duration (engine speed: 370 rpm; run 6 at 380 ihp; run 7 at 470 ihp)

bustion. Peak firing pressure was approximately 1290 psia, CWS ignition was approximately 10 deg earlier, burn rate was higher, and more energy was released earlier in the cycle. Judging from the shape of the cylinder pressure and heat release cures, combustion performance can be further optimized by varying the start of injection, rate and duration of injection, etc., and this is underway.

Effect of CWS Ignition Aids. Figure 8 shows that the diesel fuel jet cell (shown in Fig. 3) and the conventional diesel pilot injector are both effective CWS ignition aids. They both yielded approximately the same ignition delay, peak cylinder pressure, and peak burn rate. The impact that each pilot system has on emissions (especially NO_x), fuel consumption, and minimum pilot fuel quantity will be studied as part of the combustion system optimization.

Effect of Engine Load. Figure 9 illustrates the effect of load on CWS operation at two loads: 380 ihp and 470 ihp. Higher operation required a longer injection duration, but did not have a significant impact on ignition delay or peak cylinder pressure. This was expected because the early phase of the fuel injection mechanism is essentially the same regardless of load.

Assuming a mechanical efficiency of 90 percent, 470 ihp at 370 rpm corresponds to approximately 220 psi bmep. These preliminary results indicate that the LSB engine will be able to achieve full load operating on CWS. Injection and engine parameters will undergo further optimization using one cylinder, after which all six cylinders will be modified for CWS operation.

Summary

1 The six-cylinder 1800 kW Model LSB engine was modified to enable the #1 cylinder to operate on CWS, with the other five cylinders operating on DF2.

2 A CWS fuel injection system was designed and fabricated for the LSB engine. This fuel delivery system was scaled up approximately a factor of two from the previously successful JS engine CWS injection system. The same isolating-piston concept was used.

3 The modified engine was operated and full power output was achieved from the CWS cylinder. In order to boost manifold air temperature, the engine was run without the use of intercooler water.

4 Two different pilot systems gave satisfactory results: a DF2 jet cell and a conventional six-hole pilot directly injected into the combustion chamber.

5 CWS injection parameters were varied and full bmep from the CWS cylinder was achieved. However, there is potential for further optimization. The engine was operated at reduced speed to minimize drive chain vibration to the CWS cylinder cambox.

6 Emissions control equipment was designed and installed for six-cylinder CWS operation.

Acknowledgments

We acknowledge the guidance and suggestions of Cary Smith, the Contract Officer's Technical Representative of METC.

Jack Kimberley of AMBAC International provided valuable expertise in designing and supplying the injection system and making it operational. Terry Baker put the data acquisition system together and Jesse Smith supplied the expertise in operating the engine in Mt. Vernon. Al Squires and Charlie Melcher at Grove City have designed and procured respectively the modified LSB components for operation on CWS.

References

Balles, E. N., Benedek, K. R., Wilson, R. P., Jr., and Rao, A. K., 1987, "Analysis of Cylinder Pressure and Combustion Products From an Experimental Coal-Fueled Diesel Engine," *New Engine Technology for Cogeneration*, ASME ICE-Vol. 2, pp. 75–81.

Benedek, K. R., Menzies, K. T., Johnson, S. A. Wilson, R. P., Jr., Rao, A. K., and Schaub, F.S., 1989, "Emission Characteristics and Control Technology for Stationary Coal-Fueled Diesel Engines," ASME JOURNAL OF ENGINEERING FOR GAS TURBINES AND POWER, Vol. 111, pp. 507–515.

Blizzard, D. T., Schaub, F. S., and Smith, J. G., 1991, "Development of the Cooper-Bessemer CleanBurn Gas-Diesel (Duel-Fuel) Engine," *Fuels, Controls, and Aftertreatment for Low Emissions Engines*, ASME ICE-Vol. 15, pp. 87–97; ASME JOURNAL OF ENGINEERING FOR GAS TURBINES AND POWER, Vol. 114, 1992, this issue, pp. 480–487.

Mayville, R. A., Rao, A. K., and Wilson, R. P., Jr., 1990, "Cooper-Bessemer Coal-Fueled Engine System: Recent Developments in Durable Components," *Coal-Fueled Diesel Engines 1990*, ASME ICE-Vol. 12, pp. 17–22.

Mayville, R. A., Rao, A. K., and Wilson, R. P., Jr., 1991, "Durable Component Development Progress for the Cooper-Bessemer Coal-Fueled Diesel Engine," ASME *Coal-Fueled Diesel Engines—1991*, ICE-Vol. 14, pp. 23–27.

Rao, A. K., Melcher, C. H., Wilson, R. P., Jr., Balles, E. N., Schaub, F. S., and Kimberley, J. A., 1988, "Operating Results of the Cooper-Bessemer JS-1 Engine on Coal–Water Slurry," ASME JOURNAL OF ENGINEERING FOR GAS TURBINES AND POWER, Vol. 110, pp. 431–436.

Rao, A. K., Wilson, R. P., Jr., Balles, E. N., Mayville, R. A., McMillian, M. H., and Kimberley, J. A., 1989, "Cooper-Bessemer Coal-Fueled Engine System—Progress Report," *Coal-Fueled Diesel Engines*, ASME ICE-Vol. 7, pp. 9–17.

Staudt, J. E., Itse, D. C., Benson, C., Wilson, R. P., Jr., Schaub, F. S., and Rao, A. K., 1991, "Controlling Emissions From Stationary Coal-Fueled Diesel Engines," presented at the Heat Engines Conference, Morgantown Energy Technology Center, June.

Progress on the Investigation of Coal-Water Slurry Fuel Combustion in a Medium-Speed Diesel Engine: Part 5—Combustion Studies

B. D. Hsu

G. L. Confer

Z. J. Shen

General Electric Transportation Systems, Erie, PA 16531

In the GE 7FDL single-cylinder research diesel engine, coal-water slurry (CWS) fuel combustion optimization studies were conducted using electronically controlled CWS and pilot accumulator injectors. The most important performance parameters of peak firing pressure, combustion efficiency (coal burnout), and specific fuel comsumption were evaluated in relationship to CWS and pilot injection timing, CWS injector hole size, shape, and number, CWS fuel injection spray angles and injection pressure. Heat release diagrams, as well as exhaust samples (gaseous and particulate), were analyzed for each case. Interesting effects of fuel spray impingement and CWS fuel "Delayed Ignition" were observed. With the engine operating at 2.0 MPa IMEP and 1050 rpm, it was able to obtain over 99.5 percent combustion efficiency while holding the cylinder firing pressure below 17 MPa and thermal efficiency equivalent to diesel fuel operation.

Introduction

Under the sponsorship of the U.S. Department of Energy, Morgantown Energy Technology Center, GE Transportation System has been conducting a proof of concept program to use coal-water slurry (CWS) fuel to power a diesel engine locomotive since 1988. Preliminary success was obtained with a converted mechanical fuel injection equipment (FIE) 12-cylinder engine burning mostly coal-slurry fuel and powering a locomotive on the GE test Track for a short period of time. However, the mechanical FIE used by this engine could only provide about 95 percent combustion efficiency (Hsu, 1988a), and had to use a high percentage of diesel pilot fuel (Flynn et al., 1990).

As reported earlier, a high-pressure electronically controlled accumulator injector (Hsu, 1989) using a diamond compact insert nozzle (Flynn et al., 1990) was developed for this project. The improved reliability and durability of this new FIE allowed for an improved and more thorough study of combustion of CWS fuel in a diesel engine. It was decided to include a diesel pilot fuel injector in the combustion system mainly due to engine start and low load operation needs. BKM, Inc., of San Diego, CA, was contracted to develop the electronic diesel fuel pilot/starting FIE for the research engine. As a result, the experimental combustion study was very much facilitated due to the ability of changing pilot/CWS injection timings and quantities without having to stop the engine. Other parameters studied included combustion chamber configuration (by changing CWS fuel injector nozzle hole number/shape/angle), as well as injection pressure. The initial phase of this combustion study is now complete. The results have been adopted into the design of a 12-cylinder engine FIE, to be tested in 1992. This paper summarizes the main findings of this study.

The goal for this study is to maximize combustion efficiency (or carbon burnout), while maintaining tolerable peak cylinder firing pressure (P_{max}), and reasonable specific fuel consumption (SFC). High combustion efficiency is needed mainly for emissions control, although it has some effect also on SFC. It was found that due to the heat release concentration, or high relative cycle efficiency (Hsu, 1984) of the coal fuel diesel combustion, it is necessary to limit the P_{max} (Hsu, 1988b). Low engine SFC depends on high relative cycle efficiency and high combustion efficiency. However, high relative cycle efficiency usually brings high P_{max}; therefore, a compromise has to be attained to prevent engine hardware mechanical failure.

At this point, optimization of the above parameters has resulted in a 99.5 percent combustion efficiency while holding P_{max} below 17 MPa at engine full load (195 KW/cyl or 2.03 MPa indicated mean effective pressure at 1050 rpm). The corresponding SFC is 8160 kJ/IkWh, which translates into about 44 percent indicated thermal efficiency.

Contributed by the Internal Combustion Engine Division and presented at the Energy-Sources Technology Conference and Exhibition, Houston, Texas, January 26-30, 1992. Manuscript received by the Internal Combustion Engine Division August 1, 1991. Associate Technical Editor: J. A. Caton.

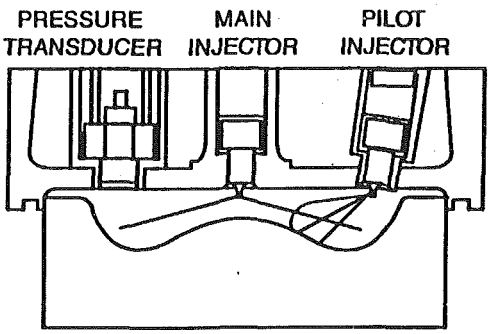

Fig. 1 Test engine combustion chamber layout

Table 1 Kentucky Blue Gem coal nominal lot analysis

Proximate Analysis		Ultimate Analysis	
% Ash	0.80	% Carbon	82.59
% Volatile	39.40	% Hydrogen	5.34
% Fixed Carbon	59.80	% Nitrogen	2.08
		% Chlorine	0.18
Particle Size		% Sulfur	1.01
Mass Mean Diameter (microns)	5.47	% Oxygen (diff.)	8.00
Heating Value	High Heating Value (kJ/kg)		34630

Experimental Hardware, Data Reduction, and CWS Fuel Used

The basic test engine and data reduction processes have been described in detail in a previous paper (Hsu and Confer, 1990). Briefly, the research single cylinder engine has a 229-mm bore, a 267-mm stroke, and a rated speed of 1050 rpm. The combustion chamber arrangement has a side-mounted pilot diesel fuel injector and a centrally placed CWS injector, as shown in Fig. 1. As mentioned previously, the pilot fuel injection system and the main CWS FIE are both electronically controlled. Their injection timings and quantities can be arbitrarily varied by the test engineer during engine operation.

The general instrumentation layout is the same as the one described earlier by Hsu (1988a). The high-speed cylinder pressure, injection pressure, and needle lift data were all collected on a crank angle basis. Fifty cycles were averaged in the digital oscilloscope for further processing. The power generated by the coal-fired cylinder was determined by the indicated kW calculated with the recorded cylinder pressure trace. Thermodynamic first-law calculations were done using cylinder pressure versus volume data to obtain average cylinder temperature and heat release. The water in the CWS was considered to evaporate instantaneously at the time of entrance into the engine cylinder at the corresponding pressure. In the heat release calculation, heat losses to the combustion chamber walls were estimated using the basic relationship outlined by Annand (1963). However, the heat transfer coefficients were modified in such a way that the total heat loss conformed with the fuel heat input rate and the combustion efficiency (carbon burnout).

The CWS combustion efficiency of each run was calculated by the ash balance method. An exhaust particulate sample was collected for each run by an absolute filter over a period of 20 minutes after the engine had stabilized on the test load. The ash/carbon ratio of the collected particulates was compared with the ash/carbon ratio in the original coal to obtain the combustion efficiency for the test run.

The CWS fuel was prepared by Otisca Industries, Inc., of New York using Kentucky Blue Gem coal. It was cleaned to 0.8 percent ash as shown in Table 1. The solid loading of the slurry used was maintained at about 49 percent by weight.

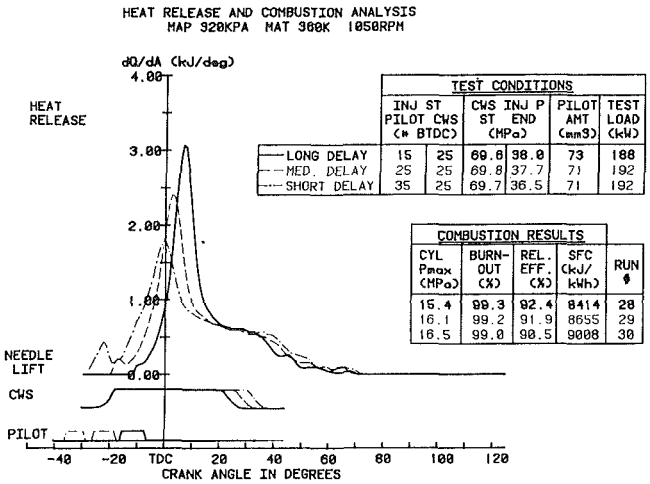

Fig. 2 "Delayed ignition" of CWS at full engine load

The "Delayed Ignition" of CWS at Full Engine Load

In a previous paper published by Hsu (1988a), it was pointed out that when pilot fuel is used to ignite CWS fuel, the starting time of combustion of the CWS fuel is dictated by the start of pilot fuel ignition. This is again investigated under engine full-load conditions (high inlet air temperature and pressure) as shown in Fig. 2. The combustion analyses of three runs using the same CWS fuel injection timing of 25 deg BTDC while varying the pilot fuel timing from 35, 25, to 15 deg before top dead center (BTDC) are displayed. As already proven by previous work, the first small peak on the heat release trace corresponds to the combustion of the pilot fuel. The start of the rise of the heat release trace that follows immediately afterward indicates the start of combustion, or ignition, of the CWS fuel. It is clearly seen that the overall start of combustion in the engine depended on the pilot fuel timing. It is also seen that, although the CWS fuel was injected at the same timing, the CWS fuel residence time before coal ignition (from the start of CWS injection to coal ignition time characterized by the start of the seocnd rise of the heat release curve) depended on the pilot fuel timing

In the right side upper table in Fig. 2, the test conditions are listed. In the lower table of "Combustion Results," the criteria set forth to investigate combustion in this study (P_{max}, combustion efficiency, and SFC) are listed. The run with 15 deg pilot injection timing had the most favorable combustion. It had the lowest P_{max}, highest combustion efficiency, and lowest SFC. Some of the results can find explanation from the heat release traces. The highest P_{max} (35 deg BTDC pilot timing case) was caused by the large amount of fuel burning BTDC. Fuel burned BTDC has a predominant effect on P_{max} over that burned after TDC (ATDC) (Hsu, 1984). The lowest SFC (15 deg BTDC pilot timing case) can be explained by the concentrated fuel combustion close to TDC, as indicated by the highest "Relative Cycle Efficiency" of 92.4 percent listed in the same table. The effect of the latter has also been explained by Hsu (1984). In Fig. 3, the cylinder pressure and temperature are plotted together with the heat release rate. The case of 15 deg BTDC pilot timing produced the highest maximum temperature occurring at about the end of the heat release period (30–40 deg ATDC), which probably contributed to the highest combustion efficiency obtained.

The difference in the shape of the three heat release traces is believed to be caused by the variance of CWS fuel residence time before coal ignition, which is shown in Table 2. The residence time of CWS before ignition appears somewhat like the "ignition delay" for diesel fuel. However, the processes involved are very different. With normal diesel fuel operation, during the ignition delay period, both a physical evaporation

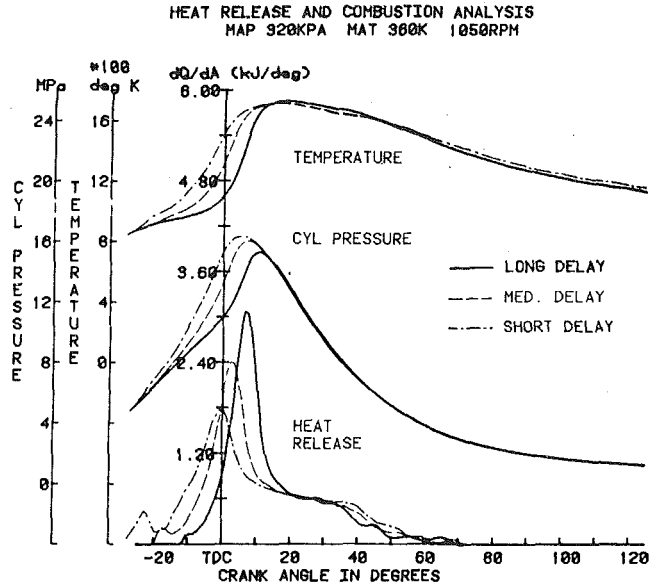

Fig. 3 Cylinder temperature and pressure with "delayed ignition"

process and a chemical kinetic reaction process take place (mainly the latter, which depends on the fuel cetane number). For CWS fuel, the residence time is mainly needed for water evaporation. This is observed both in an engine study (Hsu, 1988a) and a furnace study (Walsh et al., 1984). The amount of dehydrated coal fuel that can be burned at ignition time depends on the amount of water evaporated at that instant. Clearly, the longer residence time the CWS fuel has in the cylinder before ignition, the more water is evaporated by the heat in the cylinder. Thus, more dehydrated coal is released for combustion immediately after ignition. Hence, a very high concentrated heat release rate could appear. On the other hand, it should be pointed out that when pilot fuel is injected early and starts to burn, the average cylinder temperature becomes higher at an earlier time, which can also accelerate evaporation. This can be seen for the three cases in Fig. 3 and the average gas temperatures in the cylinder during coal residence time before ignition are listed in Table 2 as well (both in crank-angle degree and absolute time scales). However, the higher temperature has less effect on evaporation than the residence time. This can be explained, on one hand, by the simplified basic droplet evaporation relationship as follows (Kanury, 1977):

$$dW = k_1 * dt * \ln(k_2 * T_{cyl} + C)$$

where dW = increment of evaporated water mass
dt = time increment
T_{cyl} = in-cylinder temperature
k_1 = f(droplet diameter, thermal diffusivity, density)
k_2 = f(specific heat, latent heat)
C = f(specific heat, latent heat, droplet temperature)

In the above formula, it is seen that the in-cylinder temperature affects the evaporation mass in the exponential term, whereas the residence time has a direct proportional effect. On the other hand, Table 2 indicates that the difference in average gas temperature for the three cases is very small (from 940 to 920 K, about 2 percent). However, the order of magnitude of change in the residence time available for evaporation is significantly greater (from 0.95 to 2.38 ms, about 250 percent). Thus, due to having the most available dehydrated coal fuel at ignition, the case of 15 deg pilot injection producing the highest and most concentrated heat release rate is understood.

From the above analysis, it is seen that CWS fuel can be ignited by pilot fuel any time after being injected into the engine cylinder. However, the best combustion result was obtained by delaying the ignition as much as possible, as in the 15 deg pilot injection case. This can be appropriately named the "delayed ignition" case. In fact, the computer combustion model study under our general research contract also suggested the CWS fuel be injected highly in advance of the pilot fuel (Wahiduzzaman et al., 1991). In the engine tests, it was also found that when pilot injection was further retarded, self-ignition of CWS occurred, which was the limit of "delayed ignition." In such instances, pilot fuel no longer ignited the coal fuel, but rather enhanced combustion after coal self-ignition. No detrimental effect on combustion or engine performance was observed for these cases either.

Table 2 Residence time and average cylinder gas temperature before ignition

Pilot Fuel Timing Deg BTDC	CWS Fuel Res Time Deg CA (msec)	Avg Cyl Gas Temp Deg K
35	6 (0.95)	940
25	11 (1.74)	930
15	15 (2.38)	920

Wall Impingement of CWS Fuel at Full Engine Load

Since CWS self-ignition is the limit of "delayed ignition," a further study was conducted to investigate ways to increase the self-ignition delay of CWS fuel. One obvious way is to advance the injection timing of CWS fuel. Test runs were made by retarding the pilot injection timing beyond the self ignition of CWS fuel. The results of these tests are shown in Fig. 4. Clearly, ignition delay increases as CWS injection timing is advanced (lowest curve). This is evidently due to the lower mean in-cylinder compression temperature that the CWS experiences during the delay period. The mean in-cylinder temperature for the cases studied is shown in the upper curve. Interestingly, the actual ignition time in terms of crank-angle position did not change much as shown by the middle curve.

However, test results showed overly advanced injection timing, although providing very long delay, also deteriorated combustion and engine performance. The combustion analysis of the test cases is shown in Fig. 5. From the combustion results table in the lower right side of this figure, comparing the first (22 deg CWS inj., run #31) and the second (32 deg CWS inj., run #33) cases, SFC is clearly in favor of run #33, which had the longer delayed ignition. The combustion efficiencies of the two are the same, while the P_{max} of run #31 is much lower. This is because of the much lower heat release rate (solid line) due to short "delayed ignition." This trend did not hold true for further advancing the CWS injection timing from 32 deg BTDC to 42 deg, as shown by the third case (run #39, center line). For this last run, although P_{max} remained the same, the combustion efficiency and SFC started to deteriorate (from 99.5 to 99.1 percent and from 8054 to 8876 kJ/kWh, respectively). Further advancement of CWS injection timing to 47 deg BTDC (not shown in the figure) had drastically caused the combustion efficiency to drop to 98 percent and SFC to increase to over 9100 kJ/kWh.

The combustion deterioration cannot be explained by the normal pure diesel fuel operation experience. Overly advanced injection timing in diesel fuel operation brings BTDC early combustion, which leads to high P_{max}, diesel knock (long ignition delay), and bad SFC. In the coal fuel engine case, no overly early combustion is detected. By reviewing the data of

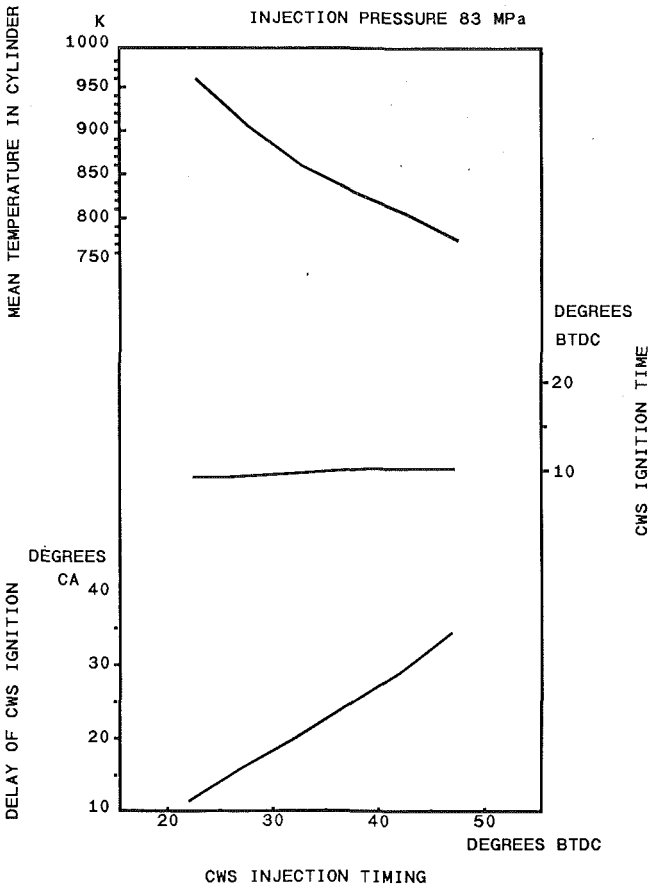

Fig. 4 CWS fuel self-ignition delay

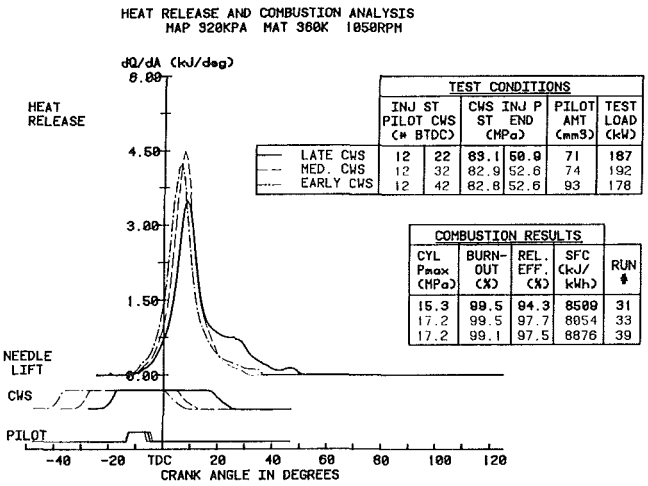

Fig. 5 CWS fuel impingement effect on combustion

a separate CWS fuel injection study included in the present contract (Caton et al., 1991), it is highly probable that the CWS fuel spray has reached the cold cylinder liner walls by the time of ignition for the very early injection timing case. This is illustratively shown in Fig. 6. Further analysis had shown that, even with the 32 deg injection case, CWS fuel spray should have hit the piston crown after less than 5 deg crank angle. The CWS was not ignited until at least 20 crank angle deg later (about 10 deg BTDC). Therefore, piston crown impingement happened well before ignition. Probably the crown temperature was high enough not to deteriorate the overall vaporization and subsequent combustion. Inspection of piston crown after engine dismantling had shown definite

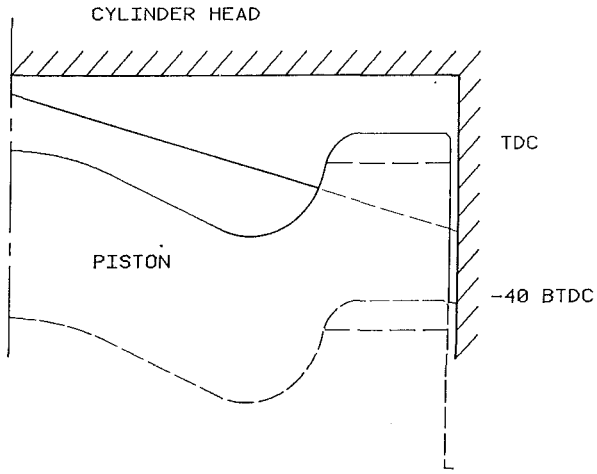

Fig. 6 Schematic of injection timing and CWS impingement

impingement marks. A major difference in the combustion of CWS and pure diesel fuel in the engine may be that for the CWS case, fuel spray impingement is not only unavoidable, but in fact is necessary (for "delayed ignition").

CWS and Pilot Injection Timing Effect at Full Engine Load

Fuel injection timing maps for full engine load operations have been generated for P_{max}, combustion efficiency, and SFC, as shown in Fig. 7. They are made by generating isometric lines using actual test results (triangles in the figure). For all three indicators, in the full load usable range, pilot fuel injection timing seems not to have a major effect. This is probably due to the fact that the combustion in the engine cylinder is mostly initiated by coal fuel self ignition. At about 37 deg BTDC CWS injection timing, maximum P_{max} can be expected with each pilot fuel injection timing. The later the pilot fuel is introduced, the smaller its contribution to raising P_{max} due to ATDC combustion. Introducing the CWS fuel before 37 deg BTDC (toward the right in the map), P_{max} is reduced because of fuel spray cylinder liner impingement hindering heat release rate. The CWS fuel "delayed ignition" effect again can be seen in the part where injection is after 37 deg BTDC (toward the left). The same explanation can be given to the combustion efficiency and SFC part of the map. However, the optimum CWS injection timings for these two indicators are not the same. This is probably because the optimum combustion efficiency depends mainly on the cylinder temperature, whereas the SFC depends on the concentration of heat release about TDC ("Relative Cycle Efficiency") and the combustion efficiency. Using this map, the injection timings of pilot and CWS fuel can be selected with the compromise needed for P_{max}, combustion efficiency, and SFC. In the present case the pilot timing is 12 and the CWS timing is 35 deg BTDC.

Combustion Chamber Configuration

The first investigation on combustion chamber configuration was to compare a 10-hole (0.40-mm diameter) CWS injector nozzle with an 8-hole (0.46-mm diameter) having the same total flow area. The combustion indicators are summarized in Fig. 8. It is seen that both injectors can have the same maximum P_{max} valve, highest combustion efficiency, and lowest SFC. However, they happened at different CWS injection timings. Normal pure diesel fuel operation experience would suggest the better "air utilization" of the 10-hole injection nozzle should indicate some advantage. Further investigation into the fuel injection rate of the nozzles had shown that due to the hole size discrepancy, the hole discharge coef-

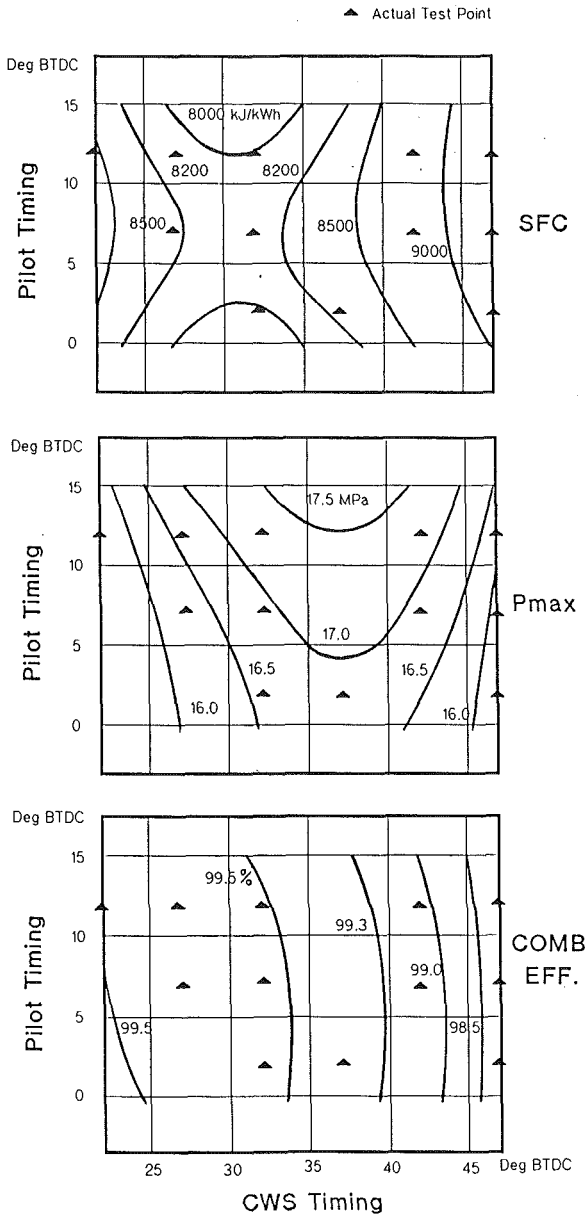

Fig. 7 Injection timing map at engine full load

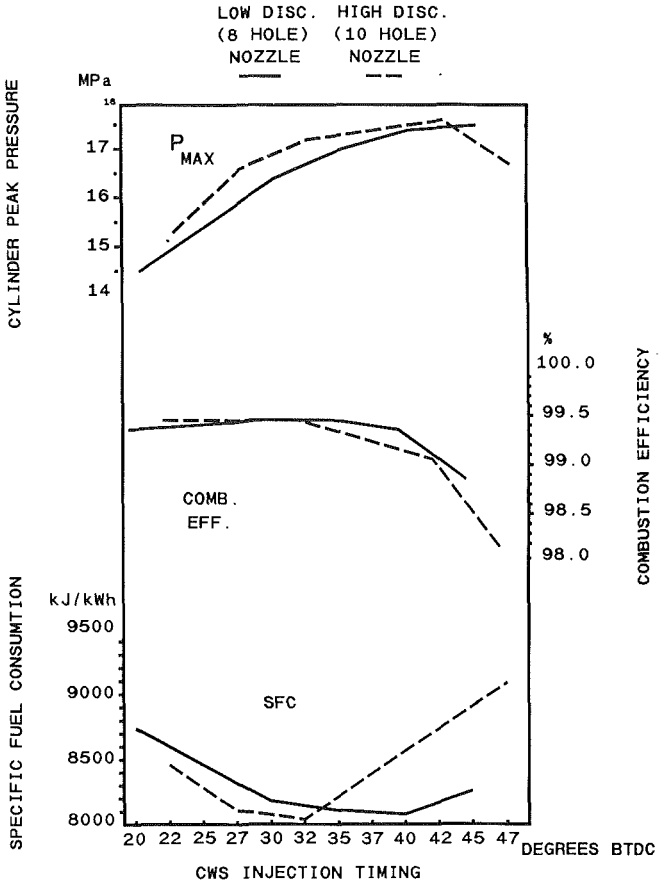

Fig. 8 Effect of injector hole discharge coefficients

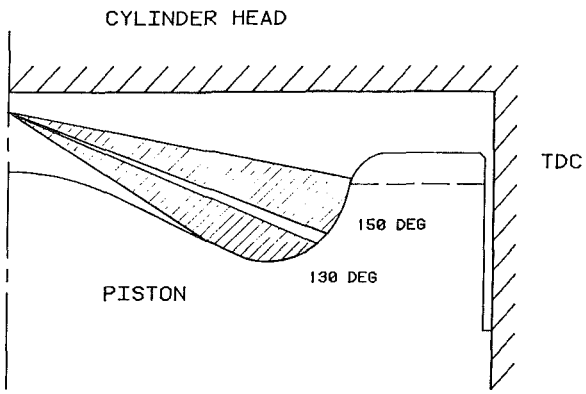

Fig. 9 Schematic of spray included angle and impingement

ficients were different (0.88 for the 0.40-mm hole and 0.80 for the 0.46-mm hole). Since they were injected with the same injection pressure of 82.7 MPa, the spray exit velocity from injector hole for the former was 333 m/s, and the latter, 300 m/s. The higher exit velocity 10-hole nozzle would hit the cylinder liner wall at a smaller injection advance angle, making its optimum value move correspondingly. This explanation suggests that for the two injectors tested, the initial air entrainment of the spray jet (hole number dependent) is not as important as the secondary atomization after spray impingement (depending on spray velocity) on the piston crown. Similar tests were done with different injector hole shapes. They included inverse trumpeted hole, rounded inner edged hole, etc. Both 8 and 10-hole nozzles of different shapes were made. All of them seemed to suggest the same conclusion of spray velocity having the dominant effect. Based on these results, the 8-hole nozzle was selected for prototype due to much less tendency to hole plugging.

An 8-hole nozzle with smaller spray included angle of 130 deg (as compared to the original 150 deg) was tested to avoid cylinder liner impingement of CWS spray. It is schematically shown in Fig. 9. Test results as compared with the original are shown in Fig. 10. It can be seen that the firing pressure was lower and the combustion efficiency never reached the previous level, although the SFC was close. However the fact that the combustion efficiency decreased was not acceptable to the combustion design. This may imply that too much attachment of the impinged CWS on the piston crown is unfavorable also. More work has to be conducted in the future to optimize CWS impingement in the combustion chamber.

Injection Pressure Effect

An investigation into CWS injection pressure was conducted early in the combustion study. The injection pressure varied between 61 to 83 MPa. The P_{max}, combustion efficiency, and SFC results are compared in Fig. 11. P_{max} and combustion efficiency are seen to increase with CWS injection pressure,

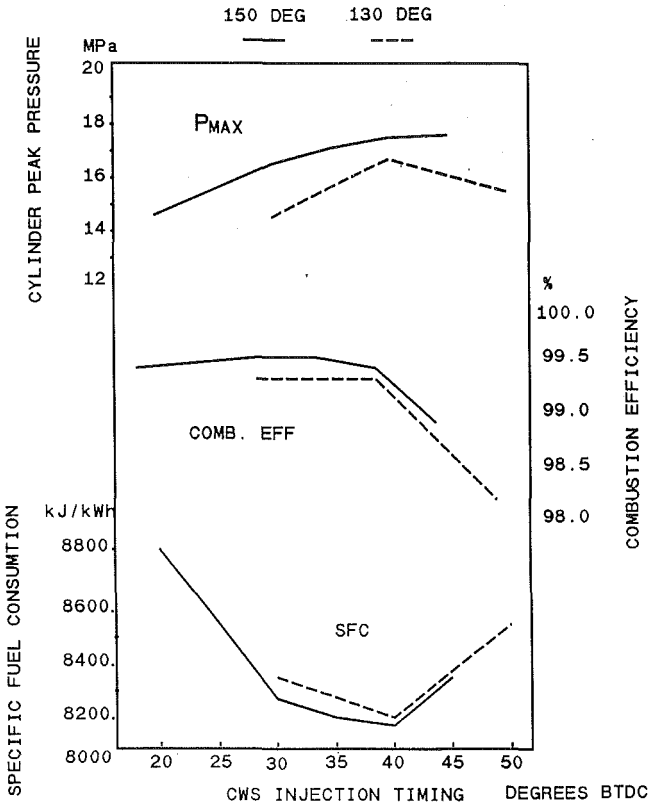

Fig. 10 Effect of injection spray included angle

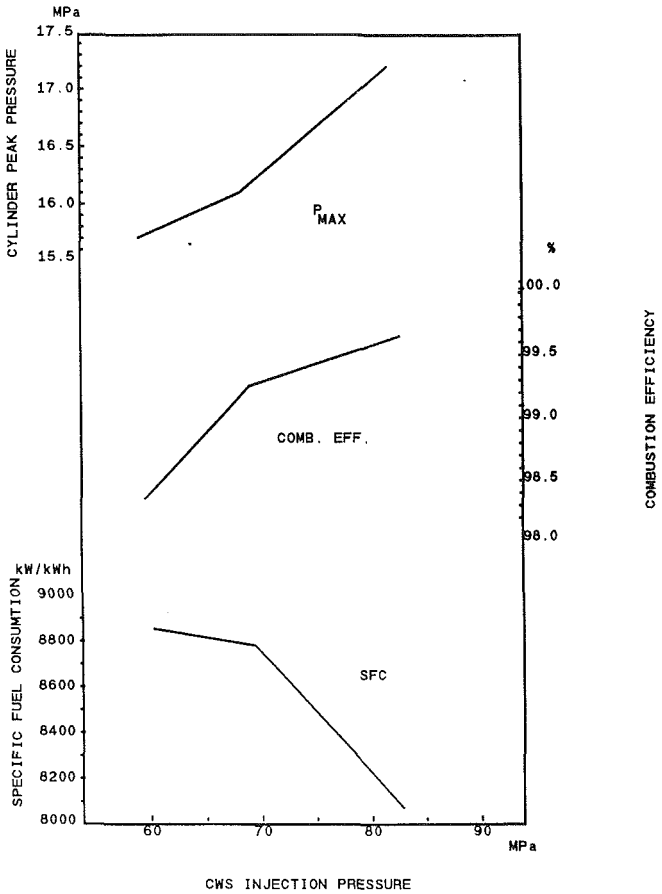

Fig. 11 Performance effect of CWS injection pressure

while SFC decreases. Within the tested range, combustion performance definitely improved when higher injection pressure was used. The calculated heat release traces together with the cylinder pressure and the injector needle lift of the three runs are shown in Fig. 12. The highest heat release rate of the highest injection pressure case is evident. The injection starting time was the same (25 deg BTDC) and the CWS fuel was ignited at about the same time (10 deg BTDC). The higher heat release rate after ignition started is both the result of better atomization and more fuel being injected into the cylinder at the same instant. It is interesting to note that from the CWS ignition to the fall off of the peak heat release, there seems to be a fairly constant duration of 35 to 40 deg crank angle. If the injection duration extends beyond the fall off period, then a hump, mentioned first by Hsu (1989), of rather slow heat release rate appears toward the end of the combustion period. It is in proportion to the extension of fuel injection duration beyond the 35 to 40 deg crank angle period.

Combustion at Engine Lower Loads

Lower load operation is characterized by very low or no boost pressure in the inlet air manifold. As explained previously (Hsu, 1988a), it is not possible to self-ignite the CWS due to the excessive temperature drop after heat is extracted to vaporize the water in fuel. Pilot diesel fuel combustion heat is necessary to raise the temperature early in the cycle for water evaporation. A typical combustion heat release pattern of the notch 2 load (naturally aspirated, 536 rpm, 300 kPa BMEP) is shown in Fig. 13. The first triangular heat release shape corresponds to the pilot diesel fuel combustion, which amounts to about 24 percent of energy as compared to about 4 percent at full engine load. The coal combustion efficiency was only about 93 percent, due to the low maximum combustion temperature of 1560 K, which is much lower than the 1900 K at full engine load. The engine operation conditions and performance results at lower loads are summarized in Table 3.

It is most interesting to note that when engine load increases, the optimum injection timing of the pilot fuel is retarded while that of CWS fuel is advanced. As anticipated, the pilot fuel amount needed becomes less when engine load is increased. The combustion efficiency increases with the engine load probably due to higher combustion and piston crown temperature.

Within the present program, a duty cycle coal usage percent target had been set for the study of overall economics of a coal fired locomotive. A typical locomotive operates about 60 percent of time at idle, which uses pure diesel fuel. Therefore, the target was set for 75 percent of coal energy consumption (25 percent diesel fuel) on a duty cycle basis. The above Table 3 type of operation can actually provide 80 percent coal usage, which exceeded the planned goal.

Summary

A detailed study of the combustion of CWS fuel in a diesel engine has been made. The important findings are as follows.

- Fully utilizing the residence time of CWS fuel in the cylinder to evaporate the water content by "delayed ignition" generally brings good combustion results. The limit of "delayed ignition" is the self-ignition of CWS without pilot fuel.
- It is advantageous to inject CWS fuel early and pilot fuel late in the cycle for "delayed ignition." The limit of CWS early injection is the fuel impingement onto the cold cylinder liner walls. When this happens, combustion deteriorates drastically.
- The residence time needed to evaporate the water content of CWS fuel is very long and the spray jet travels very fast; therefore, impingement of the CWS before ignition seems to be unavoidable. As long as high temperatures exist, as in the full engine load case, impingement of CWS onto piston crown does not seem to hurt combustion.
- Close to the optimized combustion zone for full engine

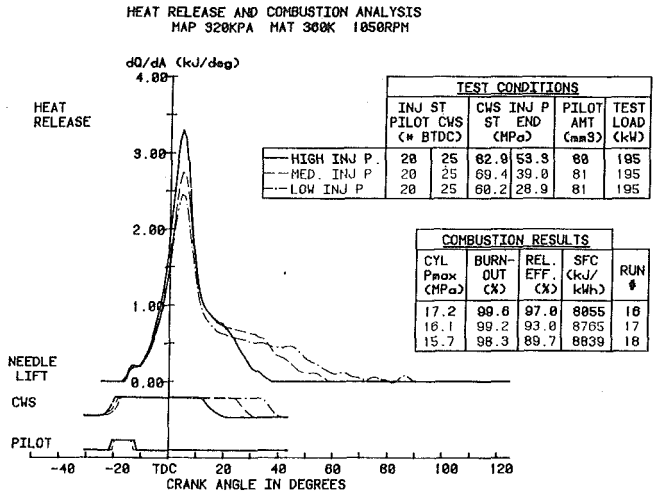

Fig. 12 Combustion effect of CWS injection pressure

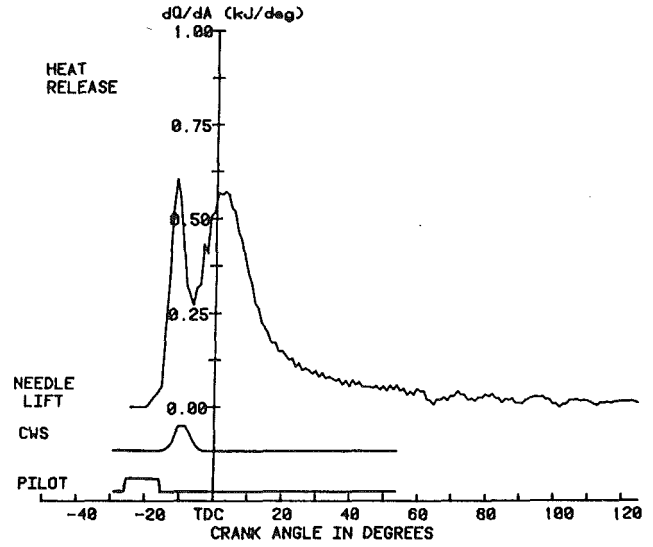

Fig. 13 Engine combustion at low engine load

load condition, the injection timing of the pilot fuel has less impact on combustion than that of CWS. The combustion efficiency can reach 99.5 percent and engine cycle efficiency is comparable to pure diesel fuel engine.

- The effect of injector hole number or shape seemed to have less effect on combustion than the spray penetration velocity. This might be due to the fact that combustion started after secondary atomization of the spray impinging on piston crown.
- Within the range tested (under 85 MPa), higher injection pressure brings better engine combustion results.
- Under low load conditions, there is not enough heat in the cylinder to evaporate the water content in CWS fuel quickly without early pilot diesel fuel combustion. CWS injection timing has to be retarded. As the engine load is increased, the injection timings of pilot and CWS fuel move in opposite directions until early CWS and late pilot are reached.

Table 3 Engine operation conditions and results

Load	Operation Conditions						Combustion Results		
	RPM	MEP MPa	Inj. Tim. BTDC		Fuel Amt Percent		Pmax MPa	Comb. Eff. %	SFC kJ/kWh
			Pilot	CWS	Pilot	CWS			
N2	620	0.30	24	15	23.8	76.2	4.9	92.8	12165
N3	880	0.49	23	15	23.9	76.1	5.5	94.9	10450
N4	880	0.56	22	15	16.9	83.1	5.9	96.5	9255
N5	960	1.03	20	20	9.2	90.8	8.2	97.5	8560
N6	960	1.35	19	20	6.7	93.3	9.9	98.5	8258
N7	960	1.71	18	25	5.0	95.0	12.3	99.0	8403
N8	1050	1.98	12	35	4.0	96.0	17.1	99.5	8159

Acknowledgment

The support and permission to publish the results of this study from GE Transportation Systems and DOE Morgantown Energy Technology Center are gratefully acknowledged. The work on which this paper is based was conducted under DOE Contract DE-AC21-88MC23174. The support of the program from the other sponsors, Norfolk Southern Corporation, Pennsylvania State Energy Development Authority, and New York State Energy Research and Development Authority is also gratefully acknowledged. The authors would like to thank their many colleagues at GE Transportation Systems and GE Corporate Research and Development for their valuable contributions. The authors would also like to thank Mr. Leland Paulson, Contracting Officer Technical Representative DOE/METC for his comments and encouragements in the course of this study.

References

Annand, W. J. D., 1963, "Heat Transfer in the Cylinder of Reciprocating Internal Combustion Engines," *Proc. Instn. Mech. Engrs.*, Vol. 177, No. 36.

Caton, J. A., Kihm, K. D., Seshadri, A. K., and Zicterman, G., 1991, "Micronized Coal Water Slurry Sprays From a Diesel Engine Positive Displacement Fuel Injection System," presented to the Combustion Institute, Control States Section, 1991 Technical Meeting, Nashville, TN, Apr.

Flynn, P. L., Hsu, B. D., and Leonard, G. L., 1990, "Coal Fueled Diesel Engine Progress at GE Transportation Systems," ASME JOURNAL OF ENGINEERING FOR GAS TURBINES AND POWER, Vol. 112, pp. 369-375.

Hsu, B. D., 1984, "Heat Release, Cycle Efficiency and Maximum Cylinder Pressure in Diesel Engine—The Use of an Extended Air Cycle Analysis," *S.A.E. Transactions*, p. 4.766.

Hsu, B. D., 1988a, "Progress on the Investigation of Coal-Water Slurry Fuel in a Medium-Speed Diesel Engine: Part 1—Ignition Studies," ASME JOURNAL OF ENGINEERING FOR GAS TURBINES AND POWER, Vol. 110, pp. 415-422.

Hsu, B. D., 1988b, "Progress on the Investigation of Coal-Water Slurry Fuel in a Medium-Speed Diesel Engine: Part 2—Preliminary Full Load Test," ASME JOURNAL OF ENGINEERING FOR GAS TURBINES AND POWER, Vol. 110, pp. 423-430.

Hsu, B. D., Leonard, G. L., and Johnson, R. N., 1989, "Progress on the Investigation of Coal-Water Slurry Fuel in a Medium-Speed Diesel Engine: Part 3—Accumulator Injector Performance," ASME JOURNAL OF ENGINEERING FOR GAS TURBINES AND POWER, Vol. 111, pp. 516-520.

Hsu, B. D., and Confer, G. L., 1991, "Progress on the Investigation of Coal-Water Slurry Fuel Combustion in a Medium Speed Diesel Engine: Part 4—Fuels Effect," *Coal Fueled Diesel Engines*, ASME ICE-Vol. 14.

Kanury, A. M., 1977, *Introduction to Combustion Phenomena*, 2nd ed., Gordon and Breach Science Publishers.

Wahiduzzaman, S., Blumberg, P. N., and Hsu, B. D., 1991, "Simulation of Significant Design and Operating Characteristics of a Coal Fueled Locomotive Diesel Engine," *Coal Fueled Diesel Engines*, ASME ICE-Vol. 14.

Walsh, P. M., Zhang, M., Farmayan, W. F., and Beer, J. M., 1984, "Ignition and Combustion of Coal-Water Slurry in a Confined Turbulent Diffusion Flame," presented at the 20th International Symposium on Combustion, Ann Arbor, MI, Aug.

Injection Characteristics of Coal-Water Slurries in Medium-Speed Diesel Equipment

L. G. Dodge

T. J. Callahan

T. W. Ryan, III

J. A. Schwalb

Southwest Research Institute,
San Antonio, TX 78228

C. E. Benson

R. P. Wilson, Jr.

Arthur D. Little, Inc.,
Cambridge, MA 02140

The injection characteristics of several micronized coal-water slurries (CWSs, where "s" implies plural) were investigated at high injection pressures (40 to 140 MPa, or 6,000 to 20,000 psi). Detailed spray characteristics including drop-size distributions and cone angles were measured using a continuous, high-pressure injection system spraying through various hole shapes and sizes into a continuous, elevated-pressure air flow. Penetration and cone angle were also measured using intermittent injection into an elevated-pressure quiescent chamber. Cone angles and fuel-air mixing increased rapidly with the relatively constant cone angles of diesel fuel. However, even at high injection pressures the CWSs mixed with air more slowly than diesel fuel at the same pressure. The narrower CWS sprays penetrated more rapidly than diesel fuel at the same injection pressures. Increasing injection pressure dramatically reduced drop sizes in the CWS sprays, while increasing injection pressure reduced drop sizes in the diesel fuel sprays more gradually. The CWSs produced larger average drop sizes than the diesel fuel at all conditions, except for some hole shapes at the highest injection pressures where the average sizes were about the same. Varying the hole shape using converging and diverging holes had a minimal impact on the spray characteristics. A turbulent jet mixing model was used to predict the penetration rate of the CWS fuel jets through different orifice sizes and into different air densities. The jet model also computes the liquid fuel-air ratio through the jet. The work reported here was abstracted from the more complete report by Schwalb et al. (1991).

Introduction

Background. For liquid-fueled diesel engines, high injection pressures generally increase the combustion performance. This high-injection pressure philosophy is also reflected in coal-fueled diesel engines in the fact that several researchers (Leonard and Fiske, 1987; Rao et al., 1988; Hsu et al., 1989) have been working toward the development of injection systems that can achieve higher injection pressures. The driving force for these development activities is the observation that increased injection pressure results in improved engine combustion performance with the coal fuels (Rao et al., 1988, 1989; Hsu et al., 1989). However, the high fuel injection pressures required for efficient combustion (e.g., ≈62 MPa or 9000 psi for the Cooper-Bessemer engine reported on here) are thought to increase wear problems in injector tips.

Objectives. This work had the following objectives:

- Evaluate the need for high injection pressures by documenting drop sizes and fuel-air mixing (cone angles and penetration rates) as a function of injection pressure.
- Determine whether alternate hole shapes could provide enhanced atomization at lower injection pressures.
- Determine the effect of coal particle size and loading on spray characteristics.

Approach

The objectives described above for the spray tests were accomplished by conducting two types of spray experiment. The detailed spray characteristics of drop-size distribution and liquid volume fraction (overall fuel-air volume ratio) were measured using a continuous high-pressure spray into an ambient temperature, elevated-pressure, flowing air stream. Measurements were made of the continuous spray with a Malvern laser-diffraction particle sizer, followed by mathematical deconvolution of the data to obtain spatially resolved data. The global spray characteristics of penetration rate and cone angle were determined using intermittent injections into an ambient-temperature, high-pressure, quiescent chamber.

Experimental Apparatus

Experimental Apparatus for Continuous Spray Tests. The apparatus used for these experiments was the standard Cooper-

Contributed by the Internal Combustion Engine Division and presented at the Energy-Sources Technology Conference and Exhibition, Houston, Texas, January 26-30, 1992. Manuscript received by the Internal Combustion Engine Division August 25, 1991. Associate Technical Editor: J. A. Caton.

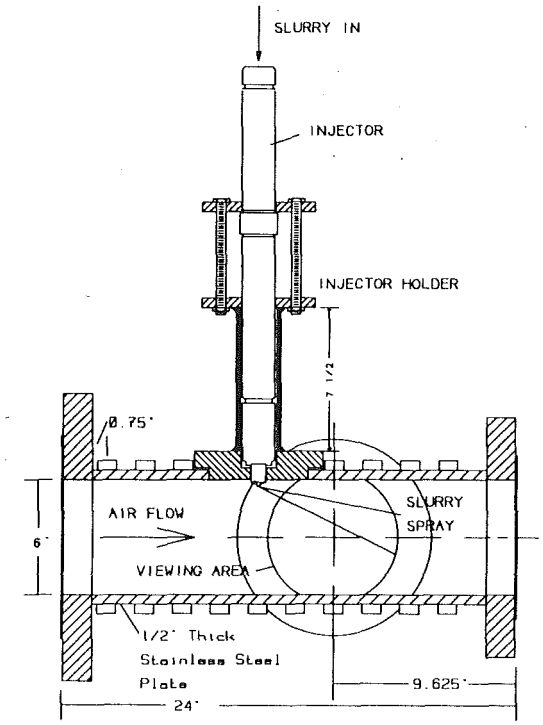

Fig. 1 Experimental apparatus for continuous spray tests into continuous high-pressure air flow

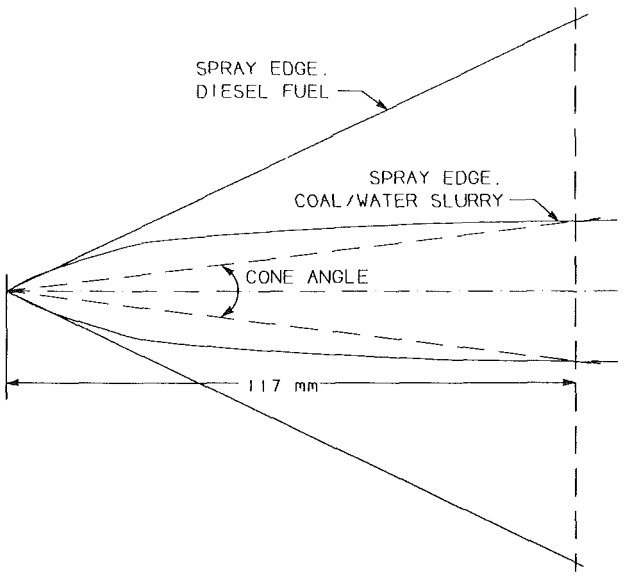

Fig. 2 Schematic showing the spray cone of the coal-water slurries compared with diesel fuel, and definition of cone angle used for continuous spray tests

Bessemer diesel injector body for the JS-1 engine, mounted into a test section that provided ambient temperature, high-pressure flowing air, as shown in Fig. 1. The test section includes large windows (175 mm diameter) on either side to allow optical access for laser diagnostic equipment. For some of these tests the standard 19-hole injector tip was used, but 18 of the 19 holes were spot welded closed to avoid spraying onto the windows of the test section, leaving a single spray for characterization. The remaining orifice has a 0.3 mm diameter with a length-to-diameter ratio (L/D) of about 5. For most of the other tests, the standard 19-hole injector tip was replaced by a modified four-hole "button-holder" tip in which three of the four holes were plugged. The "button-holder" design allowed for interchangeable nozzle orifice buttons that varied the nozzle orifice geometry. Finally, an injector tip with a 0.5 mm orifice was also used for some tests.

Fuel was supplied continuously to the nozzle at high fuel pressures by a 10:1 pressure intensifier system using a 20.7 MPa (3000 psi) hydraulic system as the power source. For the diesel spray measurements, the high-pressure side of the system was filled with standard DF-2 diesel fuel. For the coal–water slurry (CWS) measurements, the high-pressure side of the intensifier was filled with diesel fuel acting on one side of a free-floating piston that supplied pressure to the slurry on the other side of the piston. Injection pressures to 207 MPa (30,000 psi) are possible with this system. However, the pressure range of interest for this program was 41 MPa (6,000 psi) to 138 MPa (20,000 psi).

Cone angles for the sprays were determined from video recordings. There is no standard definition for cone angle by ASTM or any other standards-setting organization. This is particularly significant for the CWS sprays, for while the diesel sprays produce a cone-shaped spray with almost straight edges, the CWSs produce sprays that start out with slightly smaller initial cone angles than diesel fuels, but then bend inward until the edges are almost parallel to the spray axis, as shown schematically in Fig. 2. Water has a higher surface tension than diesel fuel by about a factor of three, and the reduced cone angle could possibly be related to the difference in surface tensions. The CWSs have other properties related to the energy required to separate closely packed particles in the relatively viscous mixture during the atomization process, and this unnamed property is somewhat analogous to surface tension and may also be related to the smaller cone angle for the CWSs. For the continuous spray tests, the cone angle was calculated as the arctangent of the spray width divided by the axial distance at the measurement location of 177 mm (4.6 in.) from the injector tip. This definition of cone angle emphasizes the narrow width of the CWS sprays near the edge of the piston bowl, but results in a smaller calculated cone angle than the initial cone angle at the injector tip.

The spray measurements reported here were performed with a Malvern Model 2600 laser-diffraction particle sizing instrument. The possibility of extended breakup distances causes problems in measurements close to the nozzle, as do the high spray densities, so these measurements were made at 152 mm (6 in.) downstream of the nozzle tip. This measurement location is slightly larger than the radius of the piston bowl of the Cooper-Bessemer engine that this nozzle is used in. The laser beam diameter was reduced from the standard 9-mm diameter to 3-mm diameter for improved spatial resolution. A computer-controlled positioner was used to traverse the instrument for measurements at various chords through the spray from the centerline to the edge of the spray in increments of 4 mm (0.157 in.). All data were reduced assuming a Rosin-Rammler distribution of drop sizes (Allen, 1981). Average drop sizes were represented by the Sauter mean diameter (SMD), also described as D_{32}, which was calculated from the Rosin-Rammler size distribution parameters (Allen, 1981). The multiple-scattering bias correction procedure of Dodge (1984) was used. These measurements were deconvoluted to convert from line-of-sight averages to spatially resolved data using the procedure of Hammond (1981).

The test matrix included sprays into air at elevated air densities to simulate injection into a diesel engine. The estimated engine conditions were an air pressure of 4.05 MPa (588 psi), an air temperatrure of 482°C (900°F), and air density of 18.7 kg/m^3. The air density rather than the air pressure is considered the significant parameter for controlling atomization. Tests at elevated air temperatures were not practical for this system, so the tests were performed at ambient temperature but with attempts to match the air density to engine conditions. Although tests were attempted at the desired air density of 18.7

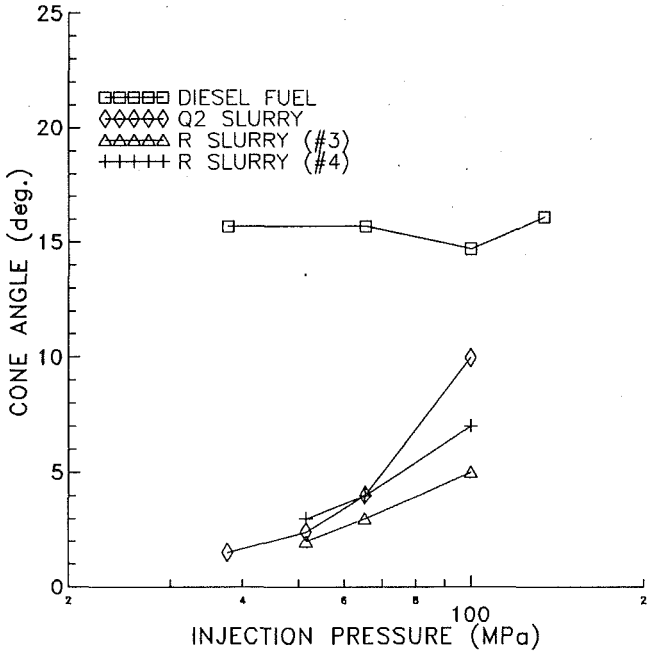

Fig. 3 Comparison of spray jet cone angles for Batch-Q2 CWS, Batch-R CWS, and diesel fuel at different injection pressures using 0.3-mm hole tip and spraying into air at 0.86 MPa (125 psia), 35°C (95°F)

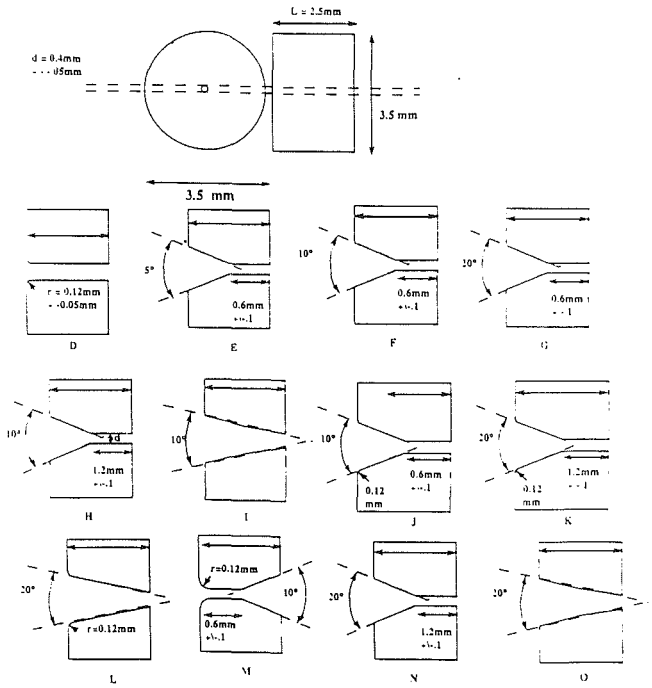

Fig. 4 Hole shapes tested for changes in atomization characteristics

kg/m^3, the maximum available air velocity at this higher air density was insufficient to keep the high-velocity fuel jet from recirculating and impinging on the window. The actual conditions were 0.862 MPa (125 psia), 38°C (100°F), and 9.7 kg/m^3 for the video and cone angle measurements, and 0.552 MPa (80 psia), 38°C (100°F), and 6.18 kg/m^3 for the drop size measurements.

Experimental Apparatus for Intermittent Injection Tests. The intermittent injection system consisted of a pump to pressurize the CWSs, a standard injector nozzle, and elevated-pressure chamber, and a high-speed movie camera. The pumping system consisted of a standard Cooper JS-1 injection pump with the cam driven by a variable speed 75 kW (100-hp) motor. The CWSs were pressurized directly by this injection pump and delivered to a 19-hole Cooper injector nozzle as used in the Cooper JS-1 engine. This injector was mounted in an ambient-temperature, elevated-pressure injection bomb. The bomb had a 0.305 m (12-in.) diameter circular cross-section with the injector centrally mounted at one end of the vessel. A 0.152 m (6-in.) diameter acrylic window was mounted at the opposite end of the vessel, slightly off-center so that an entire spray could be viewed. The injection line was instrumented to measure injection pressure with a transducer mounted at the nozzle end of the injection line. The injection nozzle was instrumented to measure needle lift using an amplifier and needle lift probe. The line pressure and needle lift data were acquired using a Nicolet four-channel digital oscilloscope. The data were acquired as a function of time that was then converted to cam angle position using a TDC pulse to reference the time-based data to cam angle.

High-speed movies were recorded with a Hycam rotating prism camera at typical framing rates of 2500 per second using high-speed film (ASA 250 and 400). For the intermittent injection tests, cone angles were determined by drawing tangents to the outer edge of the spray cone from the nozzle tip outward. This provides a measure of the initial cone angle, but resulted in angles larger than measured in the continuous spray tests.

Coal-Water Slurries. The coal-water slurries (CWSs) used in this program may be briefly described as follows. Batch-Q2 was a 52 solids wt. percent micronized CWS with a top particle size (98 wt. percent smaller) of 44 μm and a mass median diameter of 15 μm, with an ash content of less than 1.5 percent. Batch-R was a micronized CWS with a top particle size of 15 μm and a mass median size of 5 μm, with an ash content of less than 1.5 percent. Batch-R was used at several different dilutions. One batch referred to as Batch-R (#3) had a solids content of 54.0 wt. percent, but was difficult to handle and flow, and that had variable rheological properties. Limited results are shown for that batch. Batch-R (#3) was diluted with deionized water to lower its solids content to 52.0 wt. percent so that it would match the solids fraction of Batch-Q2, and this sample was labeled Batch-R (#4). Limited testing was also performed with Batch-R (#4) further diluted to 48 wt. percent and 40 wt. percent solids.

Rheological measurements were made at a range of shear rates using a concentric cylinder viscometer for shear rates of about 15 to 1500 s^{-1}, and an extrusion rheometer for shear rates from 150 to 25,000 s^{-1} (Schwalb et al., 1991). At higher shear rates presumed to be of significance to atomization, about 10,000 s^{-1}, the apparent viscosity of all the CWSs was relatively constant as a function of shear rate. For Batch-Q2 the apparent viscosity at 10,000 s^{-1} was 190 mPa-s (190 cP), Batch-R (#3) was 330 mPa-s (330 cP), and Batch-R (#4) was 150 mPa-s (150 cP) (Schwalb, 1991). The Batch-R (#4) CWSs diluted to 48 and 40 wt. percent were not characterized rheologically.

Results

Fuel–Air Mixing Rates From Continuous Spray Measurements (Cone Angles). The detailed atomization measurements performed with the continuous spray apparatus highlighted the much slower fuel-air mixing in the spray jet of the CWSs when compared with diesel fuel. Fuel-air mixing was inferred from the cone angle measurements, i.e., large cone angles implied rapid fuel-air mixing, and small cone angles implied slow mixing. As shown in Fig. 3, both the Batch-Q2 and Batch-R CWSs showed much slower fuel-air mixing than the diesel fuel. The cone angles of the CWS sprays increased rapidly with increasing injection pressure, in contrast with cone

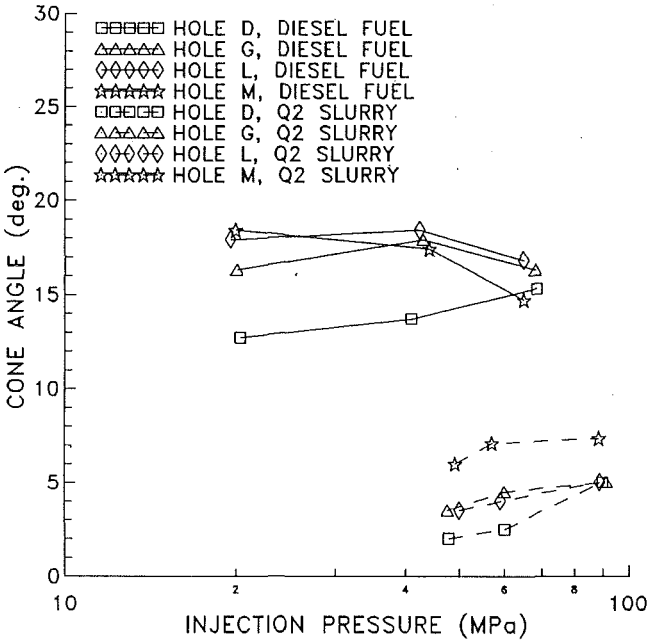

Fig. 5 Effect of hole shape on cone angle of CWS as compared with diesel fuel, spraying into air at 0.55 MPa (80 psia) and 35°C (95°F)

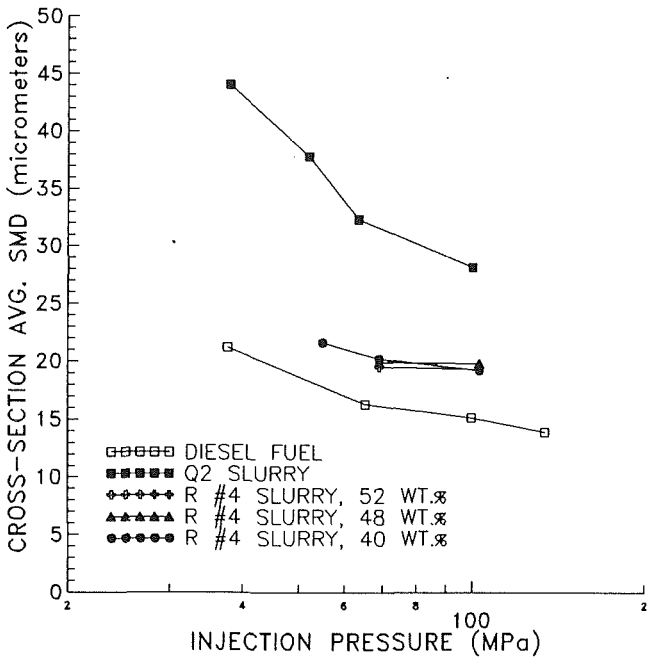

Fig. 6 Comparison of cross-section average SMDs for various injection pressures for Batch-Q2 CWS and diesel fuel spraying into air at 0.55 MPa (80 psia) and 35°C (95°F)

angles for diesel fuel that were almost constant with injection pressure. Also, while diesel fuel sprays produced almost straight-sided cone sprays, the CWSs produced sprays that initially had cone angles almost as large as diesel fuel, but then the spray jets contracted until the edges of the spray were almost parallel to the spray axis. The rapid increase in the cone angles with injection pressure for the CWSs might be the explanation for the high injection pressure requirement when using CWSs in the JS-1 engine. Both the Batch-Q2 and Batch-R CWSs showed similar spray cone angles, but the Batch-R (#4) showed consistently larger cone angles than Batch-R (#3). This trend was consistent with the fact that Batch-R (#3) had a higher loading and a higher viscosity than Batch-R (#4). Batch-Q2 and Batch-R (#4) had similar loadings and produced similar cone angles except at the highest injection pressure where Batch-Q2 had a larger cone angle.

The relatively slow air utilization by the CWS sprays, especially at lower injection pressures, led to the investigation of the spray characteristics of the twelve different hole shapes as shown in Fig. 4. The objective of this effort was to determine if these alternative hole shapes could produce equivalent or larger cone angles and equivalent or smaller average drop sizes than the standard 0.3 mm hole injector at lower injection pressures. The lower injection pressures should reduce the wear problems in the nozzle tips.

All the hole shapes shown in Fig. 4 were evaluated for spray jet cone angles at three different injection pressures ranging from about 20 to 69 MPa (3000 to 10,000 psid, where "d" indicates the differential pressure across the tip) on DF-2 diesel fuel. These measurements were made in the same apparatus as used for the standard tip, except that the four-hole nozzle holder was used with three of the four holes plugged shut. This range of injection pressures was chosen to determine if one or more of these shapes would provide enhanced atomization relative to the standard nozzle shape "D" at the lower injection pressure than required by the engine using the baseline injector tip (about 55 MPa or 8000 psid). The results for all twelve injector holes at all three pressures resulted in cone angles of 15 to 21 deg, with no discernible dependence of cone angle on hole shape or injection pressure for the diesel fuel sprays.

The standard hole shape D and the three hole shapes with the most radical hole designs, G, L, and M, were tested in the same four-hole injector using Batch-Q2 CWS, with results as shown in Fig. 5. Similar to the results with the standard 0.3 mm diameter injector, the CWS produced much smaller cone angles than diesel fuel. The cone angles with CWS were a function of injection pressure with the cone angle increasing with increasing injection pressure. Interestingly, the standard hole shape D produced a slightly smaller cone angle than the other designs on CWS, and hole shape M produced the broadest cone angle. These differences could be due to a larger effective L/D for hole shape D compared to the other shapes.

The fuel-air mixing is proportional to the spray cross-sectional area, and that is approximately proportional to the square of the cone angle. The cone angle decreased by a factor of about four for the CWSs compared to diesel fuel shown in Figs. 3 and 5. Therefore, this decrease in cone angle represents a factor of about 16 higher fuel/air ratio in the spray plume. This indicates a limited air utilization in the spray before impact with the piston bowl.

Drop Size Measurements and Liquid Volume Fraction. Drop size and liquid volume fraction measurements were made with the Malvern Model 2600 laser-diffraction particle sizer for both diesel fuel and CWSs. All measurements were made at 152 mm (6 in.) from the nozzle tip, at several radial chords for each condition. Diesel fuel sprays typically have breakup lengths on the order of 10 mm at the test conditions, while the breakup length for the CWSs is unknown. Certainly the radial spreading of the CWS sprays was much slower than for diesel fuel, and the higher surface tension and viscosity of the CWSs is expected to increase the breakup length. The spray density appeared to be even higher at locations closer to the tip, so the high extinction levels that caused high multiple-scattering corrections would have been even greater at closer measurement locations. Higher ambient pressures reduce breakup lengths and increase cone angles, but also cause more rapid deceleration of the spray. Thus, spray density is expected to remain high over any reasonable range of air densities. After converting to spatially resolved data by deconvolution, the following results were obtained. For both the diesel fuel and the CWSs, the atomization was complete at the measurement location and the radial size distribution of drops was relatively uniform, while the

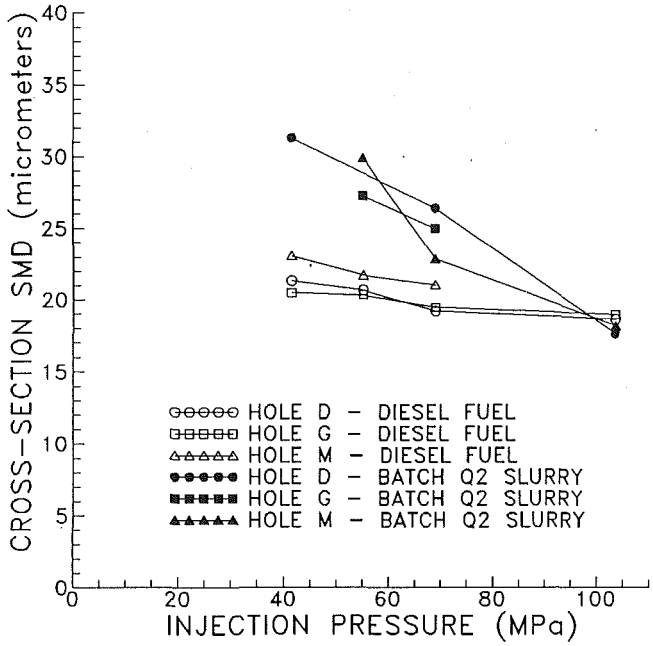

Fig. 7 Effect of hole shape on cross-section average SMD for various injection pressures for Batch-Q2 CWS and diesel fuel spraying into air at 0.55 MPa (80 psia) and 35°C (95°F)

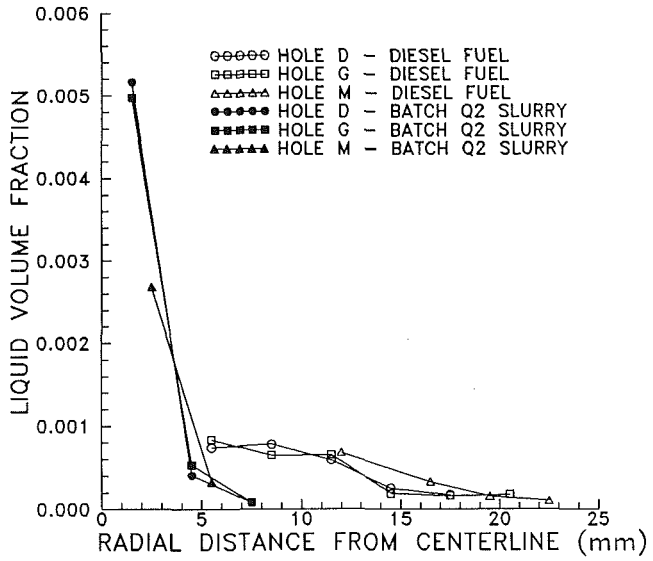

Fig. 8 Effect of hole shape on fuel-air distribution (liquid volume fraction) for Batch-Q2 CWS and diesel fuel at injection pressure of 69 MPa (10,000 psi) spraying into air at 0.55 MPa (80 psia) and 35°C (95°F)

liquid volume fraction varied radially in a profile that peaked at the centerline of the spray.

The radial profiles were averaged across the spray cross section accounting for number density and equivalent area for each annular ring (Dodge, 1988), and the results for the standard 0.3-mm tip are shown in Fig. 6. These results show that both the CWSs atomized to larger drop sizes than the diesel fuel, while Batch-R containing the smaller coal particles atomized to finer drop sizes than Batch-Q2. At the highest injection pressures, the atomization of Batch-Q2 was limited by the coal particle sizes. This statement can be illustrated by comparing the values of $D_{V0.98}$ for the dry coal particles and the drops in the spray, where $D_{V0.98}$ is that particle size for which 98 percent of the mass of the distribution is contained in particles of smaller size. For Batch-Q2, the base coal particles had a $D_{V0.98}$ of 44 μm, while the drops in the spray had a $D_{V0.98}$ of 57, 55, and 46 μm at injection pressures of 55, 69, and 103 MPa. Thus, further increases in injection pressure could not significantly reduce the $D_{V0.98}$ of the spray since the value for the drops was almost as small as for the dry coal particles. The largest coal particles ($D_{V0.98}$) for the Batch-R CWSs were 15 μm, while the $D_{V0.98}$ values for the Batch-R sprays were in the range of 39 to 62 μm.

The Batch-R CWS atomization did not vary significantly with dilution, in contrast with previous experimental measurements at this laboratory for other CWSs that showed smaller average drops at lower coal loadings. In fact, data for the 53 wt. percent CWS are coincident with the data for 48 wt. percent and are difficult to see in Fig. 6. The smaller average spray drop sizes for Batch-R when compared with Batch-Q2 CWS might be partially attributed to the smaller coal particle sizes in the Batch-R CWSs as discussed above. Differences in atomization characteristics of CWS are often correlated with high shear rate viscosity. The viscosity at a shear rate of 10,000 s^{-1} was 190 mPa s (190 cP) for Batch-Q2 and 150 mPa s (150 cP) for Batch-R (#4). Thus, the better atomization for Batch-R (#4) than Batch-Q2 could not be attributed to the small difference in high-shear rate viscosity.

Similar measurements were performed for the alternative injector hole shapes D, G, and M from Fig. 4. These results are summarized in Fig. 7, which shows that the atomization does not vary significantly with hole shape for either diesel fuel or CWSs. Further, the atomization of the CWSs is shown to improve more rapidly with increasing injection pressure than for the case of diesel fuel. Similar average drop sizes for Batch-Q2 CWS and diesel fuel were observed at injection pressures of 103 MPa (15,000 psi).

In addition to the drop size information, the laser-diffraction measurements also produced liquid volume fraction distributions. An example of the liquid volume fraction (or fuel–air) distributions is shown in Fig. 8, which is for one of the injection pressure conditions (55 MPa) shown in Fig. 7. These results were in qualitative agreement with the cone angle data discussed above, i.e., the CWSs mix more slowly with the air than does diesel fuel, and hole shape has little effect on the mixing rate.

Fuel–Air Mixing Rates Based on Penetration and Cone Angle From Intermittent Spray Tests. In addition to the continuous spray tests described above, intermittent sprays were examined to determine penetration rates and initial spray cone angles. These tests included the effect of chamber pressure (air density) on penetration rate and cone angle (Schwalb et al., 1991). The trends observed for cone angle changes with fuel type in these tests were in qualitative agreement with those discussed above. In addition to the trends discussed previously, these tests also showed that increases in air density result in increased cone angles and decreased penetration rates. For example, air densities of 8.0, 16.1, and 24.1 kg/m^3 resulted in initial cone angles close to the 0.3-mm hole injector tip of 6.2, 8.4, and 10.0 deg, while diesel fuel at the 16.1 kg/m^3 density had a cone angle of 13 deg. The differences in cone angles between CWSs and diesel fuel recorded for the intermittent tests was less than for the continuous spray tests because the cone angles for the intermittent tests were initial cone angles, while the continuous spray tests were measured 117 mm downstream of the tip (see Fig. 2). These tests also showed the cone angle for the CWS sprays to increase rapidly with increases in injection pressure.

To help understand better the effect of the reduced cone angles of CWSs on fuel–air mixing, a spray jet model based on momentum exchange between the fuel and the air was used based on the model developed by Melton (1971). Results of some example calculations are shown in Fig. 9 that shows equivalence ratio, $(\text{fuel/air})_{\text{actual}}/(\text{fuel/air})_{\text{stoichiometric}}$, as a func-

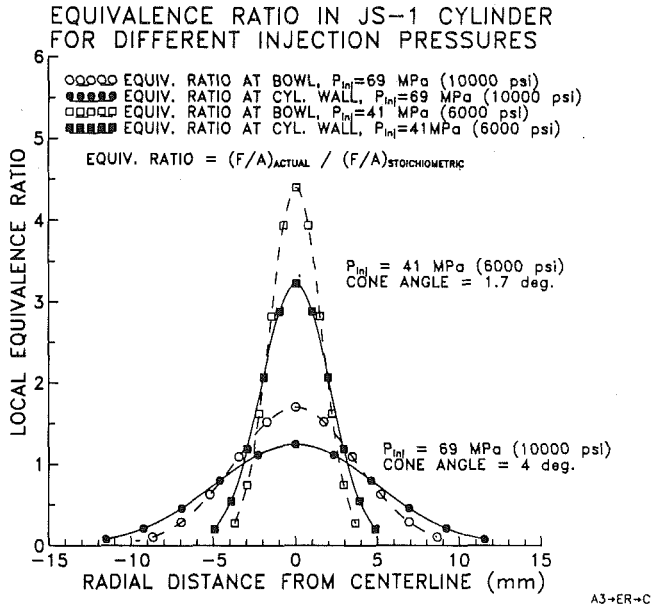

Fig. 9 Computed equivalence ratios in fuel spray jet in JS-1 engine for different injection pressures

tion of radial distance from the centerline of the spray at the piston bowl wall and at the cylinder wall for two different injection pressures. The JS-1 engine uses a standard Mexican-hat piston bowl shape, and the radius to the edge of the piston bowl is 124 mm (4.88 in.) and to the cylinder wall is 165 mm (6.5 in.). At the lower injection pressure, the cone angle for the CWS is so small that the equivalence ratio is too rich to burn cleanly and efficiently in many parts of the spray, even at the cylinder wall.

Summary and Conclusions

The atomization measurements provided an explanation of the requirement for high injection pressures ($\approx$ 60 MPa or 9000 psi) for suitable combustion performance in the Cooper-Bessemer and other similarly sized engines. At lower injection pressures the cone angles for the CWS sprays decreased significantly, to less than 3 deg, and the average drop size SMDs increased rapidly to above 35 μm. Thus, at injection pressures below 60 MPa, both the evaporation and fuel-air mixing of the CWS sprays were significantly impeded compared with the higher injection pressure sprays. Sprays of diesel fuel in the same injection equipment did not exhibit as large a dependence on injection pressure as the CWSs.

Alternative injector hole shapes had little impact on the CWS sprays, and did not offer significantly improved atomization or mixing at lower injection pressures. Thus, the concept of reducing injector hole wear by utilizing lower injection pressures with alternative hole shapes does not appear feasible. Of the injector hole designs tested, the one with the diverging hole shape appeared to have a slightly broader cone angle than the others. There was no significant change in drop size distribution for any of the hole shapes.

Limited testing with a CWS of smaller mass median diameter than that of the baseline CWS, 5 μm versus 14 μm, showed significantly smaller drop sizes for the CWS with the finer particle sizes. At the highest injection pressures, the base coal particle sizes of the CWS with the larger particles limited the drop size distribution. The CWS with the coarser coal particles had a top particle size (98 percent smaller by mass) of 44 μm, and the drop size distribution had a similar top particle size.

Future activities in this area should include: (1) development of alternative injection systems (not changes in injector hole shape) to avoid wear problems in the injector tips; (2) study of the effects of spray jet interaction with the piston bowl wall, including the effect of heat transfer on evaporation and ignition, and wall-jet mixing; and (3) further extension of diesel engine models to CWS-fueled diesel engines using the data developed in this project.

Acknowledgments

This work was funded by the Department of Energy, Morgantown Energy Technology Center, through their contract DE-AC2188MC25124 with Arthur D. Little, Inc., with a subcontract to Southwest Research Institute. Mr. William C. Smith was the contracting officer's technical representative, and his contributions are gratefully acknowledged. Mr. Michael G. Ryan performed the spray characterization measurements, and his diligent work is appreciated.

References

Allen, T., 1981, *Particle Size Measurement*, Chapman and Hall, New York, p. 139.

Dodge, L. G., 1984, "Change of Calibration of Diffraction-Based Particle Sizers in Dense Sprays," *Optical Engineering*, Vol. 23, No. 5, pp. 626–630.

Dodge, L. G., 1988, "Representation of Average Drop Sizes in Sprays," *Journal of Propulsion and Power*, Vol. 4, pp. 490–496.

Hammond, D. C., Jr., 1981, "Deconvolution Technique for Line-of-Sight Optical Scattering Measurements in Axisymmetric Sprays," *Applied Optics*, Vol. 20, p. 493.

Hsu, B. D., Leonard, G. L., and Johnson, R. N., 1989, "Progress on the Investigation of Coal-Water-Slurry Fuel Combustion in a Medium-Speed Diesel Engine: Part 3, Accumulator Injector Performance," ASME ICE-Vol. 7.

Leonard, G. L., and Fiske, G. H., 1987, "A Comparison of a Positive Displacement Fuel Injection System With an Accumulator-Based System for Coal-Fueled Diesel Engine Application," ASME Paper No. 87-ICE-32.

Melton, R. B., Jr., 1971, "Diesel Fuel Injection Viewed as a Jet Phenomenon," SAE Paper No. 710132.

Rao, A. K., Melcher, C. H., Wilson, R. P., Balles, E. N., Schaub, F. S., and Kimberly, J. A., 1988, "Operating Results of the Cooper-Bessemer JS-1 Engine on Coal Water Slurry," ASME Paper No. 88-ICE-12.

Rao, A. K., Wilson, R. P., Balles, E. N., Mayville, R. A., McMillian, M. H., and Kimberly, J. A., 1989, "Cooper-Bessemer Coal-Fueled Engine System—Progress Report," ASME ICE-Vol. 7.

Schwalb, J. A., Dodge, L. G., Ryan, T. W., III, Callahan, T. J., and Mannheimer, R. J., 1991, "Coal-Water Slurry Fueled Diesel Engine—Injector Atomization and Wear Tests," Final Report for DOE/METC Contract DE-AC2188MC25124, A. D. Little Subcontract 61366.

Coal-Water Slurry Spray Characteristics of a Positive Displacement Fuel Injection System

A. K. Seshadri

J. A. Caton

K. D. Kihm

Department of Mechanical Engineering,
Texas A&M University,
College Station, TX 77843

Experiments have been completed to characterize coal-water slurry sprays from a modified positive displacement fuel injection system of a diesel engine. The injection system includes an injection jerk pump driven by an electric motor, a specially designed diaphragm to separate the abrasive coal from the pump, and a single-hole fuel nozzle. The sprays were injected into a pressurized chamber equipped with windows. High speed movies and instantaneous fuel line pressures were obtained. For injection pressures of order 30 MPa or higher, the sprays were similar for coal-water slurry, diesel fuel, and water. The time until the center core of the spray broke up (break-up time) was determined both from the movies and from a model using the fuel line pressures. Results from these two independent procedures were in good agreement. For the base conditions, the break-up time was 0.58 and 0.50 ms for coal-water slurry and diesel fuel, respectively. The break-up times increased with increasing nozzle orifice size and with decreasing chamber density. The break-up time was not a function of coal loading for coal loadings up to 53 percent. Cone angles of the sprays were dependent on the operating conditions and fluid, as well as on the time and location of the measurement. For one set of cases studied, the time-averaged cone angle was 15.9 and 16.3 deg for coal-water slurry and diesel fuel, respectively.

Introduction

The use of coal as an alternate fuel is receiving renewed attention due to the diminishing supply of oil and its dependence on the political infrastructure. To assist the commercial development of coal-water slurry engines, the successful development of a fuel injection system is needed (Soehngen, 1976; Caton and Rosegay, 1984). A successful commercial fuel injection system must (1) provide good fuel atomization with appropriate fuel penetration and (2) be tolerant of coal-water slurry fuels (i.e., possess repeatability and durability). To progress in both these areas, fundamental information is needed on the fuel injection process of coal-water slurry fuels.

This paper is a description of a research project to determine the overall characteristics of coal-water slurry fuel sprays as a function of operating conditions and fuel specifications. The results of this study will assist coal-water slurry engine development by providing much needed insight about the fuel spray. In addition, the results will aid the development and use of coal-water slurry engine cycle simulations that require information on the fuel spray characteristics (Bell and Caton, 1988; Branyon et al., 1990; Wahiduzzaman et al., 1990). For successful cycle simulations, the evolution of the fuel spray geometry, droplet sizes, and droplet size distributions are needed as a function of time for a variety of operating conditions and fuels.

In a diesel engine injector, the pressurized liquid fuel is the primary source of energy that produces the spray. Atomization is a result of jet instability due to the relative velocity of the liquid and ambient gas. This type of injector is categorized as a single fluid pressure atomizer, in contrast to the air-assist atomizer where pressurized air is the primary source of energy for atomization. In pressure atomizers, atomization quality is controlled by the injector design, fuel properties, and injection pressure. For diesel engines, the fuel spray is injected into a confined combustion chamber that is under high-pressure and high-temperature conditions. Thus, the background air conditions are additional factors that affect the atomization quality of diesel engine injectors.

The first known study that included at least an attempt at characterizing a coal-slurry spray from a diesel engine injector was reported by Phatak and Gurney (1985). They obtained partial data on droplet size distributions from an experimental, air blast injector using coal-diesel (instead of coal-water) fuel slurries (20 or 40 percent coal by mass). Only limited data were reported, but they did show that for at least one operating condition, 80 percent of the fuel spray mass had droplet diameters of less than 20 μm for the air blast nozzle for one location and at one time. Nelson et al. (1985) obtained both

Contributed by the Internal Combustion Engine Division and presented at the Energy-Sources Technology Conference and Exhibition, Houston, Texas, January 26-30, 1992. Manuscript received by the Internal Combustion Engine Division September 3, 1991. Associate Technical Editor: J. A. Caton.

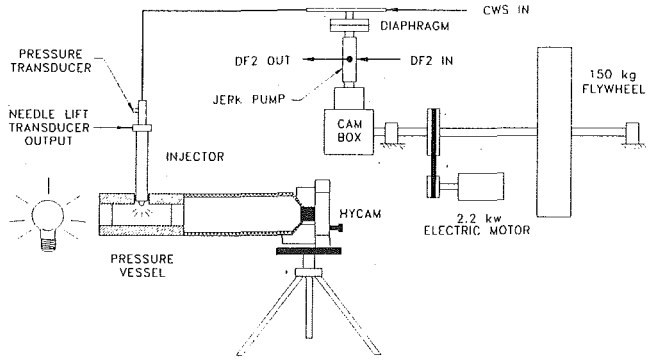

Fig. 1 Schematic diagram of the experimental system

shadowgraphs and droplet size distribution data for coal–water slurry from engine injectors. The fuel injector was a modified six-hole (0.35 mm dia) pencil nozzle (Stanadyne Roosa) with nozzle opening pressures of 5.5 and 14 MPa. For diesel fuel, 80 percent of the mass had droplet diameters less than 100 μm; whereas, for coal–water slurry, 80 percent of the mass had droplet diameters less than 400 μm. These results were for one location (32 mm from the nozzle tip) and for one time (0.5 ms after the spray tip passed). An air blast version of the nozzle showed improved (smaller droplets) performance. For both fuels, 80 percent of the mass had droplet diameters less than about 30 μm.

Yu et al. (1989) reported results from experiments that used a pneumatic, single-shot fuel delivery system. The injector was a pintle nozzle with injection pressures from 70 to 170 MPa (10,000 to 25,000 psia). The fuel was injected into a constant volume chamber which contained pressurized room temperature gas with a density of 17.5 kg/m^3. They used a laser diffraction size analyzer with a 9-mm-dia laser beam. These investigators examined two coal loadings (53 and 48 percent coal by mass) and three nozzle tip geometries, and reported their results as a function of injection velocity, fuel jet penetration distance, light transmission through the fuel spray, and mean droplet size. The average fuel injection velocity ranged from 220 to 450 m/s. They reported Sauter mean diameters (SMD) for the coal–water slurry of 25 and 54 μm for their limited tests.

Benson et al. (1991) reported results from a continuous and an intermittent injection system. The continuous injection was provided by an intensifier using a hydraulic system as a power source. The intermittent injection was provided by a jerk pump injection system. Their results indicated that cone angles of the coal–water slurry increased with the increase in the injection pressure in contrast with the cone angles for diesel fuel which were constant with injection pressure. Based on their experimental results, they estimated that the penetration time to the piston bowl was 1.3 ms and the penetration time to the cylinder wall was 2.1 ms. They also observed that the atomization of coal–water slurry did not depend on the coal loading in the slurry.

Objectives: The overall objective of this work was to characterize fully the coal–water slurry fuel sprays of a medium-speed diesel engine injection system. Specifically, the spray plume penetration as a function of time was determined for a positive-displacement fuel injection system. The penetration was determined as a function of orifice diameter, coal loading, gas density in the engine, and fuel line pressure.

Project Description

Experimental Facility. Figure 1 shows the overall injection facility for this experiment, which incorporates two fuel systems: One provides the diesel fuel used by the jerk-pump and the second provides the fuel, either diesel or slurry, which is injected by the nozzle. Figure 1 also shows the mechanical drive system, which uses an electric motor to drive a cam. Attached to the drive shaft is a large (150 kg) flywheel, which minimizes variations in the rotational speed of the cam. The cam-follower mechanism translates the rotation of the cam into the reciprocating motion needed by the jerk-pump.

The high-pressure fuel system comprises: (1) the jerk-pump, (2) the diaphragm pump, (3) a check valve mounted on the diaphragm pump, and (4) the injector nozzle. The jerk-pump is a Bendix fuel pump, which is used on many types of medium-speed diesel engines. The only modification to the pump is the addition of a diesel fuel outlet passage that enables the diesel fuel to circulate through the jerk-pump. A stainless-steel diaphragm has been inserted between the jerk-pump and the injector nozzle. The purpose of the diaphragm is to isolate the jerk-pump from the abrasive coal particles by using diesel fuel on the jerk-pump side and coal–water slurry on the nozzle side. This design is similar to that used by Leonard and Fiske (1986). The system operates in the same way as the conventional system except that in the modified system the diesel fuel that is forced out of the jerk-pump is used to increase the pressure on one side of the diaphragm. The pressure is transferred through the diaphgram to the coal–water slurry side of the pump. This forces coal-water slurry down the fuel line and into the injection nozzle. Typical injection pressures for this study were of the order of 30 MPa.

For the results reported here, the nozzle tips had only one hole. Although the full displacement of the jerk-pump was utilized, fuel line pressures were representative of multihole nozzles. This was because the volume for the overall injection system was significantly increased due to the diaphragm and additional pipe length. Actual applications have minimized this additional volume to accommodate multihole nozzles (Hsu, 1988a, 1988b; Hsu et al., 1989).

The nozzle was a standard Bendix injector used on medium-speed diesel engines. Modifications to the nozzle were limited to the installation of a needle lift transducer, increasing clearances in the needle valve assembly, and the use of custom nozzle tips. The fuel pressure was measured by the use of an in-line strain gage pressure transducer.

The custom nozzle tips allowed the use of various nozzle tip geometries with various numbers and size of orifices. Three sizes of single-hole nozzle tips were prepared for this study. The holes had a sharp-edged exit and a length-to-diameter ratio of 8. Although the details of the nozzle tip geometry are important in affecting the spray (Reitz and Bracco, 1982), this aspect was outside the scope of the present study. The nozzle holes were obtained by electro-discharge machining (EDM).

The final aspect of the injection facility is the pressurized chamber. The fuel spray was directed in one direction, while in the perpendicular direction visualization of the spray was possible through high pressure windows. The spray was backlighted through one window and photographed through the other. High speed (11,000 frames/s), 16 mm movies of the spray were obtained.

Experimental Procedures and Test Matrix. The experimental procedure included the following steps. First, the cam shaft was accelerated to a steady-state speed of 525 rpm. Next, the rack was pulled to a predetermined position and injection would begin. Finally, the movie camera was started and an electronic trigger signal was sent to the data acquisition system when the speed of the film was greater than about 3000 frames per second. This procedure would result in recordings of about 8 consecutive injections.

Table 1 lists the major experimental test parameters investigated. The base case included the following set of parameters: 50 percent (by mass) coal loading, 0.4-mm-dia nozzle tip, full

Table 1 Experimental test matrix

Case	Fuel	Tip (mm)	Rack (mm)	Density (kg/m^3)
Base	CWM50	0.4	30	25
Fuels	CWM33 CWM43 CWM55 WATER DIESEL	0.4	30	25
Tip	CWM50	0.2 0.6	30	25
Rack	CWM50	0.4	10 20	25
Density	CWM50	0.4	30	1.2 17

rack position (30 mm), and a chamber density of 25 kg/m^3 (which corresponds to the full-load conditions of the GE locomotive engine (Hsu, 1988a, 1988b; Hsu et al., 1989). The parameters that were varied were selected to represent the important features of the injection and atomization process. The fuels used included additional concentrations of coal-water slurry, water, and diesel fuel. Additional parameters that were investigated included nozzle tip diameters of 0.2 and 0.6 mm, rack positions of 10 and 20 mm, and chamber densities 1.2 and 17 kg/m^3. The nozzle tip diameters listed are nominal values and the actual values were determined by analyzing photographs from scanning electron miroscopy. The actual values are used in subsequent figures.

Results

Fuels Characterization. The basic slurry fuel was a commercially available coal-water slurry obtained from Otisca Industries. The details of this slurry have been reported elsewhere (Hsu and Confer, 1991). In summary, the base coal-water slurry contained 50 percent coal, 48 percent water, 1 percent lignosulphonate, and 1 percent Triton X-114. The coal used was a high-volatile subbituminous, which was cleaned to less than 0.8 percent ash (on a dry coal basis) with a measured Sauter mean particle diameter of 3.0 μm.

Spray Characterization. Figures 2 and 3 each show eight frames from a portion of a movie of one injection for the base case conditions for coal-water slurry and diesel fuel, respectively. The time between frames for these sets of movie frames was about 0.16 and 0.24 ms, respectively. For detailed analysis, sets of frames were selected with film rates about twice as fast. Pointers at the left of each picture were 50 mm apart and served as a reference distance for the film analysis.

From these movie frames, spray propagation and development were determined. The general qualities of the sprays were similar for the coal-water slurry and diesel fuel. The diesel fuel spray is generally broader and somewhat more stable. Other cases of coal-water slurry sprays also were obtained and are discussed elsewhere (Seshadri, 1991). As shown, the propagation for the fuel jet is rapid at the start (0–0.6 ms). This represents the period of penetration of a largely intact liquid core region. After this initial period, the liquid core breaks apart (break-up). Associated with this break-up is the development of a head vortex. This is first noted in these pictures at 0.68 ms for the coal water slurry and at 0.82 ms for the diesel fuel case. The size of the head vortex increases due to

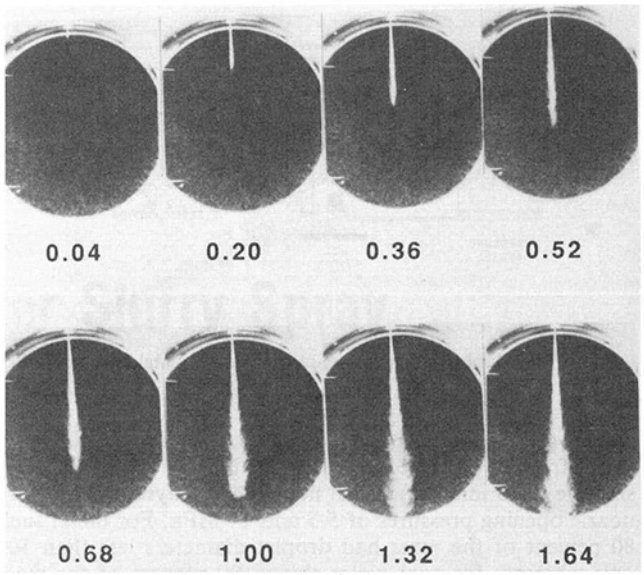

Fig. 2 Eight frames from a portion of a movie of one injection of coal-water slurry at the base case conditions (the numbers denote the time in milliseconds from the start of injection)

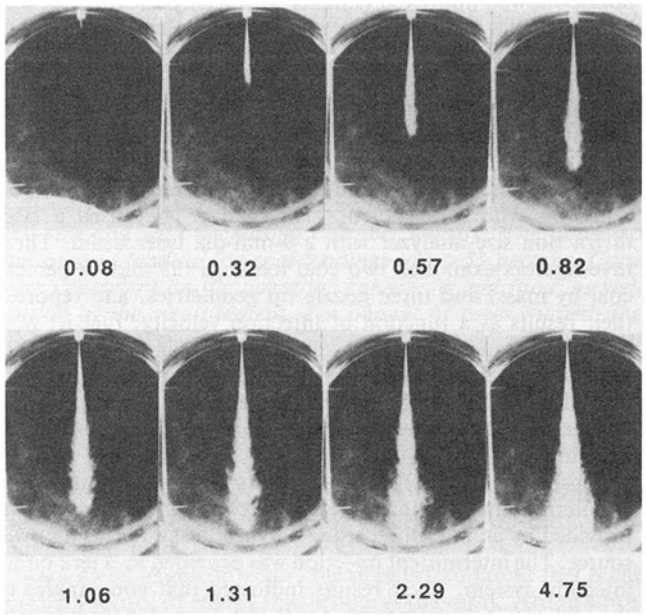

Fig. 3 Eight frames from a portion of a movie of one injection of diesel fuel at the base case conditions (the numbers denote the time in milliseconds from the start of injection)

additional fuel from the injector on one side (upstream) and due to entrained gas on the other sides. The last two frames in each of these sequences are representative of fully developed sprays for these conditions and illustrate the spray differences. Subsequent frames from these sets had shapes that fluctuated between the shapes of these two frames.

To complete the detailed analysis of the spray development, each frame of each movie set was traced using a motion analyzer. Figure 4 shows an example of the outline of the individual spray recordings for coal-water slurry for the base case conditions. The edge of the spray was selected as the location of the edge of the dark image of the spray. The maximum error in this determination was estimated as 5 percent. For this particular movie set, the time between frames was 0.101 ms. These spray shapes are superpositioned on a scaled schematic of the piston and cylinder. This schematic shows one spray

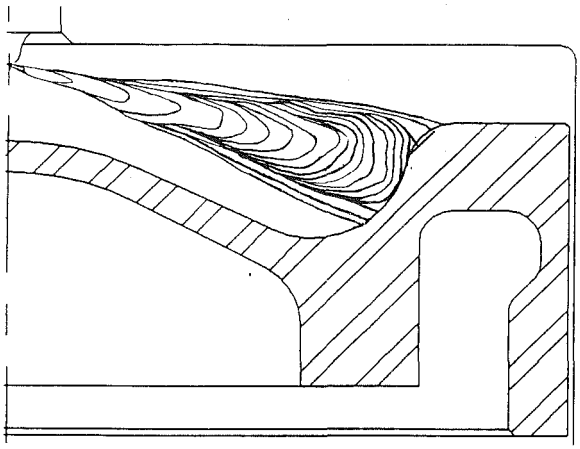

Fig. 4 Outlines of sequential spray plumes (0.101 ms apart) superpositioned on a schematic diagram of the piston and cylinder for coal-water slurry for the base case conditions

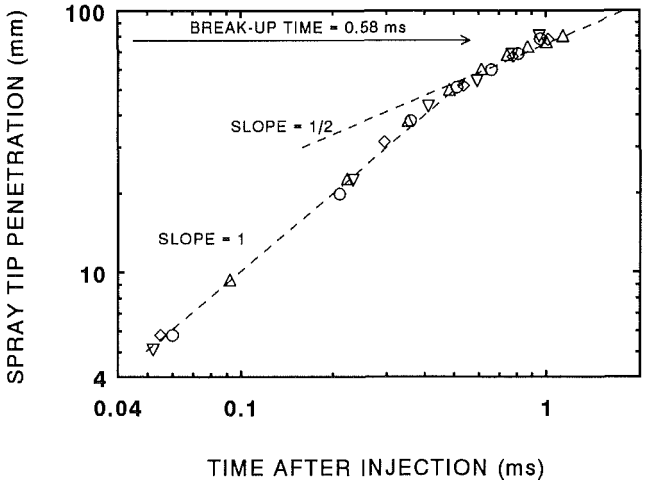

Fig. 5 Spray tip penetration as a function of time after injection for coal-water slurry for the base case conditions (the symbols represent data from four consecutive spray injections)

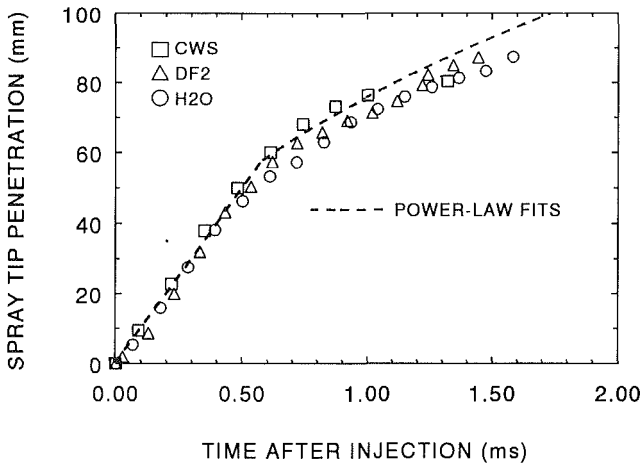

Fig. 6 Spray tip penetration as a function of time after injection for three fluids for the base case conditions

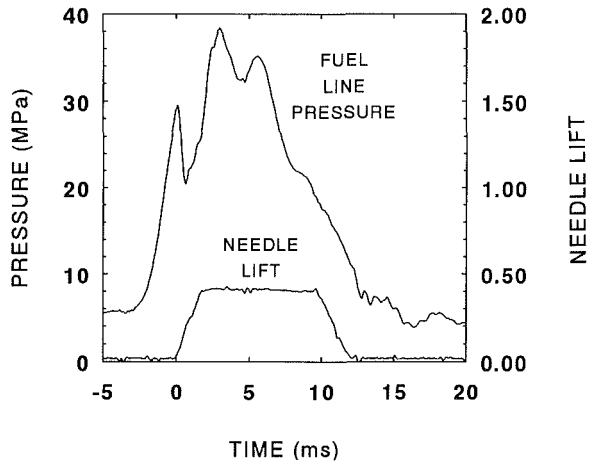

Fig. 7 Instantaneous fuel line pressure and needle lift as a function of time for coal-water slurry for the base case conditions

plume; typically eight to twenty spray plumes would be used. The typical spray plume is directed downward toward the piston at a 15 deg angle. As shown, for this case, the fuel jet would impinge on the piston bowl about 1.5 ms after the start of injection. Typical ignition delays for coal-water slurry for these conditions are greater than 1.5 ms (Hsu, 1988a, 1988b; Hsu et al., 1989) and, hence, these results indicate that at least some fuel impingement occurs. The consequences of this finding on the ignition and combustion processes in the engine are discussed by Hsu et al. (1992).

From the above spray outlines, the fuel jet penetration as a function of time was determined. Figure 5 shows the log of the fuel jet penetration distance as a function of the log of time for four consecutive injection events for the base case. As shown, the penetration distances from these four events are in good agreement with each other. When plotted in this fashion, two distinct modes of spray development may be determined. The first mode is for an intact liquid core and, for constant fuel pressure, the fuel jet penetration is linear with time. This is shown in Fig. 5 by the dashed line with slope equal to one. The second mode is for the spray after break-up of the liquid core. For this mode, penetration is proportional to time to the one-half power. In Fig. 5, this is represented by a dashed line with slope equal to one-half. The intersection of the two lines represents the time of break-up. For the base case, this was 0.58 ms for coal-water slurry and 0.50 ms for diesel fuel.

As an example of the type of information obtained from the movies, Fig. 6 shows the spray tip penetration as a function of time for three fluids: coal-water slurry, diesel fuel, and water. The dashed lines in the figure are from the previously described power-law fits. The coal-water slurry penetrated slightly faster than the other fluids and had a 0.08 ms longer break-up time. Although detailed differences such as these exist, all three fluids are in general agreement with the same power-law fits. This implies that the penetration and spray development are similar for several fluids when injected at the same conditions. Additional results for other coal concentrations substantiate these findings. The one exception was for 55 percent (by mass) coal loadings. For this case, no successful injection was achieved. Loadings as high as 53 percent, however, were successful. This implies a highly nonlinear response of fuel injection with respect to coal loadings for coal loadings above 53 percent.

In addition to the values based on the movies, the fuel jet penetration was estimated according to a model using the experimental fuel line pressures. Figure 7 shows the instantaneous fuel line pressure and needle lift as a function of time for the base case coal-water slurry conditions. As shown, fuel pressure increases and when the pressure is about 29 MPa (4300 psia) the needle lifts. The pressure decreases slightly due to the start of injection and then continues to increase. The maximum pressure is 38 MPa (5600 psia), which occurs 3.0 ms after the start of injection.

Many models exist for computing the fuel jet penetration

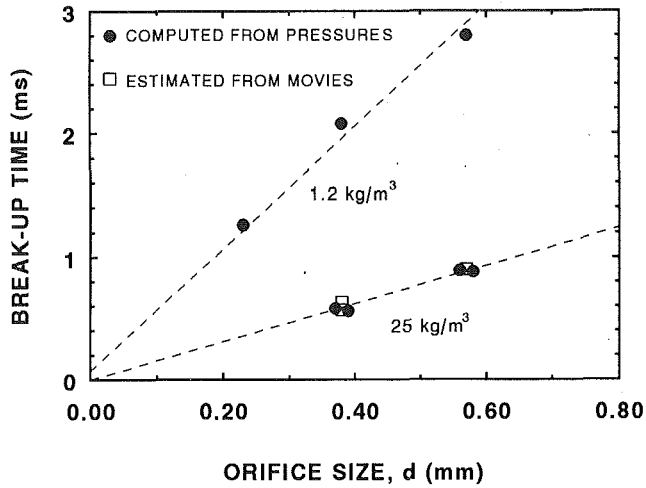

Fig. 8 Break-up time as a function of orifice size for two chamber densities for 50 percent coal-water slurry

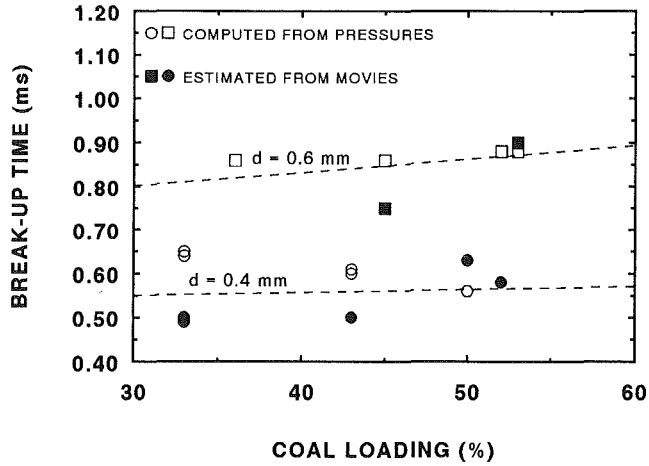

Fig. 9 Break-up time as a function of coal loading for two orifice sizes for a chamber density of 25 kg/m^3

and the break-up times using the fuel line pressure. For this study, the model described by Arai et al. (1984) was selected as representative. Further work is planned to evaluate other models. Using the instantaneous fuel line pressures and the model for jet penetration developed by Arai et al. (1984), break-up times and penetration distances were determined. This model is based on diesel fuel and the only modification was to use the correct fluid density of the coal-water slurry. The expressions for the spray tip penetration, s, are as follows (Arai et al., 1984):

$$\text{For } 0 < t < t_b,\ s = 0.39 \left(\frac{2\,\Delta P}{\rho_l}\right)_t^{0.5} \tag{1}$$

$$\text{For } t > t_b,\ s = 2.95 \left(\frac{\Delta P}{\rho_a}\right)^{0.25} (d \cdot t)^{0.5} \tag{2}$$

$$\text{where, } t_b = 28.65 \frac{\rho_l \cdot d}{(\rho_a\,\Delta P)^{0.5}} \tag{3}$$

where ΔP is the difference between the fuel line pressure and the chamber pressure, ρ_l is the density of the injected fluid, t is the time since injection, ρ_a is the density of the chamber gas, d is the nozzle orifice diameter, and t_b is the time until break-up of the spray jet.

The following discussion will focus on the effects of the major parameters of the injection process on the break-up time. The break-up time is a good indication of the quality of the atomization process. Break-up times indicate when the liquid core of the spray jet has disintegrated. The penetration of the spray, therefore, will be less rapid for short break-up times. Figure 8 shows the break-up time as a function of nozzle orifice size for two chamber densities. The symbols represent data from the movies or pressures, and the dashed lines are linear fits of the data. These results demonstrate the good agreement between the break-up times determined from he movies and the break-up times estimated from the model using the measured instantaneous fuel line pressures. As shown in Fig. 8, the break-up time increases with the increase in nozzle orifice sizes for both chamber densities of 1.2 kg/m^3 and 25 kg/m^3. As expected, as the orifice size approaches zero, the break-up time approaches zero. The effect of chamber density on the spray character is significant. For the low chamber density, the spray penetrates rapidly and does not spread out when compared to the high chamber density case. The break-up times for the low chamber density are 3.5 times greater than the break-up times for the high chamber density case.

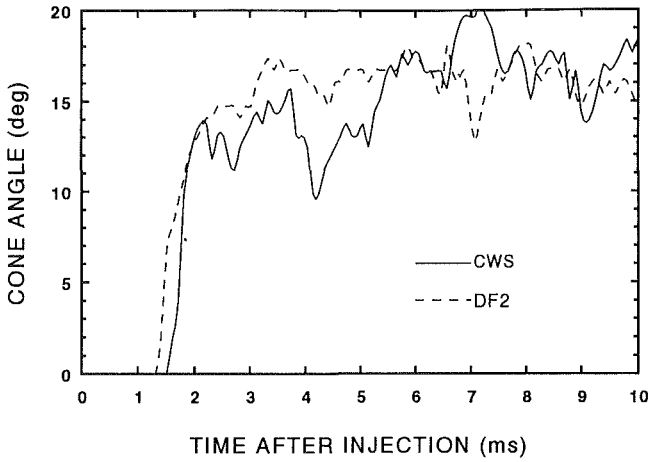

Fig. 10 Instantaneous cone angle as a function of time after injection for coal-water slurry and diesel fuel for the base case conditions

Figure 9 shows the break-up time as a function of coal loading for two nozzle orifice sizes for the base case conditions. Again, the symbols represent data from the movies or pressures, and the dashed lines are linear fits of the data. The break-up times are not significantly different from each other for the different coal loadings. The average values of the break-up time for all coal loadings were 0.55 and 0.85 ms for the 0.4 and 0.6 mm orifice sizes, respectively.

In addition to penetration distances, the cone angles of the sprays were determined from the movies. The cone angle of a spray is not well defined and no standard procedure is available. One approach is to use the arctangent of the spray width divided by the axial distance from the nozzle tip to the measurement location. For this study, the measurement location was 80 mm (200 nozzle orifice diameters) downstream from the nozzle tip. This location was selected so as to include as much of the spray as possible without being near the wall region. This distance is also representative of the distance to the piston bowl in a medium-speed diesel engine. As noted below, similar results were obtained at a measurement location of 60 mm (150 nozzle orifice diameters) downstream from the nozzle tip.

Figure 10 shows the cone angle as defined above as a function of time after injection for the base case conditions for diesel fuel and for coal-water slurry. The cone angle is similar for the two fluids for these tests. As shown, for the chosen measurement location the spray arrives at about 1.3 ms after injection. Within the next half of a millisecond, the cone angle at this location increases rapidly. For the period between 3 and 10 ms, the time-averaged cone angles for these diesel fuel and

coal-water slurry cases were 16.3 and 15.9 deg, respectively. For the nearer location (60 mm downstream of the nozzle tip), the time-averaged cone angles for the above diesel fuel and coal-water cases were 17.0 and 16.4 deg, respectively. Other tests with the coal-water slurry at these conditions resulted in narrower sprays. These narrower sprays had time-averaged cone angles of 11.2 and 13.0 deg and may be a result of needle sticking or blockage in the fuel delivery passages (Seshadri, 1991). Other investigators (Benson et al., 1991) have reported narrower coal-water slurry sprays with cone angles of between 1 and 10 deg, depending on fuel injection pressure.

The measured cone angles were unsteady with respect to time and several fluctuation frequencies exist. The high-frequency (between 5000 and 10,000 Hz) fluctuation is due to the finite movie frame rate and illustrates the frame-by-frame differences. The lower frequency (about 600 Hz) fluctuation may be a result of the wave dynamics of the injection system or from fluid instabilities associated with the atomization process. For example, these fluctuations maybe related to the time scales of large-scale fluid structures in the spray. (For reference, the injection frequency was 8.8 Hz and the pressure fluctuations were about 300 Hz.) The coal-water slurry cases resulted in larger amplitude fluctuations than for the diesel fuel cases. Note the importance of a time-averaged value as opposed to an instantaneous value even for a fully developed spray.

Additional results on the parametric effects of coal loadings, nozzle hole size, rack position, and chamber density on fuel jet penetration are available (Seshadri, 1991; Caton and Kihm, 1991) but due to space limitations, they cannot be presented here.

Summary and Conclusions

Experiments were completed to characterize coal-water slurry sprays from a modified positive displacement fuel injection system of a diesel engine. The injection system included an injection jerk-pump driven by an electric motor, a specially designed diaphragm to separate the abrasive coal from the pump, and a single-hole fuel nozzle. Injection pressures were of order 30 MPa and nozzle orifice diameters were between 0.2 and 0.6 mm. Coal-water slurry fuels with between 30 and 55 percent (by mass) coal were studied. The sprays were injected into a pressurized chamber equipped with windows. High-speed movies and instantaneous fuel line pressures were obtained. The time until the center core of the spray broke up (break-up time) was determined from both the movies and from a model using the fuel line pressure. Results from these two independent procedures were in good agreement.

The conclusions of this investigation include the following:

1 For the base conditions, the break-up time was 0.58 ms for coal-water slurry and 0.50 for diesel fuel. Break-up times increased with increasing nozzle orifice size and with decreasing chamber density.

2 The break-up time was not a significant function of coal loading for coal loadings up to 53 percent.

3 For the conditions of this study, the spray tip penetration as a function of time was similar for three fluids: coal-water slurry, diesel fuel, and water.

4 Cone angles of the sprays were dependent on the operating conditions and fluid, as well as the time and location of the measurement. The time-averaged cone angle ranged between 11.2 and 15.9 deg for the coal-water slurry and was 16.3 deg for the diesel fuel.

Future Work

The major remaining tasks of this project include additional detailed analysis of the movies and fuel pressures from the positive displacement fuel injection system. Current activities are directed at completing a similar set of experiments for an accumulator injection system. In addition to the high-speed movies and fuel line pressures, detailed droplet size measurements and high-resolution still photography will be completed.

Acknowledgments

This work was supported by a subcontract from General Electric—Transportation Systems as part of a contract with the U.S. Department of Energy, Morgantown Energy Technology Center. The contents of this paper do not necessarily reflect the views of General Electric or the Department of Energy.

References

Arai, M., Tabata, M. Hiroyasu, H., and Shimizu, M., 1984, "Disintegrating Process and Spray Characterization of Fuel Jet Injected by a Diesel Nozzle," Society of Automotive Engineers, Paper No. 840275.

Bell, S. R., and Caton, J. A., 1988, "Numerical Simulation of a Coal-Fueled, Compression-Ignition Engine," *Fuel*, Vol. 67, pp. 478-481.

Benson, C. E., Ryan, T. W., Schwalb, J. A. Dodge, L. G., and Callahan, T. J., 1991, "Coal-Water Slurry Spray Characterization," *Proceedings of the Eighth Annual Coal-Fueled Heat Engines and Gas Stream Cleanup Systems Contractors Review Meeting*, U.S. Department of Energy, Morgantown Energy Technology Center, pp. 263-272, July.

Branyon, D. P., Caton, J. A., and Annamalai, K., 1990, "Coal Fueled Diesel Cycle Simulation: The Role of Group Effects," ASME JOURNAL OF ENGINEERING FOR GAS TURBINES AND POWER, Vol. 112, pp. 391-397.

Caton, J. A., and Rosegay, K. H., 1984, "A Review and Comparison of Reciprocating Engine Operation Using Solid Fuels," *SAE Transactions*, SAE Paper No. 831362, Vol. 92, pp. 1108-1124.

Caton, J. A., Kihm, K. D., Seshadri, A. K., and Zicterman, G., 1991, "Micronized-Coal-Water Slurry Sprays from a Diesel Engine Positive Displacement Fuel Injection System," *Proceedings of the Spring Technical Meeting of the Central States Section of the Combustion Institute*, Nashville, TN, Paper No. 58, pp. 361-366.

Caton, J. A., and Kihm, K. D., 1991, "Coal-Water Slurry Spray Characteristics," *Proceedings of the Eighth Annual Coal-Fueled Heat Engines and Gas Stream Cleanup Systems Contractors Review Meeting*, U.S. Department of Energy, Morgantown Energy Technology Center, pp. 273-282, July.

Hsu, B. D., 1988a, "Progress on the Investigation of Coal-Water Slurry Fuel Combustion in Medium Speed Diesel Engine: Part 1—Ignition Studies," ASME JOURNAL OF ENGINEERING FOR GAS TURBINES AND POWER, Vol. 110, pp. 415-422.

Hsu, B. D., 1988b, "Progress on the Investigation of Coal-Water Slurry Fuel Combustion in a Medium Speed Diesel Engine: Part 2—Preliminary Full Load Test," ASME JOURNAL OF ENGINEERING FOR GAS TURBINES AND POWER, Vol. 110, pp. 423-430.

Hsu, B. D., Leonard, G. L., and Johnson, R. N., 1989, "Progress on the Investigation of Coal-Water Slurry Fuel Combustion in a Medium-Speed Diesel Engine: Part 3—Accumulator Injector Performance," in: *Coal-Fueled Diesel Engines*, M. H. McMillian and H. A. Webb, eds., ASME ICE-Vol. 7, pp. 52-67.

Hsu, B. D., and Confer, G. L., 1991, "Progress on the Investigation of Coal-Water Slurry Fuel Combustion in a Medium Speed Diesel Engine: Part 4—Fuels Effect," in: *Coal-Fueled Diesel Engines*, J. A. Caton and H. A. Webb, eds., ASME ICE-Vol. 14, pp. 1-8.

Hsu, B. D., Confer, G. L., and Shen, Z. J., 1992, "Progress on the Investigation of Coal-Water Slurry Fuel Combustion in a Medium-Speed Diesel Engine: Part 5—Combustion Studies," ASME JOURNAL OF ENGINEERING FOR GAS TURBINES AND POWER, Vol. 114, this issue, pp. 515-521.

Leonard, G. L., and Fiske, G. H., 1986, "Combustion Characteristics of Coal/Water Mixtures in a Simulated Medium-Speed Diesel Engine Environment," ASME Paper No. 86-ICE-15.

Nelson, L. P., Seeker, W. R., and Zimperman, R. A., 1985, "The Atomization, Ignition, and Combustion Characteristics of Coal Slurry Fuels in Medium-Speed Diesel Engines," Joint Central and Western States Sections, Combustion Institute, Paper No. 3-1A.

Phatak, R. G., and Gurney, M. D., 1985, "Investigation of Diesel Fuel Injection Equipment Response to Coal Slurry Fuels," ASME Paper No. 85-DGP-17.

Reitz, R. D., and Bracco, F. V., 1982, "Mechanism of Atomization of a Liquid Jet," *Physics of Fluids*, Vol. 25, No. 10, pp. 1730-1742.

Seshadri, A. K., 1991, "Characterization of Coal-Water Slurry Sprays From a Positive Displacement Fuel Injection System," Master of Science Thesis, Texas A&M University, Dec.

Soehngen, E. E., 1976, "The Development of the Coal Burning Diesel in Germany," US ERDA Report No. WA76-338F.

Wahiduzzaman, S., Blumberg, P. N., Keribar, R., and Rackmil, C. I., 1990, "A Comprehensive Model for Pilot-Ignited Coal-Water Mixture Combustion in a Direct-Injection Diesel Engine," ASME JOURNAL OF ENGINEERING FOR GAS TURBINES AND POWER, Vol. 112, pp. 384-390.

Yu, T. U., Lai, M. C., Beer, J. M., and Cheng, W. K., 1989, "Injection and Atomization of Coal-Water Slurry in High Pressure Diesel Engine Environment," in: *Coal-Fueled Diesel Engines*, M. H. McMillian and H. A. Webb, eds., ASME ICE-Vol. 7, pp. 51-60.

Implicit Numerical Model of a High-Pressure Injection System

A. E. Catania
Mem. ASME

C. Dongiovanni

A. Mittica

Dipartimento di Energetica,
Politecnico di Torino,
Torino, Italy

An implicit finite-difference numerical method has been developed and applied to the simulation of unsteady flow phenomena in a high-pressure injection system. A first-order one-step BSBT (backward space, backward time) scheme was used to obtain the difference analogue of the one-dimensional, elemental-volume averaged, partial differential equations governing the pressure-pipe flow. Second and higher-order implicit difference representations were employed for the ordinary differential equations simulating the pump and injector dynamics. The resultant nonlinear algebraic equations were solved by the Newton–Raphson method and a fast modified version of the Gaussian elimination procedure was used to solve the linearized equations. This was an extension of the Thomas solver to a multidiagonal system of algebraic equations. A compact, efficient and stable numerical algorithm was so obtained. The mathematical model takes into account the compressibility of the liquid fuel, the boundary shear, and also includes the simulation of possible cavitation occurrence at one or multiple locations in the injection system. No artificial viscosity has to be added to the solution in the vicinity of discontinuities induced by cavitation in the flow properties. The cavitation simulation is based on a simple mixture model of transient two-phase flow in pipes and can incorporate the effects of gaseous cavitation occurrence. Experimental values of the flow coefficients were used for the pump and injector and, for the latter, the dependence of the discharge coefficients on the needle lift and injection pressure was also taken into account. The model was tested and validated by comparing the numerical results with those of experiments carried out at the Fiat Research Center on a diesel-engine inline injection system, with a jerk-pump and an orifice type nozzle-injector.

Introduction

The high thermal efficiency, low emissions capabilities and increasing specific power of the diesel engine have broadened its application from the heavy to the light-duty vehicle field [1–3]. The need for maximum fuel economy while minimizing gaseous emissions, particulate and combustion-generated noise to regulation levels, has led to numerous innovations in the fuel injection system [4–9].

Numerical simulation can shorten the development time required to design and optimize a fuel injection system. It is also an investigation tool complementary to experimentation for a better knowledge of the complex nonstationary flow phenomena occurring in these systems, with particular reference to some anomalies in their operation, such as cavitation, which can seriously affect the engine performance.

Mathematical modeling has long been used as a powerful tool to study the performance of injection systems and their response to changes in design and operating parameters [10–20]. In order to make a quick analysis of a wide variety of concepts for new injection systems, a modular approach to their simulation was applied in [21].

Most of the fuel injection-system numerical models use the method of characteristics to solve the partial differential equations of the unsteady pipe flow, even including the effects of convective and friction terms. However, this method is known to present several difficulties when dealing with cavities in transient flows [22]. Although simple procedures have been developed to isolate the cavity as a separated column with the method of characteristics [23, 24], they become too cumbersome for complete system analysis [15], and in any case there is a lack of comparison with experimental data for fuel injection systems.

Other models apply explicit finite-difference schemes of second-order accuracy to the pipe-flow equations. However, like almost every second-order finite-difference scheme, these involve some difficulties in the treatment of boundaries and, furthermore, give rise to oscillations in the vicinity of discontinuities, such as those induced by cavitation phenomena in the flow properties. Second-order accurate nonoscillatory schemes have been developed only recently [25]. In all cases, for explicit schemes, the space and time computational grid increments are strictly linked up by the Courant number stability requirement and, in addition, the already restricted range of the Courant number values may be narrowed by the need to avoid a degradation of the solution quality [26].

The pump and injector, generally modeled by ordinary differential equations, are treated as boundary conditions for the

Contributed by the Internal Combustion Engine Division and presented at the Energy-Sources Technology Conference and Exhibition, Houston, Texas, January 26–30, 1992. Manuscript received by the Internal Combustion Engine Division September 1991. Paper No. 92-ICE-3. Associate Technical Editor: J. A. Caton.

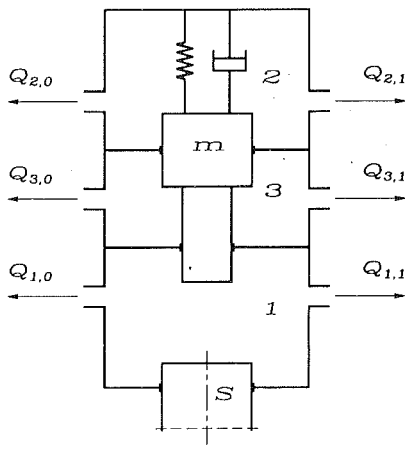

Fig. 1 Pump and injector mathematical model

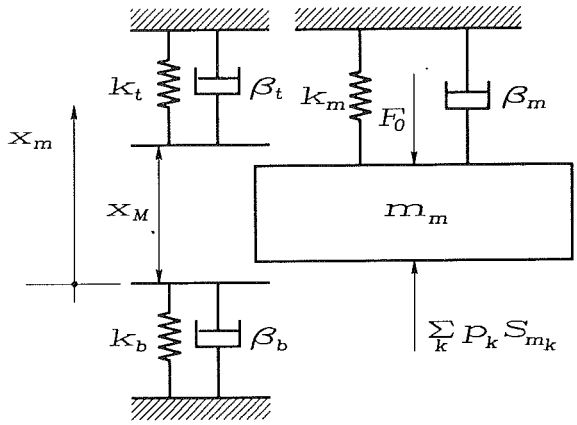

Fig. 2 Schematic of dynamics model for valves

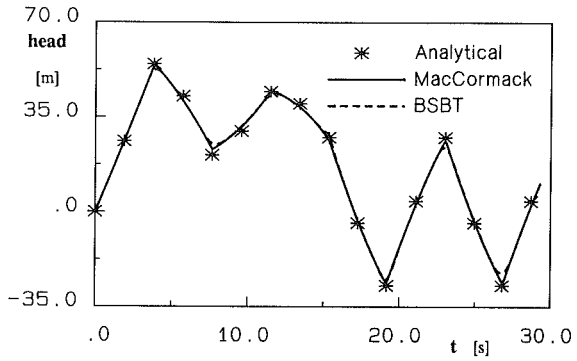

Fig. 3 Water hammer test-case results

pressure pipe. The extremely rapid response time of these components makes the solution of the boundary equations a problem of the stiff type. A fourth-order Runge–Kutta method has commonly been used to solve these equations [12, 15, 18, 21], though it requires very small time steps; a modified Eulerian predictor-corrector method was employed in [13] to reduce the step size within a fixed charateristics method time step, so as to achieve the desired accuracy level. An iterative technique was applied to explicit and implicit difference-analogue of the boundary equations in [14] and [19], respectively.

The equations simulating the pump and injector dynamics are thus solved at the same time step as the unsteady pipe-flow equations but separately from them, using different numerical techniques. Therefore, particular care must be exercised to assure a consistent and real solution of the complete differential equation set describing the whole system.

Cavitation is not generally simulated in engine fuel-injector models, but rather its effects are taken into account by rough simplifications, which neglect the mutual influence of the cavitating region on surrounding liquid properties and so lead to inconsistent solutions in the vicinity of that region, with effects that amplify in subsequent time instants. More specifically, if the pressure drops below the fuel vapor pressure, or simply zero level [14], at any point in the system, the pressure at that point is set equal to the vapor pressure. Then, either a pure reflection of the pressure wave is assumed at the boundaries of the cavitating region [14], or a local mass continuity condition is established to estimate the void fraction and consequently change the local effective bulk modulus and fluid density [10, 13, 15, 18, 21].

Most cavitation studies in steady and unsteady pipe-flow conditions refer to gaseous cavitation occurrence [27–31]. Transient gas–liquid two-phase flows in pipelines have long been simulated using different numerical schemes and mixture models [32–35]. However, in general, either drastic simplifications are accepted in the bubble-dynamics model, or semiempirical expressions are used for the wave propagation speed of the mixture, yielding satisfactory results in the specific field of application considered. A consistent wave propagation speed of the mixture is obtained in [29], though the contribution of the gas component is neglected in the momentum balance.

The main objective of the present work was to develop the

Nomenclature

a = wave propagation speed; celerity of the mixture
A = pipe cross-sectional area
C_1 = pipe constraint factor
d = pipe diameter
e = pipe wall thickness
E = bulk modulus of elasticity
E_p = Young's modulus of elasticity for pipe material
F_0 = initial spring force
k = spring rate
l = lift
L = length of pipe and injector-drilled passage
m = mass
n = engine speed
p = pressure; average cross-sectional pressure
Q = flow rate
S = surface area perpendicular to the lift axis
t = time
T = absolute temperature
u = average cross-sectional velocity of the mixture
V_0 = reference volume
x = axial distance along pipe; lift
α = average cross-sectional void fraction
β = damping
Γ = rate of gas/vapor release per unit volume of fluid
δx = length of the pipe element
Δt = time increment
Δx = distance increment
θ = cam angle
θ_0 = reference cam angle
μ = discharge coefficient
ρ = density; mixture density
τ_0 = wall shear stress

Subscripts

c = pumping chamber
d = delivery chamber
hp = half-pipe location
l = liquid phase
m = mobile element: valve, needle
n = needle
p = pipe location at injector inlet
s = plunger
v = gaseous/vapor phase

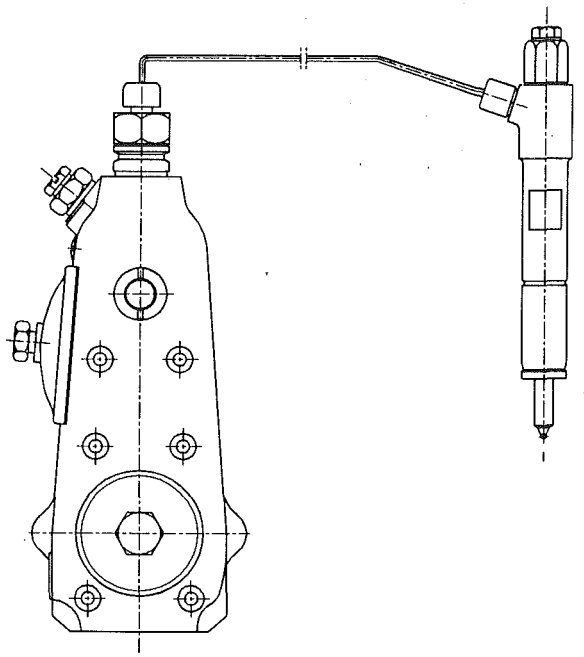

Fig. 4 Injection system layout

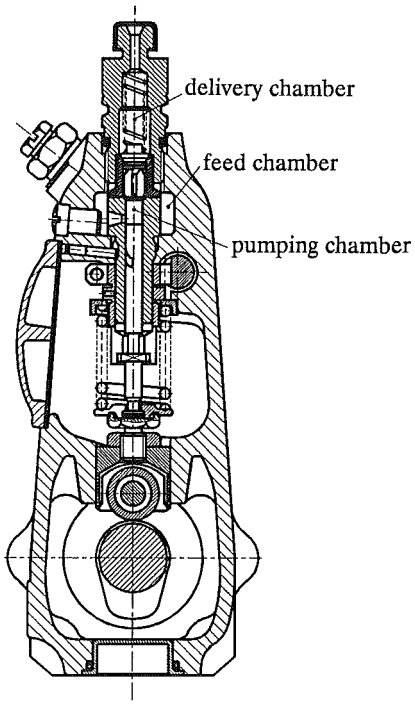

Fig. 5 In-line pump

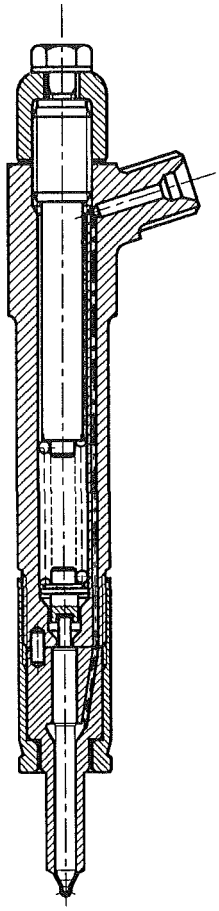

Fig. 6 Nozzle-hole injector

mathematical model of a high-pressure injection system, including the simulation of possible cavitation occurrence at one or multiple locations in the system, while essentially matching the transient pipe flow to the dynamics of the mechanical elements at its boundaries.

A one-step implicit upwind scheme of first-order accuracy was used to obtain the difference analogue of the one-dimensional, control-volume averaged, differential equations governing the high-pressure pipe flow; this scheme employs backward differences for the space and time derivatives and hence will also be referred to as the BSBT (backward space, backward time) scheme. Second and higher-order implicit difference representations, suitable to stiff type problems, were used for the ordinary differential equations simulating the pump and injector dynamics. The resultant set of nonlinear algebraic equations was solved by the Newton–Raphson method and a fast modified version of the Gaussian elimination procedure was adopted to solve the linearized equations. This was an extension of the Thomas solver to an n-diagonal ($n>5$) system of algebraic equations; in fact, the coefficient matrix of the linear equation system was easily reduced to a matrix containing a specific pattern of zeros.

A compact, efficient and stable numerical algorithm was so developed. It is particularly effective for cavitation simulation since no artificial viscosity need be added to the solution in the vicinity of discontinuities such as those induced by cavitation phenomena in the flow properties.

By comparing the numerical and analytical results obtained in a simple water hammer test case, the diffusivity of the finite-difference scheme applied to the pipe-flow simulation was found to be negligible (yielding a precision limit of less than one percent) within the range of temporal and spatial steps used in the computational grid. For comparison, the numerical results of a second-order MacCormack scheme were also included in this test case.

The proposed mathematical model can take into account the variations of the fluid density and bulk modulus of elasticity as functions of pressure and also the elasticity of the pipe, without disregarding the effect of wall friction and convective terms, in the wave propagation simulation.

The cavitation simulation is based on a simple mixture model of transient two-phase flow in pipes and can incorporate the effects of gaseous cavitation occurrence.

The computational model so developed was tested and validated by comparing the numerical results with those of experiments carried out at the Fiat Research Center on a diesel-

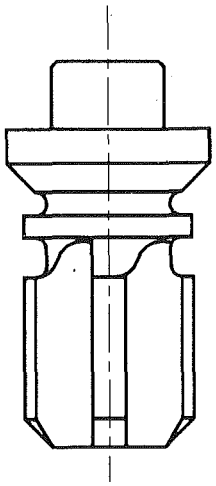

Fig. 7 Delivery valve

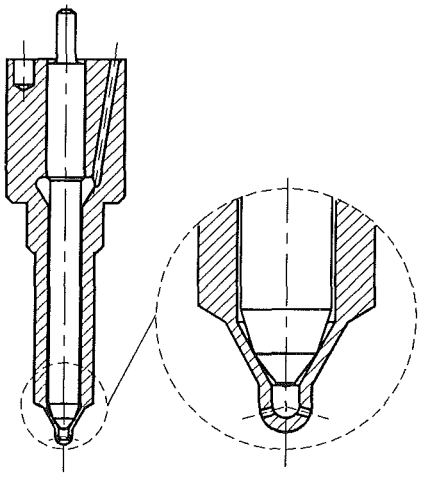

Fig. 8 Injector needle and chamber

engine injection system, with a jerk-pump and an orifice-type nozzle-injector.

Experimental values of the flow coefficients were used for the pump and injector, and the dependence of the discharge coefficients on the needle lift and injection pressure was also taken into account for the latter [36–28].

Mathematical Model

Pipe Flow. The fluid flowing in the pressure pipe is ordinarily in the liquid state, but whenever cavitation occurs it becomes a mixture of liquid phase and gaseous or vapor phase, including the presence of free gas or not. Therefore, the pipe-flow conservation equations are written, for a homogeneous, bubbly, two-phase fluid mixture, so that the pure-liquid flow equations can be directly derived from them as a particular case. A virtually isothermal flow is assumed in the present analytical model, requiring only mass and momentum conservation relations for its simulation.

Vapor cavitation takes place in regions close to vapor pressure where it is described by a dependent variable, termed the void fraction. Void growth and decay occur with passing waves through these regions. The difference in pressure across a bubble surface is neglected. Furthermore, the momentum interchange between the vapor and liquid components is ignored; thus, for momentum considerations, the vapor bubbles and liquid possess the same velocity.

An average cross-sectional representation of void fraction, mixture velocity, and component densities is employed. Therefore, following a control volume approach [39], with reference to a pipe element of cross-sectional area A and length δx, made of elastic material, the conservation of mass for the vapor component is

$$\frac{\partial}{\partial t}(\alpha\rho_v A\delta x)+\frac{\partial}{\partial x}(\alpha\rho_v uA\delta x)=\Gamma A\delta x \tag{1}$$

and for the liquid component it is given by

$$\frac{\partial}{\partial t}[(1-\alpha)\rho_l A\delta x]+\frac{\partial}{\partial x}[(1-\alpha)\rho_l uA\delta x]=-\Gamma A\delta x \tag{2}$$

having assumed an axisymmetric deformability of the pipe with a straining velocity along its axis negligible compared to the flow speed. The void fraction α is the ratio of the volume of the gaseous component per unit volume of the mixture, ρ_v is the vapor density and ρ_l the liquid density, u is the mean velocity of the mixture along the pipe axis, t is the time variable, and x the axial variable along the pipe, Γ is a source term, that is the gas/vapor production rate per unit volume.

The mixture momentum balance is, for a horizontal pipe

$$\frac{\partial u}{\partial t}+u\frac{\partial u}{\partial x}+\frac{1}{\rho}\frac{\partial p}{\partial x}=-\frac{4\tau_0}{\rho d} \tag{3}$$

in which p is the mean pressure, d is the pipe diameter, τ_0 is the wall shear stress, and ρ is the mixture density expressed by

$$\rho=\alpha\rho_v+(1-\alpha)\rho_l \tag{4}$$

By rearranging Eqs. (1) and (2), introducing the elastic properties of the vapor, liquid, and pipe material, one obtains the following mass conservation relations for the mixture and the vapor phase, respectively:

$$\left(\frac{\alpha}{\alpha_v^2}+\frac{1-\alpha}{\alpha_l^2}\right)\left(\frac{\partial p}{\partial t}+u\frac{\partial p}{\partial x}\right)+\rho\frac{\partial u}{\partial x}+$$
$$+(\rho_v-\rho_l)\left(\frac{\partial\alpha}{\partial t}+u\frac{\partial\alpha}{\partial x}\right)=0 \tag{5}$$

$$\frac{\partial\alpha}{\partial t}+u\frac{\partial\alpha}{\partial x}+\frac{\alpha}{\rho_v\alpha_v^2}\left(\frac{\partial p}{\partial t}+u\frac{\partial p}{\partial x}\right)+\alpha\frac{\partial u}{\partial x}=\frac{\Gamma}{\rho_v} \tag{6}$$

where a_v and a_l designate the isothermal celerity or wave propagation speed of the gas/vapor and liquid, respectively.

$$\frac{1}{a_v^2}=\frac{\partial\rho_v}{\partial p}\bigg|_T+\rho_v\frac{C_1 d}{E_p e}=\rho_v\left(\frac{1}{E_v}+\frac{C_1 d}{E_p e}\right) \tag{7}$$

$$\frac{1}{a_l^2}=\frac{\partial\rho_l}{\partial p}\bigg|_T+\rho_l\frac{C_1 d}{E_p e}=\rho_l\left(\frac{1}{E_l}+\frac{C_1 d}{E_p e}\right) \tag{8}$$

E_v and E_l represent the bulk modulus of elasticity for vapor and liquid, respectively, and the second term within brackets in both expressions takes into account the effects of the pipe elasticity; from stress and strain considerations one obtains, for a thin-walled pipe

$$\frac{1}{A}\frac{DA}{Dt}+\frac{1}{\delta x}\frac{D\delta x}{Dt}=\frac{C_1 d}{E_p e}\frac{Dp}{DT} \tag{9}$$

in which $\frac{D}{Dt}=\frac{\partial}{\partial t}+u\frac{\partial}{\partial x}$ indicates the Lagrangian time derivative, C_1 is a pipe constraint factor, depending on support situations for the pipe, E_p is the Young modulus of elasticity for the pipe material, and e is the pipe wall thickness.

The system of Eqs. (3), (5), and (6) can be written as

$$\frac{\partial\mathbf{w}}{\partial t}+[A]\frac{\partial\mathbf{w}}{\partial x}=\mathbf{H} \tag{10}$$

where

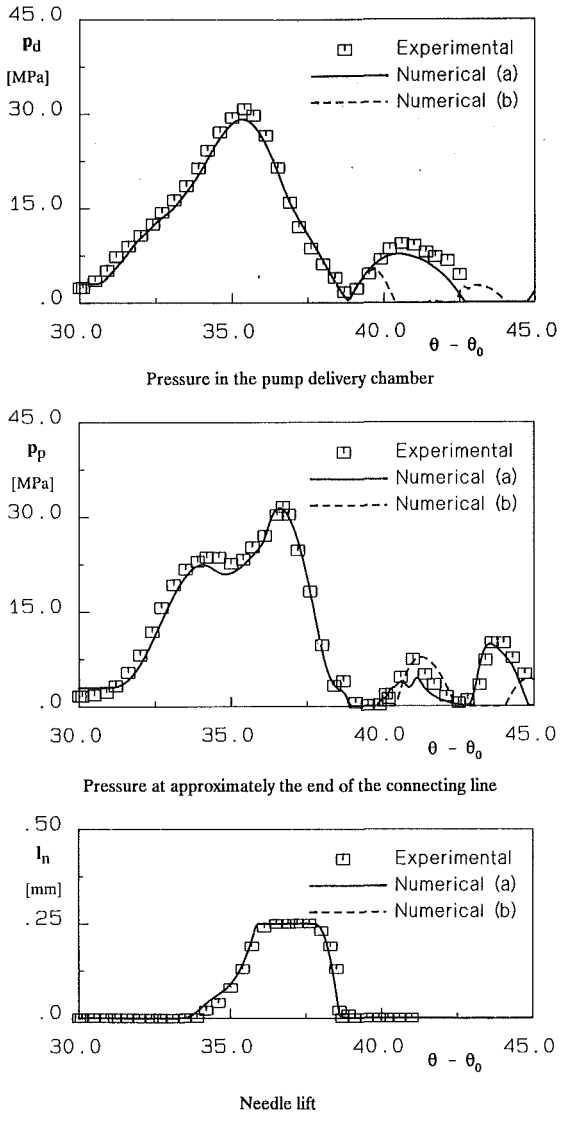

Fig. 9 Comparison of experimental and numerical results at n = 1000 rpm: (*a*) with cavitation simulation; (*b*) without cavitation simulation

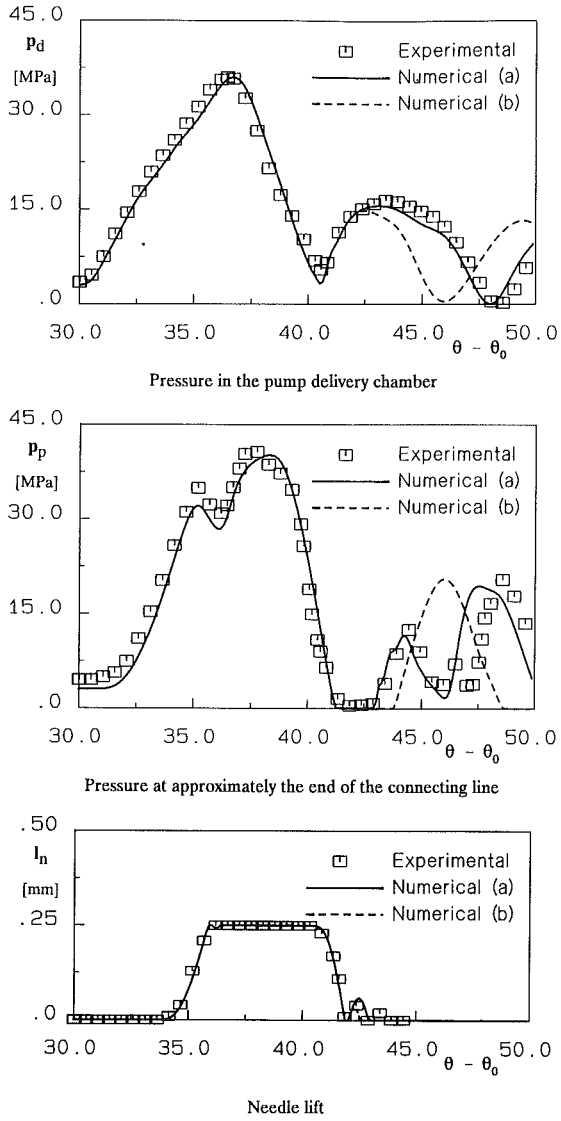

Fig. 10 Comparison of experimental and numerical results at n = 2000 rpm: (*a*) with cavitation simulation; (*b*) without cavitation simulation

$$\mathbf{w}=\begin{bmatrix} u \\ p \\ \alpha \end{bmatrix} \quad [A]=\begin{bmatrix} u & \frac{1}{\rho} & 0 \\ \rho a^2 & u & 0 \\ \alpha\left(1-\frac{\rho a^2}{\rho_v a_v^2}\right) & 0 & u \end{bmatrix}$$

$$\mathbf{H}=\begin{bmatrix} -\frac{4\tau_0}{\rho d} \\ \frac{\Gamma}{\rho_v}\left(1-\frac{\rho_v}{\rho_l}\right)\rho a^2 \\ \frac{\Gamma}{\rho_g}\left[1-\alpha\left(1-\frac{\rho_v}{\rho_l}\right)\frac{\rho a^2}{\rho_v a_v^2}\right] \end{bmatrix}$$

The variable a is defined as the wave propagation speed of the mixture and is given by

$$\frac{1}{\rho a^2}=\frac{\alpha}{\rho_v a_v^2}+\frac{1-\alpha}{\rho_l a_l^2} \tag{11}$$

It can be easily verified that the eigenvalues, λ, of the $[A]$ matrix are

$$\lambda_{1,2}=u\pm a, \quad \lambda_3=u$$

The limit cases of single-phase, liquid or gas/vapor, flow are directly derived from Eq. (10), by making the void fraction α equal to zero or one, respectively, in which cases Eq. (11) gives $a=a_l$ and $a=a_v$. Another interesting limit case, included in Eq. (10), is that of vapor cavitation development at constant pressure $p=p_v$, by considering the vapor-liquid mixture to be in thermal equilibrium. In this case, taking $\frac{Dp}{Dt}=0$, one obtains $\Gamma=\frac{\rho_l\rho_v}{\rho_l-\rho_v}\frac{\partial u}{\partial x}$ and $a=0$ in the cavitating region.

Pump and Injector. According to an ordinary lumped mass model, the continuity and compressibility equations that allow for flow rates through the concentrated and isobaric volumes of the pump and injector can be written in the form (Fig. 1)

$$\sum_{k=0}^{1} Q_{j,k}+V_{0_j}\epsilon_j=\delta_{j_0(j+2)}\cdot S_s\left(x_s\epsilon_j+\frac{dx_s}{dt}\right)+$$

$$+(-1)^j\cdot S_{m_j}\left(x_m\epsilon_j+\frac{dx_m}{dt}\right) \quad j\neq j_0, \quad j=1,2,3 \tag{12}$$

where

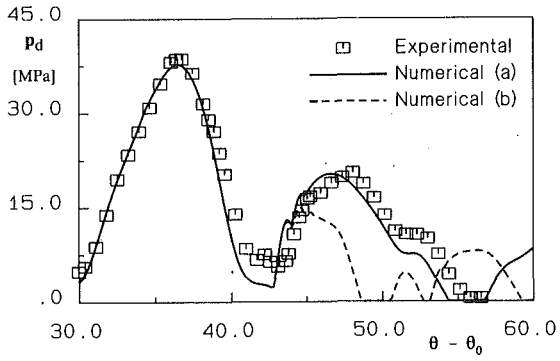

Pressure in the pump delivery chamber

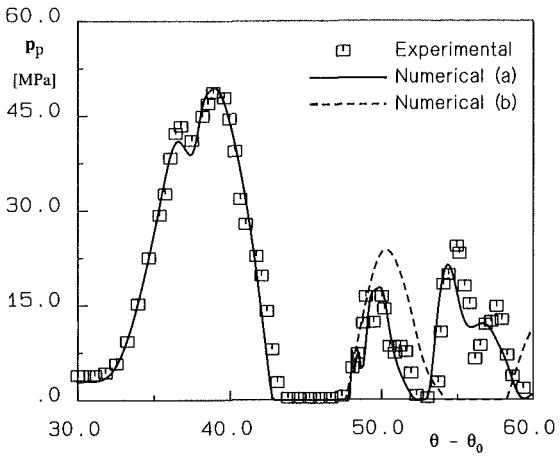

Pressure at approximately the end of the connecting line

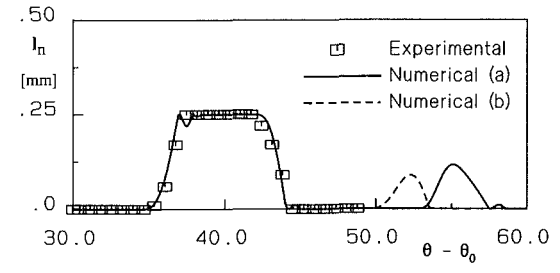

Needle lift

Fig. 11 Comparison of experimental and numerical results at n = 3000 rpm: (*a*) with cavitation simulation; (*b*) without cavitation simulation

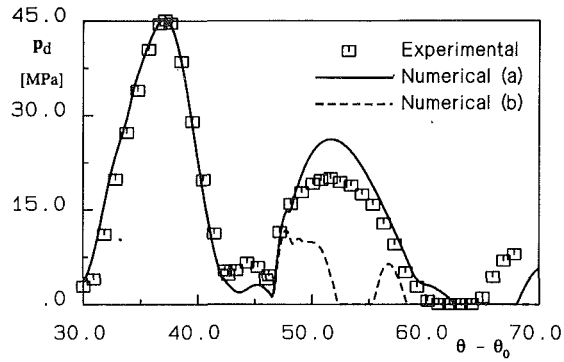

Pressure in the pump delivery chamber

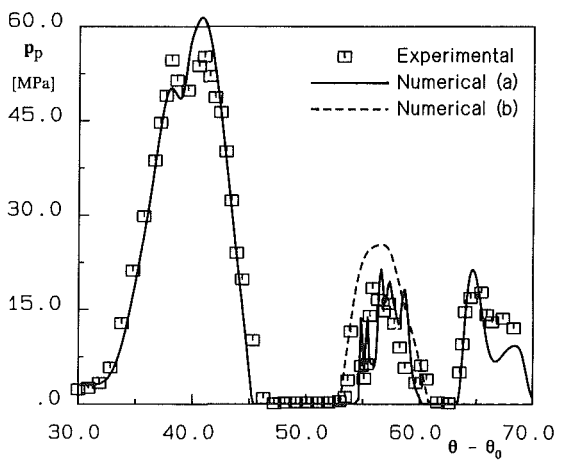

Pressure at approximately the end of the connecting line

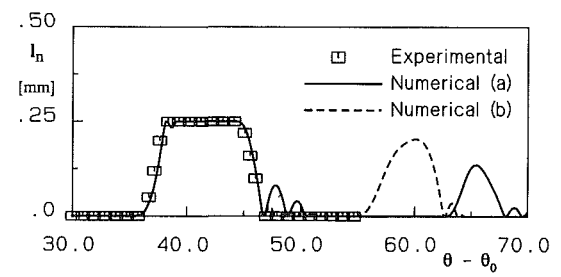

Needle lift

Fig. 12 Comparison of experimental and numerical results at n = 4000 rpm: (*a*) with cavitation simulation; (*b*) without cavitation simulation

$$Q_{j,k}=\frac{(p_j-p_{j,k})}{|p_j-p_{j,k}|}\,\mu_{j,k}A_{j,k}\sqrt{\frac{2}{\rho}\,|p_j-p_{j,k}|}$$

$$k=0,\ 1,\quad j=1,\ 2,\ 3 \tag{13}$$

$$\epsilon_j=\begin{cases}\dfrac{1}{E}\cdot\dfrac{dp_j}{dt} & p_j>p_v\\[2ex] \left(\dfrac{\rho_l}{\rho_v-\rho_l}+\alpha_j\right)^{-1}\cdot\dfrac{d\alpha_j}{dt} & p_j=p_v\end{cases} \tag{14}$$

$$\delta_{lm}=\begin{cases}1 & l=m\\ 0 & l\neq m\end{cases}$$

$$Q_{1,1}=-Q_{2,1} \qquad Q_{3,1}=-Q_{1,1}$$

pump $j_0=3$ $\quad p_{1,1}=p_2$ $\qquad$ injector $j_0=2$ $\quad p_{1,1}=p_3$

$$p_{2,1}=p_1 \qquad p_{3,1}=p_1$$

The dynamics of valves (the injector needle is also referred to as the nozzle valve) are simulated by ordinary differential equations of the second order, such as (Fig. 2)

$$m_m\frac{d^2x_m}{dt^2}+\bar{\beta}_m\frac{dx_m}{dt}+\bar{k}_m x_m+\bar{F}_0+\sum_{\substack{k=1\\k\neq j_0}}^{3}(-1)^k p_k S_{m_k}=0 \tag{15}$$

in which the terms $\bar{k}_m$, $\bar{\beta}_m$, and $\bar{F}_0$ assume the expressions

$x_m<0$ $\quad \bar{k}_m=k_m+k_b$ $\quad \bar{F}_0=F_0$ $\quad \bar{\beta}_m=\beta_m+\beta_b$

$0\le x_m\le x_M$ $\quad \bar{k}_m=k_m$ $\quad \bar{F}_0=F_0$ $\quad \bar{\beta}_m=\beta_m$

$x_M<x_m$ $\quad \bar{k}_m=k_m+k_t$ $\quad \bar{F}_0=F_0-k_t x_M$ $\quad \bar{\beta}_m=\beta_m+\beta_t$

Numerical Algorithm

A one-step BSBT (backward space, backward time) finite-difference scheme was used to discretize the partial differential Eq. (10), as follows:

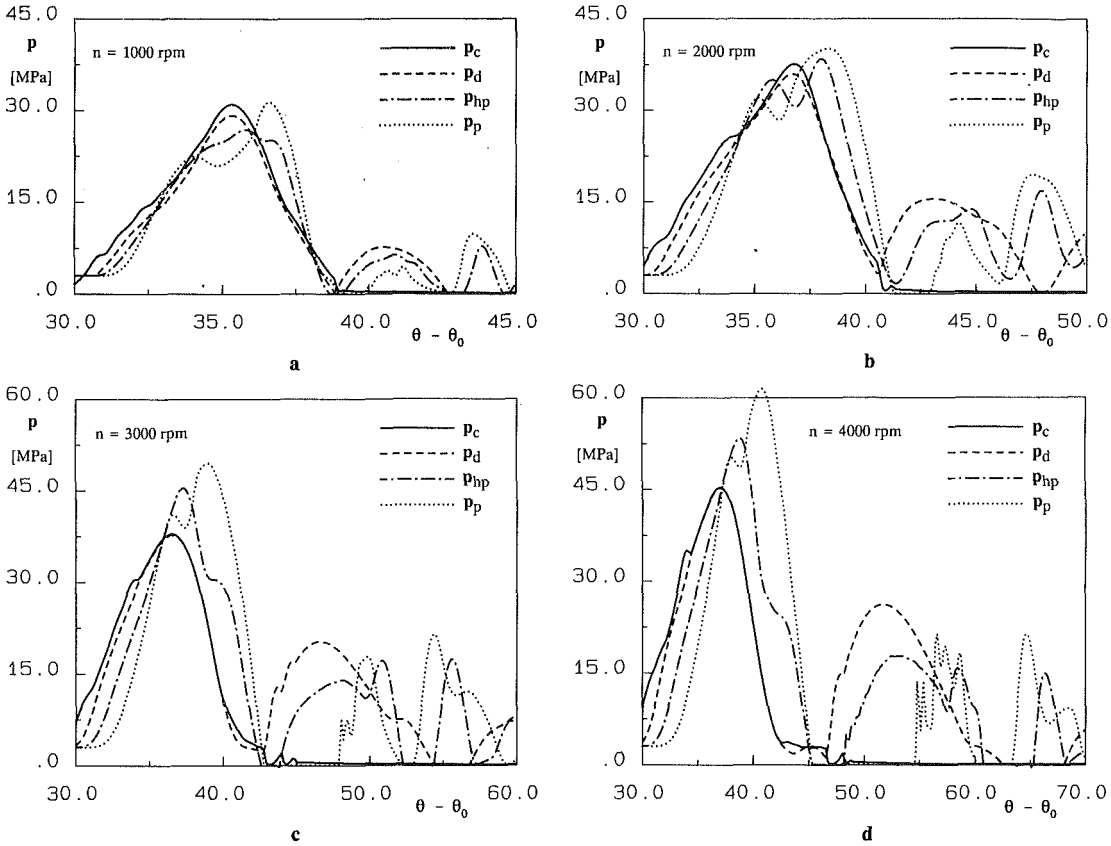

Fig. 13 Pressure distributions at different locations in the injection system

$$\left([I]+\frac{\Delta t}{\Delta x}[A]^{n+1}\right)\mathbf{w}_i^{n+1}-\frac{\Delta t}{\Delta x}[A]^{n+1}\mathbf{w}_{i-1}^{n+1}-\\ -\Delta t\mathbf{H}^{n+1}=\mathbf{w}_i^n \quad (16)$$

where the time-marching coordinate is indicated by the superscripts, and the spatial coordinate in the computational grid is indicated by the subscripts. This implicit scheme is first-order accurate with a truncation error of $O[\Delta t, \Delta x]$ and, according to a Fourier stability analysis, is unconditionally stable for all time steps.

The system of the second-order ordinary differential equations, representing the pump and injector analytical models, was preliminarily reduced to a system of the first order. Then, a BDF (backward differentiation formula) implicit multistep scheme of p-order accuracy ($p \leq 6$), was used for the finite-difference approximation of the first-order time derivatives

$$\left(\frac{dy}{dt}\right)^{n+1}=\frac{1}{\Delta t}\sum_{j=0}^{p}\alpha_j y^{n+1-j}+O(\Delta t^p) \quad (17)$$

where y is any time-function variable. In particular, for a second order accurate scheme, one has

$$\left(\frac{dy}{dt}\right)^{n+1}=\frac{1}{2\Delta t}(3y^{n+1}-4y^n+y^{n-1})+O(\Delta t^2) \quad (18)$$

The difference representation of the partial differential equations, for the pressure pipe model, and of the ordinary differential equations, for the pump and the injector model, led to a system of nonlinear algebraic equations, which can be written, in vector notation, as

$$\mathbf{F}(\mathbf{x})=0 \quad (19)$$

in which $\mathbf{x}$ is the vector of the unknown variables.

This system of nonlinear equations was solved using the Newton–Raphson iterative method, which transforms it into the following linear form:

$$[J^{(i)}]\Delta\mathbf{x}^{(i)}=-\mathbf{F}(\mathbf{x}^{(i)}) \quad (20)$$

where $\mathbf{x}^{(i)}$ is an iterative approximation of the exact solution, $[J^{(i)}]$ is the Jacobian matrix of the system, evaluated for the vector $\mathbf{x}^{(i)}$, and $\Delta\mathbf{x}^{(i)}$ the iterative correction

$$\mathbf{x}^{(i+1)}=\mathbf{x}^{(i)}+\Delta\mathbf{x}^{(i)} \quad (21)$$

The solution of the linear equation system (20), characterized by a multidiagonal matrix, was obtained by an extension of the fast Thomas solver.

Results

The test case considered to assess the diffusivity of the BSBT numerical scheme was the simple water-hammer occurrence in a horizontal pipeline, with a reservoir upstream and a valve downstream, consequent to the valve closure. The closing rate of the valve was taken to be linear in time. Figure 3 shows a result of this hydraulic transient simulation, reported as time history of the piezometric head upstream of the valve. The explicit MacCormack scheme, of second-order accuracy, was also applied to this test case, for comparison. Therefore, the numerical results in Fig. 3 refer to a unitary Courant number, which was evaluated using the largest eigenvalue of the $[A]$ matrix in Eq. (10), written for the pure liquid flow. The analytical results were obtained using the linearized water-hammer equations. By comparing the analytical and numerical results for the Courant number values, from 1.5 to 4.0, used in the injection system simulation, the diffusivity of the BSBT scheme was found to be negligible, within a precision limit of one percent, with reference to a relative elapse of time equivalent to the injection duration.

Figure 4 shows the layout of the injection system used for the model validation. The system was made up of a jerk-pump

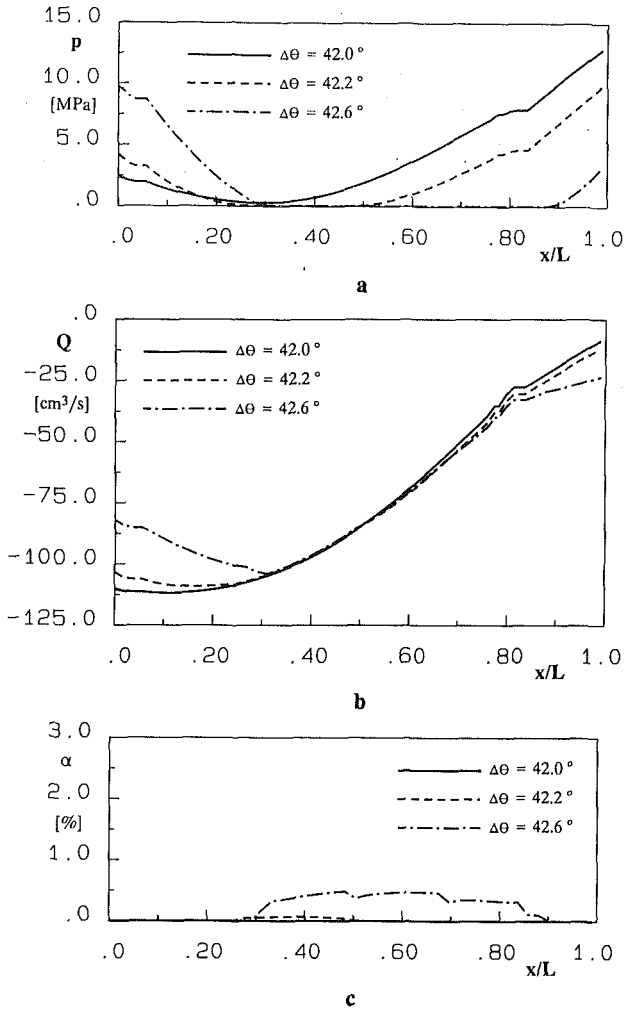

Fig. 14 Distributions of pressure (*a*), flow rate (*b*), and void fraction (*c*) along the pressure pipe

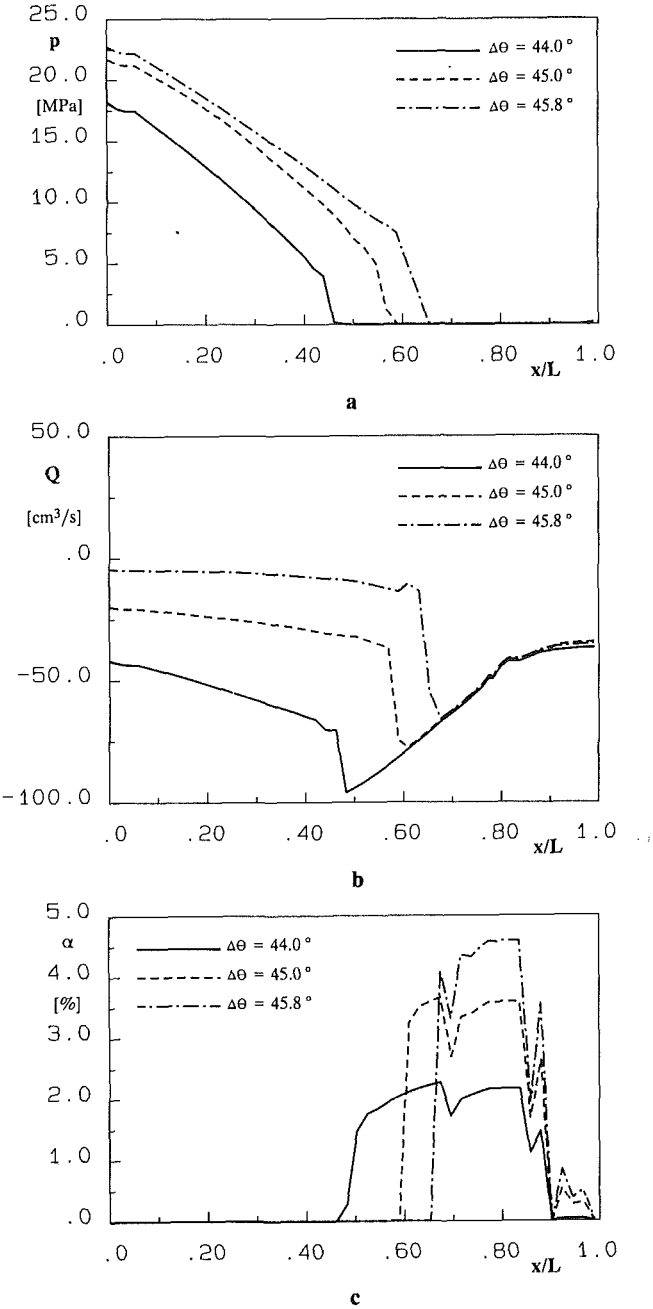

Fig. 15 Distributions of pressure (*a*), flow rate (*b*), and void fraction (*c*) along the pressure pipe

(Fig. 5), a nozzle-hole injector (Fig. 6), and their connecting line. Figure 7 shows the delivery valve of the pump. The ring on the neck of the valve gives rise to the retraction volume during the closure of the delivery chamber; this is the main cause of cavitation in the flow at the end of injection with the possible consequence of nozzle reopening and so of a secondary injection stage, especially at high speeds. Figure 8 shows the geometric features of the injector needle tip and the injection, or sac volume with two of the four holes. Experimental results on the performance of this system, for an almost constant quantity of fuel injected, showing cavitation occurrence, were provided by the Fiat Research Center, with an uncertainty that could be estimated to be within the interval of ± 10 percent.

For the simulation of the pure-liquid flow, equation system (19) was solved, at each time step, by taking the solution obtained at the previous time step as the starting solution $\mathbf{x}^{(0)}$ in the iterative procedure described by Eqs. (20) and (21). The tolerance for convergence criterion of this procedure, that is, the relative difference between two successive approximations of the exact solution, was taken to be 10^{-4}. Generally, two iterations were needed to reach convergence.

Vapor cavitation, excluding the presence of free gas, was considered to take place whenever the local unsteady pressure fell below the vapor pressure during the computation of the pure-liquid flow. As a preliminary stage of cavitation simulation, the vapor–liquid mixture was viewed to be in thermal equilibrium. For the flow simulation in the presence of cavitation, the starting solution $\mathbf{x}^{(0)}$, at any time step, was the result of an iterative process as well, the extent of the cavitating region being unknown. More specifically, the final solution obtained at the previous time step was taken to be the first initial iterative approximation of the exact solution in equation system (20); then, subsequent to the convergence of the Newton–Raphson procedure to a root of equation system (19), a new starting vector $\mathbf{x}^{(0)}$ was obtained by putting the resultant points with negative pressure in cavitation and terminating cavitation in those points with negative void fraction, and so on until reaching a physically consistent final solution. The additional simulation of gaseous cavitation is part of our continuing work in this research field.

Quasi-steady frictional losses were assumed relative to the liquid or the mixture density and velocity [29].

Figures 9–12 compare the numerical and experimental results obtained for the pressure (p_d) in the pump delivery chamber, the pressure (p_p) at approximately the end of the pipe close to the injector, and for the injector needle lift (l_n), at engine

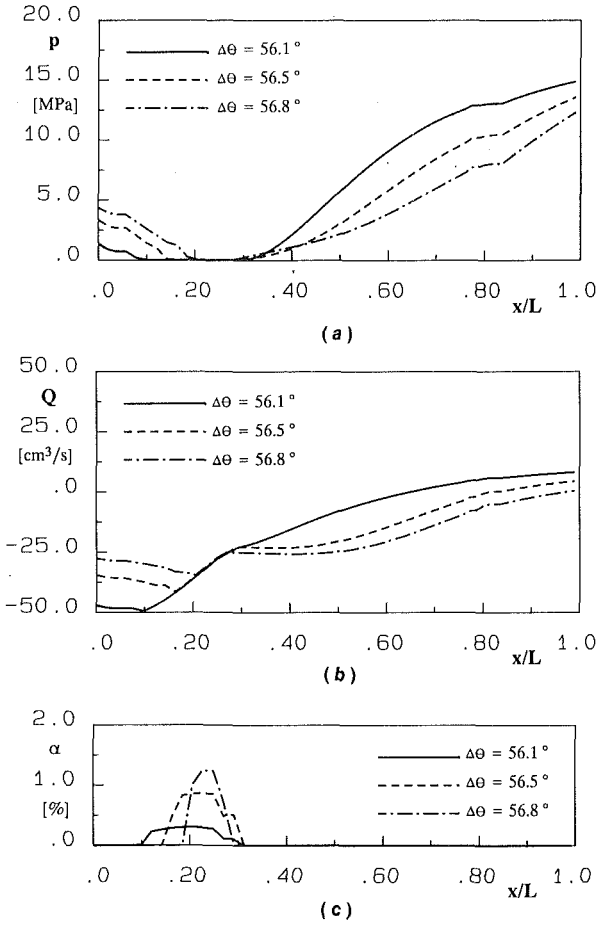

Fig. 16 Distributions of pressure (*a*), flow rate (*b*), and void fraction (*c*) along the pressure pipe

angular speeds of 1000–4000 rpm, respectively. The numerical results are reported for both cases of simulated cavitation (solid line) and of unmodeled cavitation (dashed line). In this latter case, the vapor pressure value was simply put in those points where the liquid solution gave negative pressures, as usually done in fuel-injector simulation. It is evident from these figures how the inclusion of cavitation simulation in the model may significantly alter the pressure in the secondary injection peaks following the drastic pressure reduction due to the retraction effect of the delivery valve. The pressure on the main part of the injection is virtually not influenced by the cavitation simulation. The computed quantity of fuel injected per cycle differed by less than a half percent from the measured quantity.

The injector nozzle reopening, evident in the theoretical results at 3000 and 4000 rpm, which is not reported in the experimental results, was confirmed by subsequent measurements carried out at the Fiat Research Center on the particular pump configuration considered for the model validation in the presence of cavitation.

Figure 13 reports the pressure distributions at different locations in the injection system for the different engine speeds. The subscript *c* indicates the pumping chamber, *d* the delivery chamber, *p* approximately the end of the pipe close to the injector, and *hp* the half-pipe location. The evolution of cavitating regions in the pipe is evident from this figure.

Figures 14, 15, and 16 plot the distributions of pressure (*a*), flow rate (*b*), and void fraction (*c*) along the pressure pipe at the engine speed of 3000 rpm for different instants of time corresponding to the indicated crank-angle intervals ($\Delta\theta = \theta - \theta_0$), all starting from the reference crank angle $\theta_0 = 100$ deg at the beginning of the pump plunger movement. The distance from the delivery chamber exit, normalized to the length (L) of the connecting pipe and the injector drilled passage, is reported as abscissa in these figures. The solid line in Fig. 14(*a*) represents the stage before the onset of the cavitation. The shock induced in the flow by cavitation is particularly evident in Fig. 15(*b*). These figures show three different mechanisms of cavitation propagation in the pipe.

Conclusion

The proposed mathematical model, including cavitation, is capable of analyzing transient flows in high-pressure injection systems, and so can be used as an investigation tool complementary to experimentation, for both exploring local phenomena in a specific system and performing a parametric study preliminary to the design. It is also flexible, due to its modular structure, and therefore can be applied to study the effect of different pump types on a given injector and to analyze the injection characteristics of different injectors for a given pump.

Acknowledgments

Financial support for this work was provided by C.N.R.-P.F.E.2 (Consiglio Nazionale delle Ricerche—Progetto Finalizzato Energetica 2) under contracts No. 86.00789.59. and No. 87.02166.59.

The authors would like to thank the Fiat Research Center for providing the diesel injection-system data with the related experimental results, and in particular Mr. F. Lovisolo for the detailed information.

The authors would also like to thank Dr. D. Nikitopoulos of Louisiana State University for fruitful discussions and for providing the MacCormack numerical solution of the water hammer test case considered in order to assess the diffusivity of the BSBT finite-difference scheme.

References

1 Monaghan, M. L., and McFadden, J. J., "A Light Duty Diesel for America," SAE Paper No. 750330, 1975.

2 Larkinson, E., and Jewsbury, B. R., "A Diesel Engine for Light Duty Applications," SAE Paper No. 750333, 1975.

3 Hofbauer, P., and Sator, K., "A Diesel for a Subcompact Car," SAE Paper No. 770113, 1977.

4 Parker, R. F., "Future Fuel Injection System Requirements of Diesel Engines for Mobile Power," SAE Paper No. 760125, 1976.

5 Andoh, H., and Shiraishi, K., "Influence on Injection and Combustion Phenomena by Elimination of Hole Nozzle Sac Volume," SAE Paper No. 860416, 1986.

6 Kato, T., Tsujimura, K., Shintani, M., Minami, T., and Yamaguchi, I., "Spray Characteristics and Combustion Improvement of D. I. Diesel Engine With High Pressure Fuel Injection," SAE Paper No. 890265, 1989.

7 Oblaender, K., Kollmann, K., Kraemer, M., and Kutschera, I., "The Influence of High Pressure Fuel Injection on Performance and Exhaust Emissions of a High Speed Direct Injection Diesel Engine," SAE Paper No. 890438, 1989.

8 Itoh, S., Sasaki, S., and Arai, K., "Advanced In-Line Pump for Medium-Duty Diesel Engines to Meet Future Emissions Regulations," SAE Paper No. 910182, 1991.

9 Okajima, M., Kato, M., Kano, H., Tojo, S., and Katagiri, M., "Contribution of Optimum Nozzle Design to Injection Rate Control," SAE Paper No. 910185, 1991.

10 Brown, G. W., and McCallion, H., "Simulation of an Injection System *With Delivery Pipe Cavitation Using a Digital Computer*," *IMechE, Vol. 182*, 1968, pp. 215–225.

11 Becchi, G. A., "Analytical Simulation of Fuel Injection in Diesel Engines," SAE Paper No. 710568, 1971.

12 Rosselli, A., and Badgley, P., "Simulation of the Cummins Diesel Injection System," SAE Paper No. 710570, 1971.

13 Wylie, E. B., Bolt, J. A., and El-Erian, M. F., "Diesel Fuel Injection System Simulation and Experimental Correlation," SAE Paper No. 710569, 1971.

14 Matsuoka, S., Yokota, K., Kamimoto, T., and Igoshi, M., "A Study of Fuel Injection Systems in Diesel Engines," SAE Paper No. 760551, 1976.

15 Kumar, K., Gajendra Babu, M. K., Gaur, R. R., and Garg, R. D., "A Finite Difference Scheme for the Simulation of a Fuel Injection System," SAE Paper No. 831337, 1983.

16 Pischinger, R., Staska, G., and Gao, Z., "Calculation of the Injection

Rate Curve of Diesel Injection Systems Under Cavitation Conditions" [in German], *MTZ*, Vol. 44, 1983, pp. 423–426.

17 DeLuca, L., "Numerical Approach to the Design of a Diesel Engine Injection System by an Optimization Technique," SAE Paper No. 851582, 1985.

18 Marcic, M., and Kovacic, Z., "Computer Simulation of the Diesel Fuel Injection System," SAE Paper No. 851583, 1985.

19 Gibson, D. H., "A Flexible Fuel Injection Simulation," SAE Paper No. 861567, 1986.

20 Krepec, T., To, C. H., and Lisio, C., "Investigation on Dynamic Response of a Closed Fuel Injector in a Diesel Engine at Low Speed," SAE Paper No. 880297, 1988.

21 Goyal, M., "Modular Approach to Fuel Injection System Simulation," SAE Paper No. 780162, 1978.

22 Kalkwijk, J. P. T., and Kranenburg, C., "Cavitation in Horizontal Pipe Lines Due to Water Hammer," ASCE *Journal of the Hydraulics Division*, Vol. 97, 1971, pp. 1585–1605.

23 Baltzer, R. A., "Column Separation Accompanying Liquid Transients in Pipes," ASME *Journal of Basic Engineering*, Vol. 89, 1967, pp. 837–846.

24 Streeter, V. L., "Water Hammer Analysis," ASCE *Journal of the Hydraulics Division*, Vol. 95, 1969, pp. 1959–1972.

25 Harten, A., Engquist, B., Osher, S., and Chakravarthy, S. R., "Uniformly High Order Accurate Essentially Non-oscillatory Schemes, III," *Journal of Computational Physics*, Vol. 71, 1987, pp. 231–303.

26 Anderson, D. A., Tannehill, J. C., and Pletcher, R. H., *Computational Fluid Mechanics and Heat Transfer*, McGraw-Hill, New York, 1984.

27 Weyler, M. E., Streeter, V. L., and Larsen, P. S., "An Investigation of the Effect of Cavitation Bubbles on the Momentum Loss in Transient Pipe Flow," ASME *Journal of Basic Engineering*, Vol. 93, 1971, pp. 1–10.

28 Kranenburg, C., "Gas Release During Transient Cavitation in Pipes," ASCE *Journal of the Hydraulics Division*, Vol. 100, 1974, pp. 1383–1398.

29 Wiggert, D. C., and Sundquist, M. J., "The Effect of Gaseous Cavitation on Fluid Transients," ASME *Journal of Fluids Engineering*, Vol. 101, 1979, pp. 79–86.

30 Kamiyama, S., and Yamasaki, T., "Prediction of Gaseous Cavitation Occurrence in Various Liquids Based on Two-Phase Flow Analogy," ASME *Journal of Fluids Engineering*, Vol. 103, 1981, pp. 551–556.

31 Kamiyama, S., and Yamasaki, T., "Critical Condition of Cavitation Occurrence in Various Liquids," ASME *Journal of Fluids Engineering*, Vol. 108, 1986, pp. 428–432.

32 Driels, M. R., "An Investigation of Pressure Transients in a System Containing a Liquid Capable of Air Absorption," ASME *Journal of Fluids Engineering*, Vol. 95, 1973, pp. 408–414.

33 Chaudhry, M. H., and Hussaini, M. Y., "Second-Order Accurate Explicit Finite-Difference Schemes for Waterhammer Analysis," ASME *Journal of Fluids Engineering*, Vol. 107, 1985, pp. 523–529.

34 Kohda, K., Suzukawa, Y., and Furukawa, H., "Analysis of Transient Gas-Liquid Two-Phase Flow in Pipelines," ASME *Journal of Energy Resources Technology*, Vol. 110, 1988, pp. 93–101.

35 Chaudhry, M. H., Bhallamudi, S. M., Martin, C. S., and Naghash, M., "Analysis of Transient Pressures in Bubbly, Homogeneous, Gas-Liquid Mixtures," ASME *Journal of Fluids Engineering*, Vol. 112, 1990, pp. 225–231.

36 Hardenberg, H., "The Geometrical Flow Cross Section of Hole Nozzles for Direct Injection Diesel Engines" [in German], *MTZ*, Vol. 45, 1984, pp. 427–429.

37 Hardenberg, H., "The Needle Lift Dependency of Flow Coefficients of Hole Nozzles for Direct Injection Diesel Engines" [in German], *MTZ*, Vol. 46, 1985, pp. 143–146.

38 Ziejewski, M., and Goettler, H. J., "Discharge Coefficients for Multihole Fuel Injection Nozzle for Alternate Fuels," SAE Paper No. 890448, 1989.

39 Yadigaroglu, G., and Lahey, R. T., Jr., "On the Various Forms of the Conservation Equations in Two-Phase Flow," *International Journal of Multiphase Flow*, Vol. 2, 1976, pp. 477–494.

M. Feola
Dipartimento di Ingegneria Meccanica II,
Università di Roma,
Rome, Italy

P. Pelloni
Dipartimento di Ingegneria Industriale,
Università di Parma,
Parma, Italy

G. Cantore
Istituto di Macchine,
Università di Bologna,
Bologna, Italy

G. Bella
Dipartimento di Ingegneria Meccanica II,
Università di Roma,
Rome, Italy

P. Casoli

G. Toderi

Dipartimento di Ingegneria Industriale,
Universita di Parma,
Parma, Italy

Optimization of Injection Law for Direct Injection Diesel Engine

This paper describes how different timing and shape of the injection law can influence pollutant emission of a direct injection diesel engine. The study was carried out making use of a "multizone" thermodynamic model as regards the closed valve phase, and a "filling-emptying" one as regards the open valve phase. After being calibrated by comparison with experimental data, the abovementioned model was used for injection law optimization as regards minimum pollutant concentration (NO_x and soot) in the exhaust gases with the smallest engine performance reduction possible.

Introduction

Due to lower fuel consumption associated with direct injection Diesel engines, these engines have found, lately, growing applications in both energy production fixed systems and light and heavy duty land vehicles. However, this expansion is hindered by considerable environmental pollution problems caused by this type of engine.

As a matter of fact, the typically heterogeneous characteristics of the direct injection diesel engine combustion process causes the production of high levels of pollutants, mainly soot and nitrogen oxides. This will make it difficult for the engine to be in concordance with the very strict emission standards in force in the United States and about to be introduced also in the EEC countries.

It is therefore necessary to find the best possible technical strategies for engine improvements aimed at the limitation of the abovementioned pollutant emission.

One way to limit production of pollutants is to control timing and shape of the injection law. However, with respect to the main pollutants present in the exhaust gases of a direct injection diesel engine, NO_x and soot, any changes applied to the injection law aiming at reducing nitrogen oxide emissions will cause an increase in soot production and vice versa.

This behavior suggests use of optimization techniques that, together with parameter analysis, would provide useful information about the best timing and shape of the injection law, so as to limit as much as possible the production of pollutants with little reduction in engine performances. This has led to the development by the authors of an algorithm that allows us to predict both combustion chamber pressure values and emission levels of the two pollutants to be controlled (NO_x and soot) as the main engine construction and operation parameters are varied.

The abovementioned algorithm is composed of two distinct models:

- a multizone phenomenological model for evaluation of both thermodynamic parameters (temperature and pressure) and pollutant emissions relative to the closed valve phases;
- a filling-emptying model for evaluation of the abovementioned physical and chemical parameters relative to the open valve phases.

Contributed by the International Combustion Engine Division and presented at the Energy-Sources Technology Conference and Exhibition, Houston, Texas, January 26-30, 1992. Manuscript received by the Internal Combustion Engine Division September 1991. Paper No. 92-ICE-4. Associate Technical Editor: J. A. Caton.

It must be pointed out that such an approach was preferred to both simpler single zone type algorithms and more complex ones based on fluid-dynamics for the following reasons:

- the former algorithms implied rating of heat release parameters, which would not allow an adequate predictive capability;
- the latter algorithms required a very complicated calibration procedure and long computing times; this would not allow us to obtain simple parameter analyses or to use mathematical optimization algorithms.

The model described in the following was therefore used, after calibration based on accurate comparison with experimental data, for a parametric study aimed at both the determination of the effects that different injection laws can have on performances and pollutant production, and at law optimization with respect to pollutant limitation.

Theoretical Model

The combustion phenomenological model used is based on the one proposed by Hiroyasu et al. [1-5].

The combustion process is divided into many elementary processes involving the behavior of fuel being injected into the cylinder; the latter is also split into many zones where the fuel/air mixture is considered to exist in both liquid and gaseous states. At the beginning the fuel is considered to be in the liquid state in all the cylinder zones. After a so-called "breakup time," which depends on the chemical and thermodynamic properties of each zone, air entrainment starts, the fuel is vaporized, and combustion takes place.

The spray cone is divided in both axial and radial directions into many packages, as shown in Fig. 1.

Axial package splitting represents elementary time intervals in which the overall injection time was divided; in radial package splitting there is the same amount of liquid fuel in each elementary cone. The number of radial packages was set to 10.

The rate of injected fuel, which depends on the pressure difference existing between the injector nozzle and the combustion chamber, can be computed from the following expression [3]:

$$\dot{m}_f = C_d \rho_l \left(2 \frac{(P_{\text{inj}} - P_c)}{\rho_l} \right)^{0.5} \cdot \frac{\pi d_o^2}{4} \tag{1}$$

The flow coefficient, C_d, was set to an experimentally estimated value of 0.9; this value yields the same value for total fuel input as the experimental one [5]. As previously mentioned, the spray centerline penetration can be obtained from the following empirical expressions, which are referred to a quiescent air environment:

$$t \geq t_{\text{break}} \quad s(t) = 2.95 \left(\frac{(P_{\text{inj}} - P_c)}{\rho_a} \right)^{0.25} (d_o t)^{0.5} \tag{2}$$

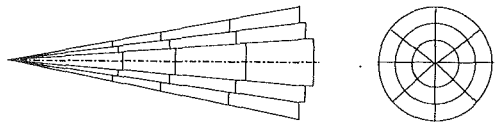

Fig. 1 Diagram of divided package of the spray

$$0 < t < t_{\text{break}} \quad s(t) = 0.39 \left(\frac{2(P_{\text{inj}} - P_c)}{\rho_l} \right)^{0.5} t \tag{3}$$

where t_{break} can be computed from:

$$t_{\text{break}} = 28.65 \frac{\rho_l d_o}{\sqrt{\rho_a (P_{\text{inj}} - P_c)}} \tag{4}$$

Representing each radial segment by the L index ($L = 1$ indicates the central package), the position of lateral packages can be determined, starting from the central one, from:

$$s_r(t) = s(t) \exp(-8.577 \times 10^{-3} (L-1)^2) \tag{5}$$

The presence of swirl in the combustion chamber affects the axial motion of spray penetration. This is taken into account by multiplying the penetration law expression, relative to quiescent air environment, by the following coefficient:

$$C_s = \left(1 + \frac{\pi r_s \text{rpm} s(t)}{30 v_{\text{inj}}} \right)^{-1} \tag{6}$$

The presence of swirl causes also spray movement of each package in the tangential direction, which can be taken into account by means of the following expression [3]:

$$r_{\text{rad}} = s(t) \left(\frac{\dot{m}_a}{\dot{m}_a + \dot{m}_f} \frac{\text{rpm} r_s \pi s(t)}{30} \right) (0.5(v_{\text{inj}} + \dot{s}(t)))^{-1} \tag{7}$$

The rate of air entrainment of each package can be determined, assuming the spray momentum in each package to be constant, from:

$$\dot{m}_f v_{\text{inj}} = (\dot{m}_f + \dot{m}_a) \frac{ds_i(t)}{dt} \tag{8}$$

When the rate of air entrainment for each package is determined, one has to take into account the way it can be affected by both the spray impingement on the piston bowl or on the cylinder walls and by ignition taking place.

When ignition starts in a package, a local pressure increase takes place, which would hinder air entrainment in the package. On the other hand, spray impingement on any surface would increase air entrainment as it causes both a decrease in spray momentum and an increase of spray surface exposed to the surrounding air. These phenomena are taken into account, in a simplified way, by multiplying the formula for the rate of air entrainment computation by two coefficients, c_f and c_w. The values of these coefficients have been rated, in accordance with the ones used by other authors [3-5], to be equal to 0.7 and 1.7, respectively.

Nomenclature

a = sound velocity, m/s
B = quantity of fuel injected per stroke, kg
C_p = specific heat at constant pressure, J/kg/K
C_v = specific heat at constant volume, J/kg/K
D = binary diffusivity, m^2/s
d_g = diameter of a droplet, m
d_o = diameter of nozzle hole, m
H_v = heat of evaporation, J/kg
k = C_p/C_v
M = molecular weight, kg/mole
m = mass, kg
Nu = Nusselt number
P = pressure, Pa
R_u = universal gas constant, J/kg/K
r_s = swirl ratio
Sh = Sherwood number
t = time, s
T = temperature, K
T_b = adiabatic flame temperature, K
v_{inj} = initial fuel injection velocity, m/s
Y_{fs} = mass fraction of vaporized fuel at the droplet surface
V = volume, m^3
λ = thermal conductivity, J/m/s/K
ρ = density, kg/m^3

Subscripts

a = air
c = cylinder
f_b = fuel burned
f = fuel evaporated
in = inlet
inj = injection
l = liquid
out = outlet
s = soot
s_f = soot formation
s_o = soot oxidation

As regards fuel evaporation, the model used in this study allows the evaluation of liquid fuel droplet mass, diameter, and temperature as a function of time [2].

The fuel droplet diameter initial value, which depends on the pressure difference existing between injector and cylinder, can be expressed as follows:

$$d_l = 23.9(P_{\text{inj}} - P_c)^{-0.135}\rho_a^{0.12}B^{0.131} \tag{9}$$

The fuel evaporation process can be simulated using the following differential equation system:

$$\frac{dT_l}{dt} = \frac{1}{m_l C_{pl}}\left(\pi d_l^2 h(T_c - T_l) + H_v \frac{dm_l}{dt}\right) \tag{10}$$

$$\frac{dm_l}{dt} = \frac{-\pi d_l^2 k^* Y_{fs}}{(1-(1+\xi)Y_{fs})} \tag{11}$$

$$\frac{dd_l}{dt} = \frac{2}{\pi\rho_l d_l^2}\left(\frac{dm_l}{dt} - \frac{\pi d_l^3}{6}\frac{d\rho_l}{dt}\right) \tag{12}$$

where h and k^* are the coefficients for global thermal exchange between fuel droplets and the surroundings and the mass exchange coefficient, respectively, which can be expressed as follows [3]:

$$h = X\left\{\pi d_l^2\left[\exp\left(\frac{X}{\text{Nu}\ \pi d_l \lambda}\right) - 1\right]\right\}^{-1} \tag{13}$$

$$k^* = -\frac{\rho_a D}{d_l}\frac{1-(1+\xi)Y_{fs}}{(1+\xi)Y_{fs}}\,SH\,\ln(1-(1+\xi)Y_{fs}) \tag{14}$$

where X, Y_{fs}, ξ, and x_f are given by:

$$X = -(C_{pf} + \xi C_{pa})\frac{dm_l}{dt}$$

$$Y_{fs} = \frac{x_f M_f}{x_f M_f + (1-x_f)M_a}$$

$$\xi = -\rho_a(1-Y_{fs})\left(\rho_l + \frac{d_l}{6}\frac{d\rho_l}{dd_l}\right)^{-1} \qquad x_f = \frac{P_f}{P_c}$$

By multiplying the amount of fuel vaporized from each droplet in a package by the number of droplets existing in that package, one can easily determine the total amount of vaporized fuel.

This can be done as it was assumed that, for every package, the behavior of all droplets contained in it is the same. The main physical and chemical properties versus temperature [6], at a fixed pressure, of the $C_{12}H_{24}$ type fuel used in this study are shown in Fig. 2.

Since it is assumed that combustion takes place at the stoichiometric condition, it can occur either in an excess fuel or in an excess air scenario. The mass of fuel burned for each computational step would therefore be:

$$\phi > 1:\ m_{fb} = \frac{m_a}{\phi_{st}} \quad \phi \le 1:\ m_{fb} = m_f \tag{15}$$

where ϕ is the package air/fuel ratio normalized with respect to the same ratio estimated in stoichiometric conditions.

The following expressions are used for the evaluation of the ignition delay [2]:

$$\tau = 4.10^{-3}P^{-2.5}\phi^{-1.04}\exp\left(\frac{4000}{T}\right) \tag{16}$$

$$\int_0^{\tau_i}\frac{1}{\tau}\,dt = 1$$

where τ_i indicates the ignition delay in the ith package.

Heat release in a package in each time interval can be determined by multiplying the fuel mass burned in that time interval by the fuel lower calorific value. Total heat release is obtained by summing the contribution of each package.

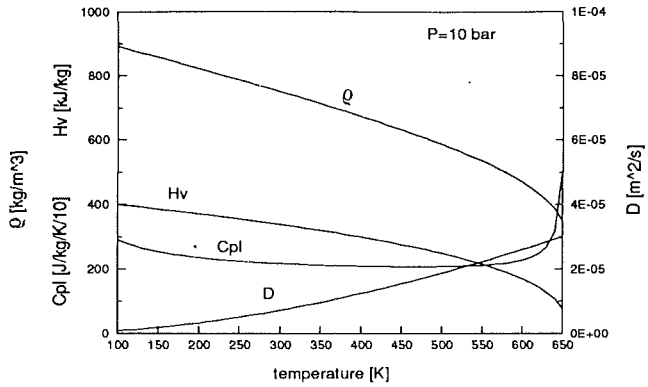

Fig. 2 Physical and chemical properties of fuel

Using the first principle of thermodynamics for an open system, the thermodynamic behavior inside a cylinder can be calculated using the following expression:

$$\frac{dP_c}{dt} = \frac{1}{V_c}(-kP_c\dot{V}_c + (k-1)(\dot{Q}_{\text{comb}} + \dot{Q}_l) + \dot{m}_{in}a_{in} - \dot{m}_{\text{out}}a_{\text{out}}) \tag{17}$$

where the subscripts comb and l indicate the amount of heat released during combustion and lost to the surroundings, respectively. The heat transfer from the hot gas to the cooled cylinder walls was rated making use of an empirical correlation [17]. The rates of flow of gases exchanged between the cylinder and the intake and exhaust ducts have been determined by means of a "filling-emptying" model [9, 10].

The differential Eqs. (10), (11), (12), and (17) can be solved using a fourth-order implicit "Runge-Kutta" method, with a one degree integration step.

As previously mentioned, it is quite clear that the use of the model described above makes it possible to evaluate thermodynamic and chemical parameters in every single package. Once the values of such parameters are known, it is possible to determine the amount of soot and nitrogen oxides produced in the cylinder during combustion.

Such production is a typical nonequilibrium process, and is therefore controlled by chemical kinetics depending on the adiabatic flame temperature. This temperature was evaluated using a procedure described in [7], assuming, as previously mentioned, every package to be homogeneous.

The post-combustion temperature behavior during the expansion phase was estimated, for each package, assuming an isentropic expansion process for the combustion products [2]. The temperature having thus been determined was afterward used in a typical Zeldovich algorithm for the computation of NO concentration. Such a procedure is well known to be based on the following chemical reactions [8, 18, 20]:

$$\begin{aligned} &N_2 + O \overset{k_1}{\leftrightarrow} NO + N \\ &N + O_2 \overset{k_2}{\leftrightarrow} NO + O \\ &N + OH \overset{k_3}{\leftrightarrow} NO + H \end{aligned} \tag{18}$$

where k_1, k_2, and k_3 are [20]:

$$\begin{aligned} k_1 &= 1.32\times 10^{13} \\ k_2 &= 1.81\times 10^{8}\ T^{1.5}\exp(-3000/T_B) \\ k_3 &= 4.2\times 10^{13} \end{aligned} \tag{19}$$

Assuming the nitrogen atom concentration to behave in a quasi-steady-state manner, the rate of change of NO concentration in the package is:

$$\frac{d[\text{NO}]}{dt} = 2R_1\frac{(1-\beta^2)}{1+\beta R_1/(R_2+R_3)} \tag{20}$$

where β represents the ratio $[NO]/[NO]_{eq}$, and $R_i (i = 1, 3)$ are given by:

$$R_1 = k_1 [NO]_{eq} [N]_{eq}$$
$$R_2 = k_2 [N]_{eq} [O_2]_{eq}$$
$$R_3 = k_3 [N]_{eq} [OH]_{eq} \quad (21)$$

The total postcombustion concentration of nitrogen oxides can be obtained by summing up the contribution of each package, and diluting this concentration with the amount of air surrounding the spray, which did not take part in the combustion process.

As regards the process of soot production, the following expression was used for every spray package [2, 11]:

$$\frac{dm_{sf}}{dt} = A_f m_{fg} p^{0.5} \exp\left(\frac{-E_f}{R_u T}\right) \quad (22)$$

where A_f and E_f are constants that can be experimentally evaluated. As regards the process of soot oxidation, the following expression was used:

$$\frac{dm_{so}}{dt} = A_o m_s \frac{p_o}{p} p^{1.8} \exp\left(\frac{-E_o}{R_u T}\right) \quad (23)$$

where A_o and E_o are constants that can be experimentally evaluated. The net quantity of soot in the cylinder at the end of the combustion process is given by the following balance equation:

$$\frac{dm}{dt} = \frac{dm_{sf}}{dt} - \frac{dm_{so}}{dt} \quad (24)$$

The above equation should be integrated from the combustion process starting time to the time when, due to the gas temperature decrease, the soot oxidation rate becomes negligible.

Analysis of Results

The capability of the previously described model to predict the pressure cycle and heat release of a direct injection diesel engine during a combustion process was verified by comparing evaluated and experimental data relative to an engine whose main geometric characteristics are shown in Table 1.

As shown in Table 2, the parameters considered during the experimental study are: angular speed (rpm), static lead, air/fuel ratio, and swirl ratio. The first four configurations listed in Table 2 are considered as reference; the remaining configurations are obtained from the reference ones by changing one parameter at a time. For each examined configuration, injection pressure curves, related to the change of a single parameter, are shown in Figs. 3–14.

The following diagrams show the cylinder pressure theoretical and experimental profiles, together with the injection pressure experimental behavior and the heat release estimated profiles. Figures 3 and 4 show results for an angular speed of 2400 rpm and fuel/air ratios of 23 and 38, respectively; a good agreement between experimental and estimated data is found.

In particular, for an air/fuel ratio of 38 (Fig. 4), the experimental and estimated behavior are practically identical, while for an air/fuel ratio of 23 (Fig. 3), the pressure values yielded by the simulation model are overestimated by about 10 bars.

In both cases, the estimated starting time of the combustion process and the angular position for the peak pressure value are in good agreement with the relative experimental data.

Figures 5 and 6 show the results obtained for a value of 3600 rpm, having kept the remaining parameters unchanged with respect to Figs. 3 and 4, respectively.

Once more it can be seen that there is good agreement between estimated and experimental data; for the air/fuel ratio value of 23 (Fig. 5), the discrepancy between estimated and experimental data is 5 bars less than in the case of Fig. 3.

Table 1 Details of the direct injection diesel engine

Bore	78 mm
Stroke	68 mm
Conrod	112 mm
Compression ratio	18.5
Diameter of nozzle hole	0.24 mm
Number of nozzle holes	4

Table 2 Configuration of functional parameters analyzed

Case	RPM	air/fuel.	swirl ratio	static injection angle
1	2400	23	2	-26
2	2400	38	2	-26
3	3600	23	2	-26
4	3600	38	2	-26
5	2400	23	2	-20
6	2400	38	2	-20
7	3600	23	2	-20
8	3600	38	2	-20
9	2400	23	1.5	-26
10	2400	38	1.5	-26
11	3600	23	1.5	-26
12	3600	38	1.5	-26

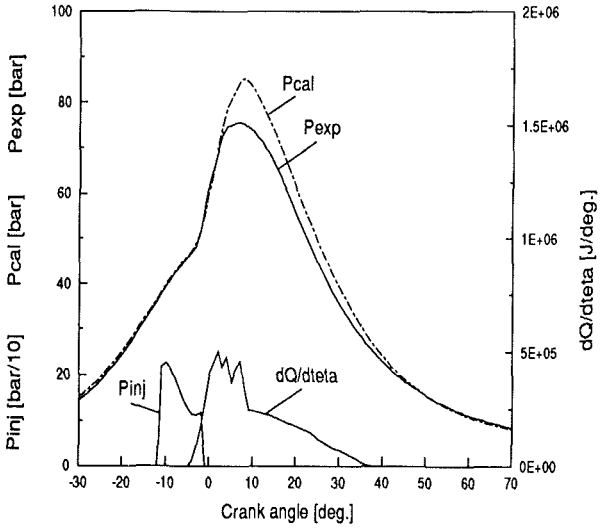

Fig. 3 Results of case 1

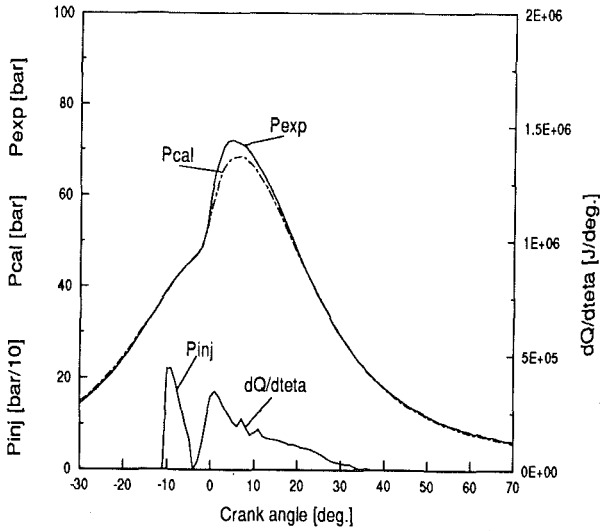

Fig. 4 Results of case 2

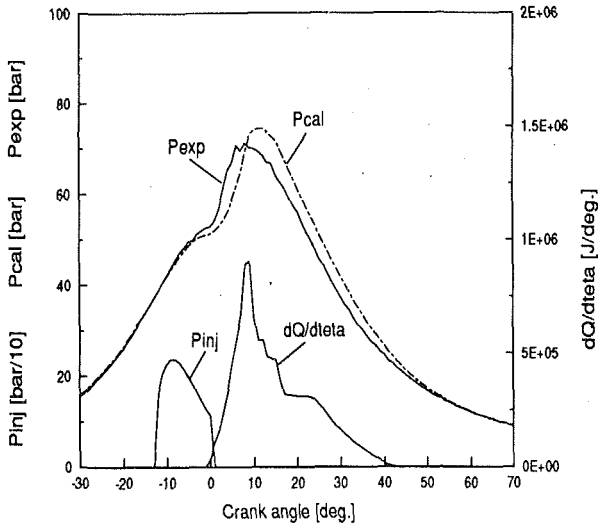

Fig. 5 Results of case 3

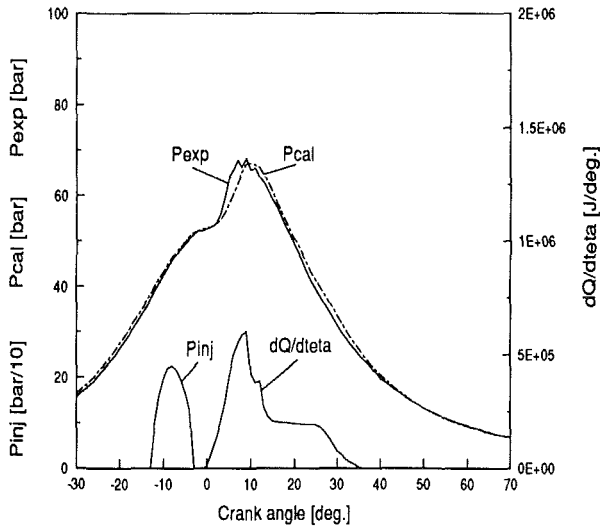

Fig. 6 Results of case 4

The effects of changing the injection lead were studied in configurations 5, 6, 7, and 8 of Table 2 and are shown in Figs. 7, 8, 9, and 10, respectively; again the simulation model showed its very good predictive capabilities.

In all combustion processes, there are two distinctive phases: one due to premixed combustion and the other due to mixed controlled combustion. The comparative analysis of the rate of change of heat release made for cases 1–4 and 5–8 shows that, as expected, a fuel injection delay causes a heat release reduction in the premixed phase and a consequent increase in the mixed controlled phase.

In Figs. 11, 12, 13, and 14 the capability of the model to predict the effect of changing the swirl ratio while keeping constant the values of the remaining variables was studied; once more a very good agreement between experimental and estimated data was found.

When the simulation model was used for the study of production of pollutants (NO and soot) it was calibrated with experimental data obtained from a direct injection diesel engine whose main geometric characteristics are shown in Table 3.

Data from this engine were used as they were readily available in the literature [2], while there were no experimental results on NO and soot production from the engine used for the indicated pressure cycle calibration.

Figure 15 shows the effects of fuel injection timing on the

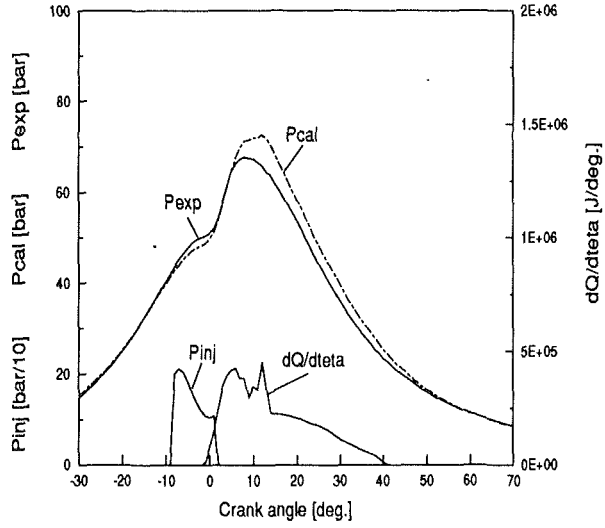

Fig. 7 Results of case 5

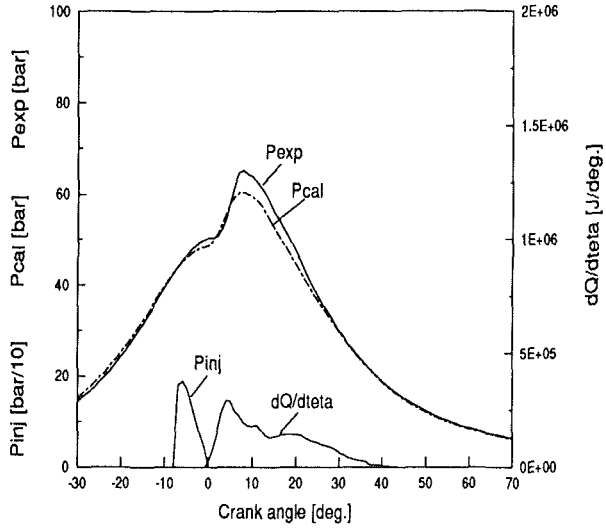

Fig. 8 Results of case 6

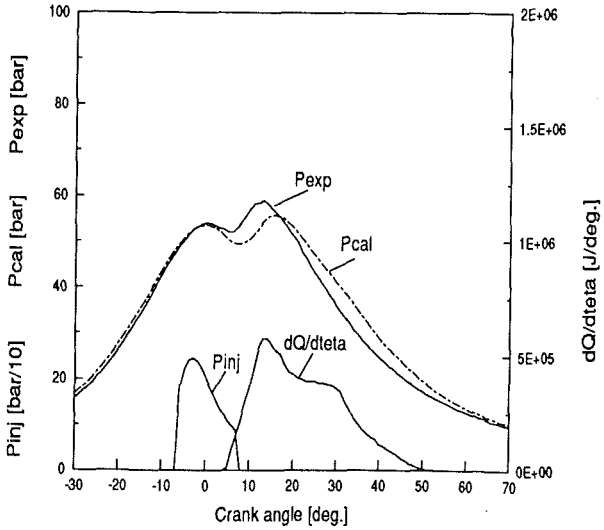

Fig. 9 Results of case 7

production of pollutants. As regards soot in particular, it can be seen that an increase in the injection lead has a beneficial effect, as the liquid fuel present in the combustion chamber has more time available to mix with air before combustion

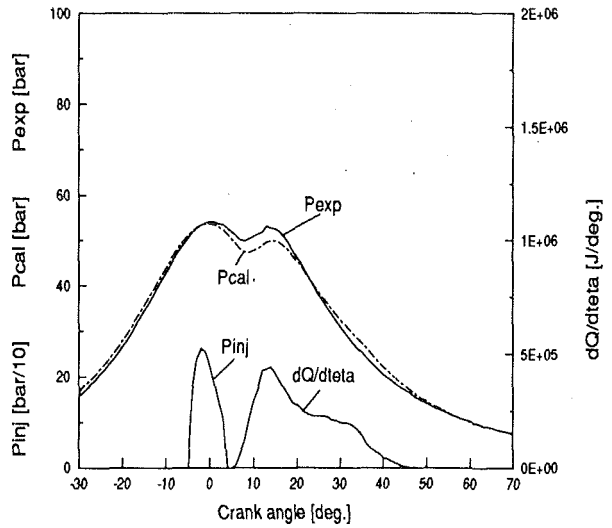

Fig. 10 Results of case 8

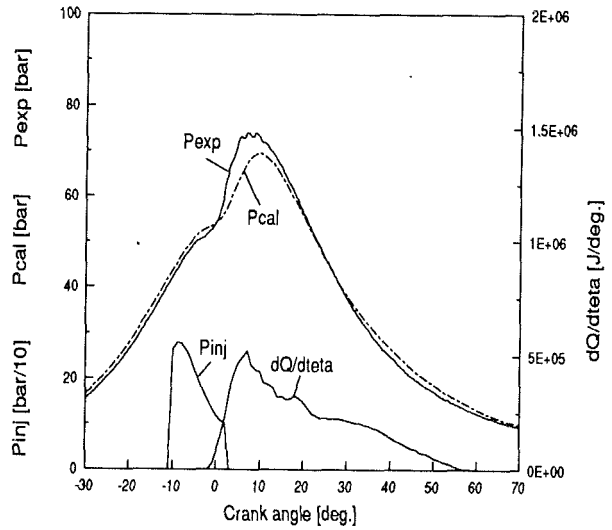

Fig. 13 Results of case 11

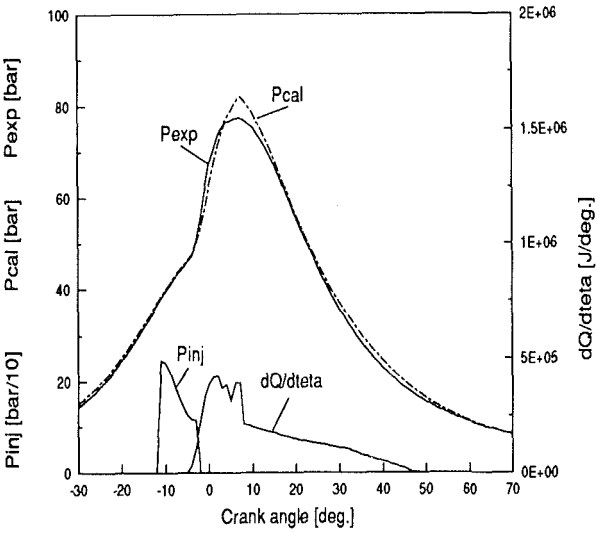

Fig. 11 Results of case 9

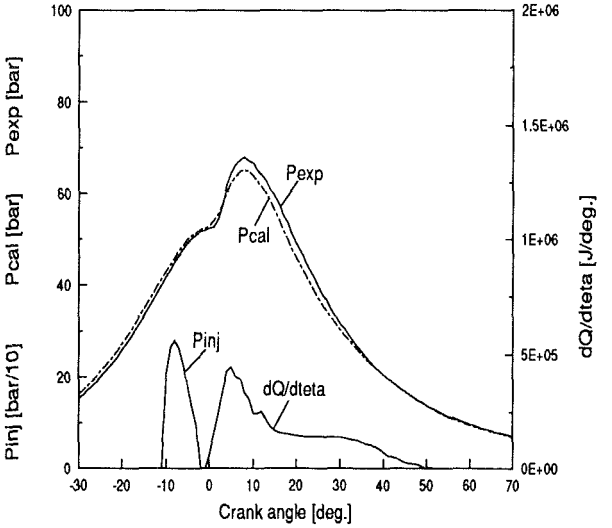

Fig. 14 Results of case 12

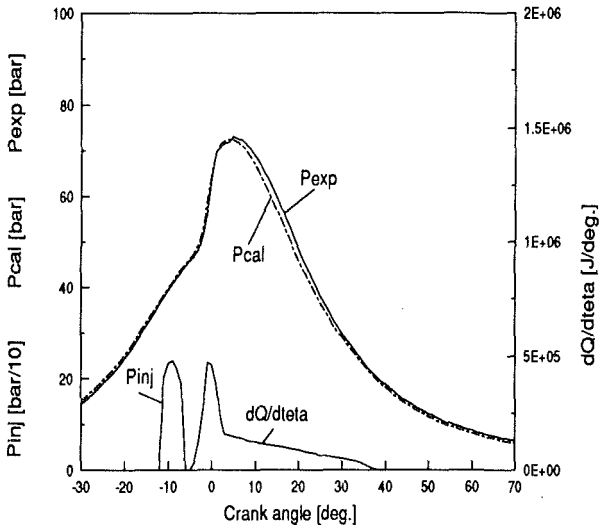

Fig. 12 Results of case 10

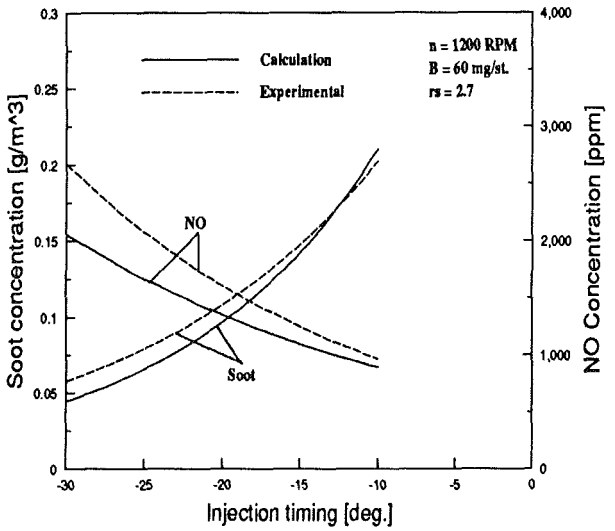

Fig. 15 Effect of injection timing on calculated and experimental soot and NO concentration

Table 3 Details of the direct injection diesel engine

Bore	135 mm
Stroke	130 mm
Conrod	230 mm
Compression ratio	15.5
Diameter of nozzle hole	0.35 mm
Number of nozzle holes	4

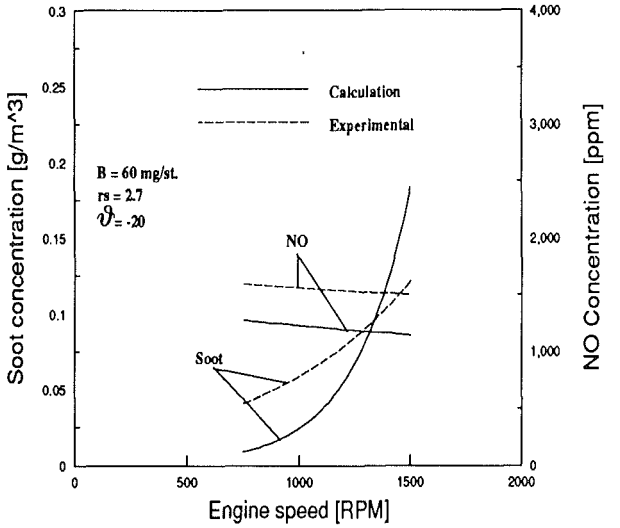

Fig. 16 Effect of engine speed on calculated and experimental soot and NO concentration

takes place. It is in fact well known that better mixing between air and fuel, together with less fuel present in the liquid phase, cause a considerable decrease in soot production [11-16].

From Fig. 15 it can be seen that, when the injection lead value is varied from -30 to -10 deg (assuming 0 deg as t.d.c.), the experimental soot production changes from about 0.06 to 0.2 g/m^3. The previously described simulation submodel yielded, under the same functional conditions, 0.05 and 0.21 g/m^3. The behavior of the estimated curve is therefore in good agreement with the experimental one.

It is worth pointing out that the empirical nature of the submodel used for the study of soot production causes its results to be very strongly dependent on constants A_f and A_o. In this study the values of such constants were set to 500 and 10,000, respectively, while E_f and E_o were set to 5.22 E+4 kJoule/kmoles and 5.85 E+4 kJoule/kmoles, respectively, as previously done by other authors [16].

The use of such correlations for a different type of engine from the one used for calibration provides, therefore, only a qualitative indication on soot production.

As regards NO, an increase in the injection lead value causes a corresponding change in the beginning of the combustion process. The latter takes place in the region of top dead center, causing an increase of gas temperature.

Therefore, as expected, the experimental values shown in Fig. 15 change from about 1000 to 2500 ppm when the injection lead value is varied from -10 to -30 deg. The corresponding theoretical values are included between 950 and 2000 ppm. Thus, as can be seen from Fig. 15, the model shows a very good predictive capability for lower injection lead values. Increasing lead values, on the other hand, causes an increase in the discrepancy between estimated and experimental data.

Engine angular speed also affects soot production, as its increase causes a decrease in available oxidation time [17-19]. Therefore, an increase of engine angular speed causes an increase of soot production, as experimentally shown in Fig. 16.

When angular speed is changed from 750 to 1500 rpm, soot production changes from 0.05 to 0.12 g/m^3. The corresponding

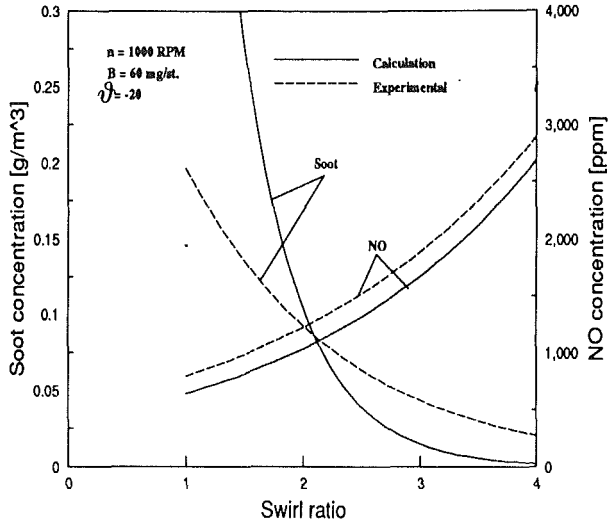

Fig. 17 Effect of swirl ratio on calculated and experimental soot and NO concentration

results yielded by the simulation model were 0.01 and 0.18 g/m^3.

The amount of produced nitrogen oxides is substantially independent from angular speed, as a decrease in available time for chemical reactions has no effect due to the very fast "freezing" of the reactions, which is always achieved in very short times [2, 20, 21]. The theoretical and experimental profiles of nitrogen oxide production as a function of angular speed are also shown in Fig. 16.

The effect of varying swirl ratio values on pollutant production was finally studied. As swirl ratio increases, fuel spray and the surrounding air can mix in a better way, thus favoring combustion in the premixed phase with respect to the mixed controlled one. It is well known that a decrease in the mixed controlled combustion phase with respect to the premixed one causes a decrease of soot production. The profiles of estimated and experimental soot production are shown in Fig. 17, which shows that the simulation model provides good results for high values of swirl ratio, while the discrepancy between estimated and experimental data increases as swirl ratio decreases.

As the premixed combustion phase is increased, the cylinder temperature also increases, thus causing the production of greater quantities of nitrogen oxide production.

The experimental and estimated trends of nitrogen oxide production, also shown in Fig. 17, are quite similar; however, the simulation model overestimates the experimentally produced quantities.

Most probably, the model's poor ability to predict nitrogen oxides, for all examined parameter configurations, is due to an underestimating of the flame temperature in each package. Such an estimate is very difficult to improve using a phenomenological type of approach.

The simulation model was also used for the analysis of the effects of different timing and shape of the injection law on engine performance and production pollutants. This was done, after proper calibration and testing of the model, through a parametric study making use of five injection laws, which are shown in Fig. 18. The pressure values in all five laws vary from a minimum of 150 bars to a maximum of 250 bars.

This latter value has been obtained in previous experimental analysis. The laws differ from each other depending on the value of the angular position corresponding to the maximum pressure value. Such angular position changes from the injection process starting time (law 1) to its final one (law 5) going through three intermediate positions (laws 2, 3, and 4) in which starting and final pressure value are set to 150 bars. The sim-

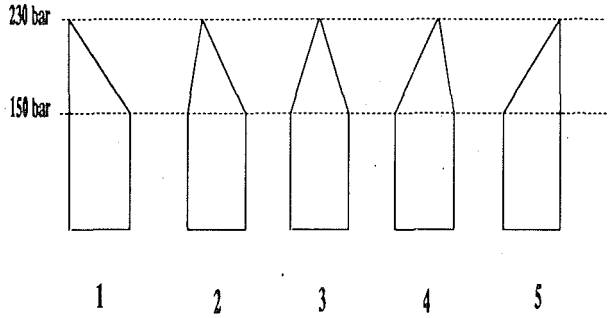

Fig. 18 Shapes of injection laws

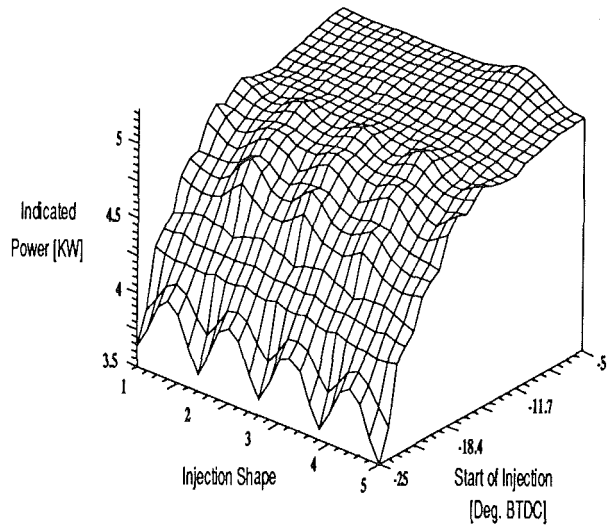

Fig. 19 Engine "indicated" power versus injection timing and shape

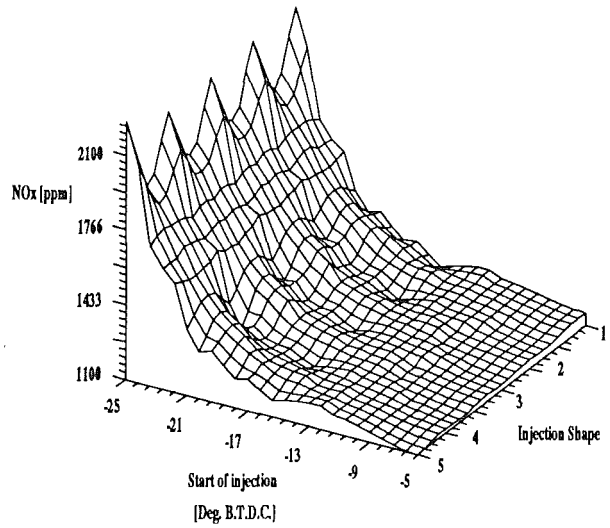

Fig. 20 NO concentration in the exhaust gas versus injection timing and shape

ulation was carried out for an angular speed 2400 rpm and an air/fuel ratio of 23.

Figure 19 shows that injection lead plays an important role on engine output power, while the injection law shape seems to have a secondary effect with respect to the lead. Figure 19 also shows that, in order to avoid excessive engine performance reduction, injection lead should be kept between about -5 to -18 deg.

Figures 20 and 21 show pollutant production, NO and soot, as a function of shape of injection law and injection lead. As

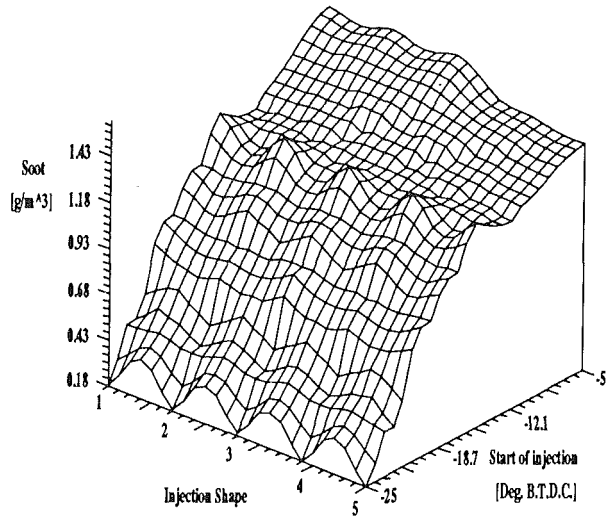

Fig. 21 Soot concentration in the exhaust gas versus injection timing and shape

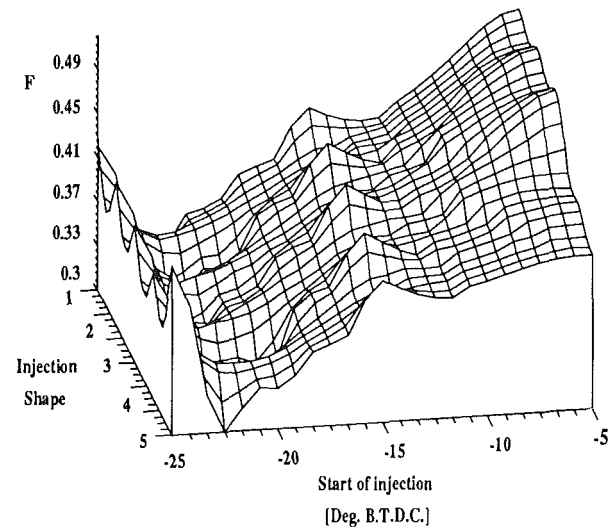

Fig. 22 Function F versus injection timing and shape

expected, and in accordance with previous results, an injection lead increase causes a chamber temperature increase, with a consequent increase in NO production.

The simulation model was also used together with a mathematical optimization routine based on a "Quasi-Newton" algorithm with the aim of minimizing the function "F" with respect to the injection law shape and lead angle. This was done at angular speeds of 2400 and 3600 rpm and with an air/fuel ratio of 23, and with the aim of keeping reductions of engine performances limited within 5 percent.

The outcome shows that, in the abovementioned conditions, the most favorable injection laws are No. 5 at 2400 rpm and No. 4 at 3600 rpm with lead angles of -15 and -22, respectively. Since these two laws inject a higher quantity of fuel in the final phase, they yield an acceptable output power level. Injection laws injecting more fuel in the initial phase of the process are not as suitable since, in order to avoid output power reduction, lead angle values cannot be increased too much; as a consequence limitation of production pollutants is impossible (see Fig. 22).

It also causes a reduced mixed controlled combustion phase, with a consequent decrease in soot production. It is worth pointing out that, for any value of the injection lead angle, injection law No. 5 seems to be the most favorable, as it allows production of the smallest quantities of soot.

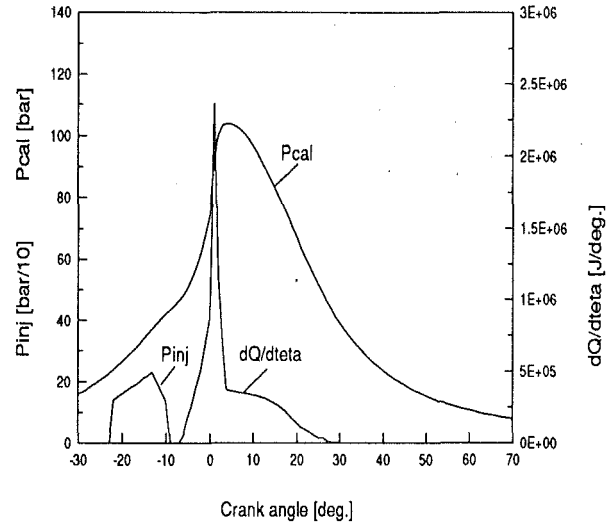

Fig. 23 Result regarding the optimum condition at 3600 rpm

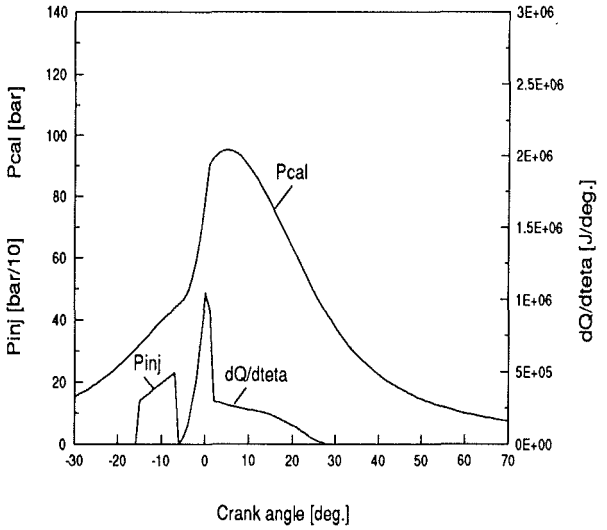

Fig. 24 Result regarding the optimum condition at 2400 rpm

Finally, Fig. 22 shows the profile of function

$$F=\frac{[NO]}{[NO]_{max}}+\frac{[soot]}{[soot]_{max}}$$

which is proportional to the engine pollutant production. From this figure one can see that pollutant production is at a minimum for a lead angle of about -23 deg. However, this value is not acceptable, as it implies excessive output power reduction with respect to the nominal one. The latter is, in the above operating conditions (2400 rpm and air/fuel ratio of 23) about 4.65 kW.

Figure 22 also shows that, for all injection lead angles, laws 4 and 5 correspond to the smallest quantities of pollutant concentration in the exhausts.

Figures 23 and 24, finally, show the behavior of the indicated pressure and heat release gradient in optimum conditions.

Conclusions

A direct injection diesel engine simulation model was used in order to study the correlation between timing and shape of the injection law and the engine performances and concentration of pollutants in the exhausts. The simulation model, a "multizone" phenomenological one for the closed valve phase and a "filling-emptying" one for the open valve phase, was calibrated and tested by comparing it with experimental data. Comparison between the result yielded by the model and experimental ones shows the model good predictive capability as regards indicated pressure cycle and pollutants (NO and soot) production. The parametric study carried out has highlighted the primary role of injection law timing on engine pollutant production with respect to the role of injection law shape. The latter, however, seems to have some influence on soot concentration in the exhaust. The abovementioned model was also used together with a "Quasi-Newton" optimization algorithm in order to find the optimum injection law minimizing pollutant production, keeping engine power output reduction within 5 percent of its nominal value. The results show the optimum injection law shapes to be the ones with increasing pressure in the final phase, which allow the use of considerable advance of injection law without excessive performances reduction. If extended to other engine configuration parameters, the proposed method can provide useful indications on injection law timing and shape so as to allow minimization of pollutant production of a direct injection diesel engine without reducing its performance too much.

References

1 Hiroyasu, H., and Kadota, T., "Models for Combustion and Formation of Nitric Oxide and Soot in Direct Injection Diesel Engines," SAE Paper No. 760129, 1976.

2 Hiroyasu, H., Kadota, T., and Arai, M., "Development and Use of a Spray Combustion Modeling to Predict Diesel Engine Efficiency and Pollutant Emissions," *Bulletin of JSME*, Vol. 26, No. 214, Apr. 1983.

3 Hiroyasu, H., Kadota, T., and Arai, M., "Supplementary Comments: Fuel Spray Characterization in Diesel Engines," *Combustion Modeling in Reciprocating Engines*, J. N. Mattavi and C. A. Amann, eds., Plenum Press, 1980.

4 Bella, G., Blasi, R., Cordiner, S., Ramos, I. J., and Rocco, V., "Predictive Capabilities of Diesel Engine Models," YSAE 891359, 1985.

5 Pelloni, P., Bettocchi, R., Bella, G., Casoli, P., and Toderi, G., "Analisi della Capacità Predittiva di un Modello Fenomenologico 'Multizone' della Fase di Combustione di un Motore Diesel D. I.," in press.

6 Reid, C. R., Prausnitz, J. M., and Poling, B. E., *The Properties of Gasses and Liquids*, McGraw-Hill, New York, 1986.

7 Bignardi, L., and Troilo, M., "Combustione a Pressione e Volume Costante di Idrocarburi del Tipo C_nH_{2n}," presented at the 23° Congresso ATI Bologna, 1968.

8 Nightingale, D. R., "A Fundamental Investigation Into the Problem of NO Formation in Diesel Engine," SAE Paper No. 750848, 1975.

9 Ferguson, C. R., *Internal Combustion Engines*, Wiley, New York, 1986.

10 Heywood, J. B., *Internal Combustion Engine Fundamentals*, McGraw-Hill, New York, 1989.

11 Nishida, K., and Hiroyasu, H., "Simplified Three Dimensional Modelling of Mixture Formation and Combustion in a D. I. Diesel Engine," SAE Paper No. 890269, 1989.

12 Smith, O. I., "Fundamentals of Soot Formation in Flames With Application to Diesel Engine Particulate Emissions," *Prog. Energy and Combustion Science*, Vol. 7, 1981, pp. 275-291.

13 Lipkea, W. H., Johnsen, J. H., and Vuk, C. T., "The Physical and Chemical Character of Diesel Particulate Emissions—Measurement Techniques and Fundamental Considerations," SAE Paper No. 780108, 1978.

14 Haynes, B. S., and Wagner, H. G., "Soot Formation," *Prog. Energy Combust. Sci.*, Vol. 7, pp. 229-273.

15 Khan, I. M., "Formation and Combustion of Carbon in a Diesel Engine," *Inst. Mech. Eng. Prog.*, Vol. 184, 1968.

16 Khan, I. M., Wang, C. H. T., and Langride, B. E., "Coagulation and Combustion of Soot Particles in Diesel Engine," *Combustion and Flames*, Vol. 17, 1971, pp. 409-419.

17 Ramos, J. I., "Internal Combustion Engine Modeling," Hemisphere Publishing Corporation, 1989.

18 Kyriakides, S. C., Dent, J. C., and Mehta, P. S., "Phenomenological Diesel Combustion Model Including Smoke and NO Emission," SAE Paper No. 860330, 1986.

19 Magnussen, B. F., "Modelling of Reaction Processes in Turbulent Flames With Special Emphasis on Soot Formation and Combustion," presented at the General Motors Symposium on Particulate Carbon Formation During Combustion, Oct. 1980.

20 Lavoie, G. A., Heywood, J. B., and Keck, J. C., "Experimental and Theoretical Study of Nitric Oxide Formation in Internal Combustion Engines," *Combustion Science in Technology*, Vol. 1, 1970.

21 Pischinger, R., and Cartellieri, W., "Combustion System Parameters and Their Effect Upon Diesel Engine Exhaust Emissions," SAE Paper No. 720756, 1972.

Variable Geometry and Waste-Gated Automotive Turbochargers: Measurements and Comparison of Turbine Performance

M. Capobianco

A. Gambarotta

Department of Energetic Engineering,
University of Genoa,
Genoa, Italy

In turbocharging automotive Diesel engines, an effective method to extend the turbine flow range and control the boost level is the use of a variable geometry turbine (VGT): This technique can be very helpful to improve the transient response of the engine and reduce exhaust emissions. In order to compare the performance of variable geometry and conventional waste-gated turbines, a thorough experimental investigation was developed on a test facility at the Department of Energetic Engineering of the University of Genoa (DINE). Two VG turbines were considered: a variable area turbine (VAT) and a variable nozzle turbine (VNT). The VG turbines were compared with a fixed geometry waste-gated turbine in both steady and unsteady flow conditions, referring to mass flow and efficiency characteristics.

Introduction

In recent years the application of exhaust turbocharging to Diesel engines has become wider and wider, since it allows for high power-weight ratios, lowering specific fuel consumption and exhaust emissions. However turbocharger matching is not a simple task for the designer, especially in the case of automotive engines, which usually operate under transient conditions.

At present most automotive turbochargers are fitted with fixed geometry nozzleless radial turbines: In those cases, although the flow range of a defined trim is fairly large, the turbine acts as a fixed restriction, and the pressure drop across it varies greatly with the mass flow rate. Since the turbine power increases with mass flow and expansion ratio, the boost pressure curve rises notably with engine speed and load. For automotive applications, where the operating conditions often vary within a wide range, the engine may have insufficient boost at low speeds and loads and be overboosted at high speeds and loads (Watson and Janota, 1982).

In order to control the boost level, a bypass valve ("waste-gate") is usually adopted, but this results in a significant loss of efficiency when operating away from the design point since a large amount of exhaust gas energy is lost. A more effective method to govern the boost level is the use of a variable geometry turbine (VGT): Changing a suitable controlling area allows the expansion ratio to be varied, and therefore the turbine power output to be varied (Flaxington and Szczupak, 1982). This technique, joined with a proper control strategy, can be very helpful to improve both steady-state performance and transient response of the engine, and reduce emissions in terms of exhaust smoke (Wallace et al., 1982; Watson and Banisoleman, 1986, 1988; Wallace et al., 1986a, 1986b; Arcoumanis et al., 1990).

Several variable area systems have been proposed by researchers and manufacturers (Flaxington and Szczupak, 1982; Hirhikawa et al., 1988; O'Connor and Smith, 1988); however, the most effective and reliable solutions seem to be based on a variation of the turbine housing throat area (variable area turbine, VAT) or on the use of a variable geometry nozzle turbine (VNT).

As a first step of a specific research program on optimization of turbocharger matching and control, a wide experimental investigation has been developed at the Department of Energetic Engineering of the University of Genoa (DINE) (jointly with the Centro Ricerche Fiat of Orbassano) in order to achieve a better knowledge of steady and unsteady flow behavior of radial turbines fitted with different variable geometry devices, in comparison with a conventional waste-gate system.

Two Garrett automotive turbochargers were considered, fitted with the same turbine wheel but with different regulating systems: a variable area turbine (Garrett VAT025) and a variable nozzle turbine (Garrett VNT025). Steady and pulsating flow performance was measured on the test facility of the DINE, with reference to different fixed settings of the variable geometry devices, and was related to those previously obtained on a quite similar fixed geometry waste-gated turbine (Garrett TB025) (Capobianco et al., 1990; Capobianco and Gambarotta, 1990).

Experimental results are presented and compared in the paper, emphasizing the influence of the control device setting on turbine steady flow performance with particular reference to

Contributed by the Internal Combustion Engine Division and presented at the Energy-Sources Technology Conference and Exhibition, Houston, Texas, January 26-30, 1992. Manuscript received by the Internal Combustion Engine Division September 30, 1991. Paper No. 92-ICE-9. Associate Technical Editor: J. A. Caton.

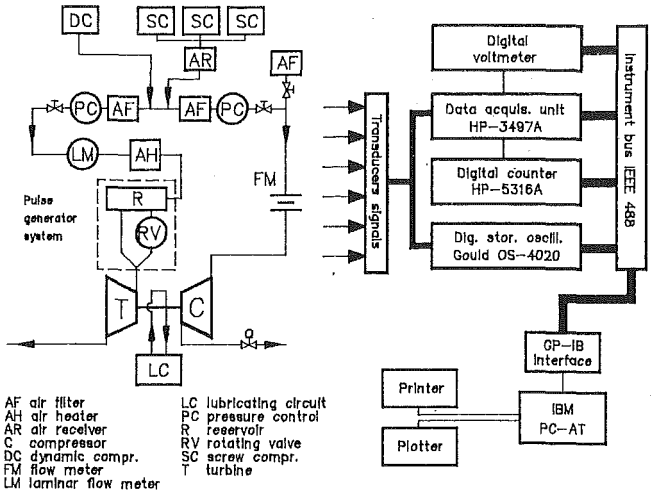

Fig. 1 Schematic of the test facility and measuring system

mass flow and efficiency. Additionally the turbine unsteady flow behavior is analyzed, referring both to pressure diagrams and average performance.

In future stages of the investigation on-engine tests and simulation models (which are now being developed at DINE) will also be considered in order to define optimized control strategies to take full advantage of VGT benefits.

Experimental Facility and Investigation Program

Measurements were performed on the DINE test rig, fully described in previous papers (Capobianco et al., 1990; Capobianco and Gambarotta, 1990), which is schematically shown in Fig. 1. In the present layout it allows us to develop steady and pulsating flow tests both on single devices and on complete intake and exhaust systems of automotive engines.

Two separate feeding lines are available: Compressed air is supplied by three screw compressors SC (with a total flow rate of 0.65 kg/s at a maximum pressure of 8 bar) or, alternatively, by a centrifugal compressor DC (with a maximum delivery of 2.2 kg/s and a compression ratio of 2.13). Pressure level in each line can be controlled by a proper regulating system.

The main feeding line is fitted with an electrical air heater AH (which allows air temperature up to 400 K) and a pulse generator system. This device, developed by the authors, makes possible an effective control of pressure oscillation characteristics, namely frequency, amplitude, and mean value. This result is obtained by mixing two flows, downstream of a small reservoir R, in one of which pressure pulses are generated by a rotating valve RV (composed of a cylindrical rotor with a diametral slot revolving inside a stator with inlet and outlet ports). Different flow area diagrams can be obtained by replacing the rotor and the stator ports, while pulse frequency can be adjusted through valve speed in the typical range of high-speed multicylinder engines (10–250 Hz). Dedicated valves allow the two flow components to mix properly, thus controlling the oscillation parameters. Recent modifications made it possible to test two entry devices (e.g., twin entry turbocharger turbines): In this case both entries can be fed with controlled pulsating flows, while the phase between the pressure pulses can be easily modified (by changing the relative angular position of the rotating valve rotors).

The experimental investigation on variable geometry turbochargers referred to in this paper was developed feeding the turbine through the main line, while the compressor was used as a dynamometer. In order to vary the compressor power at constant rotational speed, its inlet pressure was controlled by the second feeding line (Fig. 1). By this technique it was possible to investigate turbine characteristics up to higher values of the expansion ratio, while lowest values were reached by a particular device, which was mounted in place of the original compressor housing (Capobianco and Gambarotta, 1990).

Turbocharger lubrication was ensured by a dedicated circuit: Inlet oil temperature and pressure were controlled and kept constant at set levels.

Measurements were performed through an automatic data acquisition system. Pressures and temperatures were evaluated upstream and downstream of the turbine and the compressor by high frequency response strain gage transducers and by platinum resistance thermometers. Turbocharger speed and rotating valve frequency were measured by inductive probes. Turbine and compressor mass flow rate were evaluated by a laminar flow meter LM and a sharp edged orifice FM, respectively.

Data acquisition was governed by an IBM-AT computer through an HP-3497A unit. In the case of pulsating flow tests, a digital oscilloscope Gould 4020 (with 2 MHz sampling frequency and 4 kbytes internal memory) was used for recording and storage of time dependent pressure diagrams at the turbine inlet and exit. Dedicated software has been developed to control the acquisition procedure, calculate turbocharger performance parameters, and automatically plot turbine and compressor characteristics.

The investigation program was developed to analyze steady and pulsating flow behavior of turbocharger turbines fitted with variable geometry devices, and compare their performance with a conventional waste-gate system.

First the variable area turbine of a Garrett VAT025 turbocharger was considered: In this case the turbine throat area can be controlled by means of a single blade moving inside the housing (Flaxington and Szczupak, 1982; Hirhikawa et al., 1988) (Fig. 2*a*). Since the turbocharger was fitted with a waste-gate valve, this was kept closed in any operation condition.

A Garrett VNT025 turbocharger turbine with nozzle ring was also considered: Its stator area can be varied by simultaneously rotating twelve blades arranged around the peripheral portion of the turbine housing (Flaxington and Szczupak, 1982; Hirhikawa et al., 1988; O'Connor and Smith, 1988) (Fig. 2*b*). No waste-gate valve was fitted on this turbocharger.

In order to compare properly the different variable geometry systems, both turbines were quite similar (as regard wheels and related aerodynamic parameters, i.e., trim) to the waste-gated fixed geometry turbine (Garrett TB025) tested in former in-

Nomenclature

f = frequency
K = ratio between average pulsating and steady flow values
M = mass flow rate
n = rotational speed
p = pressure
P = power
t = time
T = temperature, pulse period
Δ = amplitude
ϵ = expansion ratio
η = efficiency
$\eta_t' = \eta_t \cdot \eta_m$
τ = torque

Subscripts

3 = turbine inlet
4 = turbine exit
m = mechanical
M = mass flow rate
NSF = nonsteady flow conditions
SF = steady flow conditions
P = power
t = turbine
T = stagnation conditions
τ = torque

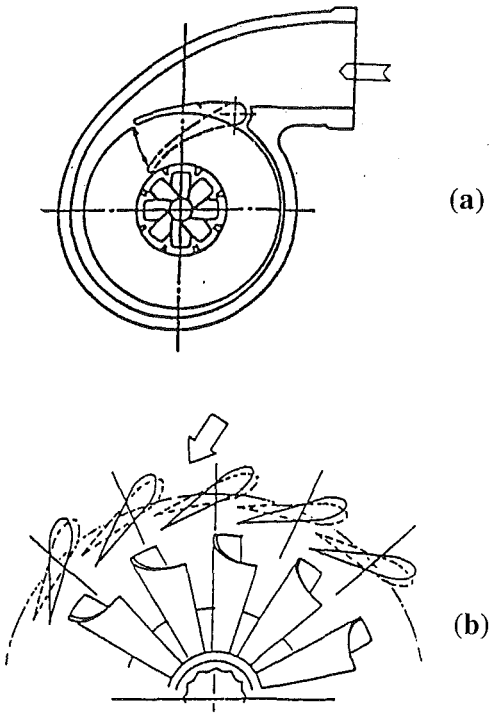

Fig. 2 Schematic of the VAT (*a*) and VNT (*b*) devices

vestigations (Capobianco et al., 1990; Capobianco and Gambarotta, 1990).

The performance of variable geometry turbines was evaluated by measuring several constant speed characteristics at different fixed settings of the regulating systems, expressed through the position of the relevant push rod. To define unequivocally this parameter and take up slack, the original spring-diaphragm actuator was replaced by a simple anchor plate, which allowed the rod to lock in the considered positions. In both cases the setting of the regulating system was related to the linear displacement of the push rod (measured with reference to two gaging surfaces) and was defined as a percentage of the total displacement of the rod, ranging from 0 to 100 percent when varying the flow area from the minimum to the maximum value.

Analysis and Comparison of Experimental Results

Steady Flow Tests. Steady flow performance of both turbines was evaluated with reference to constant speed characteristics (in term of turbine speed factor $n/\sqrt{T_{T3}}$) at different fixed settings of the variable geometry systems. As in previous investigations, four values of the speed factor were considered, ranging from 2500 to 5500 rpm $/\sqrt{K}$.

In order to account for significant positions of the variable geometry devices, "equivalent" settings were defined for both turbochargers by finding out the equality condition of mass flow curves, assuming as a reference the fixed geometry turbine (Garrett TB025) with waste-gate valve fully closed (Capobianco et al., 1990; Capobianco and Gambarotta, 1990). A very good agreement was noticed at positions of 79.2 percent for the VAT and 56.8 percent for the VNT, respectively, as is shown in Fig. 3 for a speed factor of 3500 rpm $/\sqrt{K}$. However this congruence was not found referring to the efficiency η_t' (defined as turbine isentropic efficiency η_t multiplied by turbocharger mechanical efficiency η_m, Fig. 3), which was always lower for the variable geometry turbines. Similar results were obtained for different values of turbine speed factor. This particular behavior will be analyzed later.

In order to extend performance evaluation of the two turbines, steady flow curves were also measured for different settings, equal to 0, 25, 50, 100 percent for the VAT, and to 0, 25, 45, 100 percent for the VNT. Mass flow and efficiency characteristics were defined for each setting. Figures 4 and 5 show constant-speed steady mass flow characteristics for the two variable geometry turbines.

Mass flow rate varies in a wide range for both turbochargers: At a given pressure ratio the corresponding turndown is always higher than 50 percent (while for the fixed geometry waste-gated turbine it was slightly lower).

Superimposition of characteristic curves shows a higher sen-

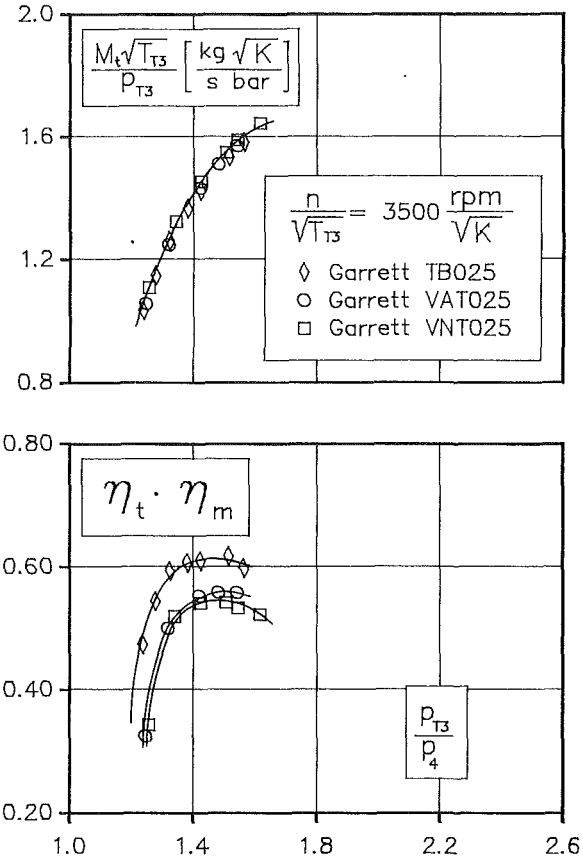

Fig. 3 Equivalence condition of mass flow characteristic curves and corresponding turbine efficiency

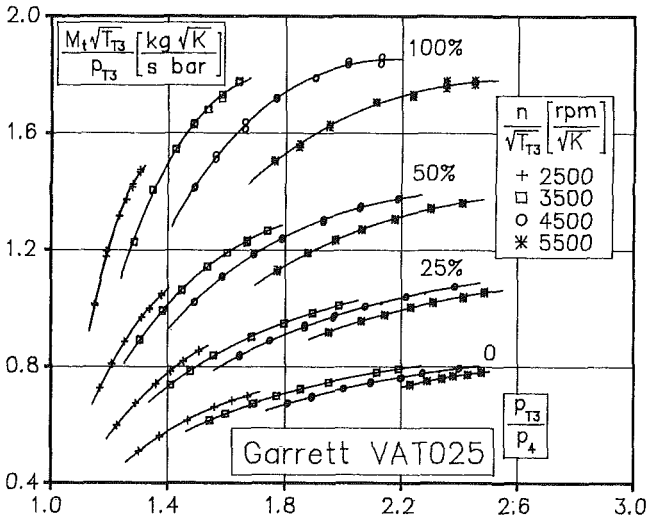

Fig. 4 Steady mass flow characteristics for the Garrett VAT025

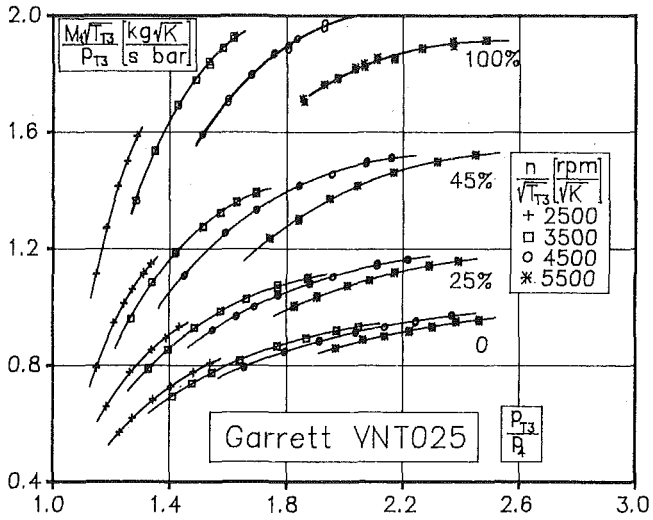

Fig. 5 Steady mass flow characteristics for the Garrett VNT025

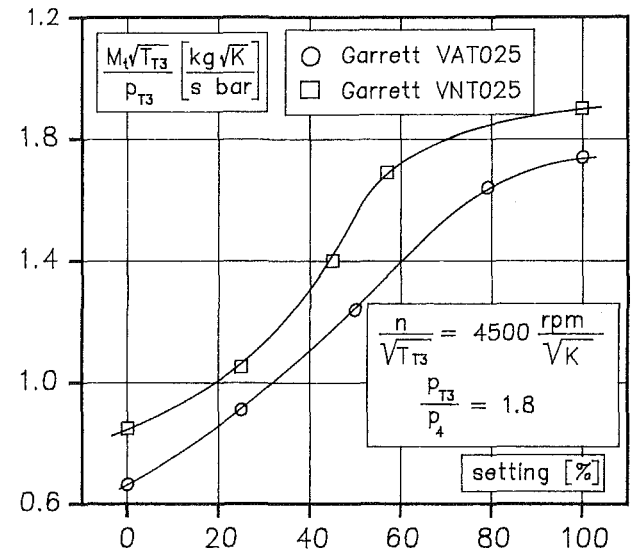

Fig. 6 Mass flow rate versus VG setting for the Garrett VAT025 and VNT025

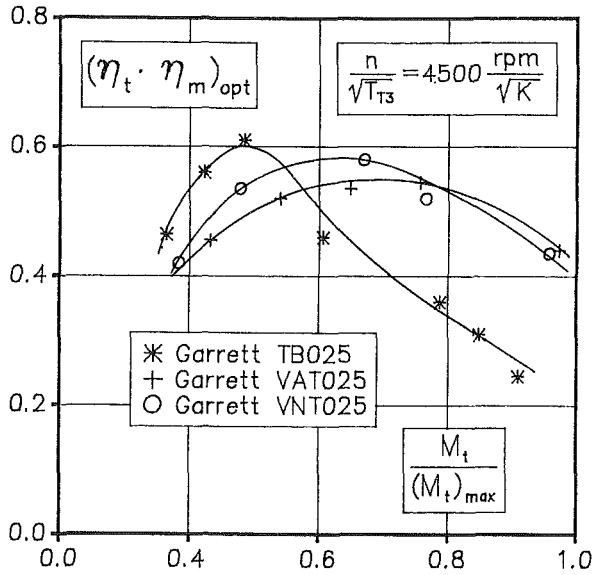

Fig. 7 Optimum efficiency values for the variable and fixed geometry turbines

sitivity (defined as the ratio of change induced in the output, i.e., mass flow rate, to the related input change, i.e., push rod position) of the regulating systems in the field of lower values of turbine flow area, particularly for the variable nozzle turbine (Fig. 5). This effect is apparent in Fig. 6, in which mass flow rate is represented versus system setting for constant values of turbine speed and expansion ratio. This peculiar behavior, not completely unexpected, may be caused by the geometric characteristics of the variable geometry devices, and must be considered in the design of the actuator system and in the definition of proper control schedules in order to take full advantage of the increased flow range (Watson and Banisoleman, 1986, 1988; Wallace et al., 1986a, 1986b; Arcoumanis et al., 1990).

For both variable geometry turbines experimental results showed a decrease of maximum efficiency η_t' compared with the fixed geometry values. This drawback may be explained as a consequence of higher losses induced by variable geometry systems: most likely incidence losses, increased surface friction (due to the additional walls), leakage losses through clearances between vanes and contour walls and, especially in the case of the variable area turbine, wake losses behind guiding vane (Flaxington and Szczupak, 1982; Hirhikawa et al., 1988). However, in the case of the fixed geometry turbine, overall efficiency η_t' drops when the control device (i.e., the waste-gate valve) is operated (Capobianco et al., 1990).

Both for VAT and for VNT the highest efficiency was obtained at an intermediate setting (maximum values of η_t' were about 0.55 and 0.60 for the variable area and variable nozzle turbine, respectively), while it decreased moving toward fully open and fully closed settings. A similar peculiar effect was pointed out by Wallace et al. (1982) and by Watson and Banisoleman (1986). This result may be due to the fact that for both turbines the scroll geometry is optimized for a particular velocity distribution achieved at an intermediate setting of the control device (Hirhikawa et al., 1988), which is the design point of the turbine housing. Besides, referring to the variable nozzle turbine, the flow in the intermediate configuration may be guided more closely by the moving vanes than in the fully open or fully closed setting (Wallace et al., 1982). The existence of a definite design operating condition may be related to the nonlinear reaction forces on the push rod, which were observed during experimental investigation.

In order to extend performance comparison and confirm previous remarks, optimum efficiency values for the different regulating systems considered in the investigation were plotted versus nondimensional mass flow rate (referred to the maximum value of each turbine) at constant turbocharger speed (Fig. 7). Results obtained for the two variable geometry and for the fixed geometry turbine were not unexpected. The highest efficiency is achieved by the fixed geometry turbine in a narrow operating range, while it drops at high mass flow rates when the waste-gate valve has to be opened. The variable nozzle turbine shows better efficiency in a wider range than the variable area one, except for highest mass flow rates. This effect may be related to different losses induced by the two control systems, with particular reference to the scroll design and to its interactions with the flow pattern (which depends on variable geometry settings) (Hirhikawa et al., 1988).

Experimental data obtained in steady flow operation represent an important starting point to define optimized control strategies to take full advantage of variables geometry turbines on their whole operating range. These results will be very useful to define proper schedules (e.g., the optimal setting for any operating condition, the initial opening condition and the rate of change of geometry setting), which will be tested and verified through direct on-engine measurements in future developments of the investigation.

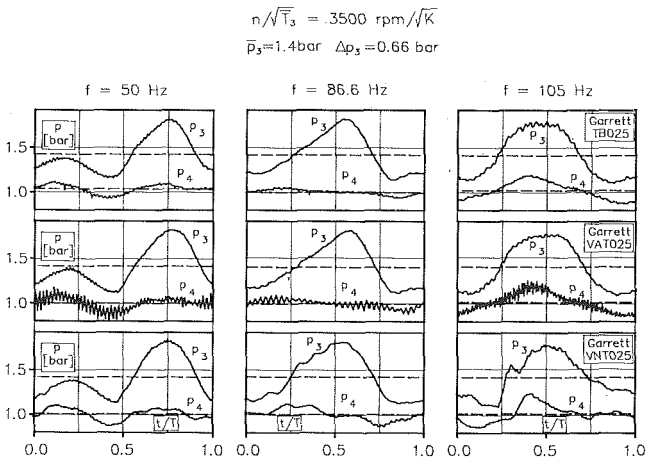

Fig. 8 Turbine experimental inlet and outlet pressure diagrams in pulsating flow conditions

Unsteady Flow Tests: Pressure Diagrams. In order to compare unsteady flow behavior of fixed and variable geometry turbines, measurements were developed with reference to the "equivalent" settings (79.2 percent for the VAT and 56.8 percent for the VNT) at a constant nondimensional speed (3500 rpm/$\sqrt{K}$). Amplitude, frequency, and mean value of pressure pulses at the turbine inlet were controlled through the pulse generator system. As in previous investigations (Capobianco et al., 1990; Capobianco and Gambarotta, 1990), with reference to real on-engine conditions, three different levels of pulse amplitude and frequency (0.30, 0.50, 0.66 bar and 50, 86.6, 105 Hz, respectively) were considered, for a constant mean inlet pressure of 1.4 bar.

Static pressure diagrams at the turbine inlet $p_3(t)$ and outlet $p_4(t)$ were recorded, while measured values of temperature, mass flow, and rotational speed were assumed as average levels over the pulse period (due to the low response characteristics of the relevant metering devices). For both turbines mean torque was evaluated on the basis of measurements on the coupled compressor.

Experimental pressure diagrams were compared with those obtained for the fixed geometry turbine: An example is reported in Fig. 8. As noticed in previous investigations, pulse shape at turbine inlet $p_3(t)$ was mainly influenced by the forcing frequency: In the case of variable nozzle turbine different pressure waveforms were often found, especially at higher pulse frequency.

Pressure signals at turbine exit $p_4(t)$ showed different alterations for each turbocharger (Fig. 8). With reference to the variable area turbine, a high frequency disturbance in exit pressure diagram $p_4(t)$ was found in every operating condition: This result might be related to the wake flow induced by the moving vane (Hirhikawa et al., 1988) and to vibrational motions of impeller blades, which may be increased due to asymmetric entry conditions caused by variable area system (Flaxington and Szczupak, 1982).

In the case of the variable nozzle turbine, pulse shape modifications with frequency are apparent both for $p_3(t)$ and $p_4(t)$: Higher amplitudes of $p_4(t)$ diagrams were found in every tested condition. These effects might be connected to the presence of wakes induced by each of the nozzle vanes, as theorized by O'Connor and Smith (1988), but they can hardly be explained without careful measurements in the inside of the turbine housing.

On this subject it would be interesting to deepen the investigation in order to analyze the influence of variable geometry setting on the propagation of pressure waves through the turbocharger turbine. Unlike the results obtained on the fixed-geometry turbine, in this case pressure diagrams showed clearly that in several operating conditions pulse amplitude at the turbine exit is not negligible. This peculiar behavior should be considered in future investigations, and particularly in the development of turbocharged engine simulation models, which take account of wave propagation phenomena in the exhaust system.

Unsteady Flow Tests: Average Turbine Performance. Starting from unsteady flow measurements, average performance of both VG turbines was evaluated and compared with steady flow results. It is important to point out that the definition of suitable methods of comparison is a very difficult task.This problem is substantial for several devices of the intake and exhaust systems of automotive engines, since they often operate in unsteady flow conditions. On the contrary, performance characteristics determined on the basis of steady flow tests are usually available and empiric correction factors are introduced to take into account flow unsteadiness.

Different procedures for relating steady and average pulsating performance of automotive turbocharger turbines have been presented and discussed in recent years in the open literature (Wallace et al., 1969; Benson, 1974, Kosuge et al., 1976; Zinner, 1978; Shamshi, 1979; Winterbone et al., 1991). If a comparison between the two flow conditions is accepted, performance analysis developed at the same level of turbine mean expansion ratio is an easy and quick procedure, since it requires only limited experimental information (i.e., inlet and outlet pressure diagrams for calculating turbine average expansion ratio) for its application.

This method was applied by the authors in previous papers (Capobianco et al., 1990; Capobianco and Gambarotta, 1990), referring to the ratios K_M and K_τ between mean pulsating mass flow and torque and the corresponding steady flow values at the same average expansion ratio. This procedure was followed in a first step of the present investigation, in order to try to point out the influence of pulse inlet amplitude and frequency on the performance of the Garrett VAT and VNT. This was possible since the experimental facility allowed tests with controlled values of the main parameters of the pulsating flow at the turbine inlet.

In order to avoid errors due to a possible nonuniform pressure distribution or to the different characteristics of measuring systems, the same pressure tappings and transducers were used both in steady and pulsating flow conditions. Transducers were mounted close to the duct wall and an appropriate geometry of tappings was chosen to reduce the passage effects (Winterbone et al., 1991).

It is important to note that the same measuring and processing procedure of pressure data should be used in steady and pulsating flow conditions with this arrangement: In fact, steady flow pressure diagrams, especially at the turbine entry, were affected by high-frequency oscillations (the amplitude of which proved to be not negligible), probably due to the impeller blades. The use of a typical steady flow measuring process, instead of recording and integration of pressure signals, might cause errors in the definition of pressure levels of the reference steady flow characteristics.

Average mass flow (K_M) and torque (K_τ) factors were calculated for the VAT and VNT in the considered operating conditions. Figures 9 and 10 show the effect of pulse amplitude and frequency on the performance of the variable geometry turbines, respectively for mass flow and torque parameters.

The analysis of the results provided by this method of comparison seems quite difficult: However, a general trend to a reduction of mass flow factors when increasing pulse amplitude, at constant frequency and mean inlet level, is apparent for both the VAT and VNT. Similar behavior was observed also in the case of the fixed-geometry turbine in a previous stage of the study and was confirmed by a subsequent experimental investigation, developed on the VAT, extended to a

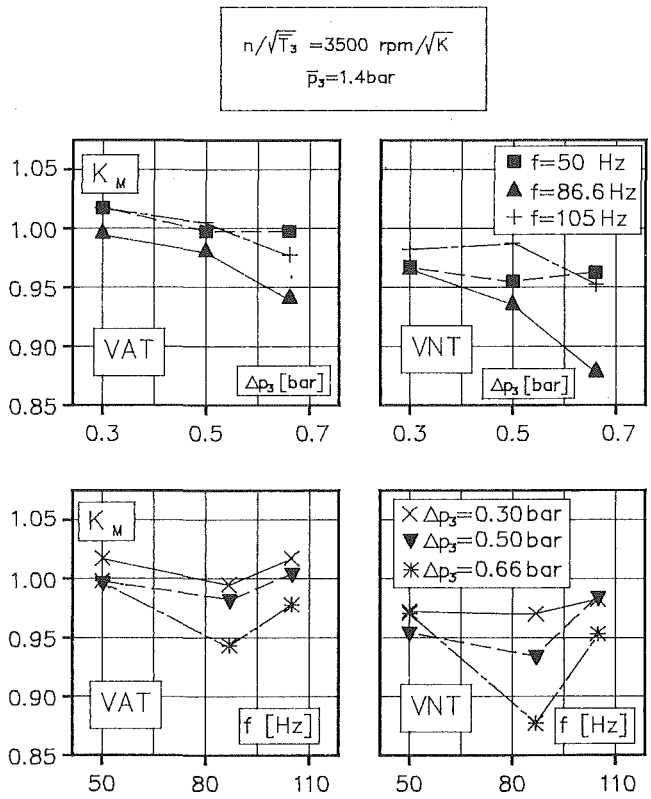

Fig. 9 Comparison between average pulsating and steady turbine mass flow

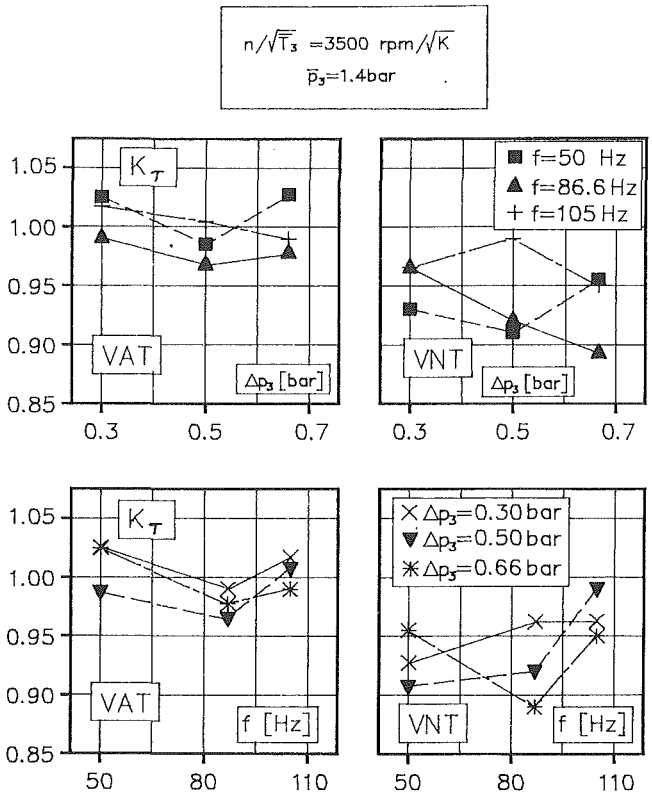

Fig. 10 Comparison between average pulsating and steady flow turbine torque

wider range of pulse amplitude values (Fig. 11). In the authors' opinion the link between mass flow factor and pulse amplitude might be explained as a quasi-steady flow effect related to the variable slope of turbine steady flow curves (Capobianco and Gambarotta, 1990).

As in the case of previous investigations performed on fixed geometry turbines (Capobianco et al., 1989; Capobianco and Gambarotta, 1990), the influence of pulse frequency on turbine unsteady performance wasn't evident. This is probably related to the observed modifications of pressure diagrams with frequency, due to the wave action in the inlet and outlet ducts.

Values of K_M and K_τ factors calculated for the VNT were generally lower than the corresponding ones for the VAT. As a hypothesis, this may be related to the different pressure diagrams measured for the two variable geometry turbines, and particularly to the higher outlet amplitudes found for the VNT.

Torque factor levels (Fig. 10) resulted in the same range of mass flow values, but any correlation with pulse amplitude and frequency is difficult to find. This may be a limitation of the method of comparing turbine performance at the same average expansion ratio.

More suitable procedures to relate steady and average pulsating performance of intake and exhaust devices of automotive engines have to be developed: A dedicated study on this subject, based on the comparison of steady and mean pulsating parameters at the same inlet energy level, is now being developed at DINE, the results of which will be discussed in a future paper.

In a first step of this investigation, turbine power in steady and pulsating flow conditions was compared for the same average nondimensional mass flow levels (related to the mean inlet energy flow rate). In the case of equal average temperature at the turbine inlet, the ratio K'_P between mean pulsating and steady turbine power (expressed in nondimensional form) is

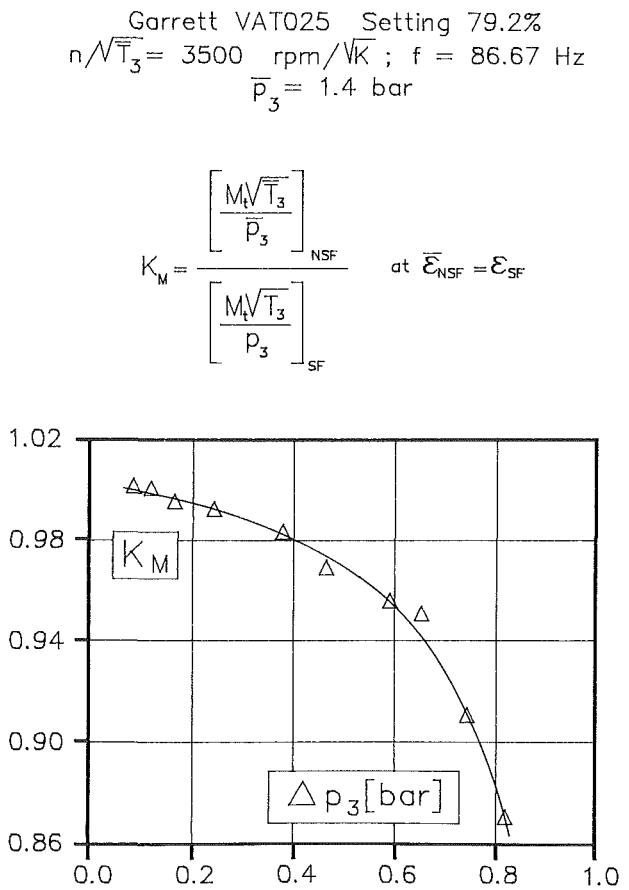

$$K_M = \frac{\left[\frac{M_t\sqrt{\bar{T}_3}}{\bar{p}_3}\right]_{NSF}}{\left[\frac{M_t\sqrt{T_3}}{p_3}\right]_{SF}} \quad \text{at } \bar{\varepsilon}_{NSF} = \varepsilon_{SF}$$

Fig. 11 Influence of pulse amplitude on average mass flow performance of VAT

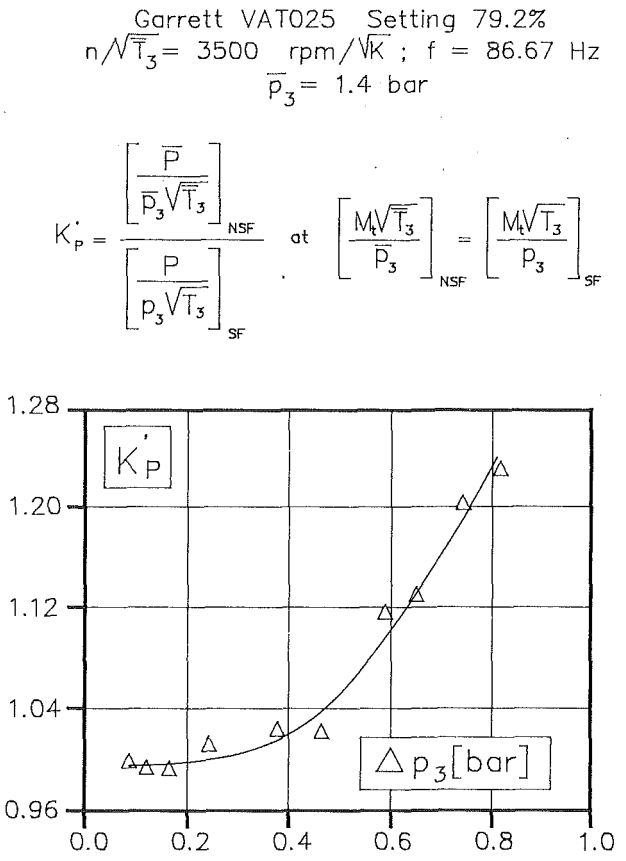

Fig. 12 Comparison of VAT steady and pulsating power at constant average mass flow rate

representative of the ratio of turbine specific work in the two flow conditions. Figure 12 shows the first results of this procedure for the Garrett VAT turbocharger, referring to the relationship between the factor K'_P and pulse amplitude at the turbine inlet, for constant values of other operating parameters. The coefficient K'_P proved to be generally above one, rising with pulse amplitude: This might be explained as an increase of turbine specific work in pulsating flow conditions, related to flow unsteadiness.

These first results are encouraging to further future development of the investigation on methods for comparing steady and average pulsating performance of automotive engine devices.

Quasi-steady-flow (q.s.f.) calculations of average pulsating turbine performance were also developed for both VAT and VNT. The relevant results generally confirmed the ones obtained in a previous stage of the investigation for the fixed geometry Garrett TB025 turbine (Capobianco and Gambarotta, 1990). Calculated performance resulted in good accordance with mean experimental values.

However, it is interesting to note that the differences between average q.s.f. levels and mean experimental pulsating performance resulted, in the case of small automotive turbocharger turbines, in the same amount of the shifting between measured steady and pulsating flow values.

Conclusions and Future Developments

A thorough experimental investigation has been developed in order to define and analyze steady and unsteady flow behavior of two different variable geometry turbocharger turbines (VAT and VNT), compared with a similar fixed geometry turbine.

As regards turbine performance, the benefits of variable geometry systems were apparent. In both cases steady flow results showed a wide mass flow operating range, with limited effects on efficiency (particularly for the VNT). Although peak efficiencies were lower in comparison with the fixed geometry turbine (because of higher losses induced by the control devices), better efficiency values were clearly achieved with reference to the whole operating range.

For both turbines the existence of a definite design point for the housing was apparent (probably due to the influence of the fixed scroll area distribution), since the highest efficiencies were obtained at intermediate settings of the variable geometry systems. This peculiar effect seems to agree with the results given by other authors (Wallace et al., 1982; Watson and Banisoleman, 1986).

In addition, turbine unsteady flow behavior was investigated by controlling frequency, amplitude, and mean value of inlet pressure pulses. For an "equivalent mass flow setting" of the control system, pressure diagrams at the turbine inlet and outlet and average turbine performance were analyzed.

Pulse shape at the turbine inlet was mainly influenced by the frequency, although somewhat affected by the variable geometry system (particularly for the VNT). In both cases, however, the presence of moving vanes seemed to introduce significant oscillations in the pressure diagrams at the turbine outlet. This effect, which may be related to wake flows induced by the vanes, doesn't agree with the common hypothesis of constant pressure downstream of a turbocharger turbine. A deeper investigation on the influence of system setting on the propagation of pressure waves through the turbine would be helpful in the development of theoretical simulation models.

Average pulsating performance of the VAT and VNT was first analyzed and compared with steady flow results at the same mean expansion ratio. The link between turbine performance and pulse characteristics (amplitude and frequency) was not evident, except for the influence of pulse amplitude on mass flow factor K_M (which showed a quasi-steady trend to a reduction of K_M when increasing pulse amplitude).

Calculated coefficients were generally lower for the VNT turbocharger: This is probably connected to the different shape and amplitude of upstream and downstream pressure diagrams measured for the vaned turbine.

In order to overcome the outlined drawbacks, a dedicated study on the methods for comparing steady and pulsating flow performance of intake and exhaust devices of automotive engines has been started and is now in progress at DINE. The results of the first step of this study are encouraging to a deeper future investigation.

The use of proper control strategies to take full advantage of VGT benefits seems to be essential. In this direction engine simulation models and experimental investigations are useful tools for the design of the control systems in order to improve steady and transient engine performance and reduce emissions.

This study represents an essential prerequisite to the progression of deeper investigation on the optimization of VGT-engine matching. On the basis of experimental data presented in the paper, a simulation model of a turbocharged Diesel engine is being developed by the authors: This will allow the analysis with reference to engine performance to be extended and, through dedicated experimental program, to define and verify optimized control systems and strategies.

Acknowledgments

The authors would like to thank Garrett S.A.-France, and particularly Mr. Luciano Bernardini, for the technical support and assistance given during the development of the experimental activity.

The authors also wish to thank the Centro Ricerche Fiat, Orbassano, for their permission to publish this paper.

References

Arcoumanis, C., Chan, S. H., and Bazari, Z., 1990, "Optimisation of the Transient Performance of a Turbocharged Diesel Engine Using Turbocharging and Fuel Injection Controls," Seminar on "Engine Transient Performance," IMechE, London.

Benson, R. S., 1974, "Nonsteady Flow in a Turbocharger Nozzleless Radial Gas Turbine," SAE Technical Paper No. 740739.

Capobianco, M., Gambarotta, A., and Cipolla, G., 1989, "Influence of the Pulsating Flow Operation on the Turbine Characteristics of a Small Internal Combustion Engine Turbocharger," presented at the 2nd International Conference on the Small Internal Combustion Engine, Paper No. C372/019, IMechE, London.

Capobianco, M., and Gambarotta, A., 1990, "Unsteady Flow Performance of Turbocharger Radial Turbines," presented at the 4th International Conference on Turbocharging and Turbochargers, Paper No. C405/017, IMechE, London.

Capobianco, M., Gambarotta, A., and Cipolla, G., 1990, "Effect of Inlet Pulsating Pressure Characteristics on Turbine Performance of an Automotive Wastegated Turbocharger," presented at the SAE International Congress and Exposition, Paper No. 900359, Detroit.

Flaxington, D., and Szczupak, D. T., 1982, "Variable Area Radial Inflow Turbine," presented at the 2nd International Conference on Turbocharging and Turbochargers, Paper No. C36/82, IMechE, London.

Hirhikawa, A., Okazaki, Y., and Busch, P., 1988, "Developments of Variable Area Radial Turbines for Small Turbochargers," presented at the SAE International Congress and Exposition, Paper No. 880120, Detroit.

Kosuge, H., Yamanaka, N., Ariga, I., and Watanabe, I., 1976, "Performance of Radial Flow Turbines Under Pulsating Flow Conditions," ASME JOURNAL OF ENGINEERING FOR POWER, Vol. 98, No. 1, pp. 53–59.

O'Connor, G. F., and Smith, M. M., 1988, "Variable Nozzle Turbochargers for Passenger Car Applications," presented at the SAE International Congress and Exposition, Paper No. 880121, Detroit.

Shamsi, S. S., 1979, "Estimating the Influence of Pulsating Flow Conditions on the Performance of a Turbine," SAE Technical Paper No. 790068.

Wallace, F. J., Adgey, J. M., and Blair, G. P., 1969, "Performance of Inward Radial Flow Turbines Under Non-steady Flow Conditions," *Proc. I. Mech. E.*, Vol. 184, Pt. 1, No. 10.

Wallace, F. J., Baghery, A., and Ziriati, M. R., 1982, "Variable Geometry Turbocharging for Transport Engines," presented at the 2nd International Conference on Turbocharging and Turbochargers, Paper No. C38/82, IMechE, London.

Wallace, F. J., Roberts, E. W., and Howard, D., 1986a, "Variable Geometry Turbocharging—Optimization and Control Under Steady State Conditions," presented at the 3rd International Conference on Turbocharging and Turbochargers, Paper No. C97/86, IMechE, London.

Wallace, F. J., Anderson, K., and Howard, D., 1986b, "Variable Geometry Turbocharging—Control Under Transient Conditions," presented at the 3rd International Conference on Turbocharging and Turbochargers, Paper No. C98/86, IMechE, London.

Watson, N., and Janota, M. S., 1982, *Turbocharging the Internal Combustion Engine*, McMillan Press, London.

Watson, N., and Banisoleman, K., 1986, "Performance of a Highly Rated Vehicle Diesel Engine With a Variable Geometry Turbocharger," presented at the 3rd International Conference on Turbocharging and Turbochargers, Paper No. C103/86, IMechE, London.

Watson, N., and Banisoleman, K., 1988, "A Variable-Geometry Turbocharger Control System for High Output Diesel Engines," presented at the SAE International Congress and Exposition, Paper No. 880118, Detroit.

Winterbone, D. E., Nikpour, B., and Frost, H., 1991, "A Contribution to the Understanding of Turbocharger Turbine Performance in Pulsating Flow," presented at the Conference on Internal Combustion Engine Research, Paper No. C433/011, IMechE, London.

Zinner, K., 1978, *Supercharging of Internal Combustion Engines*, Springer-Verlag, Berlin.

Emissions From Heavy-Duty Trucks Converted to CNG

S. G. Fritz
Department of Emissions Research,
Southwest Research Institute,
San Antonio, TX 78228-0510

R. I. Egbuonu
Energy Management Office,
City of Houston,
Houston, TX 77002

Emissions are reported for four heavy-duty trucks, which were converted to operate on compressed natural gas fuel. Two 1988 model year Ford F700 Series trucks equipped with 7.0 L gasoline engines and two 1986 model year GMC trucks equipped with DDC 8.2 L diesel engines were tested on a heavy-duty chassis dynamometer in a baseline condition and again after conversion to natural gas. The vehicles were tested over the EPA Urban Dynamometer Driving Schedule for Heavy-Duty Vehicles and at no-load curb idle. Regulated emissions of NO_x, CO, HC, and diesel particulate, along with nonmethane hydrocarbons, are reported in grams/mile. Fuel economy is reported in energy-equivalent miles per gallon of gasoline or diesel fuel.

Introduction

In 1989, the Texas Legislature mandated through Senate Bills 740 and 769 that centrally fueled fleets of ten vehicles or more should convert to a clean-burning alternative fuel. In response, the City of Houston, in cooperation with the Urban Consortium Energy Task Force (UCETF) and the Department of Energy, initiated the "Compressed Natural Gas Demonstration Project" to investigate the economic and environmental impact of utilizing CNG in fleet truck applications. In addition to funding by the Department of Energy/UCETF, various public and private partners made cash and in-kind contributions toward the project. These partners included: the Texas Governor's Energy Office, Entex (a gas utility company), Enron (a pipeline and distribution company), EPA, and Crown Services.

Implementation of this study originated under the auspices of the Fleet Management Division of the General Services Department, which is responsible for procurement, replacement, and maintenance of the majority of the City's fleet of 9000 vehicles and items of equipment. During restructuring, the project responsibility was transferred to the Energy Management Office of the Finance and Administration Department. The City's demonstration project includes nine vehicles converted to CNG. The test vehicles range from light-duty gasoline trucks to heavy-duty diesel trucks.

The project sought to measure the economic and environmental aspects of using CNG in four categories of public works vehicles: (1) heavy-duty vehicles operating on dedicated CNG, (2) medium-duty diesel/CNG conversions, (3) medium-duty gasoline/CNG conversions, and (4) light-duty gasoline/CNG conversions. The seven overall research objectives are:

- Identify the operating characteristics of CNG-fueled conversions.
- Determine the environmental effects of CNG conversions.
- Determine the cost effectiveness of using CNG as an alternative fuel in city vehicles.
- Identify maintenance concerns.
- Examine infrastructure support.
- Recommend "go or no go" decisions on conversion by vehicle class type.
- Disseminate project information of documented research.

The environmental aspects of the project involve selecting vehicles suitable for the test, emission testing of the vehicles, selection of conversion equipment, conversion of the test group vehicles, operating the vehicles over the test period, and retesting vehicle emissions. Southwest Research Institute (SwRI), under contract with the City of Houston, performed emissions testing of four trucks before and after conversion to compressed natural gas (CNG) fuel. The emission test results from the heavy-duty vehicles are the subject of this paper.

Background

Heavy-duty vehicles are designed for a variety of purposes, and use a variety of engines, transmissions, and rear-end drive arrangements. Because of these variations, EPA regulates emissions from heavy-duty *engines* rather than regulating emissions from heavy-duty *vehicles*. However, for this program, heavy-duty chassis dynamometer emission measurements are useful to assess part of the environmental impact of converting selected vehicles to run on CNG, since it tests the whole vehicle under simulated road conditions.

For emission regulatory purposes, all of the test trucks are generally referred to as "heavy-duty vehicles," to set them apart from light-duty vehicles such as cars and light-duty trucks. Emissions measured include total hydrocarbons (HC), carbon monoxide (CO), oxides of nitrogen (NO_x), carbon dioxide (CO_2), and methane (CH_4). Total hydrocarbons, as compared to methane, can be considered "reactive hydrocarbons," and

Contributed by the Internal Combustion Engine Division and presented at the Energy-Sources Technology Conference and Exhibition, Houston, Texas, January 26–30, 1992. Manuscript received by the Internal Combustion Engine Division September 27, 1991. Paper No. 92-ICE-10. Associate Technical Editor: J. A. Caton.

Fig. 1 City of Houston Ford F700 7.0 L gasoline truck

Fig. 2 City of Houston GMC 8.2 L diesel truck

are generally referred to as nonmethane hydrocarbons (NMHC). Particulate emissions were measured for those heavy-duty vehicles using diesel fuel or those replacing diesel fuel with CNG. In addition, the soluble fraction of the total particulate was assessed using an extraction process on the particulate sample (collected on a set of 90 mm filters) used to assess the rate of total particulate emissions. It is the soluble fraction of the total particulate that is generally associated with the concern for health effects related to diesel particulate.

Test Methodology

Test Vehicles. Two different types of trucks were tested in this program. Figure 1 shows one of the two Ford F700 trucks tested. The 1988 model year Ford F700 trucks were rated for a gross vehicle weight (GVW) of 24,500 pounds. They were powered with Ford 429 $in.^3$ (7.0 liter) V-8 engines rated at 200 bhp at 3600 rpm on gasoline. Both were equipped with an Allison AT-545 4-speed automatic transmission. Both trucks had approximately 25,000 miles before baseline testing.

Figure 2 shows one of the two diesel engine powered GMC trucks that was converted to dual-fuel operation. The 1986 model year GMC C7D042 trucks were rated for a gross vehicle weight (GVW) of 25,600 pounds. They were powered with DDC 500 $in.^3$ (8.2 liter) V-8 naturally aspirated engines rated at 165 bhp at 2800 rpm on diesel fuel. Both trucks were equipped with an Allison AT-545 four-speed automatic transmission. The GMC trucks each had approximately 42,000 miles before baseline testing.

CNG Engine Conversions. After baseline testing of the four trucks at SwRI in May and June of 1990, the trucks were returned to Houston where the City performed the conversions to CNG. The City then accumulated one year of field experience before the trucks were returned to SwRI for postconversion testing in April and May 1991.

The Ford trucks were equipped with a CNG conversion kit that allowed for engine operation on either gasoline or CNG, with an operator selection switch located on the dashboard. The Ford F700 trucks were equipped with three high-pressure storage tanks located under the dump truck bed. The three storage tanks were cascaded together and had a cumulative storage capacity of approximately 1800 scf when the tanks are filled to 2400 psi at 68°F. This is the energy equivalent of approximately 13 gallons of gasoline.

The GMC trucks were equipped with a dual-fuel (combined use of diesel and CNG) conversion kit. The conversion kit allowed for engine operation on either 100 percent diesel fuel or in a dual-fuel mode. In either case, the engine started and idled on 100 percent diesel. Thus, engine starting and idling characteristics were identical to unmodified trucks. In the dual-fuel mode, natural gas is introduced into the intake system, triggered by engine speed. The GMC trucks were equipped with a single high-pressure CNG storage tank located under the dump truck bed. The storage tank had a capacity of approximately 1150 scf when the tank was filled to 2400 psi at 68°F. This is the energy equivalent of approximately 8.2 gallons of diesel fuel.

Test Fuels. Tests on both F700 trucks were performed using a gasoline meeting EPA fuel specifications for emissions certification of heavy-duty gasoline engines [1]. Baseline tests on the two GMC trucks were performed using a diesel fuel meeting EPA fuel specifications for emissions certification of heavy-duty diesel engines [1].

Natural gas samples were drawn from each truck after emission testing was complete and analyzed using a gas chromatograph. Table 1 gives the properties of a typical natural gas composition and properties of the natural gas used during emission testing.

The proportion of diesel fuel to CNG used during dual-fuel operation of the GMC trucks was not determined in this test program. For emissions and fuel economy computations, it was assumed that the fuel consumed over the HDCC was 80 percent CNG and 20 percent diesel fuel.

Nomenclature

Btu = British Thermal Units
CH_4 = methane
CNG = compressed natural gas
CO = carbon monoxide
CO_2 = carbon dioxide
CVS = constant volume sampling
EPA = Environmental Protection Agency
°F = degrees Fahrenheit
GMC = General Motors Corporation
GVWR = gross vehicle weight rating
HC = hydrocarbons
HDCC = heavy-duty chassis cycle
hp = horsepower
h = hour
in^3 = cubic inches
L = liter
NMHC = nonmethane hydrocarbons
NO_x = oxides of nitrogen
psi = pounds per square inch
ROG = reactive organic gases
scf = standard cubic feet
SOF = soluble organic fraction
SwRI = Southwest Research Institute
THC = total hydrocarbons

Table 1 Natural gas composition and properties

Gas Composition	Mole or Volume %	Mass %
Methane (CH_4)	92.1	84.9
Ethane (C_2H_6)	2.5	4.3
Propane (C_3H_8)	0.4	1.0
Butane (C_4H_{10})	0.1	0.5
Nitrogen (N_2)	3.2	5.1
Carbon Dioxide (CO_2)	1.6	4.2
Other	<0.1	<0.1
Total	100	100
Property		
Gas Molecular Weight	17.38	
Gas Ideal Gas Constant - R ($ft\text{-}lb_m / lb_f \text{-}°R$)	88.87	
Fuel H/C Ratio	3.86	
Fuel Mass Fraction Carbon	0.755	
Fuel Mass Fraction Hydrogen	0.245	
Fuel Higher Heating Value (BTU/lb_m)	21,400	
Fuel Lower Heating Value (BTU/lb_m)	19,200	
Fuel Higher Heating Value (BTU/scf)	963	
Fuel Lower Heating Value (BTU/scf)	868	

Heavy-Duty Chassis Dynamometer. The heavy-duty chassis dynamometer transient emission vehicle tests were performed in accordance with procedures outlined in an EPA report titled, "Recommended Practice for Determining Exhaust Emissions From Heavy-Duty Vehicles Under Transient Conditions" [2]. Each of the trucks tested used a simulated inertia based on approximately 70 percent of the gross vehicle weight rating (GVWR). Each truck type used a common road load computed from the frontal area of the vehicle. The total dynamometer simulated inertia (test weight) for all of the trucks was 17,500 pounds. The total theoretical road load at 50 mph was 61 horsepower (hp). This theoretical road load was calculated by considering rolling resistance of 21 hp and aerodynamic influences of 40 hp as outlined in the EPA procedure, and using procedures from previous road-load simulations at SwRI [3].

Each heavy-duty vehicle group required its own sampling system configuration, chassis dynamometer tie down adjustment, and setup. Figures 3 and 4 show one of the two GMC trucks setup on the heavy-duty chassis dynamometer, with the associated truck tie-downs, exhaust system ducting, and overhead CVS dilution tunnel.

For this test program, emissions were measured for each heavy-duty vehicle over a single cold-start run and two hot-start runs over the EPA urban dynamometer driving schedule for heavy-duty vehicles illustrated in Fig. 5 [4]. This driving cycle is also known as the heavy-duty chassis cycle (HDCC). Only hot-start emission tests were run in replicate because they are generally considered more important in determining weighted composite emissions, reflecting the fact that most engines are typically cold-started only once per day. In addition, emission measurements during curb-idle operation were conducted because many trucks operating in an urban environment spend a large amount of time at this condition. The order of testing was cold-start, hot-start, curb idle, then repeat hot-start.

"Idle" emissions were quantified during a 15-min test with the transmission in "drive" and the brakes set. This test was performed after a 20-min hot soak following the first hot-start HDCC test. Note that the facility radiator blower located in front of the truck (see Fig. 4) was shut off during these idle tests. After another 20-min soak, the second hot-start HDCC test was performed.

Fig. 3 Heavy-duty chassis dynamometer test setup with GMC 8.2 L truck showing CVS dilution tunnel, analyzers, and control panel

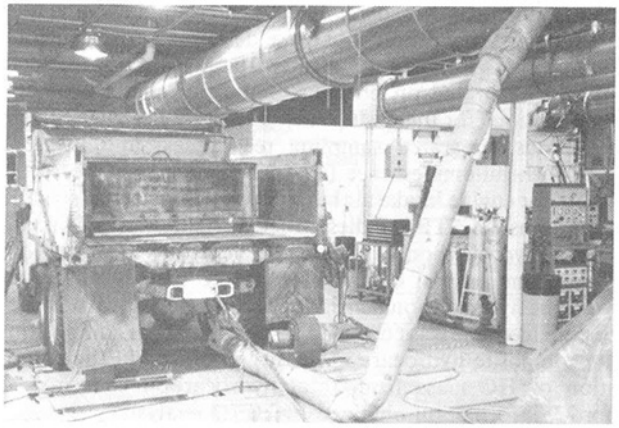

Fig. 4 Rear view of GMC 8.2 L diesel truck on chassis dynamometer showing truck tie down and exhaust ducting to overhead CVS tunnel

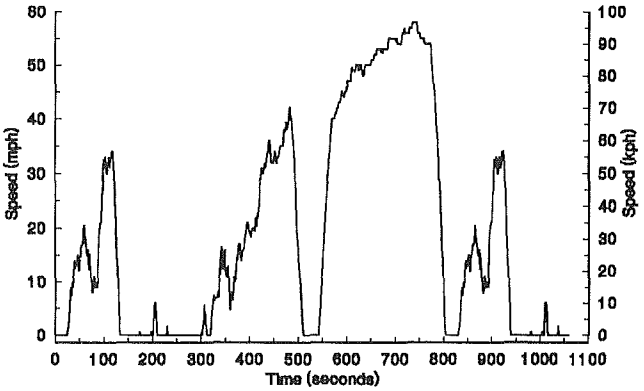

Fig. 5 EPA urban dynamometer driving schedule for heavy-duty vehicles

Analytical Procedures. The analytical procedures used throughout the tests are those outlined in the EPA report for heavy-duty chassis testing [2], and those given in the Federal Register for heavy-duty gasoline and diesel engine testing [1], and incorporated procedures adopted by the California Air Resources Board (CARB) for testing CNG-fueled heavy-duty engines [5, 6].

In general, the CARB procedures call for testing spark-ignited gasoline fueled engines that have been converted to operation on CNG as if they were still gasoline engines. Consequently, for the Ford F700 gasoline engine tests and the CNG Ford F700 tests, total hydrocarbons and NO_x were determined over each test cycle using dilute exhaust sampling techniques to accumulate a proportional sample in a bag. The total hydrocarbon concentration in the bag was measured using a Beckman 400 heated flame ionization detector (HFID), calibrated on propane. The NO_x concentrations in the bags were measured using a chemiluminescence (CL) instrument. NO_x correction factors for engine intake air humidity were applied as specified in the transient FTP for gasoline-fueled engines [1, 5].

The CARB procedures also call for testing diesel-fueled engines that have been converted to CNG as if they remained diesel engines. For this program, this meant that total hydrocarbons and NO_x concentrations in the dilute exhaust were continuously monitored over each test, and the integrated total was used to determine an average test concentration. Consequently, for the GMC diesel engine truck tests and the dual-fuel tests, total hydrocarbons were determined over each test cycle using a Beckman 402 heated flame ionization detector (HFID), calibrated on propane. Following diesel protocols, NO_x emissions for the GMC truck tests were determined using continuous integrated sampling techniques, and measured using a chemiluminescence (CL) instrument. NO_x correction factors for engine intake air humidity were applied as specified in the transient FTP for diesel-fueled engines [1, 6].

Total hydrocarbon emissions are generally assumed to be of the same general composition as the fuel used. For this work, the hydrocarbon density of 18.64 g/ft^3 per carbon atom for pure methane was corrected for the actual gas composition. The composite hydrocarbon density was used in the computation of HC mass from total hydrocarbon concentration (ppmC) information obtained by HFID analysis.

Note that the Beckman 400 and 402 instrument response factors are known to be influenced by hydrocarbon mixtures that are high in methane content. The CNG data presented for this program have not been adjusted to reflect any change in response factor. SwRI and EPA are in the process of quantifying HFID response factors for HFID instruments used to measure total hydrocarbons as specified in the various test procedures. In general, the current techniques tend to overstate methane levels about 15 percent.

In addition to total hydrocarbons, the level of reactive organic gases (ROG) was determined from proportional dilute exhaust samples for the cold and hot HDCC tests, as well as at idle. ROG are generally considered nonmethane hydrocarbons (NMHC), because methane is considered nonreactive in ozone formation. A gas chromatograph was used in determining the methane content of proportional dilute exhaust samples using SAE Method J1151 [7]. ROG or NMHC are then "total hydrocarbons" (THC) minus "methane." These calculations take into account procedures recommended by CARB for computing NMHC [8].

Concentrations of CO and CO_2 in the proportional dilute exhaust samples were determined by nondispersive infrared (NDIR) instruments [1].

Emission levels for THC, CO, CO_2, and NO_x were processed along with CVS flow parameters and truck operating parameters to compute mass emissions on the basis of distance (g/mi) and fuel usage (g/lb fuel). These computations were based on the equations specified in the Federal Register [1] for exhaust emissions from gasoline engine exhaust, ans they take into account modifications necessary for using CNG fuel as outlined in the California Code of Regulations governing certification standards of new heavy-duty vehicles fueled with natural gas [5]. These modifications include specifying a default hydrogen-to-carbon ratio of 3.802 for natural gas when detailed composition of the gas is unknown. When the actual composition of the gas is known, such as was the case in this test program, the actual hydrogen-to-carbon ratios (ranging from 3.760 to 3.909) were used in computing the emissions.

Table 2 Comparison of pre- and post-CNG conversion composite HDCC regulated emissions from two Ford F700 trucks

	Average Composite HDCC Emissions[a]					
	g/mi		g/lb fuel[b]		g/hp-hr	
	Gasoline	CNG	Gasoline	CNG	Gasoline[c]	CNG[d]
No. 16047 - CNG05						
Total Hydrocarbons	8.7	15.9	7.0	15.9	4.9	10.7
Non-Methane Hydrocarbons	8.5	3.9	6.8	3.9	4.7	2.6
Carbon Monoxide	42.1	8.1	33.8	7.7	23.7	5.2
Oxides of Nitrogen	11.0	18.2	9.0	18.2	6.3	12.2
No. 16050 - CNG06						
Total Hydrocarbons	5.4[e]	7.0	4.6[e]	6.5	3.2[e]	4.3
Non-Methane Hydrocarbons	5.2[e]	2.7	4.4[e]	1.9	2.9[e]	1.3
Carbon Monoxide	50.4[e]	24.1	44.3[e]	22.1	31.0[e]	15.3
Oxides of Nitrogen	17.5[e]	18.0	15.7[e]	16.9	11.0[e]	11.4

[a] Composite computed using 1/7(Cold HDCC) + 6/7([Hot HDCC 1 + Hot HDCC 2]/2).
[b] Fuel consumption computed from carbon balance.
[c] Estimated using an assumed bsfc of 0.70 lb/hp-hr.
[d] Estimated using an assumed bsfc of 0.67 lb/hp-hr.
[e] EGR valve malfunctioning.

Table 3 Comparison of pre- and post-CNG conversion regulated emissions at idle (in gear) from two Ford F700 trucks

	Idle (In Gear) Emissions			
	g/hr		g/lb fuel[a]	
	Gasoline	CNG	Gasoline	CNG
No. 16047 - CNG05				
Total Hydrocarbons	90.7	224	23.6	47.0
Non-Methane Hydrocarbons	90.3	52.5	23.5	11.0
Carbon Monoxide	59.1	18.3	15.4	3.8
Oxides of Nitrogen	2.3	4.2	0.6	0.9
No. 16050 - CNG06				
Total Hydrocarbons	24.3	17.4	4.8	3.0
Non-Methane Hydrocarbons	23.3	6.4	4.6	1.1
Carbon Monoxide	213	287	41.9	49.5
Oxides of Nitrogen	7.1	6.3	1.7	1.1

[a] Fuel consumption computed from carbon balance.

Test Results

Gasoline to CNG. Comparative chassis emission results from testing the two Ford F700 trucks using gasoline and CNG are given in Tables 2–4. A comparison of the average composite HDCC total hydrocarbons, nonmethane hydrocarbons, carbon monoxide, and oxides of nitrogen is given in Table 2. Inspection of these results indicates that although the total hydrocarbons were higher with the CNG trucks, both the nonmethane hydrocarbon (or ROG) and the carbon monoxide exhaust emissions were notably reduced with conversion to CNG. Emissions of NO_x increased, however.

When comparing baseline gasoline NO_x emission results to those obtained after conversion to CNG, note that the EGR valve on Truck 16050 was determined to be nonoperational after the baseline emissions were already established. Therefore, the reported NO_x level of 17.5 g/mi for Truck 16050 is higher than expected, while the 11.0 g/mi NO_x result obtained with Truck 15047 during baseline testing is likely representative of the typical NO_x level on gasoline. On CNG, NO_x emission levels of 18.2 g/mi and 18.0 g/mi were observed for the two trucks. The CNG conversion caused significantly higher com-

Table 4 Comparison of pre- and post-CNG conversion fuel economy and fuel consumption from two Ford F700 trucks

	Fuel Economy (ml/gal - equiv)[a]		Fuel Consumption (BTU/mi)		Fuel Consumption (lb/hr)[b]		Fuel Consumption (BTU/hr)	
	Gasoline[c]	CNG[d]	Gasoline[c]	CNG[d]	Gasoline	CNG	Gasoline[c]	CNG[d]
No. 16047 - CNG05								
Composite HDCC[e]	5.1	6.0	22,500	19,200	21.2	17.6	389,000	338,000
Idle (In Gear)	NA	NA	NA	NA	3.5	4.4	64,700	84,000
No. 16050 - CNG06								
Composite HDCC[e]	5.5[f]	5.3	20,600[f]	21,600	19.3[f]	18.8	354,000[f]	381,000
Idle (In Gear)	NA	NA	NA	NA	4.6	5.3	85,400	107,500

[a] CNG MPG computed assuming CNG energy equivalent to 1 gallon of baseline emissions certification gasoline (122,000 BTU/gal).
[b] Fuel consumption computed from carbon balance.
[c] LHV baseline test emissions certification gasoline = 18,400 BTU/lb (122,000 BTU/gallon).
[d] LHV of CNG used in tests is given in Table 1.
[e] Composite computed using 1/7(Cold HDCC) + 6/7([Hot HDCC 1 + Hot HDCC 2]/2).
[f] EGR valve malfunctioning.

Table 5 Comparison of pre- and post-CNG conversion composite HDCC regulated emissions from two GMC trucks

	Average Composite HDCC Emissions[a]					
	g/mi		g/lb fuel[b]		g/hp-hr	
	Diesel	Dual-Fuel	Diesel	Dual-Fuel	Diesel[c]	Dual-Fuel[d]
No. 15127 - CNG07						
Total Hydrocarbons	1.1	51	1.3	55	0.6	39
Non-Methane Hydrocarbons	1.1	7.5	1.3	8.0	0.6	5.7
Carbon Monoxide	5.4	24	6.4	25	2.8	18
Oxides of Nitrogen	13	11	16	11	7.0	8.0
Particulate	1.3	0.68	1.5	0.70	0.70	0.52
No. 15131 - CNG08						
Total Hydrocarbons	1.2	34	1.3	34	0.6	24
Non-Methane Hydrocarbons	1.2	10	1.3	10	0.6	7.2
Carbon Monoxide	6.1	17	6.6	17	3.0	12
Oxides of Nitrogen	15	11	17	11	7.5	7.7
Particulate	1.6	0.92	1.7	0.91	0.76	0.64

[a] Composite computed using 1/7(Cold HDCC) + 6/7([Hot HDCC 1 + Hot HDCC 2]/2).
[b] Fuel consumption computed from carbon balance.
[c] Estimated using an assumed bsfc of 0.45 lb/hp-hr.
[d] Estimated using an assumed bsfc of 0.71 lb/hp-hr.

Table 6 Comparison of pre- and post-CNG conversion regulated emissions at idle (in gear) from two GMC trucks

	Idle (In Gear) Emissions			
	g/hr		g/lb fuel[a]	
	Diesel	Dual-Fuel	Diesel	Dual-Fuel
No. 15127 - CNG07				
Total Hydrocarbons	10.5	10.3	2.7	2.8
Non-Methane Hydrocarbons	10.3	7.0	2.6	1.9
Carbon Monoxide	22.8	25.0	5.9	6.8
Oxides of Nitrogen	114	93.0	29.5	25.3
Particulate	2.4	2.5	0.61	0.69
No. 15030 - CNG08				
Total Hydrocarbons	13.9	23.9	3.6	6.0
Non-Methane Hydrocarbons	13.7	23.5	3.5	5.9
Carbon Monoxide	27.7	27.9	7.2	7.0
Oxides of Nitrogen	116	76.2	30.1	19.2
Particulate	2.4	2.8	0.63	0.71

[a] Fuel consumption computed from carbon balance.
[b] Dual-Fuel Conversion operates on 100% diesel fuel at idle.

posite HDCC NO_x emissions for these test vehicles, increasing NO_x approximately 60 percent over gasoline levels.

The curb idle emission results for both gasoline and CNG tests of the Ford 700 trucks are given in Table 3. Inspection of these data indicates that baseline gasoline tests with Truck 16047 resulted in normal emissions of hydrocarbons and carbon monoxide. However, the relatively high CO emissions of Truck 16050 on gasoline indicate an overly rich mixture. Similarly, relatively high CO emissions on CNG06 indicate a rich CNG-air mixture at idle. However, CNG05 appears to be much leaner at idle, with the characteristic high hydrocarbons accompanied by low CO emissions.

Idle NO_x emissions are given in Table 3 for both the baseline gasoline and CNG tests. Idle NO_x levels on a g/lb of fuel basis were approximately 1/15 to 1/20 those of composite HDCC emission levels. Therefore, caution should be exercised in judging whether or not increases or decreases in idle NO_x emissions are significant or meaningful.

Average fuel economy and fuel consumption rates are given in Table 4. Fuel economy (mpg gasoline equivalent) for the CNG configuration improved by about 18 percent for Truck 16047-CNG05 over the average composite HDCC when operating on natural gas. However, fuel economy for Truck 16050-CNG06 appears worse when operating on CNG (5.29 mpg) as compared to the baseline gasoline results (5.53 mpg). Recall that the EGR valve on Truck 16050 was inoperative during the baseline gasoline tests, and this is thought to be partly responsible for the better fuel economy demonstrated by Truck 16050 (5.53 mpg) compared to Truck 16047 (5.05 mpg) during baseline tests on gasoline. Therefore, fuel economy results from Truck 16047 are thought to be more representative results. In assessing the fuel economy implications of the CNG conversions, it may be more appropriate to compare the HDCC fuel economy results of Truck CNG06 to the baseline tests of Truck 16047, in which case the fuel economy of the CNG truck was 5 percent better. Finally, at idle, Table 4 indictes that the CNG converted trucks had 15-25 percent higher idle fuel consumption on a fuel mass basis, or a 25-30 percent higher idle energy consumption rate, than the baseline gasoline configuration.

Diesel to Dual-Fuel. Comparative chassis emission results from testing of the two GMC trucks on diesel fuel and after dual-fuel conversion (using diesel and CNG) are given in Tables 5-7. Average composite HDCC total hydrocarbons, nonmethane hydrocarbons (NMHC), carbon monoxide, and oxides of nitrogen for both configurations are given in Table 5. Inspection of these results indicate that the total hydrocarbon levels were substantially higher than baseline levels with dual-fuel trucks. Dual-fuel total hydrocarbon emissions were 30 to 50 *times* higher than the diesel baseline levels. The total hydrocarbon data indicate that 7 to 12 percent of the fuel that was supplied to the engine passed through the engine unburned. The majority of these unburned hydrocarbons were methane, generally considered nonreactive in ozone formation. The nonmethane hydrocarbons (or ROG) for the dual-fuel conversion were 7 to 10 times higher than the diesel baseline levels. Dual-fuel carbon monoxide emissions were approximately 3 to 4

Table 7 Comparison of pre- and post-dual-fuel conversion fuel economy and fuel consumption from two GMC 8.2 L trucks

	Fuel Economy (mi/gal - equiv)[a]		Fuel Consumption (BTU/mi)		Fuel Consumption (lb/hr)[b]		Fuel Consumption (BTU/hr)	
	Diesel[c]	Dual-Fuel	Diesel[c]	Dual-Fuel	Diesel	Dual-Fuel	Diesel[c]	Dual-Fuel
No. 15127 - CNG07								
Composite HDCC[d]	8.3	6.2	15,700	18,500	14.7	16.2	270,000	319,000
Idle (In Gear)	NA	NA	NA	NA	3.5	3.4	64,800	61,700
No. 15130 - CNG08								
Composite HDCC[d]	7.6	5.7	16,900	20,200	15.8	17.8	289,000	351,000
Idle (In Gear)	NA	NA	NA	NA	3.5	3.6	64,500	66,600

[a] Dual-Fuel MPG computed assuming CNG energy equivalent to 1 gallon of baseline emissions certification diesel fuel (129,000 BTU/gal).
[b] Fuel consumption computed from carbon balance.
[c] LHV baseline test emissions certification diesel = 18,300 BTU/lb (129,000 BTU/gallon).
[d] Composite computed using 1/7(Cold HDCC) + 6/7([Hot HDCC 1 + Hot HDCC 2]/2).

times diesel baseline levels. Emissions of NO_x were 15 to 25 percent lower with dual-fuel compared to baseline diesel levels. Particulate emissions were 42 to 48 percent lower with dual-fuel. However, these lower particulate levels are still well above the levels expected from current production diesel engines (0.25 g/hp-h).

Curb-idle emission results for both the diesel baseline and the dual-fuel tests of the GMC trucks are given in Table 6. As expected, the idle exhaust emissions of the dual-fuel truck were very similar to those observed during baseline testing of the trucks. Recall that the dual-fuel trucks idled on 100 percent diesel fuel. Therefore, one would not expect any change in idle emissions with the dual-fuel conversion.

Average fuel economy and fuel consumption rates are given in Table 7. Average composite HDCC fuel economy (mpg equivalent) for the dual-fuel configuration was 25 percent worse than the baseline diesel levels. The data in Table 7 indicate that the dual-fuel conversion did not affect idle fuel consumption.

Summary and Conclusions

The Department of Emissions Research of Southwest Research Institute, under contract with the City of Houston, performed heavy-duty chassis dynamometer emissions testing of four heavy-duty 9-yard dump trucks before and after conversion to compressed natural gas (CNG) fuel. Baseline testing of two Ford F700 7.4 L gasoline-powered trucks and two GMC 8.2 L diesel-powered trucks was performed in May–June 1990. After baseline emissions testing, these four vehicles were converted to CNG by the City, and one year of field trials was performed by the City. In March and April 1991, emissions testing of these CNG trucks was performed at SwRI. The principal findings of these tests were:

Ford F700 Gasoline Converted to CNG:
- Oxides of nitrogen (NO_x) emission levels were approximately 50 percent higher on CNG fuel.
- Non-methane hydrocarbon (NMHC) and carbon monoxide (CO) emission levels were 20–30 percent lower on CNG compared to gasoline.
- HDCC fuel economy was 5 percent better with CNG compared to gasoline; while idle fuel consumption was approximately 25 percent worse on CNG.

GMC Diesel Converted to Dual-Fuel (Diesel With CNG Fumigation):
- Total hydrocarbon emission levels were 30 to 50 *times* higher with dual-fuel compared to baseline diesel. Nonmethane hydrocarbon emission levels were 5–7 times higher with dual-fuel.
- Carbon monoxide emission levels were 3 to 5 times higher with dual-fuel.
- Oxides of nitrogen emission levels were reduced by approximately 50 percent with dual-fuel.
- Particulate emission levels were reduced by 50 percent with dual-fuel.
- Fuel economy was 25 percent worse with dual-fuel.

Based on these findings, the following *conclusions* can be drawn:

- The CNG conversion "kits" that were tested generally worsened exhaust emissions. Although certain pollutants were reduced with the CNG conversions for each type of truck (NMHC and CO for the gasoline conversions, and NO_x and particulate for diesel conversions), the increase in other pollutants may outweigh those reductions.
- The fuel economy penalty observed with the conversion of the diesel engine to dual-fuel operation is relatively high.

Recommendation

When considering conversion of vehicles to a fuel other than that for which the vehicle was designed, part of the purchase requirement of the conversion kit must address exhaust emission levels. Both California and Colorado have procedures for certifying that such conversion kits meet applicable emission standards.

Current Program Status—Future Work

At present, a total of nine trucks have been retrofitted or converted and are operating on CNG. Of these, two are 1983 model year GMC Brigadier heavy-duty trucks powered with new DDC 6V-92 TA engines using timed-port natural gas injection developed by Stewart and Stevenson in conjunction with Ortech International. Based on the exhaust emission test results reported herein for the two medium-duty Ford F700 gasoline trucks converted with Landi-Renzo kits, the F700s have been equipped with Impco conversion kits. In addition, based on emission results reported herein, CNG operation of the two medium-duty GMC 8.2 L diesel trucks using Landi-Renzo dual-fuel conversion kits has been suspended while an emission certified kit adaptive to the 8.2 L diesel engine is being sought. Three light-duty Chevrolet pick-up trucks (two with 5.7 L throttle-body gasoline engines, and one 5.0 L throttle-body gasoline engine) retrofitted with Landi-Renzo kits had discouraging emission test results. These vehicles have also been re-retrofitted with Impco conversion kits. The study has also been expanded to include a 1991 Dodge pickup truck retrofitted with an Impco kit, and a 1990 Dodge pickup is being retrofitted with a Stewart and Stevenson Gaseous Fuel Injection (GFI) kit for continued investigation of using CNG. Emission tests for these kits have not yet been completed.

Acknowledgments

Funding for this project was supplied from a number of sources, specifically DOE/UCETF, EPA, and the City of

Houston. The authors would like to recognize the contributions made by D. G. Robinson of the City's Fleet Management Division, and Mr. D. Huckabay of the City's Energy Management Office, as well as the following SwRI staff: Messrs. T. L. Ullman, J. G. Chessher, G. A. Harper, and W. C. Olson.

References

1 Code of Federal Regulations, Title 40, Part 86, Subpart N—Emission Regulations for New Otto-Cycle and Diesel Heavy-Duty Engines; Gaseous and Particulate Exhaust Test Procedure, July 1, 1990.

2 France, C. J., Clemmens, W., and Wysor, T., "Recommended Practice for Determining Exhaust Emissions From Heavy-Duty Vehicles Under Transient Conditions," Technical Report SDSB 79-08, Environmental Protection Agency, Feb. 1979.

3 Urban, C. M., "Dynamometer Simulation of Truck and Bus Road Horsepower for Transient Emissions Evaluations," SAE Paper No. 840349, 1984.

4 Code of Federal Regulations, Title 40, Part 86, Subpart M—Evaporative Emission Test Procedures for New Gasoline-Fueled and Methanol-Fueled Heavy-Duty Vehicles, July 1, 1990.

5 California Code of Regulations, Title 13, "California Exhaust Emission Standards and Test Procedures for 1987 and Subsequent Model Heavy-Duty Otto-Cycle Engines and Vehicles," as amended May 15, 1990.

6 California Code of Regulations, Title 13, "California Exhaust Emission Standards and Test Procedures for 1987 and Subsequent Model Heavy-Duty Diesel Engines and Vehicles," as amended May 15, 1990.

7 "Methane Measurement Using Gas Chromatography," SAE Recommended Practice, Method J1151, Oct. 1988.

8 "California Non-methane Hydrocarbon Test Procedures," CARB, as amended May 15, 1990.

9 "Standard Test Method for Heat of Combustion of Liquid Hydrocarbon Fuels by Bomb Calorimeter," ASTM Method D240-87, *ASTM Book of Standards*, Vol. 5.01.

10 Fritz, S. G., "Emissions From Heavy-Duty Trucks Converted to Compressed Natural Gas—Phase I Final Report," SwRI Report 08-3518, July 1991.

Progress in Diesel Engine Emissions Control

M. K. Khair
Southwest Research Institute,
San Antonio, TX 78228

A considerable amount of work was carried out in the mid-1980s to develop heavy-duty diesel engines that could meet limits on particulate emissions. These limits, although high by today's standards, were considered very restrictive. Some manufacturers struggled to achieve the 0.6 g/bhp-h particulate matter limit with enough margin for production variabilities and to account for the deterioration factor. Significant progress was achieved in diesel emissions control through engine and fuel system design changes. This eventually made it possible to meet a particulate level of 0.25 g/bhp-h for 1991. The next target level for particulate emissions is 0.1 g/bhp-h for the 1994 heavy-duty engine. To meet the challenge, engine developers are not only considering engine and injection system design changes but also fuel improvements and exhaust aftertreatment. This paper includes a review of past and current strategies used to control emissions in the modern diesel engine.

Introduction

In recent years, the emissions regulations and market acceptability have become strong motivators for controlling pollutants from the diesel engine. Advances in engine technology have made it possible for the diesel engine to meet very stringent emissions levels. Future standards have generated interest in other technologies such as exhaust aftertreatment, fuel composition and quality, as well as additional engine improvements. Faced with the NO_x-particulate trade-off challenge, engine manufacturers made several design choices while being concerned with the increased production cost and competition. These design choices involved many of the engine components. Some of these components having more impact on the final outcome than others. In general, the most impressive gains were achieved through changes in the combustion chamber design [1], improved fuel system characteristics [2], implementation of low-temperature charge air cooling [3], and special attention to lube oil consumption [4]. Several companies felt that electronic engine controls would be needed to meet the 1991 emissions standards for heavy-duty diesel engines. As time progressed, this notion was abandoned as several engine manufacturers managed to meet those regulations without the use of electronics. A few major diesel engine manufacturers used electronics for optimizing performance while maintaining good fuel economy [5].

Exhaust aftertreatment techniques limiting particulate emissions from diesel engines remain a topic of intense interest and development activity. Two approaches are being addressed for the upcoming 1994 heavy-duty emissions regulations. One approach is that of periodically incinerating the diesel particulate trapped in a wall-flow ceramic trap. Another approach involves the continuous catalytic oxidization of particulate matter through the use of precious metals supported on carefully selected washcoated substrates. The latter approach is similar to that of the catalytic converter that has been successfully controlling gasoline engine emissions since the mid-1970s.

Many predictions of worsening diesel fuel quality were made in the late 1970s and early 1980s [6]. In the mid- to late-1980s, considerable research work showed direct relationships between fuel composition and resultant exhaust emissions [6–8]. This determination has been recognized as being significant, prompting new legislation to control the fuel composition in an effort to reduce emissions.

This paper discusses several design changes and engine technologies adopted for the heavy-duty 1991 model year. It also reviews the two exhaust aftertreatment methods mentioned above and the impact of sulfur, cetane number, and aromatic content on engine emissions.

The Challenge of the 1991 and 1994 Heavy-Duty Diesel Standards

A common way to illustrate the 1991 and 1994 heavy-duty diesel standards is shown in Fig. 1. This stresses the trade-off between NO_x and Particulate Matter (PM). Even though HC, CO, and visible smoke are regulated, their importance to the emission control engineer is minimized. The reason is that engines meeting the PM standard should have HC, CO, and smoke emissions well within the mandated limits.

Traditionally, NO_x has been controlled by retarding injection timing. In general, this action has a negative impact on fuel economy [3]. An example of fuel economy degradation in relation to NO_x reduction is given in Fig. 2 for a midrange direct-injected diesel engine [3]. A well-developed diesel engine for the 1990s must not only meet the emissions requirements, but also must maintain competitive or superior fuel economy performance. The task of maintaining good fuel economy is especially difficult with the need to control NO_x and particulate matter.

Contributed by the Internal Combustion Engine Division and presented at the Energy-Sources Technology Conference and Exhibition, Houston, Texas, January 26–30, 1992. Manuscript received by the Internal Combustion Engine Division October 2, 1991. Paper No. 92-ICE-14. Associate Technical Editor: J. A. Caton.

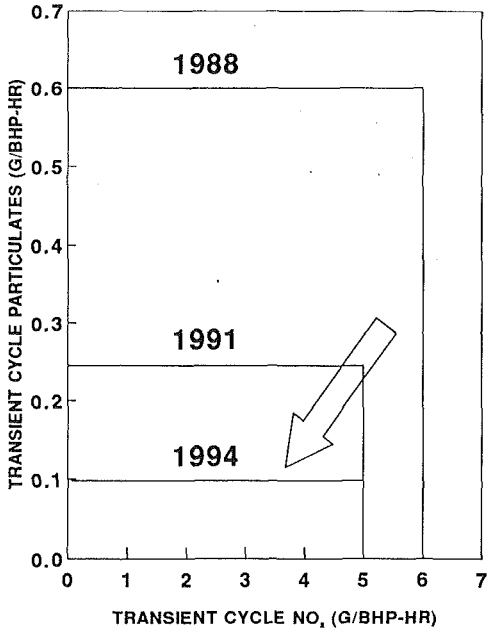

Fig. 1 Regulatory constraints for heavy-duty diesel engines

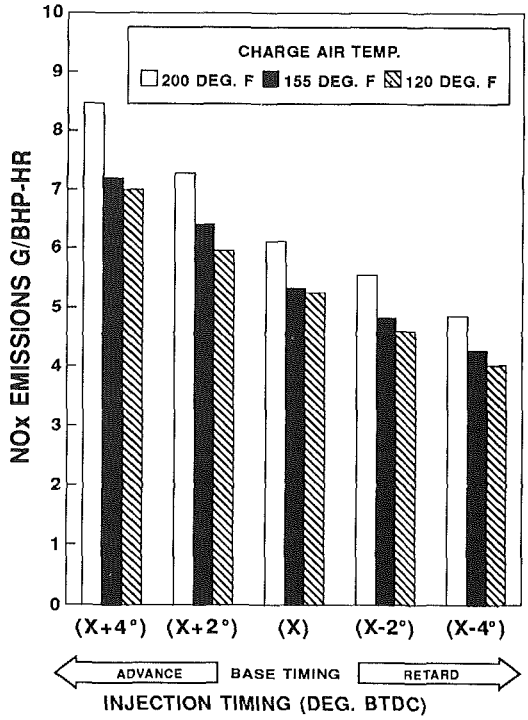

Fig. 3 Effect of injection timing and charge air temperature on NO_x emissions

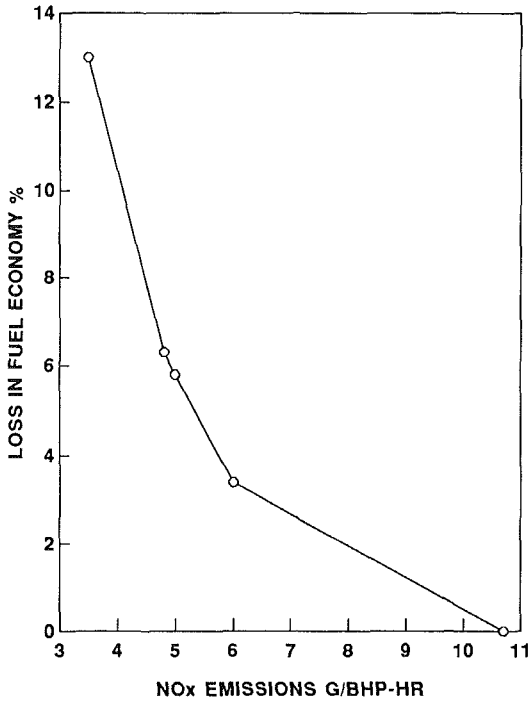

LOSS IN FE % = [(FE AT NEW LEVEL - FE AT 10.7 G/BHP-HR)/FE AT 10.7 G/BHP-HR]X100

Fig. 2 Percent fuel economy loss versus NO_x reduction

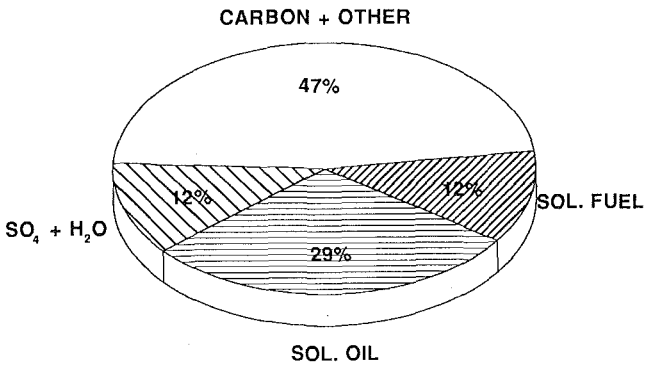

Fig. 4 Particulate composition for a heavy-duty diesel engine with low sulfur fuel without aftertreatment

Nitric oxides are a product of combustion temperature [1] and the residence time (i.e., the amount of time in the combustion cycle spent at high temperature). Two of the most significant factors affecting NO_x emissions are injection timing and charge air temperature. Figure 3 is a graphic representation of the effect of these two factors on NO_x emissions when step changes in both injection timing and intake manifold temperatures are made.

To control particulates, it was useful to study engine regimes having excessive particulate emissions. In general, the analyses of particulate samples revealed the presence of carbonaceous (soot) matter and organic compounds originating from lube oil and fuel. In addition, sulfate compounds along with bound water were found. A small portion of particulate was oil ash, other lube oil additives, and trace amounts of wear metals [9]. Figure 4 illustrates the approximate contribution of the above constituents to the total particulate from a typical pre-1991 heavy-duty direct injected diesel engine [2].

In general, particulate matter is controlled by taking measures to reduce soot (which is mostly associated with smoke) and minimize the organic contribution by reducing oil consumption while maintaining engine durability. Attention to the intake port design and its influence on swirl and flow characteristics combined with high injection pressures can yield significant gains in reducing black smoke. Working on the details of the piston ring design and the quality of the bore honing can reduce the oil contribution to particulate matter.

Meeting the 1991 Heavy-Duty Emissions Regulations

For most engine manufacturers, compliance with the 1991

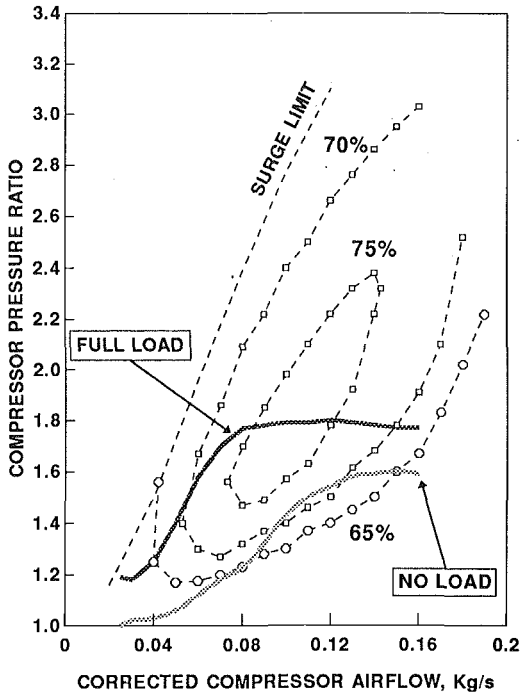

Fig. 5 Performance characteristics

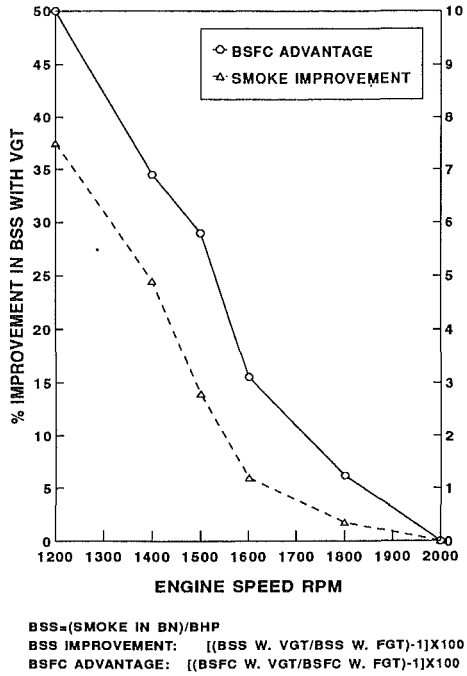

Fig. 7 Improvement in smoke and BSFC with variable geometry turbocharging of a heavy-duty DI diesel engine

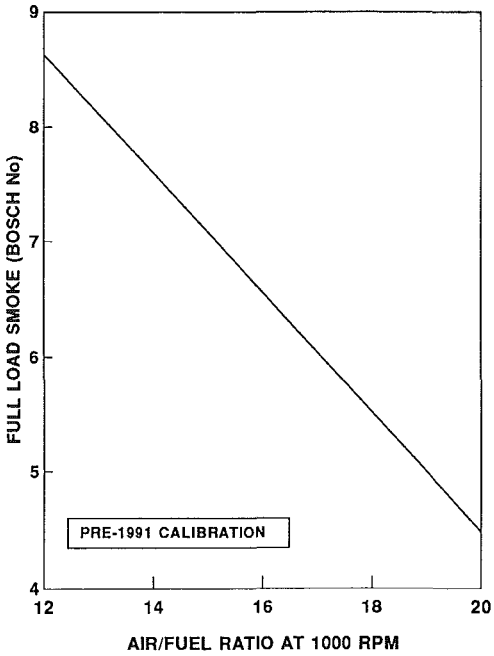

Fig. 6 Effect of A/F on full load smoke at 1000 rpm

emissions standards was attained through several design changes. This section contains a general review of these changes.

Air Induction Systems

Turbocharging. Thermodynamically, turbochargers are attractive because they recover energy that would have otherwise been exhausted into the atmosphere. In turbomachinery, low-pressure ratios, low air flows, and low mechanical efficiencies are associated with low engine speeds [10] shown in Fig. 5. Engine air supply is critical at low speeds if smoke and soot are to be controlled. Using a nonoptimized turbocharger at low engine speeds, may not provide adequate air-to-fuel ratios to control smoke. At high engine speeds, the use of a nonoptimized turbocharger may cause excessive swirling in the combustion chamber. This distorts the injection plumes and hurts fuel economy. For 1991, it was extremely important to maximize the air-to-fuel ratios at low engine speeds to control black smoke with increasing loads. Higher turbocharger speeds had to be limited to avoid the negative effect of overswirling on the mixing process and to extend the turbocharger life.

To optimize the match of turbochargers to engine needs, some manufacturers used variable geometry turbochargers in their development efforts. This "flexible" device can provide a range of pressure ratios for a given engine speed. Variable geometry turbochargers can, therefore, significantly reduce smoke especially at low speed conditions. They can also improve engine output at low speeds within a specified smoke limit. Figure 6 shows the impact of increasing air-to-fuel ratio on full-load smoke of an engine at a fixed speed of 1000 rpm. Figure 7 shows the fuel economy and smoke improvements at speeds below 2000 rpm. These improvements were recorded at higher torque outputs made possible by the characteristics of the variable geometry turbocharger. Figure 8 gives an expanded view of the smoke characteristics between the fixed (conventional) geometry turbocharger and its variable geometry counterpart. Meaningful smoke reductions were a good incentive for carefully matching the conventional turbocharger to the specific needs of the engine. Figure 9 illustrates an example of what was achieved through the optimization of the turbine housing. Using a turbine housing with a smaller aspect ratio ($\times 2$) as opposed to a baseline aspect ratio ($\times 1$), reduced smoke, especially at lower engine speeds. Similar improvements were achieved by careful optimization of the compressor aspect ratio.

Charge Air Cooling. Charge air cooling improves the specific power output of an engine by increasing the charge air density. Naturally derived benefits from this improved specific power output are better fuel economy and reduced exhaust emissions. In the past, most aftercooled engines utilized jacketwater cooling for this purpose. However, for the 1991 engines the use of air-to-air aftercooling became quite popular for medium-duty and heavy-duty diesel engines. Table 1 contains

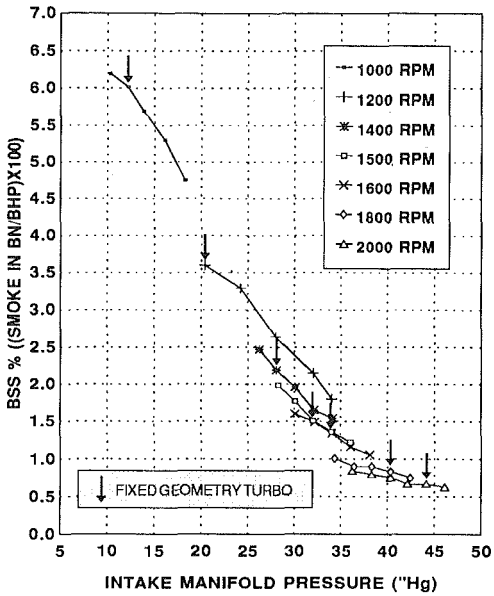

Fig. 8 Full-load smoke optimization with a variable geometry turbocharger

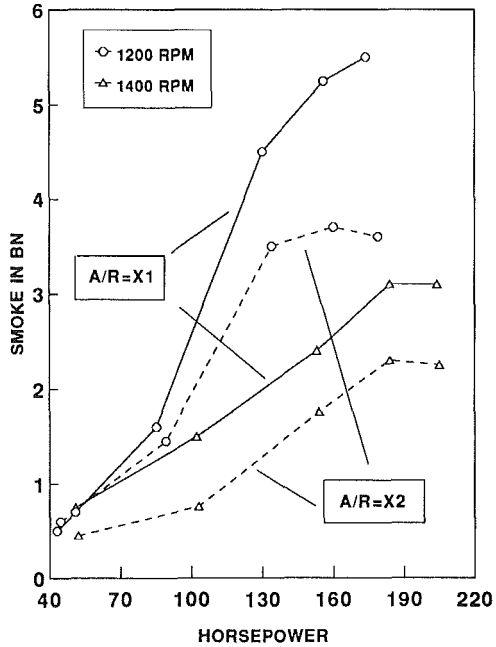

Fig. 9 Turbocharger optimization (turbine housing aspect ratio, *A/R*)

13-mode NO_x emission levels with variations to injection timing and charge air temperatures. Figure 10 shows the corresponding improvement in fuel economy associated with three charge air temperatures (120, 155, and 200°F). These temperatures were selected to represent a water jacket aftercooled engine, an air-to-air aftercooled engine, and an engine with intermediate charge air temperature. Air-to-air aftercooling also reduces the thermal loading of the engine by limiting combustion temperature extremes. This leads to extended engine life and improved reliability.

The design of the aftercooler includes proper sizing to optimize cooling and minimize the pressure drop from the turbocharger compressor to the intake manifold. All ducting from the turbocharger to the aftercooler and from the aftercooler to the intake manifold must be carefully sized and routed to avoid excessive bends and joints. The entire system must be reviewed to minimize its potential leakage under a variety of extreme engine conditions.

Table 1 Injection timing and intake manifold temperature effect on NO_x emissions

		13-MODE WEIGHTED BSNOx GM/HP-HR				
NOMINAL INT. TEMP. F / SPILL TIMING BTDC		200	REDUCTION FROM 200-155	155	REDUCTION FROM 155-120	120
ADVANCE ↑	S1	8.46	15.14%	7.18	2.5%	7.00
	S2	7.28	12.06%	6.40	7%	5.95
	(S)	6.11	12.89%	5.32	1.5%	5.24
	S3	5.54	12.99%	4.82	4.6%	4.59
↓ RETARD	S4	4.85	12.18%	4.26	5.61%	4.02
AVERAGE NOx REDUCTION		--	13.05%	--	4.24%	--

S = Standard Injection Timing

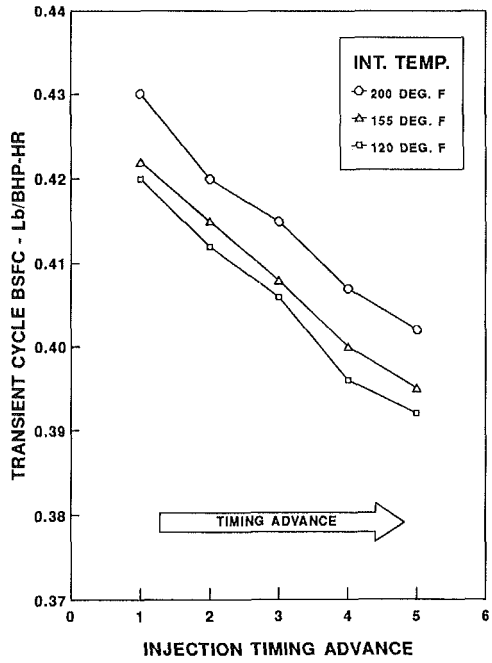

Fig. 10 Effect charge air temperature and injection timing on transient cycle economy

Intake Manifold. A considerable amount of bench test development can lead to intake manifold designs having even flow distribution to all cylinders with minimum pressure losses. The intake port shape and manifold design are often tested as a total system rather than two separate components.

In some cases, effort was expended in reducing the impact of consecutive intake valve openings on the pressure waves in the intake manifold. Segmenting the intake manifold, then grouping certain ports to the proper manifold segment can prevent the interference of unsteady air flow into the combustion chamber.

Intake Port. The mixing of fuel and air in a diesel engine has a very strong influence on its performance and emission characteristics. Diesel emission control engineers struggle with the fuel and air management to achieve optimum performance. Flow bench fixtures were used to select intake port designs that imparted good swirl or air rotation while maintaining good breathing quality. Two types of intake port designs are common. The first is known as the "tangential port" and the second as the "helical port." The former gives good breathing qualities but very little circumferential air motion to help in the mixing process. The helical port provides more air motion

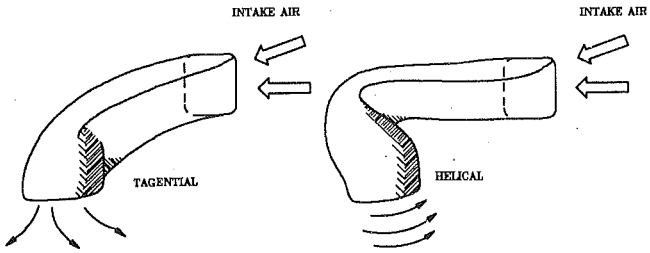

Fig. 11 Intake ports

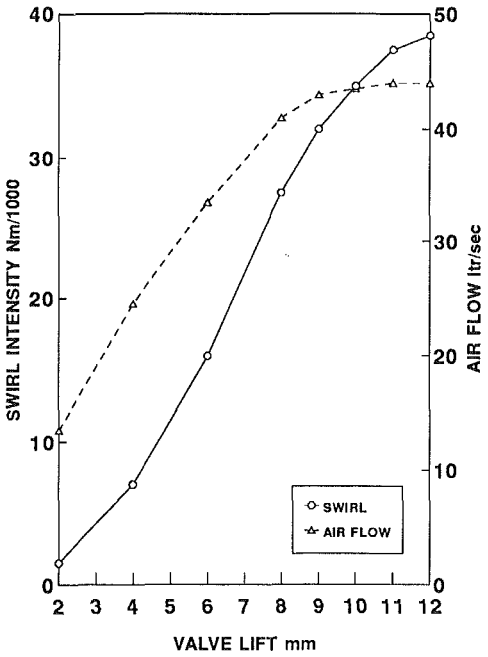

Fig. 12 Helical intake port characteristics

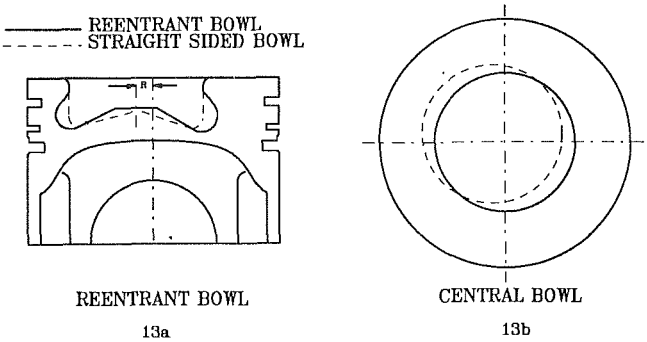

Fig. 13 Improved combustion system designs

thus assisting in the air and fuel mixing. This comes at the cost of more pressure loss than that experienced with tangential ports. An illustration of the two types of ports is shown in Fig. 11. Some engine manufacturers adopted a "quiescent combustion" system using a tangential port as opposed to the helical design associated with swirl ports. The quiescent combustion system is mostly matched with higher fuel injection pressures to optimize combustion efficiency.

Other manufacturers, especially in Japan, chose variable swirl designs. These designs allow the use of high swirl (characteristic of the helical port) at low engine speeds where it is needed. At high speeds, a variety of methods are used to reduce the swirl (to resemble the tangential port characteristics) to avoid overswirling, which can lead to the formation of soot and the loss of fuel economy [10]. Figure 12 shows the swirl and flow characteristic for a typical 1991 heavy-duty swirl port.

The Combustion System. Normally it is common to include the intake port as well as elements of the fuel injection system into the combustion system. However, for the purpose of this paper, the combustion system is defined as the zone in the cylinder where the fuel and air mix and combustion takes place. Three areas of concern for emission reductions are the shape of the combustion bowl, the location of the combustion bowl, and the compression ratio.

The Shape of the Combustion Bowl. A key point in designing the combustion bowl is that good mixing of fuel and air is achieved before the start of combustion. Turbulence in the air motion within the combustion bowl is found to be beneficial to the mixing process [11, 12]. Swirl induced by the intake port can be enhanced to create more turbulence during the compression stroke through proper design of the crater, or bowl, in the piston crown. Designs for the 1991 direct injection engines are generally described as having "re-entrant" bowl designs. Figure 13(*a*) is a representative design of a re-entrant bowl (solid line) with the traditional "straight-sided" combustion bowl design shown in the dashed line. Elements for the optimization of this design include consideration of different ratios of radii of the combustion bowl to the cylinder bore, different chamfer angles of the re-entrant lip, and different aspect (bowl diameter/bowl depth) ratios.

Location of the Combustion Bowl. Figure 13(*a*) shows an offset (*R*) between the center of the combustion bowl and that of the cylinder bore. This is typical of the pre-1991 designs. The injector tip is usually concentric with the combustion bowl. Locating the bowl in the center of the cylinder, as shown in Fig. 13(*b*), can give optimum fuel economy and sustained stable combustion at retarded injection timings through better air utilization [11].

Compression Ratio. Higher compression ratios reduce ignition delay, which reduces the fraction of the fuel burned in the premixed region and allows more injection timing retardation to control NO_x, while maintaining good NO_x-BSFC trade-off. White smoke problems are often aggravated by a combination of retarded injection timing and colder charge air. Raising the compression ratio from the 16.5:1 to 18.5:1 gave large reductions in white smoke especially under cold start and warm up operation [3].

Oil Control System. Measures to control oil consumption include bore honing and ring pack design.

Bore Honing. Figure 14 shows the particulate emissions for two identical pre-1991 engines. Engine A met the 0.6 g/bhp-h particulate standard with a reserve margin of over 30 percent. Engine B exceeded the particulate matter limit. Analysis of the particulate emissions revealed that both engines had similar insoluble particulate emissions. However, the soluble fraction of engine B was considerably larger than that of engine A. Note that the fuel-based particulate of the soluble fraction for both engines were practically the same. The oil-based particulate of engine B was twice as high as that of engine A. Investigation of the cause for the high oil particulate disclosed that the bore honing process was out of control, which led to excessive oil consumption. Therefore, special manufacturing control measures were introduced to ensure strict compliance with the bore honing specifications in terms of pattern angularity, depth, and consistency.

Ring Pack. An experiment was conducted to determine the influence of the ring pack design on particulate emissions. A key criterion in the design of the ring is its compliance. Two types of rings were used in a controlled test using the same midrange DI diesel engine. The results are shown graphically

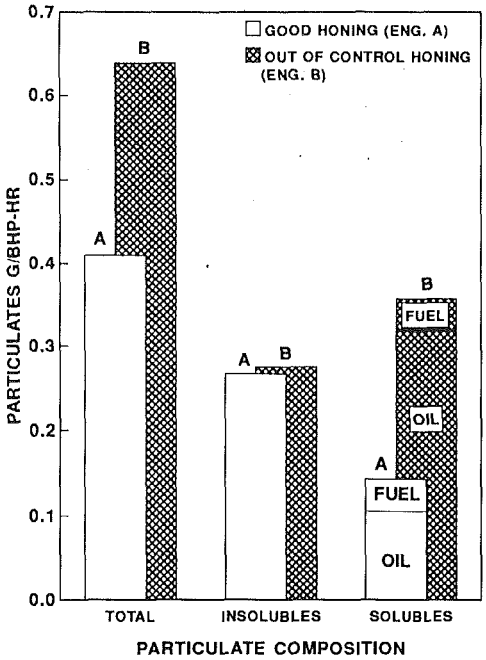

Fig. 14 Effect of bore honing on particulate composition

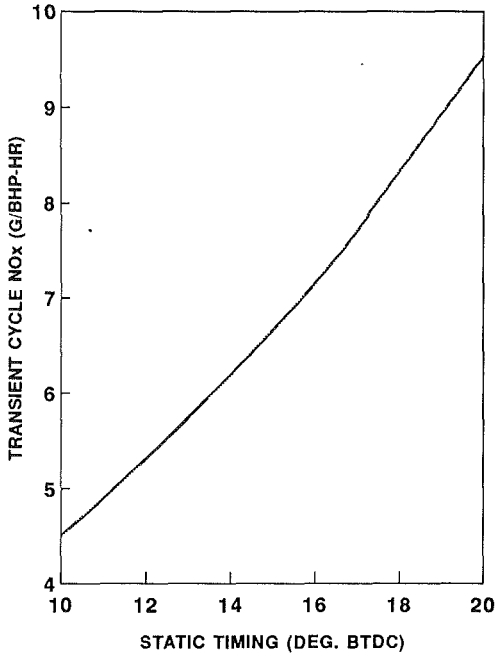

Fig. 16 Effect of injection timing on NO_x emissions (heavy-duty DI diesel engine)

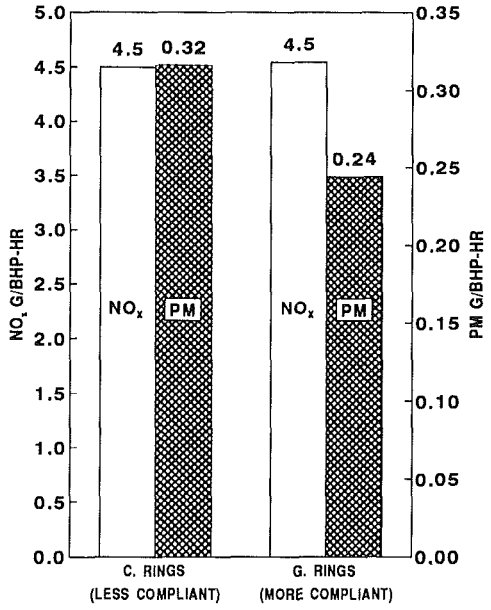

Fig. 15 Effect of ring pack

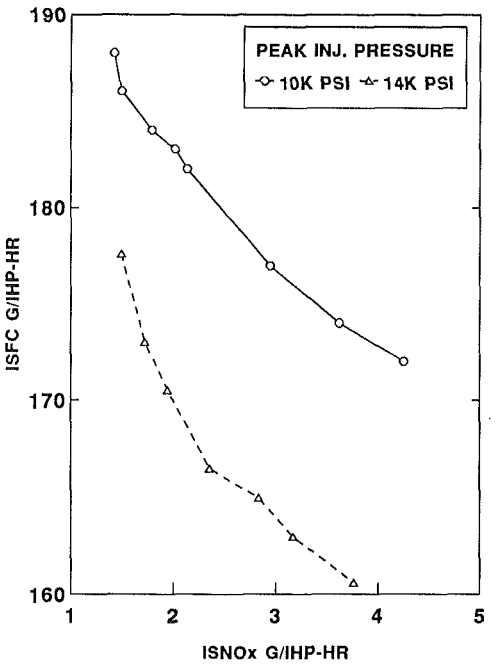

Fig. 17 Effect of injection pressure on NO_x and fuel consumption

in Fig. 15 where the type C ring was less compliant than the type G. The latter showed an average of 0.04 to 0.07 g/bhp-h advantage in composite particulate matter over type C.

The Fuel Injection System. Considerable effort went into the development of the fuel system. Components have to be selected and carefully matched to the combustion system. In this section, the following fuel system variables are reviewed:

- Injection timing
- Injection pressure
- Injection duration
- Nozzle hole configuration
- Nozzle opening pressure

Injection Timing. Injection timing is the most effective tool by which NO_x emissions are controlled [3]. Figure 16 shows the effect of injection timing on NO_x emissions for an engine having an ignition delay of about 10 crank angle degrees. Unfortunately, injection timing retardation is in conflict with good fuel economy and low particulate emissions. To reduce the fuel economy penalty associated with retarding injection timing, engineers have adopted measures to reduce the ignition delay such as using higher compression ratio and higher injection pressures [10].

Injection Pressure. The effect of injection pressure on engine performance and emission has been recognized since the early 1970s. However, some manufacturers felt that injection rate shaping was more important than injection pressure. A

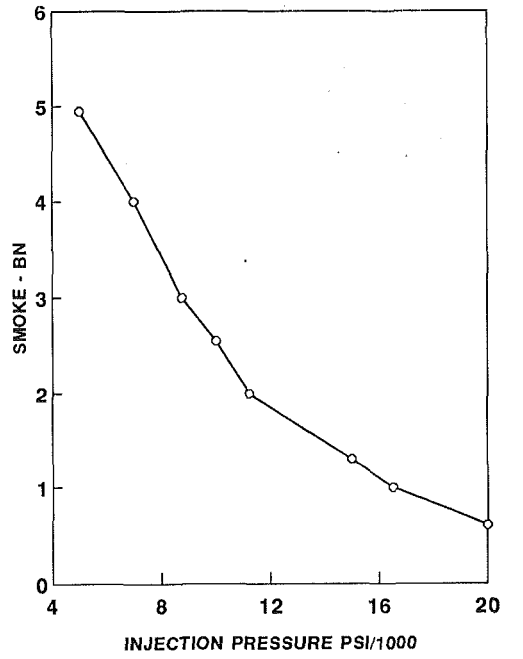

Fig. 18 Effect of injection pressure on smoke emissions

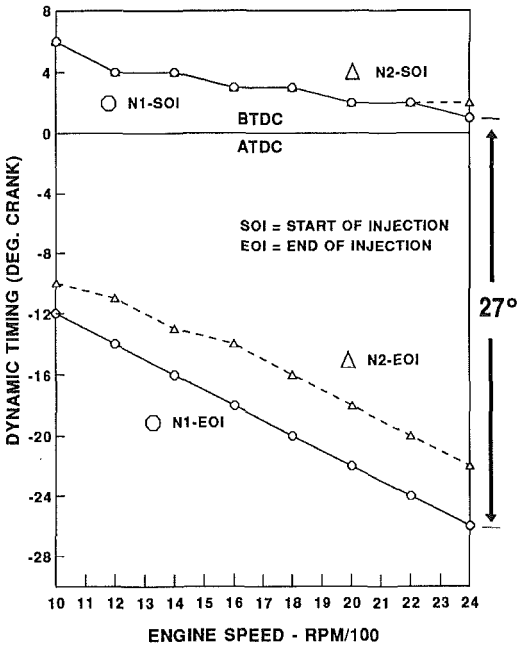

Fig. 19 Injection duration optimization as a function of nozzle hole diameter (DI swirl-type engine)

large body of work in this area has been published [1]. Changes in injection pressure lead to changes in the fuel injection rate, injection duration, and atomization as well as penetration. Therefore, it is very difficult to separate the effect of injection pressure alone from that of the rate shaping. Studies conducted to investigate this subject show that increasing injection pressure results in improved fuel economy (Fig. 17) and smoke characteristics (Fig. 18) [2]. For 1991 diesel engines, full-load rated speed injection pressure approached 15,000 psi as opposed to the pre-1991 level range of 10,000 to 11,000 psi.

Injection Duration. At one time researchers had advocated the desirability of extremely short injection durations. With the introduction of new combustion developments, more emphasis was placed on the proper matching of injection duration

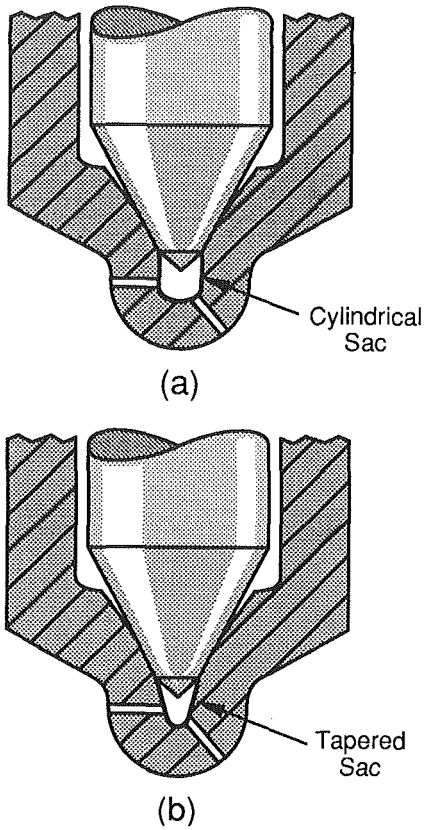

Fig. 20 Cylindrical sac (*a*) versus tapered (or conical) sac (*b*)

to the combustion system. For 1991 swirl-supported engines, an injection duration at rated speed and load conditions of approximately 25 to 30 deg crank angle was found to be optimum (see Fig. 19). Of course, this by no means suggests that injection duration is an independently controlled parameter. It is, however, a product of several choices related to the injection system and engine power output. These choices include nozzle hole size, number of nozzle holes, injection pressure, engine speed, and injected fuel quantity.

Injector Nozzle Configuration. The injector nozzle is the point of fuel delivery to the combustion chamber. Its design and placement in the cylinder head (angle of inclination) are of paramount importance to the performance and emissions characteristics of the engine. Several parametric studies have been conducted and lead to the following generalized statements describing optimized components of the nozzle configurations for 1991 direct-injection swirl engines:

- Nozzle sac volumes must be reduced to a minimum. In most cases the so-called cylindrical sac (shown in Fig. 20*a*) was adequate, but in some engines a conical design was necessary (see Fig. 20*b*).
- The number of injector holes must be optimized for the specific combustion system as well as for the injection pressure characteristics to maximize air utilization.
- The nozzle hole diameter must be selected to provide the proper fuel atomization. Figure 21 illustrates CO and particulate emission results of two different injector hole sizes. Injector B, with a hole size of 0.26 mm, exhibited higher CO and particulate emissions than injector A, which had a hole diameter of 0.25 mm.
- The length of the nozzle hole must be chosen for its contribution to fuel spray penetration. The latter together with proper atomization help in maximizing air utilization. In general, the optimum hole length was found to be 2.7 times the hole diameter [12].

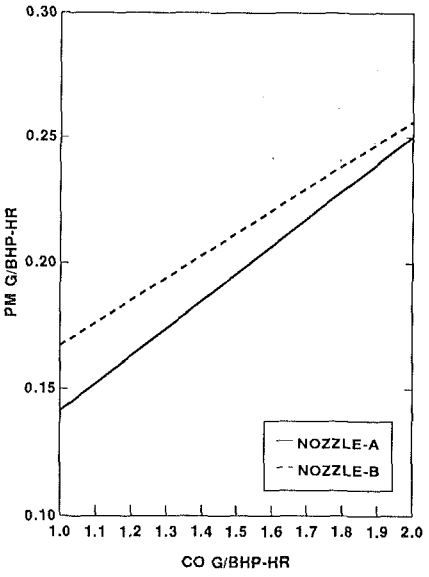

Fig. 21 Effect of nozzle hole diameter on emissions (CO/part), steady-state simulation

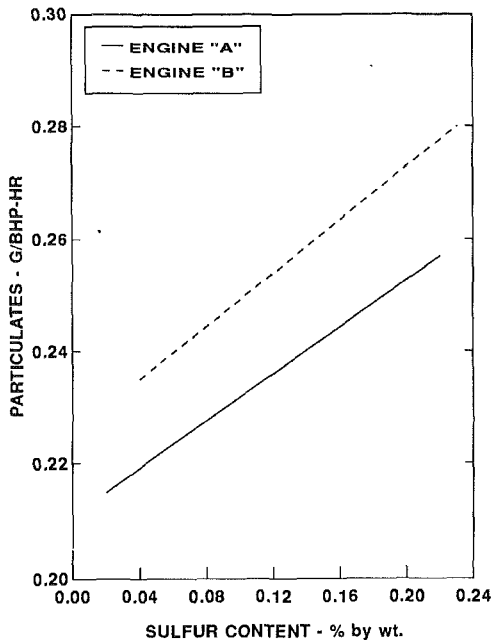

Fig. 22 Effect of sulfur on diesel particulates

• The spray cone (included) angle must be studied with regard to the specific combustion chamber and bowl design. Re-entrant type bowl design requires a smaller cone angle than traditional type bowl designs [1]. Typical reduction in the cone angle was about 10 deg from that of conventional straight sided combustion bowl designs.

• A significant amount of interaction exists between the various parameters already mentioned. The effect of some of these variables can readily be seen. However, in certain cases appreciable testing must be performed and results statistically analyzed to make the proper selection. By applying this development process, the nozzle opening pressures were raised from the pre-1991 level of 240 bars to 270–290 bars [12].

The above review of the fuel system components and their characteristics for the 1991 style engines is by no means a comprehensive account of all the changes. Some very important choices were made in the areas of delivery valves, high-pressure injection lines, the number and size of spill ports. In addition, shaping the torque curve between peak torque and rated speed, and the selection of a smoke limiter device were especially important in reducing emissions. Manufacturers that opted to include electronic controls had the additional task of optimizing the injection timing schedule. The optimization was relative to several variables such as speed, load, engine coolant temperature, and ambient temperatures. In spite of the vast improvement achieved, much remains to be done before the diesel engine can meet the emissions standards of 1994 and beyond.

The Fuel Factor. Many researchers have investigated diesel fuel quality and its impact on particulate emissions. Fuel properties most often studied include cetane number, aromatic content, and sulfur content.

Emissions of NO_x were reported to have dropped by as much as 10 percent when the cetane number was improved from 40 to 53 [6]. This NO_x reduction is generally attributed to less violent burning experienced with shorter ignition delay periods associated with high-cetane-number fuels. Most reduction in particulate emissions using high-cetane fuel results from more complete combustion, especially at low loads, and increased avoidance of lean flame-out conditions. Decreases in HC and CO emissions were also noted with high cetane number. In this case, the fuel and air mixtures do not become so lean as to reach flame-out conditions, causing partially burned fuel to escape through the exhaust.

Aromatics constitute as much as 25 to 45 percent volume of the No. 2 diesel fuel and are known to contribute disproportionately to the formation of soot. Large-molecular-weight aromatic compounds are more commonly known as polynuclear aromatics (PNA). California has legislated lower aromatic content (10 percent and 20 percent for large and small refiners, respectively) in future diesel fuel effective Oct. 1993.

Several studies were conducted to investigate the effect of sulfur on diesel particulate emissions. Figure 22 shows the result of such a test on two direct-injection diesel engines. For every 0.1 percent by weight of sulfur reduction, total particulate emissions are reduced from 0.02 to 0.025 g/bhp-h [7]. Reducing fuel sulfur also impacts the ability to apply various aftertreatment technology.

Diesel Exhaust Aftertreatment. As noted in Fig. 4, particulate matter composition has to main constituents. One constituent is insoluble particulate, which is mainly comprised of carbonaceous, sulfate, and ash particles. The other constituent is soluble particulate, which is comprised of partially burned lube oil and fuel-based particles or aerosols.

For diesel exhaust aftertreatment, particulate trap systems were the dominant solution. The operating principle of the trap is simply based on the capture and periodic incineration (or regeneration) of the carbonaceous exhaust particulates. The regeneration is often achieved through the use of heat provided by a variety of sources (fueled burners, electric heaters, engine intake throttling, etc). Regeneration is usually triggered after reaching a pre-established pressure drop measured across the trap, which is often made of a wall-flow honeycomb structure.

Central to the development of the trap system is that the regeneration must function under all operating conditions with little or no negative impact on the engine performance. This premise adds to the complexity and cost of the trap. In addition to cost and complexity issues, some doubt remains about the reliability and durability of the trap systems.

Another method of diesel exhaust aftertreatment is that of the catalytic converter. Diesel catalysis is similar to the method used for gasoline engine emission control but differs in terms of the exhaust gas composition to be controlled and the lower exhaust temperature. Catalytic aftertreatment of diesel exhaust becomes feasible with future use of low-sulfur-content diesel fuel. Using high-sulfur fuel in conjunction with oxidation cat-

Table 2 Comparison between traps and catalytic converters for diesel applications

Catalytic Converter or Trap?	
Trap	**Catalytic Converter**
Burns Carbonaceous Part.	Reduces SOF
Auxiliary regeneration required - expensive controls	No auxiliary regeneration required - no controls
Unproven durability	Deactivation concerns
Cost reduction opportunities	Cost effective
Sensitive to temperature gradient	sensitive to S in fuel

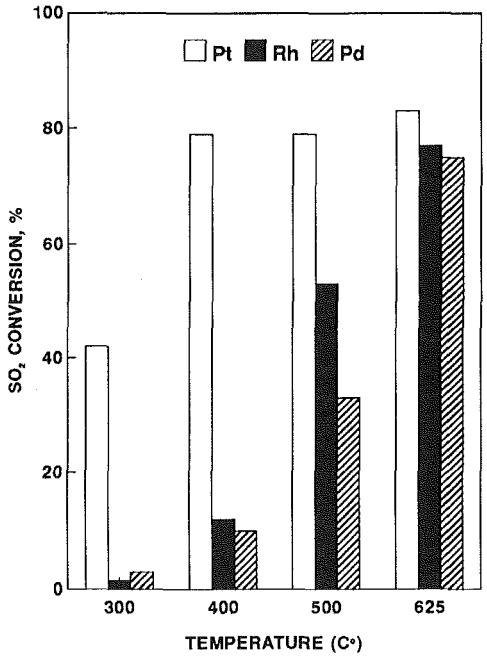

Fig. 23 Effect of noble metals on SO_2 conversion as a function of temperature

alysts leads to the formation of sulfate, thus increasing particulate mass emissions rather than decreasing them.

Catalytic aftertreatment ideally leads to the continuous oxidation of the soluble organic fraction as long as conditions are conducive for the oxidation process. The rate of oxidation of the organic fraction will depend on variables such as the composition of the catalyst washcoat and the noble metal selected as well as its loading, the space velocity, and the exhaust temperature. Other variables affecting the outcome of a catalytic aftertreatment strategy may include the type of the substrate, the location of the catalyst in the exhaust system, and the compostion of the exhaust gas itself. In summary, the effectiveness of a diesel catalytic aftertreatment system is a function of the rate of reduction of the organic fraction of total particulate, tempered by the rate of generation of sulfate emissions [13, 14]. Table 2 gives a comparison of the characteristics of both exhaust aftertreatment methods discussed above. Meanwhile, many manufacturers of heavy-duty diesel engines are attracted to the catalytic method of particulate control, due to its overall simplicity and effectiveness.

In applying catalytic aftertreatment, three factors to consider are the noble metal factor, the washcoat factor, and the substrate factor. These factors coupled with other considerations make it challenging to develop a catalytic aftertreatment system

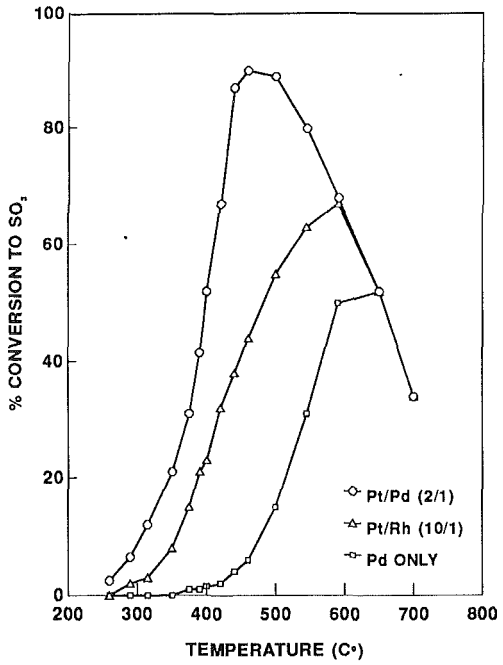

Fig. 24 Performance of three catalysts; conversion to SO_3 relative to exhaust temperature

to reduce the organic fraction, minimize the formation of sulfate, and yet preserve diesel engine performance and fuel economy.

The Noble Metal Factor. Figure 23, published in the *Platinum Metals Review* in 1989, compares the ability of various noble metals to convert sulfur dioxide into sulfur trioxide as a function of the exhaust temperature. Because the formation of sulfate is dependent on the amount of sulfur trioxide, using platinum as a diesel exhaust catalyst is expected to produce relatively high amounts of sulfate. By contrast, palladium would produce moderate amounts of sulfate emissions, even at higher exhaust temperatures compared to its platinum counterpart.

Rhodium is considered a stoichiometric NO_x reduction catalyst, and therefore is not considered the noble metal of choice for the diesel exhaust aftertreatment. However, rhodium has been used to curb the ability of platinum to produce SO_3 as shown in Fig. 24. Choosing the noble metal and its loading for a given application depends to a large extent on the composition of the exhaust and the specific objective desired. One objective may be the reduction of polynuclear aromatics (PNA) as opposed to reducing total particulates. In this case, platinum may be considered a prime choice, especially with a relatively small fraction of rhodium (Pt/Rh = 10–20:1). However if total particulate reduction is the objective, then palladium may be the preferred noble metal due to its low SO_2 to SO_3 conversion characteristics.

The Catalyst Washcoat Factor. The most important criterion for the selection of the washcoat is its capability to store and release sulfur compounds. Alumina, in various forms, is a very popular washcoat system for the gasoline exhaust aftertreatment. However, its use in the diesel exhaust environment may not be optimal because it has shown undesirable sulfate storage and release characteristics. Silica, on the other hand, has shown less sulfate storage and release capability. Therefore, it is gaining acceptance as a favored diesel catalyst washcoat system. Figure 25 shows the effect of increasing the amount of an inorganic oxide in the catalyst washcoat on the total particulate reduction. The mere substitution of alumina by silica should not be viewed as the total answer for the

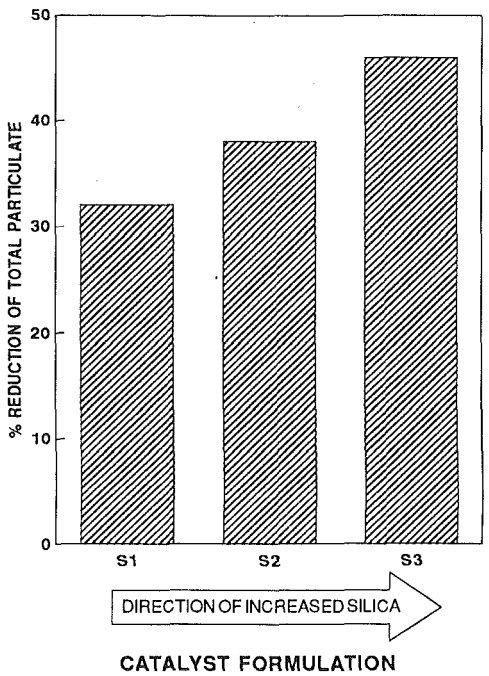

Fig. 25 Effect of washcoat on particulate reduction

washcoat effect. Inclusion of a variety of base metals such as cerium and zirconia is being investigated by several catalyst companies due to the base metal contribution in promoting and stabilizing catalyst reactions.

The Substrate Factor. The advantages and disadvantages of the substrate material (metallic versus ceramic) have been explored in [9, 15–17], and other publications. The most widely used substrates are of the thin wall ceramic honeycomb construction. In many cases, work has concentrated on the 300 or 400 cells per inch (cpi) designs. Exhaust backpressure characteristics are generally acceptable with no significant fuel economy disadvantage. Efforts to reduce backpressure, which has a negative impact on fuel economy and performance, may compromise the mechanical rigidity of the substrate. In addition, care must be taken by catalyst companies to avoid channel blockage resulting from improper washcoat processing.

The total volume of the substrate has a direct impact on the space velocity. A higher space velocity may lead to less catalytic activity due to the shorter residence time of the exhaust in the catalyst. A lower space velocity associated with higher catalyst volume could, in some cases, be detrimental for the process of sulfate storage and release. Therefore, it is important to size the catalytic converter properly.

Summary

Engine design changes including fuel system, combustion chamber, and oil consumption controls have enabled the heavy-duty diesel engine to meet the 1991 emissions standards. For 1994, the heavy-duty diesel engine will undergo further improvements of the same systems that helped it achieve 1991 emission levels. Lower sulfur content fuel is already legislated and gives new life and viability to catalytic aftertreatment of diesel exhaust. Improvements in fuel quality and composition as well as adoption of exhaust aftertreatment will be forthcoming.

References

1 Gill, A. P., "Design Choices for 1990's Low Emission Diesel Engines," SAE Paper No. 880350, 1988.

2 Mori, K., Kammikubo, H., Kawatani, T., Obara, T., Fukano, I., and Sugawara, K., "Technology for Meeting the 1991 U.S.A. Exhaust Emission Regulations on Heavy Duty Diesel Engine," SAE Paper No. 902233, 1990.

3 Khair, M. K., "Air-to-Air Intercooling of the Ford 7.8L Mid-range Truck Diesel Engine," SAE Paper No. 870534, 1987.

4 Wachter, W. F., "Analysis of Transient Emission Data of a Modelyear 1991 Heavy Duty Diesel Engine," SAE Paper No. 900443, 1990.

5 Richards, R. R., and Sibley, J. E., "Diesel Engine Emissions Control for the 1990's," SAE Paper No. 880346, 1988.

6 Knuth, H. W., and Garthe, H., "Future Diesel Fuel Compositions—Their Influence on Particulates," SAE Paper No. 881173, 1988.

7 Baranescu, R. A., "Influence of Fuel Sulfur on Diesel Particulate Emissions," SAE Paper No. 881174, 1988.

8 Ullman, T. L., Mason, R. L., and Montalvo, D. A., "Effects of Fuel Aromatics, Cetane Number, and Cetane Improver on Emissions From a 1991 Prototype Heavy-Duty Diesel Engine," SAE Paper No. 902171, 1990.

9 Ball, D. J., and Stack, R. G., "Catalyst Considerations for Diesel Converters," SAE Paper No. 902110, 1990.

10 Henein, N., and Patterson, D., "Combustion Engine Economy Performance and Emissions," Lecture notes to Ford Tractor Operations, Oct. 16–Nov. 20, 1985.

11 Dani, A. D., Nagpurkar, U. P., and Lakshminarayanan, P. A., "Universal Mixing Correlations for the Performance and Emission of Open Chamber Diesel Combustion Supported by Air Swirl," SAE Paper No. 900446, 1990.

12 Cartellieri, W. P., and Herzog, P. L., "Swirl Supported or Quiescent Combustion for 1990's Heavy-Duty DI Diesel Engines—An Analysis," SAE Paper No. 880342, 1988.

13 Horiuchi, M., Saito, K., and Ichihara, S., "Sulfur Storage and Discharge Behavior on Flow-Through Type Oxidation Catalysts," SAE Paper No. 910605, 1991.

14 Arai, M., "SOF Reduction and Sulfate Formation Characteristics by Diesel Catalyst," SAE Paper No. 910328, 1991.

15 Truex, T., Pierson, W., McKeen, D., Shelef, M., and Baker, R., "Effects of Barium Fuel Additive and Fuel Sulfur Level on Diesel Particulate Emissions," *Environmental Science and Technology*, Vol. 14, No. 9, Sept. 1980.

16 Cooper, B., and Thoss, J., "Role of NO in Diesel Particulate Emission Control," SAE Paper No. 890404, 1989.

17 Zelenka, P., Ostgathe, K., and Lox, E., "Reduction of Diesel Exhaust Emissions by Using Oxidation Catalysts," SAE Paper No. 902111, 1990.

Application of Methods for Determining Total Organic Contribution to Diesel Particulates

M. S. Newkirk
Southwest Research Institute,
San Antonio, TX 78228

This paper describes the laboratory effort to relate quantities of diesel particulate volatile organics obtained by DFI/GC™ to those obtained by traditional methods of organic analysis. Experiments were designed to investigate the potential usefulness of DFI/GC for determining the organic fraction and unburned lubricating oil contributions of diesel particulate emissions for future technology engines. A 1991 Caterpillar 3176 was used to generate samples during several heavy-duty engine test cycles, including the cold- and hot-start transient FTP and several steady-state conditions. Particulate-laden filter samples were then analyzed for organics by DFI/GC, solvent extraction, and vacuum volatilization. Results obtained using the three techniques were compared using statistical analysis techniques. Results showed that DFI/GC is extremely useful for directly determining the organic fraction of diesel particulate, and provides a better estimation of unburned lubricating oil contribution to the organic fraction than the other methods evaluated.

Introduction

Diesel particulate emissions are composed primarily of elemental carbon and organic compounds formed by incomplete combustion of fuel and oil. With new, more stringent EPA particulate emission standards scheduled for 1994, the relative contributions of unburned lubricating oil and fuel to particulate emissions have become important. Until recently, the characterization of these oil and fuel components has been costly, requiring lengthy solvent extraction and subsequent analysis.

Based on initial work done by Richardo for Volvo [1], the Department of Emissions Research at Southwest Research Institute designed and developed an improved technique for the direct analysis of unburned lubricating oil and other organic components of particulate. A dedicated gas chromatograph was modified to allow for the direct filter injection gas chromatography (DFI/GC™) analysis of a portion of the same filter used for particulate mass determination as defined by the EPA. Using DFI/GC eliminates the need for expensive and sensitivity-limiting solvent extraction procedures for determining unburned lubricating oil. Now, the more volatile organic components of particulate, which have traditionally been undetected by other methods of analysis due to excessive sample handling, are detectable.

Industry had traditionally used either particulate organic solvent extraction methods [2, 3] with subsequent gas chromatography analysis or a vacuum oven method [4] to carry out a similar determination of total organics (lubricating oil, fuel, etc.) in diesel particulate. Because these other methods of analysis have been almost exclusively used in research, it was important that a fundamental study be conducted to relate values obtained by DFI/GC to those obtained using the other methods. Therefore, establishing relationships between the quantities obtained by DFI/GC and traditional methods of analysis was the primary objective of this research project.

In order to relate the quantities obtained by the DFI/GC to the other methods of analysis, the overall scope of work shown in Table 1 was planned.

Equipment and Test Procedures

Engine Description and Setup. The 1991 Caterpillar 3176 heavy-duty diesel engine used in this program was chosen because it is a 1991 production model engine having particulate emission requirement of 0.25 g/bhp-h. In addition, this engine represented use of advanced technology. A description of engine characteristics is given in Table 2.

The engine was installed in a transient capable test cell and set up according to Federal Test Procedure requirements for transient testing. A photograph of the Caterpillar 3176 engine installed in the test cell is shown in Fig. 1.

Emission Test Procedures. The test procedures used to conduct measurements of regulated emissions were the Environmental Protection Agency (EPA) cold- and hot-start transient cycles. The transient FTP consists of a cold-start transient cycle followed by a hot-start transient cycle with a 20-min soak period between the two cycles. A graphic illustration of the EPA transient test cycle used for both cold- and hot-start emission testing is given in Fig. 2. Three steady-state conditions were also chosen as additional test points for emission sam-

Contributed by the Internal Combustion Engine Division and presented at the Energy-Sources Technology Conference and Exhibition, Houston, Texas, January 26-30, 1992. Manuscript received by the Internal Combustion Engine Division October 4, 1991. Paper No. 92-ICE-16. Associate Technical Editor: J. A. Caton.

Table 1 Summary of overall scope of work

Step	Description
1	Install 1991 technology engine in transient test cell, calibrate all instruments and map engine performance.
2	Collect 20 x 20-inch, 90 mm, and 47 mm particulate filters using hot- and cold-start EPA transient emission procedures described in the Code of Federal Regulations 40, Part 86, Subpart N.
3	Analyze selected filters by DFI/GC to determine volatile organic fraction (VOF) and lube oil percentage.
4	Analyze selected filters for total volatile fraction (TVF) using vacuum oven method.
5	Extract selected filters with methylene chloride to determine soluble organic fraction (SOF).
6	Analyze SOF samples using gas chromatograph to determine lube oil percentage.
7	Tabulate data and compare quantities obtained for VOF, TVF, and SOF.
8	Compare percentage lube oil contributions to total particulate as determined by DFI/GC and analysis of SOF.

Table 2 Engine description

Type: Caterpillar 3176	Rated Speed: 1900 rpm
Model: 1991	Peak Torque: 1275 ft-lb
Displacement: 10.3 liters	Peak Torque Speed: 1200 rpm
Rated Power: 325 hp	Idle Speed: 695 rpm (curb)
	1915 (governed)

pling. Steady-state conditions included 1100 rpm/25 percent load, 1100 rpm/50 percent load, and 1900 rpm/50 percent load. The steady-state conditions provided controlled variation to the amounts of organic fraction on the particulate filters relative to total particulate. This variation in organic fraction was important because it encompassed a large range of samples that could potentially be generated by other engines and/or test conditions.

The daily test sequence given in Table 3 began with the cold-start cycle, initiated when the engine was cranked for cold start-up. Upon completion of the cold-start transient cycle, the engine was shut down and allowed to stand (soak) for 20 min. After this hot-soak period, the hot-start cycle began with engine cranking. After the initial hot-start cycle, the engine was allowed to soak for 20 min and two additional hot-start cycles were run to provide backup data for analysis. Following the third hot-start cycle, three steady-state tests were conducted. At the conclusion of all testing, a final hot-start transient cycle was run to condition the engine for an overnight soak period. This daily sequence of testing was conducted for 8 days. Three days were preliminary tests to reduce variability. The data points and particulate samples from the remaining five sequences were used for analyses.

Emission Measurement Procedures. All emissions were determined from analyses of dilute engine exhaust using a constant volume sampling (CVS) system. The CVS system illustrated in Fig. 3 was used for both transient and steady-state test conditions. Special CVS provisions were made for obtaining two sets of 90 mm filter samples necessary for three subsequent analyses for particulate-bound organics. Although regulated gaseous emissions were not of special interest in this program, they were measured because they provided good insight into test-to-test repeatability and engine function.

Gaseous Emission Measurements. Hydrocarbon (HC) emissions were determined on a continuous basis using a heated

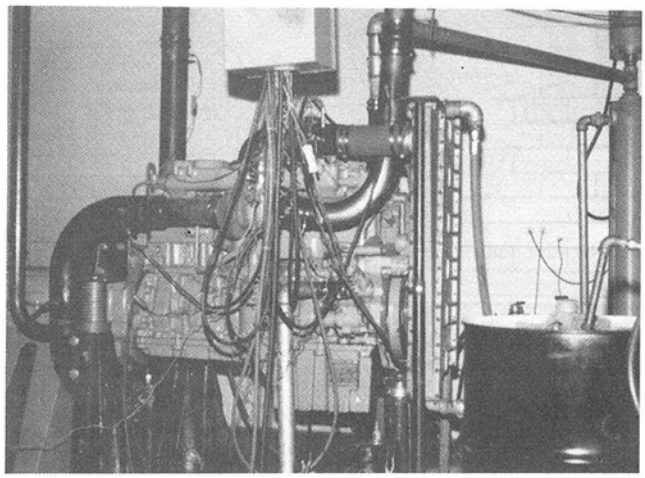

Fig. 1 Caterpillar 3176 engine installed in the test cell

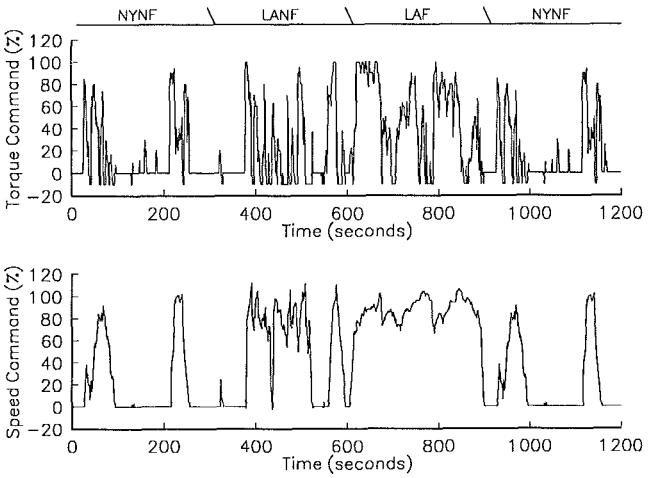

Fig. 2 Normalized speed and torque commands for the EPA transient cycle

Table 3 Summary of daily engine testing segment of the test plan

Step	Step Description
1	- Cold-Start FTP
2	- Hot-Start FTP
3	- Hot-Start FTP
4	- Hot-Start FTP
5	- 1100 rpm/25% load for 42 minutes, sample last 40 minutes
6	- 1100 rpm/50% load for 32 minutes, sample last 30 minutes
7	- 1900 rpm/50% load for 32 minutes, sample last 30 minutes
	- Prep for next day of testing

flame ionization detector (HFID), with the response integrated over time as prescribed in the FTP for transient emission testing. Hydrocarbon emissions determined from CVS dilute samples were dependent on background measurement. Background hydrocarbon levels of the CVS dilution air were determined from samples taken during the transient and steady-state tests and were relatively constant during testing. "Tunnel" background was read by the HFID sample train prior to starting the engine. The "tunnel" background was also recorded after the test had been completed and the engine turned off. For this program, the "tunnel" background levels from the start to the finish of the tests were relatively constant (within 1 ppmC of an average 7 ppmC).

Carbon monoxide (CO) and carbon dioxide (CO_2) emissions were determined from dilute exhaust samples collected using the CVS according to FTP practice using nondispersive in-

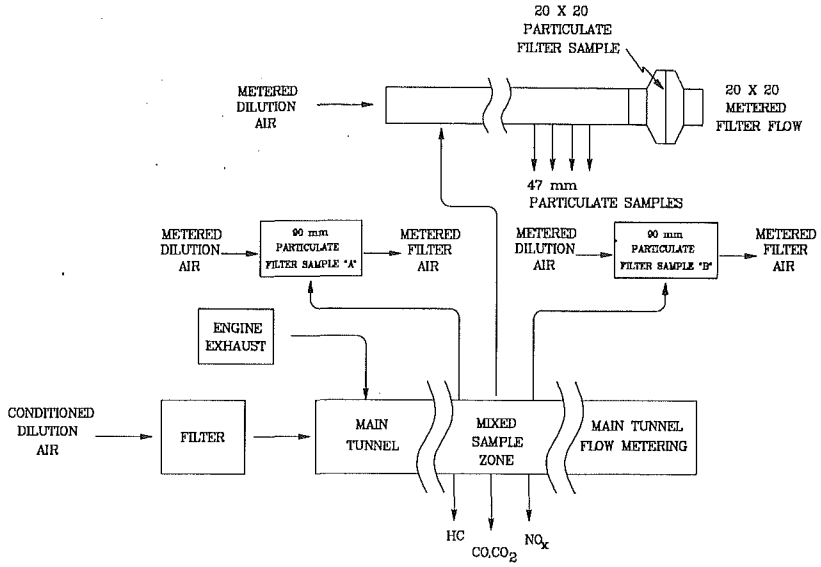

Fig. 3 Illustration of CVS and particulate sampling system

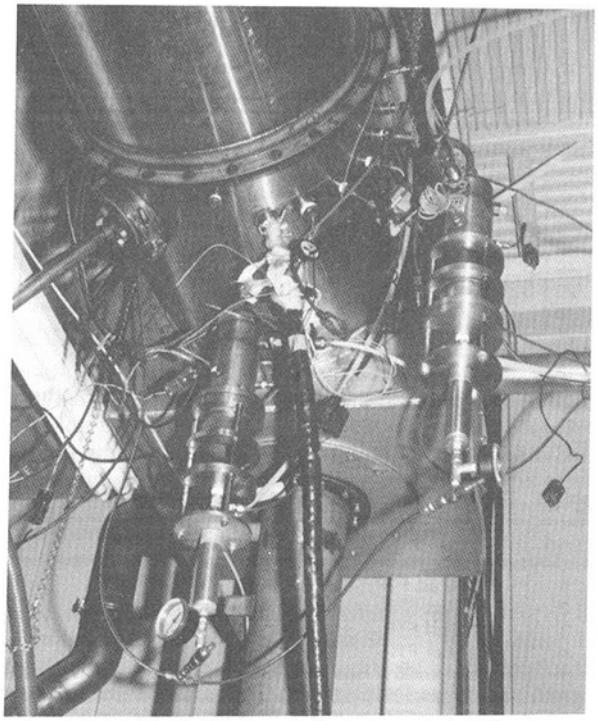

Fig. 4 90 mm dilution tunnel filter sampling system

frared (NDIR) instruments. CVS dilute oxides of nitrogen (NO_x) were determined by chemiluminescence (CL) and integrated over the applicable test cycle. Applicable NO_x correction factors for engine inlet air humidity and temperature were computed and applied per FTP practices.

Particulate Emission Measurements. Total particulate emissions were determined using a double-dilution technique specified in the EPA 1988 transient FTP for heavy-duty diesel engines. Several identical EPA-defined particulate emission samples were required for the three analytical techniques (DFI/GC, solvent extraction, and vacuum volatilization) to be investigated in this program. Therefore, two similarly configured double-dilution particulate filter sampling systems (Systems A and B) were set up to produce two sets of 90 mm filter samples as shown in Fig. 4. Each set consists of two filters in series and weight gains from both filters, one primary and one backup, were used to determine the total particulate emissions. One set of particulate filters was used for determining of SOF by solvent extraction. The other set of filters was divided and used for both the vacuum oven volatilization and the DFI/GC analysis. The two similarly configured double-dilution systems utilized dry gas meters to measure the dilution air flows and total flows across each set of two 90 mm Pallflex (T60A20) filters. During sampling air flow rates and total flow rates were set similarly for both systems (± 15 percent difference maximum) to maintain similar filter face sample temperatures. In general, the difference between filter face temperatures for cold- and hot-start did not exceed 2°C at any time during testing. Steady-state filter face temperatures were almost identical (± 1°C difference) for the two systems.

One area of concern with respect to subsequent analysis of the particulate filter samples was historically observed variations in Pallflex (T60A20) filter collection media, which cause variation in filter efficiencies, pressure drops, surface character, brittleness, etc. Often, filters from the same "batch" have exhibited different filtration characteristics, which can significantly alter particulate results and would have proven unacceptable for this project when trying to take two identical 90 mm particulate samples. In order to minimize filtration variables, all filters were cut from the same larger piece of filter material.

Preliminary hot-start emission tests were conducted to ensure that the two 90 mm double-dilution sampling systems (designated as System A and System B) were, in fact, giving approximately the same particulate filter loading levels and that the particulate emission values obtained from each system were equal (within 10 percent). Table 4 shows that the particulate mass loadings and emission rates for both systems were within 10 percent of each other.

The most important aspect was not that the particulate filters actually collected identical amounts of particulate, but rather, that both systems collected particulate material of the same composition. After all emission tests for the entire program were completed, a statistical analysis of variance (ANOVA) was conducted in order to verify that the relative contribution of organics to total particulate for both 90 mm Systems A and B were statistically from the same population. In the statistical analysis, only the organic fractions on filters A and B were considered and compared. The results of this analysis showed that no significant difference (at the 95 percent confidence level) existed between the average organic emissions at the two different filter locations. Therefore, it was concluded that the

Table 4 Results of preliminary emission tests to verify equivalence of 90 mm sampling Systems A and B

Test No.	Particulate Filter Mass, mg			Particulate Emissions, g/bhp-hr		
	System A	System B	Δ, %	System A	System B	Δ, %
HS1-01A	5.11	5.37	5	0.20	0.22	10
HS2-01A	5.69	6.02	6	0.22	0.24	8
HS3-01A	5.41	5.84	8	0.21	0.23	10

filter location did not need to be considered in any further statistical analysis and that the relative organic compositions of both filters A and B were statistically similar. Figure 5 is an illustration of the breakdown of the two sets of 90 mm particulate filters for analytical use.

Although 90 mm particulate filters were also solvent extracted to obtain a SOF value, the mass of SOF was insufficient for further analysis. Therefore, a large 20 × 20-in. particulate filter was used for sufficient organic material to be collected, solvent (Soxhlet) extracted, and subsequently analyzed for soluble organic fraction (SOF) and the contribution of lubricating oil. The 20 × 20-in. double-dilution particulate sampling system was installed to collect a large sample of total particulate on 20 × 20-in. square filters of Pallflex T60A20 material. Unlike the 90 mm sampling systems, however, the 20 × 20-in. sampling system only consisted of a single filter *without* a backup filter in series. Therefore, particulate emission rates obtained using the 20 × 20-in. system may not agree with 90 mm systems. This technique for obtaining sufficient SOF for further analysis using 20 × 20-in filters has been used traditionally in industry and therefore, it was important to consider.

Test Fuel and Engine Lubricating Oil. The fuel selected for use throughout this program was a Phillips 2D low (0.05 percent) sulfur grade fuel. The engine lubricating oil used in this program was "Caterpillar CXP 15W-40." This oil was also used as the calibration standard for all DFI/GC analyses and as the basis for determining unburned lubricating oil contributions to the organic fraction of particulate. A gas chromatography boiling point distribution of this oil is given in Fig. 6.

Organic Analysis Procedures

The main objective of this study was to relate the organic quantities obtained by DFI/GC (VOF) to more traditionally derived quantities obtained by solvent extraction (SOF) and vacuum volatilization (TVF) using 90 mm particulate filters. It should be noted that quantities of VOF, SOF, and TVF are *not* exactly the same, but they are closely related. Specifically, *Volatile Organic Fraction (VOF) is organic material that responds on an FID detector and has a boiling point of less than approximately 600°C. Soluble Organic Fraction (SOF) is any material (independent of boiling point) that is soluble in methylene chloride at the specified test conditions. Total Volatile Fraction (TVF) includes all material on a filter that can be volatilized at 225°C and 5 torr (absolute).*

DFI/GC. Direct Filter Injection Gas Chromatography (DFI/GC) analysis was developed to measure the VOF of diesel particulate emissions using the same filter collected for particle *mass* determination. In addition, the contribution of unburned lubricating oil to VOF can be determined by an interpretive procedure based on simulated distillation boiling point distribution of a fresh lubricating oil sample. It is not possible, however, to separate unburned fuel-derived particulate emissions from oxidized products of lubricating oil and oxidized fuel components because all of these components fall into the same boiling region. In fact, flame ionization detector/gas

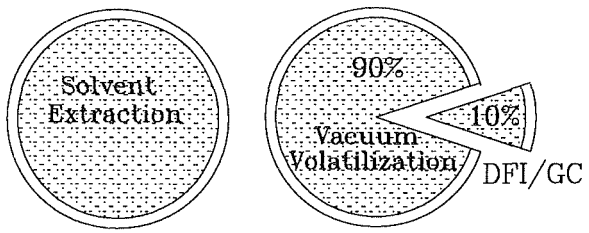

Fig. 5 Illustration of 90 mm particulate filter allocation for analysis

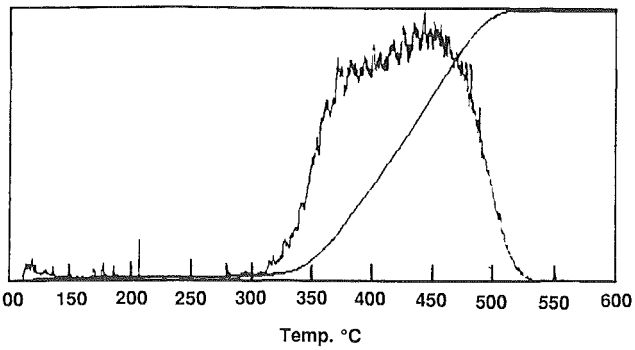

Fig. 6 Boiling point distribution of Caterpillar CSP 15W-40 engine oil

chromatography methods used to categorize a portion of the organics as "fuel" are dependent upon the analyst's definition of "fuel." For this reason, unburned fuel components, oxidized lubricating oil, and oxidized fuel components in this study were grouped together into another category called "other."

For DFI/GC analysis, a pie-shaped segment representing a 10 percent fraction of the 90 mm particulate filter was injected into the DFI/GC. An external standard of fresh lubricating oil was used to quantify the VOF and it was also used as a basis for interpreting the lubricating oil contribution to the VOF. A major advantage to the DFI/GC method over other methods is that no solvent extraction procedure is required to obtain a sample for subsequent lubricating oil determination. The DFI/GC analysis often detects some "lighter" hydrocarbons ordinarily undetected during analysis of SOF due to excessive handling and sample evaporation associated with extraction procedures.

VOF Analytical Procedure. Analysis for contribution of VOF and unburned lubricating oil to total particulate emissions was carried out by first collecting particulate matter on 90 mm Teflon-coated glass fiber (or Pallflex) filters during engine emission testing. The VOF analysis was conducted using a Perkin Elmer Model 8500 gas chromatograph (GC) equipped with a uniquely designed filter injection system and a flame ionization detector (FID) as shown in Fig. 7. The GC column for this analysis was a 15 m long by 0.53 mm o.d. DB-1 with a film thickness of 1.5 μm. The GC temperature program and operating conditions are given in Table 5 for reference.

For DFI/GC analyses in this study, a 10 percent fraction of each primary and backup particulate filter was carefully cut (Fig. 8). The primary "filter fraction" from the primary filter was stacked on top of the backup filter fraction and the set was carefully folded so that no particulate material was exposed (Fig. 9). The folded filter fractions were then placed into the injector (Fig. 10). The injector was subsequently inserted into the cool zone of the DFI/GC to allow any oxygen in the system to be purged without losing any sample by desorption. When all oxygen had been purged from the system, the injector was pushed into the hot zone of the DFI/GC where the volatile material was desorbed and deposited into the cool column (Fig. 11). The GC temperature program given in Table 5 was then

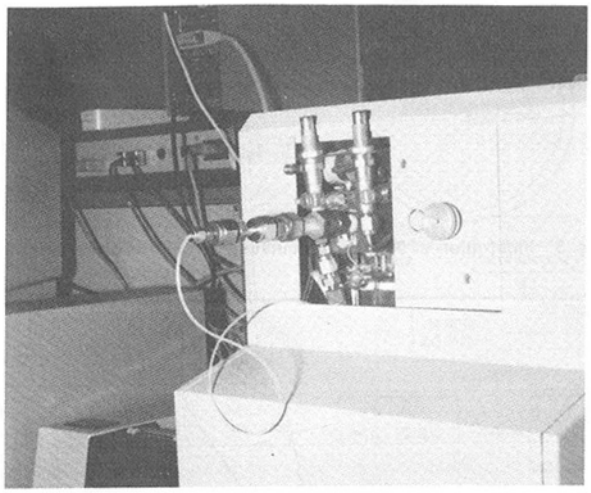

Fig. 7 View of direct filter injector

Table 5 GC temperature program and operating conditions

Cool Zone Temperature:	Ambient
Hot Zone Temperature:	380°C
Detector Temperature:	380°C
Carrier Gas:	Zero Grade Helium
Carrier Gas Flow:	17 mL/min
Temperature Program	
Initial Temperature:	40°C
Isotime:	0.5 min
Ramp Rate:	10°C/min
Final Temperature:	360°C
Isotime:	10 min

run to separate the desorbed compounds by boiling point, detecting each using an FID.

An external standard comprised of unused lubricating oil was used as a basis to quantify the VOF of a given sample. First, a sample of the oil was accurately weighed onto a 10 percent pie-shaped segment of an unused 90 mm Pallflex filter. The amount of oil was recorded, and the sample was analyzed by DFI/GC. The total raw data counts obtained from the DFI/GC analysis were proportional to the mass of oil of the filter. Thus, a conversion factor or response factor between DFI/GC counts and organics (oil) was established as a "calibration." This "calibration" was conducted at least once daily. Initially, to verify that the relationship between DFI/GC counts and the mass of oil weighed onto filters was linear, a linearity calibration study was conducted and the data are given in Table 6.

As shown in Table 6, the lubricating oil calibration was relatively linear from approximately 0 to 1 mg for organic determinations, with a maximum error of 4.0 percent. A plot of counts versus oil weight is shown in Fig. 12. The value for R-squared is 0.999. The average response factor (RF of 3.61E-09 mg/count), however, has shown linearity over a much larger range than indicated in Fig. 12. This linearity is expected because the FID on the DFI/GC system generally shows linear response.

The final calculation of the volatile organic fraction of particulates uses the following formula:

$$\text{VOF} = \left[\frac{(\text{Samp. Cts.})\ (\text{RF})}{(\text{FF})}\right]$$

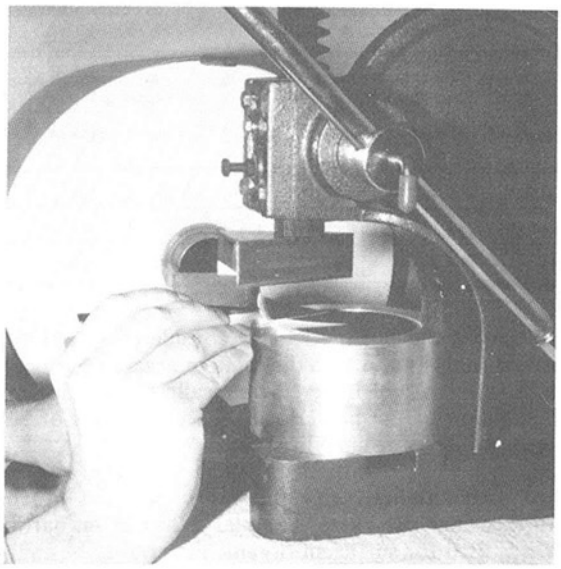

Fig. 8 10 percent pie segment cut

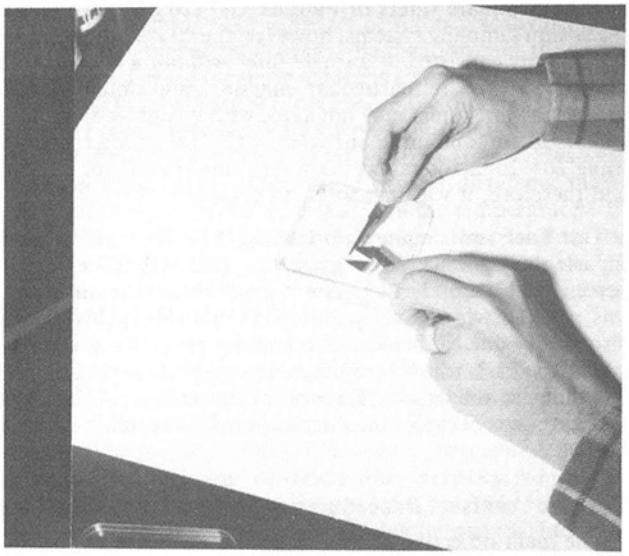

Fig. 9 Primary and backup filters stacked and folded

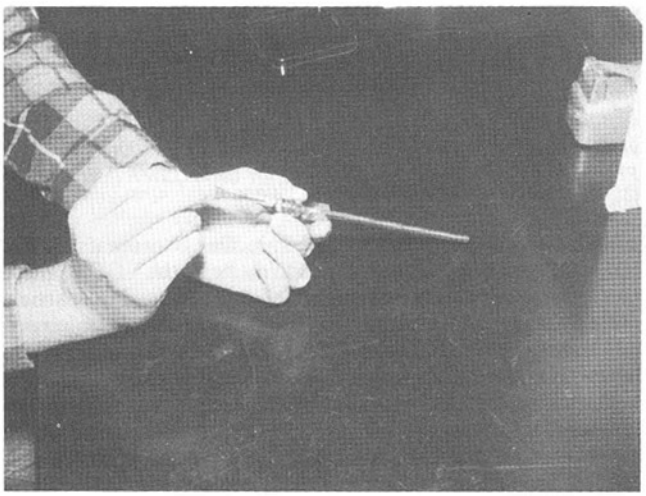

Fig. 10 Folded filter fractions placed into injector

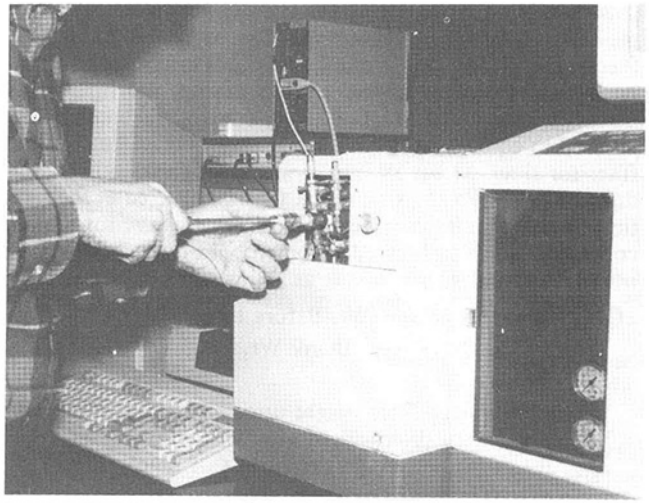

Fig. 11 Injector inserted into GC for analysis

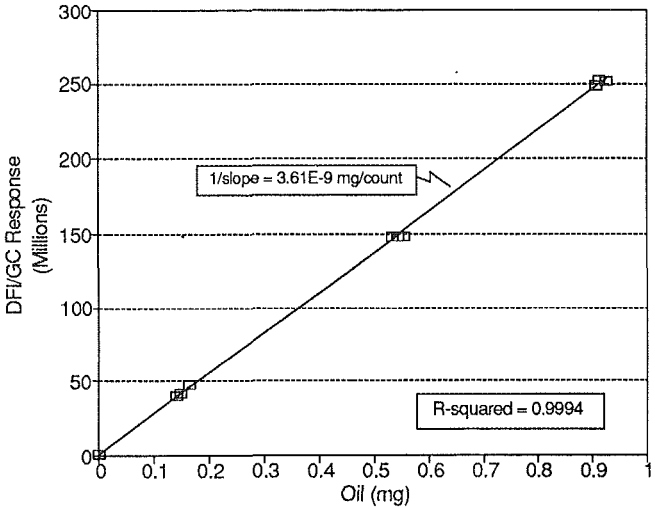

Fig. 12 Plot of area counts versus oil weight

Table 6 Linearity calibration data

Oil Weight, mg	Counts	Response Factor, mg/ct	Error[a], %
0.149	41146468	3.61E-09	0.0
0.165	47272470	3.49E-09	-3.3
0.142	40370544	3.52E-09	-2.8
0.544	147926416	3.68E-09	1.9
0.556	148016416	3.76E-09	4.0
0.534	152395952	3.50E-09	-2.9
0.925	251493776	3.69E-09	1.9
0.912	252153776	3.62E-09	0.2
0.907	248512608	3.65E-09	1.1
Average Response Factor		3.61E-09	

[a] $\%\ Error = \left(\frac{Response\ Factor - Average\ Response\ Factor}{Average\ Response\ Factor}\right) \times 100$

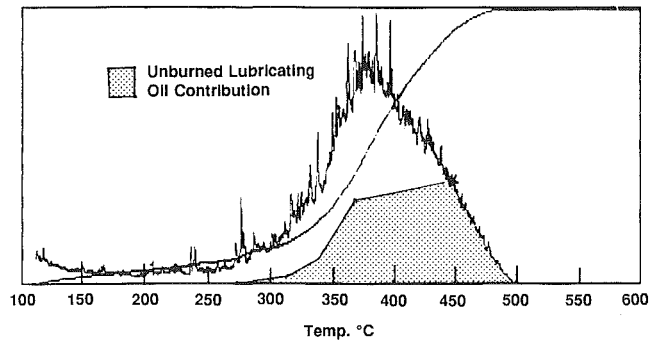

Fig. 13 Illustration of contribution of unburned lubricating oil to VOF

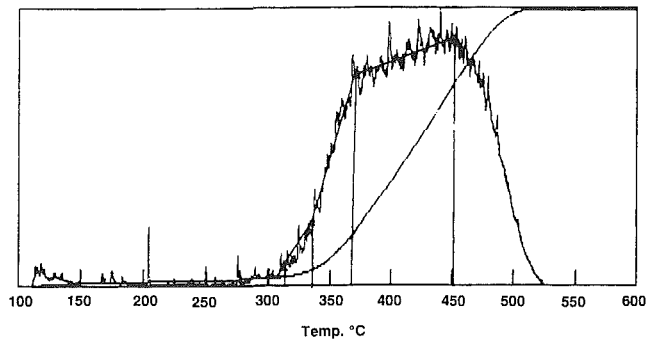

Fig. 14 DFI/GC analysis of fresh lubricating oil standard

where:

VOF = volatile organic fraction (mg/filter set)
Sample Cts = sample counts (counts/filter set)
FR = average lubricating oil response factor (mg/count)
FF = filter fraction used for analysis (dimensionless)

Given that the filter fraction is 0.1 (or 10 percent) this formula reduces to

$$VOF = (\text{Samp. Cts.})\,\frac{RF}{0.1}$$

Unburned Lubricating Oil Determination. In addition to the calculation of VOF during each DFI/GC analysis, a boiling point separation (chromatogram) of each sample was also obtained. By using the boiling point chromatogram of the sample and mathematically superimposing a boiling point chromatogram of the calibration oil onto the sample, the relative contribution of unburned lubricating oil to the VOF was determined. The shaded area of Fig. 13 illustrates the unburned lubricating oil contribution that was identified for this example. For comparative purposes, a DFI/GC analysis of a fresh lubricating oil standard is shown in Fig. 14.

For the unburned lubricating oil contribution to VOF, a maximum point on the lubricating oil chromatogram was chosen first. Next, regions of approximately linear slope were "mapped out" on the oil chromatogram. The heights of each of the points that determine the slopes of the lines were then measured relative to the baseline (which had been corrected for "column bleed"). The oil chromatogram was then approximated as a polygon. This mathematical picture, or polygon, representing the oil chromatogram was mathematically superimposed onto the sample chromatogram by using height ratios and plotting polygon points, thereby essentially negating attenuation effects. Finally, a planimeter was used to determine the area of the unburned lubricating oil on the sample chromatogram relative to the total area of the sample chromatogram. This area represented the unburned lubricating oil contribution to VOF. Any remaining area outside of the unburned lubricating oil region on the chromatogram was generally labeled as "other," and can usually be qualitatively identified based on past experience (e.g., unburned fuel, oxidized oil, etc.). It is important to note that is is *not* possible to make a specific determination of "fuel" contribution to VOF using DFI/GC or boiling point separation methods only using an FID detector, because "fuel" components fall into the same boiling range as oxidized oil and partially oxidized fuel.

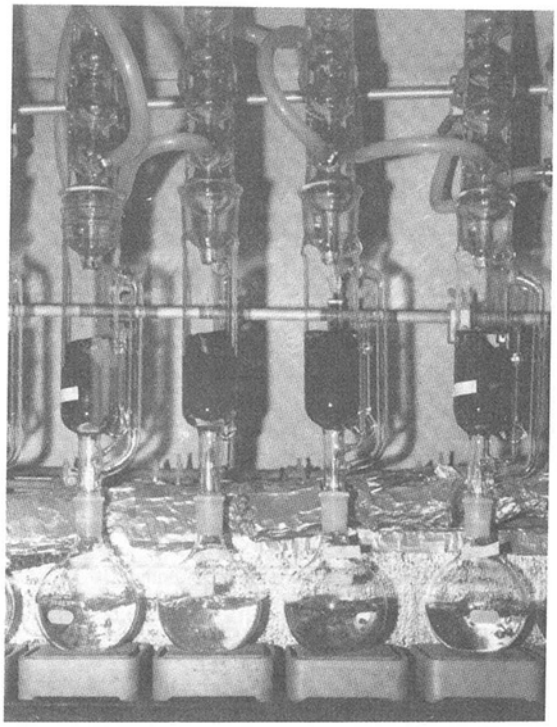

Fig. 15 Soxhlet extractors containing particulate filters

Solvent Extraction. Solvent extraction is one of the most commonly used analytical techniques for determining the total organic contribution to diesel particulate emissions. The resultant extract or soluble organic fraction (SOF) obtained from this analysis is dependent on the type of solvent used. For this program, methylene chloride was the solvent of choice because it is the most widely used.

In this study, two types of filter samples were generated for the SOF analysis: one 20 × 20-in. filter and one set of 90 mm filters (primary and backup). The 20 × 20-in. filter was needed to provide a relationship to the other analytical methods discussed in this report and to provide sufficient SOF for subsequent GC determination of lubricating oil contribution to the total SOF. However, the 90 mm particulate filter set also was used because it consists of both a primary and backup particulate filter (whereas the 20 × 20-in. does not). In addition, both the DFI/GC analysis and vacuum volatilization analysis use the 90 mm filter set.

Solvent Extraction Analytical Procedure. The analysis for SOF and unburned lubricating oil contribution to SOF was carried out by first collecting particulate material on both 20 × 20-in. and 90 mm Teflon coated glass fiber filters during engine emission tests. All particulate filters were then placed in a temperature- and humidity-controlled chamber and allowed to equilibrate for at least 4 h prior to extraction. Immediately before being extracted, each filter was carefully weighed so that the SOF could be indirectly determined by weight loss. Next, the filters were carefully folded and placed into an appropriately sized Soxhlet extractor (see Fig. 15). Both the primary and backup 90 mm filters were extracted together in the same Soxhlet apparatus because the DFI/GC and vacuum oven methods of analysis as well as the EPA total particulate emission calculations consider material collected on both filters. The filter samples were then subjected to extraction for approximately 40 cycles. The use, validation, and qualification of the extraction procedure described here have been documented by General Motors Research Laboratories and EPA [2, 3], among others.

After 40 cycles, the Soxhlet extractors were disassembled and the boiling pots containing the extracts were capped to prevent any loss by evaporation. The extracted filters were then carefully removed from the Soxhlets and allowed to dry under a nitrogen atmosphere. After drying, the filters were placed in temperature- and humidity-controlled chambers and allowed to equilibrate for no less than 4 hours. Finally, each filter (or filter set for 90 mm's) was reweighed and the SOF determined by weight loss. Blank filters extracted at the same time as the samples provided a necessary average for a blank correction factor and served as control. The overall calculation of SOF by filter weight loss is as follows:

SOF(filter weight loss) = (Wt. Before Ext.
− Wt. After Ext. − Avg. Blank Wt.)

where

Wt. Before Ext. = filter weight prior to extraction (mg)
Wt. After Ext. = filter weight after extract (mg)
Avg. Blank Wt. = average weight loss of blank filters (mg)

Since the 20 × 20-in. filters were also used to generate sufficient extract for further analysis of the lubricating oil contribution to SOF and to determine the weight of the extract (SOF) itself by direct gravimetric techniques, the extract and solvent had to be evaporated to dryness in a small weighing vial. The drying process consisted of the following steps:

1 The entire quantity of solvent and extract (approximately 400 mL) contained in the Soxhlet extractor was filtered by vacuum filtration through a 0.5 μm Teflon membrane filter to remove any particulate material that may have been washed into the solvent pot.

2 The solvent was roto-evaporated to a volume of approximately 50 mL and transferred with washings to a 100 mL beaker.

3 The beaker containing the solvent and extract was reduced under a dry nitrogen atmosphere to approximately 30 mL.

4 Portions of the solvent and extract were transferred to a single preweighed 5 mL weighing vial and reduced to dryness using dry nitrogen gas blown over the vials until all solvent (methylene choride) had evaporated.

5 The transfer and drying process was repeated until all of the extract and washings from the beaker had been transferred to the weighing vial and dried.

The vial containing only extract was then weighed to determine the final SOF directly by differential weight gain according to the following formula:

SOF(extract weight) = (Wt. Vial After
− Wt. Vial Before − Avg. Blank Wt.)

where:

Wt. Vial After = weight of vial containing dried extract (mg)
Wt. Vial Before = weight of vial before containing dried extraction (mg)
Avg. Blank Wt. = average weight of dried extract from blank filters (mg)

Unburned Lubricating Oil Determination. In addition to the gravimetric determinations of SOF, the contribution of unburned lubricating oil to the SOF also was determined by a gas chromatographic (GC) analysis similar to DFI/GC. For this GC analysis, 1 mL of carbon disulfide (CS_2) was added to each weighing vial to redissolve the diesel SOF. Methylene chloride was not used because it gives a large solvent response peak on the GC, which interferes with lubricating oil interpretations. Next, the vials containing extract and CS_2 were placed in a sonic bath for 5 min to promote complete dissolution of all of the extract in the solvent. A 1 μL aliquot of the solution was then injected into the GC and the analysis conducted using the same DB-1 column that was used for the DFI/GC analysis. The GC operating conditions were also identical to the DFI/GC analysis. The result of this GC analysis

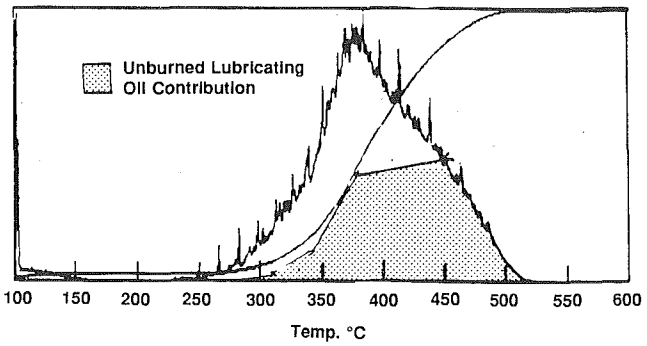

Fig. 16 Illustration of contribution of unburned lubricating oil to SOF

Table 7 Vacuum volatilization procedure

1. Condition particulate filters to be analyzed for at least 4 hours in a temperature- and humidity-controlled chamber.
2. Weigh each filter individually.
3. Preheat vacuum oven to 225°C. Maintain vacuum at pressure gauge reading between 2-5 torr above absolute vacuum.
4. Place filters on holder rack and place rack in vacuum oven.
5. Bake filters for 3 hours.
6. Remove filters from vacuum oven and replace them in temperature- and humidity-controlled chamber.
7. After at least 4 hours of equilibration, reweigh each filter and determine weight loss.

was a boiling point distribution and chromatogram of the extract. This boiling point distribution of the SOF (SOF/GC) was then compared to a lubricating oil chromatogram in the same manner as the DFI/GC analysis for unburned lubricating oil. The lubricating oil "standard" was made up by dissolving approximately 50 mg of lubricating oil in 1 mL of carbon disulfide. An example of the unburned lubricating oil contribution to the SOF using this procedure is represented by the shaded area in Fig. 16.

Like the DFI/GC analysis, it is important to note that it is *not* possible to make a determination of "fuel" contribution to SOF using a boiling point separation method that only uses an FID detector, because "fuel" components fall into the same boiling range as oxidized oil and oxidized fuel products of combustion.

Vacuum Oven Volatilization. The vacuum oven volatilization method used was adapted from an in-house procedure used by Detroit Diesel Corporation and other engine manufacturers. This procedure is used to determine the total volatile fraction (TVF) of material on a filter relative to total particulate. The vacuum volatilization procedure is described in Table 7. A photograph of the vacuum oven system used for this analysis is shown in Fig. 17.

After conducting vacuum volatilization, the calculation of TVF is as follows:

$$\text{TVF} = \left[\frac{(\text{Pre Vol. Wt.} - \text{Post Vol. Wt.})}{0.9}\right] - [\text{Avg. Blank Wt.}]$$

where:

Pre Vol. Wt. = weight of 90 percent filter segment prior to vacuum volatilization (mg)

Post Vol. Wt. = weight of 90 percent filter segment after vacuum volatilization (mg)

Avg. Blank Wt. = average weight of blank filters (mg)

Note: The "0.9" factor is introduced because only 90 percent of each sample filter was analyzed.

Prior to accepting the vacuum oven technique, 15 new pre-weighed filters were "doped" with varying amounts of lubricating oil to determine the percent recovery of the total amount of oil added to each. The results of this experiment are given in Table 8.

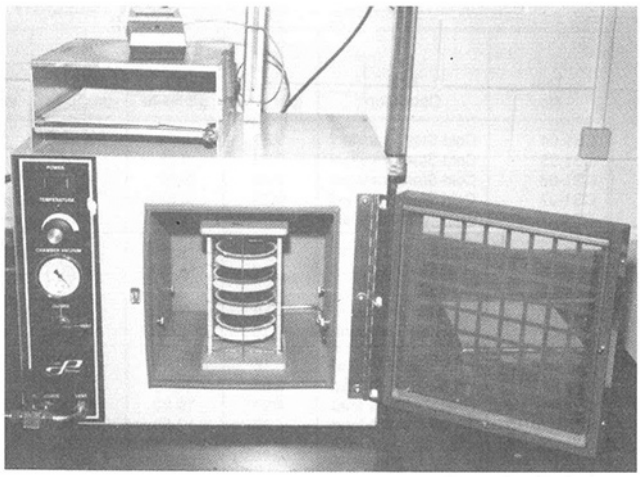

Fig. 17 Vacuum oven system

Table 8 Vacuum oven volatilization recovery experiment

Clean Filter Wt., mg[a]	Filter+Oil Wt., mg[b]	Oil Wt., mg[c]	Post Vol. Wt., mg[d]	Corrected Mass Lost, mg[e]	Recovery, %[f]
266.000	266.000	0.000	265.765	0.235[g]	--
271.880	271.880	0.000	271.679	0.201[g]	--
269.227	269.227	0.000	269.024	0.203[g]	--
270.115	270.273	0.158	269.798	0.262	166
267.400	267.538	0.138	267.130	0.195	141
266.443	266.670	0.227	266.194	0.263	116
270.165	270.743	0.578	270.000	0.530	92
270.920	271.422	0.502	270.729	0.480	96
270.610	271.155	0.545	270.442	0.500	92
266.805	267.640	0.835	266.653	0.774	93
268.145	268.984	0.839	267.987	0.784	93
266.800	267.659	0.859	266.641	0.805	94
270.255	271.374	1.119	270.169	0.992	89
267.292	268.574	1.282	267.230	1.131	88
264.970	266.184	1.214	264.864	1.107	91
268.604	270.255	1.621	268.478	1.534	95
268.843	270.620	1.777	268.810	1.597	90
266.394	268.047	1.653	266.237	1.597	97

[a] Clean Filter Wt. - Weight of unused new filter.
[b] Filter + Oil Wt. = (Clean Filter Wt.) + (Weight of "doped oil").
[c] Oil Wt.= (Filter + Oil Wt.) - (Clean Filter Wt.).
[d] Post Vol. Wt. = Weight of filter after vacuum oven volatilization.
[e] Corrected Mass Lost = (Filter + Oil Wt.) - (Post Vol. Wt.) - 0.213.
[f] Recovery = [(Mass Lost)/(Oil Wt.)] x 100.
[g] Uncorrected blank valve used to correct sample value. Average of three values = 0.213 mg/filter.

As is shown by the recovery data, this method has limited accuracy due to blank filter interference (0.213 mg), and is therefore not accurate for determinations of TVF less than about 0.5 mg/90 mm filter or 0.01 mg/cm^2 of filter stain area. However, this method is adequate for rough approximations of organics on a filter and was included in this program because it is widely used as an inexpensive tool to assess relative levels of organic contribution to particulate.

Test Results and Data Analysis

Emission Test Results. During this project, 25 valid emission tests were conducted over the five test cycles. A summary of emission results is given in Table 9. Separate values for particulate emissions are given for Systems A and B as well as the 20 × 20-in. filter system. Although particulate emissions were lower for System A relative to System B, the composition of the particulate (i.e., organic contribution) for the two sys-

Table 9 Summary of valid emission test data

Test No.	Test Condition	HC, g/bhp-hr	CO, g/bhp-hr	NO_x, g/bhp-hr	System A			System B			20x20-Inch System	
					Part., Wt., mg	Part., g/bhp-hr	Filter Eff., %	Part., Wt., mg	Part., g/bhp-hr	Filter Eff., %	Part., Wt., mg	Part., g/bhp-hr
CS1-04	Cold-Start Transient	0.29	3.48	4.36	5.862	0.24	95	6.299	0.27	95	167.1	0.29
CS1-05	Cold-Start Transient	0.32	3.58	4.28	5.781	0.22	96	6.401	0.27	95	165.8	0.28
CS1-06	Cold-Start Transient	0.26	3.92	4.32	7.110	0.26	96	6.929	0.31	95	188.4	0.33
CS1-07	Cold-Start Transient	0.25	3.34	4.28	6.769	0.23	96	6.740	0.27	94	169.8	0.29
CS1-07	Cold-Start Transient	0.19	3.49	4.24	6.620	0.24	95	6.283	0.27	96	171.3	0.28
HS1-04	Hot-Start Transient	0.16	2.83	4.29	5.198	0.21	96	5.747	0.23	96	144.7	0.25
HS1-05	Hot-Start Transient	0.17	2.79	4.18	5.099	0.19	97	5.374	0.21	99	138.9	0.23
HS1-06	Hot-Start Transient	0.11	2.87	4.19	5.917	0.21	97	5.714	0.23	97	144.0	0.24
HS1-07	Hot-Start Transient	0.18	2.80	4.20	5.680	0.18	98	5.325	0.22	96	147.1	0.25
HS1-08	Hot-Start Transient	0.16	2.65	4.11	5.478	0.19	97	5.054	0.22	97	147.0	0.24
SS1100L-04	1100 rpm/25% load	5.16	17.89	16.70	2.259	0.94	83	4.406	1.25	87	96.2	1.10
SS1100L-05	1100 rpm/25% load	3.87	14.76	13.95	4.195	0.76	84	4.232	0.89	86	92.9	0.79
SS1100L-06	1100 rpm/25% load	4.34	19.22	16.80	3.774	0.99	86	3.988	1.17	87	96.0	1.13
SS1100L-07	1100 rpm/25% load	4.92	17.53	16.57	3.669	0.86	85	3.885	1.03	85	87.1	0.98
SS1100L-08	1100 rpm/25% load	3.33	17.74	15.69	3.830	0.89	85	3.879	1.06	87	84.1	0.93
SS1100H-04	1100 rpm/50% load	0.08	2.22	4.59	8.393	0.11	98	8.884	0.13	97	212.6	0.13
SS1100H-05	1100 rpm/50% load	0.07	2.08	4.65	9.606	0.12	97	8.201	0.13	98	208.1	0.13
SS1100H-06	1100 rpm/50% load	0.09	2.32	4.73	9.539	0.13	98	8.651	0.14	98	236.3	0.15
SS1100H-07	1100 rpm/50% load	0.09	2.10	4.81	9.332	0.12	97	8.605	0.13	97	222.1	0.14
SS1100H-08	1100 rpm/50% load	0.07	2.09	4.66	9.089	0.12	98	8.404	0.13	98	222.3	0.14
SS1900H-04	1900 rpm/50% load	0.13	1.69	7.33	7.508	0.16	93	9.116	0.20	89	206.3	0.20
SS1900H-05	1900 rpm/50% load	0.36	1.67	3.58	8.601	0.17	93	8.927	0.20	93	231.7	0.23
SS1900H-06	1900 rpm/50% load	0.35	1.65	3.70	8.665	0.18	95	9.095	0.20	94	228.4	0.23
SS1900H-07	1900 rpm/50% load	0.29	1.82	3.52	9.308	0.19	92	9.655	0.22	92	240.0	0.24
SS1900H-08	1900 rpm/50% load	0.28	1.83	1.18	9.539	0.19	92	9.034	0.23	92	236.0	0.23

Table 10 Percent organics of total particulate

Test No.	90 mm Wt.[a]		20x20 Wt.[b]	20x20 Ext.[c]	Vacuum Oven[d]		DFI/GC[e]	
	Filter	SOF, %	SOF,%	SOF, %	Filter	TVF, %	Filter	VOF, %
CS1-04	B	21	18	22	A	15	A	18
CS1-05	A	22	19	22	B	21	B	19
CS1-06	B	17	16	20	A	13	A	16
CS1-07	A	19	17	--[f]	B	16	B	17
CS1-08	B	21	18	22	A	16	A	17
Average		20	18	22		16		17
HS1-04	B	18	17	20	A	12	A	16
HS1-05	A	19	19	22	B	18	B	17
HS1-06	B	14	16	20	A	11	A	17
HS1-07	A	18	17	21	B	13	B	18
HS1-08	B	16	17	21	A	14	A	19
Average		17	17	21		13		17
SS1100L-04	B	61	61	60	A	54	A	38
SS1100L-05	A	71	64	68	B	60	B	45
SS1100L-06	B	66	61	63	A	57	A	48
SS1100L-07	A	65	59	--[f]	B	53	B	41
SS1100L-08	B	65	64	66	A	53	A	44
Average		66	62	64		56		43
SS1100H-04	B	13	11	14	A	5	A	10
SS1100H-05	A	11	10	14	B	8	B	10
SS1100H-06	B	11	10	14	A	5	A	11
SS1100H-07	A	12	11	16	B	9	B	12
SS1100H-08	B	11	10	14	A	6	A	12
Average		11	11	14		7		11
SS1900H-04	B	57	57	58	A	50	A	51
SS1900H-05	A	59	58	81	B	53	B	54
SS1900H-06	B	57	58	60	A	74	A	57
SS1900H-07	A	67	64	71	B	59	B	64
SS1900H-08	B	64	64	66	A	62	A	62
Average		61	60	67		59		58

[a]Solvent extraction of 90 mm filter set--filter weight loss determination of SOF.
[b]Solvent extraction of 20x20-inch filter set--filter weight loss determination of SOF.
[c]Solvent extraction of 20x20-inch filter set--weight of extract determination of SOF.
[d]Vacuum analysis of 90% of 90 mm filter set.
[e]DFI/GC analysis of 10% of 90 mm filter set.
[f]Analysis not conducted.

tems was shown to be statistically equivalent at the 95 percent confidence level using the ANOVA statistical technique. The 20 × 20-in. filter system possibly gave different particulate emission rates because the sampling system and conditions were not as closely controlled as for Systems A and B.

Organic Analysis Results. Values for percent organics in total particulate are given in Table 10. SOF was determined for one of the 90 mm filter sets by weight loss method. For the 20 × 20-in. filters, the SOF was determined both by weight loss method and by weighting of the dried extract (SOF) directly. Vacuum oven determinations of TVF and DFI/GC determinations of VOF were conducted as previously described.

The calculation of SOF, TVF, and VOF percent of total particulate is as follows:

$$\%\text{SOF, TVF, or VOF of Total Particulate} = \frac{\text{SOF, TVF, or VOF}}{\text{Part. Wt.}} \times 100\%$$

where:

Part Wt. = weight of particulate on filter(s) (mg)

In general, average organic values determined by each method are *not* all similar over a given test cycle. The average organic percentages obtained from all methods of analysis were compared using ANOVA to determine at the 95 percent confidence level which results of analyses are different. The five test cycles used in this program (cold-start transient, hot-start transient, steady-state 1100 rpm/25 percent load, steady-state 1100 rpm/50 percent load, and steady-state 1900 rpm/50 percent load) were compared using six ANOVA analyses. The sixth ANOVA was an analysis of the composite cold- and hot-start test results.

The procedures that were found to be equivalent using multiple comparison techniques following the ANOVAs are denoted by connected asterisks. The averages are ranked from smallest to largest.

Cold-Start Transient Tests 4 5 2 1 3 *—* *—* *—*
Hot-Start Transient Tests 4 2 1 5 3 * *—*—* *
Steady-State 1100 rpm/25% Load Tests 5 4 2 3 1 * * *—* *—*
Steady-State 1100 rpm/50% Load Tests 4 2 5 1 3 * *—*—* *
Steady-State 1900 rpm/50% Load Tests 5 4 2 1 3 *—*—*—* *—*—*—*
Combined Cold- and Hot-Start Transient Tests 4 5 2 1 3 * *—*—* *

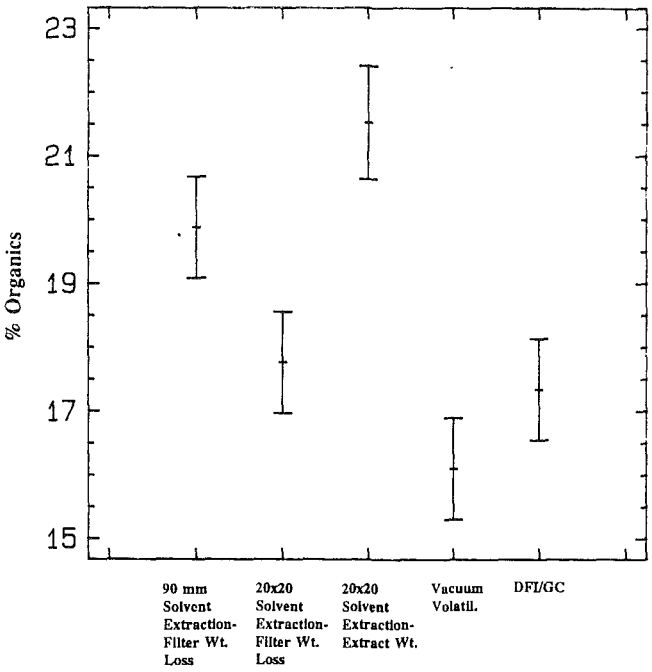

Fig. 18 Plot of averages and 95 percent confidence limits for cold-start transient test organics by analysis method

1 = Solvent extraction of 90 mm filter set—filter weight loss determination of SOF.
2 = Solvent extraction of 20 × 20-in. filter set—filter weight loss determination of SOF.
3 = Solvent extraction of 20 × 20-in. filter set—weight of extract determination of SOF.
4 = Vacuum analysis of 90 percent of 90 mm filter set.
5 = DFI/GC analysis of 10 percent of 90 mm filter set.

Figure 18 is a graphic illustration of these results. It contains a plot of all five averages and 95 percent confidence intervals about each average for organic determinations of the cold-start transient tests. Figures 19, 20, 21, and 22 are similar plots for the hot-start transient tests, steady-state condition 1100 rpm/25 percent load, 1100 rpm/50 percent load, and 1900 rpm/50 percent load, respectively. The conclusions from these plots are similar to those from the multiple comparison results. Because the cold- and hot-start transient test results are of primary importance in industry and are used to certify engines, a final analysis was run using the composite of cold- and hot-start data collected. Figure 23 is an illustration of these results.

From this statistical analysis and the accompanying plots, it is clear that different methods of analysis can give similar organic percentages for each test condition. For example, as indicated in Fig. 19, results from DFI/GC are most similar to the 90 mm and 20 × 20-in. filter extraction/weight loss analyses for the hot-start transient test. Conversely, DFI/GC appears to give different values for organics when compared to the vacuum oven method and the 20 × 20-in. extract weight method for the same test conditions. Although the five averages are *statistically* different from one another, overall the five methods of analysis provide roughly the same organic percentages. For the vacuum oven, discrepancies can likely be explained by the high blank filter weight interference values, which drastically alter results if changed slightly. The 20 × 20-in. extract weight and the 90 mm filter weight loss methods both rely on the ability accurately and repeatably to determine small weight differences. Consequently, for individual analyses, small weighing inconsistencies and physical handling errors can potentially cause large variations in SOF percentages.

Several additional observations can also be noted as a result of statistical analysis:

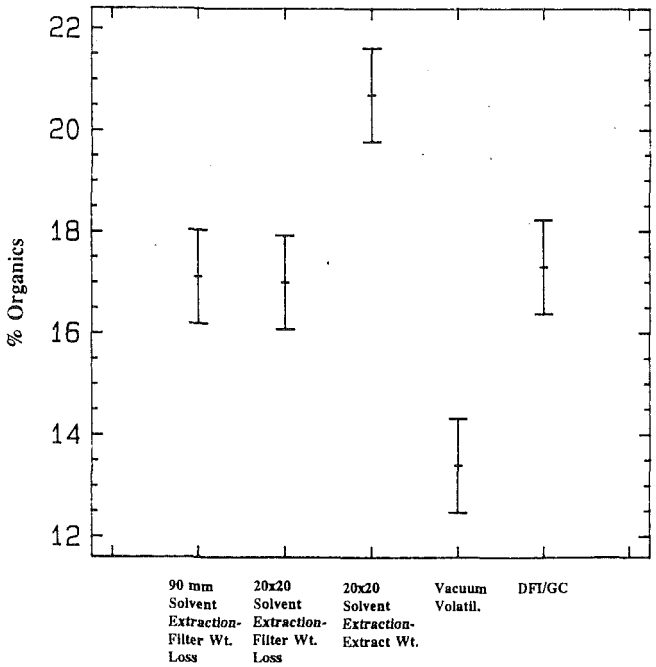

Fig. 19 Plot of averages and 95 percent confidence limits for hot-start transient test organics by analysis method

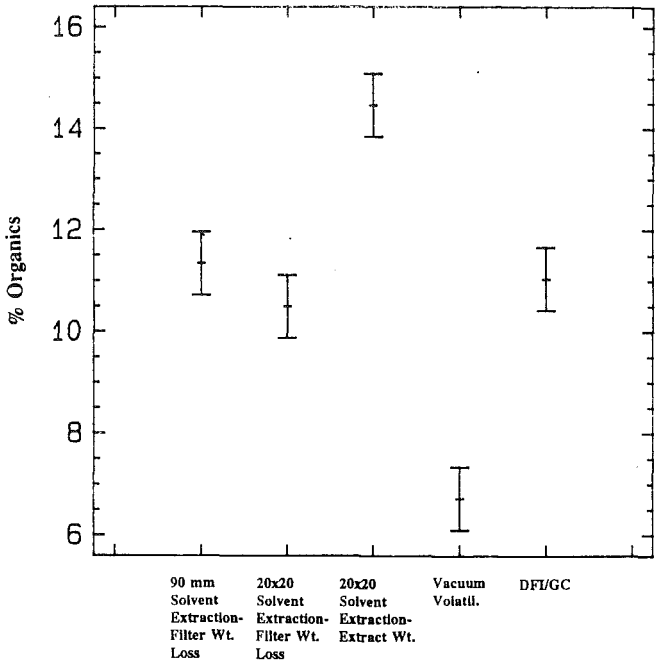

Fig. 21 Plot of averages and 95 percent confidence limits for steady-state 1100 rpm/50 percent load test organics by analysis method

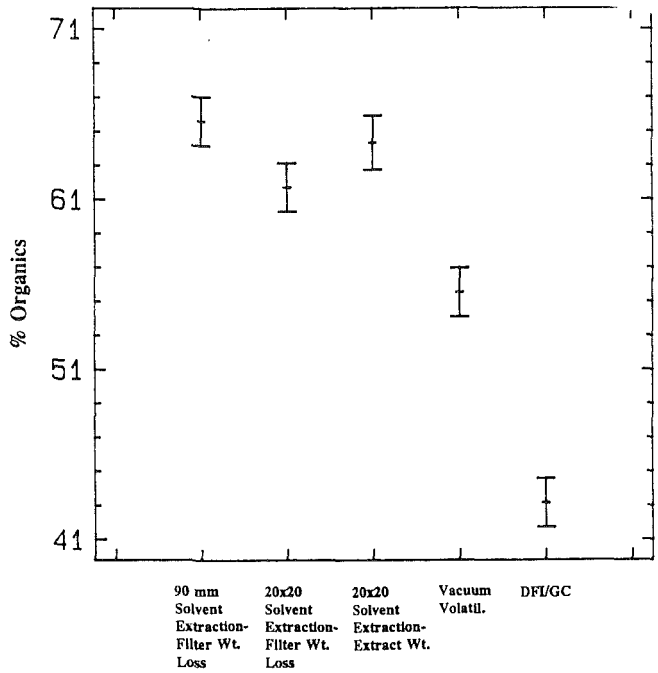

Fig. 20 Plot of averages and 95 percent confidence limits for steady-state 1100 rpm/25 percent load test organics by analysis method

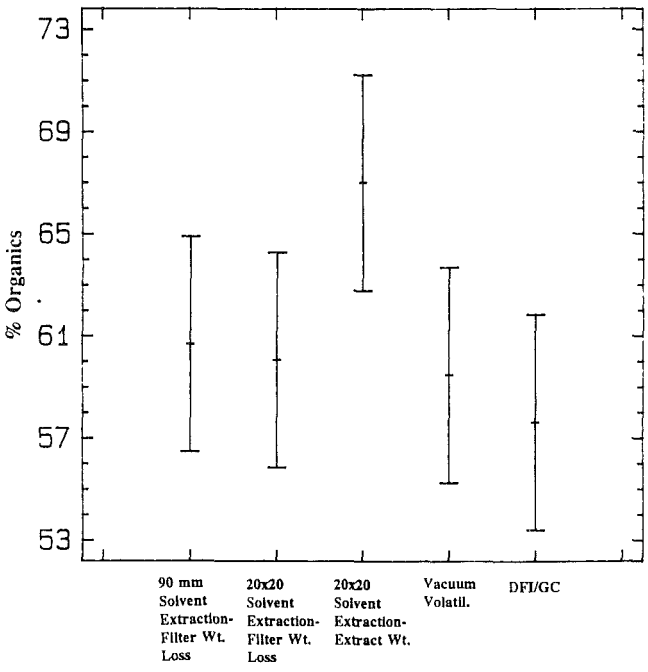

Fig. 22 Plot of averages and 95 percent confidence limits for steady-state 1900 rpm/50 percent load test organics by analysis method

- The average organic percentage from the DFI/GC method was equivalent (within the 95 percent confidence level) to the average organic percentage from the 20×20-in. solvent extraction/filter weight loss (20×20 WL) method for five of the six (including all transient) tests. The only exception was the 1100 rpm/25 percent load test.
- Both DFI/GC and 20×20 WL were also shown to be equivalent to the 90 mm filter set solvent extraction/filter weight loss (90 WL) method for four of the six tests. The exceptions in this case were the 1100 rpm/25 percent load test and the cold-start transient test.
- Overall results from the DFI/GC method most closely compare to the 20×20 WL and 90 WL methods.
- The 20×20-in. filter solvent extraction/extract weight method (20×20EW) gave statistically different averages from the DFI/GC method for *all* tests.
- The 20×20EW method also gave statistically different averages than *all* of the other methods of analysis in three of the six tests.
- The vacuum over method gave statistically different averages than *all* of the other methods in three of the six statistical tests.

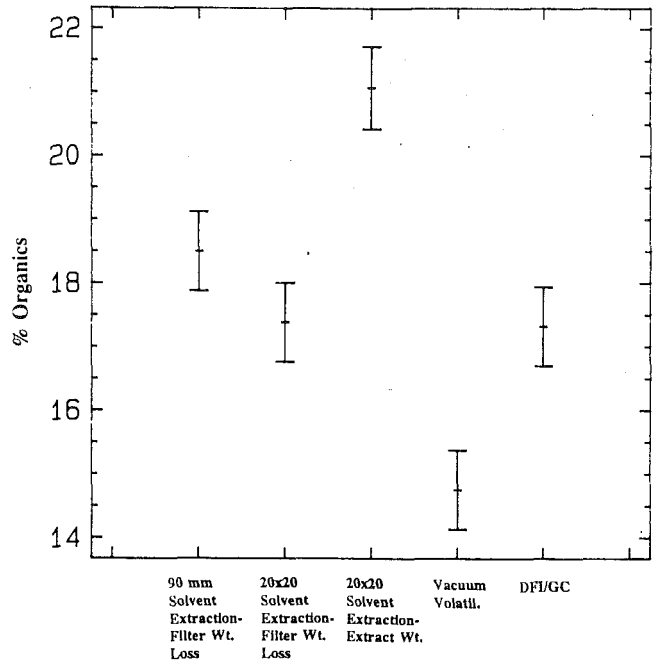

Fig. 23 Plot of averages and 95 percent confidence limits for cold- and hot-start transient test organics by analysis method

Unburned Lubricating Oil Analysis Results. Two different analyses were used in this program to determine the contribution of unburned lubricating oil to the organic portion of diesel particulate emissions. The first analysis was an interpretation of existing DFI/GC data by the method described previously. The second analysis was a GC analysis of the SOF (SOF/GC) obtained from the Soxhlet extraction of the 20 × 20-in. filter samples. This GC analysis was followed by the interpretive analysis of the GC chromatogram that was also described previously. Both the DFI/GC and SOF/GC analyses yield an unburned lubricating oil percentage of organics in the particulate; however, several important differences exist. First, the DFI/GC analysis uses both the primary *and* backup filters for analysis, whereas, the SOF/GC analysis does not. Second, the DFI/GC analysis uses directly the same EPA defined particulate filter samples (both primary and backup) that were used for mass emission determinations. The SOF/GC analysis is an *indirect* method that uses the extracted material from a *single* (no backup) filter collected under different sampling conditions than EPA-defined particulate samples. Consequently, a better representation of unburned lubricating oil contribution to the organics in particulate is expected from DFI/GC analysis.

As is evident from the data presented in Table 12, the DFI/GC typically identified a greater portion of the organic material as "other" than the SOF/GC analysis. This observation is expected for several reasons. First, organics that are volatile (and therefore detected by DFI/GC) but not soluble in methylene chloride (and therefore missed by SOF/GC), may be classified as "other." Second, as was mentioned earlier in this section, the SOF/GC analysis is an indirect analysis of the organic material from the filter. The associated extraction procedure to obtain the SOF involves a great deal of sample handling, which includes an evaporative step to completely remove all solvent and "dry" the extract prior to gravimetric determination of SOF. Consequently, it is probable that during the extensive sample handling and especially during the "drying" procedure, some of the "light ends" of the SOF that would normally be classified as "other" could be removed by evaporation with the solvent. These "light ends," however, would be detected by the DFI/GC analysis as no "drying" procedure or extensive sample workup is performed prior to analysis. Third, unlike EPA mass determinations, the SOF/GC analysis utilizes only one filter without a backup for sampling. It has been observed in previous individual DFI/GC filter analyses that "light ends" commonly classified as "other" can flow through a primary filter and not be condensed as "particulate" until reaching a secondary or backup filter. Since the SOF/GC analysis only has a primary filter to analyze, whereas the DFI/GC analysis considers both primary and backup filters, it is intuitively sound to expect a greater contribution of "other" to organic by DFI/GC than by SOF/GC. This theory is, in fact, supported by the data presented in Table 11 as every test condition shows an average of between 4 and 14 percent greater "other" contribution to organics by DFI/GC. Therefore, the consequence of both extensive handling prior to SOF/GC and the analysis of only a primary filter extract likely causes an overestimation of the unburned lubricating oil contribution to the organic fraction of the particulate. These arguments favor using the DFI/GC to quantify unburned lubricating oil contribution to diesel particulate.

Table 11 Contribution of unburned lubricating oil and "other" by DFI/GC and SOF/GC analysis

	% Oil		% Other	
Test No.	DFI/GC	SOF/GC	DFI/GC	SOF/GC
CS1-04	39	56	61	44
CS1-05	37	55	63	45
CS1-06	35	43	65	57
CS1-07	50	--[a]	50	--[a]
CS1-08	36	49	64	51
Average	**39**	**51**	**61**	**49**
HS1-04	44	51	56	49
HS1-05	33	48	67	52
HS1-06	32	54	68	46
HS1-07	43	52	57	48
HS1-08	33	51	67	49
Average	**37**	**51**	**63**	**49**
SS1100L-04	25	37	75	63
SS1100L-05	32	45	68	55
SS1100L-06	30	42	70	58
SS1100L-07	29	--[a]	71	--[a]
SS1100L-08	27	35	73	65
Average	**29**	**39**	**71**	**61**
SS1100H-04	17	37	83	63
SS1100H-05	17	29	83	71
SS1100H-06	23	35	77	65
SS1100H-07	27	26	73	74
SS1100H-08	19	28	81	72
Average	**21**	**31**	**79**	**69**
SS1900-04	77	86	23	14
SS1900-05	85	82	15	18
SS1900-06	85	87	15	13
SS1900-07	86	90	14	10
SS1900-08	77	84	23	16
Average	**82**	**86**	**18**	**14**

[a]Analysis not conducted.

References

1 Cuthbertson, R. D., et al., "Direct Analysis of Diesel Particulate-Bound Hydrocarbons by Gas Chromatography With Solid Sample Injection," SAE Paper No. 870626, 1987.

2 Swarin, S. J., "Liquid Chromatographic Determination of Benzo(*a*)pyrene in Diesel Exhaust Particulate: Verification of Collection and Analytical Methods," General Motors Research Laboratories Report GMR-3127, 1979.

3 Warner, M. A., "Filter Extraction Procedures and Results for Various EPA/ECTD Particulate Samples," EPA Report 460/3-82-008, Aug. 1982.

4 Detroit Diesel Corporation In-House Procedure.

Development of the Long-Stroke Version of the Mitsubishi SU Diesel Engine

Y. Nakamura

M. Ito

H. Arakawa

Mitsubishi Heavy Industries, Ltd.,
Sagamihara Machinery Works,
Kanagawa, Japan

A Mitsubishi S6U2 six-cylinder, in line diesel engine has been developed as a long-stroke version of the SU engine with a bore of 240 mm. This SU engine has a production record of more than 300 units. The stroke of this long-stroke version is 300 mm, compared with 260 mm for present SU engines. This paper introduces the S6U2 engine, which has now been put into regular production and describes research that has been conducted through the period of development. In the aspect of performance in particular, this paper explains reduction in fuel consumption by optimizing inlet and exhaust valve timings and improving turbocharger performance, and the reduction of NO_x by modifying the fuel injection system. In the aspect of reliability, this paper explains FEM calculation with a three-dimensional model and a stress measurement under real operation for the crankshaft. The results of stress measurement on the crankcase are also described.

Introduction of S6U2 Diesel Engine

Mitsubishi SU engine with a bore of 240 mm were developed in the latter half of the 1970's and more than 300 units of this series in total have been produced. They are now working all over the world as generating, cogeneration system, water pump driving, compressor driving, marine propulsion, and marine generating engines.

This SU engine series comprises 6- and 8-cylinder engines of in-line configuration, and 12- and 16-cylinder engines of vee configuration. It covers a power range of about 750 kW to 3680 kW at speeds of 720 rpm to 1200 rpm. The service life of the oldest SU series engine is now over 40,000 hours.

The new long-stroke, in-line, six-cylinder S6U2 engine has been developed making full use of experience through the development and the production of SU series engines and incorporating state-of-the-art technology. Table 1 shows the principal characteristics of the S6U2 engine along with those of the S6U.

Figure 1 shows the cross section of this engine and Fig. 2 shows the outer appearance of generator set. This engine has been developed under the same philosophy as SU series engines, so it retains the design features of the SU engine, such as light weight, compactness, high output, low specific fuel consumption, and high reliability. The following features have been added to the above by making its stroke longer:

1 This engine has been uprated by 15 percent at the same speed in comparison with the SU engine by making its stroke longer. Engines driving generators of 50 Hz and 60 Hz in particular can develop 1000 kW at 1000 rpm and 900 rpm as continuous service output at a generator end even for radiator specification.

Table 1 Principal characteristics of S6U2 engine

ITEM \ MODEL		*Mitsubishi S6U2*	*Mitsubishi S6U*
Type		4 stroke cycle, water cooled turbocharged, diesel engine	4 stroke cycle, water cooled turbocharged, diesel engine
Cylinder arrangement		In-line – 6	In-line – 6
Bore x stroke		ϕ 240 x 300 mm	ϕ 240 x 260 mm
Total displacement		81.4 liters	70.6 liters
Rated output/ Engine speed	50 Hz	1330 kW/1000 rpm	1160 kW/1000 rpm
	60 Hz	1200 kW/900 rpm	1230 kW/1200 rpm
Mean effective pressure		19.6 bar (1000 rpm)	17.7 bar (1200 rpm)
Piston speed		10.0 m/s (1000 rpm)	10.4 m/s (1200 rpm)
Compression ratio		13.5 : 1	12.5 : 1
Weight (dry)		8200 kg	8000 kg
Dimension length x width x height		3194 x 1379 x 2119 mm	3075 x 1410 x 2100 mm

Thanks to uprating and increases of less than 3 percent in both weight and volume in comparison with S6U, this in-line engine has a smaller specific weight of 5.6 kg/kW at maximum output and smaller specific volume as well. Figure 3 shows its power range with that of the SU series.

2 The combination of a longer stroke, a turbocharger with high efficiency that has been developed for this engine, a newly developed high-pressure injection system, and optimized inlet and exhaust valve timings has achieved specific fuel consumption as low as 193 g/kWh at rated output of bmep 19.6 bar at 1000 rpm. Figure 4 shows the standard performance curve.

3 This engine has maximal interchangeability of parts with the present SU series. Thus ease of part supply can be achieved.

Contributed by the Internal Combustion Engine Division and presented at the Energy-Sources Technology Conference and Exhibition, Houston, Texas, January 26–30, 1992. Manuscript received by the Internal Combustion Engine Division November 1, 1991, Paper No. 92-ICE-17. Associate Technical Editor: J. A. Canton.

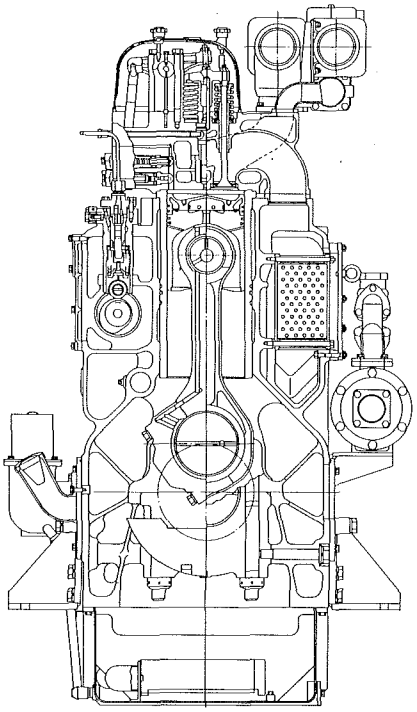

Fig. 1 Cross section

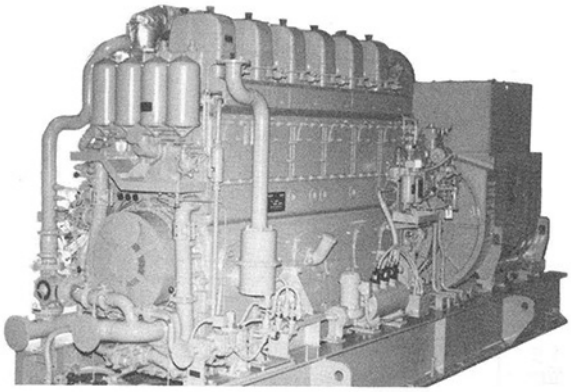

Fig. 2 Outer appearance of S6U2 gene-set

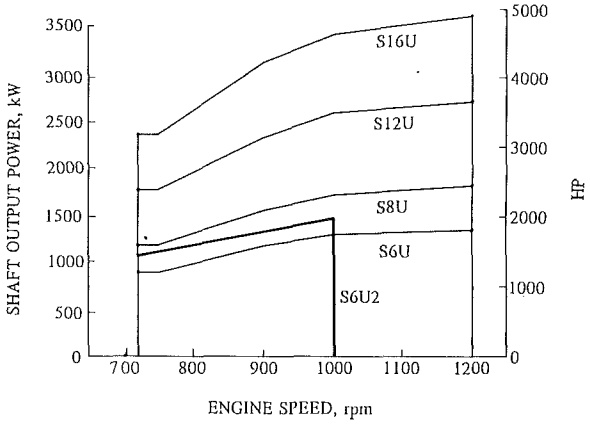

Fig. 3 SU engine output

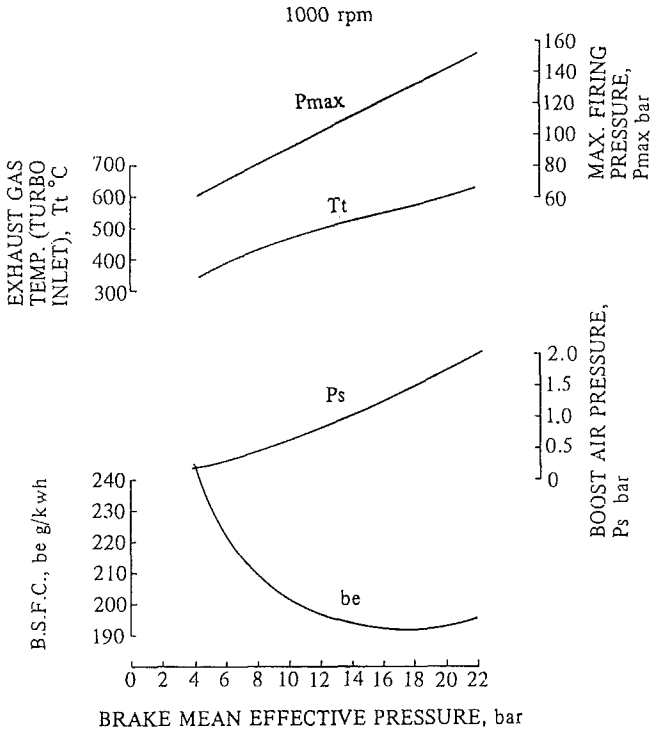

Fig. 4 S6U2 engine standard performance

That is, main parts that are different from those of the SU series engines are the crankcase (more than 90 percent of patterns are common), crankshaft, piston, connecting rod, and push rod, and most parts other than the above are readily available. Thus interchangeability of parts of more than 90 percent has been realized.

4 For reliability, no maintenance period of 3000 operating hours has now been realized by incorporating the fruits of research through the development and production phases of SU series. To confirm the reliability and durability for the parts and components different from those of present SU engines, simulation calculation by FEM, etc., and measurement at component tests, at single cylinder engine tests and at the S6U2, real engine tests under actual loads have been performed.

Reduction in Specific Fuel Consumption

From the viewpoint of maximal interchangeability of parts with SU engines, simulation calculation and single-cylinder tests have been started and performance analysis has been performed with the assumption that the fuel injection system and inlet/exhaust cam system for the S6U2 engine, which strongly influence specific fuel consumption, are those of the SU engine.

As a result, first, it has been found that the fuel injection system must be optimized and various kinds of investigation have been made. Through these investigations, the fuel injection cam and fuel injection pump have been modified and the specific fuel consumption has been lowered by 1.5 percent by raising injection pressure and shortening injection duration.

Second, inlet and exhaust timings have been optimized and the fuel consumption has been lowered by 2.8 percent by improving performance during the gas exchange period.

Third, the specific fuel consumption has further been lowered by 1.3 percent by improving the exhaust gas turbocharger.

Furthermore, the combustion mode has been changed by modifying the fuel cam to decrease NO_x emission from the viewpoint of environmental pollution control and, as a result, NO_x has been decreased by 10 to 20 percent without worsening specific fuel consumption.

Table 2 S6U2 improvement process

ITEM \ DEVELOPMENT STAGE		S6U	S6U2 (STEP 1)	S6U2 (STEP 2)	S6U2 (STEP 3)
FUEL INJECTION SYSTEM	FUEL CAM (mm/deg.)	0.55 (1.65 m/s at 1000 rpm)	0.62 (1.86 m/s at 1000 rpm)	0.62 (1.86 m/s at 1000 rpm)	0.65 (1.95 m/s at 1000 rpm)
	PLUNGER DIA. mm	ϕ18	ϕ22	ϕ22	ϕ20
	NOZZLE TIP	8 x ϕ0.37 x 150°	10 x ϕ0.40 x 155°	10 x ϕ0.40 x 155°	10 x ϕ0.40 x 155°
INLET, EXHAUST TIMING °CA		IVO 302 – IVC580 EVO 126 – EVC 404	IVO 302 – IVC580 EVO 126 – EVC 404	IVO 314 – IVC570 EVO 116 – EVC 394	IVO 314 – IVC570 EVO 116 – EVC 394
TURBOCHARGER		TC24	TC24	TD24	TD24
FUEL CONSUMPTION AT RATED OUTPUT g/kW·h		204	201	193	193
NOx % (Compared with S6U2 STEP 2)		–	–	100%	80 to 90%

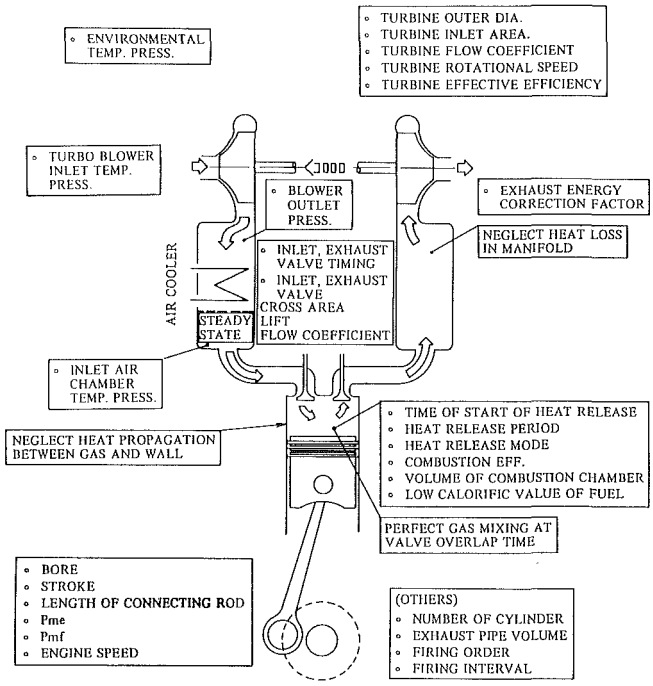

Fig. 5 Engine performance simulator

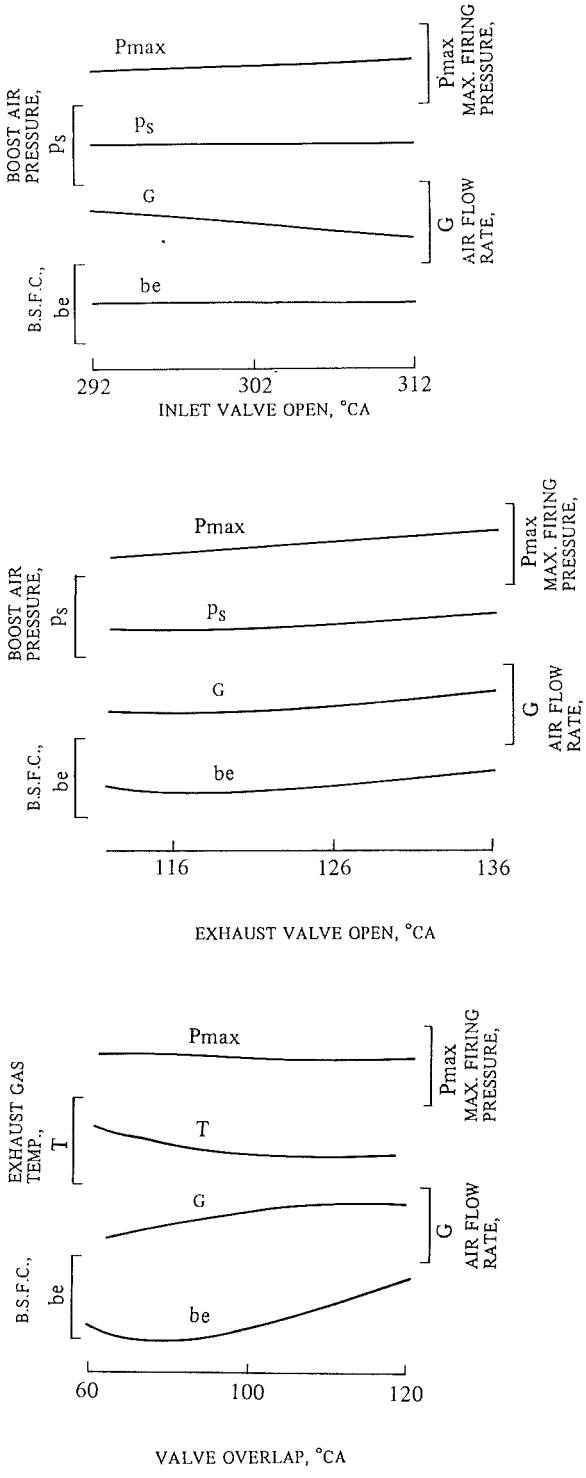

Fig. 6 Results of simulation calculation

Results of the abovementioned fuel consumption improvement and NO_x reduction are described herein-after. Table 2 summarizes the process of the improvement of fuel consumption of the S6U2 engine.

Optimization of Gas Exchange Process by Modifying Inlet and Exhaust Cam Timings. For the optimization of inlet and exhaust cam timings, optimum timings have been selected by simulation calculation with computer using a performance simulator and then their effects have been confirmed in the single cylinder engine and finally with the tests of the S6U2 engine.

1 Calculation Using a Performance Simulator. Figure 5 shows the outline of the simulator that has been developed for this engine. This simulator adopts various constants, which have been determined by collating many experimental data on the SU engines, and so has sufficiently high accuracy in coincidence with the actual engine. Using this simulator, performance calculations for the S6U2 engine have been made, changing the inlet and exhaust valve timings, and optimum timings have been selected at the rated output of bmep 19.6 bar at 1000 rpm of this engine.

As an example of the calculation results, Fig. 6 shows changes in performance with various opening timings and overlap angles of the inlet and exhaust valves. Noticeable points that can be seen here are the facts that the specific fuel consumption can be improved by advancing the opening timing of the exhaust valve from the previous 126°CA to 116°CA and that the specific fuel consumption can be minimized by keeping the overlap angle at 80°CA with a moderate rise in exhaust temperature. Figure 7 shows the best timings obtained by these tests and Fig. 8 shows low-pressure diagram with a weak spring.

As shown in Figs. 7 and 8, pumping work has been decreased by optimizing inlet and exhaust valve timings. This amount of decrease becomes larger than the loss of expansion work by advancing the exhaust valve timing.

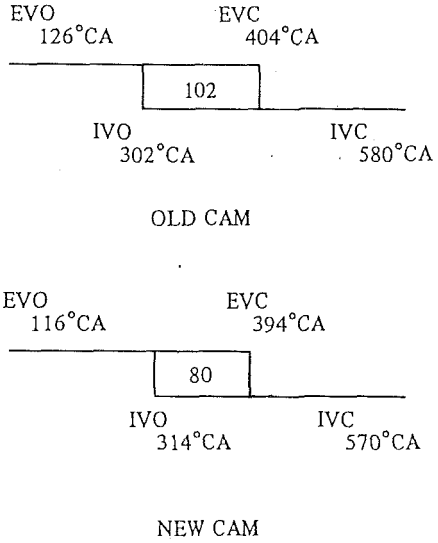

Fig. 7 Inlet, exhaust cam timing

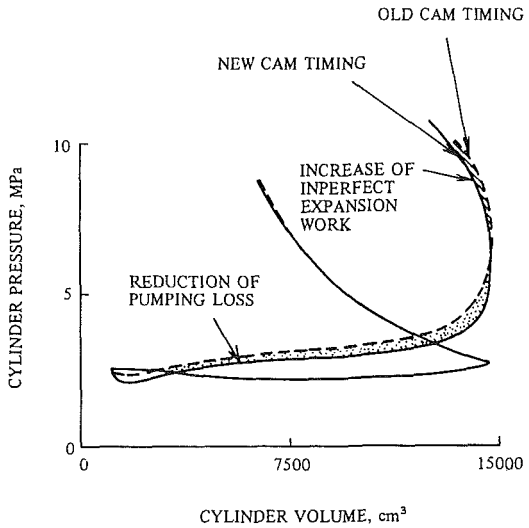

Fig. 8 Low-pressure diagram

As a result, a reduction of about 4 g/kWh in specific fuel consumption has been expected.

2 Tests With the S6U2 Engine. A camshaft with optimum cam timings that have been selected from calculation results with the abovementioned simulator has been manufactured and incorporated into the S6U2 engine. Then confirmation tests have been carried out with this engine. At that time, for the turbocharger, the optimum design of the blower side has been performed, first taking the abovementioned simulation results into consideration and aiming at the following:

(*a*) To obtain high efficiency not only on the larger but also on the smaller flow rate side.

(*b*) To give a margin against blower surging.

After many tests, this turbocharger has matched well with the engine. As a result, by changing the inlet and exhaust cam timings and turbocharger of the same S6U2 engine, a reduction of 5.5 g/kWh in specific fuel consumption has been confirmed at the rated output of bmep 19.6 bar at 1000 rpm, keeping exhaust temperature and cylinder pressure almost the same, as shown in Fig. 9. In this figure, the superiority of new cam, which corresponds to Step 2 timings in Table 2, to old cam, which corresponds to Step 1 timings in Table 2, is clearly seen.

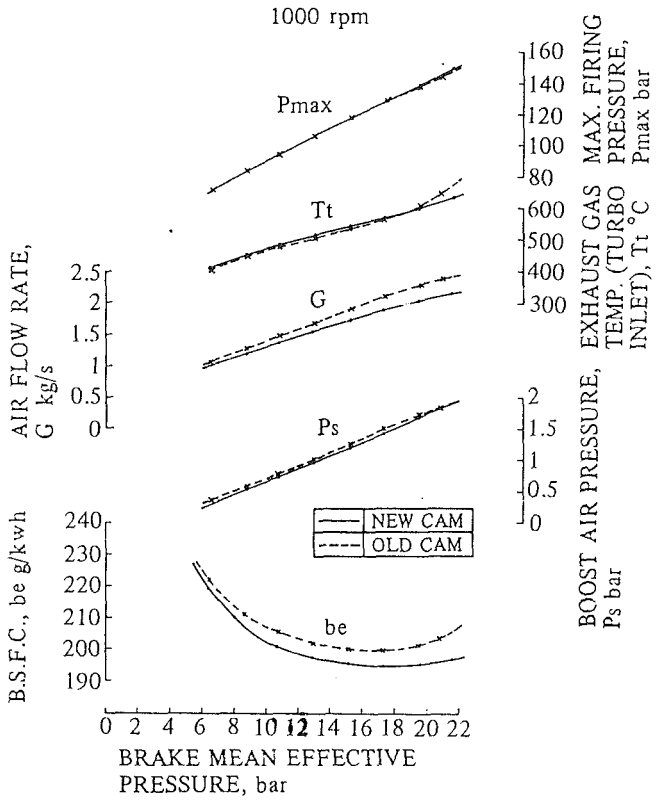

Fig. 9 S6U2 engine performance (inlet, exhaust cam comparison)

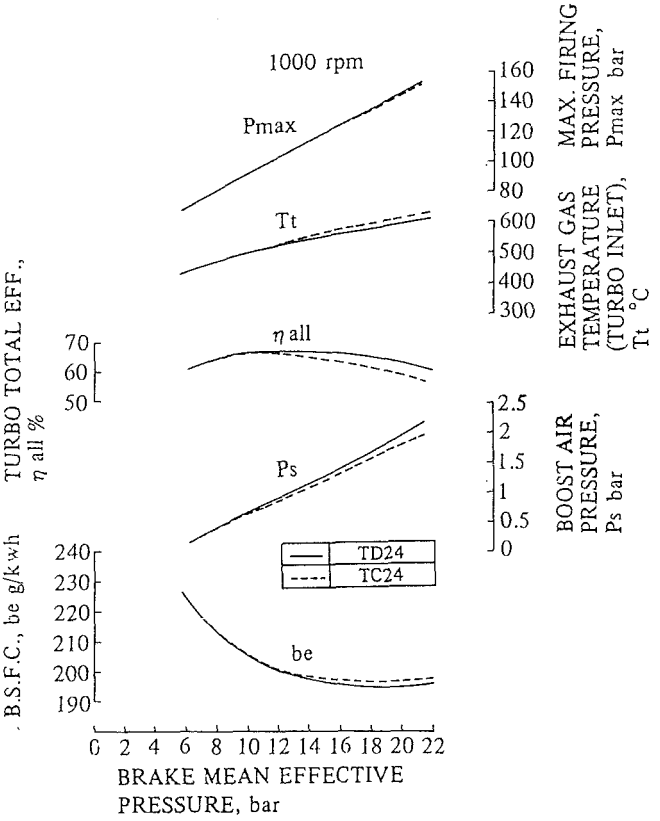

Fig. 10 S6U2 engine performance (turbocharger comparison)

Reduction in Specific Fuel Consumption by Improvement of Turbocharger. The high-efficiency TD24 turbocharger, which has a compressor wheel designed by the latest aerody-

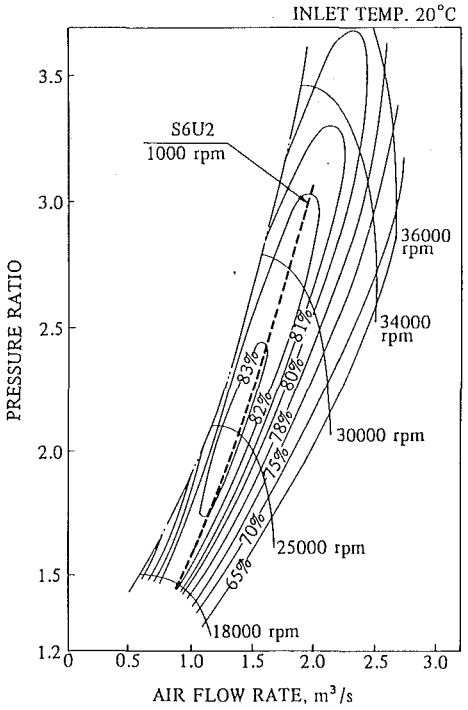

Fig. 11 TD24 compressor performance

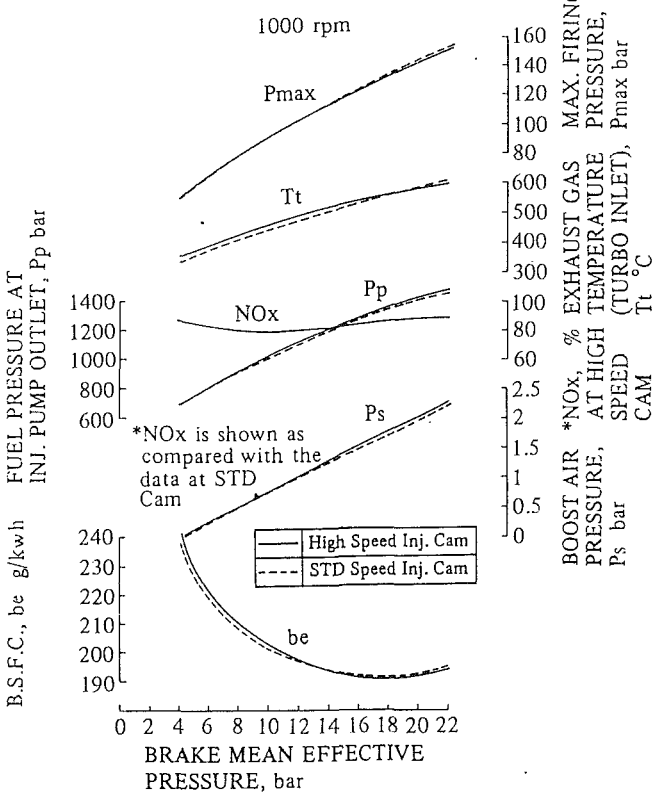

Fig. 13 S6U2 performance curve (injection cam comparison)

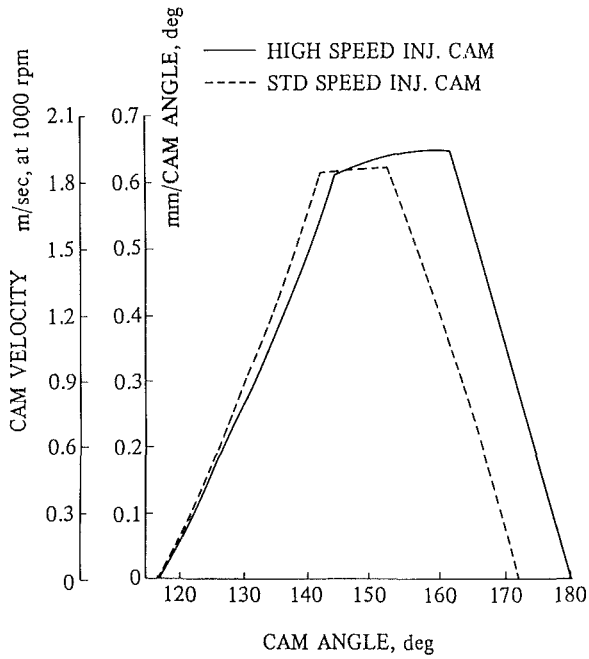

Fig. 12 Fuel injection cam

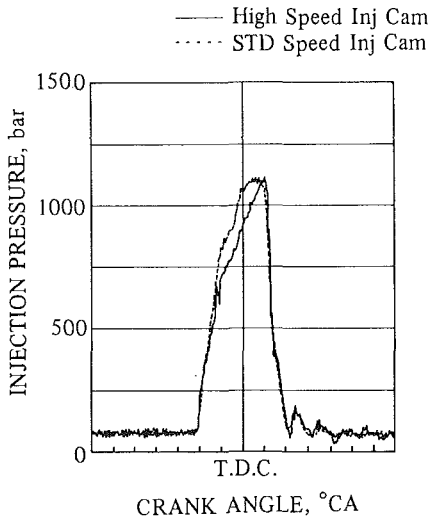

Fig. 14 Injection pressure (pme 21.5 bar)

namics, has been developed for this engine by Mitsubishi Heavy Industries Ltd. This turbocharger has been installed on the S6U2 engine, and tests with this engine have been performed to compare it with the TC24 turbocharger, which has been installed on present SU engine. As shown in Fig. 10, a reduction of 2.7 g/kWh in specific fuel consumption has finally been obtained after numbers of matching test. The improvement of about 4 percent in the overall efficiency of the turbocharger has contributed to it.

Figure 11 shows the operating line of the S6U2 engine on the compressor map of the TD24 turbocharger. It can be seen from this figure that the higher performance of this engine has been realized by making full use of the merits of the turbocharger with high efficiency over the wide range of air flow rate and boost air pressure.

Reduction of NO_x by Modification of the Fuel Injection Cam. Recently, clean diesel engines with low NO_x emission have become more and more necessary from the viewpoint of environmental pollution control. However, NO_x emission and fuel consumption are in a contradictory relationship in general and it is regarded to be difficult to improve both at the same time. Nevertheless, for the S6U2 engine, NO_x could be reduced by changing the combustion mode through modification of the fuel injection cam without sacrificing specific fuel consumption. Results are described below.

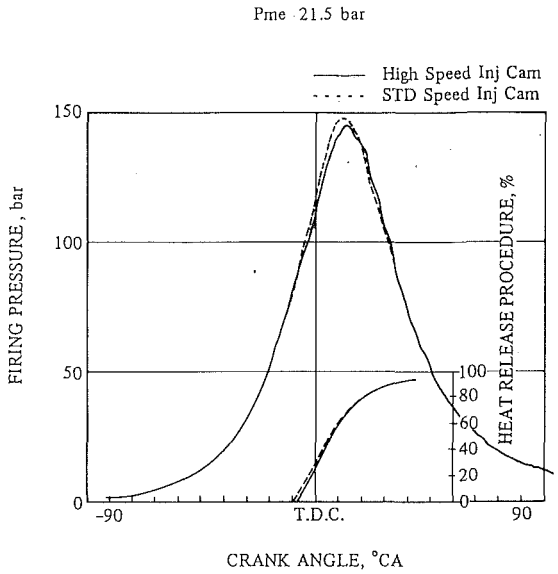

Fig. 15 Firing pressure

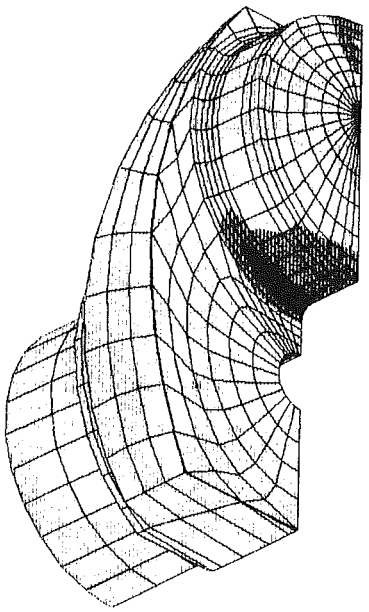

Fig. 16 Crankshaft model for FEM calculation and calculation result

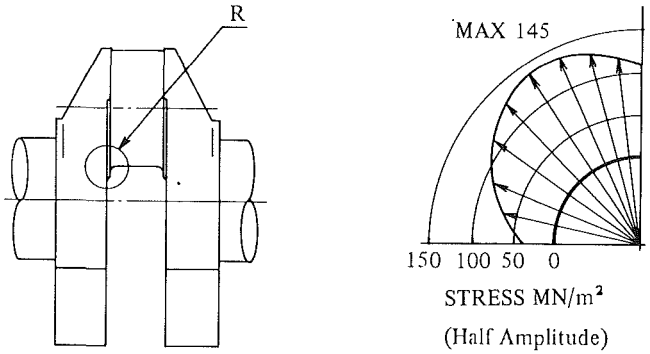

Fig. 17 S6U2 crankpin stress analysis

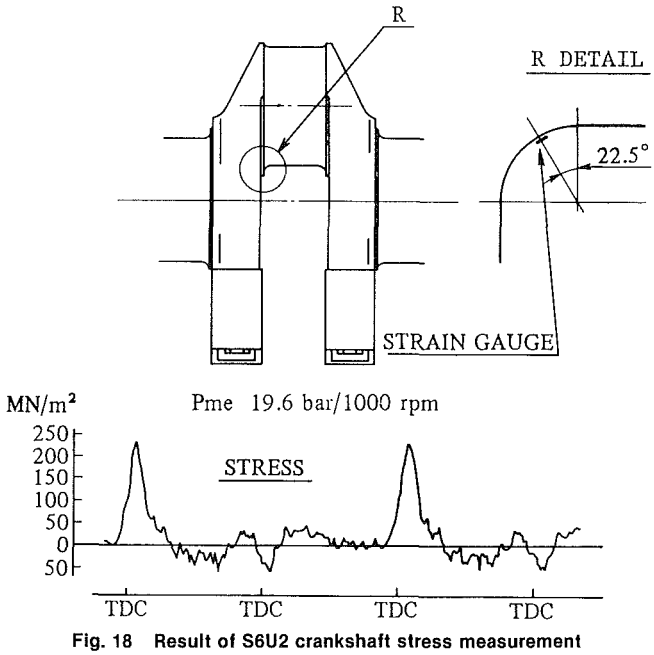

Fig. 18 Result of S6U2 crankshaft stress measurement

As seen in Fig. 12, the modified high-speed fuel injection pump cam, which corresponds to the Step 3 cam in Table 2, has such a shape that its velocity becomes higher than the STD speed cam, which corresponds to the Steps 1 and 2 fuel cam in Table 2, and its injection mode has a peak on the latter part compared with STD speed cam. Tests were performed with both cams installed in the same S6U2 engine.

As a result, NO_x has been reduced by 10 to 20 percent, keeping almost the same engine performance, such as specific fuel consumption and others. This is shown in Fig. 13. Figures 14 and 15 show injection pressure diagrams and cylinder firing pressure diagram taken at this test, respectively. It can be presumed from these figures that, in case of the modified high speed cam, combustion in an early stage has become gentle due to the moderate rise of injection pressure in an earlier stage of injection and the generation of NO_x has been suppressed. It can also be seen clearly from the heat release procedure shown in Fig. 15.

Improvement in Reliability

Three-Dimensional FEM Calculation and Stress Measurement on an Actual Engine for Crankshaft. When a stroke is made longer without changing a cylinder bore and a cylinder pitch, the crankshaft is most strongly influenced in the aspect of stress. As the stroke becomes longer, the overlap between crankpin and main journal decreases, so the bending and torsional fatigue strength of the crankpin fillet area tend to be lower.

In order to keep the safety factor of S6U2 crankshaft the same as those of SU series engine, the crankpin diameter has been increased from 180 mm for present SU engine to 190 mm and the shape of the crankweb has somewhat been modified.

Based on this design shape, FEM calculation has been performed with a three-dimensional solid model, and the stress concentration factor and stress distribution at the crankpin fillet area have been estimated accurately. In addition to this calculation, nominal bending and torsional stress calculations have been performed and been estimated with very high accuracy. In this calculation, the crankshaft is simulated as a beam that has two different sections and that is supported elastically on the base.

Thus the final shape of the crankshaft has been decided so

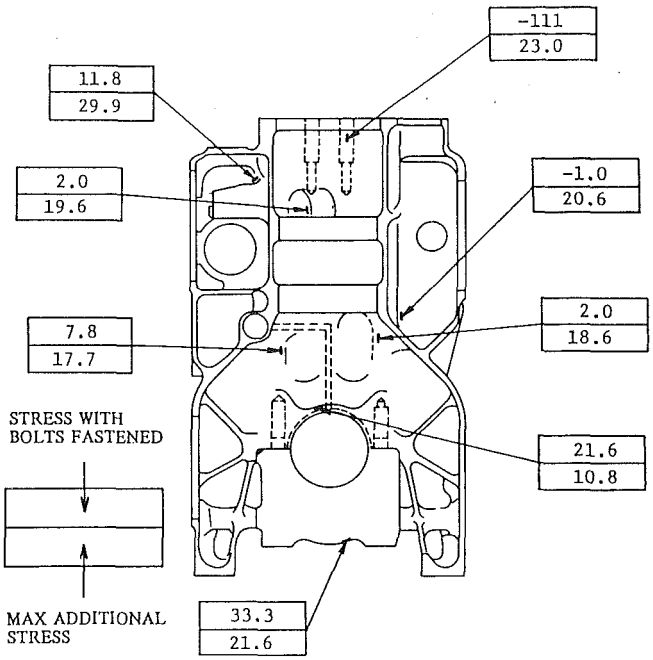

Fig. 19 S6U2 crankcase stress measurement

as to keep its stress low enough from the viewpoint of fatigue strength. Figure 16 shows a model for FEM calculation and Fig. 17 shows stress distribution obtained by calculation. These calculation methods have been applied to various crankshafts and their accuracy has been heightened by collating the results of stress measurement on many actual engines.

For this S6U2 engine also, strain gages have been put on the higher stress area, which was decided by calculation and its stress has been measured during actual operation. As shown in Fig. 18, measured stresses coincide well with expected values estimated by calculation including FEM analysis and thus the safety of the crankshaft has been confirmed.

Stress Measurement for Crankcase. The S6U2 engine has been designed so that, as far as possible, it can use the same crankcase as the S6U. This latter crankcase was designed to be compact and lightweight, and sufficiently rigid. Its effectiveness has been confirmed through many field experiences. However, since the length of the crankcase on the cylinder centerline increases with the increase of stroke, the areas where stresses were considered to increase have been modified by making full use of experience on the S6U. Although the stresses of these areas have naturally been checked by calculation using computers during the development phase of the S6U2, finally, strain gages have been put on the area where stresses are supposed to come into question and stresses have been measured during operation. Figure 19 shows the results of stress measurement during operation at rated output of bmep 19.6 bar at 1000 rpm. As seen in this figure, stresses have been equalized as a whole and they are on the same levels as those of S6U. Thus the safety of this crankcase has been confirmed.

Conclusion

The S6U2 diesel engine, which is a long-stroke version of the SU engine, has been developed with low specific fuel consumption, high reliability, and low NO_x emission by applying the fruits of research mentioned above. These features meet the requirement of not only customers but also extensive social demands in the aspect of resources and protection of environment. Further efforts to meet these demands will be made through perpetual improvement from now on.

References

Akita, H., Nakamura, Y., Ito, M., and Tanaka, M., 1989, "Improvement of Operational Reliability of 240 mm Bore Engine," presented at the 18th CIMAC.

Azuma, T., Matsumura, T., Akita, H., and Nakamura, Y., 1981, "Development of a High Speed Diesel Engine," presented at the 14th CIMAC.

Nakamura, Y., Ito, M., and Numata, A., 1990, "Capability to Burn Heavy Fuel and Kerosene for Mitsubishi 240 mm Bore SU Engine," presented at the 12th Annual Fall Technical Conference of the ASME Internal Combustion Engine Division.

Catalytic Control of NO_x, CO, and NMHC Emissions From Stationary Diesel and Dual-Fuel Engines

R. W. Bittner
Johnson Matthey,
Catalytic Systems Division,
Environmental Products,
Wayne, PA 19087

F. W. Aboujaoude
Fairbanks Morse,
Engine Division,
Beloit, WI 53511

Selective Catalytic Reduction (SCR) and oxidation catalyst technology have been applied to a stationary diesel and dual-fuel (natural gas and #2 diesel) engine for catalytic control of nitrogen oxides (NO_x), carbon monoxide (CO), and non-methane hydrocarbon (NMHC) emissions. At rated conditions, NO_x emissions have been effectively reduced by up to 90 percent, with little loss of SCR catalyst performance after 850 hours of operation. Using adequate control of the ammonia (NH_3) feed, the SCR system was capable of maintaining NH_3 slip to 10 ppm or less. CO and NMHC were reduced by 93 and 85 percent, respectively. Little soot was observed on the surface of the catalyst due to the use of a catalyst system that minimizes the buildup of heavy hydrocarbons on the catalyst surface. In addition, the catalyst structure effectively resisted the buildup of sulfur compounds that could cause premature deactivation of the catalyst.

One of the sources of NO_x, CO, and HC emissions is the combustion of fossil fuels in internal combustion engines [1]. Catalytic controls have been used effectively for many years to control these emissions from automobiles and stationary rich-burning engines. With the passage of the Clean Air Act Amendments of 1990, lean-burning heavy-duty engines such as diesel and dual-fuel engines will likely require emissions control. Catalytic technology can be effective in controlling emissions from lean-burning heavy-duty engines. A catalytic system was installed on the exhaust stream of a two-cylinder Colt-Pielstick PC2.5 engine to study its system capabilities in reducing NO_x, CO, and NMHC emissions. The catalyst system comprised a housing containing an oxidation catalyst, SCR catalyst, and an automated ammonia injection system. The demonstration took place at the Fairbanks Morse test facility in Beloit, WI. The objective was to achieve 90 percent NO_x reduction with no observable soot formation or degradation in catalyst activity.

To understand how to eliminate these emissions from the engine exhaust, a basic understanding of how NO_x, CO, and NMHC are formed is required. The formation of NO_x in internal combustion engines is primarily caused by the oxidation of N_2 in the air within the combustion chamber of the engine [2]. While both nitric oxide (NO) and nitrogen dioxide (NO_2) are formed as final products, NO is the predominant species omitted. NO_x formation is summarized by the following chemical reactions:

$$N_2 + O_2 \rightarrow 2NO \quad (1)$$

$$2NO + O_2 \rightarrow 2NO_2 \quad (2)$$

The three factors that contribute most to NO_x formation are: high combustion temperatures (needed for the high activation energy required to oxidize the stable nitrogen molecule), pressures, and oxygen availability.

The formation of CO in internal combustion engines is a result of incomplete combustion of the fuel, which occurs when there is sufficient oxygen near the hydrocarbon (fuel) molecule during combustion [3]. Also, incomplete combustion could be caused by the quenching of the hydrocarbon oxidation near a cold surface in the combustion chamber. Since diesel and natural gas fuels are predominantly hydrocarbons, some of these hydrocarbons will pass through the combustion chamber unreacted, thus retaining their original form in the exhaust stream. Other hydrocarbons will be partially oxidized and also remain in the exhaust stream.

In order to control these engine emissions, a catalytic system was constructed and is schematically shown in Fig. 1. This figure shows the catalytic system installed on the exhaust stream of the two-cylinder Colt-Pielstick engine. The exhaust gases pass through the oxidation catalyst first, then are mixed with ammonia before entering the SCR catalyst. The oxidation catalyst removes the CO and NMHC emissions by oxidizing them to CO_2 and H_2O [4]. The oxidation reactions are shown below:

$$2CO + O_2 \rightarrow 2CO_2 \quad (3)$$

$$CH_4 + 2O_2 \rightarrow CO_2 + 2H_2O \quad (4)$$

$$CnHm + O_2 \rightarrow CO_2 + H_2O \text{ (Not balanced)} \quad (5)$$

This process also results in the reduction of the heavy hydrocarbons, which minimizes the potential formation of soot on the SCR catalyst. Soot, if formed, would cause a reduction in the SCR catalyst activity. In addition, by placing the oxi-

Contributed by the Internal Combustion Engine Division and presented at the Energy-Sources Technology Conference and Exhibition, Houston, Texas, January 26-30, 1992. Manuscript received by the Internal Combustion Engine Division October 1, 1991. Paper No. 92-ICE-19. Associate Technical Editor: J. A. Caton.

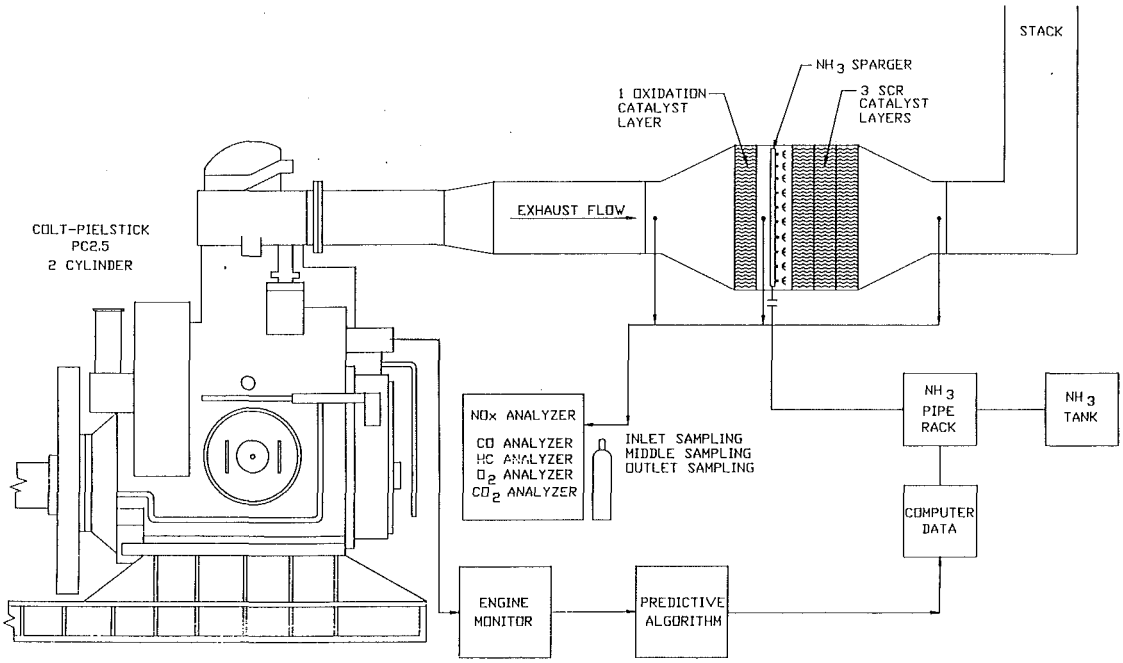

Fig. 1 Engine and catalyst system

dation catalyst upstream of the ammonia injection grid (AIG), the potential for oxidizing ammonia to form NO_x is eliminated.

To reduce NO_x emissions in the exhaust, an SCR base metal catalyst was used with ammonia (NH_3) as the reducing agent [5]. The NH_3 was injected into the exhaust stream and is intimately mixed with the exhaust. After mixing, the exhaust passed over the base metal catalyst, which resulted in the selective reduction of NO_x to form N_2 and H_2O. The principal chemical reactions are as follows:

$$6NO + 4NH_3 \rightarrow 5N_2 + 6H_2O \quad (6)$$

$$6NO_2 + 8NH_3 \rightarrow 7N_2 + 12H_2O \quad (7)$$

To achieve the desired NO_x reduction levels while minimizing NH_3 emissions, close monitoring of the NO_x emissions before and after the catalyst must be maintained with automatic control of the NH_3 feed. Insufficient supply of NH_3 would not give adequate NO_x reduction, while an excess of NH_3 would result in a large amount of NH_3 slip. After evaluation of a manual system, it was determined that an automatic control system was needed to insure maximum performance of the SCR catalyst during testing.

Experimental

System Components. The two-cylinder Colt-Pielstick PC2.5 test engine was run at the Fairbanks Morse test facility in Beloit, WI. The four-stroke test engine was lean-burn with a rated load of 1200 bhp at 514 rpm. Fairbanks Morse also supplied exhaust gas analyzers for NO_x, CO, HC, and NH_3 slip measurements. NO_x concentrations were measured using a Thermo Electron Model 10AR Chemiluminescent Analyzer. CO measurements were taken with an Infrared Industries Model IR-2200 Non-Dispersive Infrared Analyzer. Total Hydrocarbon (THC) measurements were made with a Horiba Model FIA-34A Flame Ionization Detector (FID). Methane (CH_4) was measured using a Horiba Hydrocarbon Cutter Model NMC-11A, which removed the heavy hydrocarbons from the gas samples. NMHC concentrations were then determined by subtracting the amount of CH_4 constituents from the THC measurements. Drager Detector Tubes were used to measure the amount of NH_3 slip after the catalyst.

Johnson Matthey supplied the Oxidation and SCR Catalytic System. The oxidation catalyst was composed of a precious metal coating on a metal monolith substrate. The SCR catalyst was composed of a base metal coating on a metal monolith substrate. The operating temperature range for the SCR catalyst is 600°F to 770°F. Johnson Matthey also supplied the anhydrous NH_3 delivering system, consisting of a pressurized tank, process pipe rack, and an ammonia injection grid (AIG). The ammonia control system was automated with the following equipment: Adac data acquisition system, PID controller, computer interface, orifice flow meters, differential pressure transmitters, and thermocouples. Measurements by thermocouples and differential pressure transmitters were used as input to the Adac data acquisition system to calculate the ammonia flow. The outputs of both the PID controller and the Adac data acquisition system were connected to a computer. Multiple screens on the computer were accessed to display alarms, NH_3/NO_x mole ratio, and other essential values.

Experimental Procedure. To determine the conversion efficiency required for each pollutant, the emissions of NO_x, CO, THC, NMHC, O_2, and CO_2 were measured. These tests were done at full rated load (1200 bhp at 514 rpm) to simulate power generation systems under peak conditions. Tests were performed to maximize the conversion efficiency of NO_x, CO, and NMHC by determining the effects of changing the following variables: NH_3/NO_x mole ratio, gas hourly space velocity (GHSV), and exhaust gas temperature. Emissions readings were used to determine the NH_3/NO_x mole ratio. An algorithm based on engine performance parameters and a predicted NO_x concentration for loads ranging between 50 and 100 percent was developed. The predicted NO_x value was transmitted to the computer, which references the desired NH_3/NO_x mole ratio and computed the NH_3 flow setpoint. The setpoint was compared to the actual NH_3 flow and was balanced through a PID algorithm. This automated setup resulted in accurate measurements of NH_3/NO_x mole ratio and allowed instantaneous changes in the NH_3/NO_x mole ratio setpoint during testing.

The term GHSV describes the residence time of the exhaust pollutants in the presence of the catalyst and is defined as follows:

Table 1 Typical engine exhaust gas emissions from the test engine

Constituents	Diesel Mode	Dual Fuel Mode
NOx (ppm)	1200	120
CO (ppm)	100	300
NMHC (ppm)	30	110
THC (ppm)	30	1600
O2 (%)	12	12
CO2 (%)	7	6

$$\text{GHSV } (h^{-1}) = \frac{\text{Volumetric gas flow rate (scfh)}}{\text{Catalyst volume } (ft^3)} \quad (8)$$

The higher the GHSV, the lower the residence time. For the oxidation catalyst panel the GHSV was 45,000 h^{-1}. For the three-panel SCR catalyst configuration the GHSV was 15,000 h^{-1}. The oxidation and SCR catalyst volumes were adjusted to determine the effect of varying GHSV on the conversion efficiency of the catalyst. The conversion or reduction efficiency of the catalyst is defined as the amount of NO_x, CO, and NMHC converted relative to its inlet concentration and is shown in the following equation:

$$\text{Conversion efficiency (percent)} = 100 \times \frac{[\text{Inlet}] - [\text{Outlet}]}{[\text{Inlet}]} \quad (9)$$

The effectiveness of the catalyst is generally improved with a lower rather than higher GHSV. The exhaust temperature was varied by adjusting the air/fuel ratio on the engine. A higher air/fuel ratio results in a colder exhaust.

Test Results

Table 1 lists typical exhaust gas emissions from the test engine. The table shows significant differences in exhaust emissions when operating in the diesel and dual-fuel modes. Therefore, to achieve maximum reduction of NO_x, CO, and NMHC emissions for both operating modes, the test variables, which include temperature, GHSV, and NH_3 feed, were optimized.

Oxidation Catalyst. As shown in Fig. 2, after 850 total hours of operation (230 hours in the diesel mode) the oxidation catalyst reduced the CO emissions by 90 and 93 percent, respectively, in diesel and dual-fuel modes. This was achieved at a GHSV of 45,000 h^{-1}. At a GHSV of 90,000 h^{-1}, the CO conversions were 75 percent in diesel mode and 79 percent in dual-fuel mode. The oxidation catalyst also reduced the NMHC emissions by 85 percent in diesel mode and 35 percent in dual-fuel mode at a GHSV of 45,000 h^{-1} (see Fig. 3). At a GHSV of 90,000 h^{-1}, the NHMC conversions were 70 and 15 percent, respectively, for diesel and dual-fuel modes. The reduced NMHC performance of the oxidation catalyst in dual-fuel mode can be attributed to the presence of higher concentrations of light hydrocarbons in the exhaust (from the combustion of natural gas). These NMHC's were identified as ethane and propane. For the diesel mode, however, the hydrocarbon species in the exhaust were higher molecular weight than C_3 (propane), which are easier to convert over the catalyst. The surface of the oxidation catalyst was observed to be clean of any soot or sticky particulate buildup.

SCR Catalyst. In either diesel or dual-fuel modes, the SCR catalyst was able to reduce NO_x emissions by up to 90 percent. Little loss in catalytic activity was observed after 850 total hours of operation, with the maximum conversion efficiency occurring at a GHSV of 15,000 h^{-1}. These data are shown in Figs. 4 and 5. As observed on the oxidation catalyst, the surface of the SCR catalyst was also clean of any soot or sticky particulate build up.

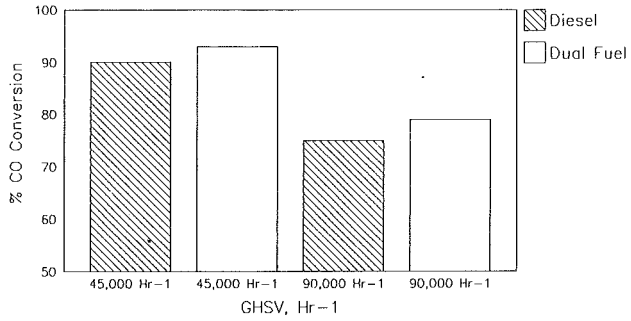

Fig. 2 Effect of GHSV on CO conversion: diesel and dual-fuel modes

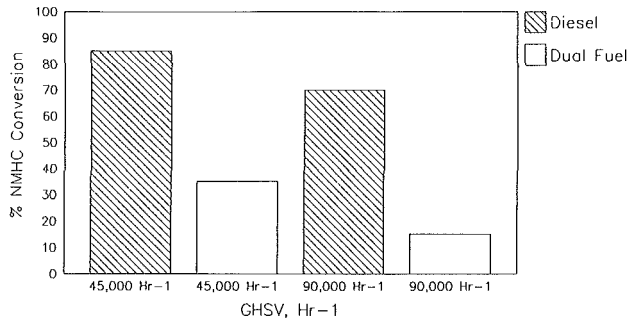

Fig. 3 Effect of GHSV on NMHC conversion: diesel and dual-fuel modes

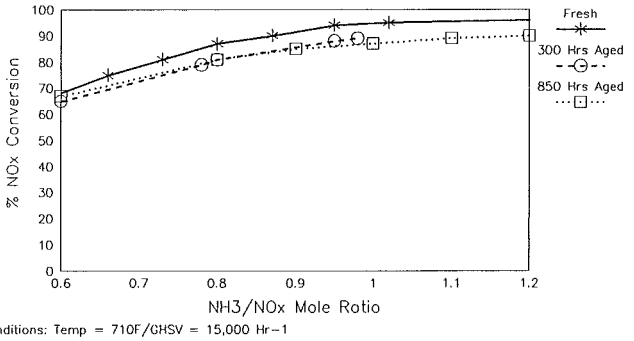

Fig. 4 SCR catalyst NO_x performance: fresh and aged (diesel mode)

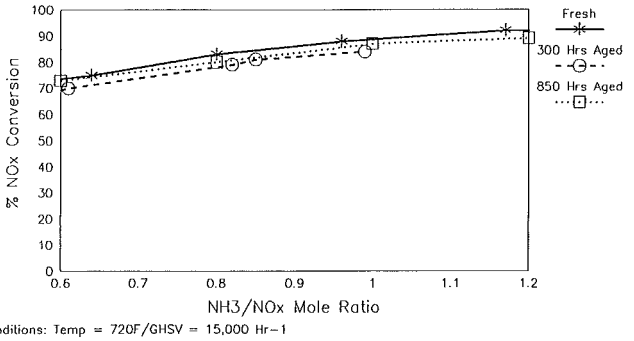

Fig. 5 SCR catalyst NO_x performance: fresh and aged (dual-fuel mode)

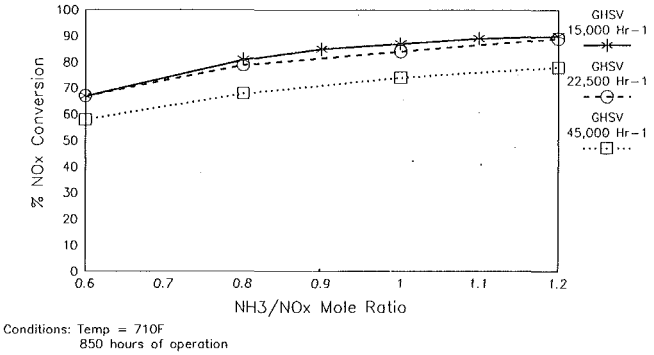

Fig. 6 Effect of GHSV on aged SCR catalyst: diesel mode

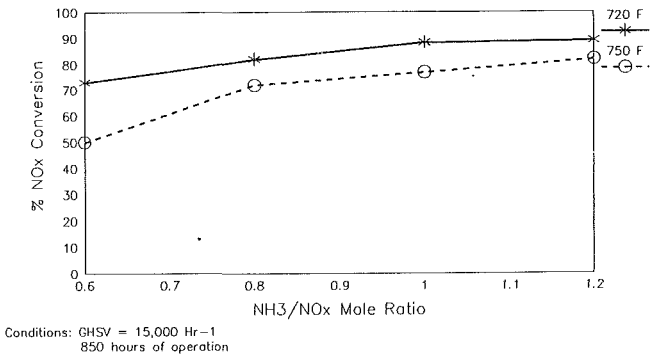

Fig. 9 Effect of temperature on aged SCR catalyst: dual-fuel mode

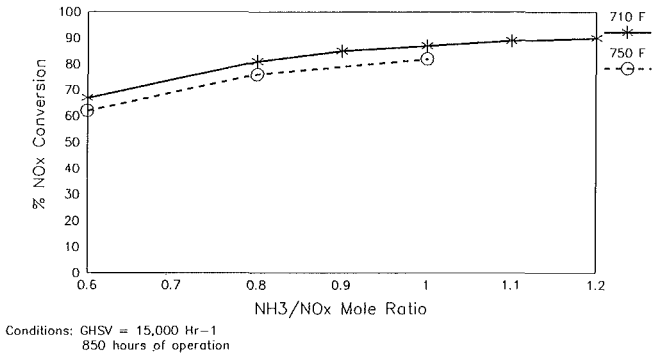

Fig. 7 Effect of temperature on aged SCR catalyst: diesel mode

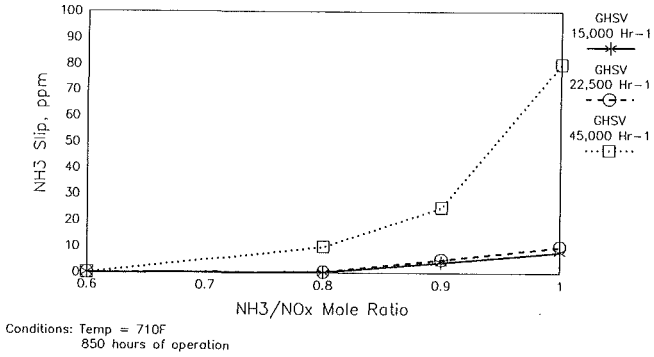

Fig. 10 Effect of GHSV on NH_3 slip: diesel mode

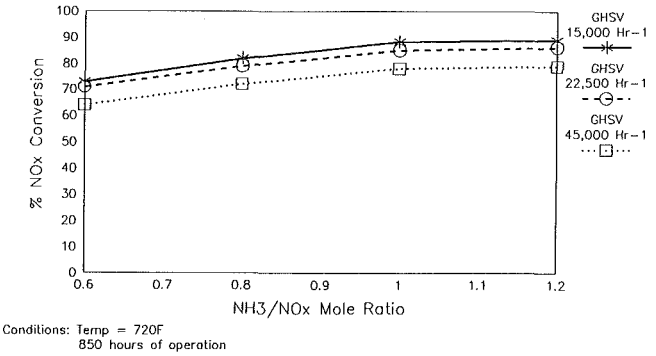

Fig. 8 Effect of GHSV on aged SCR catalyst: dual-fuel mode

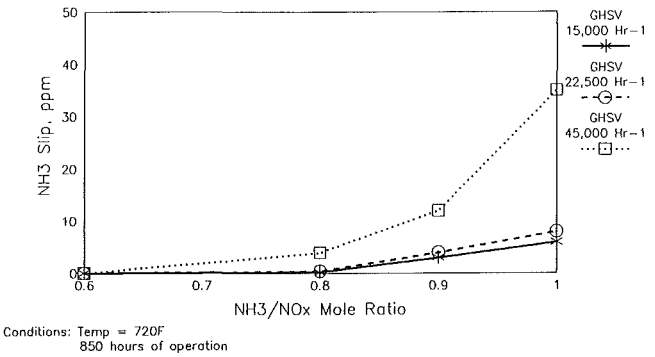

Fig. 11 Effect of GHSV on NH_3 slip: dual-fuel mode

Figure 6 shows the effect of GHSV on NO_x conversion in the diesel mode after 850 hours of operation. As expected, the NO_x conversion efficiency decreases with increasing GHSV with the maximum NO_x conversion occurring at 15,000 h^{-1}. Also in diesel mode, Fig. 7 shows the effect of exhaust temperature on NO_x conversion. The NO_x conversion efficiency was lower at 750°F, than at 710°F. Figures 8 and 9 show the same effects of GHSV and temperature, respectively, on NO_x conversion as in the case of dual-fuel mode.

The maximum NO_x conversions were achieved at NH_3/NO_x mole ratios of 1.0 or greater. Increasing the amount of ammonia injection into the exhaust stream, however, could result in excess NH_3 emissions. Therefore, it was important to determine the optimum conditions to minimize the NH_3 slip. Figures 10 and 11 show the highest amount of NH_3 slip occurring at a GHSV of 45,000 h^{-1}. The NH_3 slip at GHSVs of 22,500 h^{-1} and 15,000 h^{-1} were comparable and were 10 ppm or less in either diesel or dual-fuel modes. These data show that maximum NO_x conversions are achievable by setting the NH_3/NO_x mole ratio at 1.0 and that the resultant NH_3 slip meets the design requirements of 10 ppm or less.

Conclusions

1 The application of SCR and oxidation catalysts on lean-burning heavy-duty engines is technologically feasible to reduce NO_x, CO, and NMHC emissions at rated power.

2 The SCR catalyst reduced NO_x emissions up to 90 percent with the engine operating in diesel and dual fuel modes at rated power.

3 The SCR catalyst showed little loss in performance after 850 hours of operation.

4 In the diesel mode, maximum NO_x conversion was achieved at an exhaust temperature of 710°F and a GHSV of 15,000 h^{-1}.

5 In the dual-fuel mode, maximum NO_x conversion was achieved at an exhaust temperature of 720°F and a GHSV of 15,000 h^{-1}.

6 NH_3 slip measurements of 10 ppm and less were achieved on the SCR catalyst with a NH_3/NO_x mole ratio of 1.0 or lower.

7 No soot or sticky particulate buildup was observed on the oxidation and SCR catalysts after 230 hours of diesel operation at rated power.

8 The oxidation catalyst reduced CO emissions by as much as 90 and 93 percent with the engine operating in diesel and dual-fuel modes, respectively, at rated power.

9 The oxidation catalyst also reduced NMHC emissions by 85 and 30 percent with the engine operating in diesel and dual-fuel modes, respectively.

Acknowledgments

The authors are grateful for the full technical support in completing this demonstration and having the permission from Johnson Matthey and Fairbanks Morse to publish this paper.

References

1 Heywood, J. B., *Internal Combustion Engine Fundamentals*, McGraw-Hill, New York, 1988, p. 567.

2 Lilly, L. R. C., *Diesel Engine Reference Book*, Butterworths, 1984, Chap. 18, p. 9.

3 El-Wakil, M. M., *Powerplant Technology*, McGraw-Hill, New York, 1984, p. 716.

4 Cordonna, G. W., Kosanovich, M., and Becker, E. R., *Platinum Metals Review*, Vol. 33, No. 2, Apr. 1989.

5 Janssen, F. G., and van den Kerkohf, F. M. G., *Kema Scientific and Technical Reports*, Vol. 3, 1985, pp. 71–85.